

Identification of Flow and Transport Processes and Their Controls in the Near Surface Vadose Zone of a Clayey Glacial Till

Presented in partial fulfillment
of the requirements for the degree of
Master of Science in Hydrology

by

Craig Roepke

April 17, 1995

**Identification of Flow and Transport Processes and Their
Controls in the Near Surface Vadose Zone of a Clayey Glacial Till**

Presented in partial fulfillment
of the requirements for the degree of
Master of Science in Hydrology

by

Craig Roepke

April 17, 1995

Contents

	<u>Page</u>
Main Report	
Abstract	3
Introduction	4
Exploratory Phase	5
Testing of Hypothesized Transport Processes and Controls	6
Analysis of Transport Processes Characterization Test	
Results	8
Conclusions	13
Acknowledgments	12
References	13
Figures	14
Appendix I - Geology	
Appendix II - Infiltration	
Appendix III - Instrumentation	
Appendix IV - Colloid and Chloride Tracers	
Appendix V - Pressure Field	
Appendix VI - Dye Pulse and Excavation	

Abstract

The Transport Processes Investigation, or TPI, was developed to identify and verify site-scale transport processes and their controls in the little studied and complex vadose zone of the glacial tills underlying the Fernald Environmental Remediation Project (FEMP), in Fernald, Ohio. Based on results of an exploratory survey, an appropriate Transport Processes Characterization Test (TPCT) was designed and conducted. Analysis of data from the TPCT indicated that fracture and bioturbated macropore and megapore flow were the dominant transport processes. The TPI was able to identify the pertinent transport processes necessary for the formulation of an accurate and defensible conceptual model of flow and transport in the near-surface vadose zone. Generic modeling and sampling methods may be insufficient to identify or characterize transport processes or contaminant concentrations and distributions in such heterogeneous media.

Introduction

Site characterization has often been driven by legal and regulatory mandates requiring immediate location and monitoring of contaminant concentration distributions. This "crisis mode" may neglect an understanding of the geologic, chemical, and hydrologic processes and controls which govern flow and transport at a contaminated site. Where these processes and their controls are not well understood, simplified or inaccurate conceptual models result. Predictive simulations based upon these inadequate conceptual models and statistical sampling techniques regularly fail to correctly forecast contaminant movement, even when apparently conservative constraints and parameters have been incorporated (Lewis and Goldstein, 1982; Pearson and Konikow, 1986; Anderson and Woessner, 1992). Resulting compliance and remediation strategies may fail with associated costly legal and economic penalties.

To guard against such failure, the Transport Processes Investigation, or TPI, was developed to identify the transport processes and controls active at a site. The TPI is an initial investigative step leading to the formulation of an accurate conceptual model, providing a more thorough scientific understanding of the site, and lessening site characterization costs and time expenditures. The TPI is contained in three main steps, summarized below:

- **An exploratory phase** integrates a search of the literature and existing site data with small scale field tests and exploratory surveys of local outcrops. During this step, hypotheses are made of probable transport processes and controls, hydrostratigraphic units, and their connectivity.
- **Testing of hypothesized transport processes and controls** is accomplished by conducting appropriately designed and sited transport processes characterization tests (referred to hereafter as TPCTs). As appropriate, TPCTs employ techniques such as pump tests, infiltration and tracer studies, dye pulses and excavation, and detailed soil/rock sampling in order to thoroughly investigate the anticipated field-scale transport processes and controls.
- **Analysis of TPCT results** confirms or refutes the hypothesized transport processes and determines whether the active transport processes and controls at the site are adequately understood or if additional investigation is required.

A better understanding of how contaminant transport occurs at the site leads to more efficient sampling program design. Conditioned on the results of the TPI, decision rationales incorporating risk, uncertainty analysis, and economic value of information decision models such as Sandia Environmental Decision Support System (SEDSS) are able to further optimize characterization activities (Webb, et al., 1993). It is important to note that without an initial study of the physical processes and controls of contaminant transport, characterization and remediation efforts may proceed in an uninformed and expensive mode, controlled only by previously discovered contamination and compliance mandates.

In this paper, the results of a TPI conducted at the Fernald Environmental Management Project (FEMP) are presented. The near surface vadose zone tills at Fernald contain varied fractured and heterogeneous media, resulting in complex transport processes that provide a challenging test. The media are typical of deposits covering much of the North American continent (Keller et al., 1986; Jones et al., 1992) and have been the subject of relatively few field investigations (Bronswijk et al., 1995). In the following sections, the three phases of the TPI are discussed and conclusions as to the transport processes and controls active in the near-surface vadose zone at the site. Complete details and data are contained in Appendices. Appendix I - Geology, contains a discussion and presentation of regional geology, local outcrop surveys, and TPCT site borehole sampling and excavation. Appendix II - Infiltration, discusses infiltrometers, water supply, infiltration initiation and maintenance, and infiltration monitoring. Appendix III - Instrumentation, includes complete details of sensor array conception and design, instrument construction, and sensor installation. Appendix IV - Colloid and Chloride Tracers, contains a description of colloid and Cl^- tracer pulses and applications, soil water sampling of Cl^- tracer data, Time Domain Reflectometry (TDR) measurement of Cl^- tracer concentrations, and graphs of TDR and soil water sampler Cl^- tracer concentrations. Appendix V - Pressure Field, presents data acquisition,

reduction, results, and graphs of the pressure field in time. Appendix VI - Dye Pulse and Excavation, discusses the dye pulse and excavation of the Clay Site (Site A) and presents photos of the results.

The Exploratory Phase

During the exploratory phase, information gained from a literature search, several small preliminary tests, and a survey of local outcrops is combined, and hypotheses of transport processes are made. The literature search identified transport processes and controls common in glacial tills. Macropore or fracture flow may define fast transport pathways in layered or fractured clays (e.g., Van de Pol et al., 1976; Neretniks, 1983; Keller, et al., 1988, 1986; Ruland et al., 1991; Rudolph et al., 1991; Jones et al., 1992; McKay et al., 1993; Bronswijk et al., 1995). Media heterogeneity may also create zones of preferential flow (Neilsen et al., 1973; Vieira et al., 1981; Wagenet et al., 1984). Even in unsaturated soils without apparent or extensive macropores, preferential flow may exist due to wetting front or percolation instabilities (Bowman and Rice, 1986; Glass et al., 1988). Transport through clays in glacial tills may also be by diffusive mechanisms (Jones et al., 1992) or diffusive matrix-fracture interaction (Parker et al., 1994).

With these potential flow and transport processes in mind, a reconnaissance survey of the site was conducted. Paddys Run Creek, an intermittent stream crossing the Fernald site, afforded 2.5 km of stream cut bank for a survey of local outcrops (Refer to Figure 1). Stratigraphic units and probable transport controls were investigated and mapped. Active seeps associated with structural features and at topographically low contacts of sand and gravel channels overlying clayey units were noted (Figure 1, outcrops #8 and #5). Small scale dye infiltration tests (Figure 2) were conducted in several outcrops and confirmed transport processes such as fracture and macropore flow. Results of the exploratory survey and the preliminary tests implied a connection between small scale transport processes and larger scale geologic structural features and heterogeneity (Glass et al., 1995).

Hydrostratigraphy and hypothesized transport processes and controls

Uranium is the crucial contaminant at the Fernald site. Soluble (hexavalent) and colloidal forms of Uranium had been determined to exist on the surface and at depth at the site (Tidwell, 1993 and ITT, 1990). In either of these cases, aqueous subsurface transport processes and controls are critical, and units were consequently defined on the basis of their hydrologic, rather than geologic, characteristics. The six hydrostratigraphic units chosen are distinguished by unique flow and transport processes and controls (Table 1). Figure 3 illustrates their generalized spatial relationship. A more detailed description is given in Appendix I.

Unit	Composition	Hypothesized Transport Processes and Controls
6	Sand and gravels	Highly transmissive matrix flow
5	Topsoils and loess	Matrix flow, macropore and fracture flow, adsorption of colloids to organic material
4	Blocky structured silty clays	Matrix, fracture, and macropore flow
3	Oxidized bedded clays	Flow horizontally along bedding planes, vertically through fractures, transport through matrix by diffusion only
2	Unoxidized bedded clays	Flow through fractures, slight flow possible along tight bedding planes, diffusive flow only through matrix
1	Massive unoxidized (gray) clays	Flow through sand and gravel channels, along structural deformation, through matrix by diffusion only

Table 1. Hydrostratigraphic units and associated transport processes and controls.

Analog area selection

To minimize safety and regulatory concerns and the attendant costs, the exploratory phase also included a search for an analog to contaminated areas where the hypothesized flow and transport processes could be tested. If possible, the analog site fulfills certain criteria. An uncontaminated site permits testing without causing contaminant migration or increased procedural burden. A TPCT site in close proximity to actual contaminated areas argues for adequate analog (climate, weather, geology, etc.). Nearby outcrops for geologic mapping and interpretation are necessary, and ownership is desirable. Meeting these criteria at Fernald yielded the selection of an approximately 90 hectare, uncontaminated, client-owned field along the west side of Paddys Run Creek (Figure 1). This field, leased for dairy cow pasture, is approximately 500 m from the main uranium processing plant and within 250 m of several known locations of uranium contamination, all on the opposite, East side of Paddys Run (Figure 1). Dissection of the local glacial till by Paddys Run afforded approximately 2.5 Km of stream cut outcrops ranging in elevation from 1 m to 8 m for geologic mapping. The higher relative topographic elevation of the field suggested hydrologic separation from contaminated sites on the opposite side of Paddys Run (Figure 1).

Testing of Hypothesized Transport Processes

TPCT Design

Because the saturated conditions encountered in the near surface vadose zone during an early spring site survey may provide the worst case conditions for colloidal or dissolved contaminant transport, the test was designed to simulate saturated conditions. 2.2 meter diameter circular surface infiltrometers (Appendix VI, Plate 11) with a constant ponded head of approximately 5 cm. water created a steady-state saturated flow field. Cl^- , analog colloid, and dye tracers introduced through the infiltrometers were intended to reflect preferential flow.

Results from the exploratory phase suggested active transport processes would be macropore flow through insect, worm, and root holes; rapid transport along bedding planes, structural features, and through fractures; preferential flow through highly transmissive sand and gravel stringers and channels; and diffusive transport between macropores and clay matrices. To investigate these hypothesized features, an intensive sampling array was used, consisting of forty-four sampling points in a 3-D, 10 m diameter, 2 to 3 m deep, radial arrangement (Figures 4 and 5). Each 50 cm. long by 10 cm. diameter sampling point contained a Time Domain Reflectometry (TDR) probe, a tensiometer, a colloid sampler, and a suction soil water sampler, all in a fine sand pack. The sampling points were sealed from intra-borehole flow with bentonite. The 50 cm. long by 10 cm. diameter dimensions of the sampling point instrument packs were intended to permit interception of the anticipated macropore and fracture network without requiring integration of results over such large volumes as to render spatial definition of flow paths impossible. The use of sand in the instrument packs provided a high conductivity medium to facilitate sampling and interception of macropores.

The transducer-equipped tensiometers installed at each sampling point monitored the pressure field via a microprocessor-controlled, automatic data acquisition system at fifteen minute intervals throughout the test. Measurement of the pressure field was designed to allow definition of the overall flow field and to detect preferential flow. Transducers monitored by this system also supplied rain gage and infiltration rate measurements. The TDR probes served as passive monitors of Cl^- tracer movement, while the soil water suction and colloid samplers provided active monitoring of Cl^- and colloid distributions. Soil moisture was not of prime importance under the saturated conditions generated by the ponded infiltration, and TDR soil moisture measurements were made only to determine if the desired saturated conditions did indeed exist.

Because the test site(s) must not only contain media and features relevant to the anticipated transport processes, but also be suitable for implementation of the TPCTs, final selection of specific test site(s) is dependent upon the final TPCT design. Several candidate sites for TPCTs were located within the analog area during a reconnaissance in the early spring. In late May a number of exploratory holes were augered. Based on samples from the exploratory holes, two sites were chosen for TPCTs. Together, the two sites contained distinct geologic sequences and media that represented both the major hydrostratigraphic units and all the hypothesized transport process and their controls (Figures 1 and 5).

The Sand Site was composed of topsoils and loess (Unit 5) overlying blocky structured clays (Unit 4). Beneath these units was a large, unconsolidated body of sand and gravels (Unit 6). Instrument boreholes penetrated the sands and gravels only to a depth below ground surface of approximately 2.5 meters before the

walls collapsed. Bedded clays (Units 2 and 3) were encountered at the Sand Site only in isolated samples above the sand and gravel unit.

The Clay Site contained a hydrostratigraphic sequence including all of the units at the Sand Site plus horizontal beds of oxidized and unoxidized clays (Units 3 and 2) extending across the site and overlying the massive unoxidized gray clays (Unit 1). The sands and gravels of Unit 6 were evidenced as stringers and one sand channel penetrating Unit 1, not in a large sand body as at the Sand Site.

The elevation of the upper and lower sampling levels (Figure 5) was determined by the stratigraphy encountered during sampling at each site. At the Clay Site, the upper levels were contained in the oxidized layered clays (Unit 3) approximately 2 meters below ground surface, with the lower levels located at approximately 3 meters depth in the layered oxidized clays (Unit 2) or at the upper surface of the massive unoxidized clay (Unit 1). At the Sand Site, the upper level instrument packs were located in the blocky structured silty clays (Unit 4) at approximately 1.1 meters depth, while the lower level packs were contained in the underlying sands and gravels (Unit 6) at approximately 2.1 meters depth.

TPCT Implementation

Infiltration was initiated at both the Clay and Sand Sites in mid June by pouring water into the circular infiltrometers and simultaneously opening the water supply valves, creating an essentially instantaneous ponded head of 5 cm. Infiltration was continued uninterrupted at both TPCT sites till late August, sixty-six days after the start.

Five days after the start of infiltration, when steady state conditions had been achieved, an analog colloid pulse was introduced at the Clay Site. The pulse was composed of 260 mL (2% solids) of 1 μm blue fluorescent Interfacial Dynamics Corporation latex microspheres and 25 mL (2% solids) of .2 μm yellow fluorescent microspheres. The water supply to the infiltrometer was first shut off and the analog colloids well mixed into the water within the infiltrometer. Infiltration was resumed after the water containing the colloid pulse had dropped to the ground surface inside the infiltrometer. A pulse of 25 mL (2% solids) of Interfacial Dynamics Corporation .2 μm yellow fluorescent microspheres was introduced in the same manner into the Sand Site.

Six days after the start of infiltration, clean water supply was halted, and the water level in the Clay Site infiltrometer was allowed to drop to the ground surface. Before any de-saturation occurred, a 0.1M CaCl_2 tracer solution was poured from containers into the infiltrometer, quickly re-establishing the 5 cm. ponded level. Infiltration of the Cl^- tracer was continued from a site supply tank. The next day, the same procedure was followed at the Sand Site. After infiltration of 1,534 Liters in 48 hours, the Cl^- tracer pulse at the Clay Site was terminated and infiltration of clean water resumed. The total Cl^- pulse at the Sand Site was 1,209 Liters in 53 hours. The lower Cl^- tracer flow rate into the Sand Site may have been the result of greater degradation of the conductivity of the infiltrometer surface by algae in the water supply (Refer to **Infiltration** results, below).

Sixty-two days from the start of infiltration, FD&C Red #3 dye was added to the Clay Site infiltrometer supply tanks. After infiltration of 400 gallons of dye at the Clay Site TPCT in four days, infiltration was simultaneously terminated at both the Clay and Sand Sites. Three days later, excavation of the Clay Site was begun. Excavation proceeded down and into the lowermost massive gray clay (Unit 1). The excavation was accomplished using both a back hoe and hand tools. The back hoe rapidly removed one foot to two foot layers, and was followed by a detailed examination using hand tools. This process ensured that complete and detailed transport features would be revealed. The final excavation was approximately 20 m in diameter at the surface, sloping to a 5 m diameter floor at 5.1 m depth.

Analysis of TPCT Results

Analysis of data from the TPCTs confirmed the existence of our hypothesized transport processes and yielded a much improved understanding of their active controls at the Fernald site (Figure 6). The major results from each type of measurement are presented below.

Infiltration

Figure 7 presents the infiltration rates of both the Clay Site and the Sand Site in time. The maximum daily average infiltration rate at the Clay Site was 2.23 cm/hr, attained approximately 570 hours after the start of infiltration. From this point, infiltration asymptotically declined to 0.74 cm/hr. During the dye pulse at the Clay Site, the infiltration rate again experienced a decline from 0.74 cm/hr to 0.57 cm/hr. The dye pulse was created by infiltrating dissolved powdered dye, and the resulting suspension apparently had a detrimental effect on the transport ability of the system, especially the topsoil matrix where the majority of the dye was captured (Plate 19, Appendix VI). The maximum daily average infiltration rate for the Sand Site was 2.85 cm/hr, attained after approximately 514 hours of infiltration. After reaching this maximum, the infiltration rate declined to approximately 0.73 cm/hr.

Various explanations have been proposed for the pattern of infiltration rate change in time shown in Figure 7. DeBano (1969) noted that the decrease in conductivity resulting from water repellent soils diminished with time as the soil wetted and can produce the delayed rise in infiltration rate experienced. One hundred sixty water drop penetration time tests on were conducted on samples distributed within the upper two layers of soil at each site. In all samples, the water drop penetrated immediately upon contact with the soil. A careful contact between the water drop and the soil resulted in soil particles attaching to the water drop while the water drop was still attached to the hypodermic syringe/dropper, indicating a hydrophilic contact angle of zero. Muckel (1959) suggested that this pattern of rapid decrease followed by the rise and second decline shown in Figure 7 rate is caused by entrapment of air, dissolution of the entrained air, and subsequent biological degradation of the hydraulic conductivity.

Changes in the upper and lower boundary conditions of the flow system are the likely cause for the pattern. The regulatory constraints in effect at the site prevented the use of even a mild algacide in the infiltrator supply water. The warm and sunny summer conditions and the translucent polyethylene water supply tanks produced 35 °C. water temperatures and resulted in persistent algae growth in both the supply tanks and the infiltrators. The rise to maximum infiltration rate began approximately 100 hours after the introduction of the Cl⁻ pulse, when algae growth was observed to be strongly reduced. The subsequent decrease in infiltration rates began approximately 400 hours after the start of the tracer, when the Cl⁻ was essentially flushed from the system and algae growth in the infiltrator and site supply tanks resumed (See Figure 7).

The long time, steady-state infiltration rate will approach the 1-D saturated hydraulic conductivity (Rubin, J. and R. Steinhardt, 1963). In 1-D flow perpendicular to layering, K_{eff} is expressed by the harmonic mean and should be controlled by the conductivity of the least conductive layer. At the Sand Site, these limiting layers are the silts and loess with saturated conductivities ranging from 10^{-5} cm/s to 10^{-7} cm/s. Conductivity values are from Freeze and Cherry (1979). At the Clay Site, the limiting media are the clays with conductivities ranging from 10^{-7} cm/s to 10^{-11} cm/s. However, infiltration rates after five hundred hours of infiltration approached 10^{-3} cm/s at both sites, exceeding the limiting conductivities by almost two to eight orders of magnitude. The difference between expected and realized infiltration rates is likely due to macropore and megapore flow, lateral flow through fractures and along bedding planes, and flow through highly transmissive sand and gravel stringers and channels (See Tracer and Dye Pulse and Excavation discussions below). The similarity between infiltration rates at the two geologically different sites can be explained by the controlling effect of the upper boundary conditions of the flow system, as noted in the discussion above of algae growth.

Sixty-one thousand liters of water were infiltrated in sixty-six days at the Clay Site, and 78,000 liters of water were infiltrated over the same period at the Sand Site. These large quantities of infiltrated water imply a well-drained flow system. No evidence of moisture at the surface was found anywhere outside the infiltrator during the entire test, also implying an effective, interconnected subsurface transport-pathway system capable of significant transport from the surface to depth or laterally (e.g., via the seeps into Paddys Run Creek noted during the exploratory phase).

Additionally, the accepted bulk conductivity of the surface soils (10^{-5} cm/s to 10^{-7} cm/s), is less by half an order of magnitude than even the lowest infiltration rates experienced (at the Clay Site after introduction of the

dye pulse). This suggests that infiltration even in the generally homogeneous upper layers was controlled by flow through transport pathways that remained unaffected by clogging with the suspended dye; e.g., macropores such as root hole, wormhole, and fractures.

Pressure head field

The pressure head field across the instrument array showed a general pattern of mounding beneath the infiltrometer, with local head perturbations of -10 to -5 cm distinguishing areas of preferential flow (Figure 8). The majority of sampling points showed rapid response to rainfall events (Figure 9). The rise in head was often ten times the amount of precipitation. McWhorter (1971), Bianchi and Haskell (1968), and others have attributed this response to an increase in air pressure from confinement of air between the water table and an advancing, saturated air wetting front. Given the well-connected and well-drained nature of the flow system, the preponderance of dye tracer flow through macropores (See Dye Pulse and Excavation below), and the negligible viscosity of air, it is unlikely such a simplistic explanation is adequate. It is possible that filling of the macropores feeding the sampling points resulted in the observed pressure head response. Topp and Davis (1981) found that rainfall events with magnitudes as small as 1 cm. and intensities as low as 1 cm./hr resulted in flow through clay fractures. If soil air pressure increases were responsible for the increase in pressure head measurement, all sampling points across the array should have demonstrated equal times and magnitudes of rise. However, the time and magnitude response was quite variable (Figure 10). The natural spread in macropore density and connectivity is a probable cause for the range in both time and magnitude responses, both within and between the sites.

The variation in macropore density and connectivity is also demonstrated by the response of individual sampling points to soil water suction sampling. Points showing a low magnitude response to rainfall events typically required a long time for re-equilibration after soil water sampling, suggesting they were not connected to a ready source of water or air. Sampling points showing a rapid and relatively large response to rainfall events usually recovered quickly from sampling suctions (Figure 11). The response to rainfall events, and the recovery from soil water sampling, is likely proportional to the degree of connection to the surface and/or a rapid flow pathway.

Plots of changes in total potential over the period of the tests at individual instrument locations in both the Clay and the Sand Site exhibit trends mimicking the change in infiltration rate (See Figure 12). This correspondence supports the proposition that algae constriction of water passages at the upper boundary (infiltrometer surface) of the flow system combined with abundant drainage from the lower boundaries to control the patterns of change in infiltration rate and head.

Tracer concentration field

Both soil water sampler and TDR measurement of Cl⁻ tracer concentration distributions showed that tracer movement at both sites was initially vertical downward immediately below the infiltrometer, then moved laterally in irregular spatial and temporal patterns. The lateral distribution of tracer concentrations began sooner at the more layered and heterogeneous Clay Site than at the Sand Site and continued almost ten days longer. Both the downward and lateral Cl⁻ tracer movement at the Clay Site appeared to follow definite pathways (Figure 13). The bulk of Cl⁻ tracer at the Sand Site remained directly below the infiltrometer twice as long as at the Clay Site, and the lateral distribution was more homogeneous (Figure 13).

One sampling point 2 m below the infiltrometer in the Clay Site was directly intercepted by a wormhole (See Dye Pulse and Excavation below). The Cl⁻ tracer arrived at this sampling point with a peak concentration of C/Co > .85 after only 41 minutes for a solute velocity = v_s = 2 m/41 min ≅ 8.1 x 10⁻² cm/s. Solute travel velocities for sampling points directly below the infiltrometer at the Clay Site and Sand Sites are given in Table 2, below:

	Max (cm/s):	Min (cm/s):	Avg (cm/s):
Clay Site:	8.1 x 10 ⁻²	2.3 x 10 ⁻⁴	7.3 x 10 ⁻³
Sand Site:	6.7 x 10 ⁻⁴	9.7 x 10 ⁻⁵	2.2 x 10 ⁻⁴

Table 2. Solute travel times at the Clay and Sand Sites.

While the more sandy and less heterogeneous sequence at the Sand Site (Figure 5) is conventionally modeled as more conductive than the layered clay sequence at the Clay Site, average solute transport at the Clay Site was over an order of magnitude faster. This suggests that flow through macropores and zones of preferential flow, rather than through the matrix, provides the bulk of solute transport. Breakthrough curves at both sites, but especially at the Clay Site, displayed a long tail, implying the expected diffusion from macropores and fractures into a clayey matrix and the resultant retardation of solute movement out of the system (Figure 14).

The differences in TDR versus suction lysimeter peak arrival times and magnitudes can be used to identify preferential flow. The artificial flow field generated when a suction is applied during soil water sampling, combined with the instrument and macropore geometry illustrated in Figure 15a, yields faster arrival times and higher peaks at the suction lysimeter. The effect is illustrated in the results from sampling site A31-80U (Figure 15b). The opposite result may also be gathered from the soil water sampler, TDR probe, and transport pathway relationship illustrated in Figure 16a. In this configuration, the suction applied to the soil water sampler causes solutes to arrive first at the TDR probe and in greater concentration. The repeated peaks displayed by the TDR trace correspond exactly to soil water sampling times, further evidence that the gradient induced by soil water sampling caused flow past the TDR probe from a preferential flow path. In either of the situations displayed above, the evidence for fast transport pathways is apparent. Repeated peaks in breakthrough curves are also strong evidence for the existence of preferential or secondary transport pathways. Figure 17 illustrates the contributions of both a primary and secondary solute transport pathway.

Colloid Tracer

Soil water samples for colloid concentration analysis were captured in 15 mL glass sampling bottles to prevent adhesion of the microspheres to the polyethylene sample bottles used for Cl^- tracer capture. The samples were transported to Los Alamos National Laboratory for testing. By the time testing could be accomplished, the fluorescent materials had degraded to the extent that no definable measurements could be made, though fluorescent microspheres were detected in most tested samples. Previous use of the microspheres and communication with the manufacturer had not uncovered this deficiency and more reliable analog colloids are under development at Los Alamos National laboratories.

Dye Pulse and Excavation

The dye pulse and subsequent excavation of the Clay Site presented striking visualization of flow processes and transport pathways, and confirmed data from the instrument array. A vertically integrated plan view of dye-stained transport pathways is shown in Figure 18. This sketch displays only the main occurrences of macropore and preferential flowpaths.

The matrix of the uppermost layer of topsoils and loess was heavily infused with dye (Plate 19, Appendix VI), while vertical root, worm, and insect macropores and fractures transported the dye tracer through the underlying blocky structured clays (Plates 29 to 39, Appendix VI). The matrix of this unit was stained only in the immediate vicinity of active macropores and transmissive fractures, indicating that transport bypassed the bulk of the Unit 4 matrix. This staining of the matrix in the near vicinity of the macropores (Plate 34, Appendix VI) confirmed the potential for diffusive transport and retardation, as inferred above from the analysis of the Cl^- tracer results (Figure 14). As hypothesized, lateral transport along horizontal fractures and bedding planes was noted both in the oxidized bedded clays of Unit 3 and in the unoxidized bedded clays of Unit 2. Numerous instances of dye-stained vertical and horizontal fractures were noted in bedded clays (Plates 51 and 54, Appendix VI).

In addition to these expected features, pipe-like pathways approximately 2 cm by 3 cm in cross sectional area, were found extending from just beneath the topsoil to depth. These large macropores were later identified as crayfish burrows that are endemic to the area (Plates 40, 80 to 84, and Figure 18). Dye-filled crayfish burrows and burrow complexes connected the topsoils to fracture networks in the bedded clays, to depths 2 meters below the water table in spring and early summer. These pathways are each capable of transmitting much more than the maximum flux observed passing through the infiltrometers. Stone (1993) notes that crayfish vertically extend these "hardened," and "long-persisting" burrows to maintain contact with a lowering water table, and he also notes that their connectivity allows rapid lateral flow irrespective of antecedent moisture. Sampling points at 3 m depth in the southern quadrant of the Clay Site never measured any significant Cl^- tracer, though a large number of dye-stained crayfish burrow complexes were found there (Figure 18). It is probable that all tracer moving through this quadrant in the lower depths was transported via these crayfish burrows, none of which was

intercepted by sampling points. These and all other bioturbated pathways ended in the unoxidized layered clays of Unit 2. A cursory 15 minute inspection of the surrounding field after completion of the excavation discovered three instances of crayfish burrows at the surface (Plates 104 to 109). A single surface entrance usually indicates an underlying burrow complex (Stone, 1993).

Dye transport through numerous silty sand and sand and gravel stringers was discovered (Plates 44, 87, and 102). These highly transmissive transport pathways were common, and penetrated to the deepest extent of the Clay Site excavation. A sand stringer which discharged dyed water was discovered at 2.8 m depth penetrating the unoxidized layered clays of Unit 3 (Plates 77 and 78). Further excavation revealed connection to a glacially inserted large silty sand body (mixture of Units 6 and 4) located in the Northwest quadrant of the Clay Site (Plate 76 and Figure 18).

At the depths where Unit 1 was first encountered (3 to 5 meters), the dye pulse was diluted to an extent that no confident association could be made between the infiltrated dye pulse and flowpaths. However, when excavated samples of Unit 1 were broken open, they often split along planes that appeared to be shear or remnant bedding features. These fracture planes were typically covered with a fine sand, indicating flow had occurred at some time in the past. A few of these fracture planes contained red dye from a secondary dye pulse initiated after excavation to approximately 3 meters, affirming that flow at low gradients was possible through this unit (Plates 55 and 103).

Conclusions

The Transport Processes Investigation proved an effective, expeditious, and relatively inexpensive tool to identify the active flow and transport processes. The following conclusions are made.

Transport Processes and controls:

- The dominant flow and transport pathways from the topsoil to the bedded clays are vertical bioturbated macropores and fractures. These pathways are capable of rapid and abundant transport during most of the year, when essentially saturated conditions exist or when rainfall events are of sufficient magnitude to enter the macropore system.
- The bedded clays support a pervasive network of transmissive horizontal and vertical fractures and are hydrologically connected to the surface primarily by vertical fractures and macropores passing through the topsoil and blocky structured clays.
- Channels and stringers of sands and gravels provide localized zones of preferential flow and are often interconnected by fractures and macropores.
- Some crayfish burrows are continuous from the surface through the bedded clays and intersect fracture networks in the clays. Crayfish burrows provide rapid transport pathways to the lowest annual levels of the water table, allowing contaminants to bypass extensive volumes of the near surface media. In some areas they may be the primary avenues for transport. In clayey and highly heterogeneous media, contaminant transport may go undetected even with an intensive sampling scheme.
- This glacial depositional environment is extensively reworked and deformed, and highly transmissive sand and gravel channels and fracture zones penetrate portions of all hydrostratigraphic units. Shear and fracture zones, discontinuities, and sand and gravel channels discovered in the massive unoxidized clays may render the "gray clay" flow barrier ineffective.
- Seeps found during the exploratory geologic survey may be representative of significant lateral field-scale transport pathways.

Implications for sampling, modeling, and remediation:

- At least four simultaneous and interrelated flow and transport processes must be addressed in any conceptual model: diffusive transport and retardation from matrix-macropore interaction in fine-grained materials such as layered and massive clays; highly transmissive matrix flow through sandy channels and stringers and slower transport through finer-grained matrices; macropore flow through small fractures, root holes, and wormholes; and pipe flow through large megapores such as crayfish burrows.
- The well drained nature of both the Clay and Sand Sites indicates that modeling of contaminant flow and transport in the near-surface vadose zone at Fernald must acknowledge the potential for extensive lateral and vertical (3-D) movement.

- Generic predictive models based on conventional statistical analysis and simplifying assumptions of flow and transport will not likely reflect the active rapid transport processes or controls.
- Significant pockets of contamination and rapid transport pathways may go undiscovered by conventional sampling techniques. Conventional statistical analysis based on classical sampling methods may easily allow subsurface transport pathways and pockets of contamination to go unmodeled.

To fully characterize the active transport processes and their effect on contaminant migration, further studies are necessary:

- The connectivity and the transport processes and pathways between the near-surface vadose zone, the deeper media, and the underlying confined aquifer must be conclusively determined.
- Larger scale and longer term tracer tests investigating the lateral and vertical transport processes should be performed, preferably under natural conditions.

Acknowledgments

I would like to acknowledge the contributions of the following individuals and organizations. Kim Nuhfer of FERMCO provided administrative, logistical, and planning support. Cliff Lee of FERMCO aided in geological sampling and instrumentation support. The efforts of the leaders of the Site Sampling Team, Mike Stott and Tim Smith, and that of the members, Nick Jansen, Bill Neyer, Jenny Milchert, and Andy Cleeter were invaluable. Jim Brainard, Mike Mann, Bob Holt, and Kelly Kriel of SNL provided invaluable field assistance and support. Support for this demonstration was provided by the DOE Technology Development Landfill Waste Area program.

References

- Anderson, M. P. and W. W. Woessner. 1992. *Applied Groundwater Modeling*. Academic Press, Inc, San Diego.
- Beven, K., and P. Germann. 1982. Macropores and water flow in soils. *Water Resources Research*. v. 18, pp. 1311-1325.
- Bianchi, W. C. and E. E. Haskell Jr. 1968. Air in the Vadose Zone as it Affects Water Movements Beneath a Recharge Basin. *Water Resources Research*. v. 2, pp. 315-322.
- Bowman, R. S. and R. C. Rice. 1986. Transport of conservative tracers in the field under intermittent flood irrigation. *Water Resources Research*. v. 22, pp. 1531-1536.
- Bronswijk, J. J. B., Hamminga, W., and K. Oostindie. 1995. Field scale solute transport in a heavy clay soil. *Water Res. Res.* v. 31. pp 517-526.
- DeBano, L. F. 1969. Water repellent soils: A worldwide concern in management of soil and vegetation. *Agricultural Science Review*. v. 7, pp. 11-18.
- Fernald Environmental Management Project. 1993. USID : Uranium in Soils Integrated Demonstration Program. Prepared for the U. S. DOE, Oak Ridge Operations Office.
- Freeze, R. A., and J. A. Cherry. 1979. *Groundwater*, Prentice-Hall, Inc, Englewood Cliffs, New Jersey.
- Glass, R. J., Brainard, J., Roepke, C., and M. Mann. 1995. Preliminary Subsurface Transport Pathway Characterization Test: Data Report Summer 1993. Prepared for Fernald Environmental Restoration Management Corp. and the DOE Office of Technology Development, Cincinnati, Ohio.
- Glass, R. J., T. S. Steenhuis, and J. Y. Parlange. 1988. Wetting front instability as a rapid and far-reaching hydrologic process in the vadose zone. *Journal of Contaminant Hydrology*. v. 3, pp. 207-226.
- ITT. 1990 Remedial Investigation Report for Operable Unit 3. Feed Materials Production Center, Fernald, Ohio. Prepared for U. S. DOE
- Jones, L., Lemar, T., and T. Chin-Ta. 1992. Results of Two Pumping Tests in Wisconsin Age Weathered Till in Iowa. *Groundwater*. v. 30, pp. 529-538.
- Kachanoski, R. G., E. Pringle, and A. Ward. 1992. Field measurement of solute travel times using time domain reflectometry. *Soil Science Society of Am. Journal*. v. 56, pp. 46-52.
- Keller, C. K., van der Kamp, G., and J. A. Cherry. 1986. Fracture Permeability and Groundwater Flow in Clayey Till Near Saskatoon, Saskatchewan. *Canadian Geotechnical Journal*. v. 23, pp. 229-239.
- Keller, C. K., van der Kamp, G., and J. A. Cherry. 1988. Hydrogeology of Two Saskatchewan Tills, I. Fractures, Bulk Permeability, and Spatial Variability of Downward Flow. *Journal of Hydrology*. v. 101, pp. 97-121.
- Lewis, B. D. and F. S. Goldstein. 1982. Evaluation of a predictive ground-water solute-transport model at the Idaho National Engineering Laboratory, Idaho, USGS, Water-Resources Investigations Report 86-4022, 71 p.
- McKay, L. D., Cherry, J. A., and R. W. Gillham. 1993. Field experiments in a fractured clay till 1. Hydraulic conductivity and fracture aperture. *Water Resources Research*. v. 29, pp 1149-1162.
- McWhorter, D. B. 1971. Infiltration Affected by Flow of Air, Colorado State University Hydrol. Paper 49, Fort Collins, CO
- Muckel, D. C. 1959. Replenishment of Ground Water Supplies by Artificial Means, U. S. Dept. of Agric., Agric. Res. Service Tech. Bull. 1195.
- Neretniks, I. 1983. A note on fracture flow dispersion mechanisms in the ground. *Water Resources Research*. v. 19, pp. 364-370.
- Nielsen, D. R., and J. W. Biggar, and K. T. Erh. 1973. Spatial variability of field-measured soil-water properties. *Hilgardia*. v. 42, pp. 215-259.
- Person, M. and L. F. Konikow. 1986. Reclaibration and predictive reliability of a solute transport model of an irrigated stream-aquifer system. *Journal of Hydrol.* v. 87, pp. 145-165.
- Richard, T. and T. S. Steenhuis. 1988. Tile drain sampling of preferential flow on field scale. *Journal of Contaminant Hydrology*. v. 3.
- Rubin, J. and R. Steinhardt. 1963. Soil water relations during rain infiltration: I. Theory. *Soil Science Society of America Proceedings*, 27.
- Rudolph, D. L., Cherry, J. A., and R. N. Farvolden. 1991. *Water Resources Research*. v. 27, pp. 2187-2201.
- Ruland, W. W., Cherry, J. A., and Stan Feenstra. 1991. The Depth of Fractures and Active Ground-Water Flow in a Clayey Till Plain Southwestern Ontario. *Ground Water*. v. 29, pp. 405-417.
- Stone, E. L. 1993. Soil Burrowing and Mixing by Crayfish. *Soil Science Society of America Journal*. v. 57, pp. 1096-1099.
- Tidwell, V. C., Cunnane, J. C., Gill, V. R., Lee, S. Y., Morris, D. E., Nickleson, M. D., and D. L. Perry. 1993. Uranium in Soils Integrated Demonstration Project: Soil Characterization Project Report. Prepared for Fernald Environmental Management Restoration Corp., Cinn, OH.
- Topp, G. C. and J. L. Davis. 1981. Detecting infiltration of water through soil cracks by time domain reflectometry. *Geoderma*. v. 26. pp 13-23
- Van de Pol, R. M., Wierenga, P. J., and D. R. Nielsen. 1977. Solute movement in a field. *Soil Science Society of America Journal*. v. 41, pp. 10-13.
- Vieira, S. R., D. R. Nielsen, and J. W. Biggar. 1981. Spatial variability of field measured infiltration rate. *Soil Science Society of America Journal*. v. 45, pp. 1040-1048.
- Wagenet, R. J., R. E. Knighton, and E. Bressler. 1984. Soil chemical and physical effects on spatial variability of hydraulic conductivity. *Soil Science*. v. 137, pp. 252-262.
- Webb, E.K., S. Conrad, and R. Breeden. 1993. A probabilistic approach to site characterization for the Superfund Program. in: R. Chawla (ed.) *Proceedings Federal Environmental Restoration Conference and Exhibition, May 25-27, 1993, Washington D.C., Hazardous Materials Control Resources Institute*, p. 321-327.

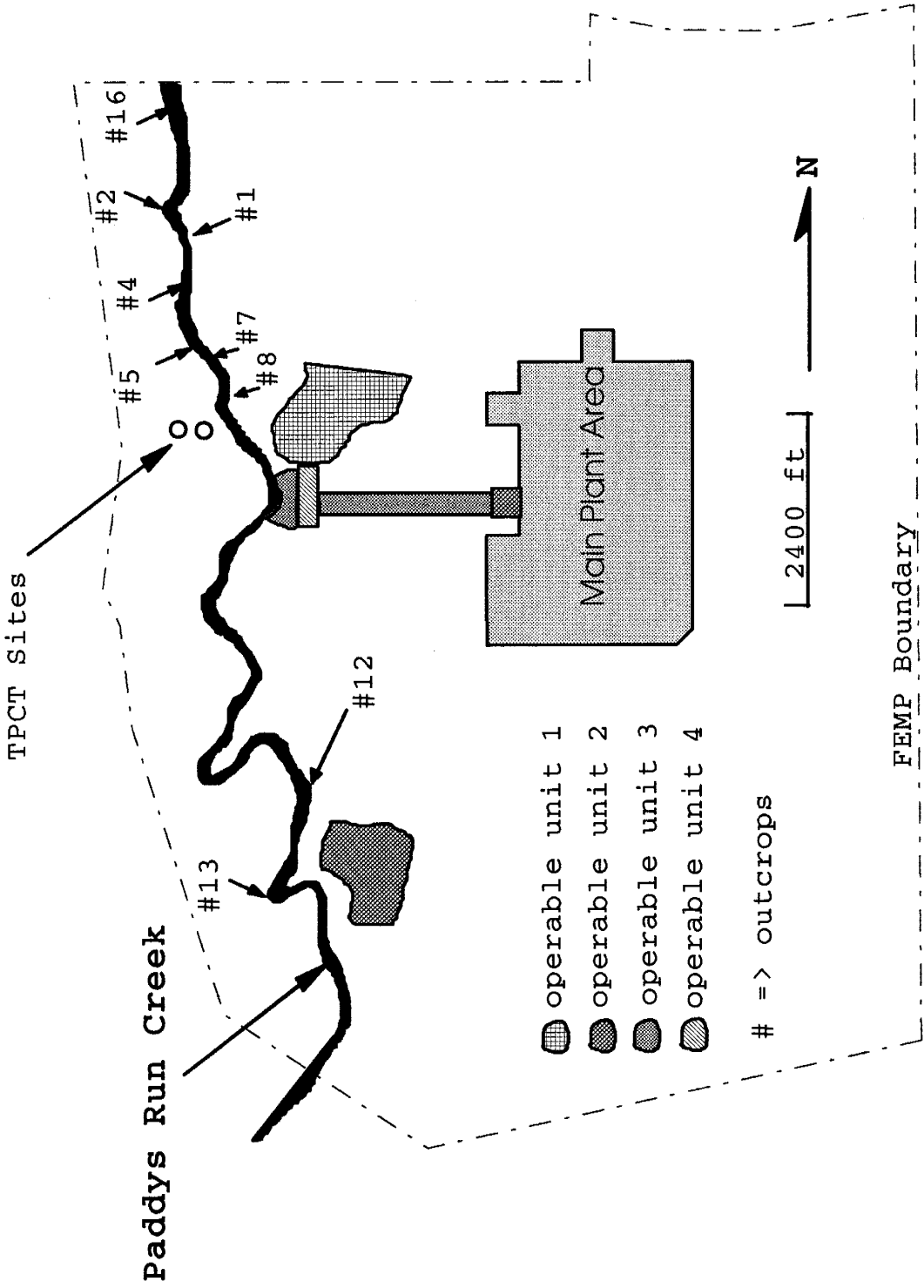


Figure 1. Surveyed outcrop locations along Paddy's Run in relation to location of main plant and Operable (contaminated) Units.

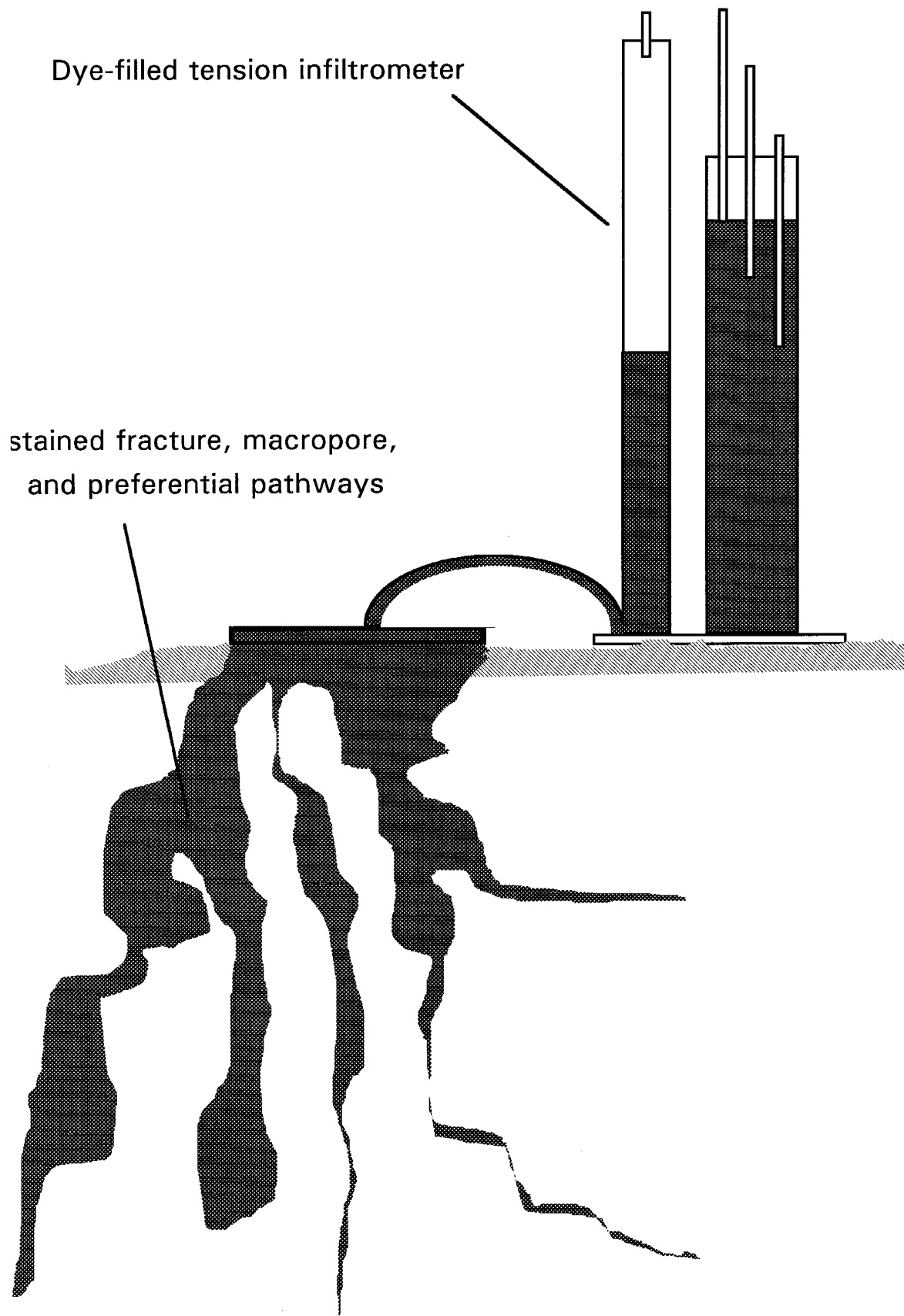


Figure 2. Initial small scale tests identified possible transport processes.

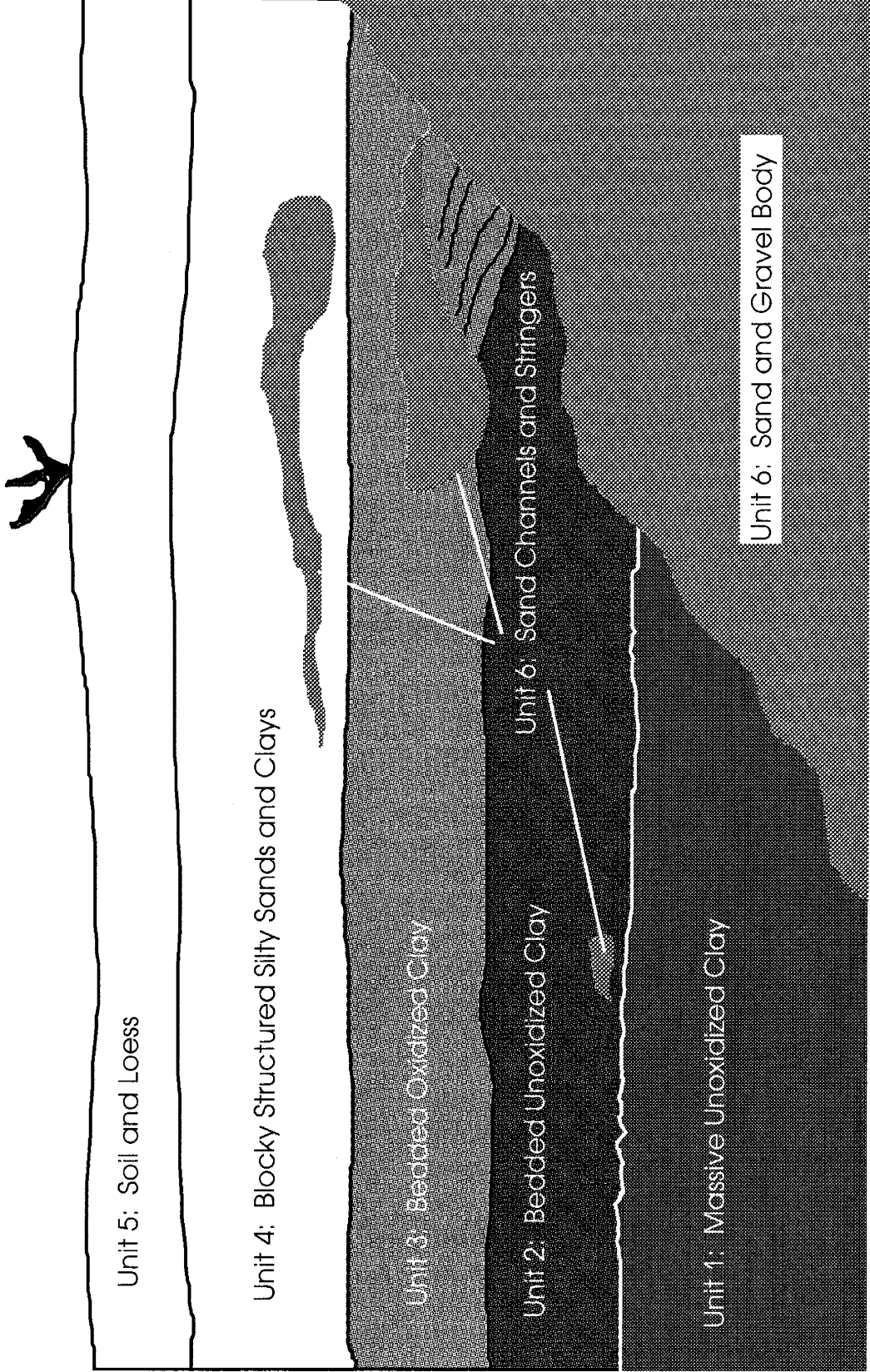


Figure 3. Generalized relationship of the six hydrostratigraphic units.

Clay Site Sampling Array

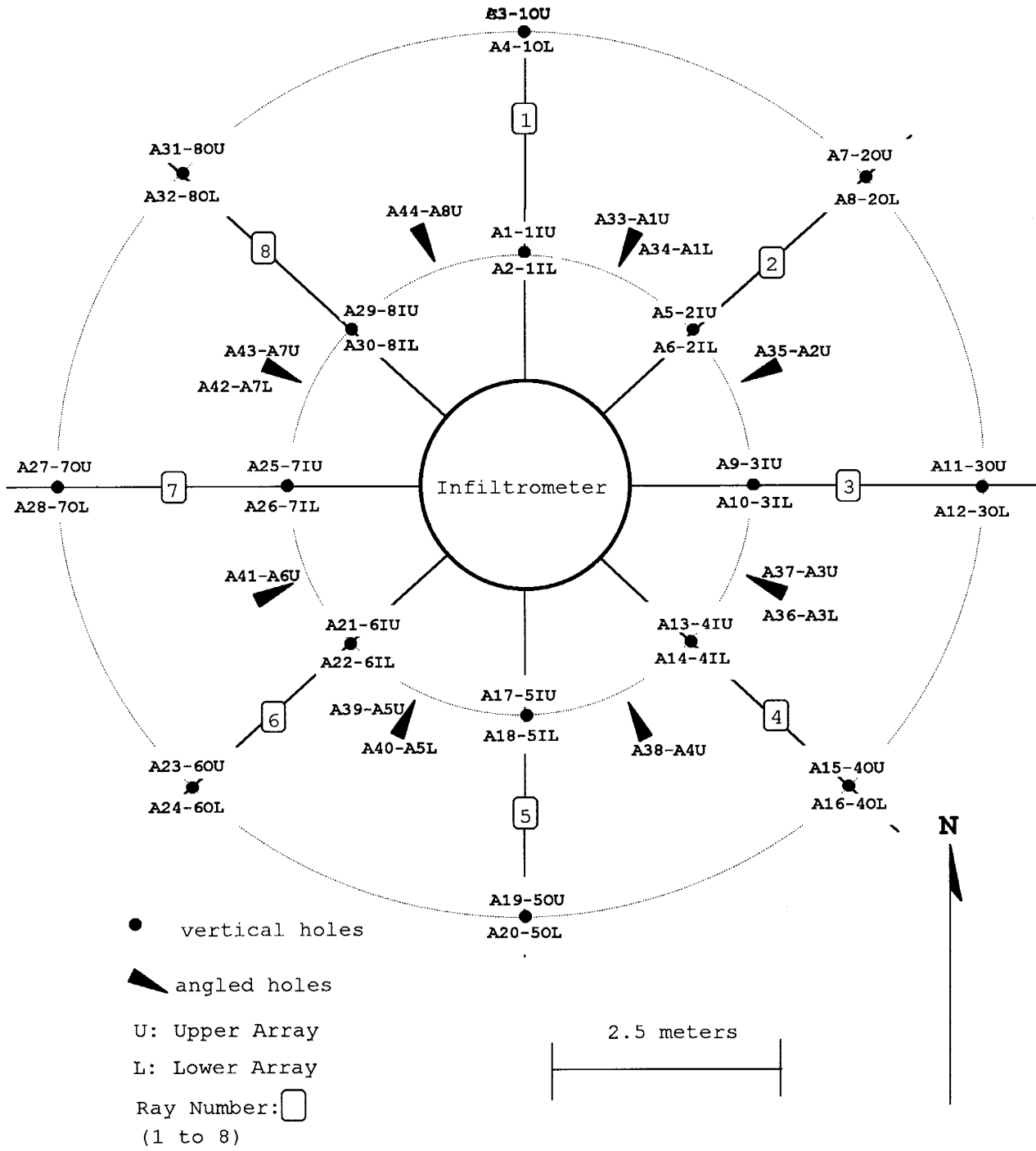


Figure 4. Clay Site instrument array. The plan layout of the sampling points is identical at the Sand Site.

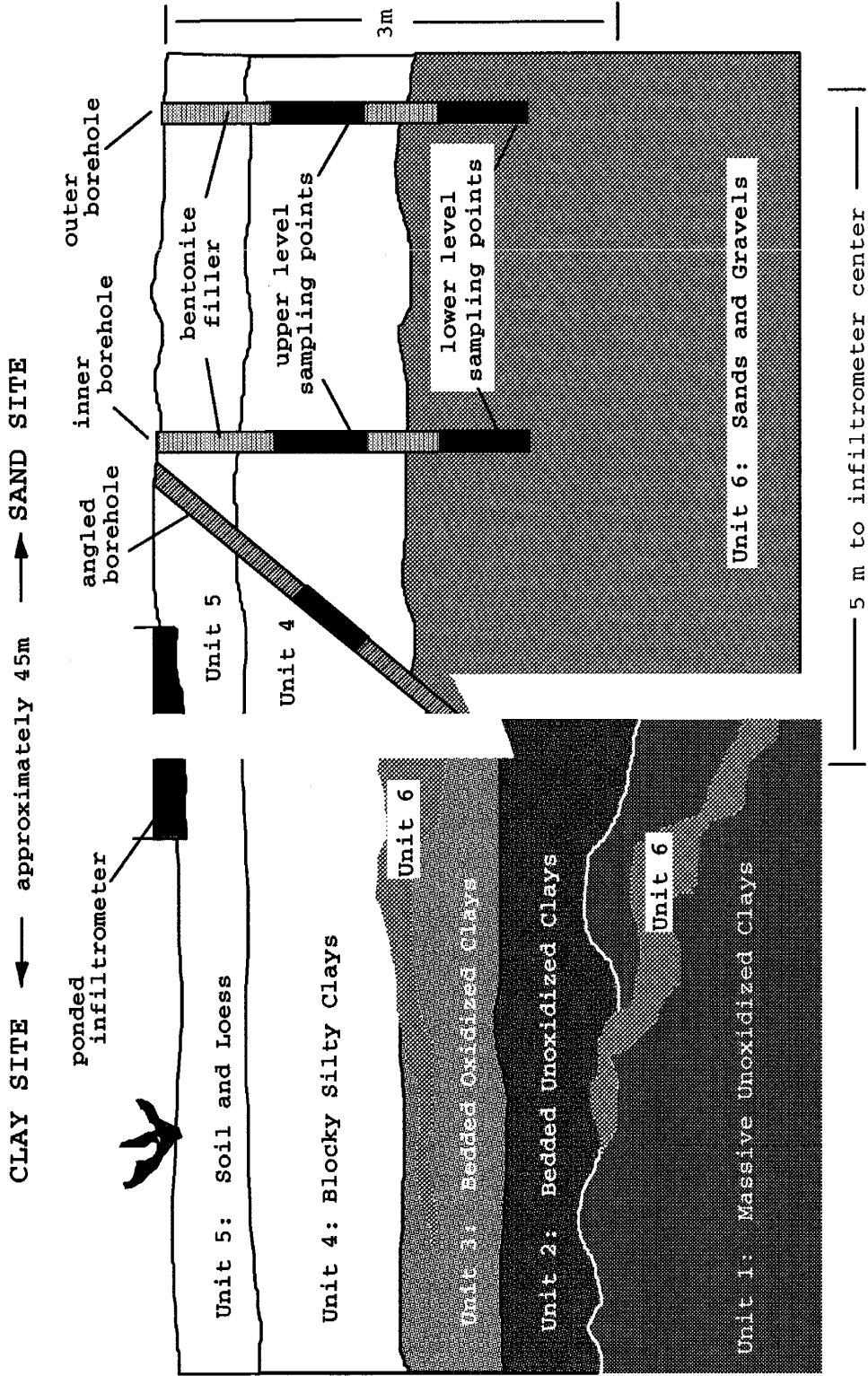


Figure 5. Hydrostratigraphic units at the Clay and Sand Sites. A cross section of the instrument array at the Sand Site is also shown. The instrument array at the Clay Site is identical except the upper and lower level instrument packs are approximately 1 m deeper, with the lower packs just above Unit 1.

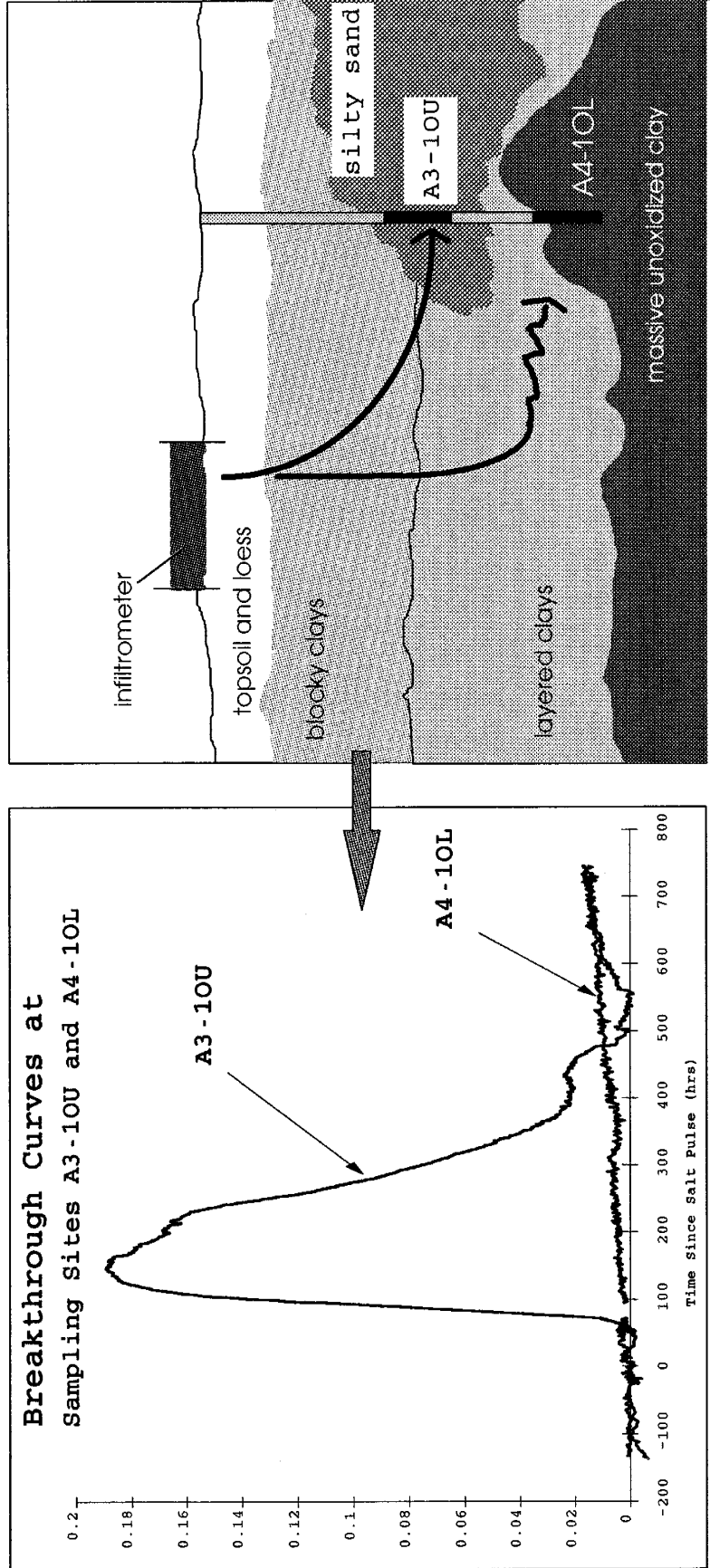


Figure 6. Sampling data reflected actual transport processes and controls.

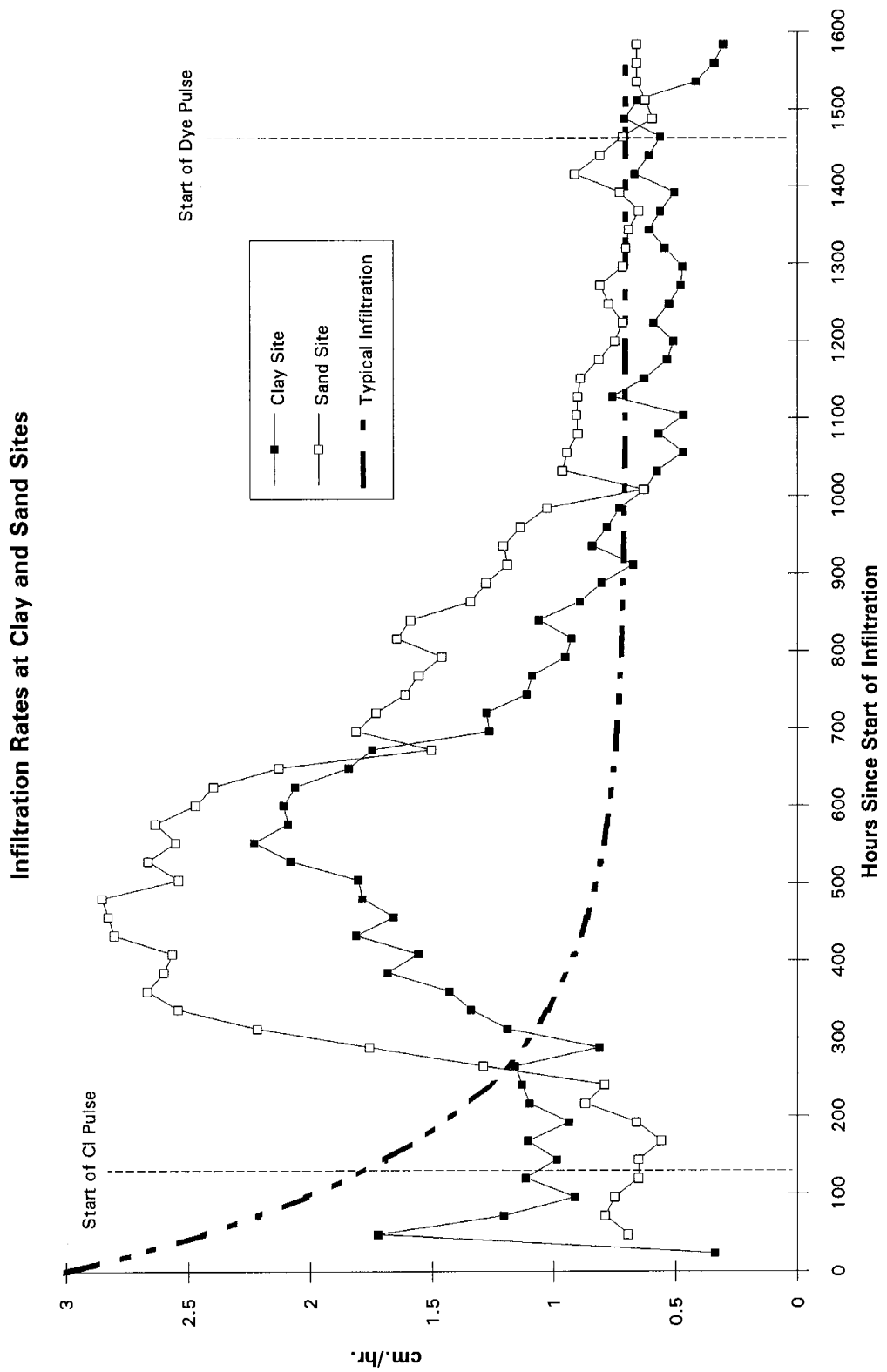


Figure 7. Infiltration rates at the Clay and Sand Sites.

Clay Site, 3 Meter Level
Head in Meters Below Infiltrometer Surface
500 Hours After Start of Infiltration

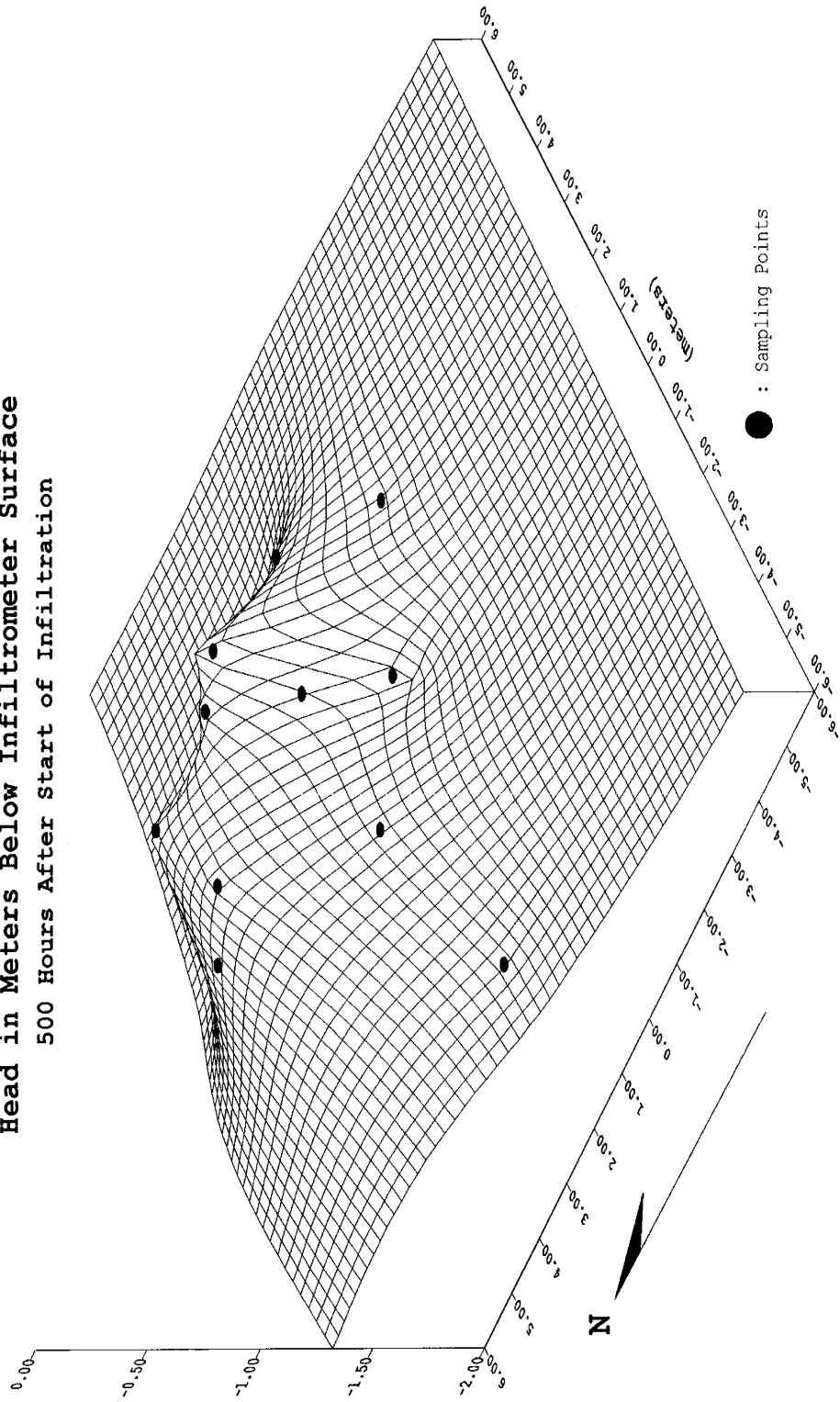


Figure 8. Pressure head surface plot at the 3 meter (lower) level of the Clay Site tensiometer array 500 hours after start of infiltration. The 2.2 meter ponded surface infiltrometer would be above the plot, centered at (0.0, 0.0, 0.0).

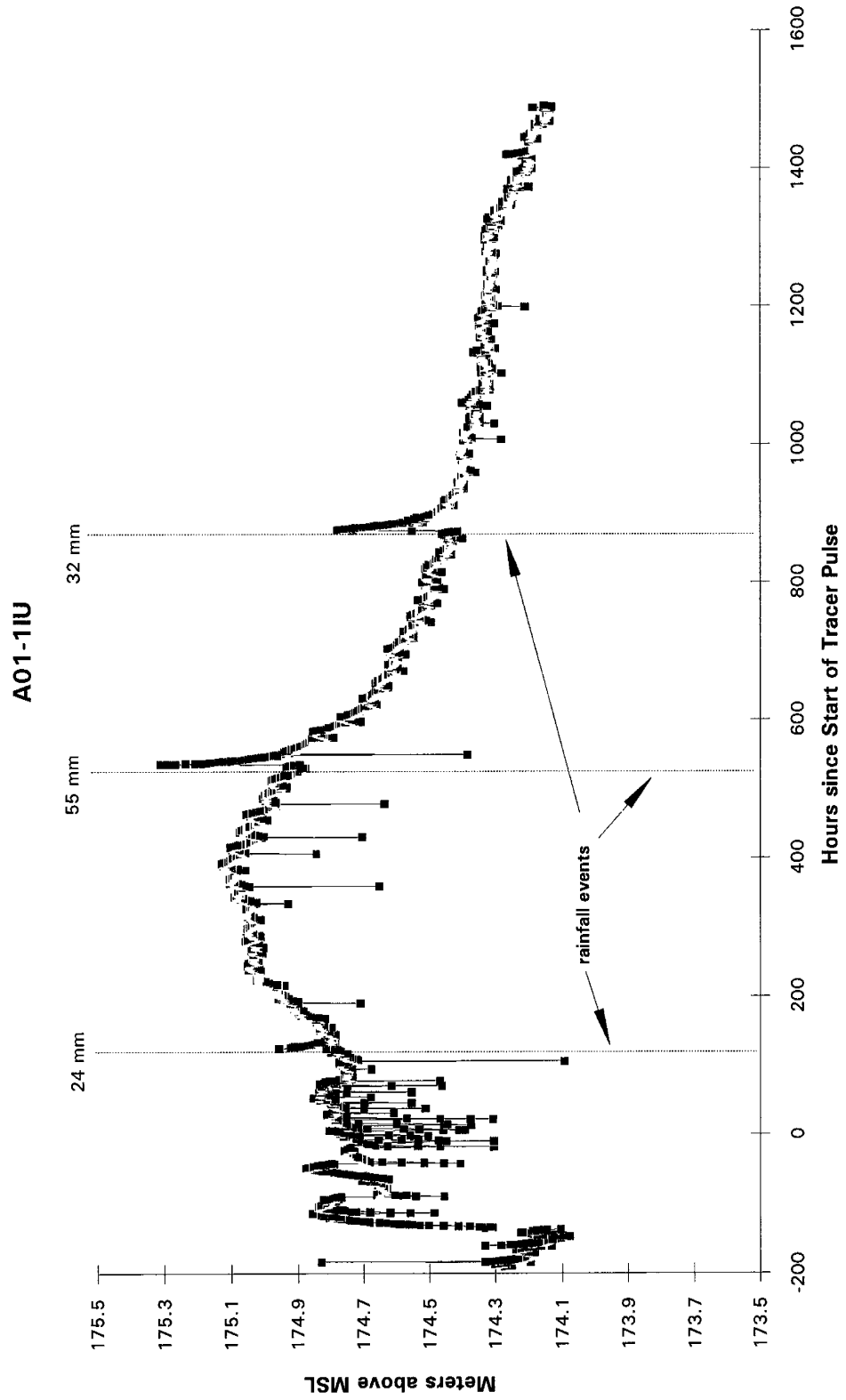


Figure 9. Potentiometric head and response to rainfall events at sampling point A1-IU, Site A.

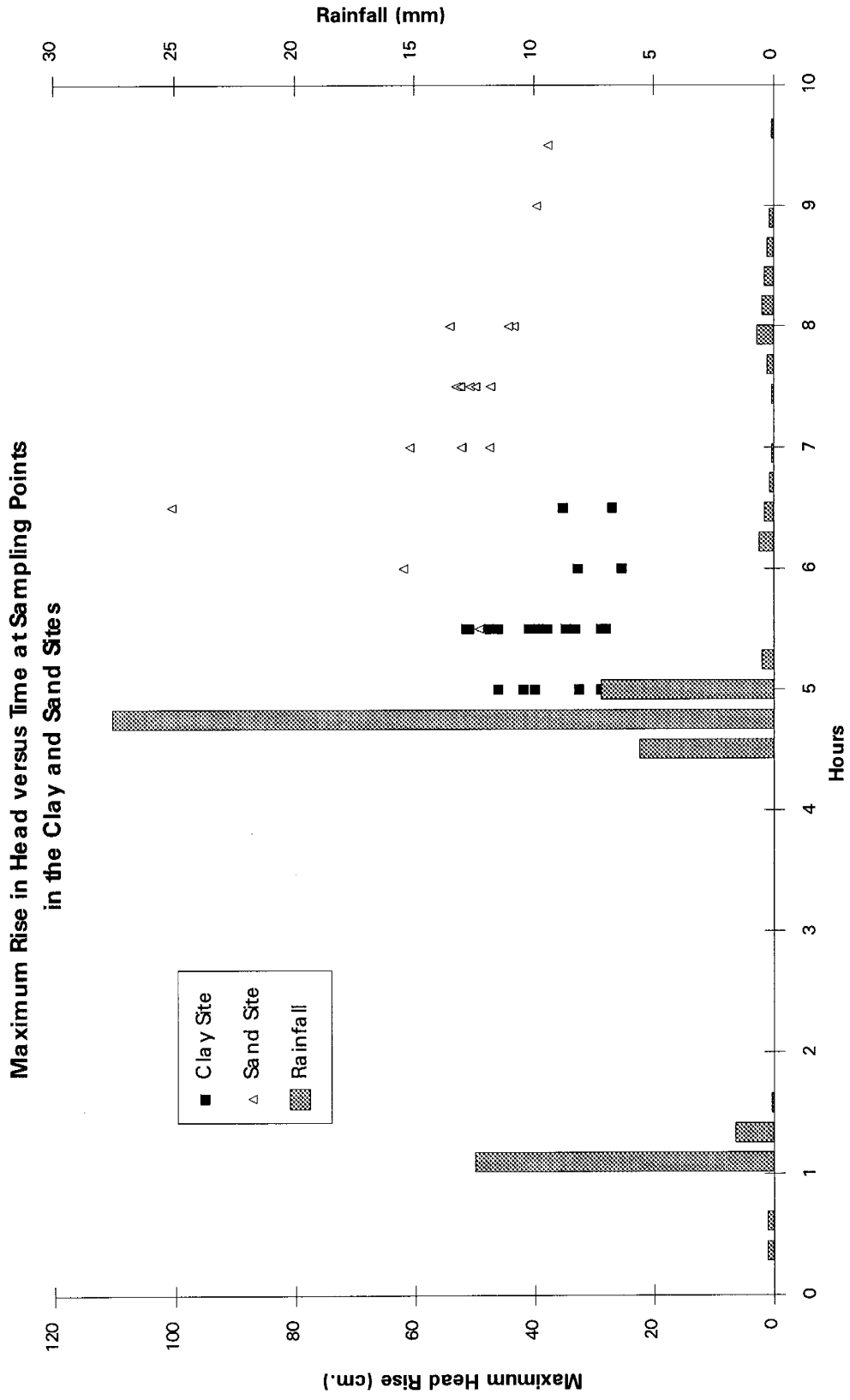


Figure 10. Variability of maximum head rise and time at the Clay and Sand Sites during a rainfall event.

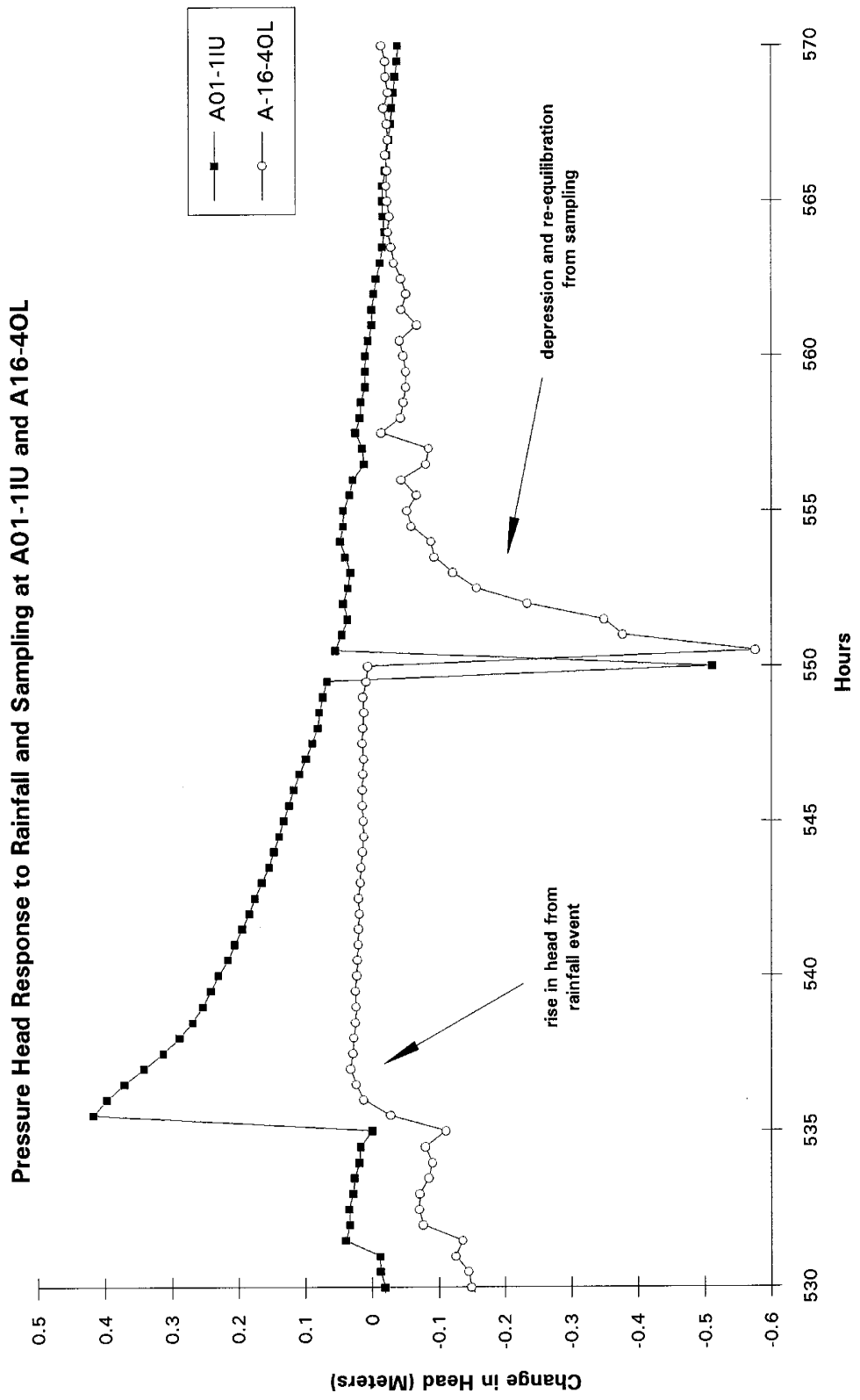


Figure 11. Pressure potential response to rainfall and re-equilibration from soil water sampling at a point connected to macropores (A01-1IU) and at an isolated sampling point (A16-4OL).

Correspondence of Infiltration Rate and Head at Sampling Point A1-1IU

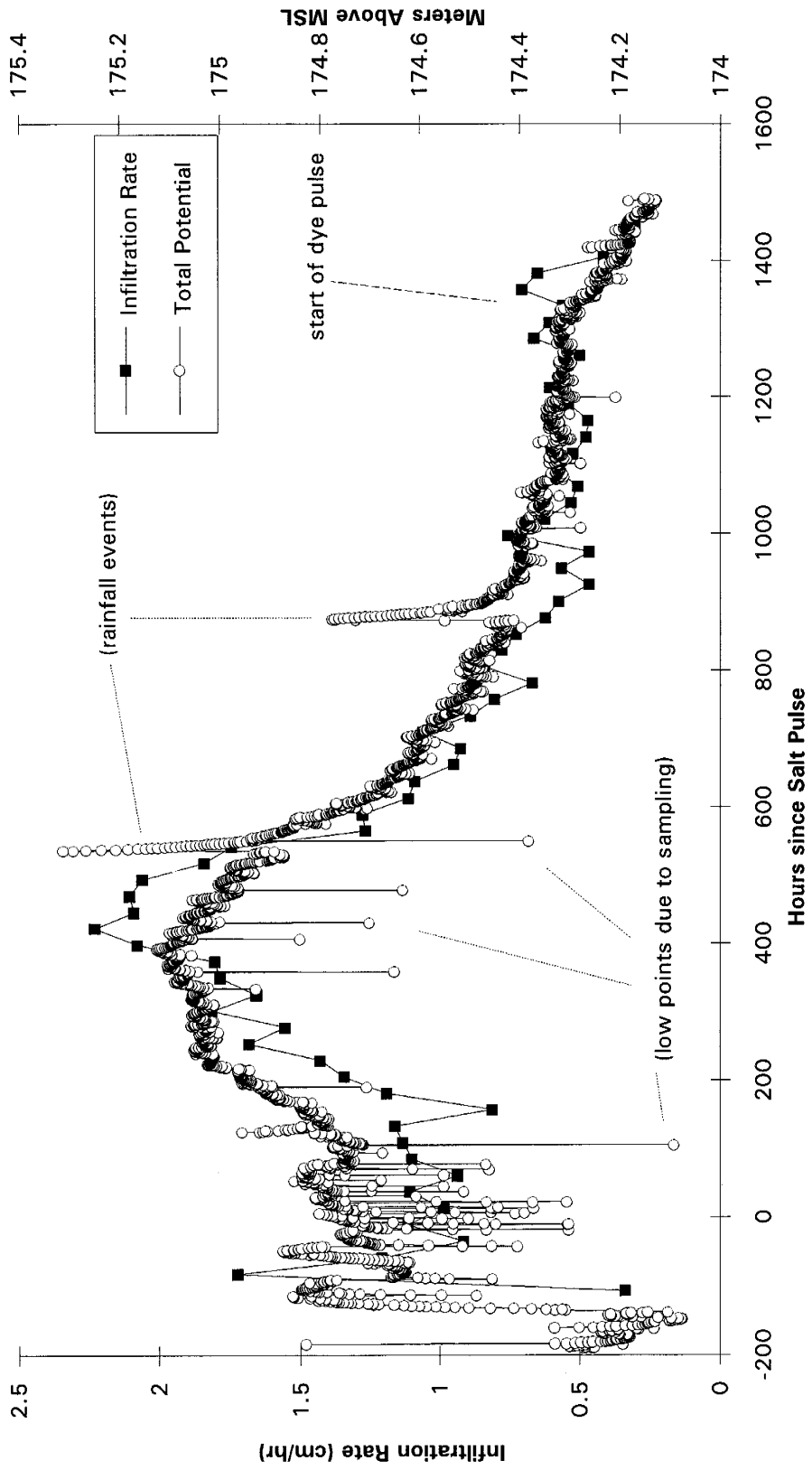


Figure 12. Correspondence of trends between infiltration rate and changes in total potential.

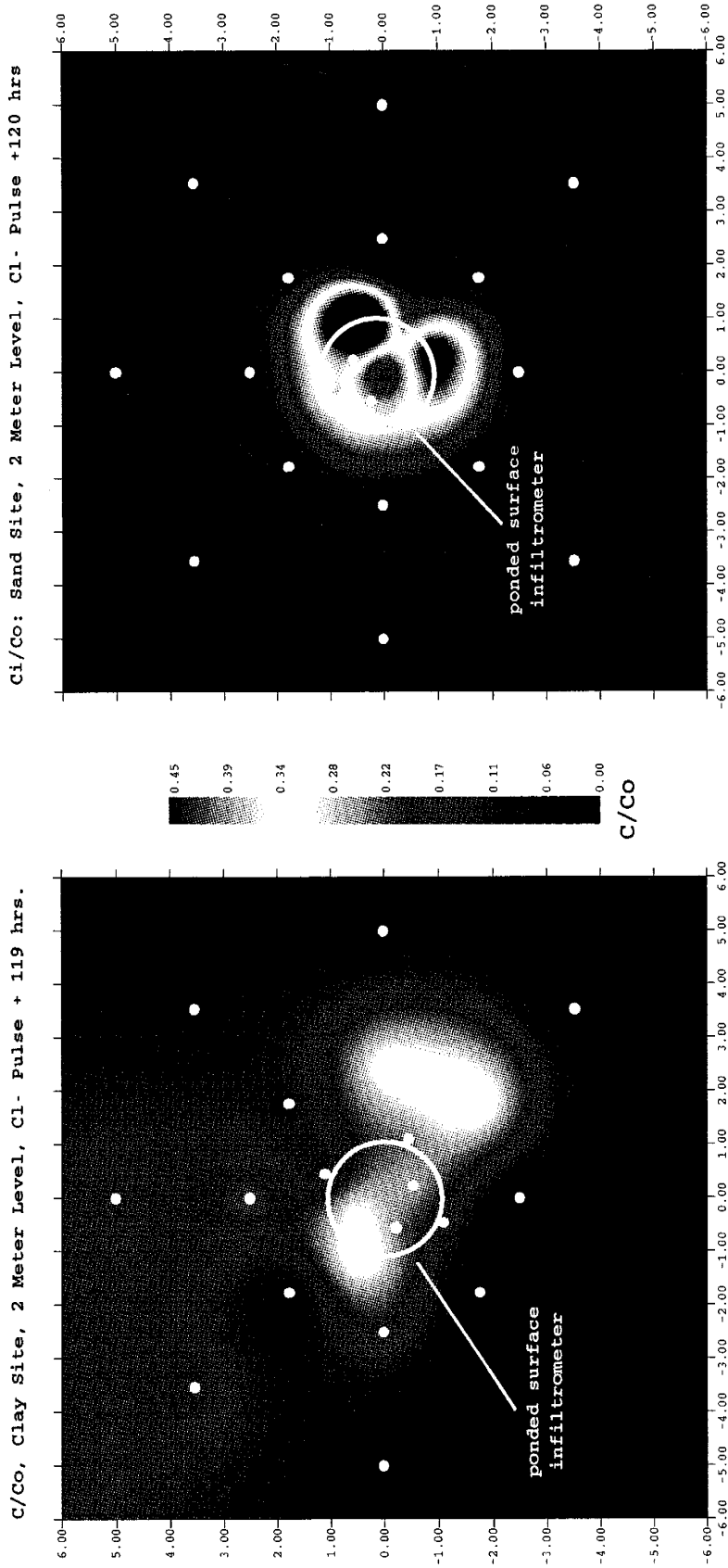


Figure 13. Cl^- tracer concentrations distribution at the 2 meter level of the Clay and Sand Sites 119 and 120 hours after start of the Cl^- pulse. White dots are operational sampling points. The 2.2 m diameter surface infiltrrometer is shown centered in the figure. The flow to the upper left at the Clay Site is moving through a transmissive body of sandy silts deposited by glacial processes among the clays normally encountered at that depth (See Figure 18).

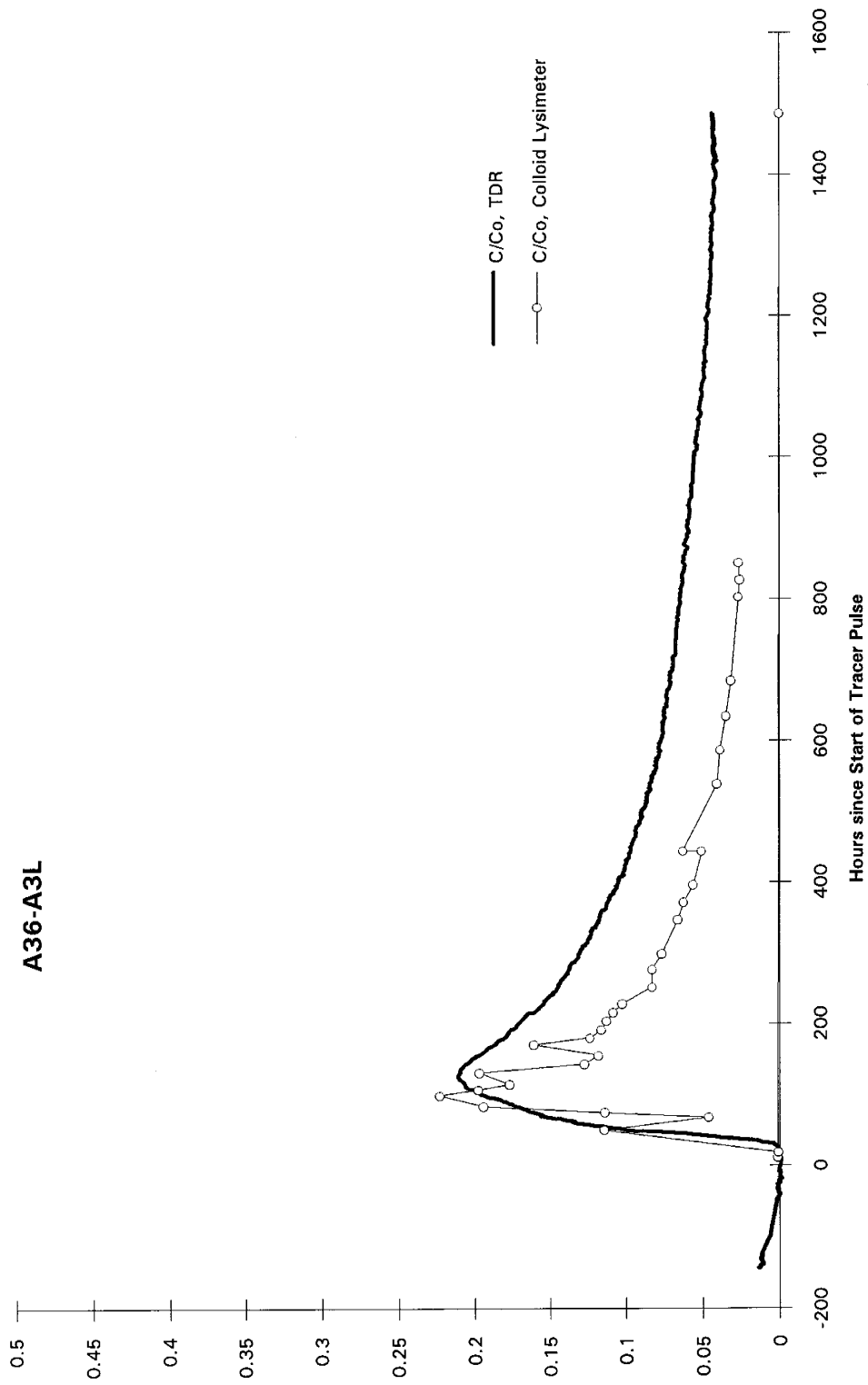


Figure 14. Most breakthrough curves exhibited a long tail indicative of retardation from matrix-macropore diffusive interaction.

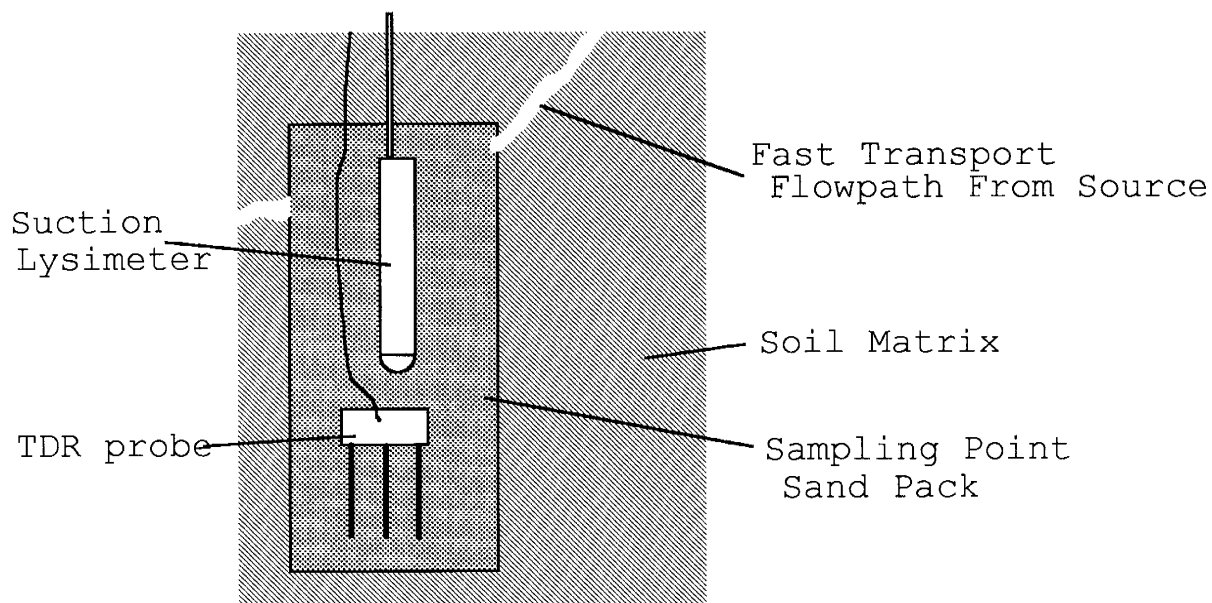


Figure 15a. Soil water sampler between transport pathway and probe.

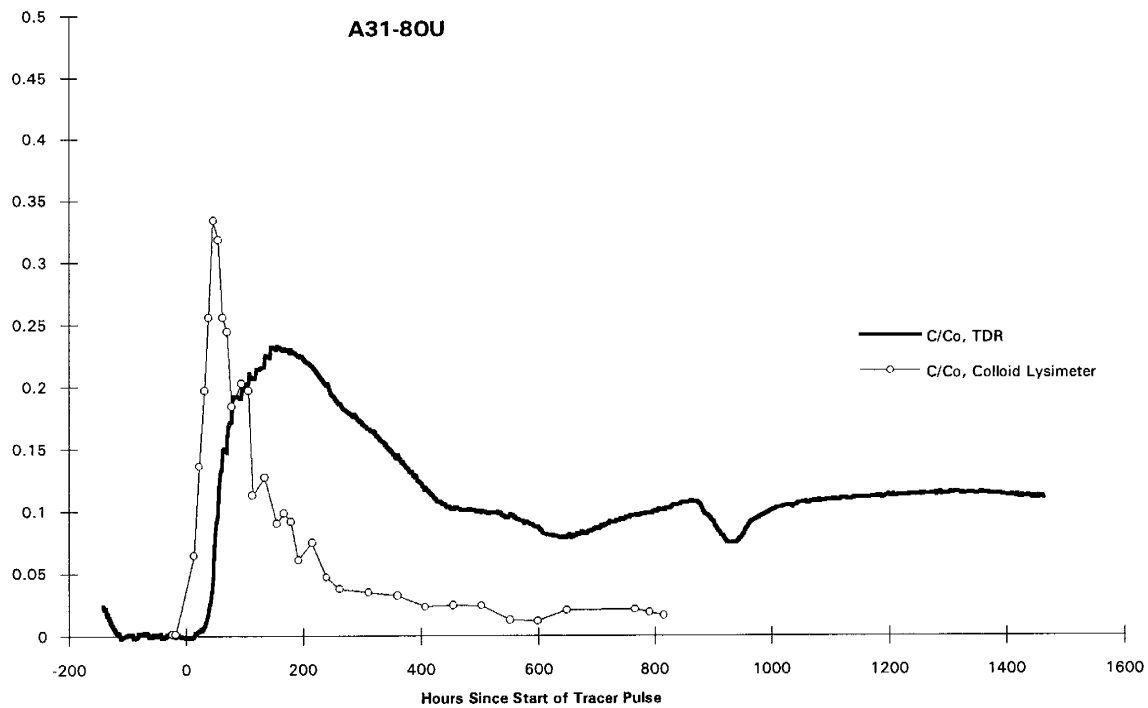


Figure 15b. Differences in arrival times and peaks due to TDR probe, suction lysimeter, and fast transport flow path geometry which favor suction lysimeter.

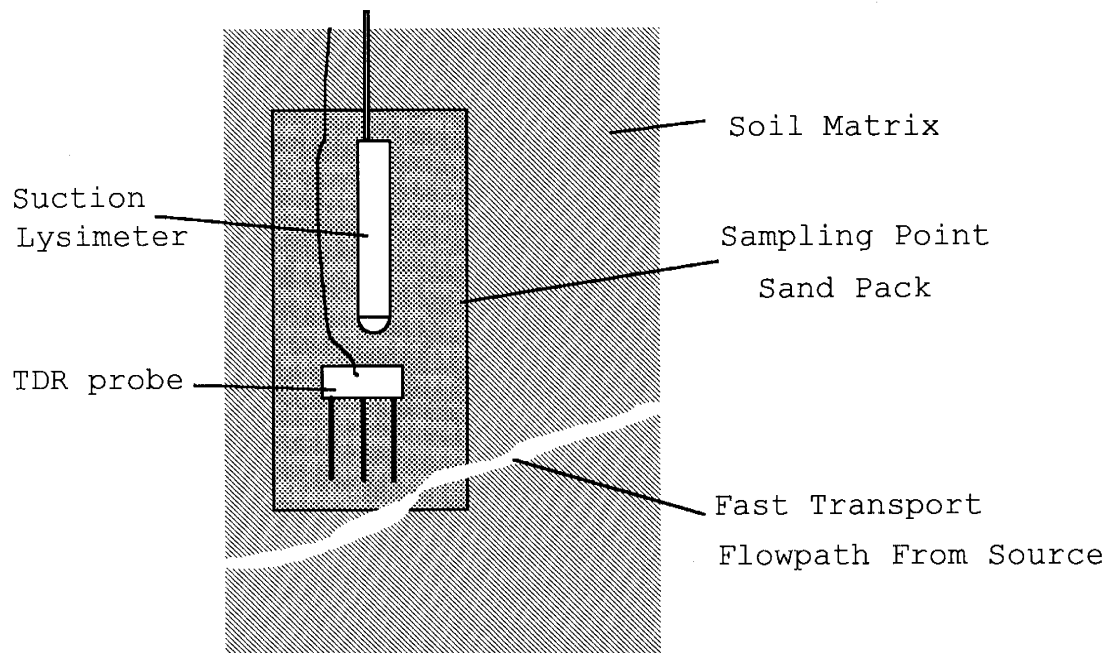


Figure 16a. TDR probe between transport pathway and soil water sampler.

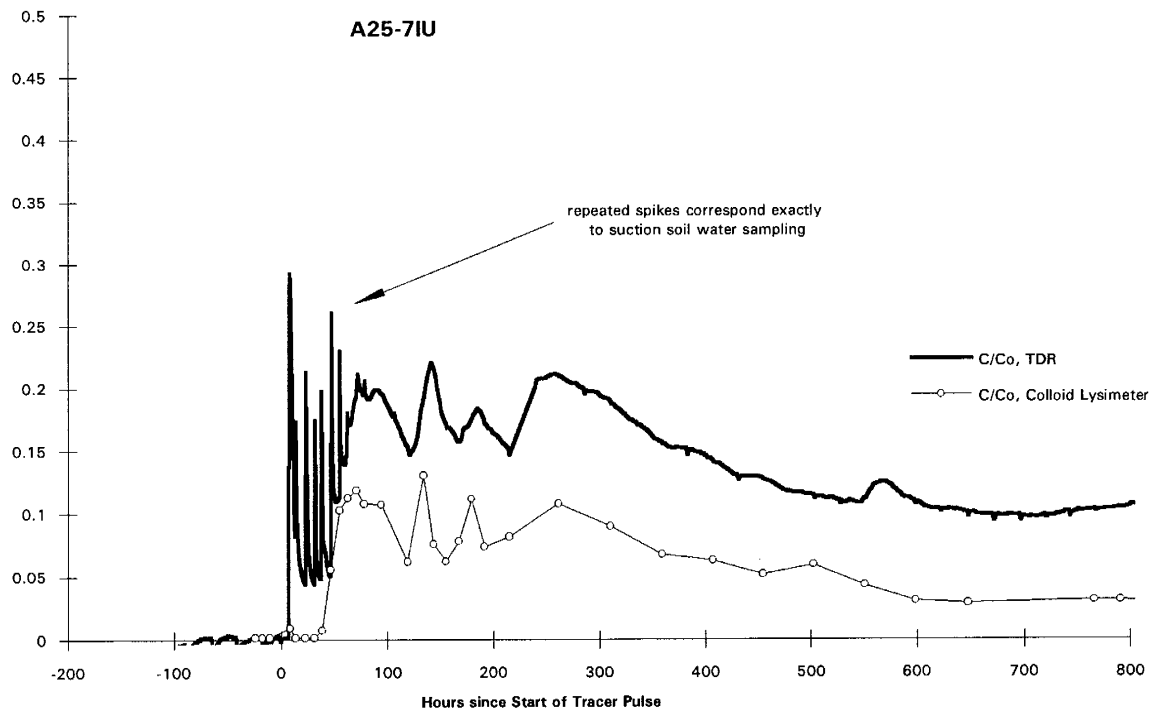


Figure 16b. Faster arrival times at the TDR and higher peaks due to the favorable location of a fast transport pathway which favors solute transport past the TDR probe.

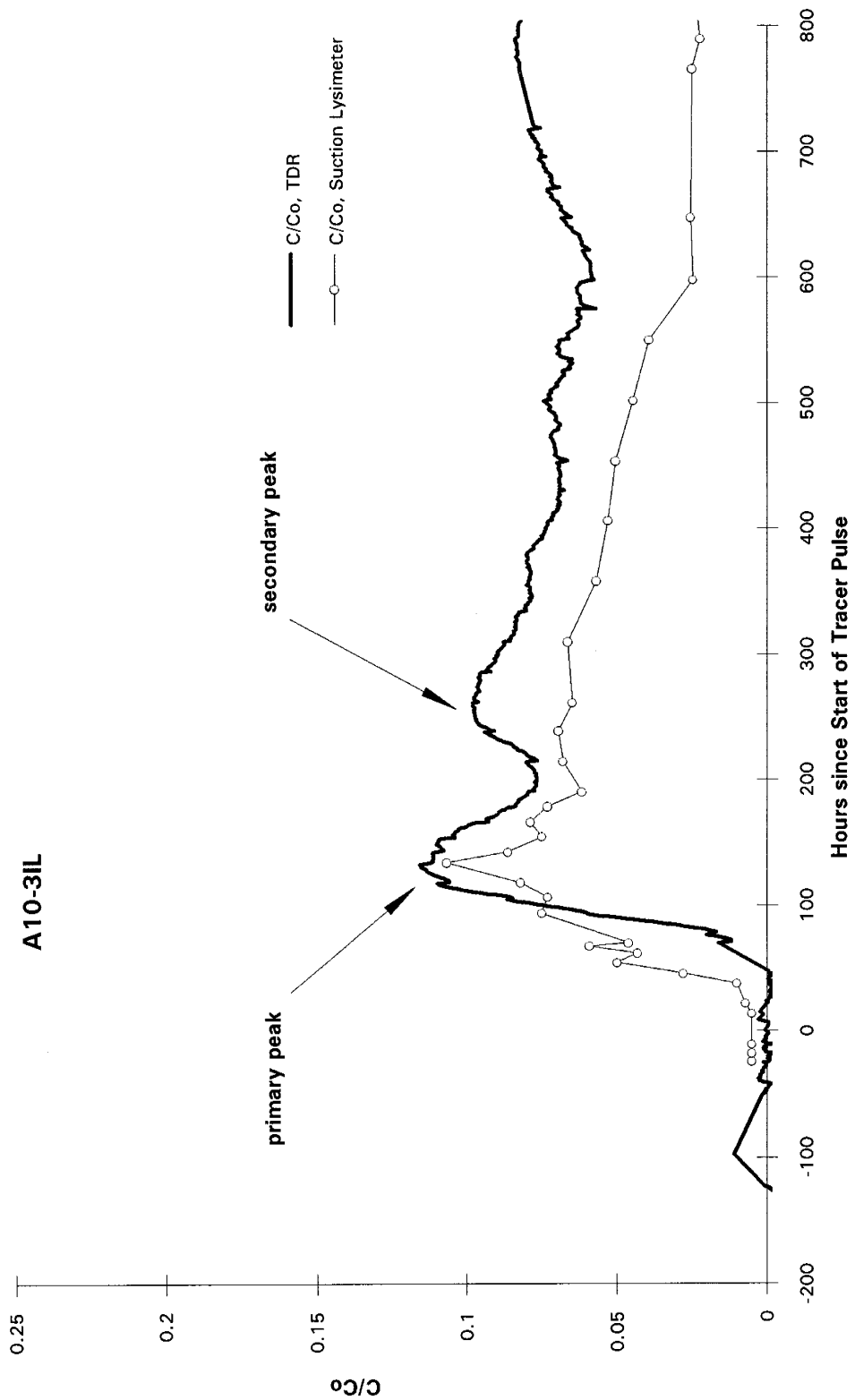
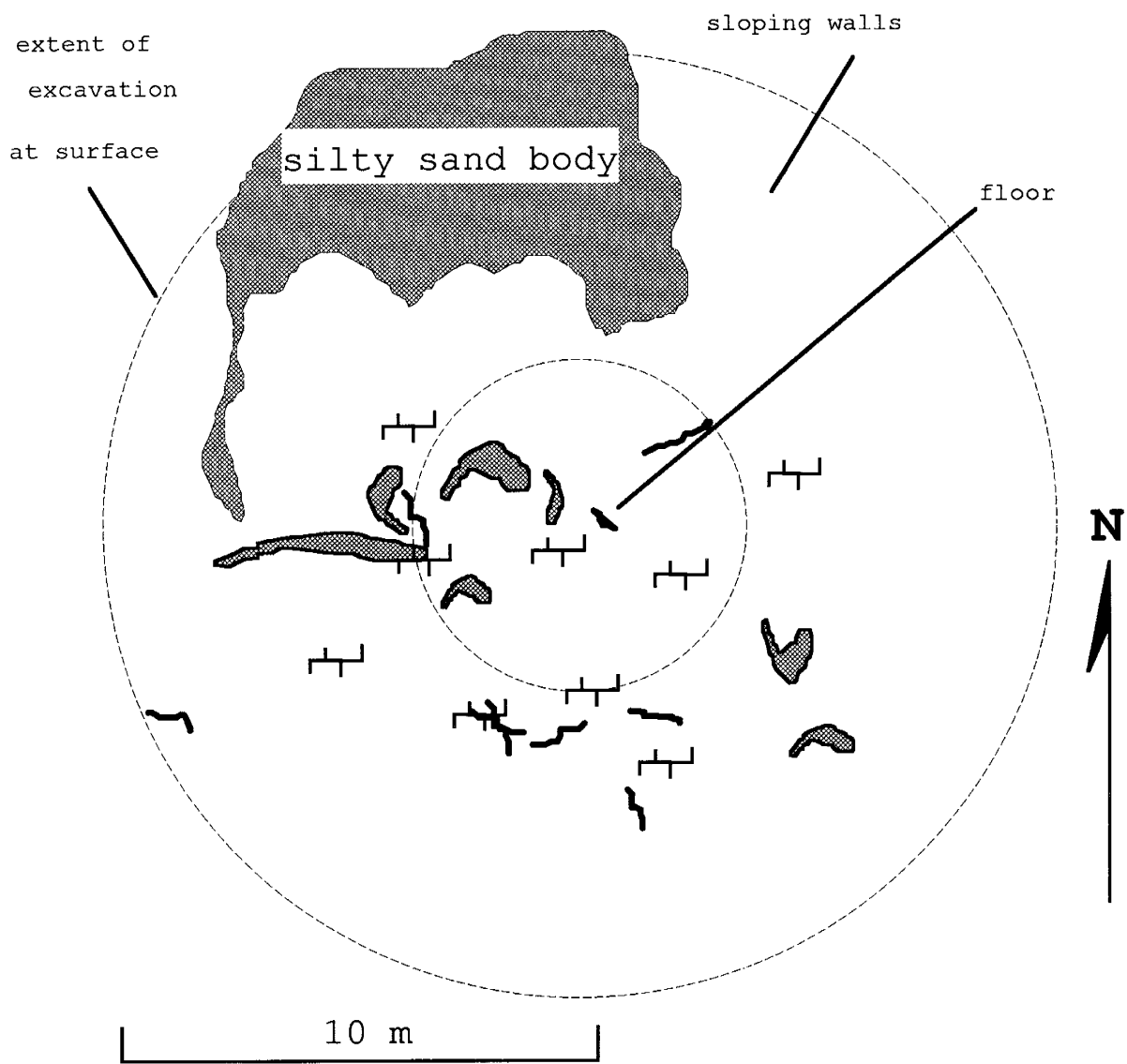


Figure 17. Repeated peaks in the Cl^- breakthrough curve from initial and secondary flowpaths.



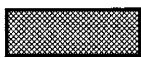
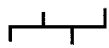

-  : preferential flow through sandy inclusions (Unit 6)
-  : active flow through fractures
-  : crayfish burrows

Figure 18. Plan view of excavation at Clay Site (Site A) showing major occurrences of macropore, fracture, and preferential flow. Features are integrated over the depth of the excavation.

Appendix I - Geology

<u>Section</u>	<u>Page</u>
Introduction and Regional Geology	2
Outcrop mapping of Paddys Run	4
TPCT Site Geology	9
Figures	15
Descriptive Tables and Cross-Sections	21

Introduction and Regional Geology

The Fernald site is located in the New Haven Trough, a classic paleo glacial valley cut into Ordovician aged bedrock of shales and limestones. The preponderance of sediments are composed of glacial tills and outwash deposits. The ancestral Ohio river eroded into the bedrock of the New Haven Trough. A later ice sheet advance diverted its original flow, and the abandoned drainages filled with fluvial sands and gravels. These sands and gravels form the present day Great Miami Aquifer, the major source of groundwater in the Fernald region. Sand and gravel deposits underlying the FEMP typically range from 40 to 60 meters in thickness. During the glacial fluctuations, these aquifer deposits were covered by deformed and heterogeneous deposits of loess, clays, silts, sands, and gravels typical of the glaciofluvial, glaciolacustrine, and glaciomarine environments.

We have divided the media encountered in the mapping, sampling, and excavation portions of the test into six main *hydrostratigraphic* units. These units are grouped according to their hydrologic flow and transport characteristics and may not have any relationship to geologic morphology and genetic or depositional processes. A sketch illustrating the general relationship of the six units at Site A (Clay Site) is shown in Figure 1. Plates referred to are contained in Appendix V.

Unit	Composition	Hypothesized Transport Processes and Controls
6	Sand and gravels	Highly transmissive matrix flow
5	Topsoils and loess	Matric flow, macropore and fracture flow, adsorption of colloids to organic material
4	Blocky structured silty clays	Matrix, fracture, and macropore flow
3	Oxidized bedded clays	Flow horizontally along bedding planes, vertically through fractures, transport by diffusion only through matrix
2	Unoxidized bedded clays	Flow through fractures, slight flow possible along bedding planes, diffusive flow only through matrix
1	Massive unoxidized (gray) cl	Flow through sand and gravel channels, along structural deformation, through matrix by diffusion only

Table 1. Hydrostratigraphic Units and associated transport processes and controls.

Unit 6 is composed of sand and gravel diamicts of varied glaciofluvial, glaciolacustrine, fluvial, and lacustrine origin. All of the units below except Unit 5 were intersected at some location by channels or stringers of Unit 6 (Plates 77, 78, and 102). The sands and gravels of this unit were generally loosely compacted and provided the most transmissive avenue for transport through any unit matrix.

Unit 5 is the uppermost unit and consists of the topsoil and silty loess comprising the bulk of the rooted zone. Flow through this unit is controlled primarily by plant material and bioturbation. Worm and root holes in this unit provided avenues for fast transport of water

and tracers (Plate 31) while plant and other organic matter captured much if not most of the colloid and dye tracers (Plate 19).

Unit Four consisted of blocky structured silty clays and sandy silts apparently derived from paleosols. Flow in this unit was primarily vertical and aided by bioturbation, root holes, and pervasive systems of interconnected fractures (Plates 20 and 38).

Unit 3 was composed of bedded and laminated oxidized clays and silty clays (Plate 47). The first significant radial flow was noticed in this unit, along bedding planes and laminae. Layers of transmissive and easily eroded carbonate deposits were apparent at some levels (Plate 36). Bedding planes, fractures, and laminae in this unit were heavily stained with iron and manganese oxides (Plate 54). Sand and gravel inclusions were encountered, providing zones of both radial and vertical preferential flow (Plate 44). The majority of crayfish burrows (Plate 40) occurred in this unit, and wormholes penetrated the unit.

Unit 2 was composed of layered and bedded unoxidized clays. Although appearing massive during cursory sample examination, hand excavation and thorough sample examination revealed this unit to be heavily bedded and laminated (Plate 68). Horizontal fracture surfaces and bedding planes were often oxidized or covered with fine sands implying past flow and transport (Plate 50). Large vertical fractures (~ 1 cm width) could be found filled with medium sands. Crayfish burrows were not found beneath this unit.

Unit 1 embodied massive unoxidized clay with frequent and irregular gravels, pebbles, and cobbles. When excavated, large masses of this unit broke apart along fracture planes which could be remnant bedding planes or shear and stress fractures. Transport of the dye tracer was possible through these fracture planes, though sand and gravel inclusions appeared to provide a more capable route (Plates 102 and 103).

Due to the demands of scale and definition, geologic mapping of local outcrops and the infiltration site required that these units be subdivided at the site scale and sometimes combined at the local outcrop scale. Over the entire study area, proportions of sands, silts, and clays were not constant in most units, especially in Units 4 and 5, where they were highly variable.

Available references on the geology and hydrology of the glacial tills include the Remedial Investigation Report for Operable Unit 3 (ITT, 1990) and the summary report from the FEMP Industrial Workshop on Characterization on the Vadose Zone.

A brief geologic history of the FEMP site is given in the RIR (ITT, 1990) as well as general descriptions of the Great Miami Aquifer. The Preliminary Subsurface Transport Pathway Characterization Test: Data Report Summer 1993 summarizes the geology at a test site located 50 m to the northeast of Site A.

Outcrop mapping of Paddys Run

As part of the Subsurface Transport Pathways Characterization Test at Fernald, exposures of Wisconsin Age glacial deposits (Shelbyville Till) in Paddy's Run were geologically mapped in mid August, 1994. All accessible outcrops of usable size were mapped and described. In general, the exposures showed considerable geologic heterogeneity and the mapping unit geometry was complex. Only four outcrops, outcrops #5, #8, #12, and #13 (Figure 2), showed complete or nearly complete sequences of the Shelbyville Till. The remaining outcrops are not complete because they were eroded during the development of the Paddy's Run terrace. During the geologic mapping, nine lithofacies of the six hydrostratigraphic units were identified. Seeps, seepage face conditions, and locations were observed. The lithofacies encountered are briefly described below. Maps and complete descriptions of these outcrops are presented in the next section. Colors are described according to the Munsell color charts.

Matrix-Supported, Argillaceous Diamict (Hydrostratigraphic Unit 1)

The matrix-supported, argillaceous diamict (Dma) lithofacies is a calcareous, matrix supported deposit containing angular, blocky to tabular pebbles and cobbles of fossiliferous limestone and dolomite. The matrix consists of poorly sorted, sandy mud. The Dma lithofacies is usually massive or structureless (Dma-m). Stratification (Dma-s) is rare within the matrix, although irregular, discontinuous, and deformed interbeds of sand and laminae of silt are common. Sand interbeds vary in thickness from a less than an inch (2 cm) to over 4.5 ft. (1.4 m), but most are a few inches (cm) thick. Some thin beds of sand contain clay inter laminae. Planar features, marked by a pavement of limestone and dolomite cobbles wedged into the deformed underlying Dma, are persistent across several outcrops. Some of these cobbles show a weak imbrication toward the south. The Dma is light gray (5 Y 7/1 to 5 Y 7/2) when dry to gray (5 Y 6/1 to 10 YR 5/1) or light olive gray (5 Y 6/2) when moist. Along the upper contacts and some internal contacts with sand interbeds, the Dma is light olive brown (2.5 Y 5/3 to 2.5 Y 5/6), pale yellow (2.5 Y 7/2), or brown (10 YR 5/3).

Deformation structures are common within the Dma. Strata and inter strata, when present, are often deformed into flame structures or contorted drag folds indicating shear toward the south. Shear planes showing separation and displacement are common. At some outcrops (e.g., outcrops #5 and #8), series of reverse faults with over 5 ft. (1.5 m) of slip are over thrust toward the south indicating horizontal compression in the north-south direction.

The Dma is typically massive and breaks along irregular planes forming a blocky surface. Subvertical fractures are common locally and the matrix material along the fractures is often light olive brown (2.5 Y 5/3 to 2.5 Y 5/6), pale yellow (2.5 Y 7/2), or brown (10 YR 5/3), indicating possible oxidation and the potential for flow and transport.

Both the upper and lower contacts of the Dma are spatially variable, and the Dma is not uniformly distributed along Paddys Run. In the northernmost outcrops (e.g., outcrops #16, #3, and #2), the Dma is overlain by a stratified gravel lithofacies. In this area the upper contact is erosional and slightly undulatory, and local channels tens of feet (m) wide and up to 3 ft (1 m)

deep are down cut into the Dma. The erosional surface truncates shear surfaces and probable over thrust faults. The Dma is truncated erosionally by the stratified gravel lithofacies in the northern part of outcrop #2. Channels within the stratified gravel lithofacies occur at the northern or southern edge of the outcrops, and it is possible that the channels cut through most of the Dma and that topographic highs (outcrops) are only present where channels do not occur. In the north of the study area, the Dma overlies the stratified sandy diamict and massive sandy diamict lithofacies. The lower contact is deformed and undulatory over 2.5 ft. (0.75 m) and shows load deformation.

Further to the south (outcrops #1 and #4), the Dma is overlain by a gravel lag and massive sandy silt lithofacies, and the upper contact is erosional, sharp, and undulates over 2.5 ft (0.75 m). Along the north edge of outcrop #1, a channel in the stratified gravel lithofacies significantly thins the Dma. The Dma overlies the bioturbated sand and silt lithofacies.

At outcrop #5, the Dma is overlain by a complicated and deformed mix of sandy diamict, gravel, and pebbly sand lithofacies. A highly deformed unit of Dma inter bedded with sand overlies massive Dma-m along the south side of the outcrop #5. Complications at outcrop #5 are due to preserved shear structures and over thrust faults affecting the upper contact of the Dma and the overlying materials. The lower contact of the Dma lithofacies is not visible at outcrop #5.

At outcrop #6, the Dma is absent. At outcrop #7, the Dma is again overlain by the gravel lithofacies and the upper contact is erosional. The Dma overlies the sandy diamict lithofacies, and the lower contact is sharp, undulatory and shows load deformation.

Further south (outcrop #8), the Dma lithofacies again shows complicated relationships with the overlying materials. Shear structures (over thrusts or flame structures) display over 4 ft. (1.2 m) of vertical displacement. A lenticular zone of cross laminated sand is surrounded by Dma and appears to have been wedged into the Dma as a solid mass. A very thick bed of sand, over 2.5 ft (0.75 m) to 0.5 ft (0.15 m) thick, subdivides the Dma lithofacies. The Dma overlies the great Miami aquifer (GMA), but the contact zone is obscured.

The southernmost exposures of the Dma occur at outcrops #12 and #13. In these locations, the Dma lithofacies directly overlies the GMA and underlies sandy diamict and sand. The upper contacts are sharp and undulatory.

Matrix Supported, Sandy Diamict Lithofacies (Hydrostratigraphic Unit 6)

The matrix supported, sandy diamict lithofacies (Dms) consists of poorly sorted, sand dominated matrix with subrounded to subangular granules, pebbles, and cobbles, including limestone, dolomite, and siliclasts. The Dms lithofacies rarely displays structure and is described as massive, although some clasts show alignment along deformation at the basal contact. The Dms is typically brown (10 YR 4/3) when wet.

The Dms lithofacies has a limited distribution within Paddys Run, and is confined to two northern outcrops: outcrops #2, and #3. In outcrop #3, the Dms lithofacies occurs at the base

of the outcrop and is overlain by the Dma lithofacies. The upper contact is sharp and undulatory. Evidence of erosion is not present. In outcrop #2, the Dms lithofacies is bounded on the top by the gravel lithofacies and on the bottom by the clast supported, sandy diamict lithofacies. Along the north side of outcrop #2, a thin tongue of Dma overlies the Dms. The upper contact is clearly erosional and local channels down cut into the Dms. The basal contact of the Dms is deformed from loading and undulatory over 3.5 ft (1 m).

Clast Supported, Sandy Diamict Lithofacies (Hydrostratigraphic Unit 6)

The clast supported, sandy diamict (Dcs) is calcareous and displays a poorly sorted sand matrix with subrounded to subangular granules, pebbles, and cobbles. Locally, some clasts are tabular and very angular. The Dcs displays horizontal to subhorizontal parallel very thin to thin beds (Dcs-h), planar cross-beds (Dcs-p), and trough cross-beds. Strata packages show lenticular bounding surfaces and are up to 2 ft (0.6 m) thick. Low angle cross cutting relationships are common at bounding surfaces. Some bar forms are almost completely exposed and are over 40 ft. (12) long in the outcrop plane. The Dcs ranges from reddish yellow (7.5 YR 6/6) to light yellowish brown (2.5 Y 6/4) when dry.

The Dcs occurs at the base of outcrops #2 and #7. At these locations, the lower contact is not observed. The upper contacts show load deformation and undulate over 4 ft. The Dcs is overlain by Dms at outcrop #2 and Dma at outcrop #7. At outcrop #5, Dcs is weakly stratified, overlies the Dma, and is associated with deformed and sheared areas with over thrust.

Inter bedded Matrix Supported, Argillaceous Diamict/Sand Lithofacies (Hydrostratigraphic Units 1 and 6)

The inter bedded matrix supported, argillaceous diamict/sand (Dma/S) lithofacies consists of Dma (major component) with up to 8 cm thick interbeds of silt, very fine to very coarse sand with some granules and pebbles. Structure was not observed in the sandy component of the lithofacies. The Dma component contains some subhorizontally oriented planar surfaces marked by pebbles and cobbles of limestone and dolomite. The Dma breaks along blocky, slickensided surfaces. The Dma/S is generally grayish brown (10 YR 5/2) when wet.

The Dma/S lithofacies is a major part of the exposure at outcrop #5. Dma/S overlies Dma, and the contact was partly obscured.

Pebbly Sand Lithofacies (Hydrostratigraphic Unit 6)

The pebbly sand (Sp) lithofacies consists of poorly sorted sand and subangular to subrounded pebbles. It typically displays planar cross beds and horizontal laminae to very thin beds. Low angle cross cutting relationships are evident in some exposures. Frequently contains interbeds of silt and clay to 5 cm thick. The color varies from yellowish brown (10 YR 5/4) to light gray (5 Y 7/2) when dry. The silt component is light yellowish brown (2.5 Y 6/3) when wet.

The Sp lithofacies occurs as a tilted, angular wedges within the Dms lithofacies at north part of outcrop #5 and between the laminated mud lithofacies (top) and Dma lithofacies (bottom) at

the south part of outcrop #5. A lens shaped form of Sp, with dipping strata, occurs near the top of outcrop #8 and is bounded on all sides by Dma.

Sand Lithofacies (Hydrostratigraphic Unit 6)

The sand lithofacies encompasses a variety of mapping units showing different sedimentary structures. Typically, the sand is poorly sorted and calcareous. Grain sizes vary but the sand lithofacies usually consists of very fine to coarse sand. Sand may display horizontal laminations (Sh) and contain interbeds of silt to 4 cm thick when associated with the Dma lithofacies. Structureless and mottled sand (Sm) is laterally equivalent to Dcs and Dms at outcrop #1. Sand stringers and interbeds within the Dma units may be considered small scale examples of the Sl lithofacies.

At outcrop #13, sand is rippled (Sr). The Sr lithofacies consists of inter bedded with poorly sorted sand, well sorted sand, and silt. The lower 3 to 6 in. of Sr consists of granule and pebbly sand with wavy to contorted thin laminae that shows some soft sediment deformation and shear. Well sorted, fine sand showing ripple cross laminae sets to 1 to 3 cm high and ripple drift cross laminae with stoss and lee preservation. Ripple sets are typically capped by clay drapes. Soft sediment deformation due to loading is abundant including flame structures and cm scale shear displacements.

The sand lithofacies is present in various locations within Paddys Run. At outcrop #1, Sm occurs at the base of the outcrop and is overlain by Dma. At outcrop #7, a thin bed of Sm is overlain by the sand and gravel lithofacies and underlain by the Dma lithofacies. Sl overlies Dma and underlies the Sp lithofacies and the laminated mud lithofacies at outcrop #8. At outcrop #13 and possibly outcrop #12, Sr and Sl with soft sediment deformation and shear directly underlay the laminated mud lithofacies and overlie the Dma at outcrop #13 and the Sp or Dms lithofacies at outcrop #12.

Laminated Mud Lithofacies (Hydrostratigraphic Units 2 and 3)

The laminated mud lithofacies (Fl) consists of horizontally laminated to thinly laminated silt and clay couplets. In general, strata are flat, parallel to wavy, and locally contorted and disrupted. The lower few cm of Fl are often slightly brecciated. Adhesion ripples are present locally. The color of Fl ranges from grayish brown (10 YR 5/2) to light gray (10 YR 7/2 to 2.5 Y 7/1).

The Fl lithofacies are only present at outcrops #5, #8, #12, and #13 and overly a variety of other lithofacies. At outcrop #5, only a small erosional remnant of the Fl lithofacies is preserved, and it overlies the Dms and Dcs lithofacies. At outcrop #13, the Fl lithofacies overlies the Sr lithofacies.

Sand and Gravel Lithofacies (Hydrostratigraphic Unit 6)

The sand and gravel (S/G) lithofacies consists of matrix supported, massive (Sm/Gm), horizontally stratified (Sh/Gh), planar cross stratified (Sp/Gp), or trough cross stratified (St/Gt) pebble to cobble gravel inter bedded with poorly sorted sand. Most clasts tabular and vary from angular to subrounded. Many clasts show strong imbrication toward the south. Packages separated by erosional bounding surfaces show distinct bar morphology. Strata

within some sand interbeds drape over channel forms cut into the underlying gravel. Sand interbeds display flat strata, low angle tangential cross strata, and planar cross strata. Where sand dominates, gravel occurs as lags. In general, the sand and gravel lithofacies appears to fine upward as the gravel content decreases. The lower contact of this lithofacies is sharp and erosional, and channel forms are frequent along the edges of outcrops.

Except for outcrops #8, #12, and # 13, the sand and gravel lithofacies is present at all outcrops mapped. These outcrops occur where the river bank has cut into the first terrace of Paddy's Run. In the southern most outcrops, the lithofacies displays less gravel.

Blocky Structured Silt/Sand Lithofacies (Hydrostratigraphic Unit 4)

The silt/sand (Si/S) lithofacies consists of argillaceous silt and sand. It is frequently mottled, shows a blocky texture, and may display peds. Strata are evident locally but are poorly preserved. The lower contact may show a pebble lag. The unit typically grades upward into the root zone.

The Si/S lithofacies is present at all mapped outcrops in Paddy's Run. In some circumstances, it is completely incorporated into the root zone. It appears to blanket a variety of lithofacies, and is the youngest outcrop deposit mapped. Strata occur infrequently in topographically low areas.

Seepage Face Locations in Paddy's Run

During the mapping of Paddy's Run, seepage faces were observed only in outcrops #5 and #8. Seeps were observed at the upper contact of the Dma lithofacies and along sand interbeds within the Dma lithofacies. Because of local cover and slump, the volumetric flux from these seeps could not be estimated. Seeps do not always occur within oxidized sediments. At outcrop #5, seeps occur from gray (presumably reduced) sand in gray Dma. In addition, many oxidized fracture surfaces show no seepage. Therefore, the reduction/oxidation status of the sediment is not always a definitive indicator of modern flow paths. Seeps along the upper contact of the Dma occurred in topographically low areas where sands were in contact with the Dma. These topographically low areas display features consistent with large scale shear, over thrusting, or emplacement of frozen blocks by sub glacial processes. The three dimensional geometry of these features is unknown, but it is clear they provide paths for preferential groundwater flow and transport.

TPCT Site Geology

In an effort to obtain information on the geology of the near surface vadose zone in the glacial deposits within the study area, seventeen geologic cross-sections, six at each infiltration site, three between the infiltration sites, and two from unused candidate Transport Processes Characterization Tests (TPCTs) were constructed from visual descriptions of approximately 800 hand augered samples (Figures 3, 4, and 5). Additional insight on the geology was obtained during excavation of the clay site which permitted direct observation of the glacial till. Eight lithofacies were identified and used to construct geologic cross-sections. These lithofacies are designated as cross-section units (CS Unit #) and are described independently of the lithofacie units in the Outcrop Mapping section above.

Preliminary augering throughout the study area was undertaken to locate two suitable TPCTs. The final sites were chosen because the deposits found below each site together represented the transport processes and controls that we wished to investigate. Site A (the Clay Site) consists of several distinct clay lithofacies in the upper 3.5 m while Site C (the Sand Site) consists of 2 to 3 clay lithofacies overlying saturated silty sands and gravels. The sites were located approximately 45 m apart on an approximate east west line. A plan view of the study area showing the two infiltration sites, preliminary augered holes, and unused candidate sites is given in Figure 3.

Sampling location layout

All samples were collected at one foot intervals during hand augering of 2 inch diameter boreholes using a mud head auger. Boreholes in which instruments were installed were later reamed to 4 inches with a mud head auger.

Two circular cross-sections along the sampling rings (Figure 5) and four radial cross-sections running through the center of each infiltrometer were constructed from samples taken during instrument installation borings at each Transport Pathways Characterization Test (TPCT) site. The radial sections are designated according to their compass direction (East-West, Northwest-Southeast, North-South, and Northeast-Southwest) and the circular cross sections are designated Inner and Outer Rings. Additional holes were augered around each site exclusively for the purpose of extending radial cross-sections. Three East-West cross-sections were constructed from three rows of augered holes between the two TPCT sites. The cross-sections from these holes are designated North Medial, Central Medial, and, South Medial. A plan view of the instrument borings at the TPCTs is shown in Figure 5 and an overview showing both TPCTs, additional borings around the TPCTs and the medial borings between the TPCTs is shown in Figure 4.

Other cross-sections were constructed from samples collected at two other candidate infiltration sites (Figure 3). Four holes were augered at each of the candidate sites to correspond with the north, south, east, and west holes on the outer ring of Site A and B. Three other holes, P-1, P-2, and P-3 were augered while searching for suitable TPCTs. Hole P-1 was augered between the 1993 site and the clay site and two other holes, P-2 and P-3,

were augered to the southwest of the clay site (Figure 3). The geologic cross-sections associated with the infiltration sites document the contrasting geology of the two infiltration sites as well as the transition between the sites. Information from the holes augered at unused TPCT sites yield geologic information over a scale of several hundred meters. All cross-sections were constructed from sample descriptions organized into description tables.

Sample description and categorization methods

Because of the similar textures displayed by many samples, other features were used for classification. At shallow depths, where weathered clays predominated and original geological features could not be discerned, color was used as the primary criteria. At intermediate depths at the clay site and along the medial cross-sections, color as well as bedding and carbonate deposits aided in classification.

Using the above criteria, eight distinct lithofacies were identified from which the cross-sections were constructed. Table 1 correlates cross-sectional unit numbers, general descriptions, and distinguishing features for the eight cross-sectional lithofacies (CS Units) and sub-units. Table 2 lists abbreviations used in the descriptive tables (Tables 3 - 20) and describes features used to classify samples.

The descriptive tables are named and arranged in the same manner as the cross-sections. The characteristics of the augered samples that aided in classification, as well as the final classification (CS Unit #), are read down the left hand side of each descriptive table. The sample characteristics used for classification include consistency, texture, and color. Finally, other features are noted that were important to classification (apparent degree of saturation for instance) or that were observed often enough to warrant mentioning (mottling, stains, CaCO₃ etc.)

The description of the geology begins at Clay Site with the inner and outer ring cross-sections. The geology at the Sand Site as well as the transition between the sites is then contrasted to that of the Site A. The field scale geology is then discussed in light of the descriptions at and between the infiltration sites.

Clay Site Geology

Identification of lithofacies at the clay site was greatly aided by the excavation of the site (Appendix VI). The excavation was carried out by a large track hoe with a back hoe attachment. The track hoe had a long reach so that a 10 m diameter by 4m deep hole could be excavated with all but one section of the walls exposed (Appendix VI, Plate 87). Seven geologic lithofacies were identified from the excavation and hand augered samples from the Clay Site. Five of the units form a layer cake (Figure 6), while the sixth (Hydrostratigraphic Unit 6) forms an anomalous silty sand body in the northwest section of the infiltration site and is present in stringers and one sand and gravel channel. The following seven cross-sectional lithofacies used to construct cross-sections at the Clay Site.

Soil and Loess (CS Unit 1, Hydrostratigraphic Unit 5)

The upper most unit (classified 1A in the description tables) consist of a yellowish brown silty clay (loamy) which in augered samples consisted of very fine to medium (< 20 mm) crumbs. As viewed from the exposures in the pit, the thickness of this unit varied from 15 to 20 cm.

Blocky Structured Silty Clays (CS Unit 2, Hydrostratigraphic Unit 4)

The next CS Unit consists of 1 to 1.5 m of predominantly blocky silty clays with occasional 1 to 4 cm thick beds of sands. No primary geologic structure could be discerned in this unit, but the blocky structure was readily observable in pit exposures. Subtle mottles of gold, grays, and greens could be discerned when the samples were viewed close up. When viewed at a comfortable arms length the mottles could not be discerned and the color of the sample matched the Munsell soil color charts fairly well. Augered samples typically contained medium to coarse blocks which roughly correspond to the size of blocks observed in the pit exposures. Manganese deposits are found in many of the augered samples and are probably more common than indicated in the cross-section tables.

Two continuous color bands could be discerned in this lithofacies in pit exposure: a lighter upper band and slightly darker lower band of approximately equal thickness. Augered samples from the upper band have a Munsell soil color chart 10YR hue while the lower have a 2.5Y hue. Both colors were not consistently observed in the augered samples. This discrepancy between observations from the pit exposures and the samples may be due to the lack of resolution and accuracy in obtaining samples at desecrate intervals.

Interbedded/Laminated Oxidized Silty Clays (CS Unit 3, Hydrostratigraphic Unit 3)

The third lithofacie consists of a 2 to 3 m thick sequence of bedded silty clay. Bedding characteristics in this unit change with depth. In the upper part of this lithofacie beds 1 to 3 cm thick and interbedded laminations are apparent, while towards the bottom, the laminations give way to diffuse layering and the beds thicken to 3 to 7 cm. In general, the beds are comprised of light gray, pale brown, pale yellow, to white mottled silty clay containing variable amounts of calcium carbonate. In many locations the fractures as well as bedding planes are heavily stained with iron oxide and magnesium (Appendix VI, Plate 54). Numerous vertical fracture planes connect planer surfaces of the well defined beds.

Bedded Oxidized Silty Clay (CS Unit 4, Hydrostratigraphic Unit 3)

The next lower cross-sectional unit consists of a bedded brown silty clay distinguished from the interbedded deposits by the lack of laminations and thicker beds (generally 4 to 8 cm thick) with less color variation and by lack of obvious CaCO₃. In general these beds show a slight change in hue from the overlying beds although comparison with the Munsell color charts failed to reveal a consistent color change.

Bedded Oxidized to Unoxidized Silty Clays (CS Unit 5 and 6, Hydrostratigraphic Units 3 and 2)

CS Unit 5 marks the transition to between the overlying “weathered” deposits and the underlying “gray clay”. Samples from CS unit 5 are generally olive brown while those from CS Unit 6 are dark gray to dark grayish brown. These lithofacies are combined because

excavation revealed that the transition between the oxidized (as indicated by brown colors) and the unoxidized deposits (gray colors) is gradational.

Both of these lithofacies are bedded to varying degrees, the bedding being defined by thin silt layers (<1mm). Stained partings (iron oxide and manganese oxide) are found in hand samples as through out samples taken from both of these lithofacies. Thin sand and pebble lenses are occasionally encountered in the lower part of this unit.

Sandy Clay to Clayey Sand (CS Unit 7*, Hydrostratigraphic Unit 6)

Upon excavation, an anomalous sand body was intersected on the northeast sector of the infiltration site (Plates 74, 75, 76, and 87). In general this lithofacie contains lightly compacted sandy clay and clayey sand. Sandy deposits were found at other locations, but the dark brown color, sharp contacts with surrounding lithofacies, and the cohesive nature of the matrix is unique.

Clay Site excavation

Correlation between the cross-sections constructed from samples at the Clay Site (See Cross-Sections and Descriptive Tables) and the geology observed in the pit is good, except in the northeast corner where the anomalous sand body was exhumed during excavation. This sand body forms sharp contacts with the surrounding lithofacies and truncates the Bedded/laminated deposits where it thickens to the north (Plate 87). From this point the sand body becomes thicker and the contact is roughly parallel to the bedding of Unit 3. The sand body continues to the north and east, though the eastern contact was buried under the access ramp constructed for the track hoe. A stringer from this body extended to the most westerly outer lower instrument pack location (Plate 77). This sand body extended outside of the outer ring and the only augered sample collected came from the sample taken at the western sampling point.

Further excavation of the central part of the pit revealed extensive areas of stained partings in the gray clay (Plate 103). Non stained silt filled partings were also observed. A final excavation in the bottom of the pit in the form of a 2 m deep gouge exposed massive gray clay interrupted by a brown sand channel (Plate 102).

Sand Site Geology

Of the lithofacies found at the Clay Site, only CS Units 1, 2, and 7 were also noted at the Sand Site. CS Units 1 and 2 were layered across the site over a large sand and gravel deposit (CS Units 7 and 8).

Soil and Loess (CS Unit 1, Hydrostratigraphic Unit 5)

The top soil encountered at the sand site was also encountered at the clay site. However, the Soil and Loess at the sand sight exhibited a slightly darker hue (10YR versus 2.5YR) than at the clay site. Unit 1B does have the same fine to medium sized crumb of unit 1A and, other than the slight color change, is similar in appearance.

Blocky Structured Silty Clay (CS Unit 2, Hydrostratigraphic Unit 4)

Samples comprising this unit were similar to lithofacies at the clay site except that the subtle mottle of gold, grays, and greens were more intense.

The interbedded deposits found at the sand site were not readily apparent the clay site. However, when CaCO_3 was observed in augered samples, they were classified as interbedded deposits.

Sands and Gravels (CS Unit 7 and 8, Hydrostratigraphic Unit 6)

These lithofacies are grouped together because they generally grade from silty, sandy, clayey deposits (CS Unit 7) in the upper part to sands and gravels (CS Unit 8) towards the bottom. All samples collected from both of these lithofacies were fully saturated. Samples fitting into from these lithofacies were typically monochromatic and matched the indicated Munsell color almost exactly.

In contrast to the clayey sands of the anomalous sand body at (CS Unit 7*), samples from this unit are much lighter in color and have a much softer consistency.

Sand Site Cross-sections

As indicated by the inner and outer ring Sand Site Cross-Sections, the infiltrometer was placed directly over a saturated zone with intervening CS Unit 1 and CS Unit 2. CS Units 3, 5, and 6 are missing in all samples taken from the instrument hole borings except at the C-3 hole where CS Unit 3 is present. CS Units 3, 5, and 6 do reappear to the south of the site in the North-South cross-section. Unit 3 appears in the two farthest east sampling location on the East-West cross-section (C-3 Outer and C-P3). Unit 3 also appears at the southwest corner in the northeast-southwest cross-section (C-P6).

Comparison of Geology Between Sites A and C

In comparing the sand and clay site cross-sections, several differences are obvious. First, the blocky structured silty clays of CS Unit 2 is generally thicker at the Sand Site than it is at the Clay Site. Secondly, saturated deposits of sands and gravels were encountered at a fairly shallow depth at the sand site, but not at the clay site. Finally, Several lithofacies identified at the clay site are missing at the sand site, especially within the inner and outer ring sampling locations.

Medial Cross-section Geology

The medial cross-sections were constructed from sample holes located approximately 3 m apart (Figure 4). These cross-sections reveal that saturated deposits of clays, sands, and gravels (CS Units 7 and 8) are common between the two sites. Less common is the brownish to gray clay at the depths augered. The bedded and laminated clays (CS Unit 3), on the other hand, tend to be present between the infiltration sites while thickly bedded deposits (CS Unit 4) appear to pinch out completely. Also the blocky structured silty clays of CS Unit 2 appear to maintain an approximate thickness of 2 feet between the sites.

Field Scale Geology

Inspection of the Preliminary test hole geology shows that the lithofacies described at the Clay Site may be found up to 50 m north of the infiltration sites in test holes P2 and P3. Farther to

the north of the infiltration sites, samples from candidate test sites exhibit the same lithofacies as found at the Sand Site (Figure 3).

Summary of TPCT site geology

The subsurface at and between the infiltration sites shows considerable variations in the upper 3 to 4 meters. All lithofacies, except the anomalous sand body at the clay site, were observed either at the candidate test sites or the preliminary hole sites. Correlations between the two infiltration sites were made possible with the three sets of medial holes augered between them, but correlations on larger scales may be impossible because of strong heterogeneities commonly present in glacial deposits. This is born out by outcrops in Paddys Run and by the presence of the anomalous sand body at the clay site. Thus, direct correlation of lithofacies at the field or larger scales may not be justified without more extensive geologic investigation.

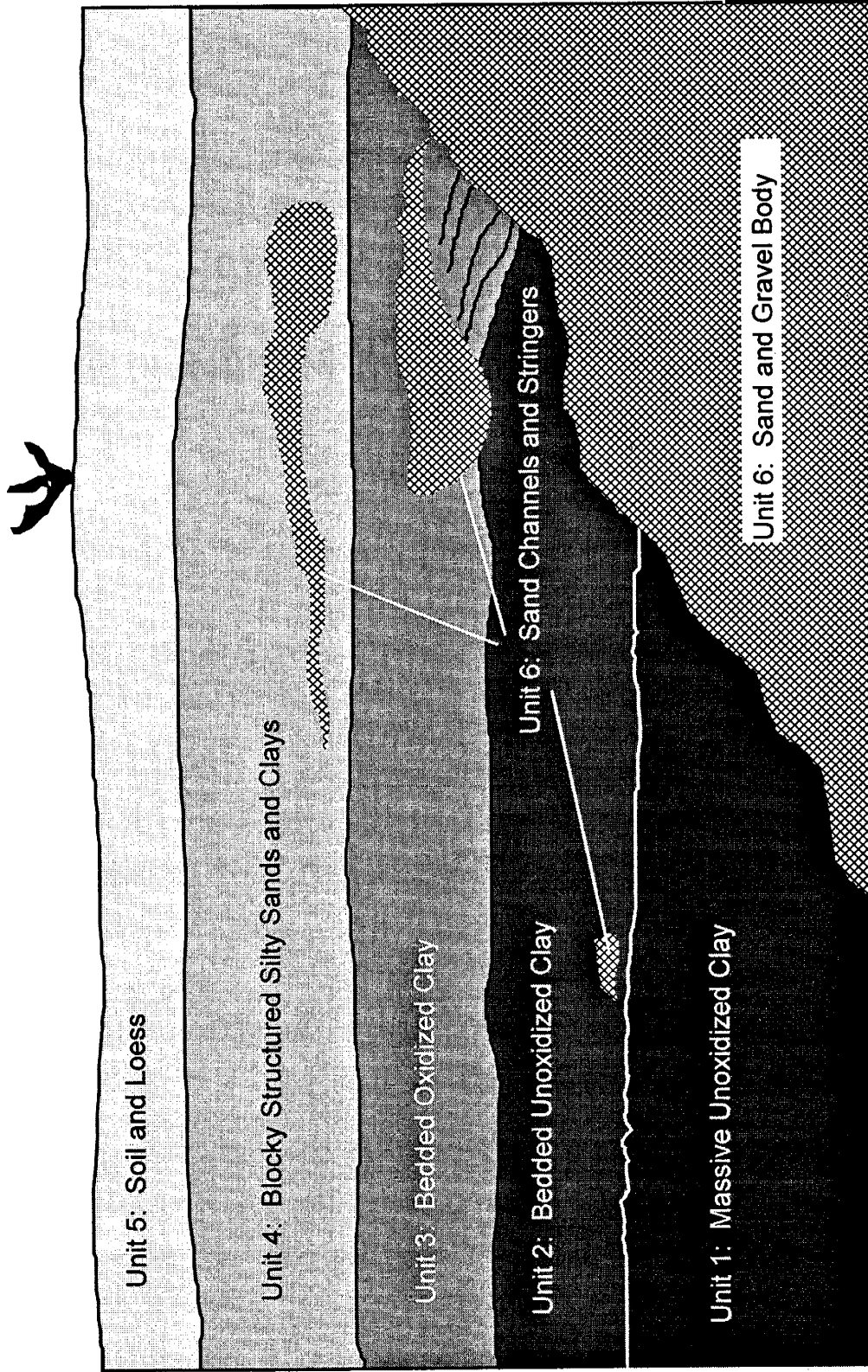


Figure 1. General relationship of hydrostratigraphic units.

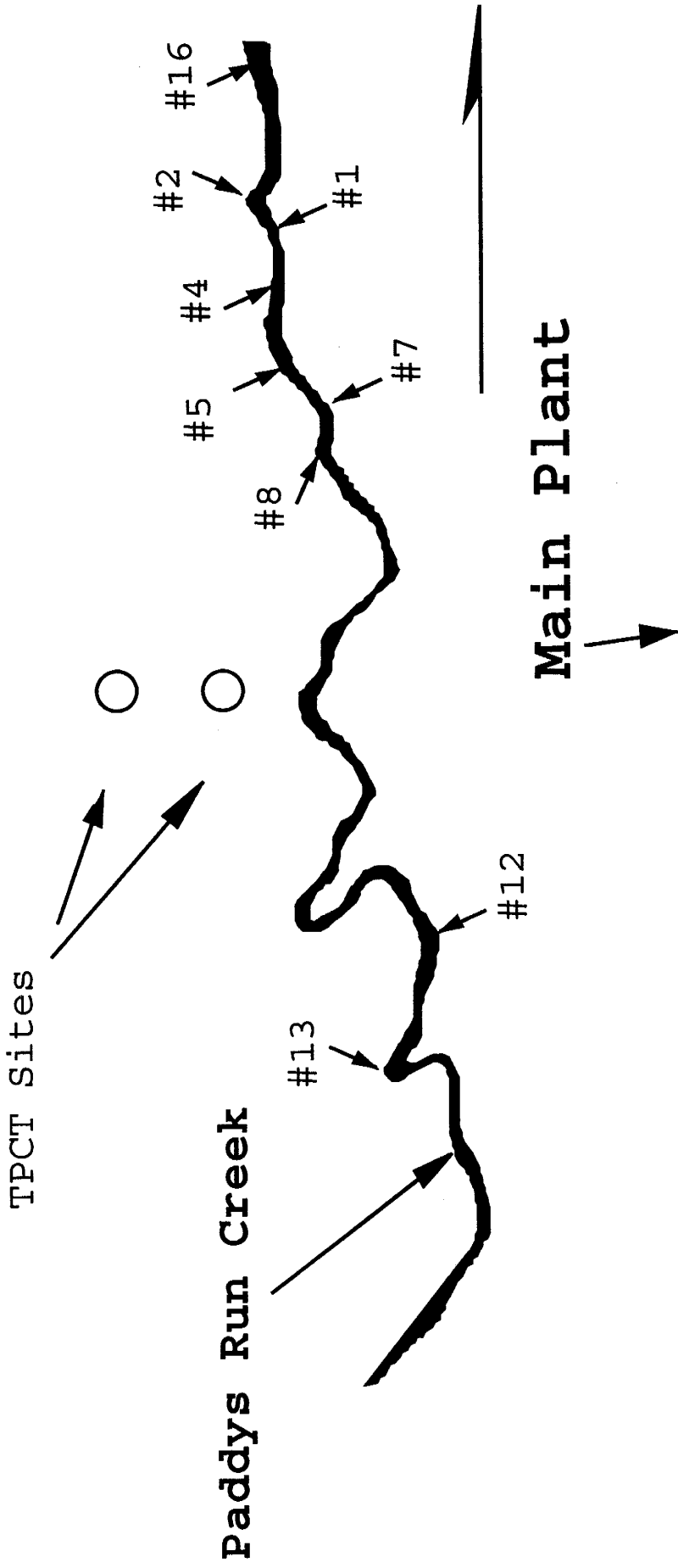


Figure 2. Outcrop locations along Paddy's Run.

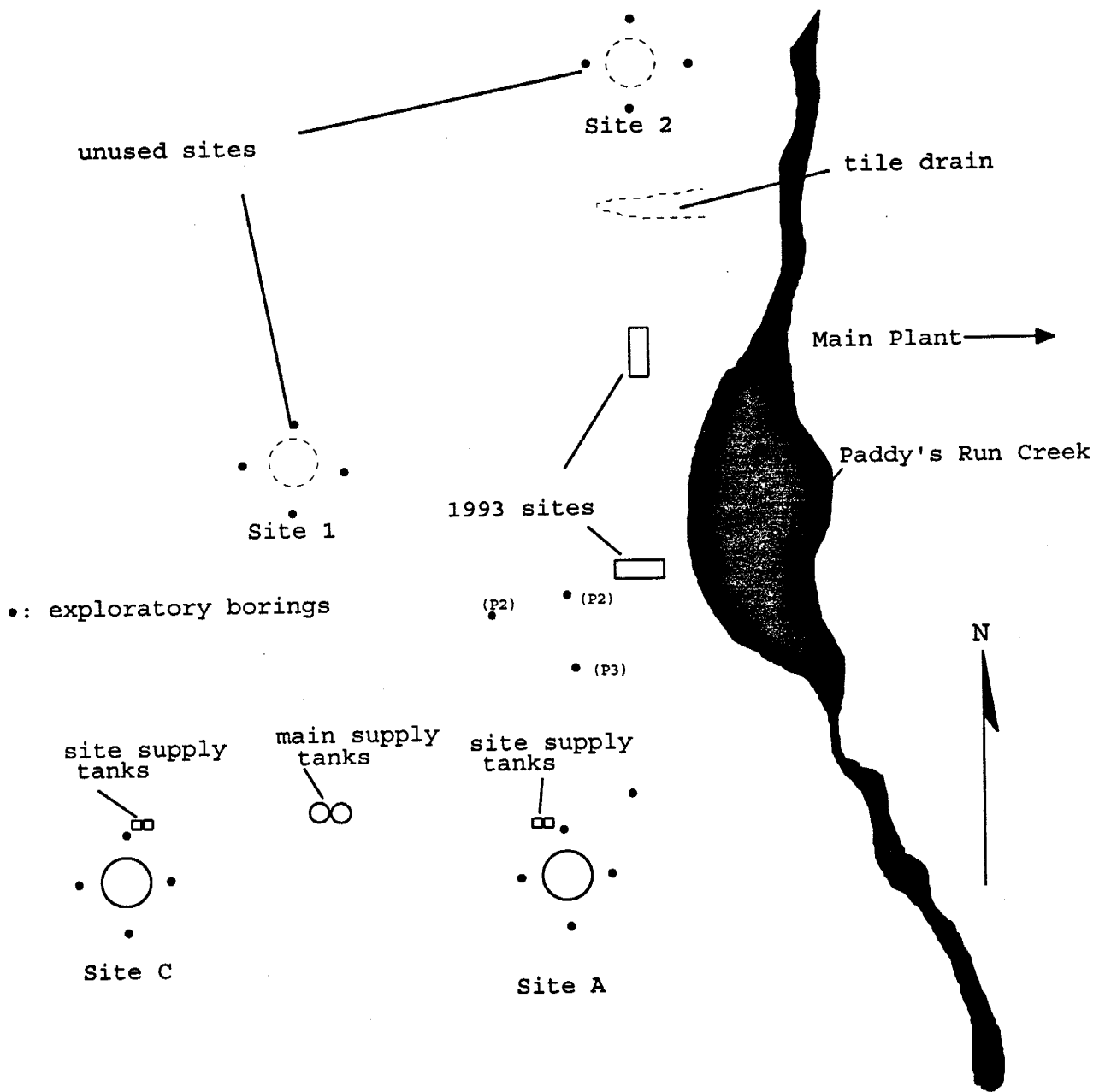


Figure 3. Location of 1994 Infiltration Stress Tests sites.

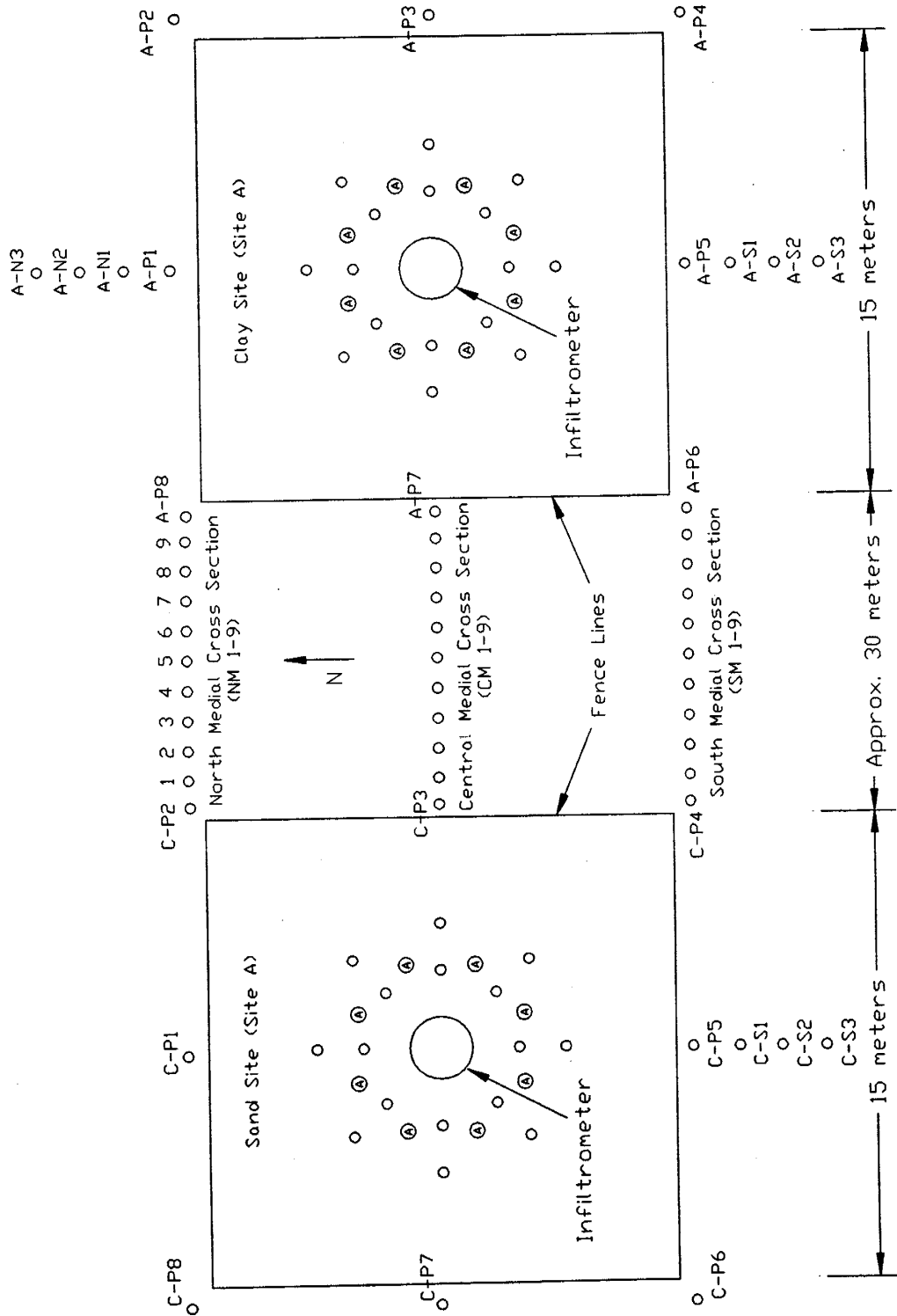


Figure 4. Plan view of sampling holes.

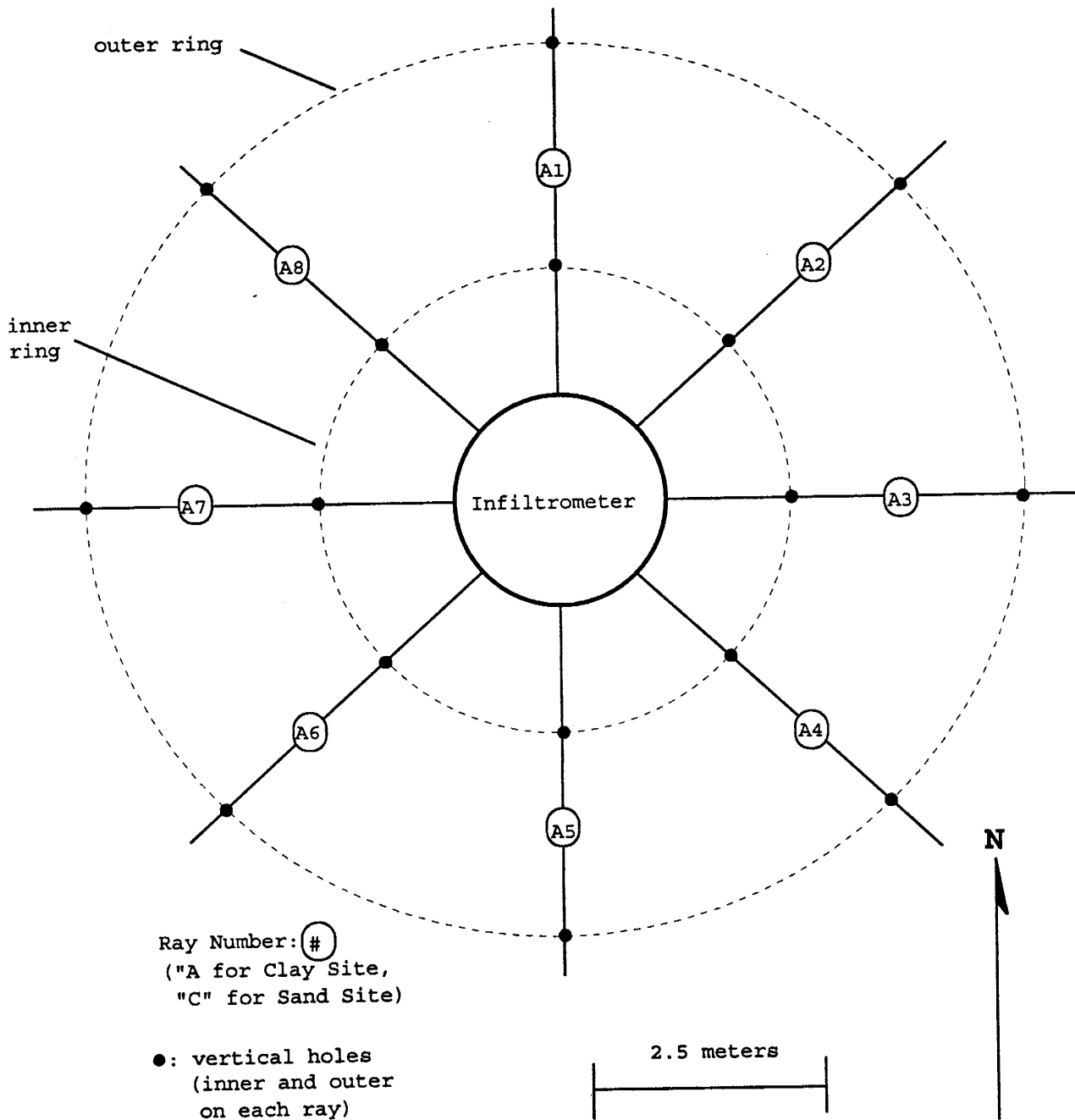


Figure 5. Location of sampling holes at the Clay and Sand TPCT sites.

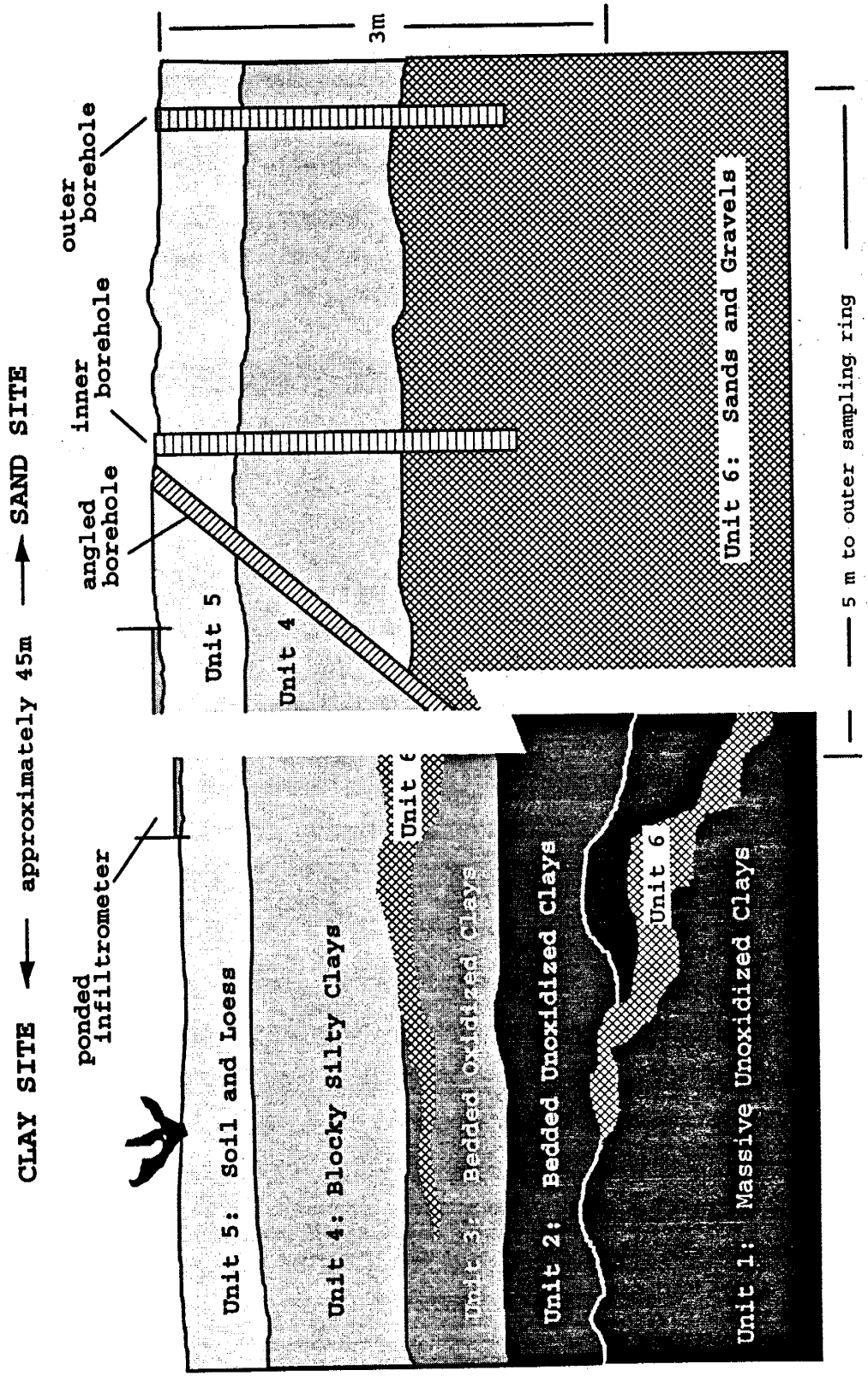
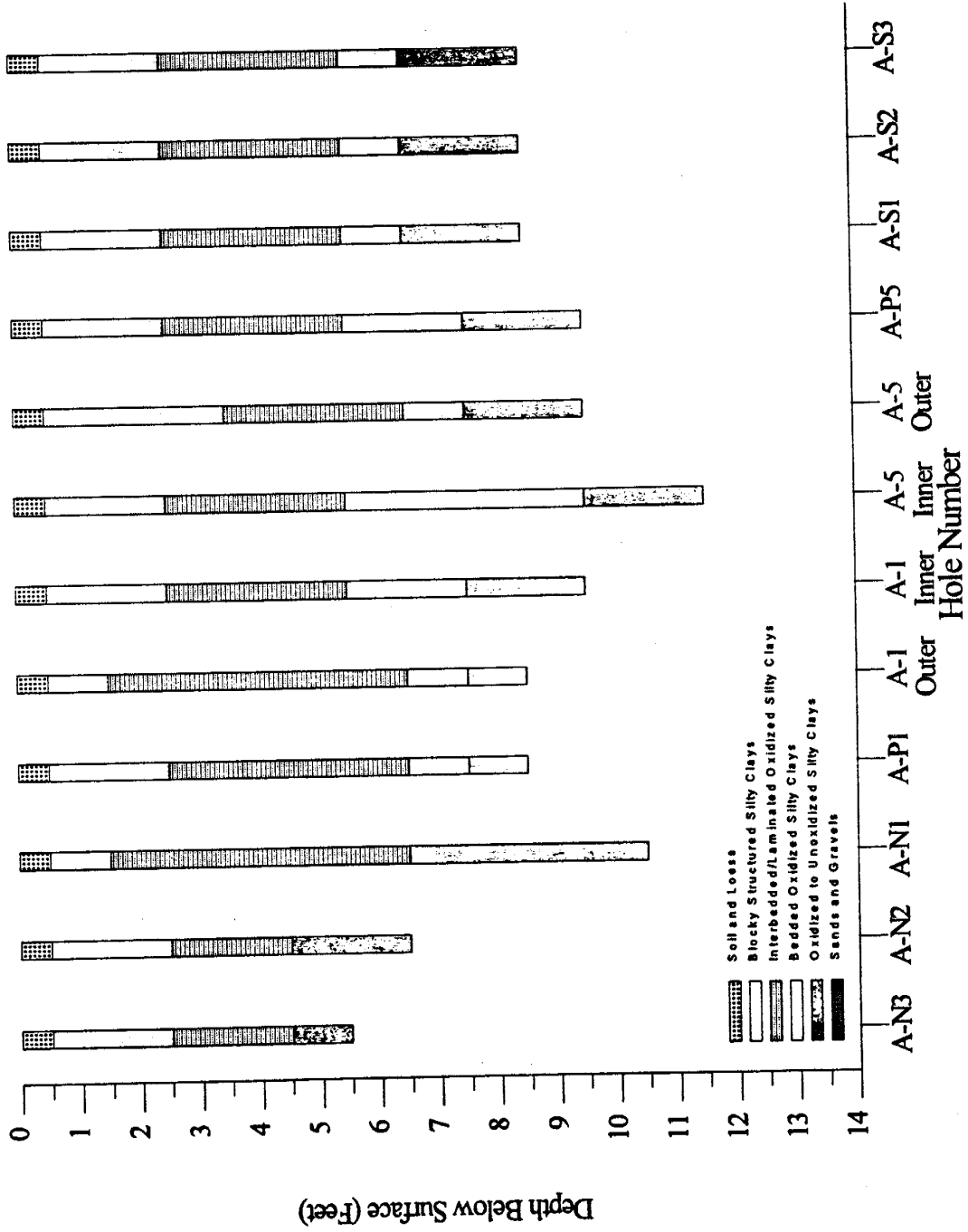


Figure 6. Hydrostratigraphic units at the "Clay" and "Sand" Sites. A cross section of the instrument borings used for sample collection is shown at the Sand Site. Sampling holes at the Clay Site are identical except they extend approximately 1 m deeper, ending just above Unit 1.

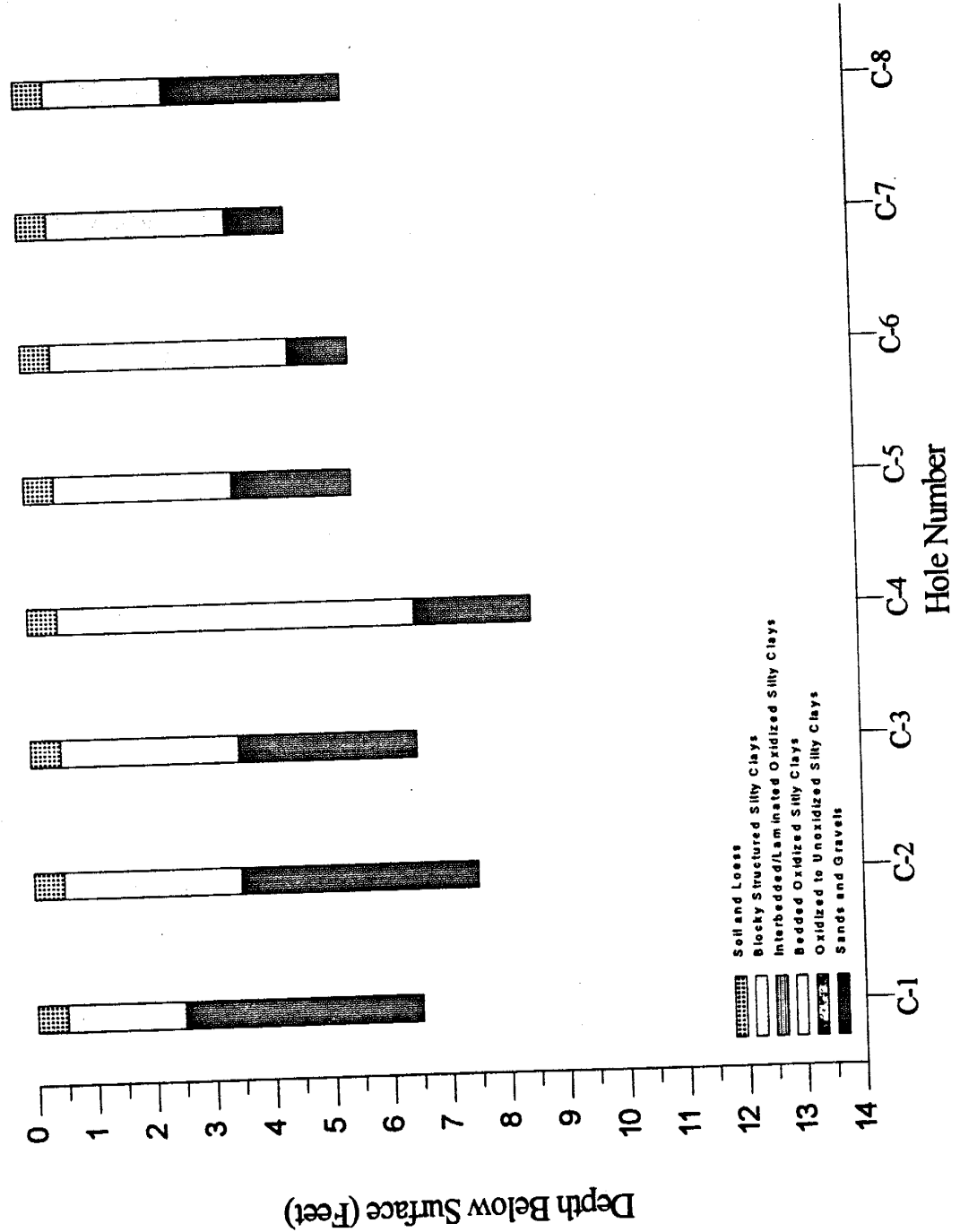
Clay Site (Site A) North-South Cross-section



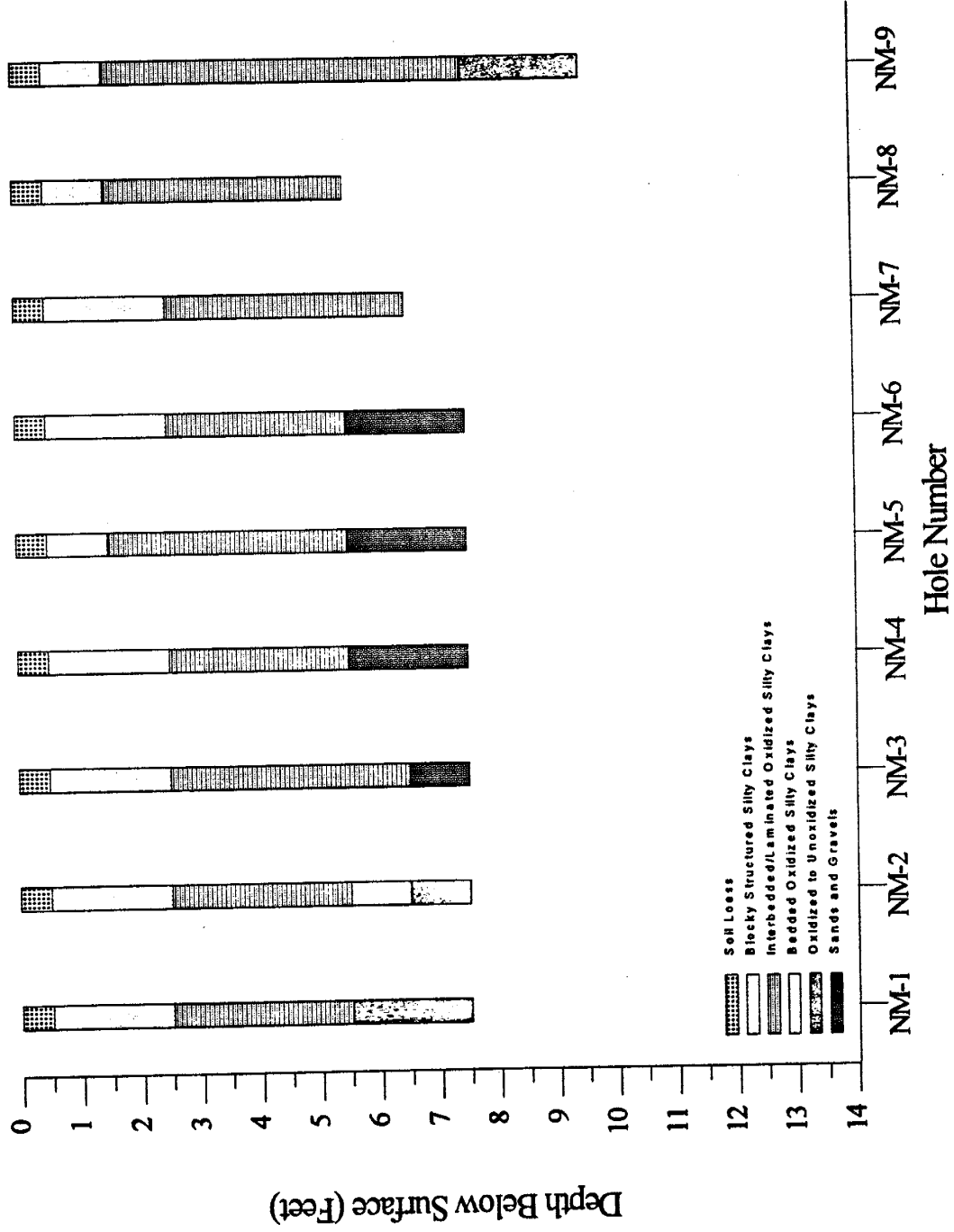
Clay Site North South Cross-section

	A-N3	A-N2	A-N1	A-P1	A-1 OUTER	A-1 INNER	A-5 INNER	A-5 OUTER	A-P5	A-S1	A-S2	A-S3
1 R. CS Unit #	1A	1A	1A	1A	1A	1A	1A	1B	1A	1A	1A	1A
Consistency	SoB/V Friable	SoB/V Friable	SoB/V Friable	SoB/V Friable	SoB/V Friable	SoB/V Friable	SoB/V Friable	SoB/V Friable	SoB/V Friable	SoB/V Friable	SoB/V Friable	SoB/V Friable
Texture	SC	SC	SC	SC	SC	SC	SC	SC	SC	SC	SC	SC
Color	10YR5/6	10YR5/6	10YR5/6	10YR5/6	10YR5/6	10YR5/6	10YR4/6	2.5Y6/4	10YR5/6	10YR5/6	10YR5/6	10YR5/6
Other Features	Dry, O	Dry, O	Dry, O	Dry, O	Dry, O	Dry, O	Dry, O	Dry, O	Dry, O	Dry, O	Dry, O	Dry, O
2 R. CS Unit #	2A	2A	2A	2A	2A	2A	2A	2B	2A	2A	2A	2A
Consistency	SoB/V Friable	SoB/V Friable	SR-SI Hid/Plastic	SoB/V Friable	SoB/V Friable	SoB/V Friable	SoB/V Friable	SR-SI Hid/Plastic	SR-SI Hid/Plastic	SR-SI Hid/Plastic	SR-SI Hid/Plastic	SoB/V Friable
Texture	SC	SC	SC	SC	SC	SC	SC	SC	SC	SC	SC	SC
Color	10YR5/6	10YR5/6	10YR3/6	10YR4/6	10YR4/6, 4/6	10YR4/6	10YR4/6	2.5Y4/4	10YR4/6	10YR4/6	10YR4/6	10YR4/6
Other Features	Dmp, O Dmp, Mn	Dmp, O	Dmp, Mn	Dmp, O	Dmp, CxCO3	Dmp, O	Dmp, CxCO3, O	Dmp, O	Dmp, O	Dmp, O, Mn	Dmp, O, Mn	Dmp, O CxCO3, Mn
3 R. CS Unit #	3A	3A	3A	3A	3A	3A	3A	3B	3A	3A	3A	3A
Consistency	SoB/V Friable	SR-SI Hid/Plastic	SR-SI Hid/Plastic	SR-SI Hid/Plastic	SR-SI Hid/Plastic	SR-SI Hid/Plastic	SR-SI Hid/Plastic	SR-SI Hid/Plastic	SR-SI Hid/Plastic	SR-SI Hid/Plastic	SR-SI Hid/Plastic	SR-SI Hid/Plastic
Texture	SC	SC	SC	SC	SC	SC	SC	SC	SC	SC	SC	SC
Color	10YR4/4	2.5Y5/4	2.5Y5/4	2.5Y4/4	2.5Y5/4	2.5Y4/4	2.5Y4/4	2.5Y4/4	2.5Y5/4	2.5Y5/4	2.5Y5/4	10YR4/4
Other Features	10YR4/4	Dmp, CxCO3	Dmp, CxCO3	Dmp, Mn	Dmp, CxCO3	Dmp, Mn	Dmp, O	Dmp	Dmp	Dmp, Mn	Dmp, Mn	Dmp, Mn
4 R. CS Unit #	4B	4A	4A	4A	4A	4A	4A	4B	4A	4A	4A	4A
Consistency	SoB/V Friable	SR-SI Hid/Plastic	SR-SI Hid/Plastic	SR-SI Hid/Plastic	SR-SI Hid/Plastic	SR-SI Hid/Plastic	SR-SI Hid/Plastic	SR-SI Hid/Plastic	SR-SI Hid/Plastic	SR-SI Hid/Plastic	SR-SI Hid/Plastic	SoB/V Friable
Texture	SC, S, P	SC	SC	SC	SC	SC	SC	SC	SC	SC	SC	SC
Color	2.5Y5/4	2.5Y5/4	2.5Y5/4	2.5Y5/4, 6/2	2.5Y5/4	2.5Y5/4, 6/4	2.5Y5/4	2.5Y4/4	2.5Y5/4	2.5Y5/4	2.5Y5/4	2.5Y5/4
Other Features	Dmp	Dmp	Dmp	Dmp, CxCO3	Dmp, CxCO3	Dmp, CxCO3	Dmp, CxCO3	Dmp, CxCO3	Dmp, CxCO3	Dmp, CxCO3	Dmp, CxCO3	Dmp, CxCO3
5 R. CS Unit #	5A	5A	5A	5B	5A	5A	5A	5A	5A	5A	5A	5A
Consistency	SR-SI Hid/Plastic	SR-SI Hid/Plastic	SR-SI Hid/Plastic	SR-SI Hid/Plastic	SR-SI Hid/Plastic	SR-SI Hid/Plastic	SR-SI Hid/Plastic	SR-SI Hid/Plastic	SR-SI Hid/Plastic	SR-SI Hid/Plastic	SR-SI Hid/Plastic	SR-SI Hid/Plastic
Texture	SC	SC	SC	SC, S	SC	SC	SC	SC	SC	SC	SC	SC
Color	2.5Y5/4, 7/2	2.5Y5/4	2.5Y4/4	2.5Y5/4	2.5Y5/4	2.5Y5/4	2.5Y5/4	2.5Y5/4	2.5Y5/4	2.5Y5/4, 6/2, 8/1	2.5Y5/4, 7/3	2.5Y5/4
Other Features	Dmp	Dmp, CxCO3, SP	Dmp	Sat	Dmp, CxCO3	Dmp, CxCO3	Dmp, Mn	Dmp, CxCO3, Mn	Dmp, CxCO3	Dmp, CxCO3	Dmp, CxCO3, Mn	Dmp, CxCO3, Mn
6 R. CS Unit #	6D	6A	6B	6B	6B	6B	6B	6A	6A	6A	6A	6A
Consistency	V SR/V Sticky	SR-SI Hid/Plastic	SR-SI Hid/Plastic	SR-SI Hid/Plastic	SR-SI Hid/Plastic	SR-SI Hid/Plastic	SR-SI Hid/Plastic	SR-SI Hid/Plastic	SR-SI Hid/Plastic	SR-SI Hid/Plastic	SR-SI Hid/Plastic	SR-SI Hid/Plastic
Texture	SC, S, P, G	SC, S, P, G	SC, S, P, G	SC, S, P	SC, G	SC, S	SC	SC	SC	SC	SC	SC
Color	2.5Y5/4	2.5Y4/4	2.5Y4/3	2.5Y5/4	2.5Y5/4	2.5Y5/4	2.5Y5/4	2.5Y5/4	2.5Y5/4	2.5Y5/4	2.5Y5/4	2.5Y5/4
Other Features	Sat	Sat	Dmp	Dmp	Dmp, CxCO3	Dmp, CxCO3	Dmp, CxCO3	Dmp, CxCO3	Dmp, CxCO3	Dmp, CxCO3	Dmp, CxCO3, SP	Dmp, SP, Mn
7 R. CS Unit #	7A	7A	7B	7B	7B	7B	7B	7A	7A	7A	7A	7A
Consistency	SR-SI Hid/Plastic	SR-SI Hid/Plastic	SR-SI Hid/Plastic	SR-SI Hid/Plastic	SR-SI Hid/Plastic	SR-SI Hid/Plastic	SR-SI Hid/Plastic	SR-SI Hid/Plastic	SR-SI Hid/Plastic	SR-SI Hid/Plastic	SR-SI Hid/Plastic	SR-SI Hid/Plastic
Texture	SC, P	SC, P	SC, S, P	SC, S, P	SC, S, P	SC, S, P	SC, S, P	SC	SC	SC	SC	SC
Color	2.5Y5/4	2.5Y4/3	2.5Y4/3	2.5Y5/4	2.5Y5/4	2.5Y4/4	2.5Y4/4	2.5Y5/4	2.5Y5/4	2.5Y5/4	2.5Y5/4, 5YR4/4	2.5Y5/4, 8/2, 7/3
Other Features	Sat	Sat	Dmp	Dmp	Dmp	Dmp	Dmp	Dmp, CxCO3	Dmp, SP	Dmp, SP	Dmp, SP, Mn	Dmp, SP, Mn
8 R. CS Unit #	8D	8B	8B	8B	8A	8A	8A	8A	8A	8A	8A	8A
Consistency	SR-SI Hid/Plastic	SR-SI Hid/Plastic	SR-SI Hid/Plastic	SR-SI Hid/Plastic	SR-SI Hid/Plastic	SR-SI Hid/Plastic	SR-SI Hid/Plastic	SR-SI Hid/Plastic	SR-SI Hid/Plastic	SR-SI Hid/Plastic	SR-SI Hid/Plastic	SR-SI Hid/Plastic
Texture	SC, S	SC, S, P	SC, S, P	SC, S, P	SC	SC	SC	SC	SC	SC	SC	SC
Color	2.5Y5/4	2.5Y5/4	2.5Y5/4	2.5Y4/4	2.5Y4/4	2.5Y5/3	2.5Y5/4	2.5Y5/4	2.5Y5/4	2.5Y5/4	2.5Y5/4	2.5Y5/3
Other Features	Sat	Sat	Dmp, SP	Dmp, SP	Dmp	Dmp, SP	Dmp	Dmp, SP	Dmp, SP	Dmp, SP	Dmp, SP, Mn	Dmp
9 R. CS Unit #	9A	9B	9B	9B	9A	9A	9A	9A	9A	9A	9A	9A
Consistency	SR-SI Hid/Plastic	SR-SI Hid/Plastic	SR-SI Hid/Plastic	SR-SI Hid/Plastic	SR-SI Hid/Plastic	SR-SI Hid/Plastic	SR-SI Hid/Plastic	SR-SI Hid/Plastic	SR-SI Hid/Plastic	SR-SI Hid/Plastic	SR-SI Hid/Plastic	SR-SI Hid/Plastic
Texture	SC, S	SC, S	SC, S	SC, S	SC	SC	SC	SC	SC	SC	SC	SC
Color	2.5Y5/4	2.5Y5/4	2.5Y5/4	2.5Y4/1	2.5Y4/2	2.5Y5/2	2.5Y5/3	2.5Y5/3	2.5Y5/4	2.5Y5/2	2.5Y5/2	2.5Y4/2
Other Features	Dmp, SP	Dmp, SP	Dmp, SP	Dmp, SP	Dmp	Dmp, SP	Dmp, SP	Dmp, SP	Dmp, SP	Dmp, SP	Dmp, SP	Dmp
10 R. CS Unit #	10A	10A	10A	10A	10A	10A	10A	10A	10A	10A	10A	10A
Consistency	V SR/V Sticky	SR-SI Hid/Plastic	SR-SI Hid/Plastic	SR-SI Hid/Plastic	SR-SI Hid/Plastic	SR-SI Hid/Plastic	SR-SI Hid/Plastic	SR-SI Hid/Plastic	SR-SI Hid/Plastic	SR-SI Hid/Plastic	SR-SI Hid/Plastic	SR-SI Hid/Plastic
Texture	SC, P	SC, P	SC, P	SC, P	SC, P	SC, P	SC	SC	SC	SC	SC	SC
Color	2.5Y5/3	2.5Y5/3	2.5Y5/3	2.5Y5/3	2.5Y5/3	2.5Y5/3	2.5Y5/2	2.5Y5/3	2.5Y5/2	2.5Y5/2	2.5Y5/2	2.5Y4/2
Other Features	Sat	Sat	Sat	Sat	Dmp	Dmp	Dmp, SP	Dmp, SP	Dmp, SP	Dmp, SP	Dmp, SP	Dmp

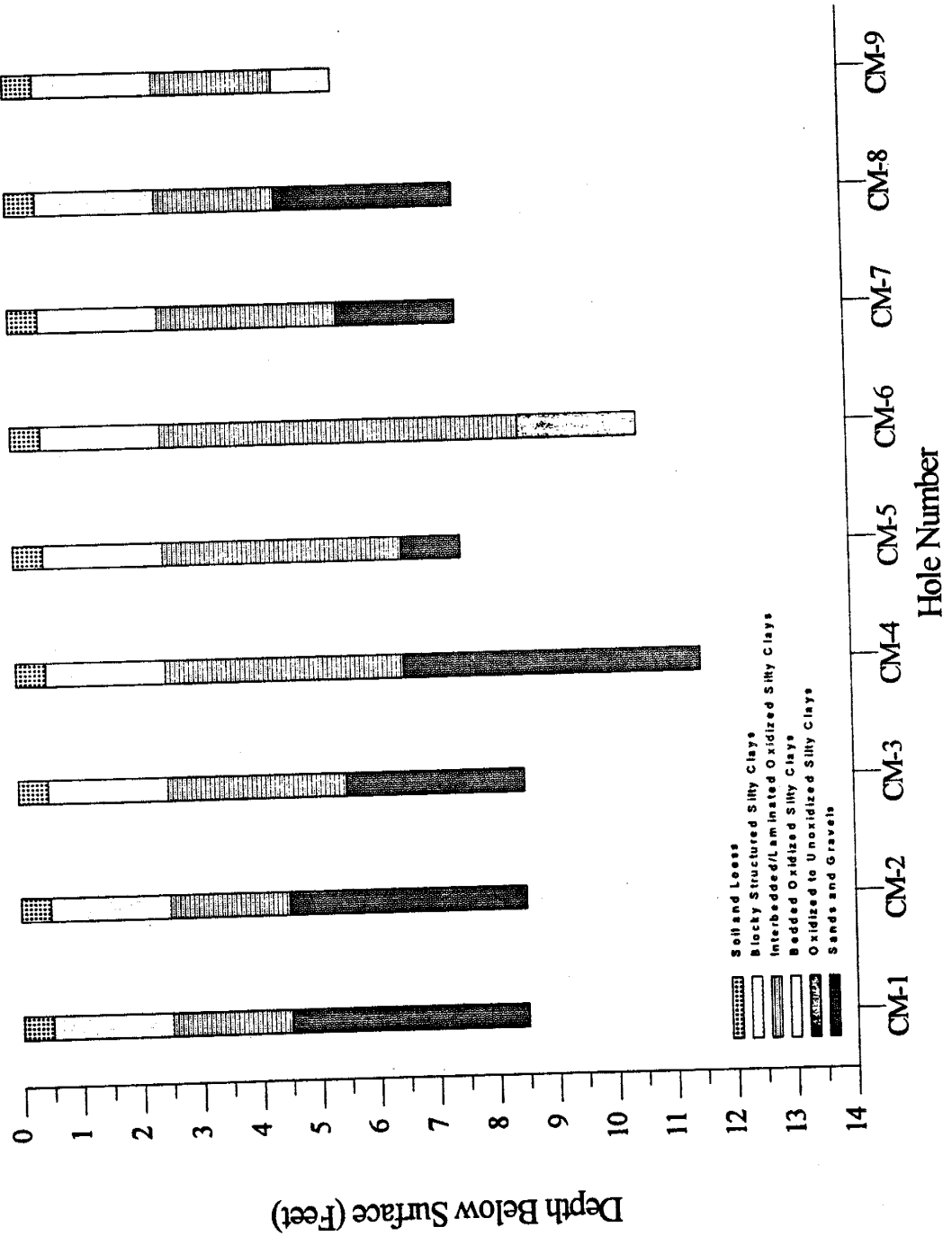
Sand Site (Site C) Inner Ring Cross-section



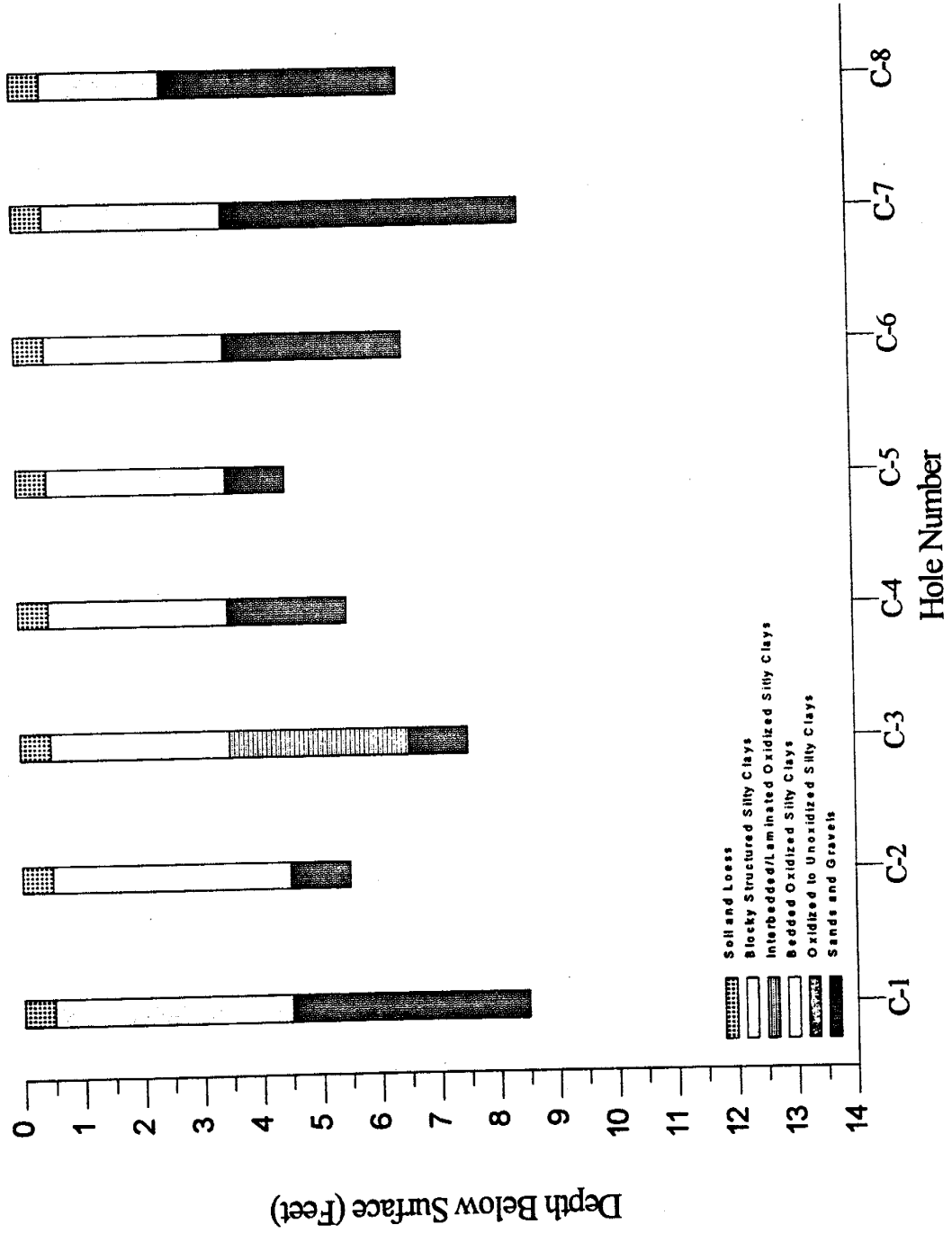
North Medial Cross-section



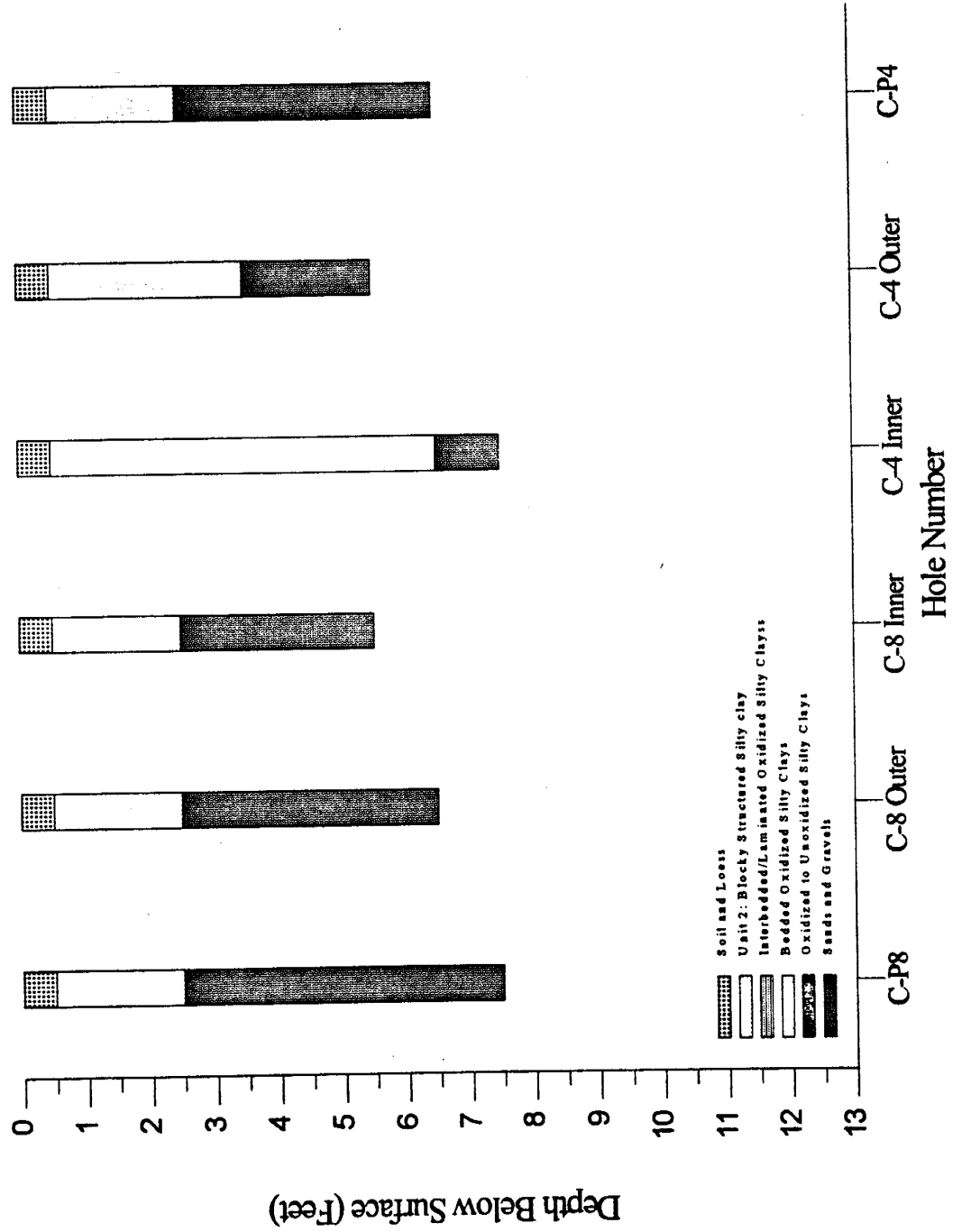
Central Medial Cross-section



Sand Site (Site C) Outer Ring Cross-section



Sand Site (Site C) Northwest-Southeast Cross-section



Sand Site Northwest-Southeast Cross-section

Depth/Hole #	C-P8	C-8 OUTER	C-8 INNER	C-4 INNER	C-4 OUTER	IA	C-P4
1 R. CS Unit #	IB	SoBV Friable	SoBV Friable	SoBV Friable	SoBV Friable	SoBV Friable	IA
Consistency	SC	SC	SC	SC	SC	SC	SC
Texture	2.5Y7/4	10YR5/6	10YR5/6	2.5Y6/3	2.5Y5/3	10YR4/6	10YR4/6
Color	Dry, O	Dry, O	Dry, O	Dry, O	Dry, O	Dry, O	Dry, O
Other Features							
2 R. CS Unit #	2A	2B	2A	2B	2A	2A	2A
Consistency	SR-SI Hrd/Plastic	SR-SI Hrd/Plastic	SR-SI Hrd/Plastic	SR-SI Hrd/Plastic	SR-SI Hrd/Plastic	SR-SI Hrd/Plastic	SR-SI Hrd/Plastic
Texture	SC	SC	SC	SC	SC	SC	SC
Color	10YR6/6, 5/8	2.5Y5/6	10YR4/6	2.5Y6/3, 7.5YR5/8	10YR4/6, 4A	10YR4/4	10YR4/4
Other Features	Dmp, O	Dmp, O	Dmp, Mn	Dmp, CaCO3	Dmp, CaCO3	Dmp, CaCO3	Dmp, CaCO3
3 R. CS Unit #	2B	2B	2B	2B	2B	2A	2A
Consistency	SR-SI Hrd/Plastic	SR-SI Hrd/Plastic	SR-SI Hrd/Plastic	SR-SI Hrd/Plastic	SR-SI Hrd/Plastic	SR-SI Hrd/Plastic	SR-SI Hrd/Plastic
Texture	SC	SC	SC	SC	SC	SC, P	SC, P
Color	2.5Y5/4	2.5Y4/4	2.5Y4/4	2.5Y4/4, 7.5YR5/8	2.5Y4/4, 7.5YR6/8	10YR4/6	10YR4/6
Other Features	Dmp, Mn	Dmp, O	Dmp, Mn	Dmp, CaCO3, Mn	Dmp	Dmp, Mn	Dmp, Mn
4 R. CS Unit #	7A	7D	7B	7B	7B	7A	7A
Consistency	V SBV Sticky	V SBV Sticky	V SBV Sticky	SR-SI Hrd/Plastic	SR-SI Hrd/Plastic	SR-SI Hrd/Plastic	SR-SI Hrd/Plastic
Texture	SC	SC, S, P, G	SC, S	SC	SC	SC	SC
Color	2.5Y5/4	2.5Y4.4	2.5Y4.4	2.5YR5/3, 7.5YR5/6	2.5Y5/3, 10YR 5/8	2.5Y4/4	2.5Y4/4
Other Features	Sat	Sat	Sat	Dmp, Mn	Dmp, CaCO3, Mn	Sat	Sat
5 R. CS Unit #	8A	7D	8B	8B	7B	7B	7B
Consistency	NA/Soupy	NA/Soupy	NA/Soupy	SR-SI Hrd/Plastic	SR-SI Hrd/Plastic	SR-SI Hrd/Plastic	SR-SI Hrd/Plastic
Texture	SC, S, P, G	SC, S, P, G	SC, S	SC	SC	SC, S	SC, S
Color	2.5Y5/4	2.5Y5/4	2.5Y5/4	2.5Y4/3, 7.5YR5/6	2.5Y5/4	2.5Y4/4	2.5Y4/4
Other Features	Sat	Sat	Sat	Dmp	Sat	Sat	Sat
6 R. CS Unit #	8A	7D	8C	8C	7B	7C	7C
Consistency	NA/Soupy	V SBV sticky	NA/Soupy	SR-SI Hrd/Plastic	V SBV sticky	V SBV sticky	V SBV sticky
Texture	SC, S, P, G	SC, S, P, G	SR, S	SC, P	S, SC	SC, S, P	SC, S, P
Color	2.5Y5/4	2.5Y5/4	2.5Y5/4	2.5YR5/2, 7.5YR5/6	2.5Y5/4	2.5Y5/4	2.5Y5/4
Other Features	Sat	Sat	Sat	Dmp	Sat	Sat	Sat
7 R. CS Unit #	8A	7D					
Consistency	NA/Soupy	V SBV Sticky		SR-SI Hrd/Plastic		V SBV sticky	V SBV sticky
Texture	SC, S, P, G	SC, S, P, G		SC, P		SC, S	SC, S
Color	2.5Y5/4	2.5Y5/4		2.5Y4/3, 5YR5/8		2.5Y5/4	2.5Y5/4
Other Features	Sat	Sat		Dmp		Sat	Sat
8 R. CS Unit #	8D						
Consistency	NA/Soupy						
Texture	SR, S, P, G						
Color	2.5Y5/4						
Other Features	Sat						

Sand Site Northeast-Southwest Cross-section

Depth / Hole #	C-P6	C-6 OUTER	C-6 INNER	C-2 INNER	C-2 OUTER	C-P2
1 R. CS Unit #	IB	IA	IB	IB	IB	IB
Consistency	Soft/Friable	Soft/Friable	Soft/Friable	Soft/Friable	Soft/Friable	Soft/Friable
Texture	SC	SC	SC	SC	SC	SC
Color	2.5Y6/3	10YR5/6, 2.5Y6/3	2.5Y5/3	2.5Y4/3, 5/4	2.5Y4/2	2.5Y7/2
Other Features	Dry, O	Dry, O	Dry, O	Dry, O	Dry, O	Dry, O
2 R. CS Unit #	2A	2B	2A	2B	2A	2A
Consistency	SR-SI Hid/Plastic	SR-SI Hid/Plastic	SR-SI Hid/Plastic	SR-SI Hid/Plastic	SR-SI Hid/Plastic	SR-SI Hid/Plastic
Texture	SC	SC	SC	SC	SC	SC
Color	10YR4/6	2.5Y4/4	10YR3/6, 2.5Y5/4	2.5Y4/4	10YR4/6, 4/4	10YR4/4, 7.5YR4/6
Other Features	Dmp, Mn	Dmp, O, CaCO3, Mn	Dmp, CaCO3	Dmp, Mn	Dmp, Mn	Dmp
3 R. CS Unit #	2A	2B	2B	2B	2A	2A
Consistency	SR-SI Hid/Plastic	SR-SI Hid/Plastic	SR-SI Hid/Plastic	SR-SI Hid/Plastic	SR-SI Hid/Plastic	SR-SI Hid/Plastic
Texture	SC	SC	SC	SC	SC	SC
Color	10YR4/6, 2.5Y4/2	2.5Y4/4, 7.5YR5/8	2.5Y5/4	2.5Y4/4, 5/6	10YR5/4	10YR5/6, 7.5YR5/8
Other Features	Dmp, Mn	Dmp, Mn	Dmp, Mn	Dmp, Mn	Dmp, Mn	Dmp, Mn
4 R. CS Unit #	2B	2B	2B	2B	2B	2B
Consistency	SR-SI Hid/Plastic	SR-SI Hid/Plastic	SR-SI Hid/Plastic	SR-SI Hid/Plastic	SR-SI Hid/Plastic	SR-SI Hid/Plastic
Texture	SC	SC, S	SC, S	SC, S	SC	SC
Color	2.5Y5/4	2.5Y4/4	2.5Y4/4, 4/2	2.5Y4/4, 6/3	2.5Y5/4, 7/6	2.5Y5/4, 7.5YR5/8
Other Features	Dmp, Mn	Dmp	Sat	Dmp	Dmp, CaCO3	Dmp
5 R. CS Unit #	IB	7B	7B	7B	2B	1A
Consistency	SR-SI Hid/Plastic	SR-SI Hid/Plastic	SR-SI Hid/Plastic	SR-SI Hid/Plastic	SR-SI Hid/Plastic	SR-SI Hid/Plastic
Texture	SC, S	SC, S	SC, S	SC	SC, S	SC
Color	10YR5/6, 2.5Y5/4	2.5Y4/4	2.5Y4/4	2.5Y4/4, 6/3	2.5Y5/6	2.5Y5/2, 7.5YR6/6
Other Features	Dmp, Mn	Sat	Sat	Dmp	Dmp	Dmp, CaCO3
6 R. CS Unit #	7B	7D	7D	7B	7B	1A
Consistency	SR-SI Hid/Plastic	SR-SI Hid/Plastic	V SRV Sticky	V SRV sticky	V SRV sticky	SR-SI Hid/Plastic
Texture	SC, S	SC, S, P, G	SC, S, P, G	SC, S	SC, S	SC
Color	2.5Y4/4	2.5Y5/4	2.5Y4/4	2.5Y5/4	2.5Y5/4	2.5YR5/4, 6/2
Other Features	Sat	Sat	Sat	Sat	Sat	Sat
7 R. CS Unit #	8A	7D	7C	7B	7B	1B
Consistency	NA/Sloopy	SR-SI Hid/Plastic	SR-SI Hid/Plastic	SR-SI Hid/Plastic	V SRV sticky	V SRV sticky
Texture	SC, S	SC, S, P, G	SC, S, G	SC, S	SC, S	SC, S
Color	2.5Y4/4	2.5Y5/4	2.5Y4/4	2.5Y5/4	2.5Y5/4	2.5Y5/2, 7.5YR5/8
Other Features	Sat	Sat	Sat	Sat	Sat	Dmp, CaCO3
8 R. CS Unit #	8D	8B	8A	7D	7D	7B
Consistency	NA/Sloopy	NA/Sloopy	SR-SI Hid/Plastic	V SRV sticky	V SRV sticky	V SRV sticky
Texture	SR, S, P, G	SR, S	SR, S	SC, S, P, G	SC, S, P, G	SC, S
Color	2.5Y4/4	2.5Y4/4	2.5Y4/4	2.5Y5/4	2.5Y5/4	2.5Y4/4
Other Features	Dmp	Sat	Sat	Sat	Sat	Sat
9 R. CS Unit #	7C	7D	7D	7D	7D	7B
Consistency	V SRV Sticky	V SRV sticky	V SRV sticky	V SRV sticky	V SRV sticky	V SRV sticky
Texture	SC, S, P	SC, S, P	SC, S, P, G	SC, S, P, G	SC, S, P, G	SC, S
Color	2.5Y5/4	2.5Y5/4	2.5Y5/4	2.5Y5/4	2.5Y5/4	2.5Y4/4
Other Features	Sat	Sat	Sat	Sat	Sat	Sat
10 R. CS Unit #	7C	7D	7D	7D	7D	7B
Consistency	V SRV Sticky	V SRV sticky	V SRV sticky	V SRV sticky	V SRV sticky	V SRV sticky
Texture	SC, S, P	SC, S, P	SC, S, P, G	SC, S, P, G	SC, S, P, G	SC, S
Color	2.5Y5/4	2.5Y5/4	2.5Y5/4	2.5Y5/4	2.5Y5/4	2.5Y4/4
Other Features	Sat	Sat	Sat	Sat	Sat	Sat

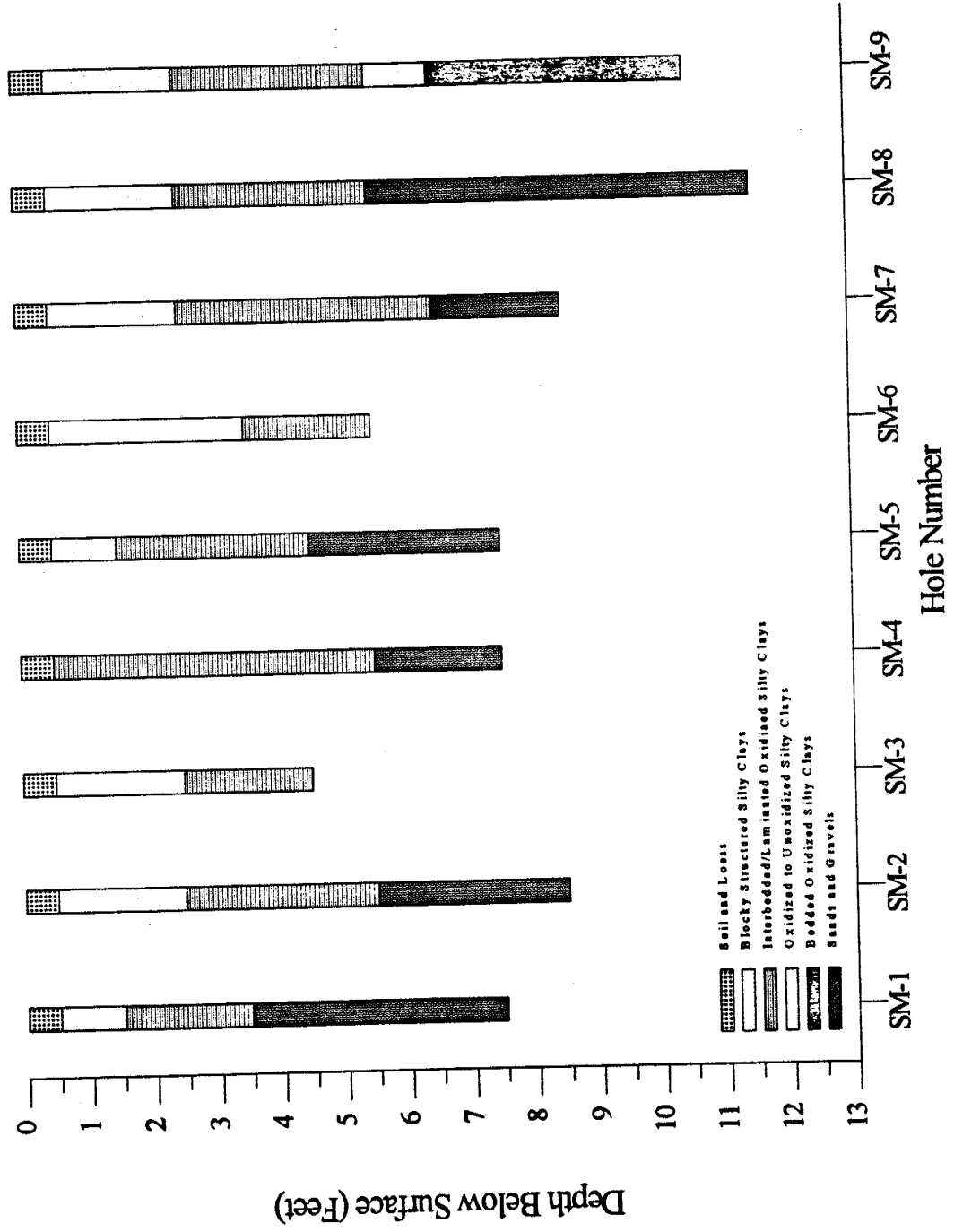
Central Medial Cross-section

	CM1	CM2	CM3	CM4	CM5	CM6	CM7	CM8	CM9
1 R. CS Unit #	1B	1B	1A	1A	1A	1A	1A	1B	1A
Consistency	Soft/V Fiable	Soft/V Fiable	Soft/V Fiable	Soft/V Fiable	Soft/V Fiable	Soft/V Fiable	Soft/V Fiable	Soft/V Fiable	Soft/V Fiable
Texture	SC	SC	SC	SC	SC	SC	SC	SC	SC
Color	2.5Y6/4	2.5Y6/4	10YR5/6	10YR5/6	10YR5/6	10YR5/6	10YR5/6	2.5Y6/4	10YR5/8
Other Features	Dry, O	Dry, O	Dry, O	Dry, O	Dry, O	Dry, O	Dry, O	Dry, O	Dry, O
2 R. CS Unit #	2A	2B	2B	2A	2A	2B	2B	2B	2B
Consistency	SI Hd/V Fiable	SI Hd/V Fiable	SR-SI Hd/Plastic	SR-SI Hd/Plastic	SR-SI Hd/Plastic	SR-SI Hd/Plastic	SR-SI Hd/Plastic	SI Hd/V Fiable	SI Hd/V Fiable
Texture	SC	SC	SC	SC	SC	SC	SC	SC	SC
Color	10YR5/4	2.5Y5/4, 5/6	2.5Y5/4, 7.5YR5/8	10YR5/6	10YR5/6	2.5Y5/4	2.5Y4/4	2.5Y5/4	2.5Y5/4
Other Features	Sat, Mn	Dmp, O, Mn	Dmp, Mn	Dmp, O, Mn	Dmp, O, Mn	Dmp, Mn	Dmp, CxCO3, Mn	Dmp, O, Mn	Dmp, O, Mn
3 R. CS Unit #	2B	2B	2B	2B	2B	2B	2B	2B	2B
Consistency	SR-SI Hd/Plastic	SR-SI Hd/Plastic	SR-SI Hd/Plastic	SR-SI Hd/Plastic	SR-SI Hd/Plastic	SI Hd/V Fiable	SI Hd/V Fiable	SR-SI Hd/Plastic	SR-SI Hd/Plastic
Texture	SC	SC	SC	SC	SC	SC	SC	SC	SC
Color	2.5Y4/4	2.5Y5/6	2.5Y6/4	2.5Y5/6	2.5Y5/6	2.5Y5/4	2.5Y4/4	2.5Y6/6	2.5Y4/6
Other Features	OB, Dmp, Mn	Dmp, Mn	Dmp, Mn	Dmp, Mn	Dmp, Mn	Dmp	Dmp	Dmp, Mn	Dmp, Mn
4 R. CS Unit #	3A	3A	3A	3A	3A	3A	3A	3A	3A
Consistency	SR-SI Hd/Plastic	SR-SI Hd/Plastic	SI Hd/V Fiable	SR-SI Hd/Plastic	SR-SI Hd/Plastic	SR-SI Hd/Plastic	SR-SI Hd/Plastic	SR-SI Hd/Plastic	SR-SI Hd/Plastic
Texture	SC	SC	SC	SC	SC	SC	SC	SC	SC
Color	2.5Y6/4	2.5Y5/6	2.5Y6/4	2.5Y6/4	2.5Y6/4, 8/2	2.5Y6/4, 7/1	2.5Y6/4, 6/2	2.5Y6/6	10YR5/6, 2.5Y6/3
Other Features	Dmp	Dmp	Dmp, CxCO3	Dmp, CxCO3	Dmp, CxCO3	Dmp, CxCO3	Dmp, CxCO3	Dmp, CxCO3	Dmp, Mn
5 R. CS Unit #	3A	3A	3A	3A	3A	3A	3A	3A	3A
Consistency	SR-SI Hd/Plastic	SR-SI Hd/Plastic	SR-SI Hd/Plastic	SR-SI Hd/Plastic	SR-SI Hd/Plastic	V SR/V Sticky	SR-SI Hd/Plastic	SR-SI Hd/Plastic	SR-SI Hd/Plastic
Texture	SC	SC	SC	SC	SC	SC	SC	SC	SC
Color	2.5Y5/4	2.5Y6/6	2.5Y6/4	2.5Y6/4, 5/4	2.5Y6/4, 5/4	2.5Y4/4	2.5Y6/2	2.5Y6/6	2.5Y6/4
Other Features	Dmp, CxCO3, Mn	Dmp, CxCO3	Dmp, CxCO3	Dmp, CxCO3	Dmp, CxCO3	Sat	Dmp, CxCO3	Dmp, Mn	Dmp, CxCO3
6 R. CS Unit #	4A	4A	4A	4A	4A	4A	4A	4A	4A
Consistency	NA/Soupy	SR-SI Hd/Plastic	SR-SI Hd/Plastic	SR-SI Hd/Plastic	SR-SI Hd/Plastic	V SR/Plastic	SR-SI Hd/Plastic	NA/Soupy	SR-SI Hd/Plastic
Texture	SC, S	SC	SC	SC	SC	SC	SC	SC	SC
Color	2.5Y5/4	2.5Y5/4	2.5Y5/4 6/3	2.5Y6/4 6/6 7/1	10YR5/8 2.5Y5/4	2.5Y5/4	2.5Y6/2 6/4	2.5Y5/6	2.5Y4/4
Other Features	Sat	Dmp, CxCO3	Dmp, SP, CxCO3	Dmp, CxCO3	Sat	Dmp, CxCO3	Sat	Dmp, CxCO3, Mn	Dmp, CxCO3, Mn
7 R. CS Unit #	8A	7B	7B	8A	8A	8A	8A	8A	8A
Consistency	NA/Soupy	SR-SI Hd/Plastic	SR-SI Hd/Plastic	SR-SI Hd/Plastic	V SR/Sticky	V SR/Sticky	NA/Soupy	V SR/V Plastic	V SR/V Plastic
Texture	SC, S	SC, S	SC, S	SC, S	SC, S	SC, S	SC, S	SC	SC
Color	2.5Y5/4	2.5Y5/3	2.5Y5/4	2.5Y5/4, 6/2	2.5Y5/4	2.5Y4/4	2.5Y4/4	2.5Y4/4	2.5Y4/4
Other Features	Sat	Dmp	Sat	Dmp, CxCO3, Mn	Dmp	Dmp, Mn	Sat	Sat	Sat
8 R. CS Unit #	8A	8A	8B	8A	8B	8B	8A	8A	8A
Consistency	NA/Soupy	NA/Soupy	SR-SI Hd/Plastic	NA/Soupy	NA/Soupy	SR-SI Hd/Plastic	NA/Soupy	NA/Soupy	NA/Soupy
Texture	SC, S	SC, S	S, SC	S, SH	S, SH	SC, S	S, SC	S, SC	S, SC
Color	2.5Y5/4	2.5Y5/4	2.5Y5/4	2.5Y5/4	2.5Y5/4	2.5Y5/4	2.5Y5/4	2.5Y5/4	2.5Y5/4
Other Features	Sat	Sat	Sat	Sat	Sat	Dmp, SP	Sat	Sat	Sat
9 R. CS Unit #	8B	8B	8B	8A	8A	8A	8A	8A	8A
Consistency	NA/Soupy	NA/Soupy	V SR/V Plastic	NA/Soupy	SR-SI Hd/Plastic	SR-SI Hd/Plastic	SR-SI Hd/Plastic	NA/Soupy	SR-SI Hd/Plastic
Texture	SH, S	SH, S	SH, S	S, SC	S, SC	SC, S	SC, S	S, SC	S, SC
Color	2.5Y5/4	2.5Y5/4	2.5Y5/4	2.5Y5/4	2.5Y5/4	2.5Y4/3	2.5Y5/4	2.5Y5/4	2.5Y5/4
Other Features	Sat	Sat	Dmp, SP	Sat	Sat	Dmp	Sat	Sat	Sat
10 R. CS Unit #	8B	8B	8A	8A	8A	8A	8A	8A	8A
Consistency	NA/Soupy	NA/Soupy	NA/Soupy	NA/Soupy	SR-SI Hd/Plastic	SR-SI Hd/Plastic	SR-SI Hd/Plastic	NA/Soupy	SR-SI Hd/Plastic
Texture	SH, S	SH, S	SH, S	SC, S	SC, S	SC, S	SC, S	S, SC	S, SC
Color	2.5Y5/4	2.5Y5/4	2.5Y5/4	2.5Y5/4	2.5Y5/4	2.5Y4/3	2.5Y5/4	2.5Y4/3	2.5Y4/3
Other Features	Sat	Sat	Dmp, SP	Sat	Sat	Dmp	Sat	Sat	Sat

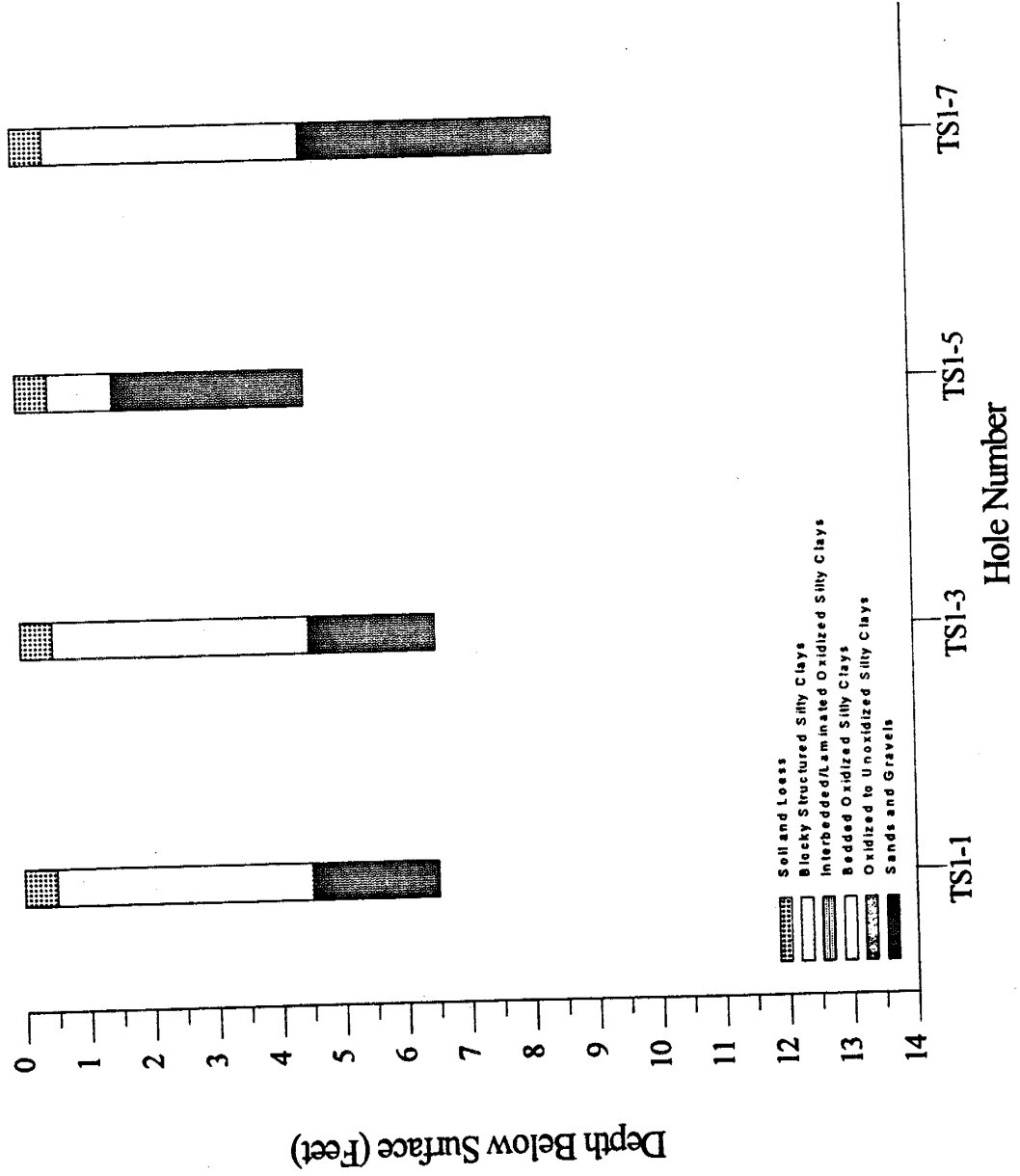
Central Medial Cross-section

	CM1	CM2	CM3	CM4	CM5	CM6	CM7	CM8	CM9
Depth / Hole #									
11 R. CS Unit #				RB		NA			
Consistency				N/A Soupy		SR-SI Hydro Plastic			
Texture				SH. S		SC			
Color				2.5Y5/4		2.5Y3/2			
Other Features				Sat		Dmp			
12 R. CS Unit #				7D					
Consistency				SR-SI Hydro Plastic					
Texture				SC, S, P					
Color				2.5Y5/3					
Other Features				Sat					

South Medial Cross-section



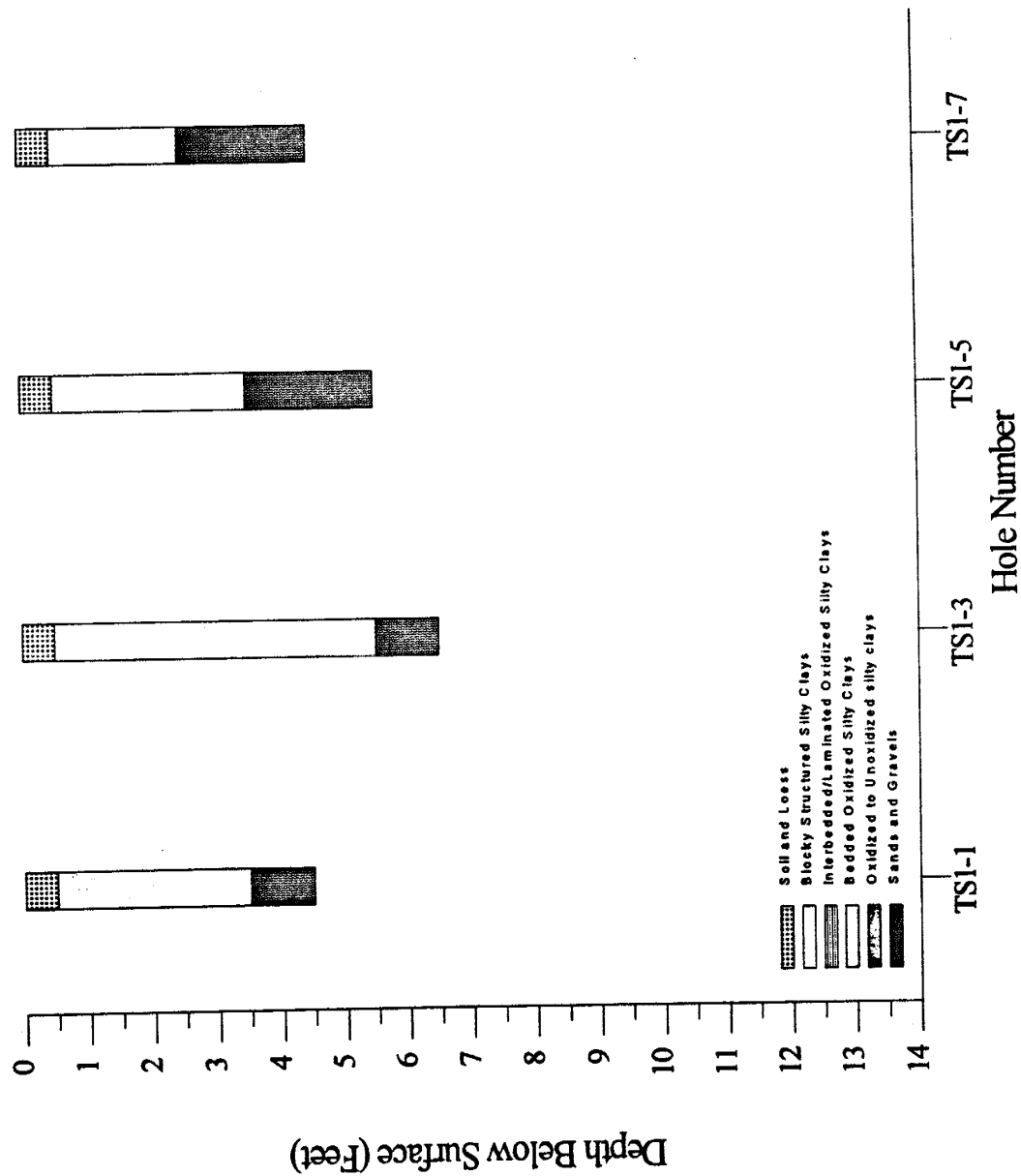
Test Site 1 Outer Ring Cross-section



Test Site 1 Cross-section

Depth / Hole #	TS1-2	TS1-6	TS1-10	TS1-14
1 ft. CS Unit #	1A	1B	1B	1A
Consistency	Soft/V Friable	Soft/V Friable	Soft/V Friable	Soft/V Friable
Texture	SC	SC	SC	SC
Color	10YR5/4	2.5YR5/6	2.5YR6/4	10YR6/6
Other Features	Dry, O	Dry, O	Dry, O	Dry, O
2 ft. CS Unit #	2A	2A	2A	2A
Consistency	Soft/V Friable	Soft/V Friable	Soft/V Friable	Soft/V Friable
Texture	SC	SC	SC	SC
Color	10YR4/4	10YR4/4	10YR4/4	10YR5/6
Other Features	Dmp	Dmp	Dmp, O, Mn	Dmp, O, Mn
3 ft. CS Unit #	2A	2A	6A	2A
Consistency	Sr-Si Hd/Sl Plastic	Sr-Si Hd/Sl Plastic	N/A/Sony	Sr-Si Hd/Sl Plastic
Texture	SC	SC	SC	SC
Color	10YR4/4	10YR4/4	10Y0/4/4	10YR5/6
Other Features	Dmp, Mn	Dmp, CaCO3	Sat	Dmp, O, Mn
4 ft. CS Unit #	2A	2B	8A	2A
Consistency	Sr-Si Hd/Sl Plastic	Sr-Si Hd/Sl Plastic	N/A/Sony	Sr-Si Hd/Sl Plastic
Texture	SC	SC	N/A/Sony	SC
Color	10YR4/4	2.5Y5/6, 2.5Y7/2	2.5Y4/4	10YR4/4, 10YR6/2
Other Features	Dmp, Mn	Dmp, CaCO3	Sat	Dmp, CaCO3
5 ft. CS Unit #	2B	2A	8C	2A
Consistency	Sr-Si Hd/Sl Plastic	Sr-Si Hd/Sl Plastic	N/A/Sony	Sr-Si Hd/Sl Plastic
Texture	SC	SC	Sr, S, P	SC
Color	2.5Y5/4	10YR4/4	2.5Y4/4	10YR4/4, 10YR6/2
Other Features	Dmp	Dmp, CaCO3, Mn	Sat	Dmp, CaCO3
6 ft. CS Unit #	7A	7B		8A
Consistency	V SNV Sticky	V SNV Sticky		N/A/Sony
Texture	SC	SC, S		SC, S, P
Color	2.5Y4/4	2.5Y4/4		10YR5/4
Other Features	Sat	Sat		Sat
7 ft. CS Unit #	7A	7C		8A
Consistency	V SNV Sticky	V SNV Plastic		N/A/Sony
Texture	SC	SC, S, P		SC, S, P
Color	2.5Y4/4	2.5Y4/4		10YR5/4
Other Features	Sat	Sat		Sat
8 ft. CS Unit #				9A
Consistency				N/A/Sony
Texture				SC, S, P
Color				10YR5/4
Other Features				Sat
9 ft. CS Unit #				9C
Consistency				N/A/Sony
Texture				Sr, S, P
Color				10YR5/4
Other Features				Sat

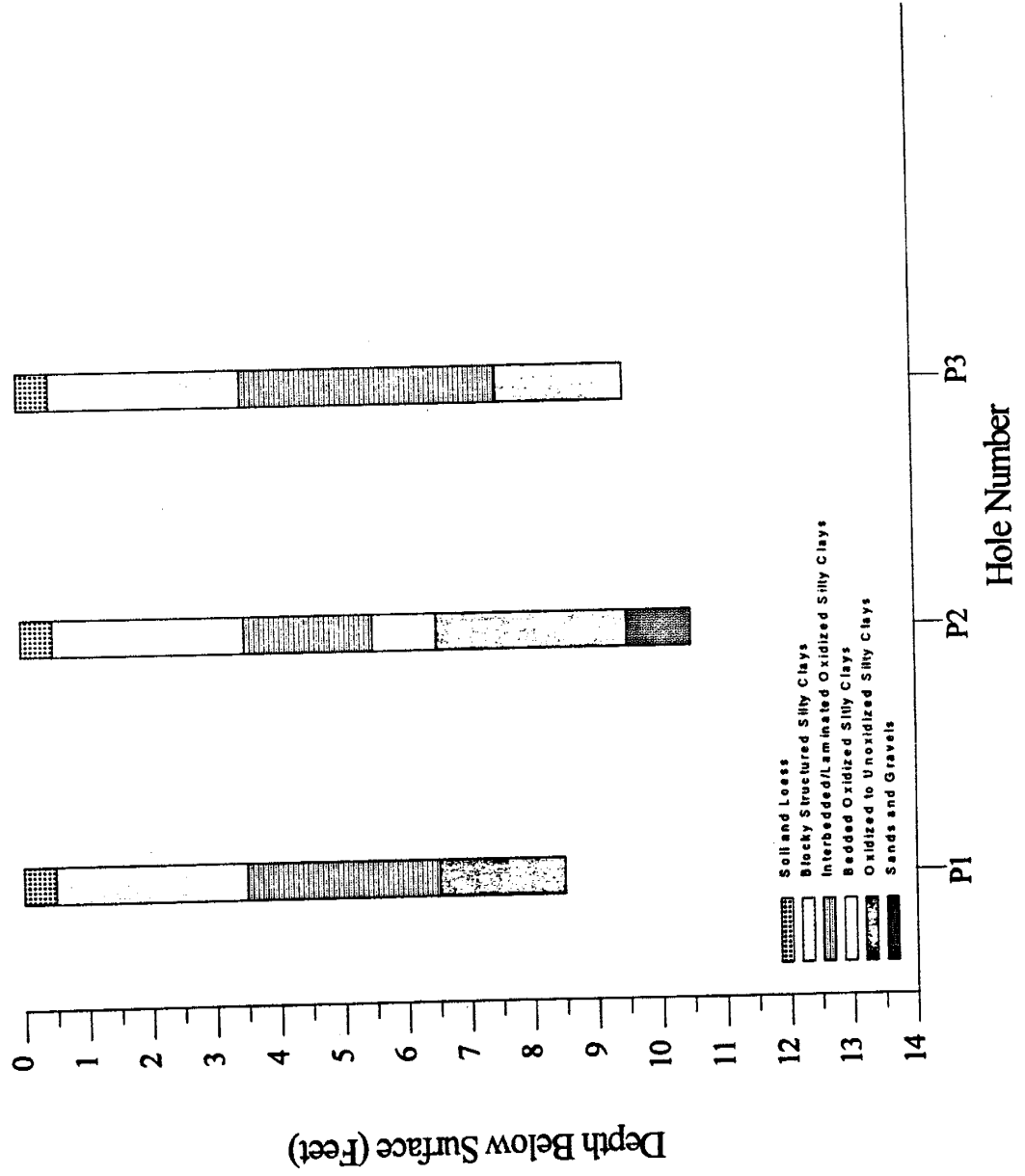
Test Site 2 Outer Ring Cross-section



Test Site 2 Cross-section

Depth / Hole #	TS2-2	TS2-6	TS2-10	TS2-14
1 ft. CS Unit #	1A	1A	1B	1B
Consistency	Soft/Friable	Soft/Friable	Soft/Friable	Soft/Friable
Texture	SC	SC	SC	SC
Color	10YR6/6	10YR5/4	2.5Y5/4	2.5Y5/4
Other Features	Dry, O	Dry, O	Dry, O	Dry, O
2 ft. CS Unit #	2A	2A	2A	2B
Consistency	Soft/Friable	Soft/Friable	Soft/Friable	Soft/Friable
Texture	SC	SC	SC	SC
Color	10YR4/6	10YR4/4	10YR4/4	2.5Y4/4
Other Features	Dmp. Mn	Dmp. Mn	Dmp. Mn	Dmp. Mn
3 ft. CS Unit #	2A	2B	2B	2B
Consistency	S-M S/SLC	Stk-SI Hrd/SI Plastic	Stk-SI Hrd/SI Plastic	Stk-SI Hrd/SI Plastic
Texture	SC	SC	SC	SC
Color	10YR4/4	2.5Y5/4	2.5Y4/4	2.5Y4/4
Other Features	Dmp. Mn	Dmp. Mn	Dmp. Mn	Dmp. Mn
4 ft. CS Unit #	2B	2B	2B	7A
Consistency	S/P	Stk-SI Hrd/SI Plastic	Stk-SI Hrd/SI Plastic	V-SMV Sticky
Texture	SC	SC	SC	SC
Color	2.5Y5/4	2.5Y5/4	2.5Y4/4	2.5Y4/4
Other Features	Dmp. Mn	Dmp. Mn	Dmp. Mn	Sat
5 ft. CS Unit #	7A	2B	7A	3A
Consistency	V-SMV Sticky	Stk-SI Hrd/SI Plastic	V-SMV Sticky	V-SMV Sticky
Texture	SC	SC	SC	SC
Color	2.5Y4/4	2.5Y5/4	2.5Y4/4	2.5Y4/4
Other Features	Sat	Dmp. Mn	Sat	Sat
6 ft. CS Unit #		2B	7A	
Consistency		Stk-SI Hrd/SI Plastic	V-SMV Sticky	
Texture		SC	SC	
Color		2.5Y5/4	2.5Y4/4	
Other Features		Dmp. Mn	Sat	
7 ft. CS Unit #		7A		
Consistency		V-SMV Sticky		
Texture		SC		
Color		2.5Y4/4		
Other Features		Sat		

Preliminary Test Holes



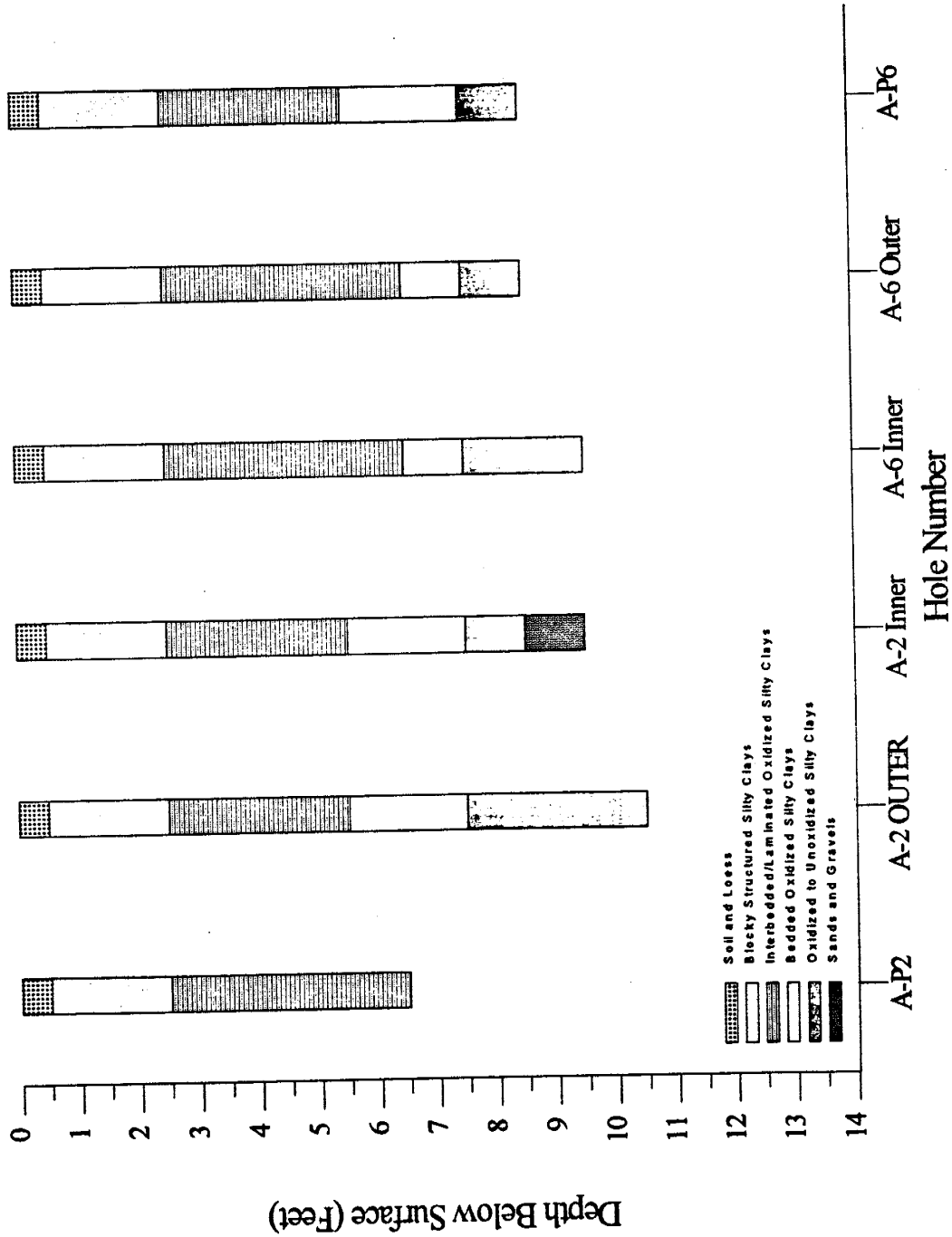
Preliminary Holes

	P1	P2	P5
Depth / Hole #	1B	1B	1A
1 ft. CS Unit #	SoftV Friable	SoftV Friable	SoftV Friable
Consistency	SC	SC	SC
Texture	2.5Y 6/4	2.5Y 6/4	10YR5/8
Color	Dry, O	Dry, O	Dry, O
Other Features			
2 ft. CS Unit #	2B	2A	2A
Consistency	SoftV Friable	SoftV Friable	SoftV Friable
Texture	SC	SC	SC
Color	2.5Y 4/4	10YR4/4	10YR4/6
Other Features	Dmp. Mn	Dmp. Mn	Dmp
3 ft. CS Unit #	2B	2A	2A
Consistency	S-MSLC	Sr-Si Hyd/Si Plastic	Sr-Si Hyd/Si Plastic
Texture	SC	SC	SC
Color	2.5Y 4/4	10YR4/4	10YR4/6
Other Features	Dmp. Mn	Dmp. Mn	Dmp. Mn
4 ft. CS Unit #	2B	2B	2B
Consistency	Sr-Si Hyd/Si Plastic	Sr-Si Hyd/Si Plastic	Sr-Si Hyd/Si Plastic
Texture	SC	SC	SC
Color	2.5Y 5/4	2.5Y 5/4	2.5Y 4/4
Other Features	Dmp	Dmp. Mn	Dmp
5 ft. CS Unit #	3A	3A	3B
Consistency	Sr-Si Hyd/Si Plastic	Sr-Si Hyd/Si Plastic	Sr-Si Hyd/Si Plastic
Texture	SC	SC	SSC
Color	2.5Y 6/4, 6/6	2.5Y 5/4, 7/2	2.5Y 5/4, 2.5Y 7/3
Other Features	Dmp. CaCO3	Dmp. CaCO3	Dmp. CaCO3
6 ft. CS Unit #	3A	3A	3A
Consistency	Sr-Si Hyd/Si Plastic	Sr-Si Hyd/Si Plastic	Sr-Si Hyd/Si Plastic
Texture	SC	SC	SC
Color	2.5Y 6/4, 7/4, 5YR5/4	2.5Y 5/4, 7/2	2.5Y 4/4
Other Features	SP, CaCO3	Dmp. CaCO3	Dmp
7 ft. CS Unit #	3A	4A	3A
Consistency	Sr-Si Hyd/Si Plastic	Sr-Si Hyd/Si Plastic	Sr-Si Hyd/Si Plastic
Texture	SC	SC	SC
Color	2.5Y 5/4	2.5Y 5/4	2.5Y 4/4
Other Features	Mn	Dmp. SP	Dmp
8 ft. CS Unit #	5A	5A	3A
Consistency	Sr-Si Hyd/Si Plastic	Sr-Si Hyd/Si Plastic	Sr-Si Hyd/Si Plastic
Texture	SC	SC	SC
Color	2.5Y 3/6	2.5Y 4/3	2.5Y 4/4
Other Features	Dmp. S P	Dmp. SP	Dmp
9 ft. CS Unit #	5A	5A	5A
Consistency	Sr-Si Hyd/Si Plastic	Sr-Si Hyd/Si Plastic	V SoftV Plastic
Texture	SC	SC	SC
Color	2.5Y 4/2	2.5Y 4/3	2.5Y 4/3
Other Features	Dmp	Dmp. SP, Mn	Dmp. SP
10 ft. CS Unit #		5A	6A
Consistency		Sr-Si Hyd/Si Plastic	Sr-Si Hyd/Si Plastic
Texture		SC	SC
Color		2.5Y 4/4	2.5Y 4/1
Other Features		Dmp	Dmp

Preliminary Holes

Depth / Hole #	P1	P2	P5
11 ft. CS Unit # Consistency Texture Color Other Features		7A Sn-Si Hyd/SI Plastic SC 2.5Y4/1 Dmp	

Clay Site (Site A) Northeast-Southwest Cross-section



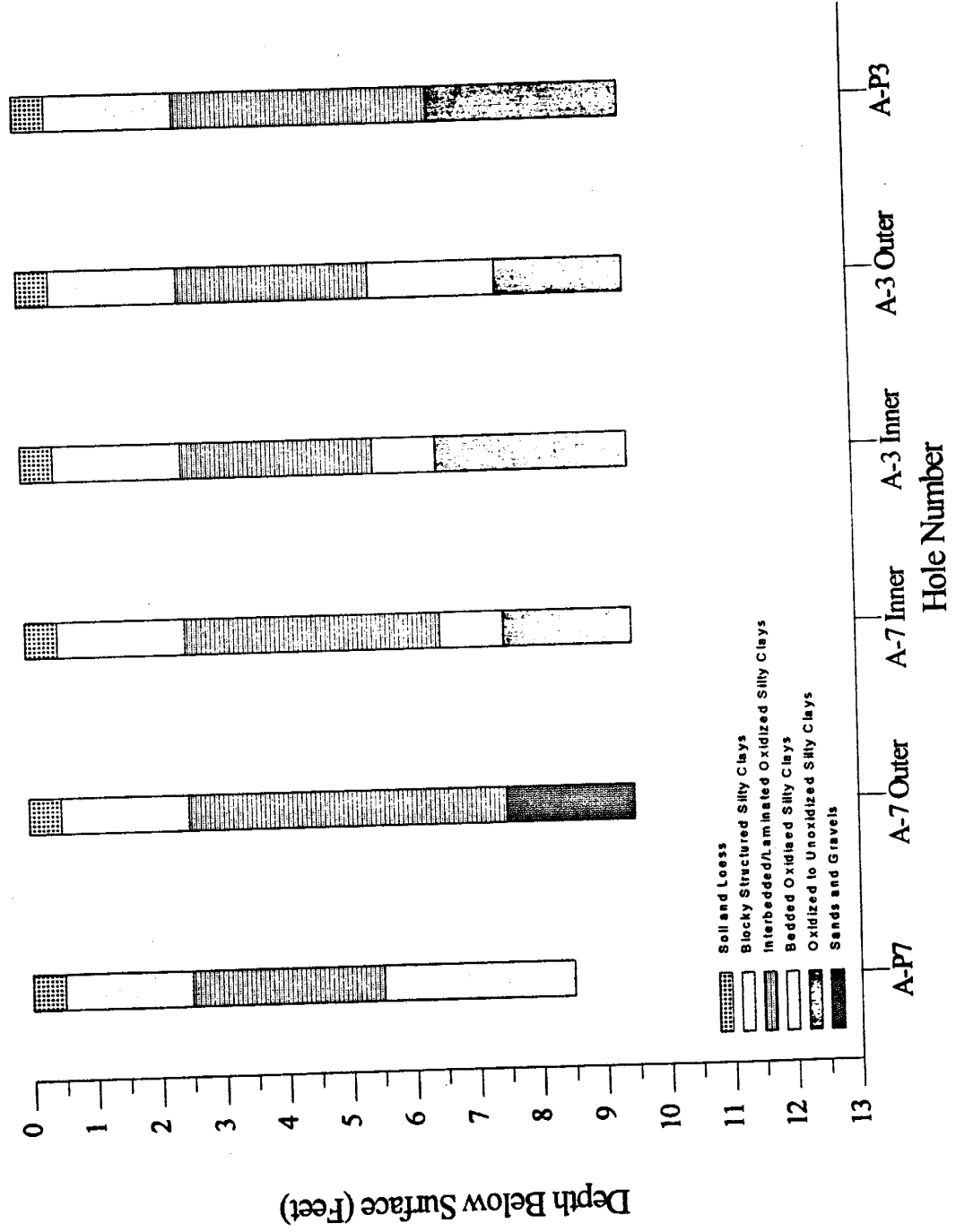
Clay Site Northeast-Southwest Cross-section

Depth/Hole #	A-22	A-2 OUTER	A-2 INNER	A-6 INNER	A-6 OUTER	A-26
1 R. CS Unit #	1A	1A	1A	1A	1A	1A
Consistency	SoB/V Friable	SoB/V Friable	SoB/V Friable	SoB/V Friable	SoB/V Friable	SoB/V Friable
Texture	SC	SC	SC	SC	SC	SC
Color	10YR5/6	10YR5/6	10YR5/6	10YR5/4	10YR6/6	10YR5/6
Other Features	Dry, O	Dry, O	Dry, O	Dry, O	Dry, O	Dry, O
2 R. CS Unit #	2A	2A	2A	2A	2A	2A
Consistency	SR-SI Hid/Plastic	SR-SI Hid/Plastic	SR-SI Hid/Plastic	SR-SI Hid/Plastic	SR-SI Hid/Plastic	SR-SI Hid/Plastic
Texture	SC	SC	SC	SC	SC	SC
Color	10YR4/6	10YR4/6	10YR4/6	10YR4/6	10YR4/6, 4/4	10YR4/6
Other Features	Dmp, O	Dmp, O	Dmp, O	Dmp, Mh, O	Dmp, Mn	Dmp, O
3 R. CS Unit #	2B	2B	2A	2B	2A	2A
Consistency	SR-SI Hid/Plastic	SR-SI Hid/Plastic	SR-SI Hid/Plastic	SR-SI Hid/Plastic	SR-SI Hid/Plastic	SR-SI Hid/Plastic
Texture	SC	SC	SC	SC	SC	SC
Color	2.5Y5/4	2.5Y5/4	2.5Y4/4	2.5Y4/4	10YR4/6	10YR3/6
Other Features	Dmp, Mn	Dmp, O	Dmp, Mn	Dmp, Mn	Dmp, O, Mn	Dmp, CaCO3
4 R. CS Unit #	3A	3A	3A	3A	3A	3A
Consistency	SR-SI Hid/Plastic	SR-SI Hid/Plastic	SoB/V Friable	SR-SI Hid/Plastic	SR-SI Hid/Plastic	SR-SI Hid/Plastic
Texture	SC	SC	SoB/V Friable	SC	SC	SC
Color	2.5Y5/4	2.5Y5/4, 6/4	2.5Y5/4	2.5Y5/4, 7/4	2.5Y5/4, 5/6	2.5Y5/4
Other Features	CxCO3, Dmp, Mn	Dmp, CaCO3	Dmp, O	Dmp, CaCO3	Dmp, CaCO3	Dmp, CaCO3
5 R. CS Unit #	3A	3A	3A	3A	3A	3A
Consistency	SR-SI Hid/Plastic	SR-SI Hid/Plastic	SR-SI Hid/Plastic	SR-SI Hid/Plastic	SR-SI Hid/Plastic	SR-SI Hid/Plastic
Texture	SC	SC	SC	SC	SC	SC
Color	2.5Y5/4	2.5Y5/4, 7/8	2.5Y4/4	2.5Y4/4	2.5Y5/4, 5/6	2.5Y6R, 6/1, 8/1
Other Features	Dmp, CaCO3	Dmp, CaCO3	Dmp	Dmp, Mn	Dmp, SP	Dmp, CaCO3
6 R. CS Unit #	3A	3A	3A	3A	3A	3A
Consistency	SR-SI Hid/Plastic	SR-SI Hid/Plastic	SR-SI Hid/Plastic	SR-SI Hid/Plastic	SR-SI Hid/Plastic	SR-SI Hid/Plastic
Texture	SC	SC	SC	SC	SC	SC
Color	2.5Y5/4, 6/2, 7/2	2.5Y5/6	2.5Y5/4	2.5Y7/3	2.5Y5/4, 3/6, 6/2	2.5Y6/4
Other Features	Dmp, CaCO3	Dmp, CaCO3	Dmp, CaCO3	Dmp, CaCO3	Dmp, CaCO3	Dmp, CaCO3
7 R. CS Unit #	3A	4A	4A	3A	3A	4B
Consistency	SR-SI Hid/Plastic	SR-SI Hid/Plastic	SR-SI Hid/Plastic	SR-SI Hid/Plastic	SR-SI Hid/Plastic	V SoB/V Sticky
Texture	SC	SC	SC	SC	SC	SC, C
Color	2.5Y5/4, 7/2	2.5Y5/4, 5YR5/8	2.5Y5/4	2.5Y5/4	2.5Y5/4	2.5Y5/4
Other Features	Dmp, CaCO3	Dmp, SP, Mn	Dmp, SP, Mn	Dmp, CaCO3, Mn	Dmp, CaCO3	Sh, SP, Mn
8 R. CS Unit #	4A	4A	4A	4A	4A	4A
Consistency	SR-SI Hid/Plastic	SR-SI Hid/Plastic	SR-SI Hid/Plastic	SR-SI Hid/Plastic	SR-SI Hid/Plastic	SR-SI Hid/Plastic
Texture	SC	SC	SC	SC	SC	SC
Color	2.5Y5/4	2.5Y 3/4	2.5Y5/4	2.5Y5/4	2.5Y5/4, 5YR4/6	2.5Y5/4
Other Features	Dmp, Mn	Dmp, Mn	Dmp	Dmp, SP	Dmp, SP	Dmp, SP, Mn
9 R. CS Unit #	5A	5A	5A	5A	5A	5A
Consistency	SR-SI Hid/Plastic	SR-SI Hid/Plastic	SR-SI Hid/Plastic	SR-SI Hid/Plastic	SR-SI Hid/Plastic	SR-SI Hid/Plastic
Texture	SC	SC	SC	SC	SC	SC
Color	2.5Y4/4, 5YR4/6	2.5Y5/2	2.5Y5/2	2.5Y4/3	2.5Y4/3	2.5Y4/3
Other Features	Dmp, SP, Mn	Dmp, SP	Dmp, SP	Dmp, SP, Mn	Dmp	Dmp, SP, Mn
10 R. CS Unit #	6B	6B	6D	6A	6A	6A
Consistency	SR-SI Hid/Plastic	SR-SI Hid/Plastic	V SoB/V Sticky	SR-SI Hid/Plastic	SR-SI Hid/Plastic	SR-SI Hid/Plastic
Texture	SC, S	SC, S, P, G	SC, S, P, G	SC	SC	SC
Color	2.5Y4/1, 5, 5YR3/4	2.5Y4/4	2.5Y4/4	2.5Y4/2	2.5Y4/2	2.5Y4/4
Other Features	Dmp	Dmp	Sat	Dmp	Dmp	Dmp

Clay Site Northeast-Southwest Cross-section

Depth / Hole #	A-P2	A-2 OUTER	A-3 INNER	A-6 INNER	A-6 OUTER	A-P6
11 R. CS Unit # Consistency Texture Color Other Features		SB SRS-51 Hyd/Plastic S.C. 5 2.5YR/2.5YR/4/4 Dmp				

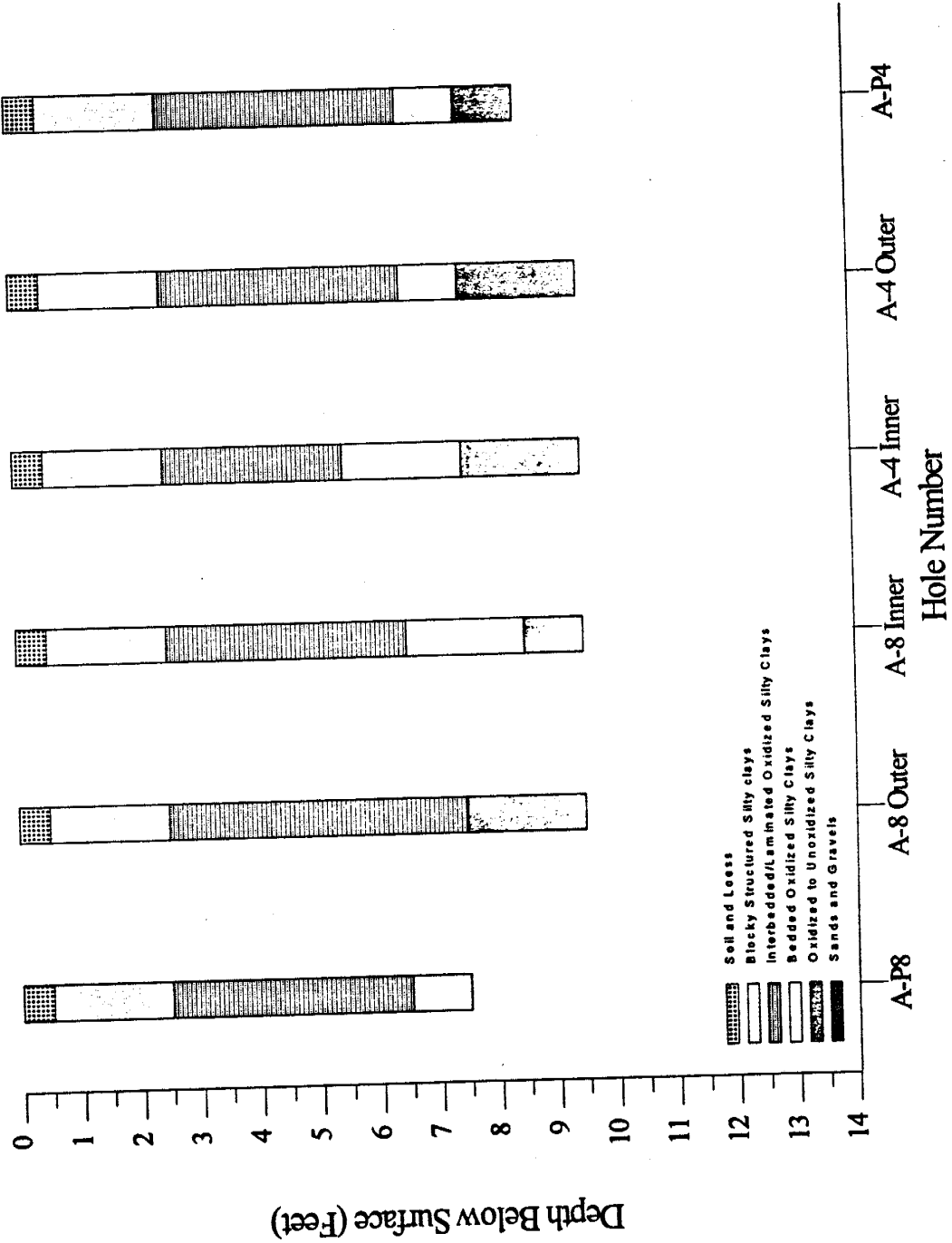
Clay Site (Site A) East-West Cross-section



Clay Site East-West Cross-section

Depth / Hole #	A-P7	A7 OUTER	A7 INNER	A3 INNER	A3 OUTER	A-P3
1 R. CS Unit #	1A	1A	1A	1A	1A	1A
Consistency	So/VP Friable	So/VP Friable	So/VP Friable	So/VP Friable	So/VP Friable	So/VP Friable
Texture	SC	SC	SC	SC	SC	SC
Color	10YR5/6	10YR5/6	10YR5/6	10YR5/6	10YR5/6	10YR5/6
Other Features	Dry, O	Dry, O	Dry, O	Dry, O	Dry, O	Dry, O
2 R. CS Unit #	2A	2A	2A	2A	2A	2A
Consistency	WCRB	Sr-SI Hrd/Plastic	Sr-SI Hrd/Plastic	Sr-SI Hrd/Plastic	Sr-SI Hrd/Plastic	Sr-SI Hrd/Plastic
Texture	SC	SC	SC	SC	SC	SC
Color	10YR4/6	10YR4/6	10YR4/6	10YR4/6	10YR4/6 4A	10YR4/6
Other Features	Sat, Mn	Dmp, O	Dmp, O, Mn	Dmp, O	Dmp	Dmp
3 R. CS Unit #	3A	3A	3A	3A	3A	3A
Consistency	Sr-SI Hrd/Plastic	Sr-SI Hrd/Plastic	Sr-SI Hrd/Plastic	Sr-SI Hrd/Plastic	Sr-SI Hrd/Plastic	Sr-SI Hrd/Plastic
Texture	SC	SC	SC	SC	SC	SC
Color	10YR 3/4	10YR4/4	10YR4/4	10YR5/6	10YR3/6	2.5Y5/4
Other Features	Dmp, O, Mn	Dmp, O, Mn	Dmp, O, Mn	Sat	Dmp	Dmp, O
4 R. CS Unit #	4A	4A	4A	4A	4A	4A
Consistency	Sr-SI Hrd/Plastic	Sr-SI Hrd/Plastic	Sr-SI Hrd/Plastic	Sr-SI Hrd/Plastic	Sr-SI Hrd/Plastic	Sr-SI Hrd/Plastic
Texture	SC	SC	SC	SC	SC	SC
Color	2.5Y5/4	10YR4/6	2.5Y5/4, 7/4	2.5Y5/4, 7/3	2.5Y5/4, 7/4	2.5Y5/4
Other Features	Dmp	Dmp, CaCO3, Mn	Dmp, CaCO3	Dmp, CaCO3	Dmp, CaCO3	Dmp, CaCO3
5 R. CS Unit #	5A	5A	5A	5A	5A	5A
Consistency	Sr-SI Hrd/Plastic	Sr-SI Hrd/Plastic	Sr-SI Hrd/Plastic	Sr-SI Hrd/Plastic	Sr-SI Hrd/Plastic	Sr-SI Hrd/Plastic
Texture	SC	SC	SC	SC	SC	SC
Color	2.5Y5/4, 7/3	2.5Y5/4, 7/4	2.5Y5/4	2.5Y5/4, 7/4	2.5Y4/4, 8/3	2.5Y5/4, 6/2
Other Features	Dmp, CaCO3	Dmp	Dmp	Dmp, CaCO3	Dmp, CaCO3	Dmp, CaCO3, Mn
6 R. CS Unit #	6A	6A	6A	6A	6A	6A
Consistency	Sr-SI Hrd/Plastic	Sr-SI Hrd/Plastic	Sr-SI Hrd/Plastic	Sr-SI Hrd/Plastic	Sr-SI Hrd/Plastic	Sr-SI Hrd/Plastic
Texture	SC	SC	SC	SC	SC	SC
Color	2.5Y5/4	2.5Y5/4, 8/3	2.5Y5/4	2.5Y5/4	2.5Y5/4	2.5Y5/4, 7/3
Other Features	Dmp, CaCO3	Dmp, CaCO3	Dmp	Dmp	Dmp	Sat
7 R. CS Unit #	7A	7A	7A	7A	7A	7A
Consistency	Sr-SI Hrd/Plastic	Sr-SI Hrd/Plastic	Sr-SI Hrd/Plastic	Sr-SI Hrd/Plastic	Sr-SI Hrd/Plastic	Sr-SI Hrd/Plastic
Texture	SC, S	SC	SC	SC	SC	SC
Color	2.5Y5/4	2.5Y5/4	2.5Y5/4, 5YR6/8	2.5Y5/4	2.5Y5/4	2.5Y5/4
Other Features	Sat	Dmp	Dmp, SP, Mn	Dmp, Mn	Dmp, SP, Mn	Dmp, CaCO3
8 R. CS Unit #	8A	8A	8A	8A	8A	8A
Consistency	Sr-SI Hrd/Plastic	Sr-SI Hrd/Plastic	Sr-SI Hrd/Plastic	Sr-SI Hrd/Plastic	Sr-SI Hrd/Plastic	Sr-SI Hrd/Plastic
Texture	SC, S	SC	SC	SC	SC	SC
Color	2.5Y5/4	2.5Y5/4	2.5Y5/4, 5YR5/6	2.5Y5/3	2.5Y5/3, 5YR5/8	2.5YR5/2
Other Features	Dmp	Dmp	Dmp, SP, Mn	Dmp, SP	Dmp, SP	Dmp, SP
9 R. CS Unit #	9A	9A	9A	9A	9A	9A
Consistency	Sr-SI Hrd/Plastic	Sr-SI Hrd/Plastic	Sr-SI Hrd/Plastic	Sr-SI Hrd/Plastic	Sr-SI Hrd/Plastic	Sr-SI Hrd/Plastic
Texture	SC, S, P	SC, S	SC, S	SC	SC	SC
Color	2.5Y5/4	2.5Y5/4	2.5Y4/2	2.5Y5/2	2.5Y4/3	2.5YR4/2
Other Features	Sat	Sat	Dmp, SP	Dmp, SP	Dmp, SP	Dmp, SP, Mn
10 R. CS Unit #	10A	10A	10A	10A	10A	10A
Consistency	Sr-SI Hrd/Plastic	Sr-SI Hrd/Plastic	Sr-SI Hrd/Plastic	Sr-SI Hrd/Plastic	Sr-SI Hrd/Plastic	Sr-SI Hrd/Plastic
Texture	SC, S	SC, S	SC, S	SC	SC	SC
Color	2.5Y3/1	2.5Y5/2	2.5Y5/2	2.5Y5/1, 5/2	2.5Y4/2, 4/3	2.5Y4/2, 5YR3/4
Other Features	Dmp	Sat	Dmp	Dmp	Dmp	Dmp

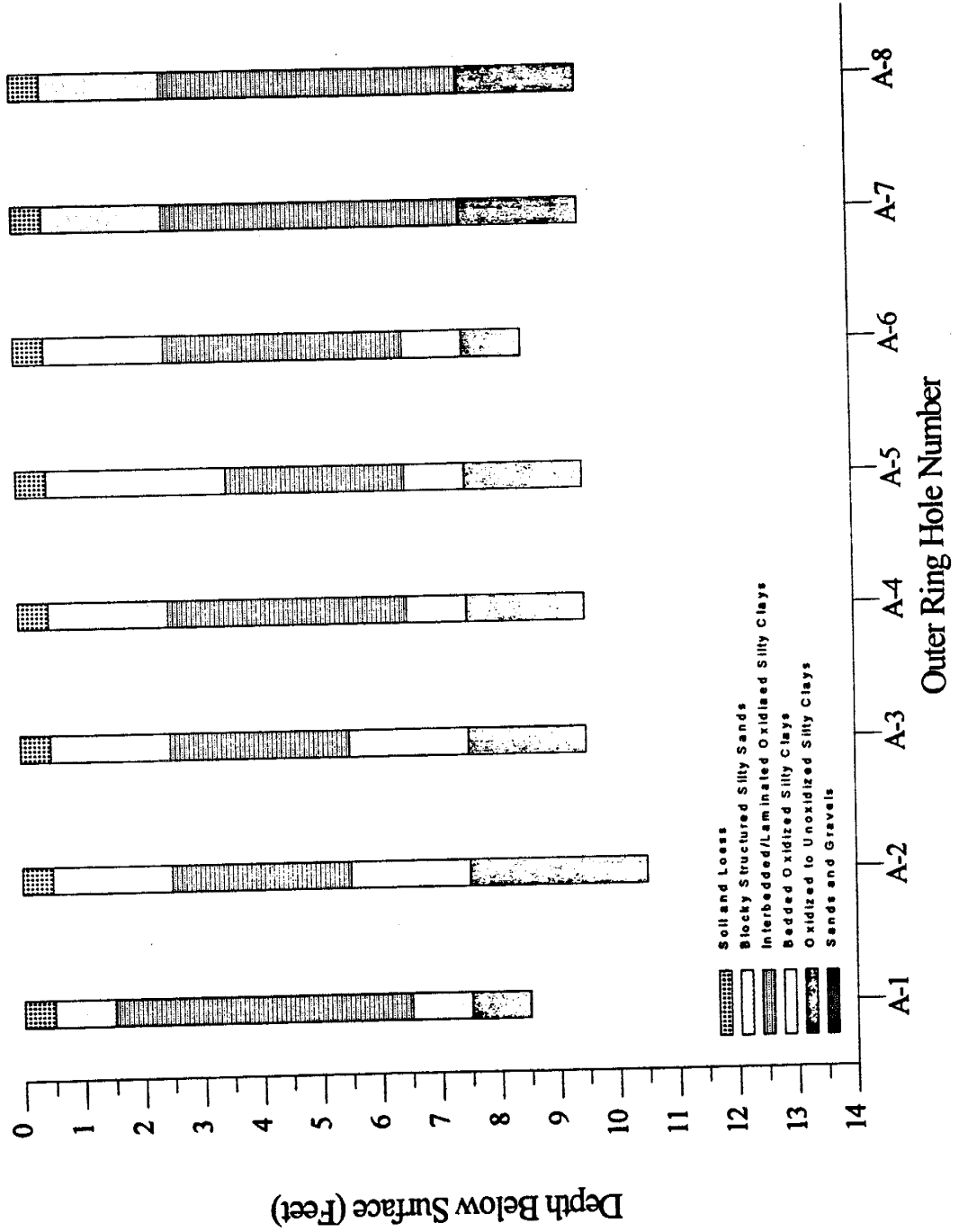
Clay Site (Site A) Northwest-Southeast Cross-section



Clay Site Northwest-Southeast Cross-section

Depth / Hole #	A-P8	A-8 OUTER	A-8 INNER	A-4 INNER	A-4 OUTER	A-P4
1 R. CS Unit #	1A	1A	1A	1A	1A	1A
Consistency	Soft/V Friable	Soft/V Friable	Soft/V Friable	Soft/V Friable	Soft/V Friable	Soft/V Friable
Texture	SC	SC	SC	SC	SC	SC
Color	10YR5/6	10YR5/8	10YR5/6	10YR5/6	10YR4/6	10YR5/6
Other Features	Dry, O	Dry, O	Dry, O	Dry, O	Dry, O	Dry, O
2 R. CS Unit #	2A	2A	2A	2A	2A	2A
Consistency	SR-SI Hrd/Plastic	SR-SI Hrd/Plastic	SR-SI Hrd/Plastic	SR-SI Hrd/Plastic	SR-SI Hrd/Plastic	SR-SI Hrd/Plastic
Texture	SC	SC	SC	SC	SC	SC
Color	10YR4/6	10YR5/4	10YR4/6	10YR4/4	10YR4/6	10YR4/6
Other Features	Sat, Mn	Dmp, Mn	Dmp, Mn	Dmp, Mn	Dmp	Dmp, O
3 R. CS Unit #	3A	3A	3A	3A	3A	3A
Consistency	SR-SI Hrd/Plastic	SR-SI Hrd/Plastic	SR-SI Hrd/Plastic	SR-SI Hrd/Plastic	SR-SI Hrd/Plastic	SR-SI Hrd/Plastic
Texture	SC	SC	SC	SC	SC	SC
Color	10YR3/6	10YR5/4	10YR5/4	2.5Y4/4	2.5Y4/4	10YR3/6
Other Features	Dmp, Mn	Dmp, Mn	Dmp, O	Dmp	Dmp	Dmp, O
4 R. CS Unit #	4A	4A	4A	4A	4A	4A
Consistency	SR-SI Hrd/Plastic	SR-SI Hrd/Plastic	SR-SI Hrd/Plastic	SR-SI Hrd/Plastic	SR-SI Hrd/Plastic	SR-SI Hrd/Plastic
Texture	SC	SC	SC	SC	SC	SC
Color	2.5Y5/4, 6/2	2.5Y5/4	2.5Y5/4	2.5Y5/4	2.5Y5/4	2.5Y5/4, 6/1
Other Features	Dmp, CaCO3	Dmp, CaCO3	Dmp, CaCO3	Dmp, CaCO3	Dmp, CaCO3	Dmp, CaCO3
5 R. CS Unit #	5A	5A	5A	5A	5A	5A
Consistency	SR-SI Hrd/Plastic	SR-SI Hrd/Plastic	SR-SI Hrd/Plastic	SR-SI Hrd/Plastic	SR-SI Hrd/Plastic	SR-SI Hrd/Plastic
Texture	SC	SC	SC	SC	SC	SC
Color	2.5Y5/4, 5/2	2.5Y5/4	2.5Y5/4, 6/2, 7/4	2.5Y5/4	2.5Y5/4, 7/2, 7/4	2.5Y5/4, 5/4
Other Features	Dmp, CaCO3	Dmp, CaCO3	Dmp, CaCO3	Dmp	Dmp, CaCO3	Dmp
6 R. CS Unit #	6A	6A	6A	6A	6A	6A
Consistency	SR-SI Hrd/Plastic	SR-SI Hrd/Plastic	SR-SI Hrd/Plastic	SR-SI Hrd/Plastic	SR-SI Hrd/Plastic	SR-SI Hrd/Plastic
Texture	SC	SC	SC	SC	SC	SC
Color	7.5YR5/6, 2.5Y5/4	2.5Y5/4	2.5Y5/4	2.5Y5/4	2.5Y6/4	2.5Y5/6, 6/2
Other Features	Dmp, CaCO3, Mn	Dmp, SP, Mn	Dmp, CaCO3	Dmp, CaCO3	Sat, CaCO3	Dmp, CaCO3, SP, Mn
7 R. CS Unit #	7A	7A	7A	7A	7A	7A
Consistency	SR-SI Hrd/Plastic	V SD/Plastic	SR-SI Hrd/Plastic	SR-SI Hrd/Plastic	SR-SI Hrd/Plastic	V SD/Plastic
Texture	SC	SC	SC	SC	SC	SC
Color	2.5Y4/4	2.5Y4/4	2.5Y4/4	2.5Y4/4	2.5Y4/4	2.5Y3/4, 5YR3/4
Other Features	Dmp, CaCO3, SP, Mn	Dmp	Dmp, SP, Mn	Dmp, SP, Mn	Dmp	Dmp, SP
8 R. CS Unit #	8A	8A	8A	8A	8A	8A
Consistency	SR-SI Hrd/Plastic	SR-SI Hrd/Plastic	SR-SI Hrd/Plastic	SR-SI Hrd/Plastic	SR-SI Hrd/Plastic	SR-SI Hrd/Plastic
Texture	SC, S, P	SC	SC	SC	SC	SC
Color	10YR5/6	2.5Y4/4	5YR5/8	2.5Y5/4	2.5Y5/4	2.5Y4/4
Other Features	Dmp	Dmp	Dmp, SP, Mn	Dmp, SP, Mn	Dmp	Dmp, SP, Mn
9 R. CS Unit #	9A	9A	9A	9A	9A	9A
Consistency	SR-SI Hrd/Plastic	SR-SI Hrd/Plastic	SR-SI Hrd/Plastic	SR-SI Hrd/Plastic	SR-SI Hrd/Plastic	SR-SI Hrd/Plastic
Texture	SC, S, P, G	SC, S, P	SC, S, P, G	SC	SC	C
Color	2.5Y4/3	2.5Y4/3	2.5Y4/4	2.5Y5/3	2.5Y5/3	2.5Y4/3, 4/2
Other Features	Dmp	Dmp, SP	Dmp, SP	Dmp	Dmp	Dmp, SP, Mn
10 R. CS Unit #	10A	10A	10A	10A	10A	10A
Consistency	SR-SI Hrd/Plastic	SR-SI Hrd/Plastic	SR-SI Hrd/Plastic	SR-SI Hrd/Plastic	SR-SI Hrd/Plastic	SR-SI Hrd/Plastic
Texture	SC	S, SC	SC	SC	SC	SC
Color	2.5Y4/2	2.5Y4/3	2.5Y4/3	2.5Y5/2	2.5Y4/3	2.5Y4/3
Other Features	Dmp, SP, Mn	Dmp	Dmp	Dmp	Dmp	Dmp

Clay Site (Site A) Outer Ring Cross-section



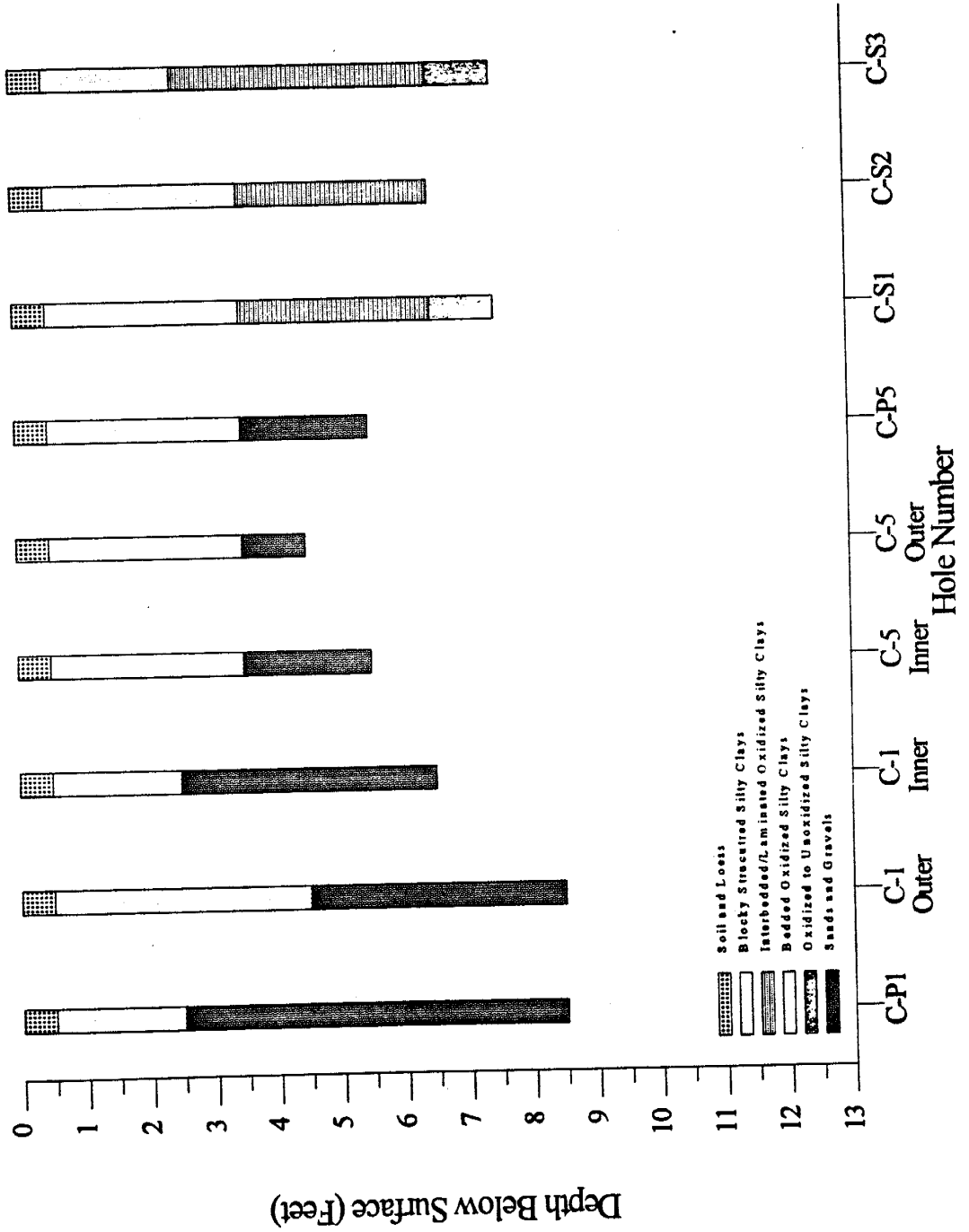
Clay Site Outer Ring Cross-section

Depth / Hole #	A-1 OUTER	A-2 OUTER	A-3 OUTER	A-4 OUTER	A-5 OUTER	A-6 OUTER	A-7 OUTER	A-8 OUTER
11 ft. CS Unit # Consistency Texture Color Other Features		6B SAS1 Hd/Plastic SC. 5 D.5Y4/2.5YR4/4 Dmp						

Clay Site Inner Ring Cross-section

Depth / Hole #	A-1 INNER	A-2 INNER	A-3 INNER	A-4 INNER	A-5 INNER	A-6 INNER	A-7 INNER	A-8 INNER
1 R. CS Unit #	1A	1A	1A	1A	1A	1A	1A	1A
Consistency	So/VP Friable	So/VP Friable	So/VP Friable	So/VP Friable	So/VP Friable	So/VP Friable	So/VP Friable	So/VP Friable
Texture	SC	SC	SC	SC	SC	SC	SL	SC
Color	10YR5/6	10YR5/6	10YR5/6	10YR5/6	10YR4/6	10YR5/4	10YR5/6	10YR5/8
Other Features	Dry, O	Dry, O	Dry, O	Dry, O	Dry, O	Dry, O	Dry, O	Dry, O
2 R. CS Unit #	2A	2A	2A	2A	2A	2A	2A	2A
Consistency	So/VP Friable	So/VP Friable	SR-SI Hid/Plastic	SR-SI Hid/Plastic	So/VP Friable	SR-SI Hid/Plastic	SR-SI Hid/Plastic	SR-SI Hid/Plastic
Texture	SC	SC	SC	SC	SC	SC	SC	SC
Color	10YR4/6	10YR4/6	10YR4/6	10YR4/4	10YR4/6	10YR4/6	10YR4/6	10YR4/6
Other Features	Dmp, O	Dmp, O	Dmp, O	Dmp, Mn	Dmp, CaCO3	Dmp, O, Mn	Dmp, O, Mn	Dmp, O
3 R. CS Unit #	2B	2A	2A	2B	2B	2B	2A	2B
Consistency	SR-SI Hid/Plastic	SR-SI Hid/Plastic	SR-SI Hid/Plastic	SR-SI Hid/Plastic	SR-SI Hid/Plastic	SR-SI Hid/Plastic	SR-SI Hid/Plastic	SR-SI Hid/Plastic
Texture	SC	SC	SC	SC	SC	SC	SC	SC
Color	2.5Y4/4	10YR4/6	10YR5/6	2.5Y4/4	2.5Y4/4	2.5Y4/4	10YR4/4	2.5Y5/4
Other Features	Dmp, Mn	Dmp, O	Sat	Dmp	Dmp, O	Dmp, Mn	Dmp, O, Mn	Dmp, O
4 R. CS Unit #	3A	3A	3A	3A	3A	3A	3A	3A
Consistency	SR-SI Hid/Plastic	So/VP Friable	SR-SI Hid/Plastic	SR-SI Hid/Plastic	SR-SI Hid/Plastic	SR-SI Hid/Plastic	SR-SI Hid/Plastic	SR-SI Hid/Plastic
Texture	SC	SC	SC	SC	SC	SC	SC	SC
Color	2.5Y5/4 6A	2.5Y5/4	2.5Y4/4, 7/3	2.5Y5/4	2.5Y5/4	2.5Y5/4, 7/4	2.5Y4/4, 7/4	2.5Y5/4
Other Features	Dmp, CaCO3	Dmp, O, CaCO3	Dmp, CaCO3	Dmp, CaCO3	Dmp, CaCO3	Dmp, CaCO3	Dmp, CaCO3	Dmp, CaCO3
5 R. CS Unit #	3A	3A	3A	3A	3A	3A	3A	3A
Consistency	SR-SI Hid/Plastic	SR-SI Hid/Plastic	SR-SI Hid/Plastic	SR-SI Hid/Plastic	SR-SI Hid/Plastic	SR-SI Hid/Plastic	SR-SI Hid/Plastic	SR-SI Hid/Plastic
Texture	SC	SC	SC	SC	SC	SC	SC	SC
Color	2.5Y5/4	2.5Y4/4	2.5Y5/4 7/4	2.5Y5/4	2.5Y5/4	2.5Y4/4	2.5Y5/4	2.5Y4/4, 6Z, 7/4
Other Features	Dmp, Mn, CaCO3	Dmp, CaCO3	Dmp, CaCO3	Dmp	Dmp, Mn	Dmp, Mn	Dmp, O	Dmp, CaCO3
6 R. CS Unit #	3A	3A	3A	3A	3A	3A	3A	3A
Consistency	SR-SI Hid/Plastic	SR-SI Hid/Plastic	SR-SI Hid/Plastic	SR-SI Hid/Plastic	SR-SI Hid/Plastic	SR-SI Hid/Plastic	SR-SI Hid/Plastic	SR-SI Hid/Plastic
Texture	SC	SC	SC	SC	SC	SC	SC	SC
Color	2.5Y5/4	2.5Y5/4	2.5Y5/4	2.5Y5/4	2.5Y5/4	2.5Y7/3	2.5Y5/4	2.5Y5/4
Other Features	Dmp, CaCO3	Dmp, CaCO3	Sat	Dmp, CaCO3	Dmp	Dmp, CaCO3	Dmp	Sat, CaCO3
7 R. CS Unit #	4B	4A	4A	4A	4A	4A	4A	4A
Consistency	V SR/Sticky	SR-SI Hid/Plastic	SR-SI Hid/Plastic	SR-SI Hid/Plastic	SR-SI Hid/Plastic	SR-SI Hid/Plastic	SR-SI Hid/Plastic	V SR/Plastic
Texture	SC, S	SC	SC	SC	SC	SC	SC	SC
Color	2.5Y5/4	2.5Y5/4	2.5Y5/4	2.5Y4/4	2.5Y5/4	2.5Y5/4	2.5Y5/4, 5YR6/8	2.5Y5/4
Other Features	Dmp, SP	Dmp, SP, Mn	Dmp, Mn	Dmp, SP, Mn	Dmp	Dmp, Mn, CaCO3	Dmp, SP, Mn	Dmp, SP, Mn
8 R. CS Unit #	4A	4A	4A	4A	4A	4A	4A	4A
Consistency	SR-SI Hid/Plastic	SR-SI Hid/Plastic	SR-SI Hid/Plastic	SR-SI Hid/Plastic	SR-SI Hid/Plastic	SR-SI Hid/Plastic	SR-SI Hid/Plastic	SR-SI Hid/Plastic
Texture	SC	SC	SC	SC	SC	SC	SC	SC
Color	2.5Y5/3	2.5Y5/4	2.5Y5/3	2.5Y5/4	2.5Y5/4	2.5Y5/4	2.5Y5/4, 5YR5/6	5YR5/8
Other Features	Dmp, SP	Dmp, SP	Dmp, SP	Dmp, SP, Mn	Dmp	Dmp, SP	Dmp, SP, Mn	Dmp, SP, Mn
9 R. CS Unit #	5A	5A	5A	5A	5A	5A	5B	4B
Consistency	SR-SI Hid/Plastic	SR-SI Hid/Plastic	V So/VP Plastic	SR-SI Hid/Plastic	SR-SI Hid/Plastic	SR-SI Hid/Plastic	SR-SI Hid/Plastic	SR-SI Hid/Plastic
Texture	SC	SC	SC	SC	SC	SC	S	SD, S, P, G
Color	2.5Y5/2	2.5Y5/2	2.5Y5/2	2.5Y5/3	2.5Y5/3	2.5Y4/3	2.5Y4/2	2.5Y4/4
Other Features	Dmp, SP	Dmp, SP	Dmp, SP	Dmp	Dmp, SP	Dmp, SP, Mn	Dmp, SP	Dmp
10 R. CS Unit #	6B	6D	5A	6A	5A	6A	5A	6B
Consistency	SR-SI Hid/Plastic	V SR/Sticky	SR-SI Hid/Plastic	SR-SI Hid/Plastic	SR-SI Hid/Plastic	SR-SI Hid/Plastic	SR-SI Hid/Plastic	SR-SI Hid/Plastic
Texture	SC, P	SC, S, P, G	SC	SC	SC	SC	SC	S, SC
Color	2.5Y5/1	2.5Y4/4	2.5Y5/1, 5/2	2.5Y5/2	2.5Y5/2	2.5Y5/2	2.5Y5/2	2.5Y4/3
Other Features	Dmp	Dmp	Dmp	Dmp, SP	Dmp	Dmp	Dmp	Dmp

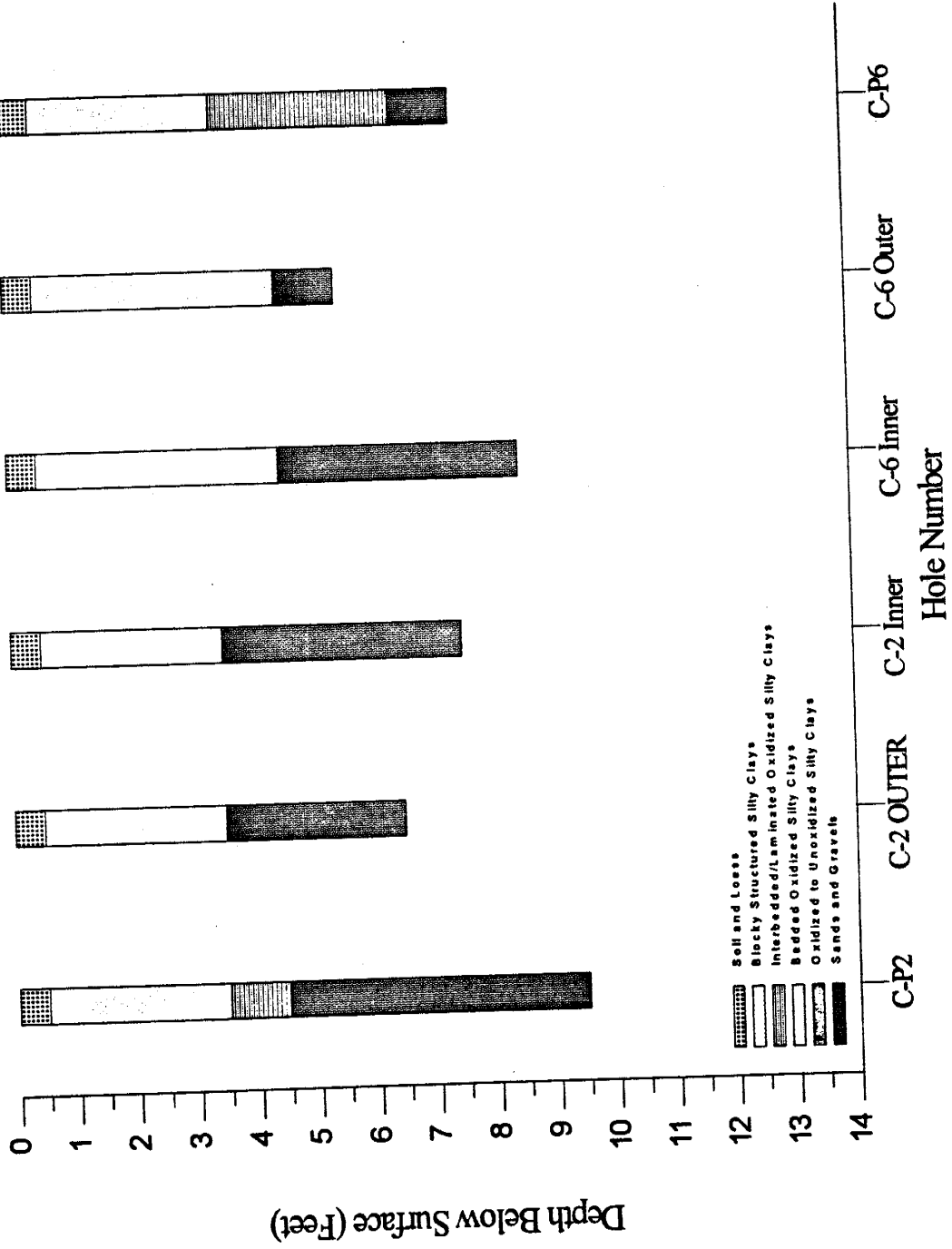
Sand Site (Site C) North South Cross-section



Sand Site North-South Cross Cross-section

Depth / Hole #	C-P1	C-1 OUTER	C-1 INNER	C-5 INNER	C-5 OUTER	C-PS	C-S1	C-S1	C-S1	C-S1
1 R. CS Unit #	IB	IB	IB	IB	IB	IB	IA	IB	IB	IB
Consistency	SoBV Friable	SoBV Friable	SoBV Friable	SoBV Friable	SoBV Friable	SoBV Friable	SoBV Friable	SoBV Friable	SoBV Friable	SoBV Friable
Texture	SC	SC	SC	SC	SC	SC	SC	SC	SC	SC
Color	2.5Y7/4	2.5Y6/3	2.5Y5/2	2.5Y5/2	2.5Y6/3	2.5Y6/4	10YR6/6	2.5Y7/4	2.5Y7/4	2.5Y7/4
Other Features	Dry, O	Dry, O	Dry, O	Dry, O	Dry, O	Dry, O	Dry, O	Dry, O	Dry, O	Dry, O
2 R. CS Unit #	2A	2B	2B	2A	2A	2A	2A	2A	2A	2A
Consistency	SR-SI Hrd/Plastic	SR-SI Hrd/Plastic	SR-SI Hrd/Plastic	SR-SI Hrd/Plastic	SR-SI Hrd/Plastic	SR-SI Hrd/Plastic	SR-SI Hrd/Plastic	SR-SI Hrd/Plastic	SR-SI Hrd/Plastic	SR-SI Hrd/Plastic
Texture	SC	SC	SC	SC	SC	SC	SC	SC	SC	SC
Color	10YR4/6	2.5Y5/6	2.5YR4/6	10YR4/6	10YR5/6, 2.5Y4/3	10YR5/6	10YR4/4	10YR4/6	10YR4/6	10YR4/6
Other Features	Dmp, Mn	Dmp, O, Mn	Dmp, O	Dmp, O	Dmp	Dmp	Dmp, Mn, CaCO3	Dmp	Dmp	Dmp
3 R. CS Unit #	2B	2B	2B	2B	2A	2A	2A	2A	2A	2A
Consistency	SR-SI Hrd/Plastic	SR-SI Hrd/Plastic	SR-SI Hrd/Plastic	SR-SI Hrd/Plastic	SR-SI Hrd/Plastic	SR-SI Hrd/Plastic	SR-SI Hrd/Plastic	SR-SI Hrd/Plastic	SR-SI Hrd/Plastic	SR-SI Hrd/Plastic
Texture	SC	SC	SC	SC	SC	SC	SC	SC	SC	SC
Color	2.5Y4/6	2.5Y4/4	2.5Y4/3, 7.5YR5/6	2.5Y4/4, 7.5YR5/8	10YR5/8, 5/6	10YR5/8, 2.5Y5/6	10YR4/4	10YR4/6	10YR4/6	10YR4/6
Other Features	Dmp, O, Mn	Dmp, Mn	Dmp, O, Mn	Dmp	Dmp	Dmp	Dmp	Dmp	Dmp	Dmp, CaCO3
4 R. CS Unit #	7B	2B	7B	2B	2A	2B	2B	2B	2B	2B
Consistency	V SBV Sticky	SR-SI Hrd/Plastic	SR-SI Hrd/Plastic	SR-SI Hrd/Plastic	SR-SI Hrd/Plastic	SR-SI Hrd/Plastic	SR-SI Hrd/Plastic	SR-SI Hrd/Plastic	SR-SI Hrd/Plastic	SR-SI Hrd/Plastic
Texture	SC, S	SC	SC, S	SC	SC	SC	S, CS	S, SC	S, SC	S, SC
Color	2.5Y5/6	2.5Y4/4	2.5Y5/4	2.5Y4/2, 7.5YR5/8	2.5YR4/3, 10YR5/6	2.5Y4/3, 10YR4/3	2.5Y5/4	2.5Y 4/6	2.5Y 4/4	2.5Y 4/4
Other Features	Sat, Mn	Sat, Mn	Sat	Dmp, Mn	Dmp	Dmp	Dmp	Dmp	Dmp	Dmp
5 R. CS Unit #	7B	2B	7A	7B	8D	7C	7B	3A	3B	3B
Consistency	V SBV Sticky	SR-SI Hrd/Plastic	NA/Soupy	V SBV Sticky	NA/Soupy	SR-SI Hrd/Plastic	SR-SI Hrd/Plastic	SR-SI Hrd/Plastic	SR-SI Hrd/Plastic	SR-SI Hrd/Plastic
Texture	SC, S	SC	SC, S	SC, S	SH, S, P, G	SC, S, P	S, P, G, SC	S, SC, P, G	S, SC, P, G	S, SC, P, G
Color	2.5Y4/4	2.5Y5/5	2.5Y4/4	7.5YR5/8	2.5Y5/4	2.5Y5/4	2.5Y4/4	2.5Y4/4	2.5Y4/4	2.5Y4/4
Other Features	Sat	Dmp	Sat	Sat	Sat	Sat	Dmp	Dmp	Dmp	Dmp
6 R. CS Unit #	7C	7B	8A	7D	8A	8A	8A	3B	3B	3B
Consistency	SR-SI Hrd/Plastic	V SBV Sticky	NA/Soupy	V SBV Sticky	NA/Soupy	NA/Soupy	NA/Soupy	SoBV Friable	SoBV Friable	SoBV Friable
Texture	SC, S, P	SC, S	SC, S	SC, S, P, G	SC, S, P, G	SC, S, P, G	S, P, G, SC	S, P, G, SC	S, P, G, SC	S, P, G, SC
Color	2.5Y4/4	2.5Y5/4	2.5Y5/4	2.5Y4/4	2.5Y5/4	2.5Y5/4	2.5Y4/4	2.5Y4/4	2.5Y4/4	2.5Y4/4
Other Features	Sat	Sat	Sat	Sat	Sat	Sat	Dmp	Dmp	Dmp	Dmp
7 R. CS Unit #	8A	8A	8C	8A	8A	8A	8A	3B	3B	3B
Consistency	NA/Soupy	V SBV Sticky	NA/Soupy	V SBV Sticky	NA/Soupy	NA/Soupy	SR-SI Hrd/Plastic	V SBV Plastic	V SBV Plastic	SR-SI Hrd/Plastic
Texture	S, SC, G, P	SC, S, P, G	SIL, S, G	SC, S, P, G	SC, S, P, G	SC, S, P, G	SC, S, P	SC, S, P	SC, S, P	SC, S, P
Color	2.5Y4/4	2.5Y5/4	2.5Y5/4	2.5Y4/4	2.5Y5/4	2.5Y5/4	2.5Y4/4	2.5Y4/4	2.5Y4/4	2.5Y4/4
Other Features	Sat	Sat	Sat	Sat	Sat	Sat	Dmp	Dmp	Dmp	Dmp
8 R. CS Unit #	8A	8D	8A	8D	8D	8A	8A	3B	3B	3B
Consistency	V SBV Sticky	NA/Soupy	NA/Soupy	V SBV Sticky	NA/Soupy	NA/Soupy	SR-SI Hrd/Plastic	V SBV Plastic	V SBV Plastic	SR-SI Hrd/Plastic
Texture	SC, S, P, G	SC, S, P, G	SC, S, P, G	SC, S, P, G	SC, S, P, G	SC, S, P, G	SC, S, P	SC, S, P	SC, S, P	SC, S, P
Color	2.5Y4/4	2.5Y5/4	2.5Y5/4	2.5Y4/4	2.5Y5/4	2.5Y5/4	2.5Y4/4	2.5Y4/4	2.5Y4/4	2.5Y4/4
Other Features	Sat	Sat	Sat	Sat	Sat	Sat	Dmp	Dmp	Dmp	Dmp
9 R. CS Unit #	8D	8D	8D	8D	8D	8D	8A	3B	3B	3B
Consistency	NA/Soupy	NA/Soupy	NA/Soupy	V SBV Sticky	NA/Soupy	NA/Soupy	SR-SI Hrd/Plastic	V SBV Plastic	V SBV Plastic	SR-SI Hrd/Plastic
Texture	SIL, S, P, G	SIL, S, P, G	SIL, S, P, G	SIL, S, P, G	SIL, S, P, G	SIL, S, P, G	SC, S, P	SC, S, P	SC, S, P	SC, S, P
Color	2.5Y 4/4	2.5Y5/4	2.5Y5/4	2.5Y5/4	2.5Y5/4	2.5Y5/4	2.5Y4/1	2.5Y4/1	2.5Y4/1	2.5Y4/1
Other Features	Sat	Sat	Sat	Sat	Sat	Sat	Dmp	Dmp	Dmp	Dmp

Sand Site (Site C) Northeast-Southwest Cross-section



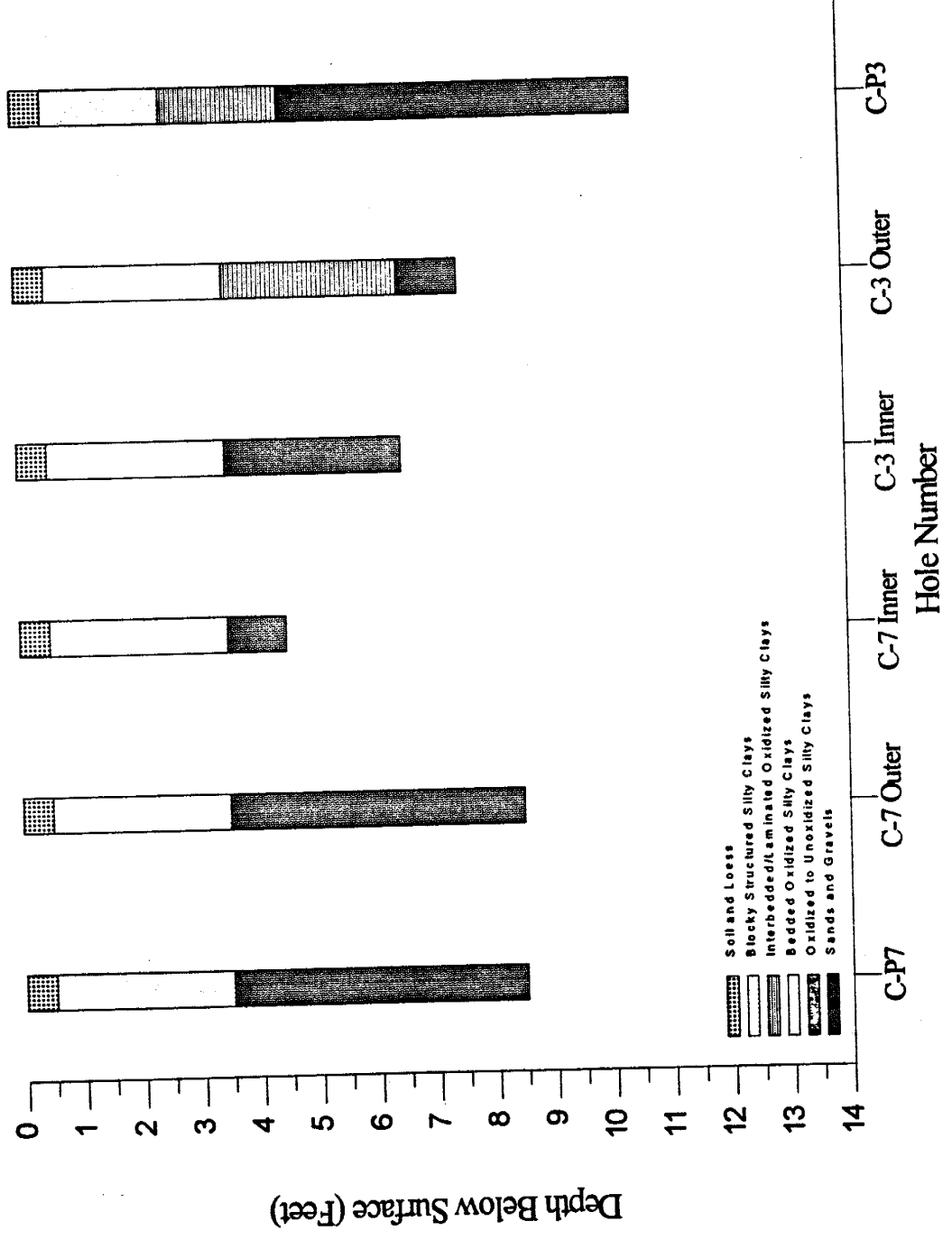
Sand Site Northwest-Southeast Cross-section

Depth / Hole #	C-18	C-8 OUTER	C-8 INNER	C-4 INNER	C-4 OUTER	C-14
1 R. CS Unit #	1B	1B	1A	1B	1B	1A
Consistency	Soft/V Friable	Soft/V Friable	Soft/V Friable	Soft/V Friable	Soft/V Friable	Soft/V Friable
Texture	SC	SC	SC	SC	SC	SC
Color	2.5Y7/4	2.5Y5/3	10YR5/6	2.5Y6/3	2.5Y5/3	10YR4/6
Other Features	Dry, O	Dry, O	Dry, O	Dry, O	Dry, O	Dry, O
2 R. CS Unit #	2A	2B	2A	2B	2A	2A
Consistency	SR-SI Hrd/Plastic	SR-SI Hrd/Plastic	SR-SI Hrd/Plastic	SR-SI Hrd/Plastic	SR-SI Hrd/Plastic	SR-SI Hrd/Plastic
Texture	SC	SC	SC	SC	SC	SC
Color	10YR6/6, 5R	2.5Y5/6	10YR4/6	2.5Y6/3, 7.5YR5/8	10YR4/6, 4Y	10YR4/4
Other Features	Dmp, O	Dmp, O	Dmp, Mn	Dmp, CaCO3	Dmp, CaCO3	Dmp, CaCO3
3 R. CS Unit #	2B	2B	2B	2B	2B	2A
Consistency	SR-SI Hrd/Plastic	SR-SI Hrd/Plastic	SR-SI Hrd/Plastic	SR-SI Hrd/Plastic	SR-SI Hrd/Plastic	SR-SI Hrd/Plastic
Texture	SC	SC	SC	SC	SC	SC, P
Color	2.5Y5/4	2.5Y4/4	2.5Y4/4	2.5Y4/4, 7.5YR5/8	2.5Y4/4, 7.5YR6/8	10YR4/6
Other Features	Dmp, Mn	Dmp, O	Dmp, Mn	Dmp, CaCO3, Mn	Dmp	Dmp, Mn
4 R. CS Unit #	7A	7D	7B	7B	7A	7A
Consistency	V SBV Sticky	V SBV Sticky	V SBV Sticky	SR-SI Hrd/Plastic	SR-SI Hrd/Plastic	SR-SI Hrd/Plastic
Texture	SC	SC, S, P, G	SC, S	SC	SC	SC
Color	2.5Y5/4	2.5Y4, 4	2.5Y4/4	2.5YR5/3, 7.5YR5/6	2.5Y5/3, 10YR 5/8	2.5Y4/4
Other Features	Sat	Sat	Sat	Dmp, Mn	Dmp, CaCO3, Mn	Sat
5 R. CS Unit #	8A	7D	8B	7B	7B	7B
Consistency	NA/Sloppy	NA/Sloppy	NA/Sloppy	SR-SI Hrd/Plastic	SR-SI Hrd/Plastic	SR-SI Hrd/Plastic
Texture	SC, S, P, G	SC, S, P, G	SC, S	SC	SC, S	SC, S
Color	2.5Y5/4	2.5Y5/4	2.5Y5/4	2.5Y4/3, 7.5YR5/6	2.5Y5/4	2.5Y4/4
Other Features	Sat	Sat	Sat	Dmp	Sat	Sat
6 R. CS Unit #	8A	7D	8C	7B	7B	7C
Consistency	NA/Sloppy	V SBV Sticky	NA/Sloppy	SR-SI Hrd/Plastic	V SBV Sticky	V SBV Sticky
Texture	SC, S, P, G	SC, S, P, G	SR, S	SC, P	SC, S, SC	SC, S, P
Color	2.5Y5/4	2.5Y5/4	2.5Y5/4	2.5YR5/2, 7.5YR5/6	2.5Y5/4	2.5Y5/4
Other Features	Sat	Sat	Sat	Dmp	Sat	Sat
7 R. CS Unit #	8A	7D		7B		7B
Consistency	NA/Sloppy	V SBV Sticky		SR-SI Hrd/Plastic		V SBV Sticky
Texture	SC, S, P, G	SC, S, P, G		SC, P		SC, S
Color	2.5Y5/4	2.5Y5/4		2.5Y4/3, 5YR5/8		2.5Y5/4
Other Features	Sat	Sat		Dmp		Sat
8 R. CS Unit #	8D					
Consistency	NA/Sloppy					
Texture	SR, S, P, G					
Color	2.5Y5/4					
Other Features	Sat					

Sand Site Northeast-Southwest Cross-section

Depth / Hole #	C-P6	C-6 OUTER	C-6 INNER	C-2 INNER	C-2 OUTER	C-P2
1 R. CS Unit #	1B	1A	1B	1B	1B	1B
Consistency	So/Plv Friable	So/Plv Friable	So/Plv Friable	So/Plv Friable	So/Plv Friable	So/Plv Friable
Texture	SC	SC	SC	SC	SC	SC
Color	2.5Y6/3	10YR5/6, 2.5Y6/3	2.5Y5/3	2.5Y4/8, 5A	2.5Y4/2	2.5Y7/2
Other Features	Dry, O	Dry, O	Dry, O	Dry, O	Dry, O	Dry, O
2 R. CS Unit #	2A	2B	2A	2B	2A	2A
Consistency	SR-SI Hid/Plastic	SR-SI Hid/Plastic	SR-SI Hid/Plastic	SR-SI Hid/Plastic	SR-SI Hid/Plastic	SR-SI Hid/Plastic
Texture	SC	SC	SC	SC	SC	SC
Color	10YR4/6	2.5Y4/4	10YR5/8, 2.5Y5/4	2.5Y4/4	10YR4/6, 4/4	10YR4/4, 7.5YR6/6
Other Features	Dmp, Mn	Dmp, O, CaCO3, Mn	Dmp, CaCO3	Dmp, Mn	Dmp, Mn	Dmp
3 R. CS Unit #	2A	2B	2B	2A	2A	2A
Consistency	SR-SI Hid/Plastic	SR-SI Hid/Plastic	SR-SI Hid/Plastic	SR-SI Hid/Plastic	SR-SI Hid/Plastic	SR-SI Hid/Plastic
Texture	SC	SC	SC	SC	SC	SC
Color	10YR3/6, 2.5Y4/2	2.5Y4/4, 7.5YR3/8	2.5Y5/4	2.5Y4/4, 5/6	10YR5/4	10YR5/6, 7.5YR5/8
Other Features	Dmp, Mn	Dmp, Mn	Dmp, Mn	Dmp, Mn	Dmp, Mn	Dmp, Mn
4 R. CS Unit #	2B	2B	2B	2B	2B	2B
Consistency	SR-SI Hid/Plastic	SR-SI Hid/Plastic	SR-SI Hid/Plastic	SR-SI Hid/Plastic	SR-SI Hid/Plastic	SR-SI Hid/Plastic
Texture	SC	SC, S	SC, S	SC, S	SC	SC
Color	2.5Y5/4	2.5Y4/4	2.5Y4/4, 4/2	2.5Y4/4, 6/3	2.5Y5/4, 7/6	2.5Y5/4, 7.5YR5/8
Other Features	Dmp, Mn	Dmp	Sat	Dmp	Dmp, CaCO3	Dmp
5 R. CS Unit #	1B	7B	7B	2B	2B	3A
Consistency	SR-SI Hid/Plastic	SR-SI Hid/Plastic	SR-SI Hid/Plastic	SR-SI Hid/Plastic	SR-SI Hid/Plastic	SR-SI Hid/Plastic
Texture	SC, S	SC, S	SC, S	SC, S	SC	SC
Color	10YR5/6, 2.5Y5/4	2.5Y4/4	2.5Y4/4	2.5Y4/4, 6/3	2.5Y5/6	2.5Y5/2, 7.5YR6/6
Other Features	Dmp, Mn	Sat	Sat	Dmp	Dmp	Dmp, CaCO3
6 R. CS Unit #	7B	7D	7D	7B	7B	1A
Consistency	SR-SI Hid/Plastic	SR-SI Hid/Plastic	SR-SI Hid/Plastic	V SRV Sticky	V SRV Sticky	SR-SI Hid/Plastic
Texture	SC, S	SC, S, P, G	SC, S, P, G	SC, S	SC, S	SC
Color	2.5Y4/4	2.5Y5/4	2.5Y4/4	2.5Y3/4	2.5Y5/4	2.5YR5/4, 6/2
Other Features	Sat	Sat	Sat	Sat	Sat	Sat
7 R. CS Unit #	8A	7D	7C	7B	7B	1B
Consistency	NA/Sloopy	SR-SI Hid/Plastic	SR-SI Hid/Plastic	SR-SI Hid/Plastic	SR-SI Hid/Plastic	V SRV Sticky
Texture	SC, S	SC, S, P, G	SC, S, G	SC, S	SC, S	SC, S
Color	2.5Y4/4	2.5Y5/4	2.5Y4/4	2.5Y5/4	2.5Y5/4	2.5Y5/2, 7.5YR5/8
Other Features	Sat	Sat	Sat	Sat	Sat	Dmp, CaCO3
8 R. CS Unit #	8D	8B	8B	7D	7D	7B
Consistency	NA/Sloopy	NA/Sloopy	NA/Sloopy	V SRV Sticky	V SRV Sticky	V SRV Sticky
Texture	Slt, S, P, G	Slt, S, P, G	Slt, S	SC, S, P, G	SC, S, P, G	SC, S
Color	2.5Y4/4	2.5Y4/4	2.5Y4/4	2.5Y5/4	2.5Y5/4	2.5Y4/4
Other Features	Dmp	Sat	Sat	Sat	Sat	Sat
9 R. CS Unit #	7C			7D		
Consistency	V SRV Sticky			V SRV Sticky		
Texture	SC, S, P			SC, S, P, G		
Color	2.5Y5/4			2.5Y5/4		
Other Features	Sat			Sat		
10 R. CS Unit #	7C					
Consistency	V SRV Sticky			V SRV Sticky		
Texture	SC, S, P			SC, S, P, G		
Color	2.5Y5/4			2.5Y5/4		
Other Features	Sat			Sat		

Sand Site (Site C) East-West Cross-section



Sand Site East - West Cross-section

Depth / Hole #	C-17	C-7 OUTER	C-7 INNER	C-3 INNER	C-3 OUTER	C-F3
1 R. CS Unit #	1A	1A	1A	1B	1B	1B
Consistency	So/IV Friable	SR-SI Hid/Plastic	So/IV Friable	So/IV Friable	So/IV Friable	So/IV Friable
Texture	SC	SC	SC	SC	SC	SC
Color	10YR5/6	10YR5/6	10YR5/6	2.5Y5/3	2.5Y5/2	2.5Y6/3
Other Features	Dry, O	Dry, O	Dry, O	Dry, O	Dry, O	Dry, O
2 R. CS Unit #	2A	2A	2A	2B	2B	2B
Consistency	SR-SI Hid/Plastic	SR-SI Hid/Plastic	SR-SI Hid/Plastic	SR-SI Hid/Plastic	SR-SI Hid/Plastic	SR-SI Hid/Plastic
Texture	SC	SC	SC	SC	SC	SC
Color	10YR5/6	10YR5/6	10YR5/8	2.5Y4/4	2.5Y5/3	2.5Y5/3
Other Features	Dmp. O, Mn	Dmp. Mn	Dmp. O	Dmp. CxCO3	Dmp. O	Dmp. Mn
3 R. CS Unit #	3A	3A	3A	3B	3B	3A
Consistency	SR-SI Hid/Plastic	SR-SI Hid/Plastic	SR-SI Hid/Plastic	SR-SI Hid/Plastic	SR-SI Hid/Plastic	SR-SI Hid/Plastic
Texture	SC	C	SC	SC	SC	SC
Color	10YR5/6	2.5Y4/4	2.5Y4/4	2.5Y4/4	2.5Y4/4	2.5Y4/3
Other Features	Dmp	Dmp. Mn	Dmp. O	Dmp. Mn	Dmp	Dmp. Mn
4 R. CS Unit #	4A	4A	4A	4B	4B	4A
Consistency	SR-SI Hid/Plastic	SR-SI Hid/Plastic	SR-SI Hid/Plastic	SR-SI Hid/Plastic	SR-SI Hid/Plastic	SR-SI Hid/Plastic
Texture	S, SC	SC	SC, S	SC	SC	SC
Color	2.5Y5/6, 6/2	2.5Y4/4	2.5Y4/4	2.5Y4/4	2.5Y4/4, 10YR5/8	2.5Y5/4
Other Features	Dmp, CxCO3	Dmp	Dmp	Dmp	Dmp. Mn	Dmp
5 R. CS Unit #	5B	5B	5B	5B	5B	5A
Consistency	NA/Soupy	NA/Soupy	NA/Soupy	V SRV Sticky	SR-SI Hid/Plastic	SR-SI Hid/Plastic
Texture	SC, S	SC, S	SR, S	SC, S	SC, S, P	SC
Color	2.5Y5/4	2.5Y4/4	2.5Y5/4	2.5Y5/4	2.5Y4/4	2.5Y5/4 6/1, 10YR6/6
Other Features	Sat	Sat	Sat	Sat	Sat	Dmp, CxCO3, Mn
6 R. CS Unit #	6B	6B	6B	7D	7B	6A
Consistency	SR-SI Hid/Plastic	NA/Soupy	SR-SI Hid/Plastic	V SRV Sticky	SR-SI Hid/Plastic	V SRV Sticky
Texture	S, SC	SC, S, P, G	SC, S, P, G	SC, S, P, G	SC, S, G, P	S, SC
Color	2.5YR3/4	2.5Y4/4	2.5Y4/4	2.5Y5/4	2.5Y4/4	2.5Y4/4
Other Features	Sat	Sat	Sat	Sat	Sat	Sat
7 R. CS Unit #	7A	7A	7A	7B	7B	7A
Consistency	NA/Soupy	NA/Soupy	NA/Soupy	V SRV Sticky	V SRV Sticky	V SRV Sticky
Texture	SC, S, G	SC, S, P, G	SC, S, P, G	SC, S	SC, S, P, G	SC, S
Color	2.5Y5/4	2.5Y5/4	2.5Y5/4	2.5Y4/4	2.5Y4/4	2.5Y4/4
Other Features	Sat	Sat	Sat	Sat	Sat	Sat
8 R. CS Unit #	8A	8A	8A	7D	7D	8A
Consistency	NA/Soupy	NA/Soupy	NA/Soupy	V SRV Sticky	V SRV Sticky	NA/Soupy
Texture	SC, S, P, G	SC, S, P, G	SC, S, P, G	SC, S, P, O	SC, S, P, O	SC, S
Color	10YR3/4	2.5Y5/4	2.5Y5/4	2.5Y4/4	2.5Y4/4	2.5Y4/4
Other Features	Sat	Sat	Sat	Sat	Sat	Sat
9 R. CS Unit #	9C	9D	9C			9A
Consistency	NA/Soupy	NA/Soupy	SR, S, G			NA/Soupy
Texture	Sit, S, G	Sit, S, G	Sit, S, P, G			SC, S
Color	2.5Y5/4	2.5Y5/4	2.5Y5/4			2.5Y4/4
Other Features	Sat	Sat	Sat			Sat
10 R. CS Unit #						10B
Consistency						NA/Soupy
Texture						Sit, S
Color						2.5Y4/4
Other Features						Sat

Sand Site East - West Cross-section

Depth / Hole #	C-P7	C-7 OUTER	C-7 INNER	C-3 INNER	C-3 OUTER	C-P3
11 ft. CS Unit # Consistency Texture Color Other Features						BB N/A/ropy SILS 2.3Y4/2, 4/3 Sat

Appendix II - Infiltration

<u>Section</u>	<u>Page</u>
Infiltrimeters and water supply	2
Infiltration initiation and maintenance	2
Infiltration monitoring and calculation of infiltration rate	2
Results	3
Figures	6

Infiltrometers and water supply

Each infiltration site utilized a 2.2 m diameter single ring surface infiltrometer (Figure 1). The ponded head in the infiltrometer was kept at a constant 5 cm level by a manifold of four float valves supplied by two 500 gallon site supply tanks. The site supply tanks were refilled as needed from two 2500 gallon main supply tanks. Water was delivered by truck to fill the main supply tanks. Ametec brand model PSCL-SI, 20 micron filters were placed between the main supply tanks and the 500 gallon site tanks to filter out particulates from the water supply.

The infiltrometers were constructed of three sheets of polyethylene fastened end to end to form a ring 2.2 meters in diameter and 40.3 cm high. Gaskets and silicone sealer prevented leakage at joints. To form a seal between the infiltrometer ring and the soil, a circular trench approximately 10 cm deep and 5 cm wide was filled with granular bentonite. The infiltrometer ring was set into the bentonite seal. No leakage was observed from inside the infiltrometer to the surface soils directly outside. The inside edge of the infiltrometer was covered with a four inch wide sand border to prevent contamination of the soil surface inside the infiltrometer by expanding bentonite.

Infiltration initiation and maintenance

Infiltration was initiated at 1415, 15 June 1994, by pouring four 133 liter containers of water into the infiltrometers and simultaneously opening the water supply valves, yielding an initial and essentially instantaneous ponded head of 5 cm. The undisturbed soil surface was protected from scouring by placing splash deflectors under the flow valves and the areas where the large containers were emptied into the infiltrometer. These deflectors were removed after initial filling of the infiltrometer.

Infiltration was continued uninterrupted for the time of the test. Four Ryan Herco rinse tank float valves plumbed to the site supply tanks maintained a constant average ponded head of 5 cm above the infiltration surface. Infiltration was terminated at both sites on 1130, 20 August, 1994.

Infiltration monitoring and calculation of infiltration rate

Two pressure transducers were placed in the bottom of each site supply tank (Figure 2). The mV readings from the pressure transducers were taken every fifteen minutes for the duration of infiltration. The mV readings were translated into pressure head of water in the tanks (See Appendix V - Pressure Field, for a complete discussion of conversion of transducer mV readings to pressure heads). The height of water in each reservoir tank was equal to the pressure head at the transducers in the tank bottom, and was multiplied by the rectangular area of the tank to yield volume of water in liters. To simplify calculations, the tanks were never filled beyond the height of the constant rectangular area of the tanks (approximately 385 gallons). The sum of volume change over time equaled the cumulative infiltration. Volume changes in time were used to calculate the flux through the infiltrometer in centimeters of water:

$$i = \frac{\Delta V}{\Delta t} * \frac{1}{A}, \text{ where } \Delta V = \text{volume change [cm}^3\text{]}$$

$$i = \text{infiltration rate } \left[\frac{\text{cm}}{\text{hr}} \right]$$

$$\Delta t = \text{time change [hr]}$$

$$A = \text{area of the infiltrometer [cm}^2\text{]}$$

Use of pressure transducers to monitor water height in the reservoir tanks was less accurate than if flow meters had been used for the following reasons:

1. Actual flow to the infiltrometer could not be accurately determined during the time tanks were being refilled, cleaned of algae, or when tracers were added.
2. In some periods of very low or no flow, pressure readings indicated negative flow, either from measurement error or expansion of water during increases in temperature.

Algae growth in both the site and main water supply tanks was a significant problem. The translucent tanks and sunny summer weather created 95 °F. water temperatures in the infiltrometers. Combined with poor water quality, this produced the ideal conditions for algae growth. At the termination of the test, thick algae growth covered the bottoms of the site supply tanks and extended two feet up the side walls. Because of regulatory concerns, the algae growth could not be properly controlled with available algaecides (Refer to Project Implementation at a DOE Facility in Main Report). Algae undoubtedly was infiltrated into the test sites.

Results

Figure 3 graphs the infiltration rates of both Site A (Clay Site) and Site C (Sand Site) in time. The maximum daily average infiltration rate at Site A was 2.23 cm/hr, attained approximately 570 hours after the start of infiltration (430 hours after the start of the Cl⁻ tracer pulse). From this point, infiltration steadily declined to approach 0.72 cm/hr at steady state. During the dye pulse, the infiltration rate at Site A again experienced a significant decline to approximately 0.53 cm/hr (Figure 3). The maximum daily average infiltration rate for Site C (Sand Site) was 2.85 cm/hr, attained approximately 514 hours after the beginning of infiltration (350 hours after initiation of the Cl⁻ tracer pulse). The infiltration rate at the Site C also declined to approximately 0.73 cm/hr at long time. Both the initial rise after the Cl⁻ tracer pulse and a following decline were experienced sooner at Site C than at Site A. This is likely because of the higher sand content in the topsoils at Site C, and resulting higher effective conductivity.

The similarity between trends and magnitudes of infiltration rates at Site A and Site C is striking (Figure 3). The pattern of sharp decline after initial rise, followed by renewed rise and steady decline which was observed at Site A was also apparent at Site C. Site C initially experienced a lesser infiltration rate than Site A, but after introduction of the Cl⁻ tracer pulse,

the rate at Site C exceeded that at Site A and maintained a slightly higher level until after almost 1200 hours of infiltration when long time steady state had been attained (Figure 3). It is obvious that at both sites the same mechanism exists for controlling the pattern of infiltration rate change in time.

This pattern in undisturbed soils of rapid initial rise, sharp decline, renewed rise, and final steady decline may be controlled by biological, physical, or geologic mechanisms. The pattern observed in this test has been noted by a number of researchers. Muckel (1959) attributed the second rise in infiltration rate to the displacement of entrained air followed by a steady decline in rate due to biological and chemical activity constricting pores. Hantush (1967) modeled the mounding of uniformly percolated water as the inverse to pumping well draw down. The change of infiltration rate with time mimics these models well (See Muckel, 1959, his Figure 18).

Besides mounding of water or dissolution of entrapped air, the growth of algae in the water supply tanks and infiltrometers may provide a biological mechanism producing the pattern shown in Figure 2. The proliferation of algae was inevitable given the 95 °F. temperature of the supply water caused by a combination of translucent supply tanks and the hot and sunny summer weather. The rise in infiltration rates begins approximately two hundred hours after the introduction of the Cl⁻ tracer pulse, when conditions for algal growth throughout the site would be minimal, and infiltration rates decline again approximately four hundred hours after the tracer pulse, when the Cl⁻ tracer was essentially flushed from the system. An algae build up in the infiltrated surface and upper subsurface passages would create an upper boundary condition inhibiting infiltration into the flow system. A striking similarity in trends between infiltration rate and change in total potential is also displayed (Figure 4). A decrease in infiltration due to algae clogging flow passages and a corresponding decrease in total head lends weight to the theory that changing conditions at the upper boundary caused the observed pattern in infiltration rate (See also Appendix V, for a discussion of the correlation between infiltration rates and total head across the array).

A sharp decline in the infiltration rate was also observed during the dye pulse at Site A, beginning about 1400 hours after the salt pulse (Figure 2). The dye pulse was created by infiltrating dissolved powdered dye, and the resulting suspension apparently had a detrimental effect on the transport ability of the system, especially in the topsoil layer where the majority of the dye was captured (Plate 19, Appendix VI). This dye capture may be analogous to the infiltration constricting effect of algae growth.

Media heterogeneity and macropore or fracture flow could also have influenced infiltration. The infiltration rate would be expected to slow as infiltrated water moved into less transmissive media or features. Most of the media investigated by the stress test was essentially saturated at Site A, and an increase in infiltration rate due to saturation of the matrix about fractures or minor macropores would be expected to be small. The media at Site C was unsaturated to a slightly greater depth than at Site A, and the lower initial infiltration rate at Site C could be partly a function of less flow through fractures and macropores in the initially unsaturated near surface layers. Unfortunately, because of problems with water quality and summer

temperatures and the resultant algae growth and its effect on the infiltrometer boundary conditions, no definitive answer can be provided to explain the pattern of infiltration rate change with time.

The worst case scenario for flow and transport occurs under saturated conditions. The essential saturation of the sites to the surface (standing water) was experienced during a field inspection in early spring, and water levels (standing water in boreholes) in late May were noted only 1 m below the surface at Site C. It is not unreasonable to assume that saturated or essentially saturated conditions exist on site for a significant portion of the year. At long time, the infiltration rate will closely approach the saturated hydraulic conductivity (Rubin, J. and R. Steinhardt, 1963).

Under these conditions, the maximum bulk saturated conductivity at both sites may be estimated to approach 10^{-3} cm/s in the near surface zone investigated by the infiltration tests. The range of saturated hydraulic conductivity commonly accepted for sands is 10^{-4} to 1 cm/s, for silty sand 10^{-5} to 10^{-3} cm/s, for silt and loess 10^{-7} to 10^{-5} cm/s, for glacial till 10^{-12} to 10^{-5} cm/s, and for unweathered clay 10^{-13} to 10^{-9} cm/s. Values are from Freeze and Cherry (1979). Because vertical flow perpendicular to layering precludes any but the lowest conductivity layers from dominating, K_{eff} would necessarily be near the lower end of the above ranges. At Site C, the silts and loess would be the least conductive media encountered. The maximum infiltration rates experienced at Site C exceed the conductivities of these least transmissive media by two to four orders of magnitude. At Site A, the massive clays present the lowest conductivities. Infiltration rates at Site A exceed the expected conductivity by two to eight orders of magnitude. It is apparent that preferential flow through zones of higher conductivity media and structural and bioturbated fast transport pathways play an important role.

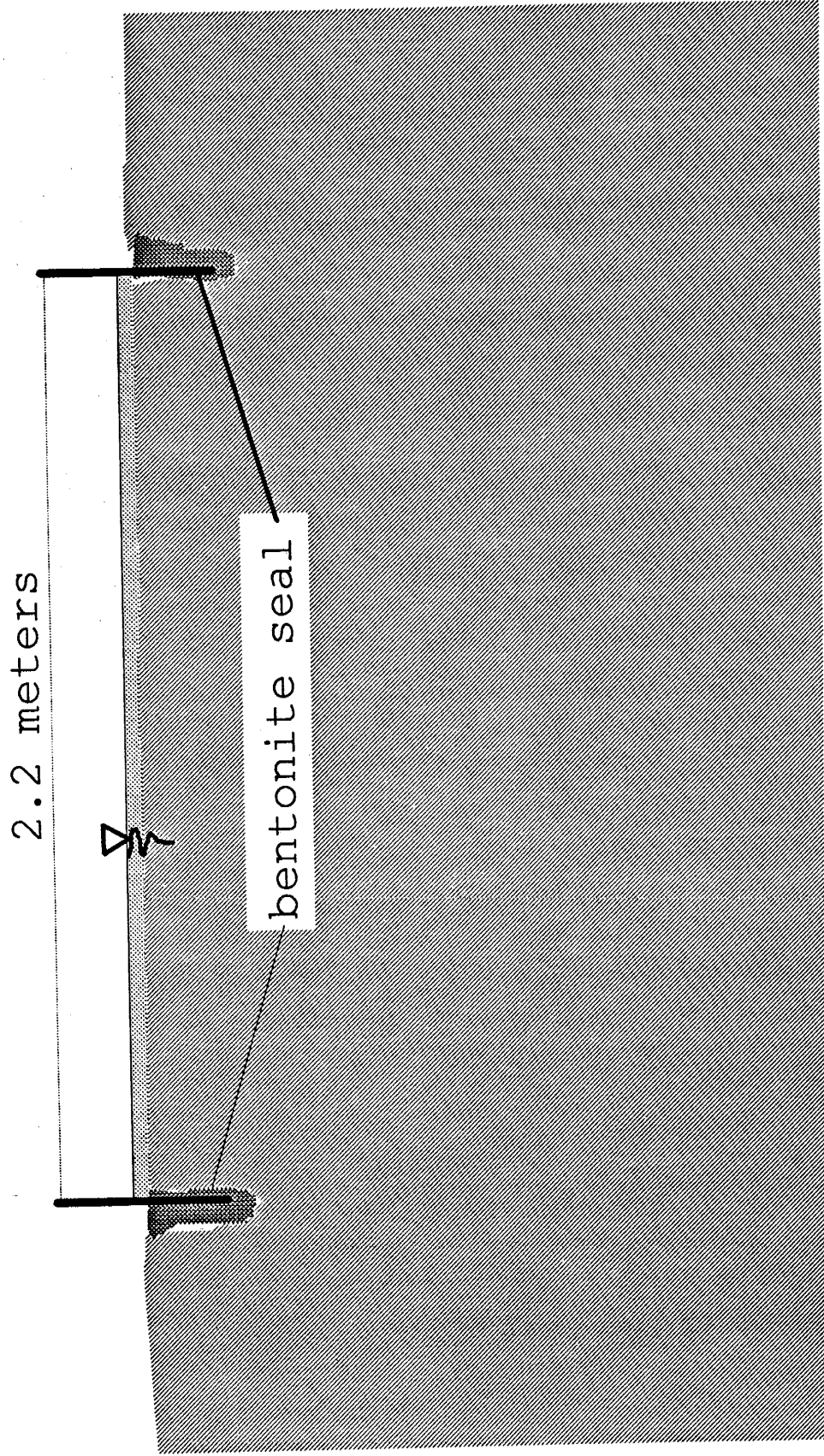


Figure 1. Ponded surface infiltrometer. The ponded level was kept at a constant 5 cm.

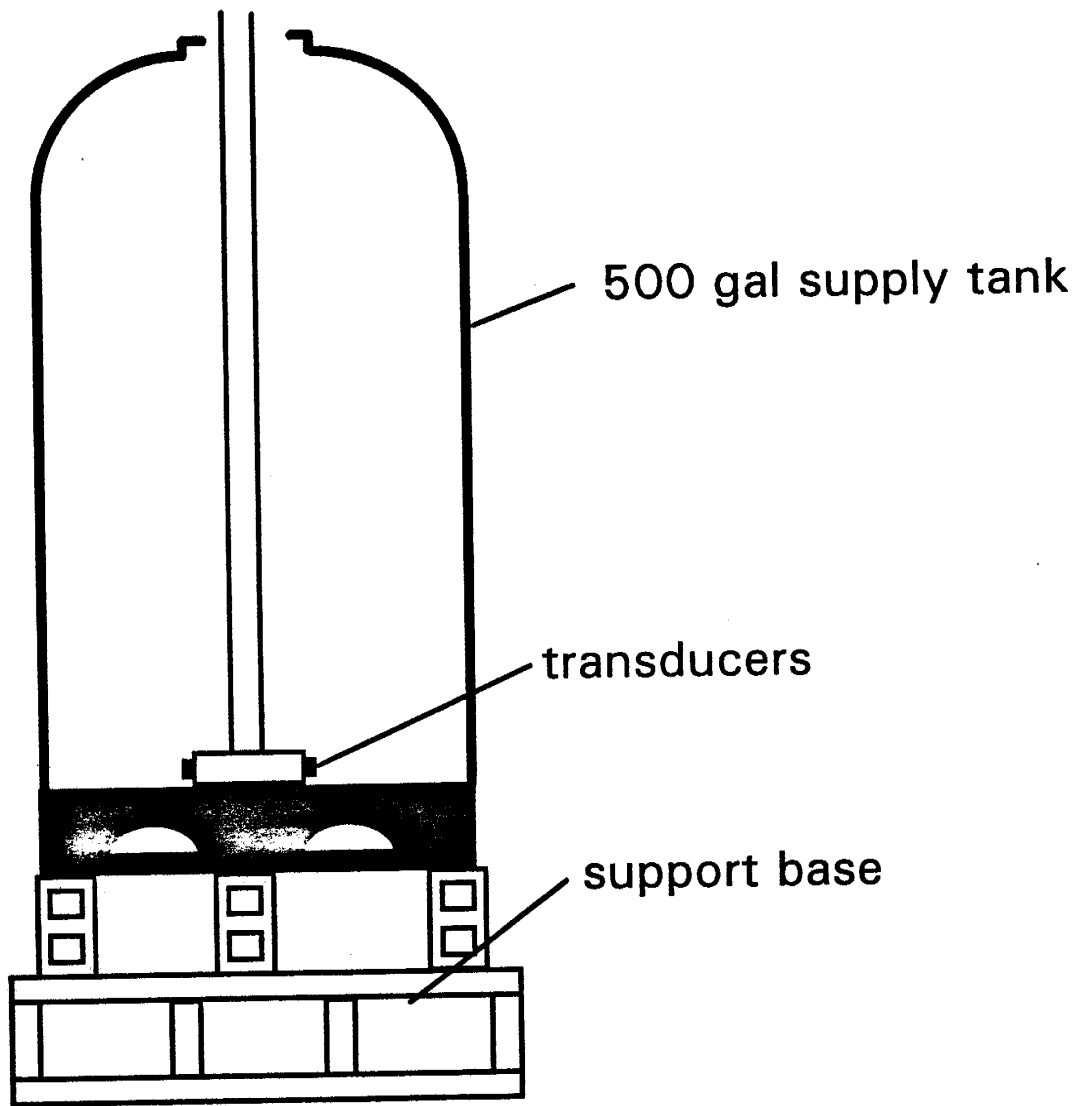


Figure 2. Site supply tanks.

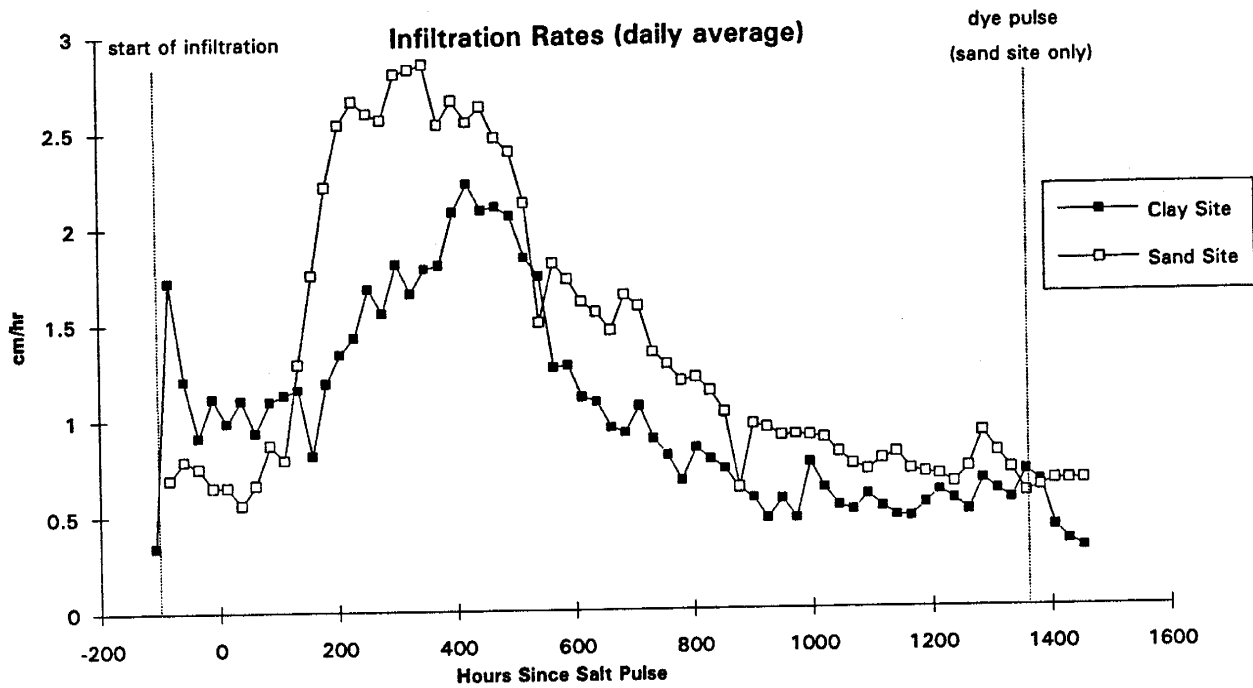


Figure 3. Infiltration rates in time at Site A and Site C.

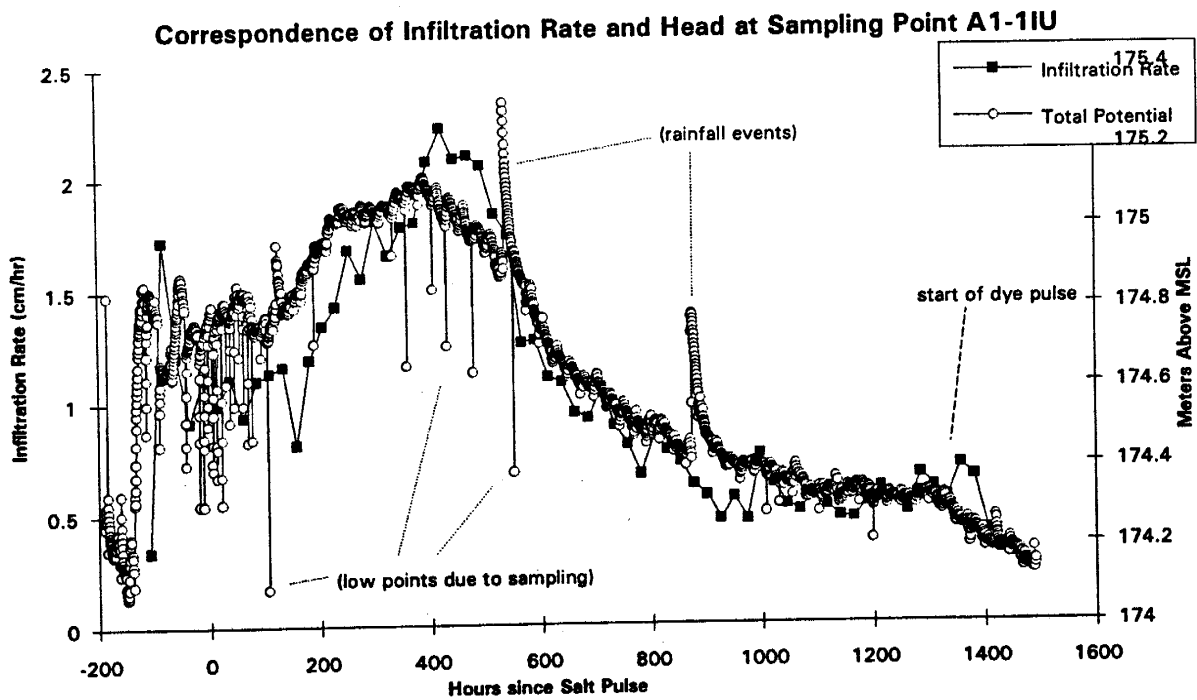


Figure 4. Correspondence of trends between infiltration rate and changes in total potential.

Appendix III - TPCT Design and Instrumentation

<u>Section</u>	<u>Page</u>
Sensor Array Design	2
Instrument Construction	2
Instrument Installation	3
Figures	4

Sensor Array Design

The investigations completed in the summer of 1993 (Glass et al., 1995) and the results of exploratory investigations during 1994 demonstrated that the oxidized tills at the FEMP are capable of significant ground water flow through fractures, zones of preferential flow, and bioturbated macropores. A primary concern in investigation of transport processes is the interception of active preferential and fast transport pathways. If the scale of instrumentation is Brobdingnadian, significant heterogeneity and fast transport pathways may never be illuminated. If the scale of instrumentation is Lilliputian, detail will be conserved but data may reflect only the small scale matric characteristics and not the effective hydraulic parameters (Neuzil, 1994; Keller, 1989). The array must be designed to resolve data without compelling integration over such large portions of the array that three dimensional understanding of flow and solute transport processes would not be possible.

The sensor array developed for the Transport Processes Characterization Tests (TPCTs) was designed to minimize these concerns. Each sampling point instrument pack contained a tensiometer (Figure 1), a Time Domain Reflectometry (TDR) probe (Figure 1), and suction lysimeter and colloid soil water samplers (Figure 2). All sensors were situated in close proximity within a 50 cm section of the 10 cm diameter borehole (Figure 3). Each sampling point was filled with a 50/50 mixture of #8 fine sand and #4 filter pack sand. Siting all instruments in close proximity allowed comparison of different types of measurements at an identical location and time throughout the sampling array. The sand filler minimized effects of material property changes due to media differences across the array and provided a transmissive media to allow transport of tracers to the various sensors. The sampling points were sealed from intra borehole flow with bentonite (Figures 3 and 4). With forty-four sampling points in a single 10 meter diameter by 3 meter deep array (Figures 4, 5, 5a, and 5b), the 50 cm length by 10 cm diameter sampling point configuration was designed to allow both spatially defined data and also interception of active macropores. The colloid and suction lysimeters allowed active collection of soil water samples for laboratory analysis of tracer concentrations. The TDR probes allowed passive measurement of tracer concentrations. Tensiometers gathered soil matric pressures.

At the termination of the TPCTs, Site A was subjected to a dye pulse and then excavated to allow visualization of the active preferential flow paths and confirm sensor interpretation and fast transport pathways identified by the instrumentation array.

Instrument construction

Colloid and suction lysimeter samplers were designed and constructed by Sandia National Laboratory personnel from PVC pipe, acrylic and PVC tubing, polyethylene filters, and solute resistant 1 bar 653X02-B1M3 SoilMoisture Equipment ceramic cups, all non-reactive materials (Figure 2).

Tensiometers were constructed of 3/4" PVC pipe, 1/2" polycarbonate sight glass and Soil Measurement Systems rubber septums, and SoilMoisture Equipment 655X01B1M1 ceramic

porous cups. Transducers, sight glasses, and auxiliary valves were fitted in PVC pipe "tees" (Figure 1). The sight glasses allowed technicians to check for full water levels and as a check for leaking tensiometers. Tensiometers were filled by removing the sight glass septum. The tensiometer design is complicated and experienced a bothersome failure rate. A simpler design is being developed and tested.

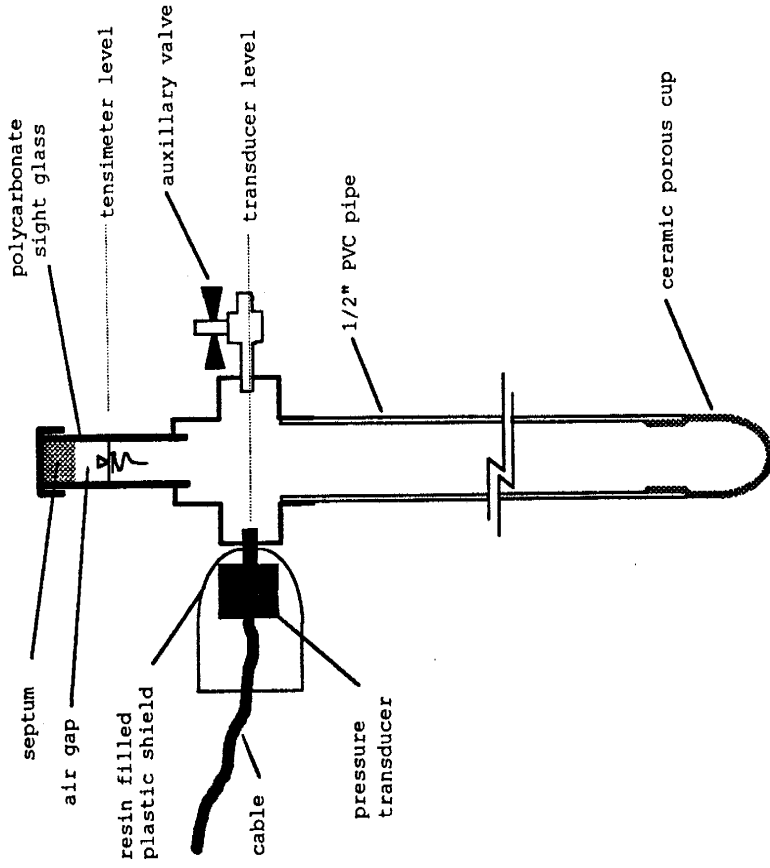
The TDR probes used were three prong models with 5/16"x 6" stainless steel prongs in 2"x 3"x4" polycarbonate blocks (Figure 1). Signal transmission was over Alpha brand RG58-A low noise coaxial cable. The relatively short and thick prongs were chosen to accentuate signal return, which has been shown to be a problem in clays with significant layer charge (See Glass et al., 1995).

Instrument Installation

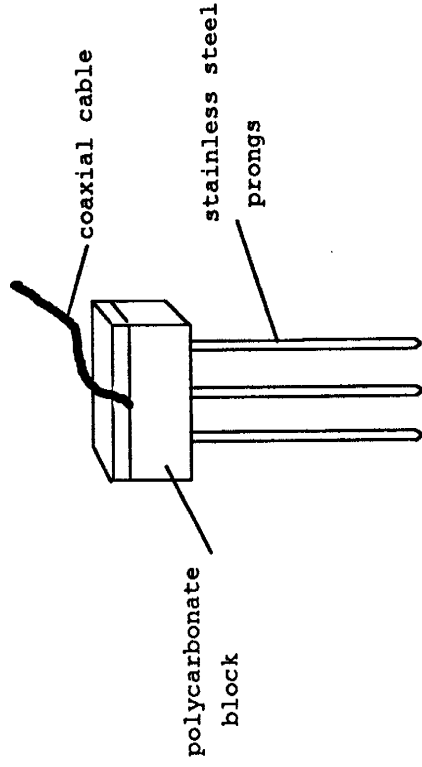
Sampling station locations for each site were located and flagged on the surface. Initial borings were made with 2" hand augers to provide samples for geologic interpretation and analysis. Boreholes were then enlarged to 4" with either a "Little Beaver" gasoline engine powered hydraulic continuous flight auger, or 4" bucket hand augers. The "Little Beaver" auger caused a significant layer of cuttings to adhere to the borehole sides, especially where standing water or saturated materials were encountered. This skin was removed by scraping and then reborings with four inch hand augers.

After completion of the instrument borehole, approximately six inches of a mixture of equal parts of #8 Fine and #4 Filter Pack sand was deposited in the bottom. The TDR probe was then inserted in the sand. The suction lysimeter was taped to the tensiometer and lowered until just above the TDR probe. A spacer was inserted between the tensiometer and suction lysimeter to prevent voids and ensure proper operation of both instruments. The colloid sampler was taped to the 3/8" PVC pipe protecting the TDR probe's coaxial cable, and lowered into the borehole until it also was just above the TDR probe. The sampling point was then filled with sand and the borehole sealed with granular bentonite (Figures 3 and 4). In boreholes used for bi-level sampling points, the bentonite fill was halted at the lower elevation of the upper pack and the above procedure was repeated, with bentonite filler above the sand pack continuing to the surface (Figure 4). Upon excavation, it was apparent that voids in the sand pack had been avoided, and that the bentonite had swelled and succeeded in preventing intra borehole flow between the upper and lower sampling points (Appendix VI, Plate 49).

The TDR probes could have been inserted in the parent material. However, under the saturated conditions generated by the ponded infiltrometer, changing soil moistures in the parent material were not important, and TDR soil moisture measurements were taken only to ensure that saturated conditions in the instruments packs did indeed occur. Situating the TDR probes in the sand pack also allowed comparison of passive TDR and active soil water sampler tracer concentrations.



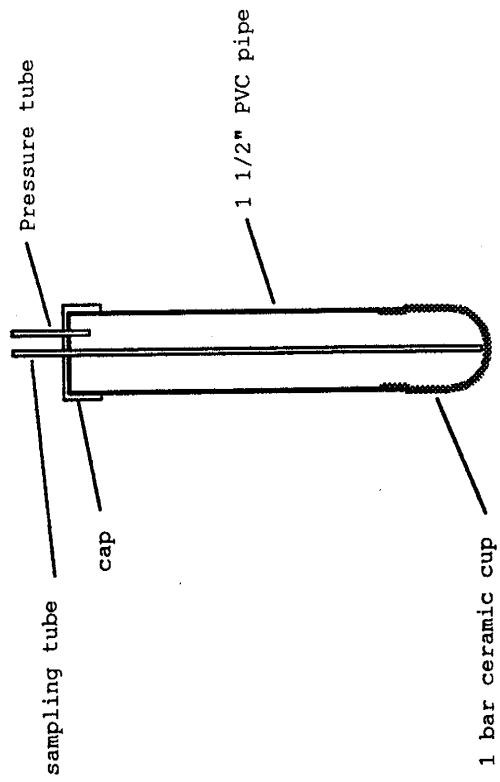
Tensiometer



TDR Probe

Figure 1. Tensiometer and TDR probe construction.

Suction Lysimeter Sampler



colloid sampler

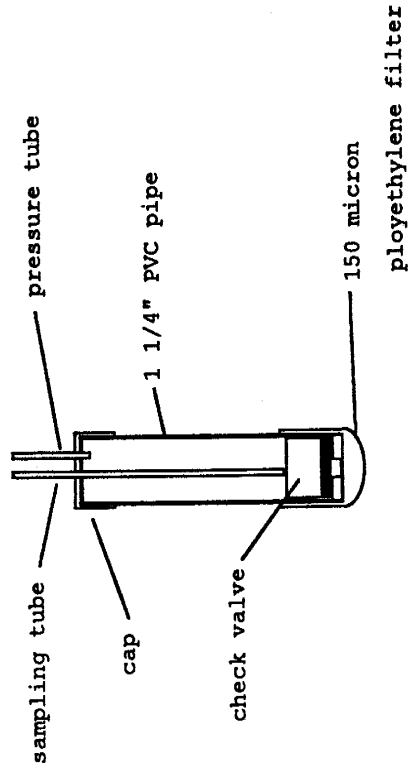


Figure 2. Suction lysimeter and colloid soil water samplers.

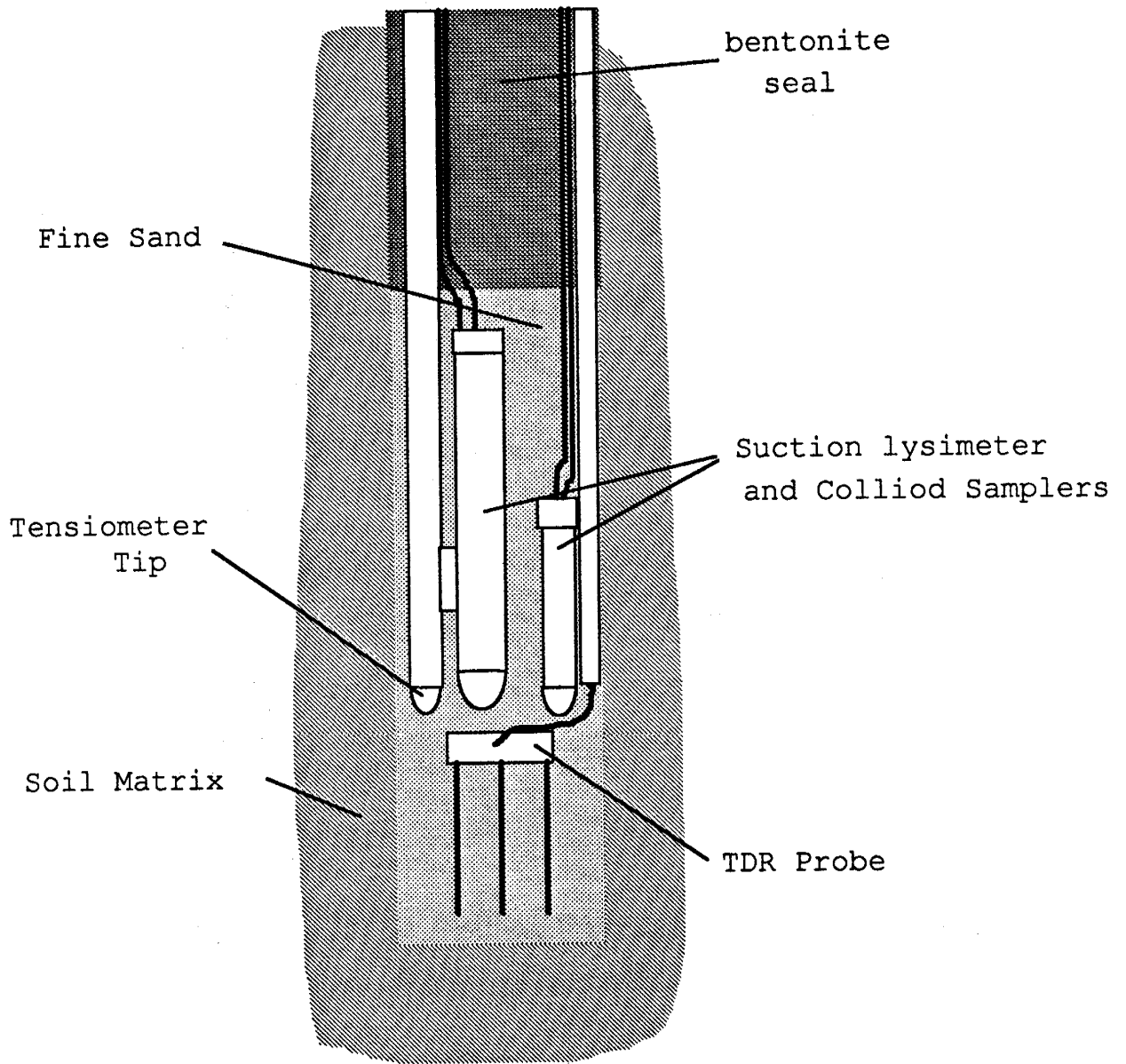


Figure 3. Sampling point instrumentation package.

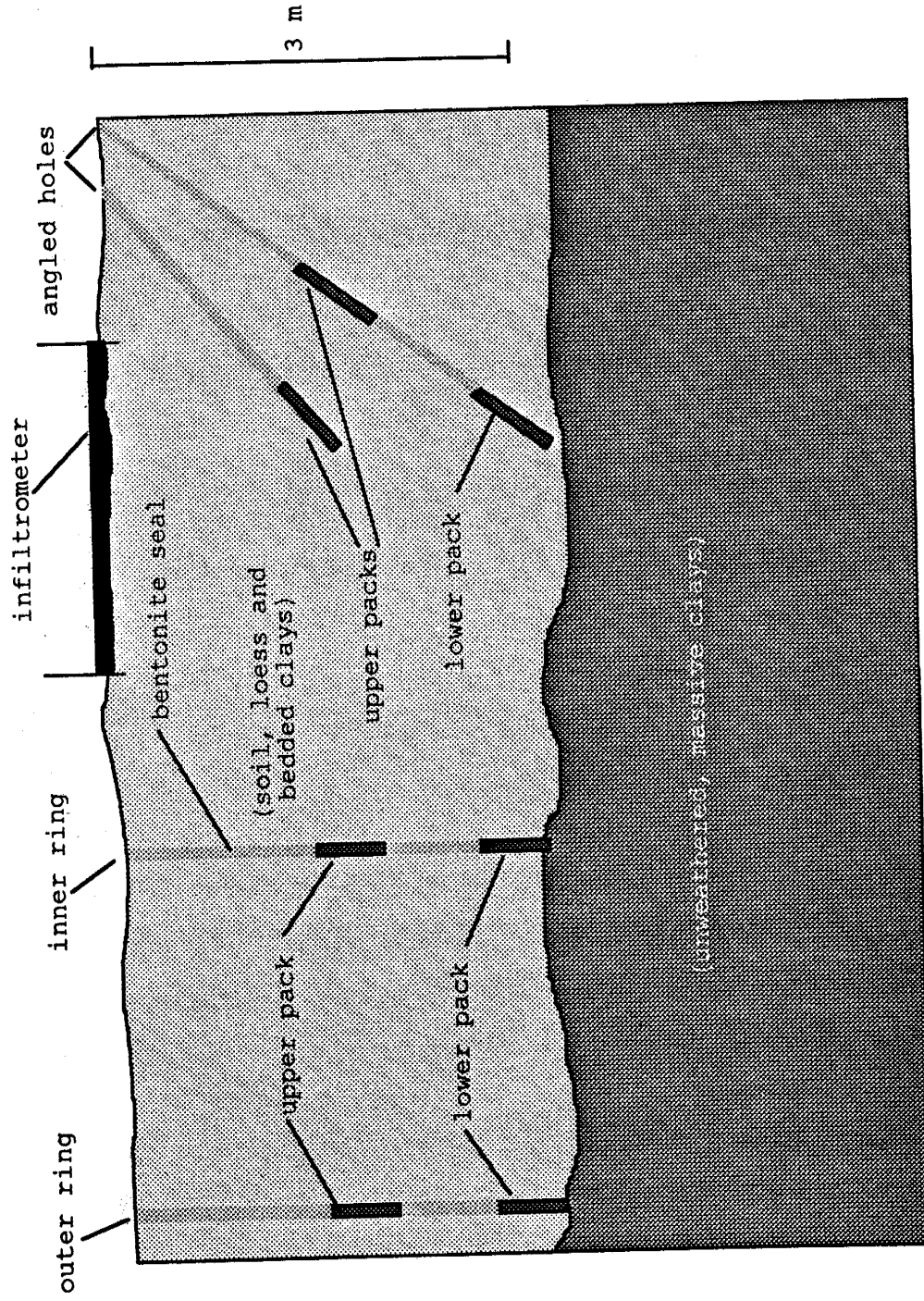


Figure 4. Cross section of ponded infiltrometer and instrumentation array at Site A. The instrument array at Site C is identical, but the geology is different.

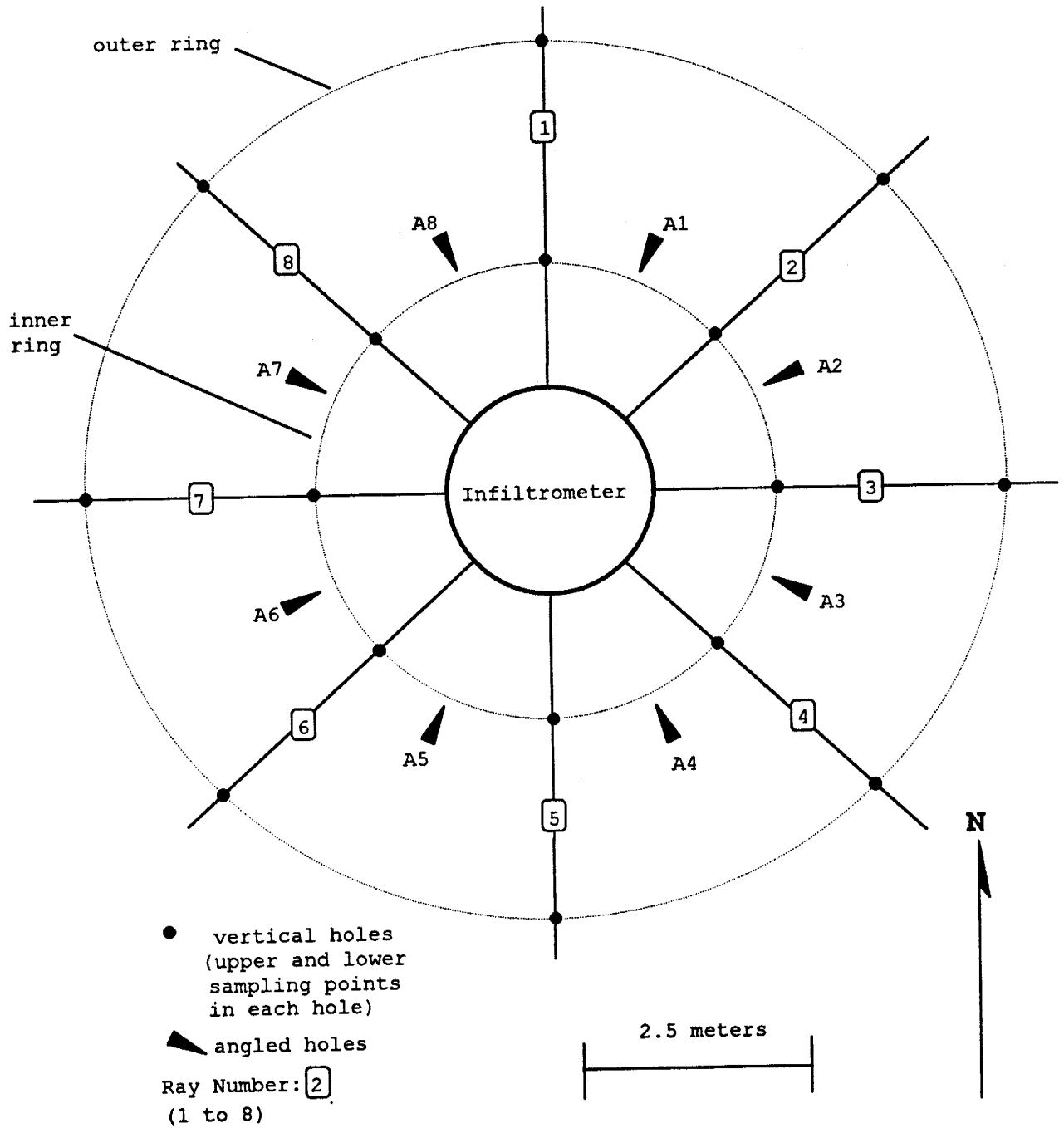


Figure 3. Site instrumentation array.

Site A (Clay Site) Map

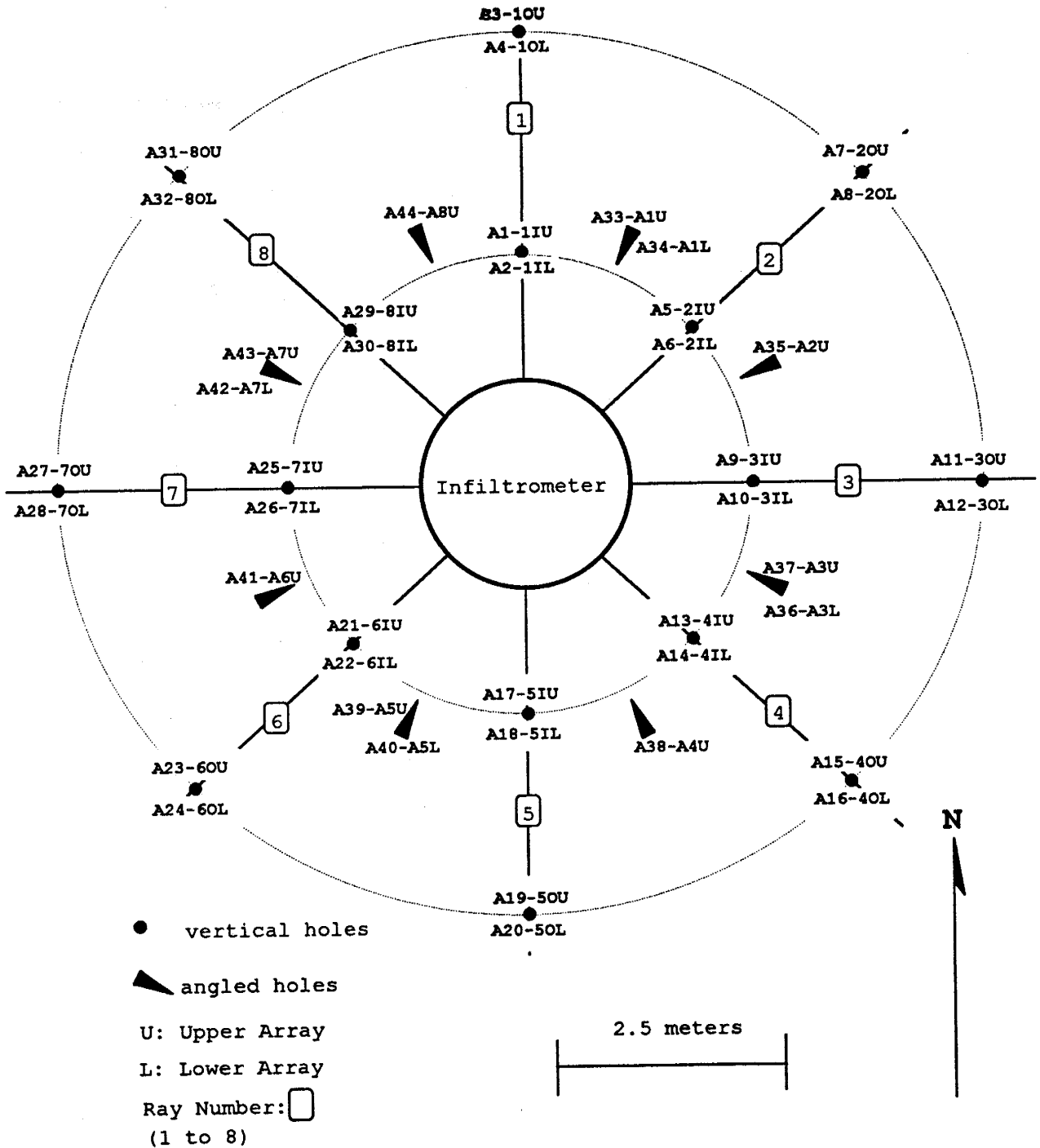


Figure 5a. Site A sampling point layout.

Site C (Sand Site) Map

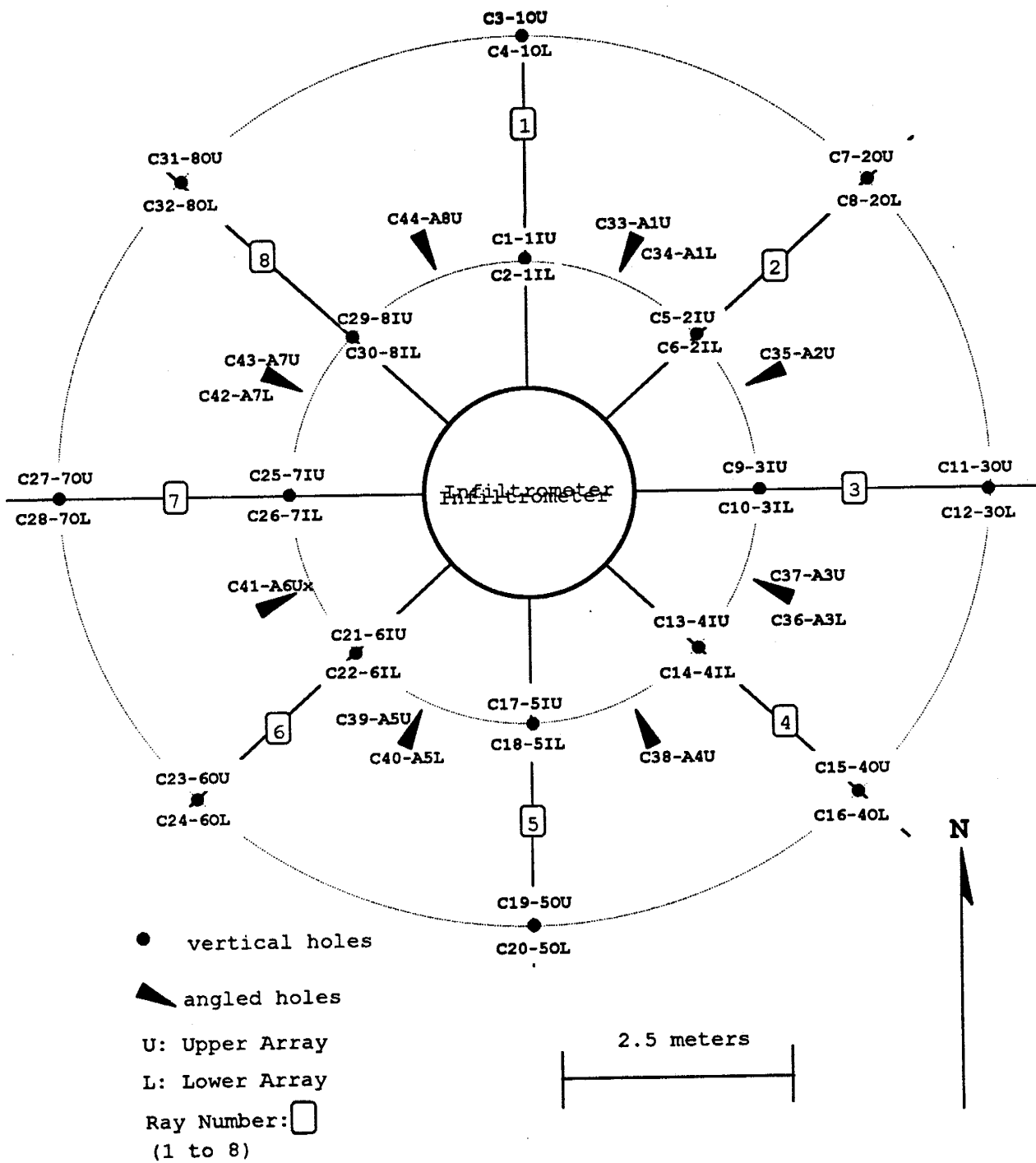


Figure 5b. Site C sampling point layout.

Appendix IV - Colloid and Chloride Tracers

<u>Section</u>	<u>Page</u>
Colloid Tracer	2
Cl ⁻ Tracer Application	2
Soil water Sampling Cl ⁻ Tracer Concentrations	4
Time Domain Reflectometry Measurement of Cl ⁻ Tracer Concentrations	7
Results	11
Tables	14
Figures	18
Graphs of Tracer Concentrations, Site A (Clay Site)	28
Graphs of Tracer Concentrations, Site C (Sand Site)	75

The Transport Processes Characterization Tests (TPCTs) conducted at Paddys Run in Fernald, Ohio were performed as a demonstration of the Transport Processes Investigation (TPI). To provide concentration distribution fields which could be used to determine fast transport pathways and zones of preferential flow, Cl^- and analog colloid tracer pulses were applied at each TPCT site. These pulses were monitored by Time Domain Reflectometry and soil water samplers across radial, bi-level forty-four sampling point instrument arrays (Refer to Appendix III).

Analog Colloid Tracer

A analog colloid tracer pulse composed of 260 mL (2% solids) of 1 mm blue fluorescent and 25 mL (2% solids) of .2 mm yellow Interfacial Dynamics Corporations latex fluorescent microspheres was introduced into the Site A (Clay Site) infiltrometer at 1030 June 20. The water supply to the infiltrometer was shut off on introduction of the analog colloids and resumed after the water containing the analog colloid pulse had dropped to the ground surface in the infiltrometer approximately 5 hours later. A pulse of 25 mL of Interfacial Dynamics Corporations .2 mm yellow fluorescent microspheres was introduced in the same manner into the Site C (Sand Site) infiltrometer at 1030 June 21.

Soil water samples were captured in 15 mL glass sampling bottles to prevent possible adhesion of the microspheres to the polyethylene sample bottles being used for Cl^- tracer capture. The samples were transported to Los Alamos National Laboratory in New Mexico for testing. By the time testing was performed, the fluorescent materials had degraded to the extent that no definable measurement of concentrations could be made, though fluorescent microspheres were detected in the tested samples.

Cl^- Tracer Application

To allow instrumentation identification of transport pathways at the test site, a 0.1M calcium chloride tracer was applied as a pulse through the ponded infiltrometers at Site A (Clay Site) and Site C (Sand Site). The changing salinity concentrations were monitored by TDR and aqueous salinity sampling at forty-four sampling points at each site (Figures 1 and 2). The changing concentrations were graphed in time for each sampling location. A complete set of graphs of the solute transport in time at each sampling point is shown in the last two sections of this appendix.

At the TPCT sites, 12.6 Kg of powdered commercial grade calcium chloride was dissolved in a 50 gallon drum and added to a site supply tank. Water was pumped into the tank to provide 300 gallons total volume of a well mixed 0.1 M CaCl_2 solution. Prior to the introduction of the tracer, the water level in the infiltrometer was reduced as near as possible to ground level without allowing any portion of the infiltrated surface to become unsaturated. The Cl^- tracer was then immediately introduced into the infiltrometer. The tracer pulse was begun at Site A on 1030, June 21 by pouring three 133 liter containers filled with 0.1M CaCl_2 into the infiltrometer and simultaneously opening the valve to the site tank containing the Cl^- solution. An essentially instantaneous 5 cm ponded level in the infiltrometer was attained. Splash

deflectors were used to prevent scouring of the infiltrated surface. The float valves in the infiltrometer maintained a constant 5 cm ponded level of the Cl^- solution flowing from the site supply tank, duplicating infiltration conditions prior to the introduction of the tracer pulse. On 1030, June 22, the same procedure was followed for Site C. Samples were taken from the infiltrometers as part of the normal chloride sampling routine, and used to determine the maximum initial Cl^- tracer concentration, C_0 . C_0 at Site C was determined as 6572 mg/L and 5558 mg/L at Site A. The disparity between the sites, and between the Cl^- target concentration of 7090 mg/L, is caused by topographical pockets of clean water contained within the infiltrometers and absorption of water vapor from the air by the CaCl_2 . The tracer pulses were terminated approximately 48 hours after the start of application. The total salt pulse at Site A was 1534 Liters, and the total salt pulse at Site C was 1209 Liters.

Soil Water Sampler Measurement of Tracer Concentrations

During the TPCTs, Cl⁻ tracer samples were actively collected by means of soil water samplers. The samples were analyzed to determine the concentrations of analog colloid and Cl⁻ tracers used during the test. The discussion in this section concerns sampling procedures, analysis techniques, and compensation for errors. A complete set of graphs of soil water sampler Cl⁻ concentrations for each sampling point at each TPCT presented in the last section of this appendix.

Collection of Cl⁻ samples by soil water samplers

Soil water samples for solute and analog colloid concentration analysis were gathered from either the colloid or suction lysimeter soil water samplers. Because of the ease of operation and the lesser suction which needed to be applied, samples for both the analog colloid and Cl⁻ tracers were obtained from the colloid samplers where possible.

For both samplers, an identical procedure was followed. The sampling and pressure tubes (see Figures 3 and 4) were opened and a positive air pressure was applied to the sampler via the pressure tube with a bicycle-type vacuum/pressure pump, model 2006G, manufactured by SoilMoisture Equipment Corporation. Any soil water which had entered the sampler since the last sampling period was blown from the sampler. The sampling tube was then closed and a negative pressure was induced in the sampler via the pressure tube, after which the pressure tube was closed. After all samplers in the array had been cleansed of old water and a suction applied, usually taking 30 to 60 minutes, a fresh soil water sample was obtained. The sampling and pressure tubes were opened, and a positive pressure was again applied to the pressure tube, forcing out the fresh soil water sample through the sample tube. To prevent cross contamination during sampling of other points, both sampling and pressure tubes were kept closed except when actually sampling.

For Cl⁻ tracer analysis, the sample was captured in Nalgene brand polyethylene sample bottles. Sampling was done by two person teams, one person operating the pressure/vacuum pump and the other filling the sample bottle from the sampling tube. This procedure delivered a sample concentration in a 30 to 60 minute time span. The frequency of sampling is given in Table 1. One week prior to the introduction of the Cl⁻ tracer, sampling was carried out to establish baseline concentrations and introduce the sampling crew to the technique and procedure. The sampling frequency during this period was once per 24 hours.

The initial *in situ* soil water temperature was cold enough that "Sharpie" brand permanent markers did not adhere to the Nalgene bottles. On early samples the labeling was easily rubbed off. Sample bottles were re labeled with paper labels, and a few samples from the first days after the salt pulse may have been mislabeled in the process. Paper labels were used the remainder of the sampling period. Any sample with unreadable or questionable labeling was not analyzed.

The samples were shipped from Fernald, Ohio to Sandia National Laboratories in Albuquerque, New Mexico via Federal Express. The chloride tracer samples were then analyzed for chloride concentration.

Analysis of Cl⁻ concentrations in soil water samples

Salinity concentrations in mg/L were obtained with an Orion Benchtop pH/ISE Meter model 920A and a model 94-17B chloride combination electrode. The two probes of the combination electrode were inserted into the unagitated sample bottle and held just above the bottle bottom until the reading stabilized. The readings were manually entered, along with date, time and location, into a spreadsheet program. The probes were then rinsed with deionized water and immersed into two 5 liter Nalgene bottles of deionized water. Excess water was shaken from the probes and the sides of the probes wiped with a Kim-wipe before the probes were inserted into the next sample.

Sample Run 1

Analysis of Cl⁻ tracer concentrations from soil water samplers was done in three batches or runs. Sample Run 1 refers to the majority of the 2341 sample analyses. Samples in this run were analyzed without benefit of buffering with an Ion Strength Adjuster (ISA) solution (See Sample Run 2 below). Calibration standards were prepared by diluting the Orion chloride standard solution number 941706 with deionized water. The instrument calibration was done according to manufacturer's recommendations on page 8 of the Orion *Chloride Electrode Instruction Manual*. On page 6 of the Orion Chloride Electrode instruction manual it is recommended that re calibration of the instrument be performed every two hours during normal operation. A drift in the instrument calibration occurs between calibrations and was noticed when periodically analyzing the standards to verify calibration. Quantification of drift error was accomplished by comparing the salinity concentration measurements of the standards immediately after re calibration (S_i) to the salinity concentration measurements of the same standards immediately before the next calibration (S_f). Results are given in Table 2. After analysis the samples were archived for future reference.

Sample Run 2

Sample Run 2 refers to the test of the Ion Strength Adjuster (ISA), and accompanying error analysis. The ISA, a buffering solution, was obtained from Orion with the understanding that the instrument readings would be returned quicker and accuracy would be enhanced. The ISA solution is 5 M sodium nitrate which lowers the pH to an optimal level and complexes out interfering ions. The ISA solution was added as 2 mL per 100 mL of sample, or 0.30 mL for the 15 mL samples used in this test. To check the efficacy of the ISA solution, four sampling points in site A were chosen for re analysis. Using the ISA solution, Cl⁻ concentrations were rechecked from the start of the Cl⁻ pulse to the end of the samples available at the time of the test. The comparison of ISA versus non-ISA analyses are shown at four sampling points in Figures 5 to 8. The ISA and non ISA concentration analyses showed good correspondence at low concentrations, but significant variation was observed when measuring peak concentrations.

A blind comparison test was also done during Sample Run 2 by inserting at least nine known solutions of each calibration concentration into the normal sampling process. The standard solutions for the error analysis were made from reagent grade sodium chloride and distilled water. The concentrations were introduced into the normal sampling stream. Table 3 gives the statistical analysis of the results of the blind test. Results of the drift error analysis and the blind test indicated re calibration could be performed using only the smallest standard (3.545 mg/L). This provided acceptable readings when the re calibration was rechecked against all standards.

Sample Run 3

The results from Sample Run 2 prompted re analysis samples from twenty-four hours before and to twenty-four after peaks, obvious inconsistencies, and questionable data in the salinity breakthrough curves. Four hundred and fifty seven samples were selected for re analysis. Of the four hundred fifty seven samples in Run 3, two hundred eighty nine comparisons were possible between the unbuffered analyses of Run 1 and the buffered analyses of Run 3. Buffered results from Sample Run 2 were incorporated into the data set yielding a final total of 371 buffered/unbuffered time and sampling point correlations. The results of the buffered and unbuffered assays are plotted against each other in Figure 9. The resulting regression equation of "Buffered = 1.055*Unbuffered + 7.978" (shown in Figure 9) was used to adjust the mg/L salinity concentrations of unbuffered samples. The R² value for the regression equation is .975. The greatest deviation is shown at peak values. Because all peak concentrations were re analyzed, this disparity does not affect final values or data interpretations.

Time Domain Reflectometry Measurement of Cl-Tracer Concentration

Time Domain Reflectometry, or TDR, is a relatively new but accepted method of monitoring both soil moisture and soil water salinity. Utilizing an automated signal generator and multiplexed switches controlled by a microprocessor (Refer to Glass et al, 1995), it provides an efficient method of monitoring these essential hydraulic variables in both time and space. Building on the scoping study conducted the previous year, fully automated data acquisition systems were constructed and installed at the 1994 TPCTs. A full set of TDR graphs for each sampling point is presented in the last section of this appendix.

The system used at Site C consisted of a Tektronics 1502B signal generator and receiver, a JFW 32 port automated coaxial cable switch, an array of thirty-two three prong probes (Figure 10), and a Compaq "Contura" 486-25X laptop computer for system control and data acquisition. Data for the calculation of soil moisture and soil water salinity at Site A was gathered by two separate systems, each with a Tektronics 1502B signal generator and receiver, a single automated 24 port JFW coaxial cable switch, an array of twenty-four three prong probes, and a Compaq "Contura" 486-25X laptop computer for system control and data acquisition. All systems were battery powered with two deep cycle 120 amp hour marine batteries, which were replaced with fully charged units every two days.

Soil moisture analysis

Soil moisture calculations were accomplished using the algorithm developed by Topp et al (1980). The data reduction algorithms used were sufficiently accurate to render soil moisture measurements with an repeatability of plus or minus .015. Soil moisture measurements reflect soil moistures within the instrument sand packs (See Appendix III) and were used only to determine that conditions were saturated or essentially saturated. TDR soil moisture and soil water tracer concentration measurements in time, with corresponding soil water sampler concentrations, are presented for both Site A and Site C in the last section of this appendix.

TDR soil water salinity analysis

Analysis of the reflected TDR wave form may also be used to calculate soil water salinity concentrations (Dasberg and Dalton, 1985; Kachanoski et al., 1992, and Wraith et al., 1993). The TDR systems used in the TPCTs were controlled by a software program configured to gather information which would yield both soil moisture content and soil water salinity concentrations.

Salinity analysis was initially attempted utilizing the method of Wraith et al (1993) :

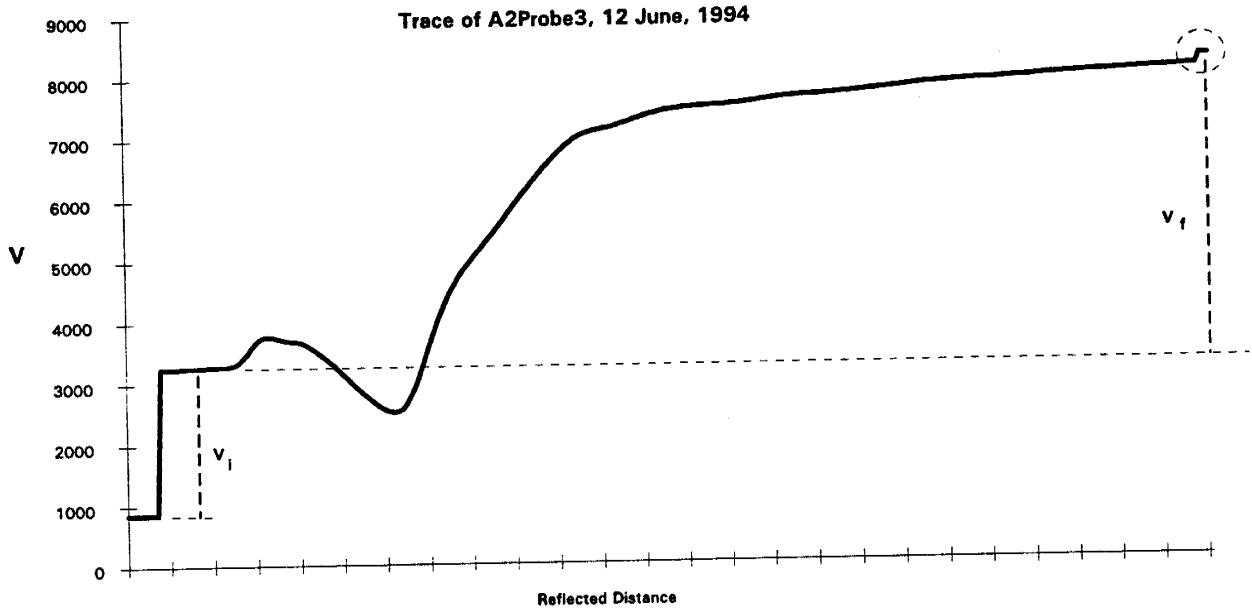
$$\sigma = \frac{f_t}{Z_1} K, \text{ with}$$

σ = bulk soil electrical conductivity
 Z_1 = the resistive impedance
 K = probe geometric constant
 f_t = a temperature correction factor

The resistive or load impedance, Z_L , is computed using:

$$Z_L = Z_o \frac{(V_i + V_f)}{(V_i - V_f)} \quad \text{where } \begin{array}{l} Z_o = \text{transmission line nominal impedance} \\ V_i = \text{the incident voltage} \\ V_f = \text{the final voltage} \end{array}$$

V_i and V_f are measured as illustrated below:



The figure above is the actual trace of the reflected TDR wave form at sampling point A3-10U, 12 June, 1994, showing values of the reflected incident (V_i) and final voltage (V_f) values.

It is apparent from the relative magnitudes of V_i and V_f above, that the quantity $(V_i - V_f)$ will be negative, rendering both resistive impedance, Z_L , and the bulk soil conductivity, σ , also negative. Correspondence with Jon Wraith disclosed no apparent reason for this seeming impossibility. A study of Wraith et al. (1993), Nadler et al. (1991), Dalton et al. (1984), and Kachanoski et al. (1992) found that the potential existed in all methods for the calculation of negative soil conductivities. Thus, an alternative approach was needed. Since the change in soil water conductivity is indirectly proportional to the change in V_f , we adopted an empirical relationship:

$$\frac{C}{C_o} = \frac{1}{R} \frac{(V_{f_o} - V_{i_o}) - (V_{f_i} - V_{i_i})}{(V_{f_o} - V_{i_o})} = \frac{1}{R} \frac{(V_{f_o} - V_{f_i}) - (V_{i_o} - V_{i_i})}{(V_{f_o} - V_{i_o})}$$

where:

- C = concentration at the probe some time during the tracer pulse
- C_o = initial concentration of tracer the start of the pulse
- V_{f_t} = final reflected voltage at some time during the tracer pulse
- V_{f_o} = final reflected voltage at the start of the tracer pulse
- V_{i_t} = initial reflected voltage at some time during the tracer pulse
- V_{i_o} = initial reflected voltage at the start of the tracer pulse
- R = an empirical correction factor

In the above equation, the quantity $(V_{f_o} - V_{f_t})$ represents the drop in the final reflected voltage due to the increase in soil water salinity, the quantity $(V_{i_o} - V_{i_t})$ normalizes the changes due to effects on the system other than changes in soil water salinity, and the quantity $(V_{f_o} - V_{i_o})$ represents the difference between incident and final reflected voltages at a baseline concentration. The baseline concentration chosen was the average of $(V_f - V_i)$ for the twenty four hours immediately prior to the introduction of the salt pulse.

Comparison of TDR and soil water sampler concentrations

This approach provided excellent correspondence with soil water sampler results in cases where a significant breakthrough curve was found, especially during the rising limb and peaks. A comparison of TDR and soil water sampler C/Co ratios at sampling point A36-A3L throughout the period of the test is shown in Figure 11. A complete set of graphs of simultaneous soil water sampler and TDR tracer concentrations are presented in the last section of this appendix.

While the early time trends and peak values of soil water sampler and TDR concentrations correspond well, there is a definite disparity in values following peak concentrations. Changing soil and soil water temperatures due to the infiltration of warmer (95° F.) water from the ponded infiltrometer, chemical perturbation of the media, and colloidal influences may be responsible for this deviation..

Soil water temperatures were not taken during the test, but temperatures during early sampling were low enough to cause the normally reliable "Sharpie" brand markers to fail in labeling polyethylene sample bottles when filled with *in situ* soil water samples. The basic theories allowing conversion of TDR data to soil water conductivities all recognize the effect of temperature (Dasberg and Dalton, 1985; Kachanoski et al., 1992; and Wraith et al., 1993). The divergence between TDR and suction lysimeter measurements increases with time, as would be expected for increasing soil water temperatures.

Another reason for the deviation may be measurement by TDR of ion concentrations other than Cl⁻. It is reasonable to assume that the infiltrated Cl⁻ ions would exchange with other ions present in the soil matrix; e. g., $\text{CaCO}_3 + 2\text{Cl}^- \rightleftharpoons \text{CaCl}_2 + \text{CO}_3^{2-}$. This would yield soil

water with an total ion concentration greater than just the Cl^- concentration. Because the TDR measurement is a reflection of the bulk soil water conductivity, this additional ion concentration would be reflected in the TDR measurements but not in the ion specific Cl^- analysis of soil water samples.

Colloidal influences may also play a part. During boring of the sampling points, disruption of the soil matrix is inevitable. The agrillaceous nature of the soil resulted in high concentrations of suspended clay particles in many sample points. It is possible that clay colloids may have been flushed from the matrix and transport pathways by the infiltration itself. Because the baseline C/C_0 ratio was taken as the twenty-four hours immediately preceding the salt pulse when the colloid suspension would still be relatively high, a changing colloid density may also influence TDR measurements as fresh water from infiltration flushed sampling points. Laboratory experiments are ongoing to define and quantify the source or sources of the differences between soil water sampler and TDR solute concentration measurements.

Lack of data in unsaturated conditions

A TDR system configured to deliver valid data over a large range of soil moistures will not provide great resolution and accuracy at any particular soil moisture. Because the TPCT simulates the worst case saturated conditions, the TDR system was optimized for saturated or near saturated media. This provided greater resolution of both relative salinity concentrations and soil moistures. In instances where the instrument packs did not approach saturation, primarily the upper outer ring sampling points and some of the upper inner ring sampling points at Site C, the TDR settings resulted in off scale readings (noted as "bad data" in plots).

Results

Cl⁻ Tracer Movement

A study of tracer concentration movement in time at Site A shows a definite westerly radial trend. Solute concentrations appear to initially increase in the upper level instrument packs located in the silty sand body in the Northwest quadrant of the site. Peak concentrations then occur in the lower level instrument packs in the Northeast (A6-2IL, Figure 1) and then quickly decrease. This initial northeast movement was followed by concentration increases due West in the lower packs of Ray 7 (A26-7IL and A28-7OL, Figure 1) where concentrations peak and then decline to almost zero after approximately 500 hours.

The higher Cl⁻ tracer concentrations at the 2 meter level in Site A generally occur in the silty sand body located in the Northwest quadrant of the site (Refer to Appendix I, TPCT Site Geology Section and Appendix VI - Dye Pulse and Excavation). The peak tracer concentration observed in the upper sampling pack (2 m level) of the outer ring at the Northwest ray (Ray 8, sampling point A31-8OU, peak C/Co = .35) was greater than the peak concentration observed in the sampling pack immediately below at the 3 m level (sampling point A32-8OL, peak C/Co = .12) and almost equivalent to the concentrations observed in the lower sampling points on the outer and inner rings of the West ray (Ray 7, sampling points A26-7IL and A28-7OL), indicating that the Cl⁻ tracer may have moved preferentially through the silty sand body in the Northwest quadrant of the site at the upper level, then down to the lower level in the West, bypassing the lower Northwest level almost entirely. This would be consistent with the glacial emplacement of the sand body between units of layered clays. The site excavation (See Appendix VI) revealed that sand stringers from this silty sand body penetrated the bedded clays of Units 2 and 3 and that one emerged at sampling site A28-7OL, three meters below the surface. Pink dyed water (Appendix VI, Plates 77 and 78) could be discerned seeping from the sand stringer at this location and the salinity concentrations at this sampling point were both higher and sooner arrived than at any adjacent sampling sites at the three meter level, or at the sampling site directly overhead at the two meter level (Refer to the graphs of tracer concentration in time at the end of this appendix).

The lack of any significant tracer concentration sensed by the sampling points in the South and Southeast portion of the site may be a true reflection of the flow direction or a result of transport through unintercepted active fractures and crayfish burrows, frequently encountered in that region during excavation (See Plates 56, 81, 82, and 83 in Appendix VI). Where bioturbated fast transport pathways and zones of preferential flow exist, interception by tracer sampling instrumentation may be disproportionate. Because of the dominance of preferential flow and fast transport pathways and the relatively small volumes intercepted by the instrument packs, such trends must be treated with caution.

Movement of tracers at Site C was less complex. Peak concentrations are contained in the volume almost directly beneath the infiltrometer until approximately 120 hours. Concentrations then increase horizontally over the area of the sampling array, with slightly higher concentrations in Northeast and Southwest sampling locations. Concentrations do not

decline to negligible levels until over 800 hours after the beginning of the tracer pulse. It would appear that tracer movement is initially downward and then spreads laterally, moving preferentially to the Northeast and Southwest directions. Other than directly under the infiltrometer, the peak concentrations at Site C never reach the same levels as in Site A. The Cl^- tracer also takes longer to disperse at Site C. As with Site A, the small volume of media investigated by the sampling array and the possibility of preferential flow dictates that these patterns must be viewed cautiously.

In both sites the Cl^- tracer movement can be discerned moving at first vertically through the topsoils and blocky structured silty clays of Units 5 and 4 and then spreading laterally at depth. As the tracer flow at Site A encountered the planar structures of the bedded clays of Units 3 and 2 (refer to Figure 5, Main Report), it began moving horizontally, notwithstanding the initial lateral flow through the silty sand body in the Northwest upper levels of the site.

TDR indications of preferential flow

Sampling point A35-A2U was intercepted by a worm hole (Plate 30). Forty-five minutes after introduction of the Cl^- tracer into the infiltrometer 2 m overhead, TDR measurement of relative tracer concentration went almost instantaneously off scale ($C/C_0 > 0.45$, Figure 12), indicating the presence of a fast transport pathway at that location. Direct interception of sampling packs by such transport pathways is rare even with the intense instrumentation of the TPCTs, but other means are possible to determine the existence of fast transport pathways and preferential flow.

Repeated peaks in breakthrough curves are also strong evidence for the existence of preferential flowpaths or secondary transport pathways. Figure 13 illustrates the contributions of both a primary and secondary solute transport pathway.

The artificial flow field induced by the 70 to 80 PSI suction placed on soil water samplers during the sampling process has an effect on tracer concentration distributions in time. Differential measurement by TDR and soil water samplers of peak magnitudes and arrival times may be used to postulate the existence of preferential flow paths. Where the soil water sampler is between the tracer source and the TDR probe, the tracer will be drawn preferentially to the soil water sampler while at the same time clean water will be pulled past the TDR probe. The effect is illustrated in the results from sampling site A31-8OU (Figures 14a and 14b). The flow field induced by active soil water sampling results in higher peaks and earlier arrival times at the suction lysimeter than the TDR. In the comparison of TDR and soil water sampler tracer concentrations where a significant breakthrough curve was experienced, 7 times in Site A and 3 times in Site C the soil water sampler yielded significantly earlier breakthrough times and higher peak concentrations than the TDR probe.

The opposite result may also be gathered from the pathway geometry illustrated in Figure 15a. In this configuration, the suction applied to the soil water sampler would cause solutes to arrive first and in greater concentrations at the TDR probe, as happened at sampling point A25-7IU (Figure 15b). The abrupt and repeated peaks displayed in the TDR trace correspond to soil water sampling times, as the flow field induced by sampling drew Cl^- tracer from a fast

transport pathway past the TDR probe. This situation arose 3 times at Site C, and 4 times in Site A and is a clear indicator of preferential flow or fast transport flowpaths. In any of the situations displayed above, the evidence for preferential flowpaths is apparent.

Tables

A blind comparison test was performed by introducing at least nine solutions of each calibration concentration into the normal sampling process. The standard solutions for the error analysis were made from reagent grade sodium chloride and distilled water. The concentrations were introduced into the normal sampling stream. Table 1 is the statistical representation of the results of the blind comparison.

Blind Test

Bottle Number	standard (mg/L)	measured (mg/L)
9	3.545	3.12
5	3.545	3.24
30	3.545	3.29
26	3.545	3.41
7	3.545	3.43
28	3.545	3.43
1	3.545	3.51
24	3.545	3.88
3	3.545	4.08
6	35.45	31.5
10	35.45	32.5
27	35.45	32.9
2	35.45	33.2
29	35.45	34
25	35.45	34
4	35.45	34.8
8	35.45	35.1
23	35.45	35.7

Bottle Number	standard (mg/L)	measured (mg/L)
13	354.5	303
11	354.5	334
17	354.5	334
15	354.5	348
32	354.5	350
38	354.5	352
34	354.5	356
19	354.5	357
36	354.5	361
40	354.5	371
20	3545	3390
37	3545	3410
12	3545	3550
35	3545	3550
14	3545	3560
33	3545	3580
18	3545	3630
16	3545	3670
39	3545	3750
31	3545	3840

Blind Test Statistics

Standard (mg/L)	Maximum (mg/L)	Minimum (mg/L)	Average (mg/L)	Standard Deviation (mg/L)	Standard Deviation as % of Standard
3.55	4.08	3.12	3.49	0.31	8.66
35.45	35.70	31.50	33.74	1.35	3.80
354.50	371.00	303.00	346.60	19.03	5.37
3545.00	3840.00	3390.0	3593.0	138.49	3.91

Table 1. Blind test measurements.

To quantify the calibration drift, the sample analysis procedure was documented over the four days of July 27, 28, 29, and August 1, 1994. The procedure consisted of the following:

- the calibration was carried out as usual
- the meter was checked against the standards as a reference (S_i)
- after approximately two hours the standards were measured again (S_f)
- the drift, $S_i - S_f$, was then quantified

Results are given below:

Si	Sf	Si - Sf
3.545	2.09	1.455
3.545	2.71	0.835
3.545	5.48	1.935
3.545	0.858	2.687
3.545	3.67	0.125
3.545	9.11	5.565
3.545	3.83	0.285
35.45	32.2	3.25
35.45	31.8	3.65
35.45	34.26	1.19
35.45	32.8	2.65
35.45	35.5	0.05
35.45	40.2	4.75
35.45	41	5.55

Si	Sf	Si - Sf
354.5	352	2.5
354.5	343	11.5
354.5	350	4.5
354.5	354	0.5
354.5	352	2.5
354.5	371	16.5
354.5	351	3.5
3545	3520	25
3545	3410	135
3545	3420	125
3545	3400	145
3545	3620	75
3545	3720	175
3545	3610	65

Measurement of Drift (Si-Sf) Results

Standar	Minimu	Maximu	Averag	Standar Deviatio	Standard Deviation Standard
3.545	0.125	5.565	1.841	1.8761	52.92373
35.45	0.05	5.55	3.0128	1.9213	5.41994
354.5	0.5	16.5	5.9285	5.8268	1.643686
3545	25	175	106.42	52.734	1.487581

Table 2. Results of the Calibration Drift Analysis.

The following tables show the arrival and peak concentration times from the tracer test.

Location	t Start	C Start	t Peak	C Peak	t End	C End	t Total
A1	38.43	94.3	69.53	1263.41	622.05	111.49	583.62
A10	46.18	34.44	190.53	367.04	622.2	115.362	576.02
A11	Baseline Only						
A12	Baseline Only						
A13	333.95	61.15	430.1	85.35			
A14	216.08	34.04	286.23	138.6	815.2	24.37	599.12
A15	Baseline Only						
A16	Baseline Only						
A17	54.87	68.03	526.17	241.2			
A18	Baseline Only						
A2	45.87	140.53	78.2	1089.17	573.92	111.49	528.05
A20	Baseline Only						
A21	78.78	52.54	285.5	256.69	671.95	107.33	593.17
A22	Baseline Only						
A24	Baseline Only						
A25	62.38	55.25	94.55	620	622.53	174.41	560.15
A26	37.57	1369.89	78.92	1882.93	574.78	145.37	537.21
A27	Baseline Only						
A28	46.82	96	118.4	2124.93	574.85	76.64	528.03
A29	32.45	95.23	37.63	450.29			
A3	37.02	528.7	117.52	972.04	573.97	92.13	536.95
A30	38.4	2040	47.62	28.3	622.65	159.89	
A31	37.67	343.81	70.72	1540	430.85	135.69	393.18
A32	62.55	50.6	178.97	543.22	622.68	139.56	560.13
A33	37.5	600.33	86.52	1130	575.13	104.71	537.63
A34	37.33	1270	79.22	2370	790.63	53.8	753.3
A35	No Data						
A36	37.83	257	86.55	1240	790.68	149	752.85
A37	37.87	1002.05	79.22	1880	383.78	193.77	345.91
A38	37.88	194.74	79.25	1360	383.83	28.7	345.95
A39	47.33	1500	79.32	3620	334.9	131	287.57
A4	Baseline Only						
A40	37.92	103.75	131	425.12	384.03	47.89	346.11
A41	37.95	385.43	71.17	3810	622.97	24.37	585.02
A42	37.97	136.66	118.93	801	672.75	126.98	634.78
A43	38	235	167.9	1331.17	384.2	71.3	346.2
A44	38.02	4340	71.3	4850	479.22	52	441.2
A5	37.07	124.07	101.5	769	574.02	164.73	536.95
A6	37.1	842.33	78.35	2212.05	662.15	128.91	625.05
A7	62.08	34.63	285.13	182.15	622.17	46.92	560.09
A8	Baseline Only						
A9	32.23	146.34	86.23	2480	574.12	150.21	541.89

Table 3. Site A. Start, Peak, and End Time(t) and Concentration(C) of the Pulse.

Location	t Start	C Start	t Peak	C Peak	t End	C End	t Total
C10	136.22	27.76	219.67	326.39	651.92	50.51	515.7
C11	Baseline Only						
C12	97.9	39.86	170.08	322.51	651.93	138.95	554.03
C14	Baseline Only						
C16	Baseline Only						
C17	No Data						
C18	158.73	55.25	266.38	342	747.37	55.93	588.64
C19	No Data						
C2	194	71.5	218.08	329.29	554.75	38.31	360.75
C20	410.7	44.7	532.02	85.35			
C21	No Data						
C22	195.12	31.24	458.95	578	747.4	105.39	552.28
C23	No Data						
C24	220.28	50.5	244.13	433	602.38	66.28	382.1
C25	No Data						
C26	213.19	96.3	362.2	308	602.42	67.4	389.23
C27	No Data						
C28	314.28	128.91	506.92	169.57	747.48	68.51	433.2
C3	No Data						
C30	266.52	59	362.33	132			
C31	No Data						
C32	532.12	47.7	771.17	87			
C33	No Data						
C34	52.5	129.88	110.68	2020	458.83	61.44	406.33
C35	76.58	82.55	266.63	342	554.63	24.37	478.05
C36	34.52	101	76.6	2750	458.55	59.702	424.03
C37	No Data						
C38	52.62	1120	76.62	2150	363.67	44.7	311.05
C4	Baseline Only						
C40	52.62	503.53	76.63	1810	363.33	24.37	310.71
C41	28.17	459.97	76.65	4012.53	206.52	98.6	178.35
C42	52.68	35.99	110.82	924.61	410.43	24.37	357.75
C43	No Data						
C44	No Data						
C5	No Data						
C6	82.28	39.08	170.07	653.57	458.85	66.28	376.57
C7	No Data						
C8	266.37	34.05	338.65	107.42	770.82	46.05	504.45
C9	No Data						

Table 4. Site C Start, Peak, and End Time(t) and Concentration(C) of the Salt Pulse.

Site A Map

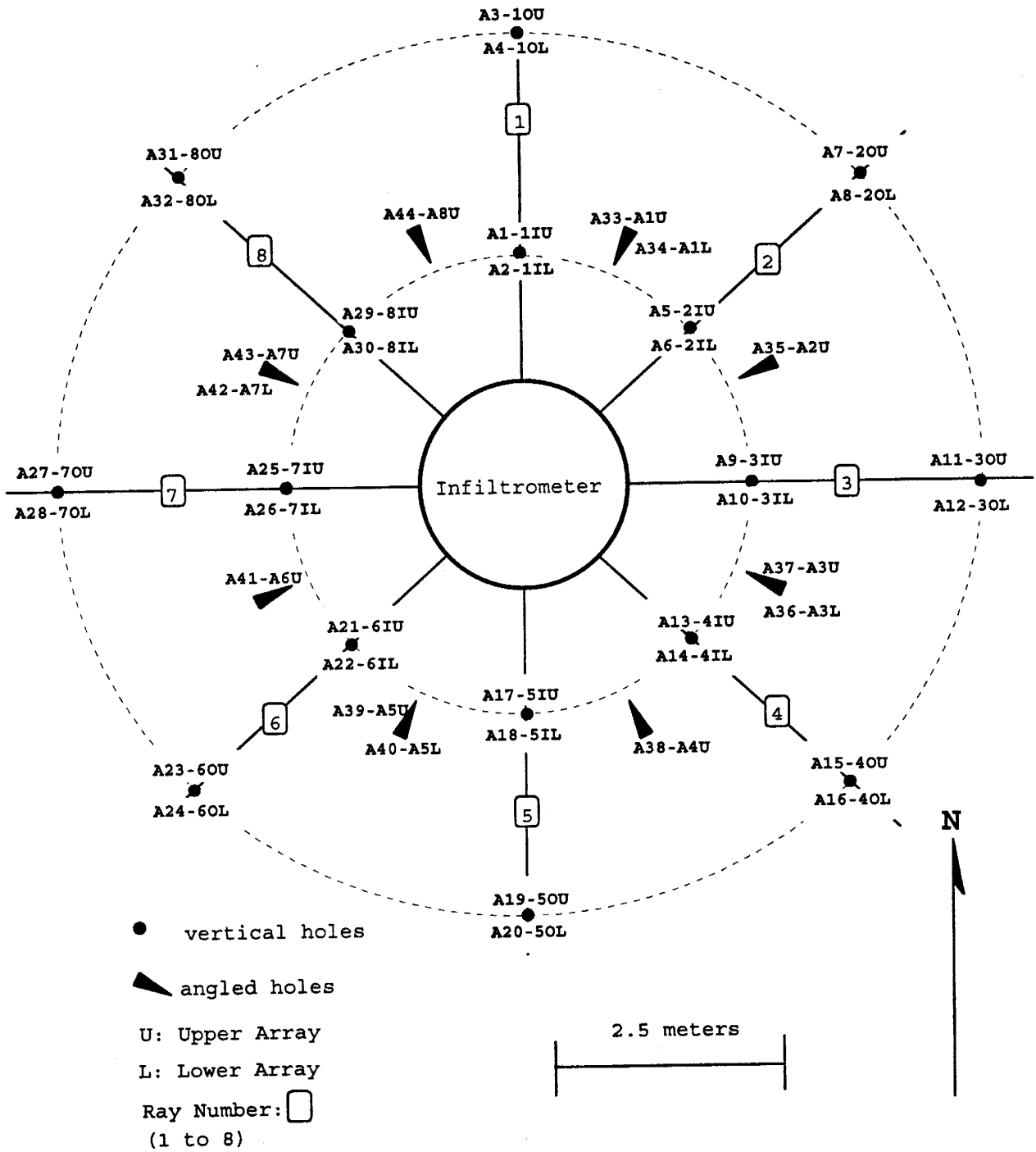


Figure 1. Site A sampling point layout.

Site C Map

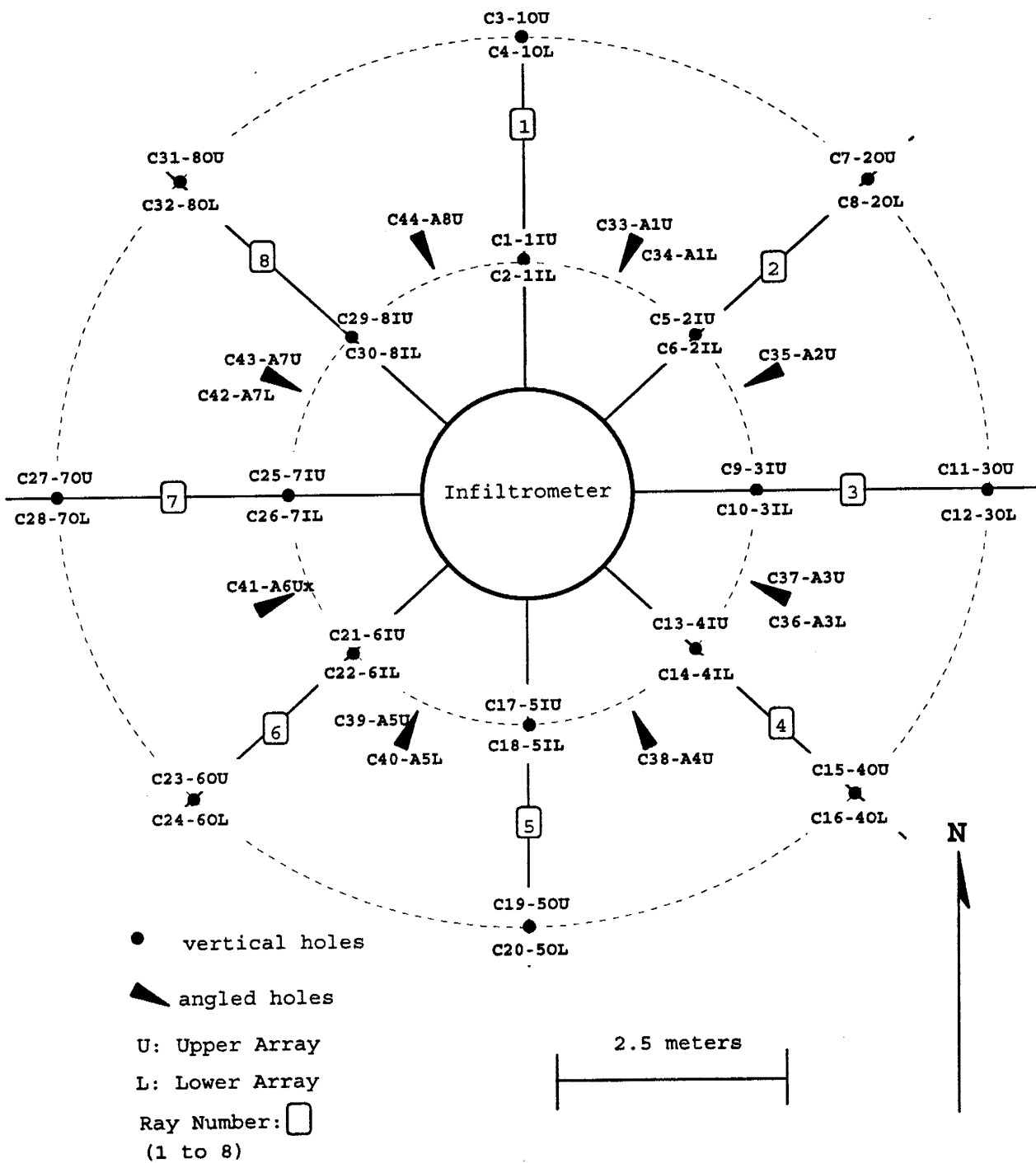


Figure 2. Site C sampling point layout.

Suction Lysimeter Sampler

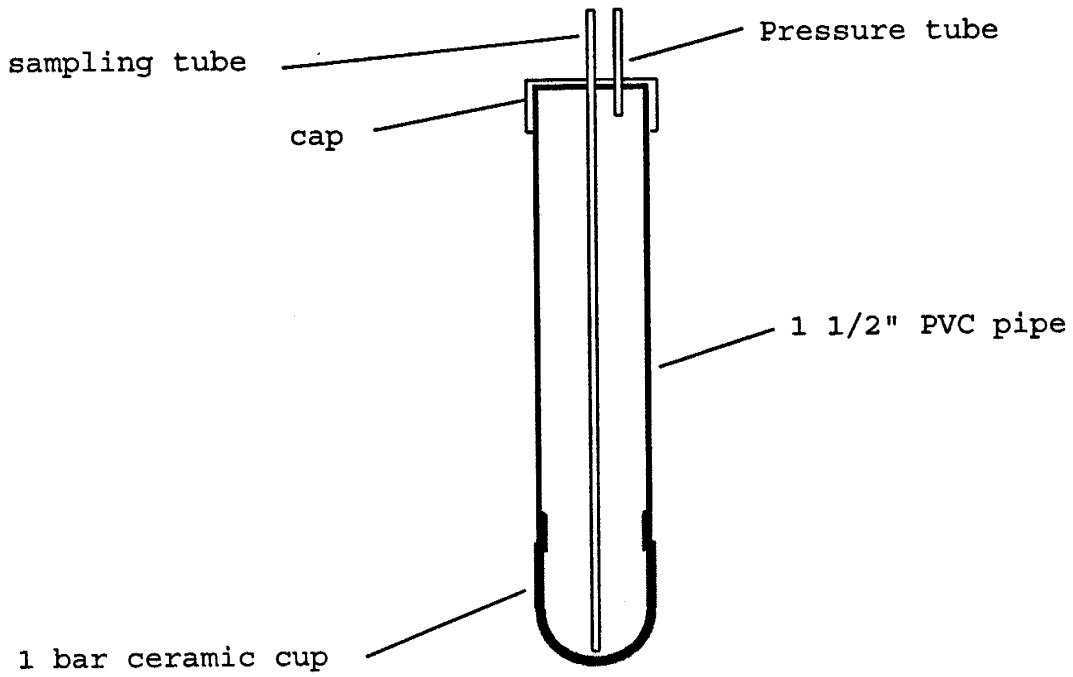


Figure 3. Suction lysimeter.

colloid sampler

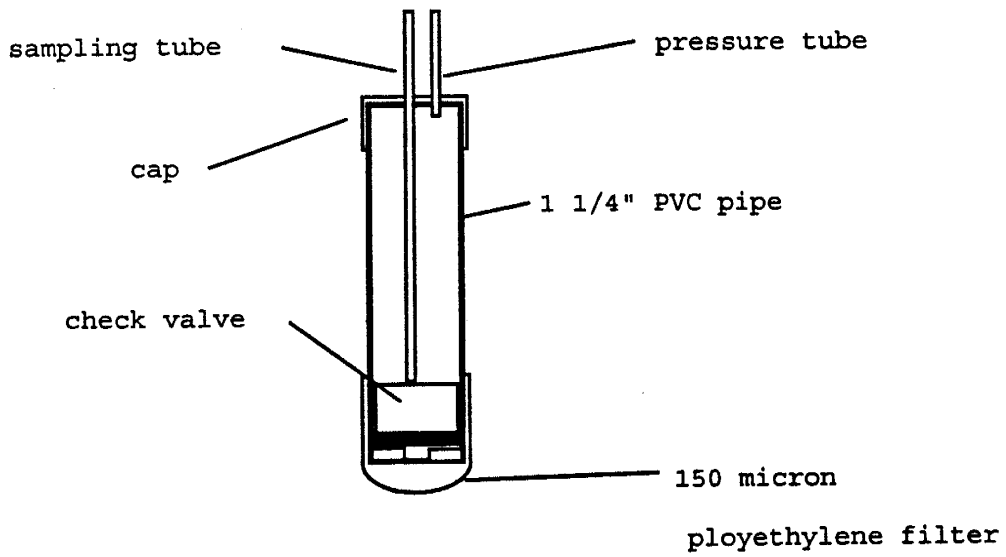


Figure 4. Colloid sampler

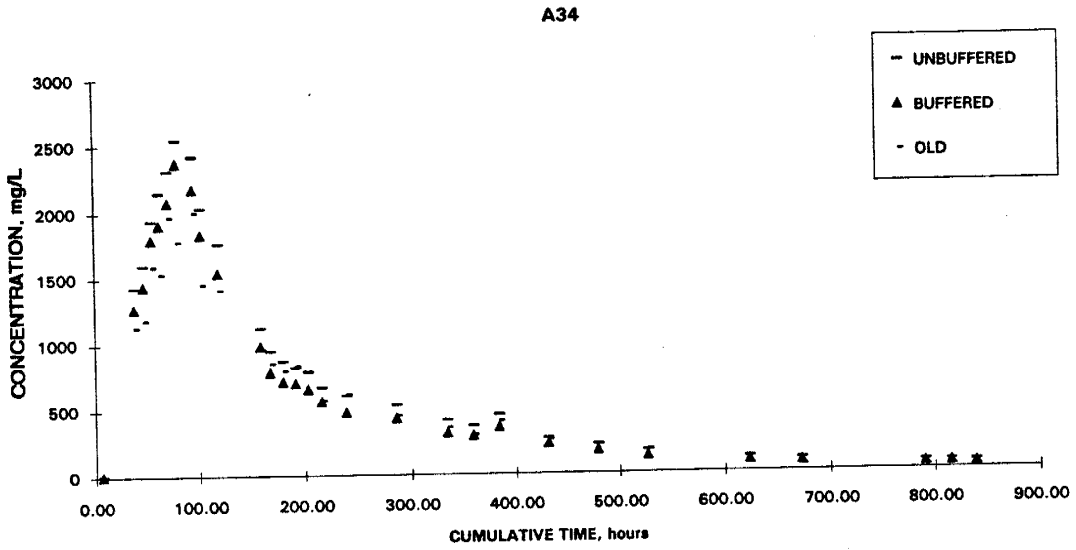


Figure 5. Graphical Results of Sample Run 2. Site A34.

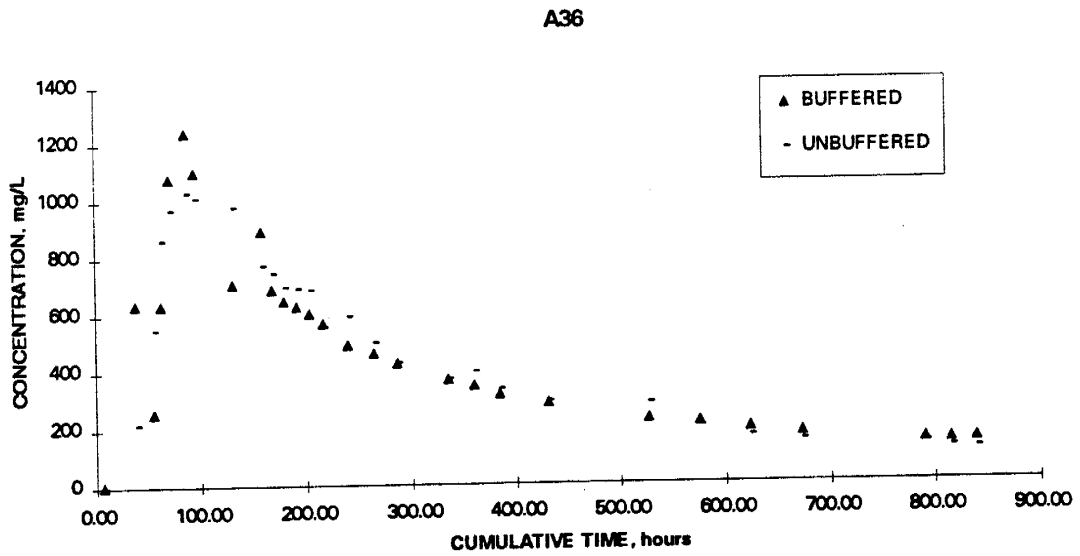


Figure 6. Graphical Results of Sample Run 2. Site A36.

A39

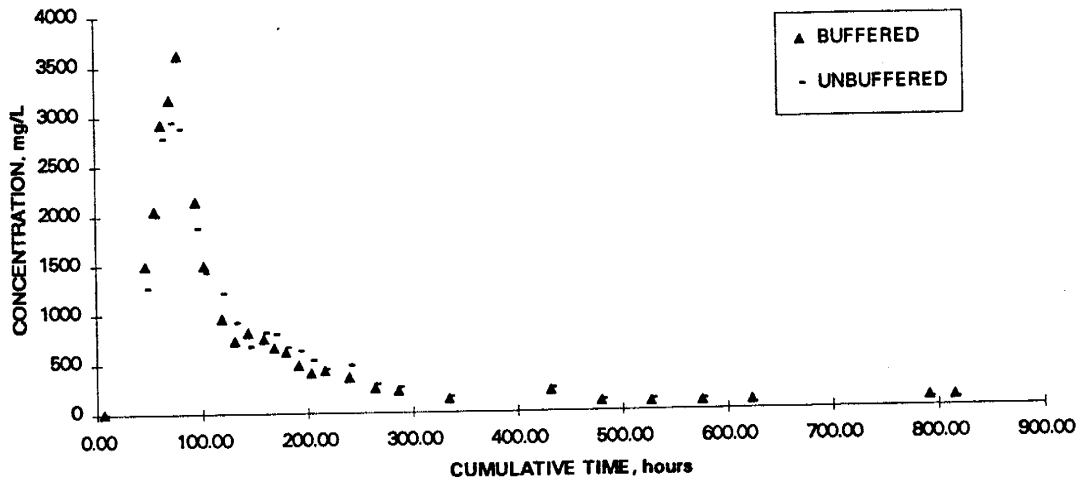


Figure 7. Graphical Results of Sample Run 2. Site A39.

A44

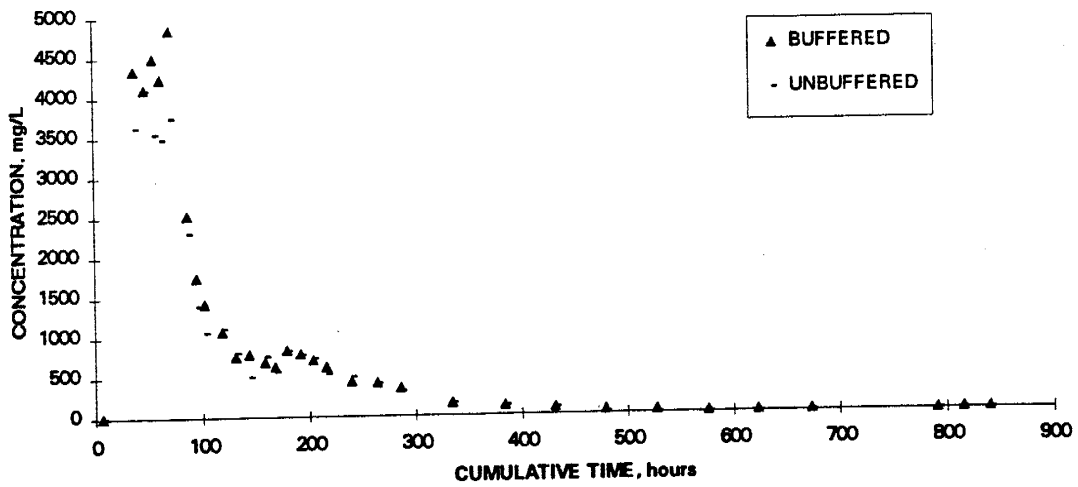


Figure 8. Graphical Results of Sample Run 2. Site A44.

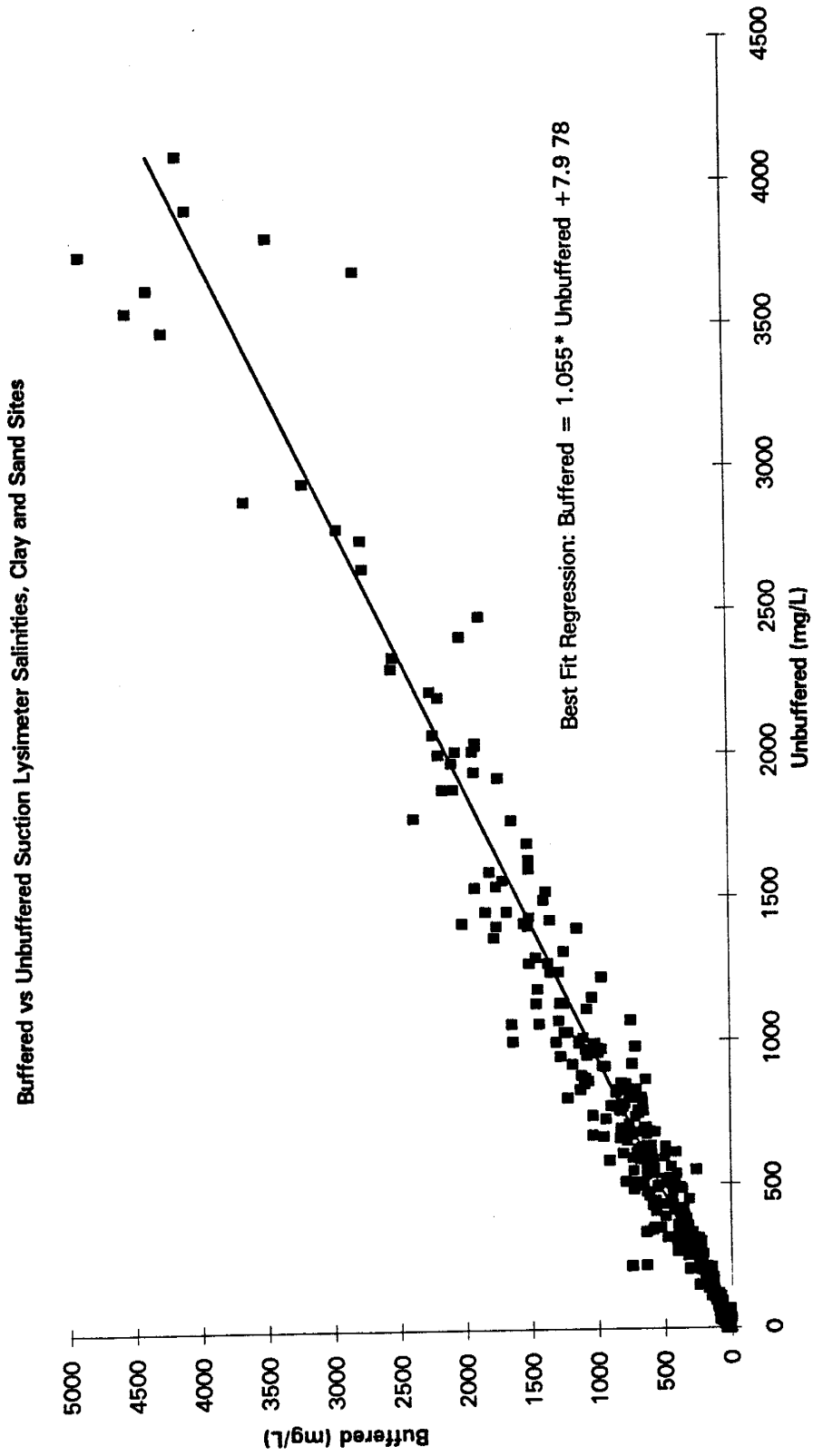


Figure 9. Regression of unbuffered (non-ISA) versus buffered (ISA) salinity analyses.

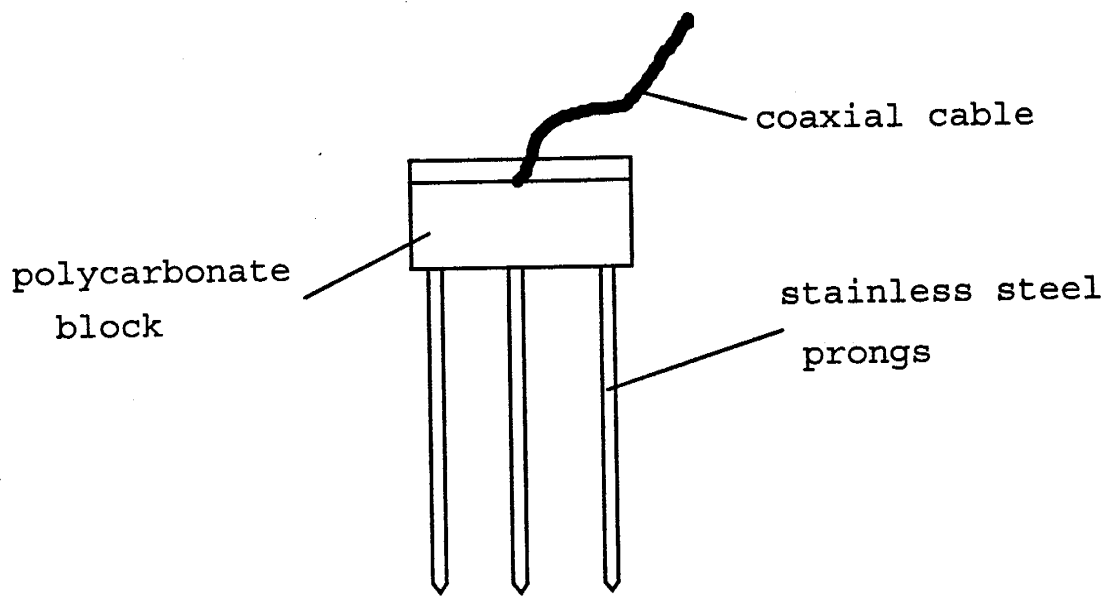
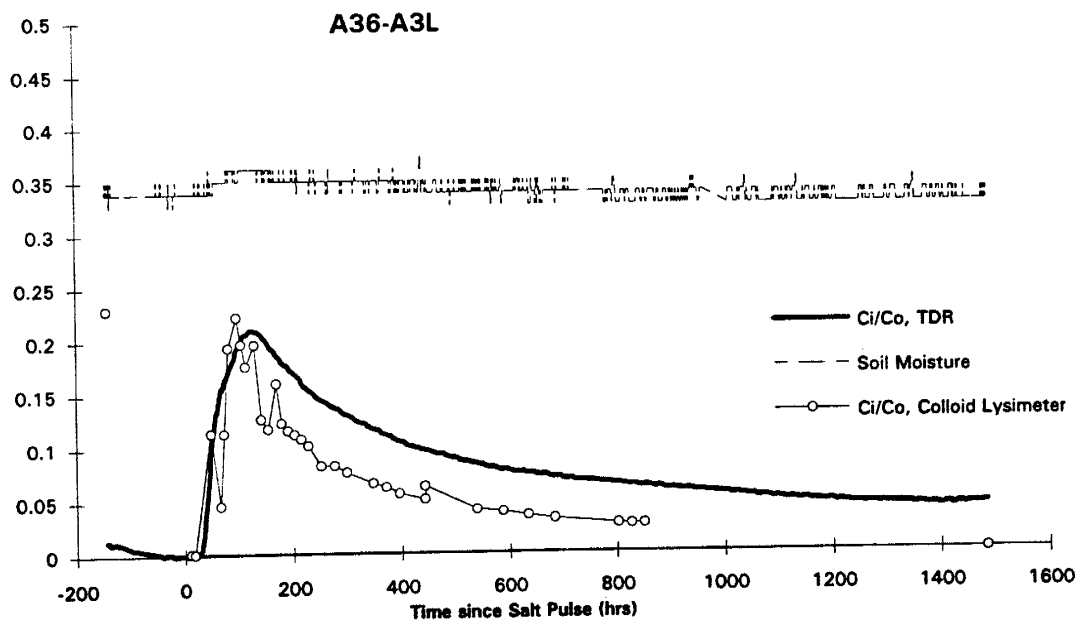


Figure 10. Time Domain Reflectometry probe.



S

Figure 11. Salinity breakthrough curves from TDR and suction lysimeter sampling.

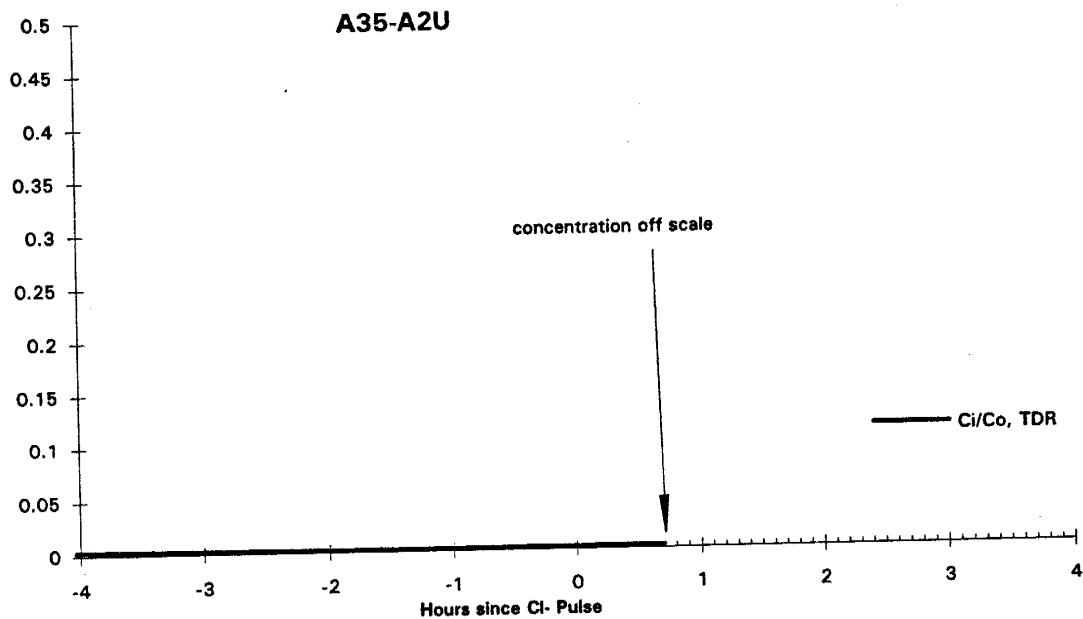


Figure 12. TDR trace showing arrival of Cl^- pulse at sampling site A35-A2U via worm hole forty-two minutes after Cl^- introduction in the infiltrrometer.

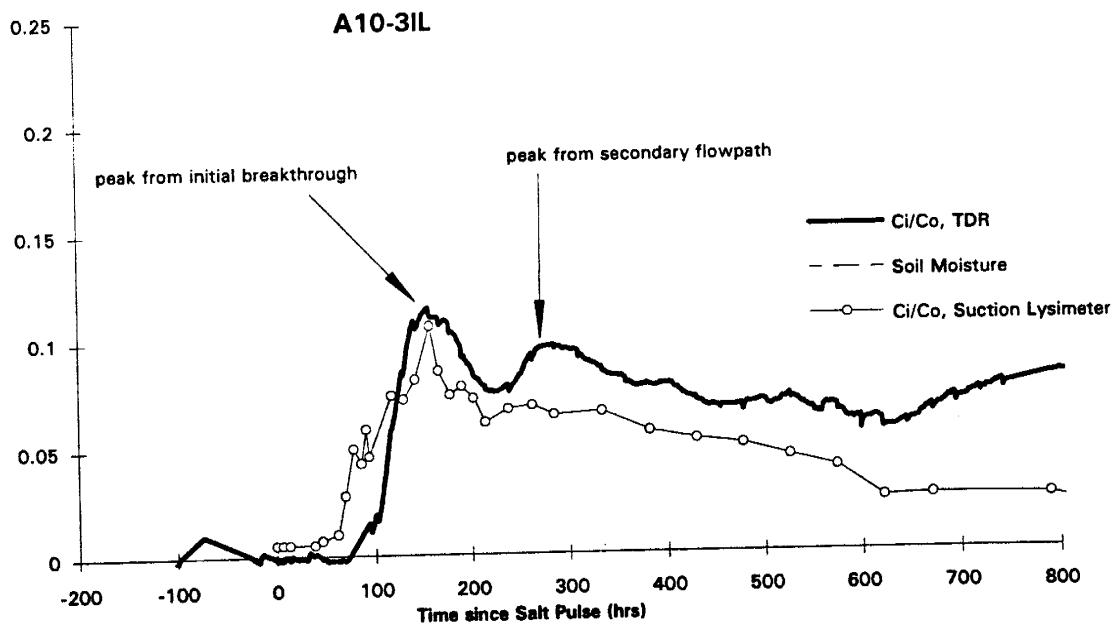


Figure 13. Repeated peaks in the solute concentration breakthrough curve from primary and secondary flowpaths

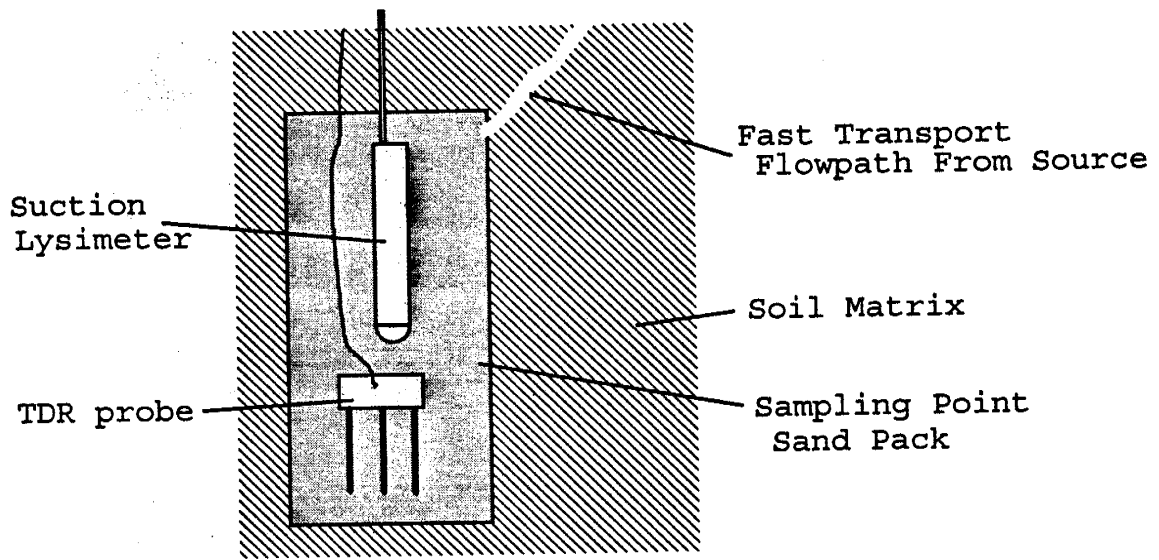


Figure 14a. Soil water sampler between transport pathway and probe.

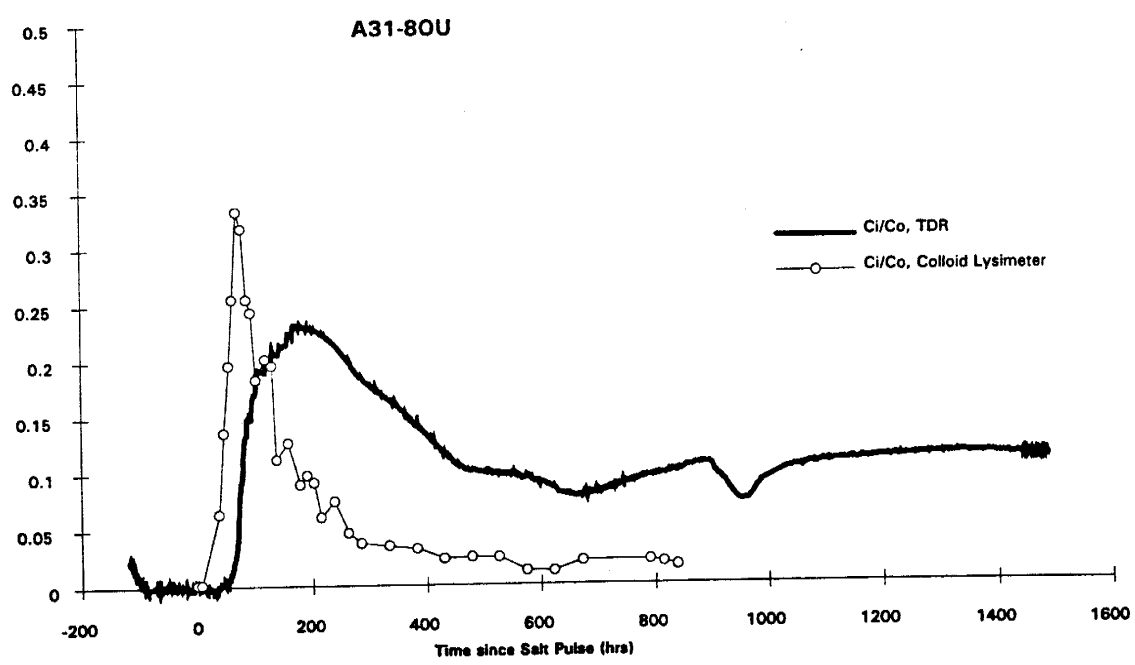


Figure 14b. Differences in arrival times and peaks due to TDR probe, suction lysimeter, and fast transport flow path geometry which favor suction lysimeter.

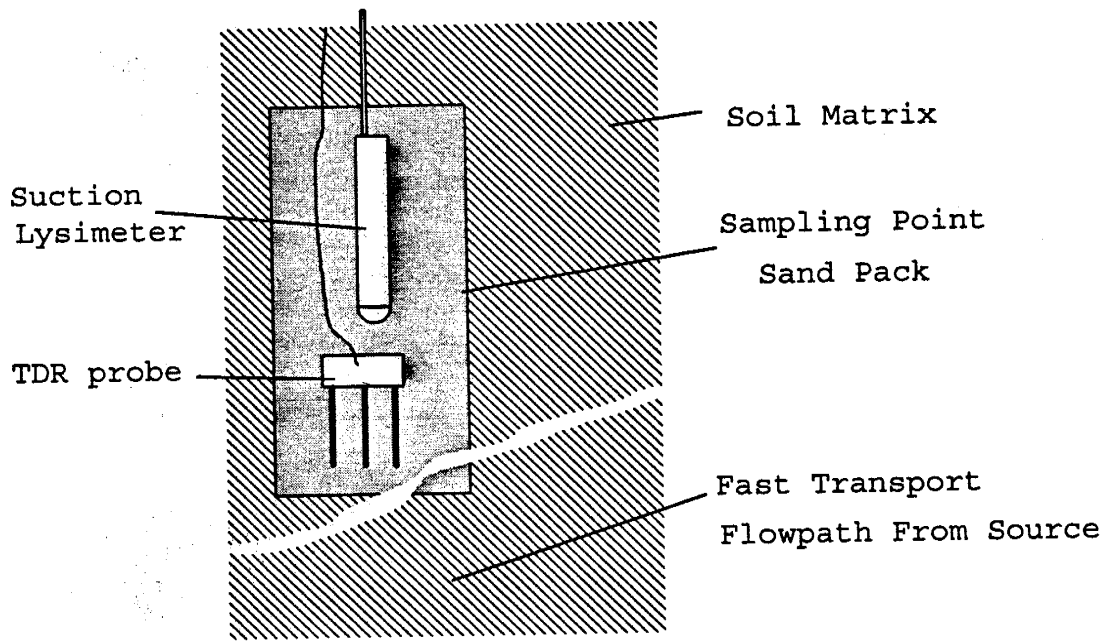


Figure 15a. TDR probe between transport pathway and soil water sampler.

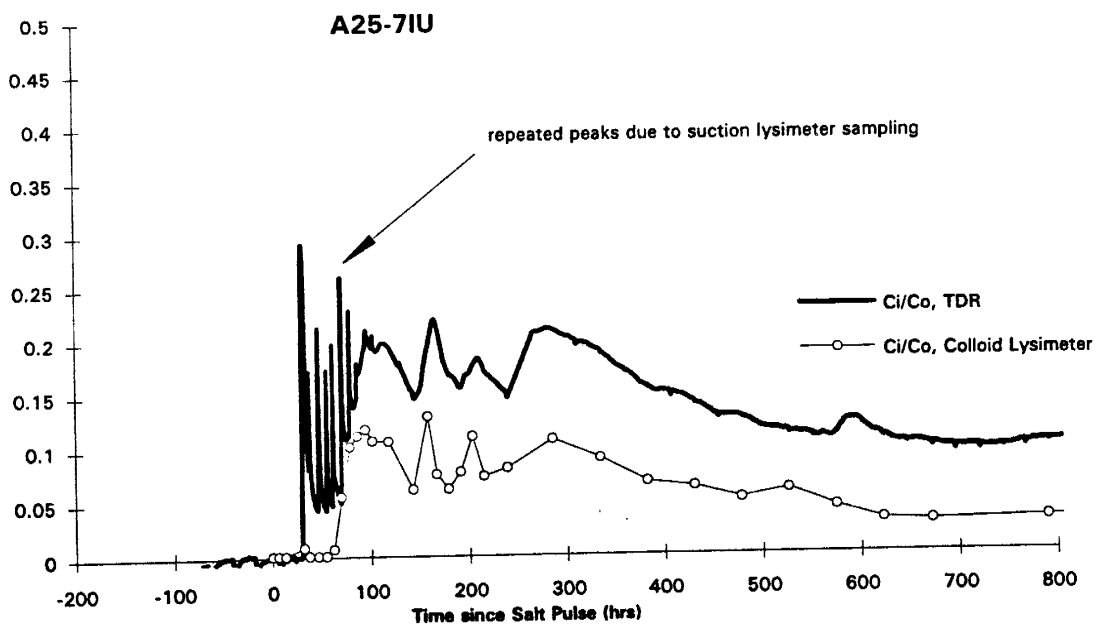
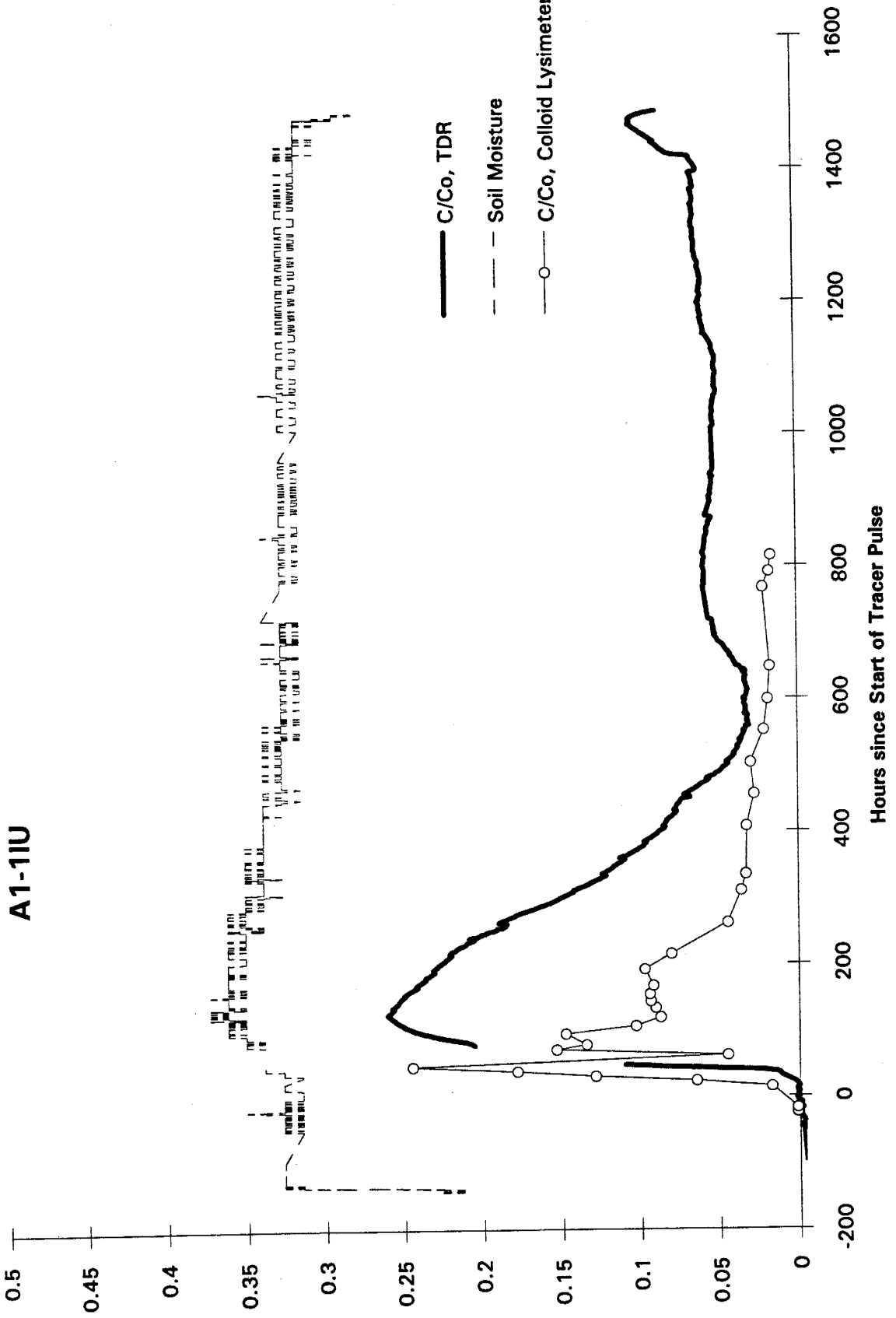
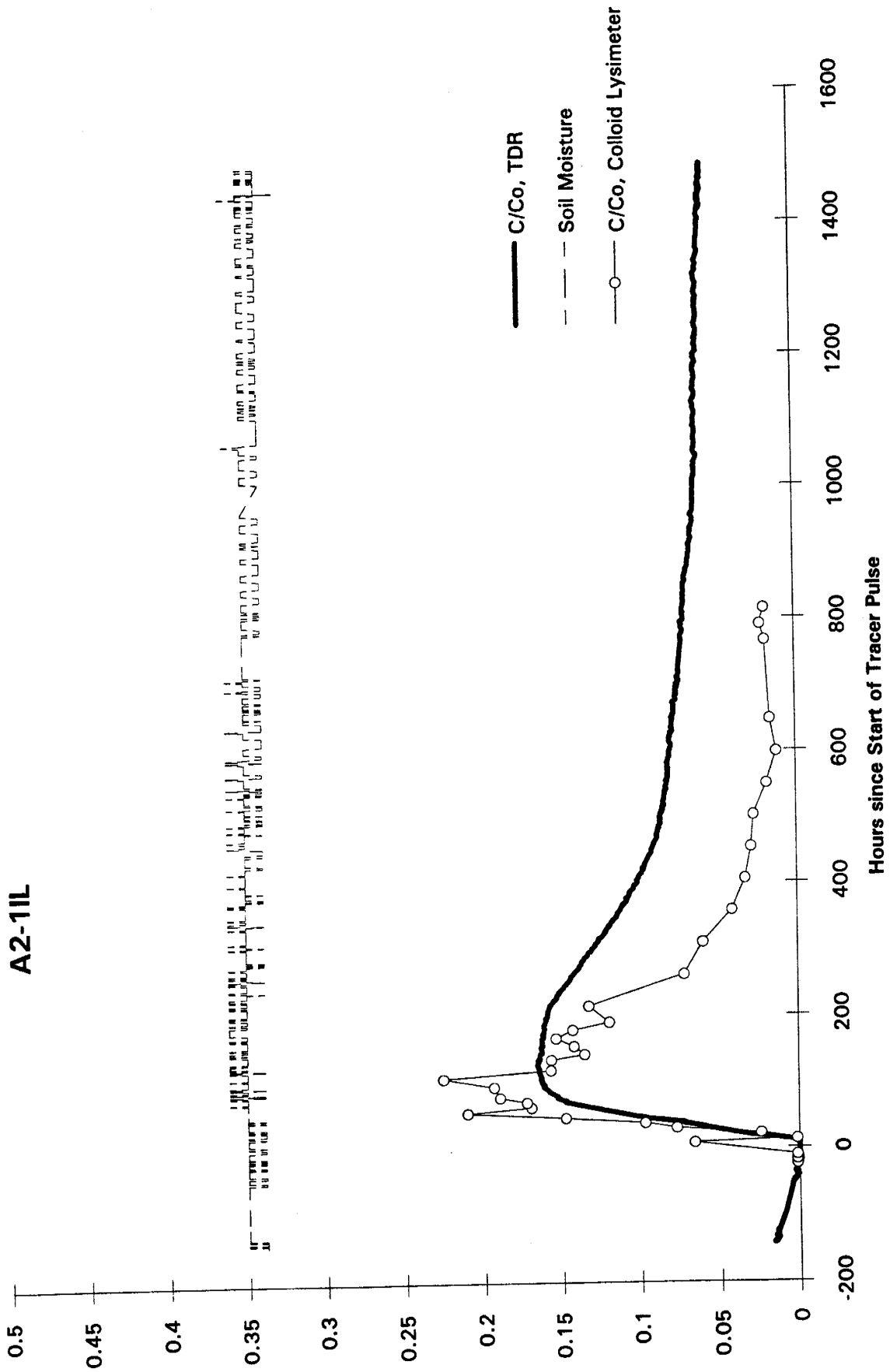


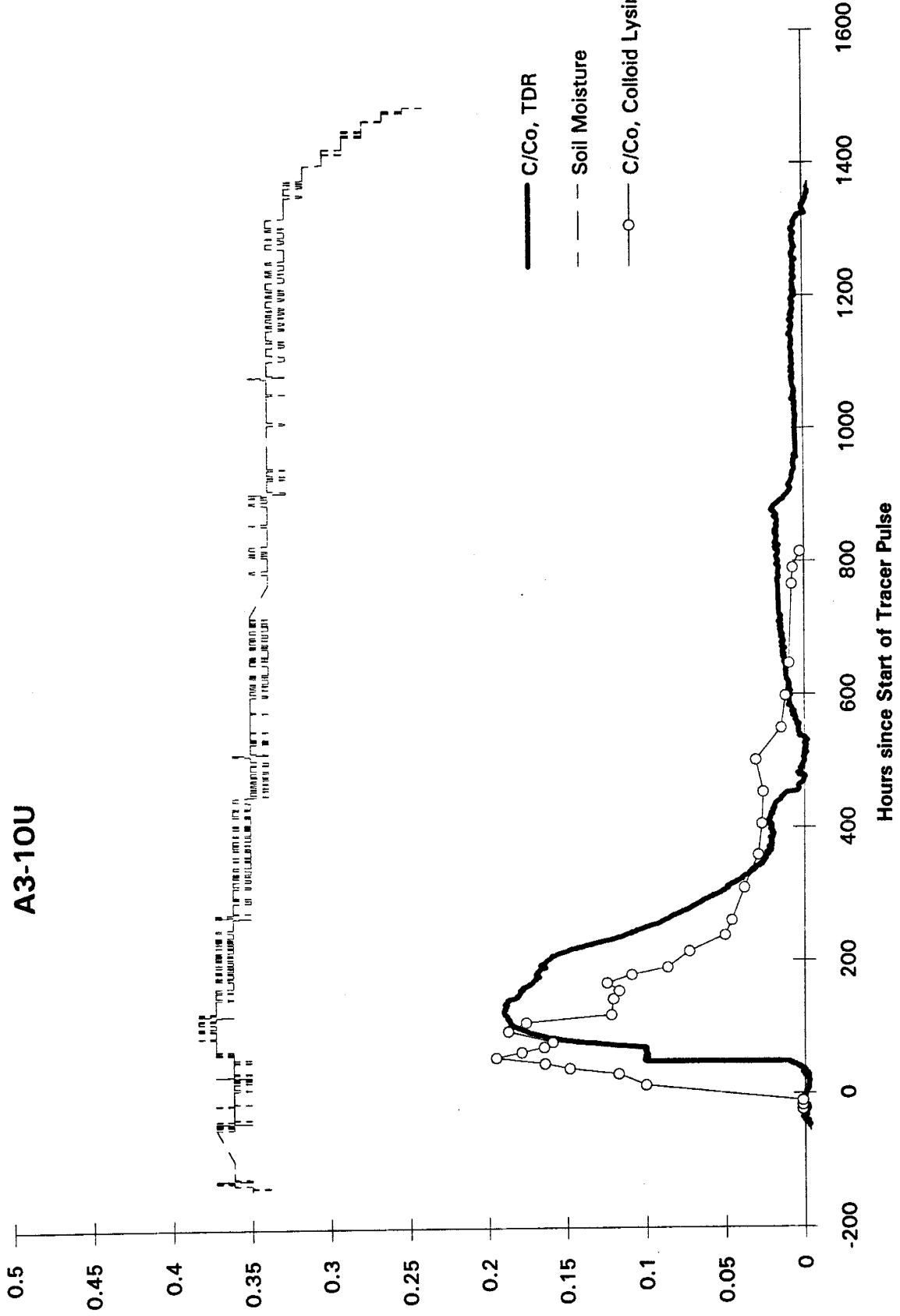
Figure 15b. Faster arrival times at the TDR and higher peaks due to the favorable location of a fast transport pathway which favors solute transport past the TDR probe.



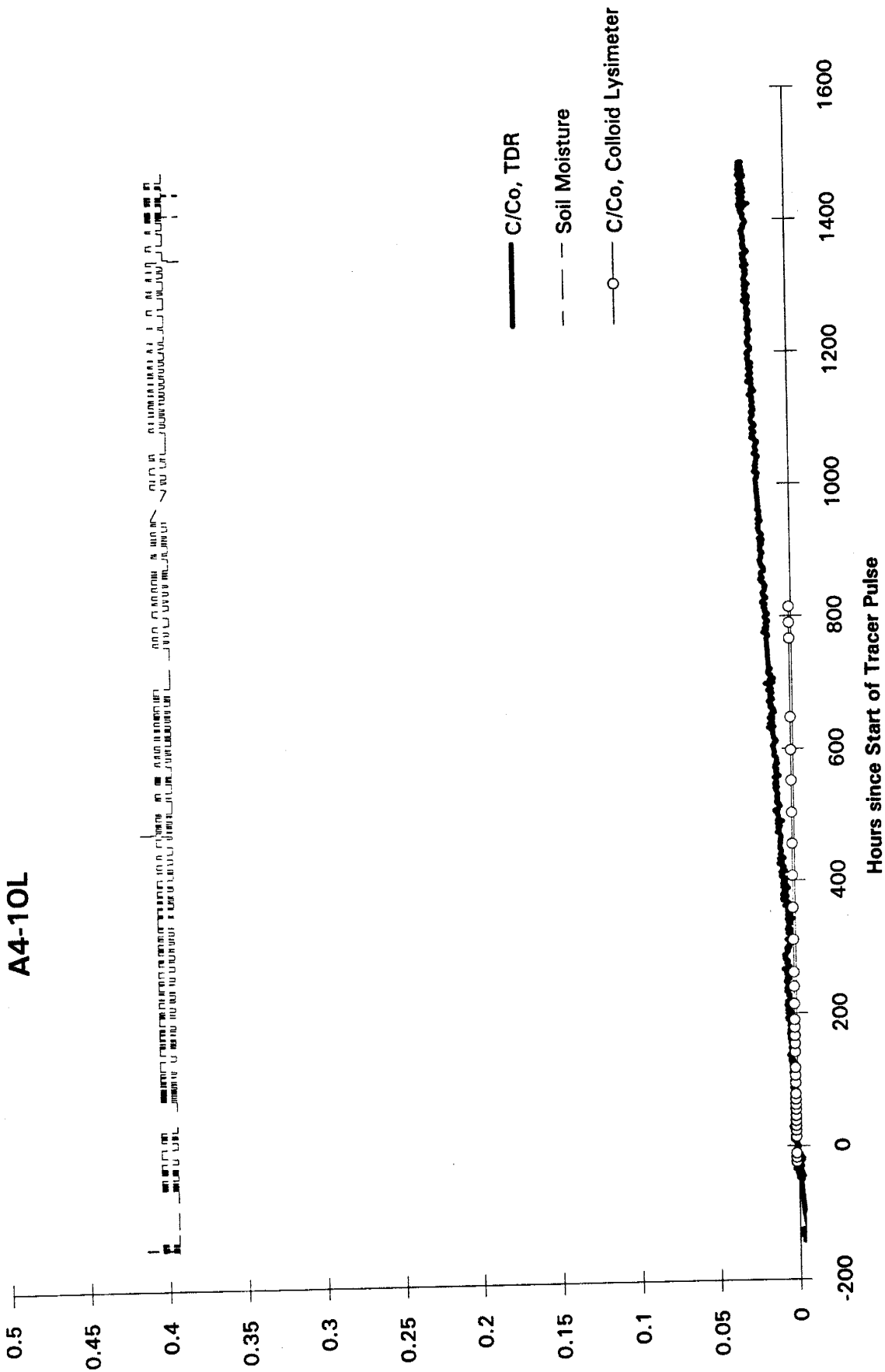
A2-11L



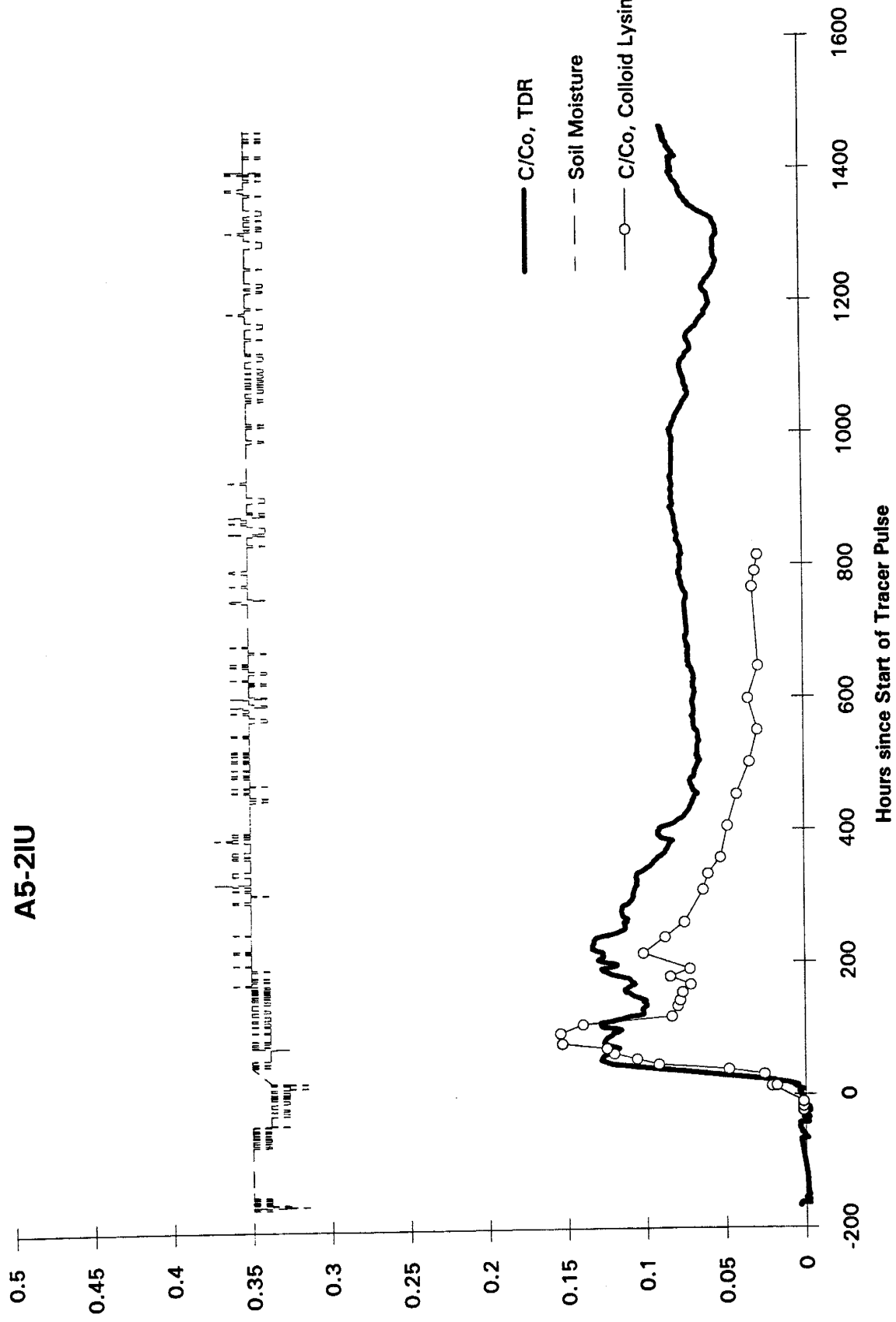
A3-10U



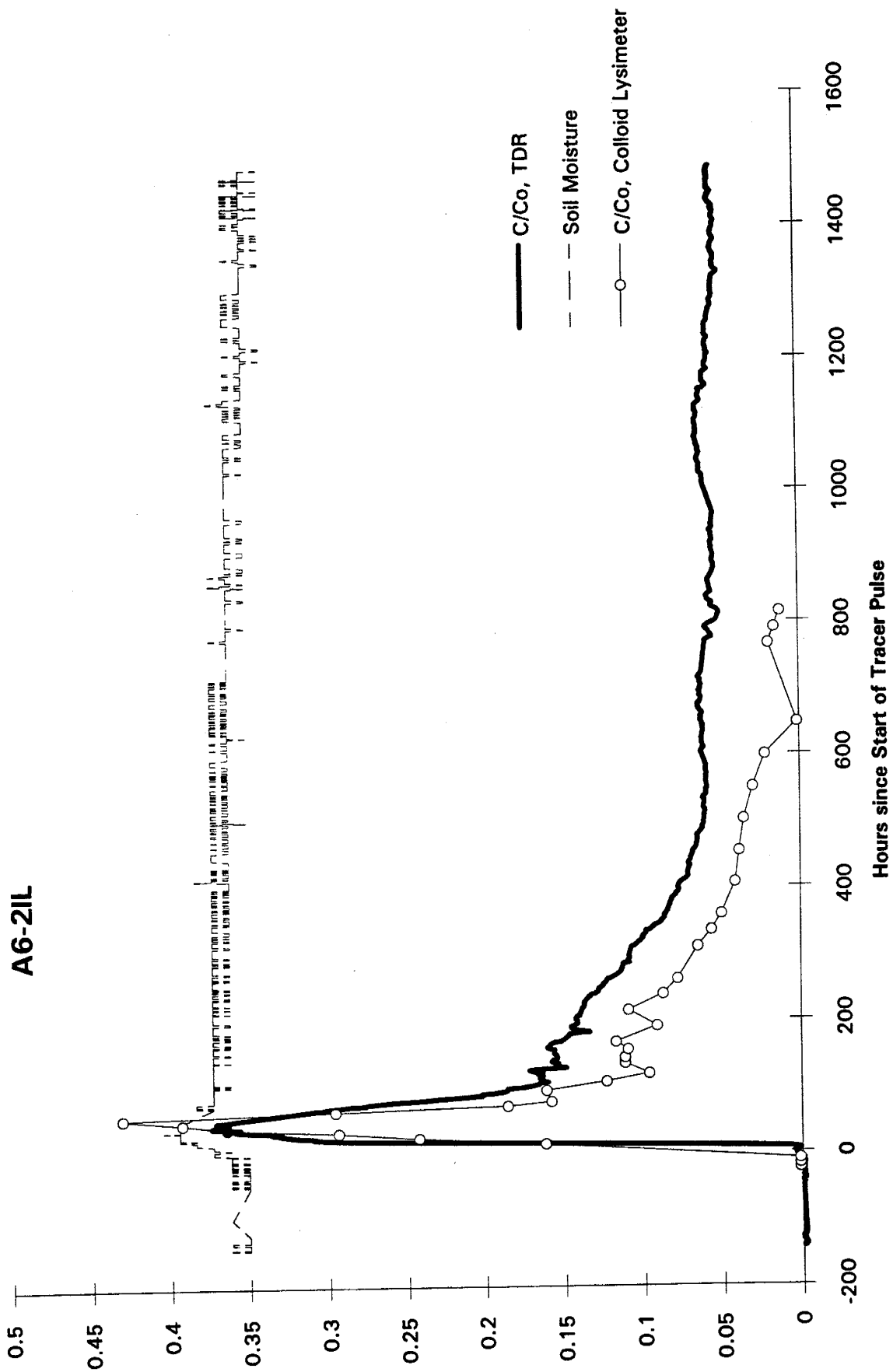
A4-10L



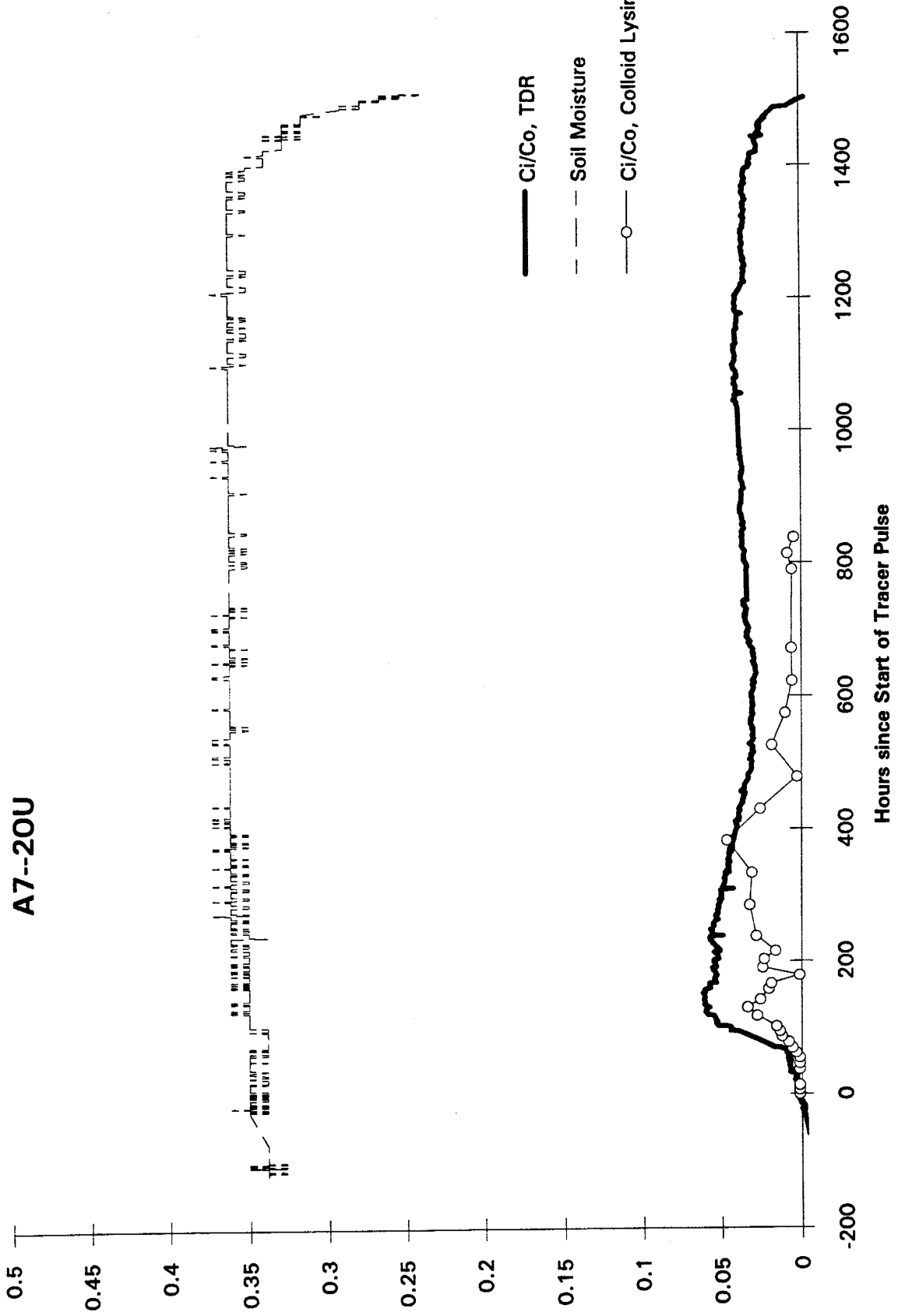
A5-2IU



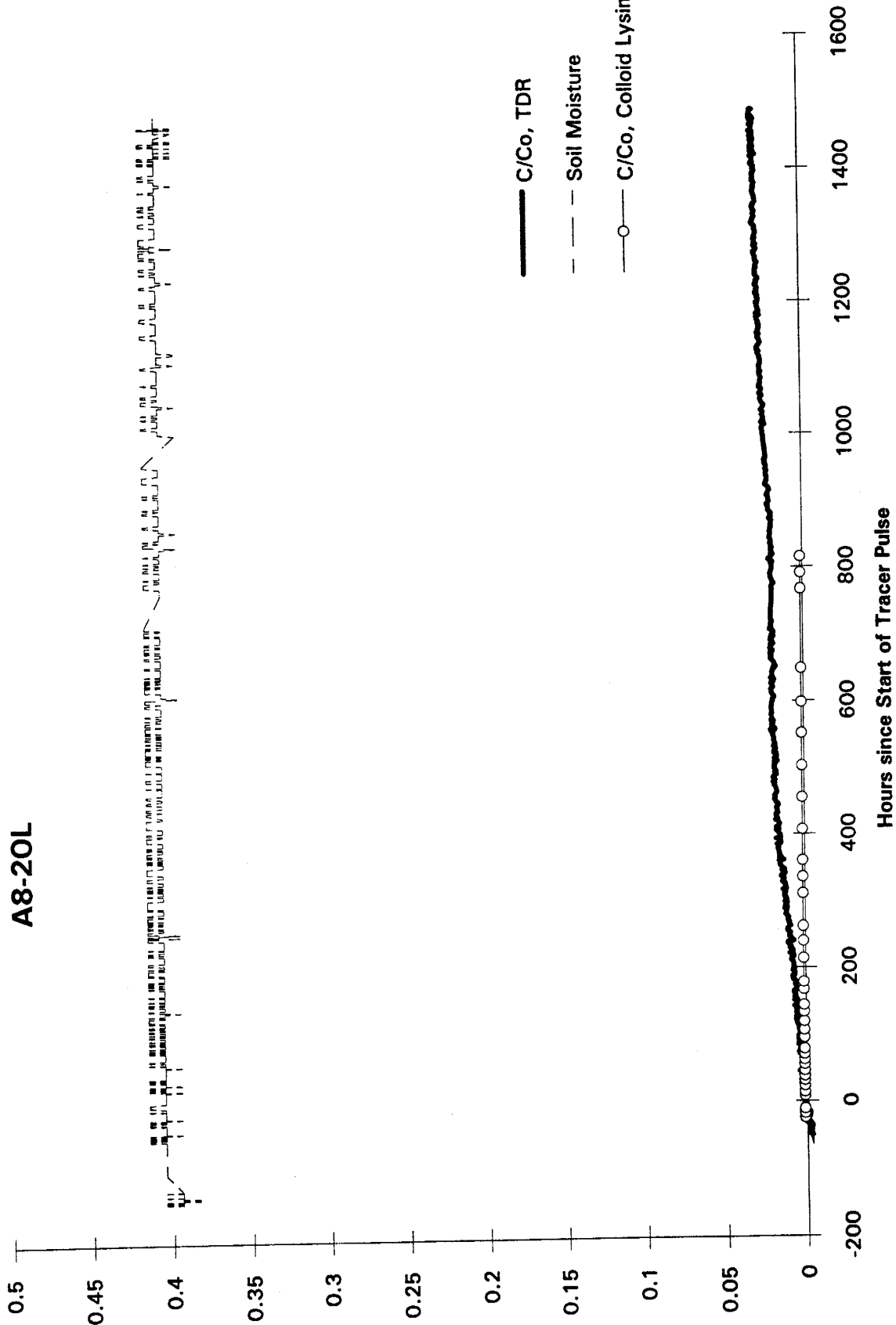
A6-2IL

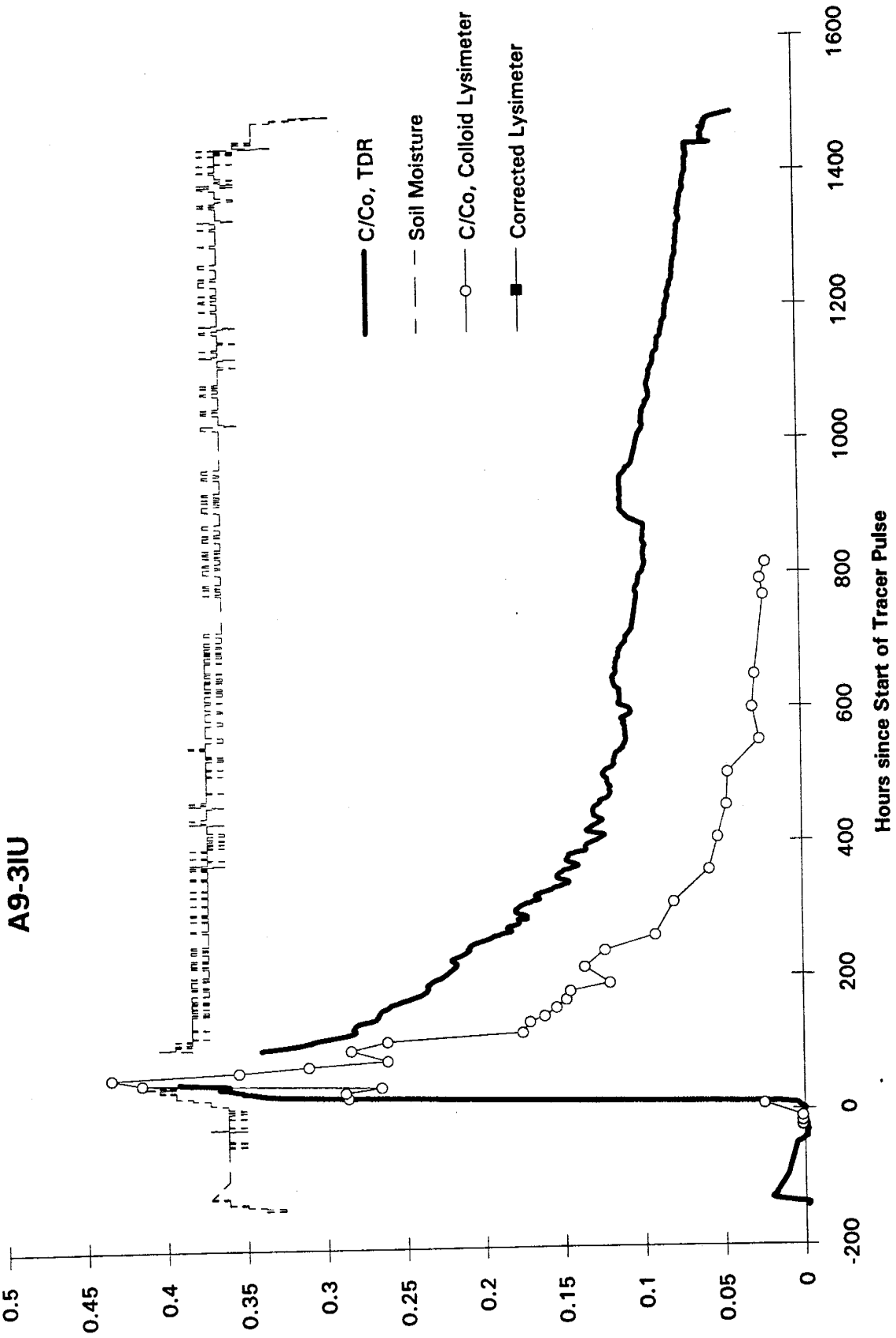


A7--20U

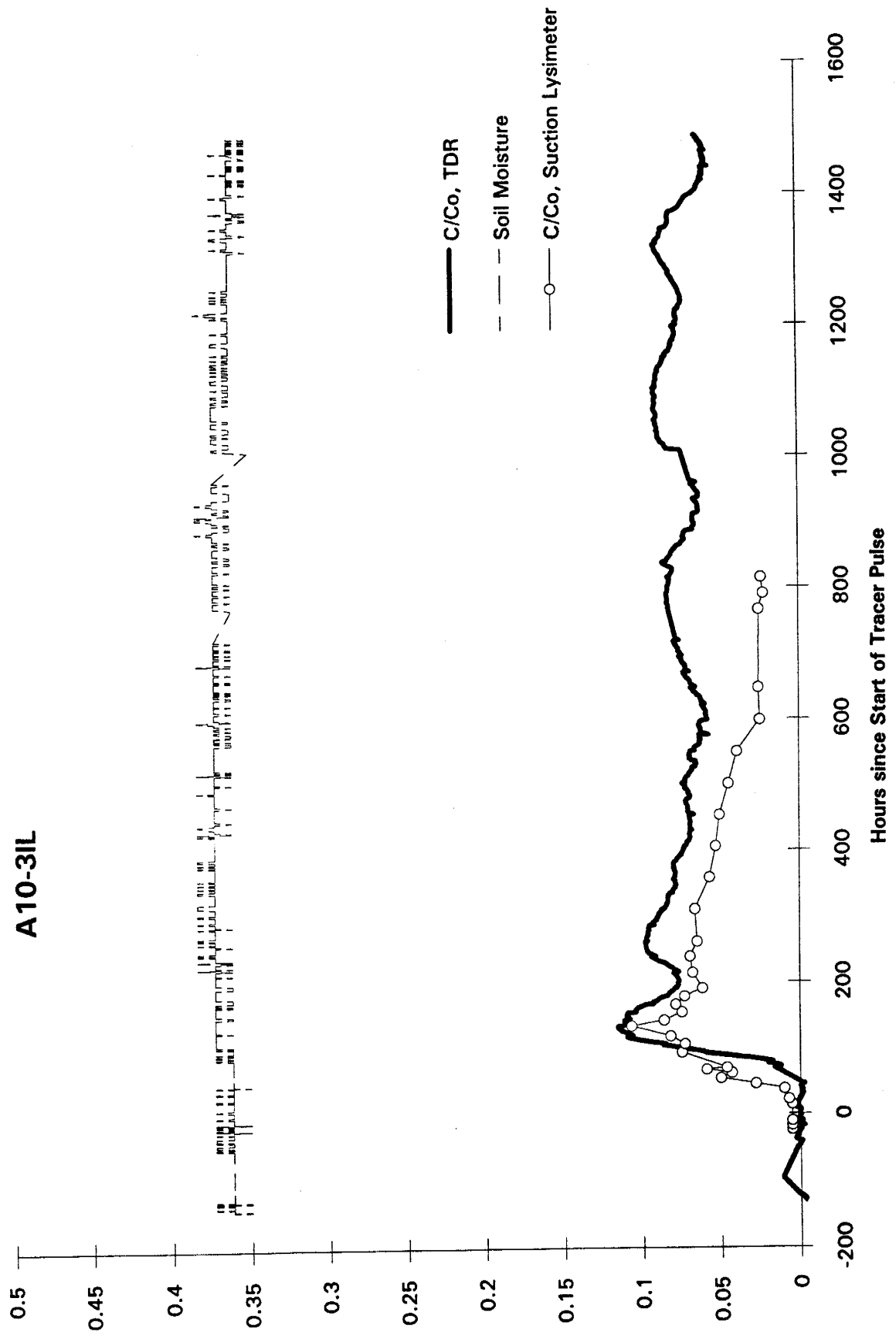


A8-20L

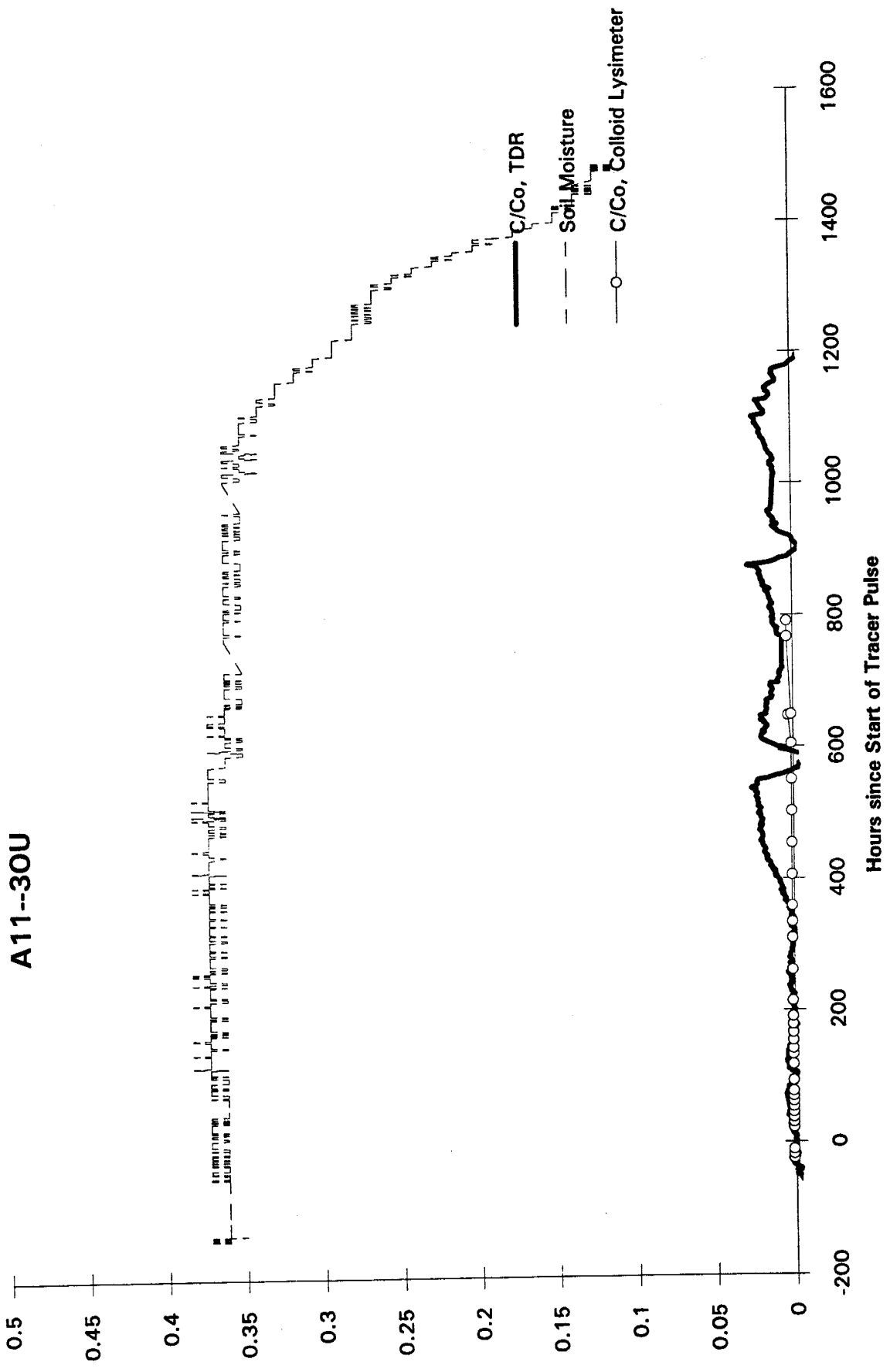




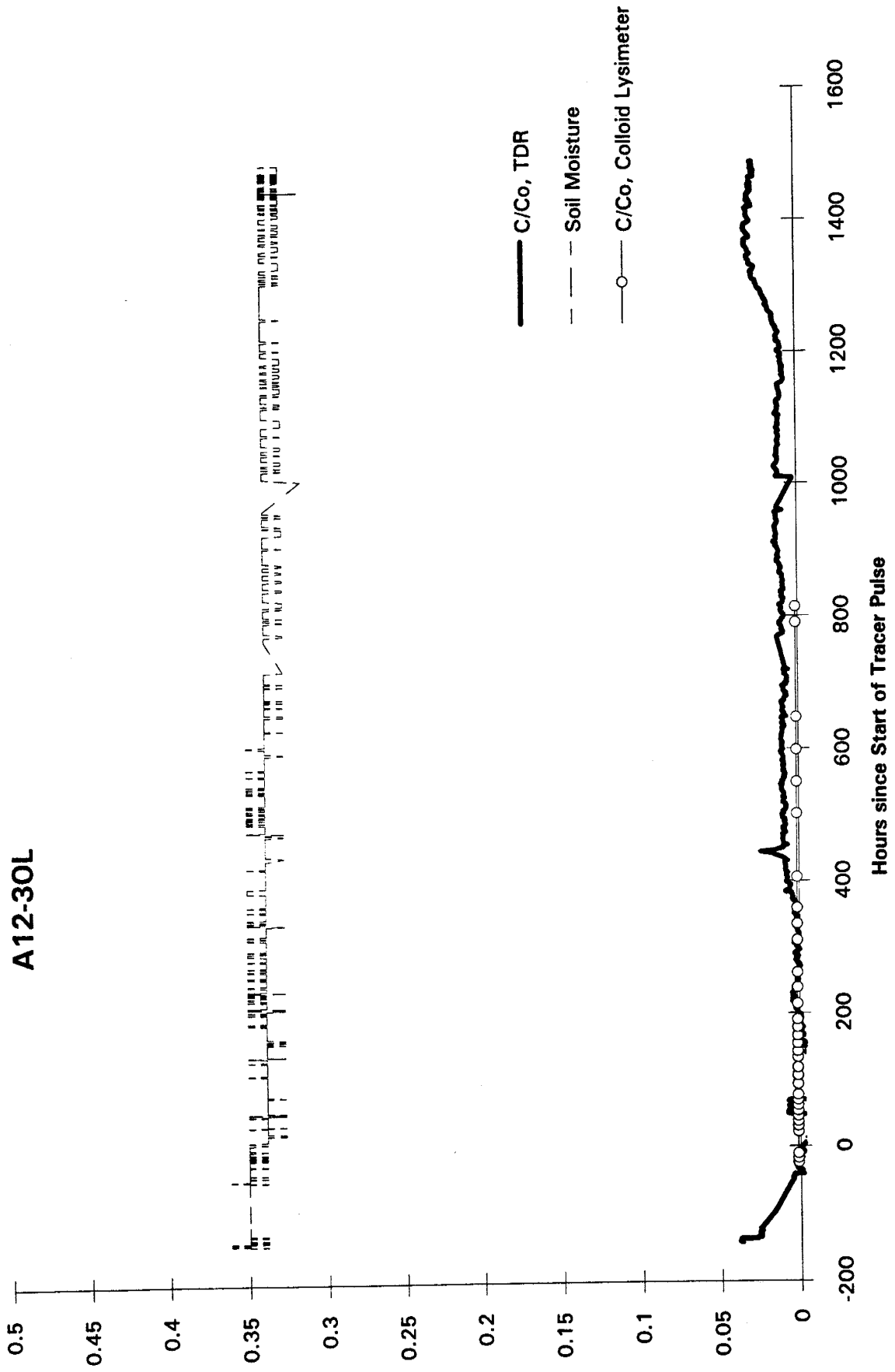
A10-3IL



A11--30U

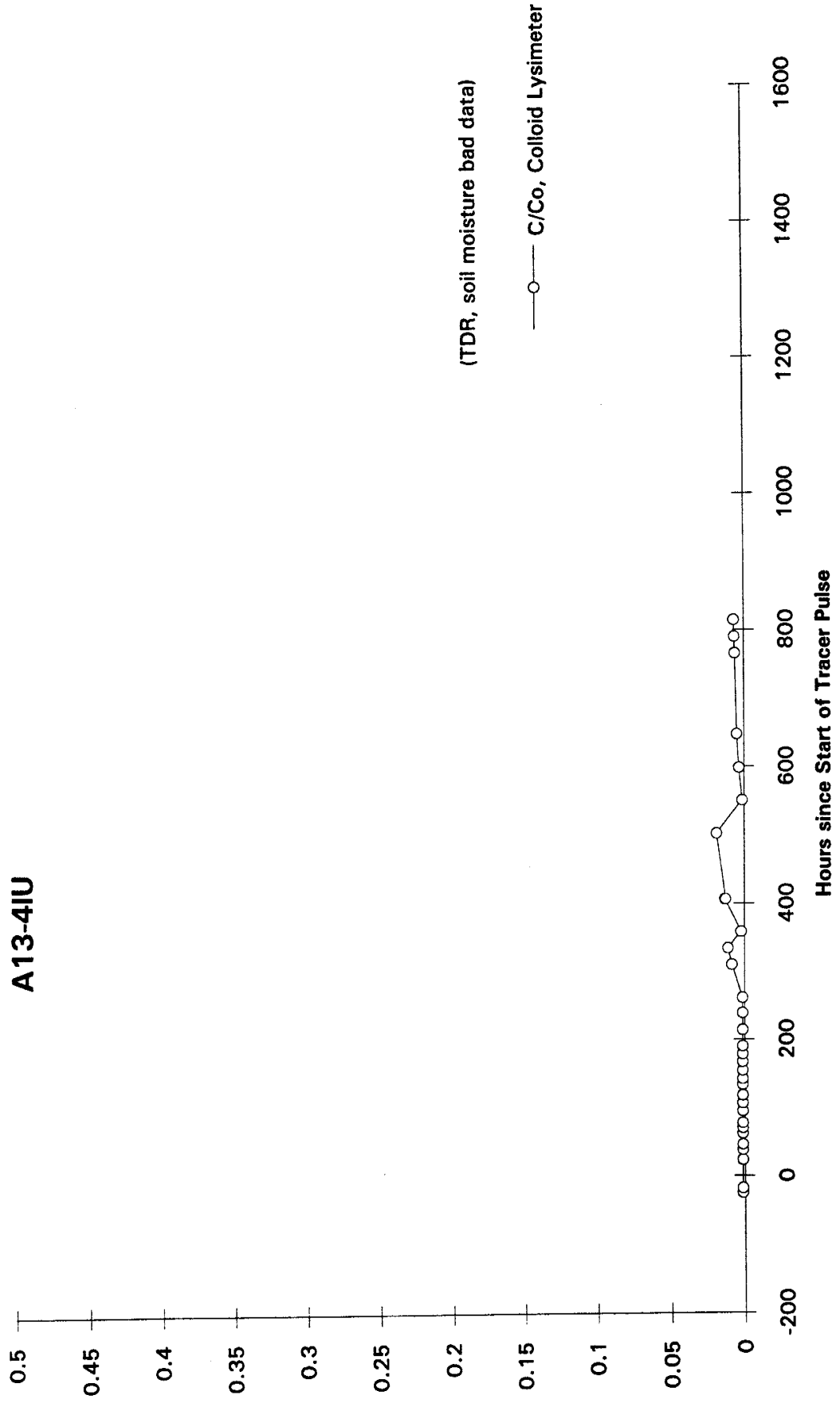


A12-30L

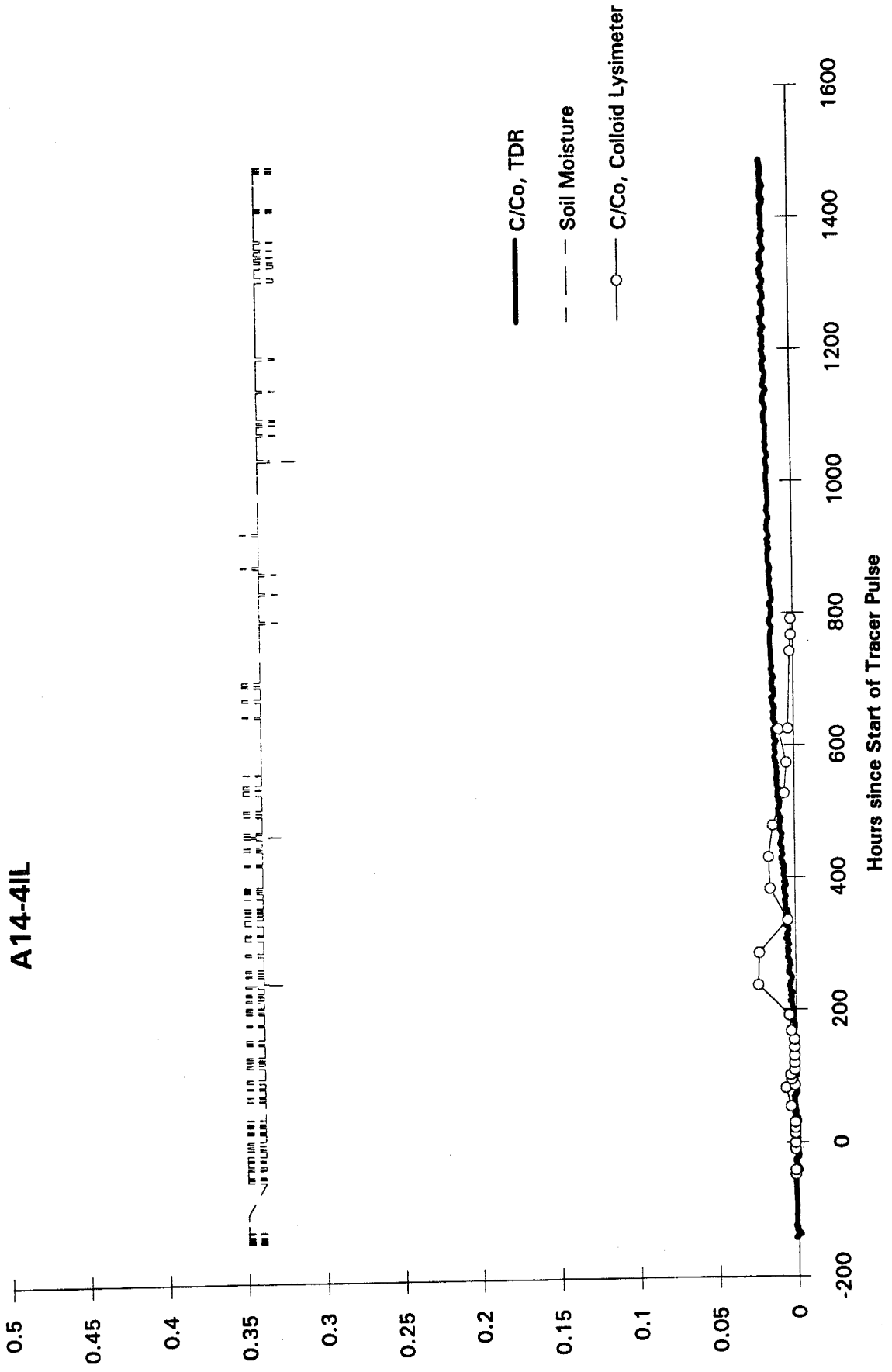


C/Co, Colloid Lysimeter

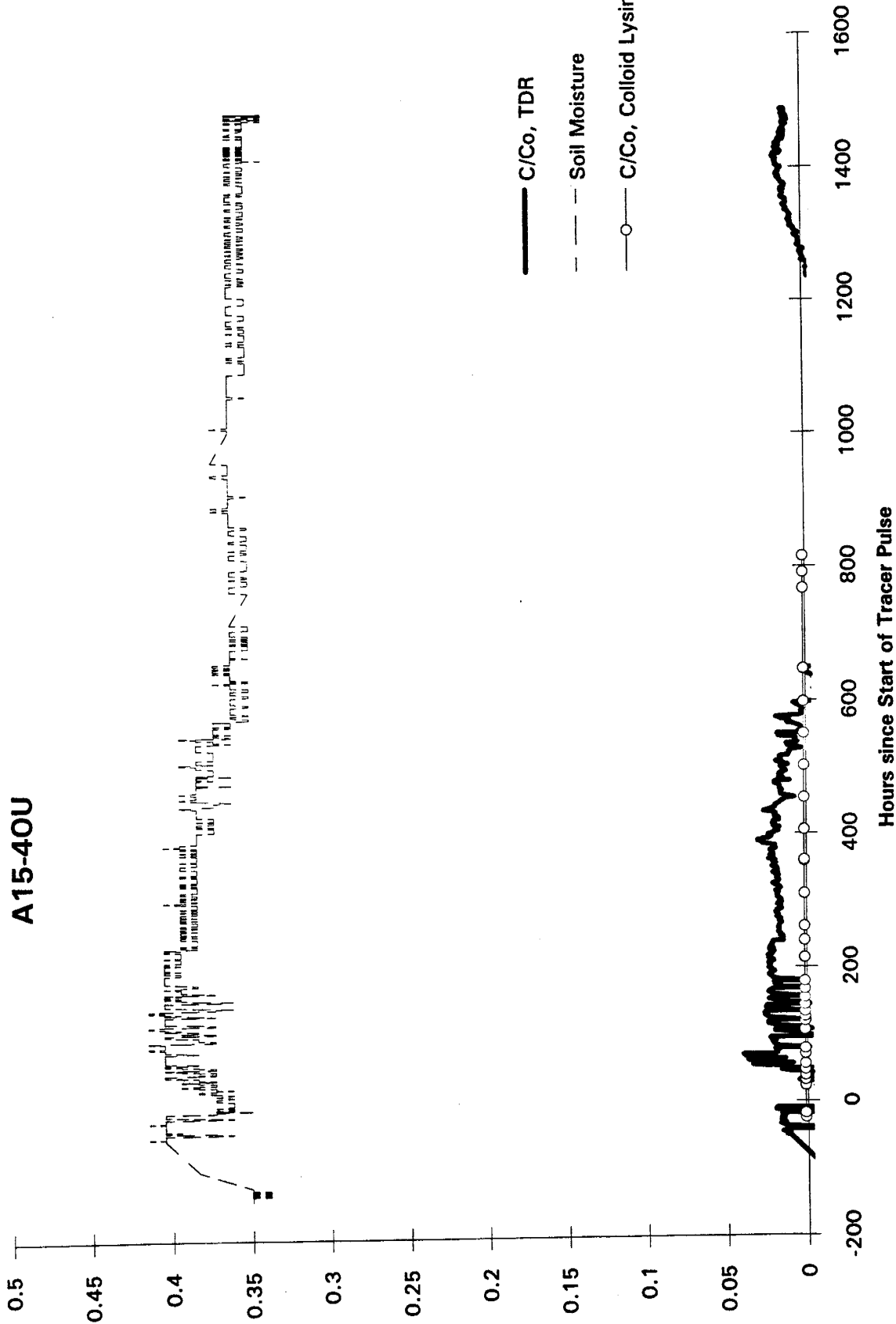
A13-4IU



A14-4IL

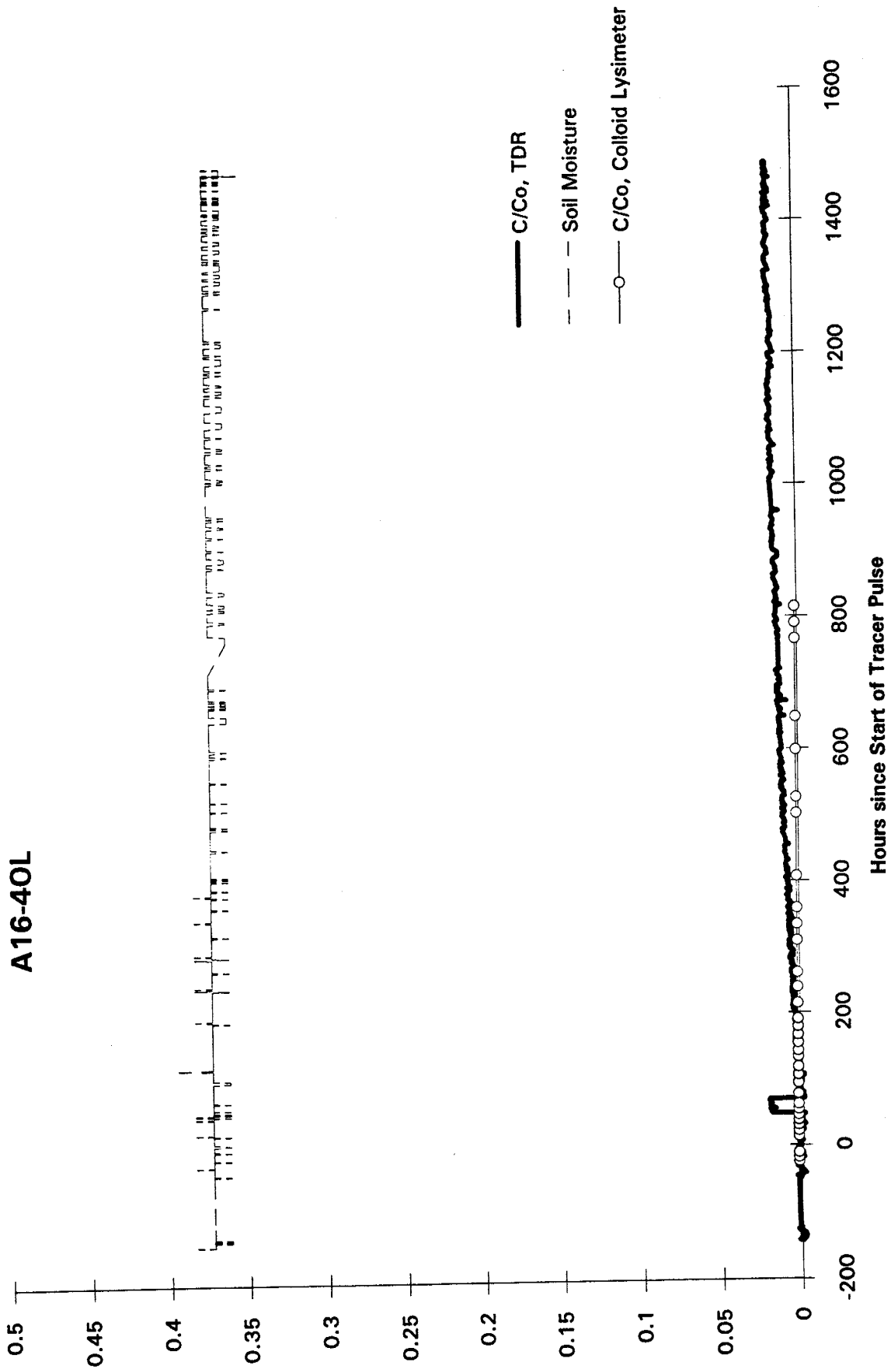


A15-40U

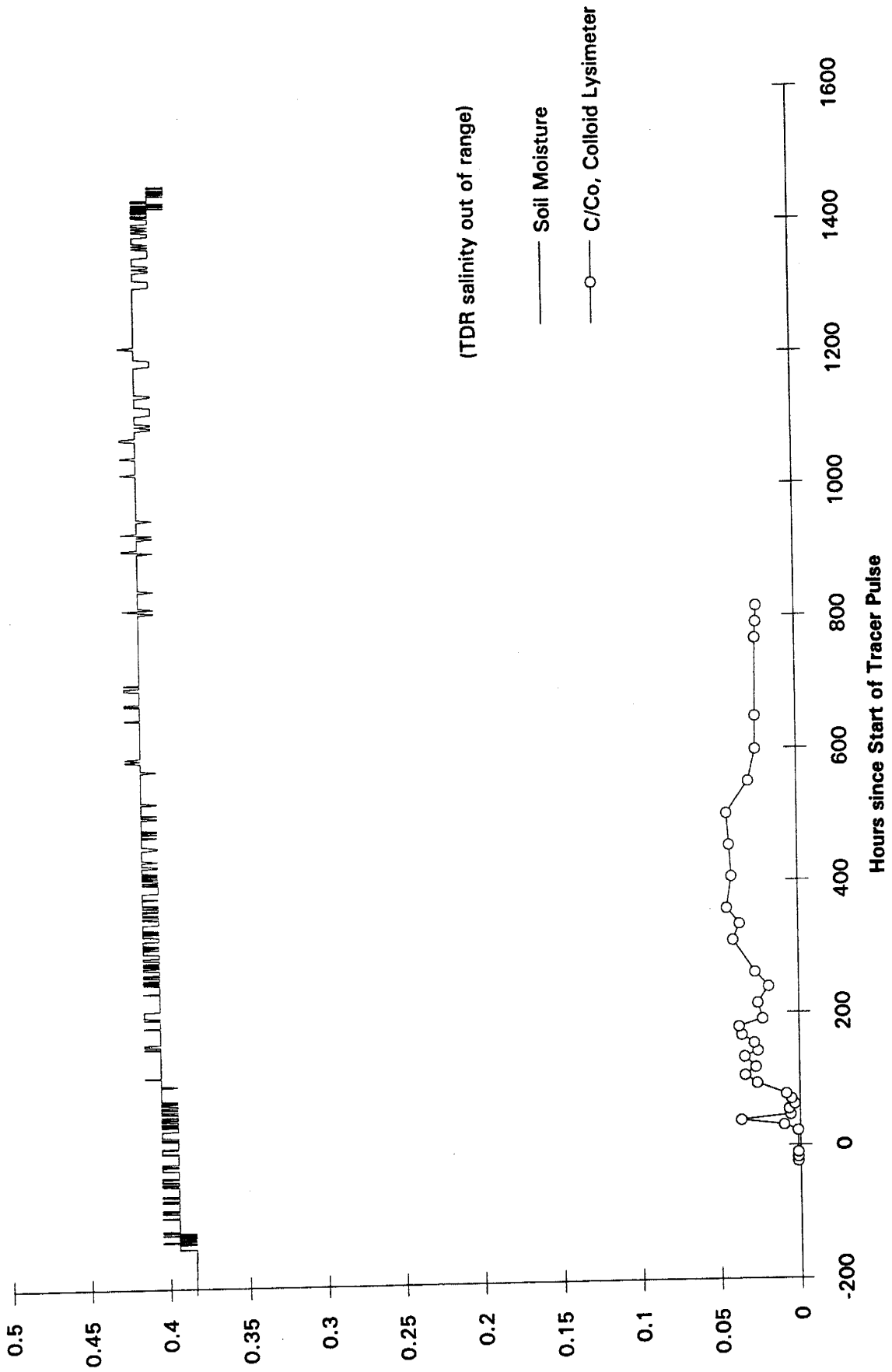


— C/Co, TDR
 - - - Soil Moisture
 —○— C/Co, Colloid Lysimeter

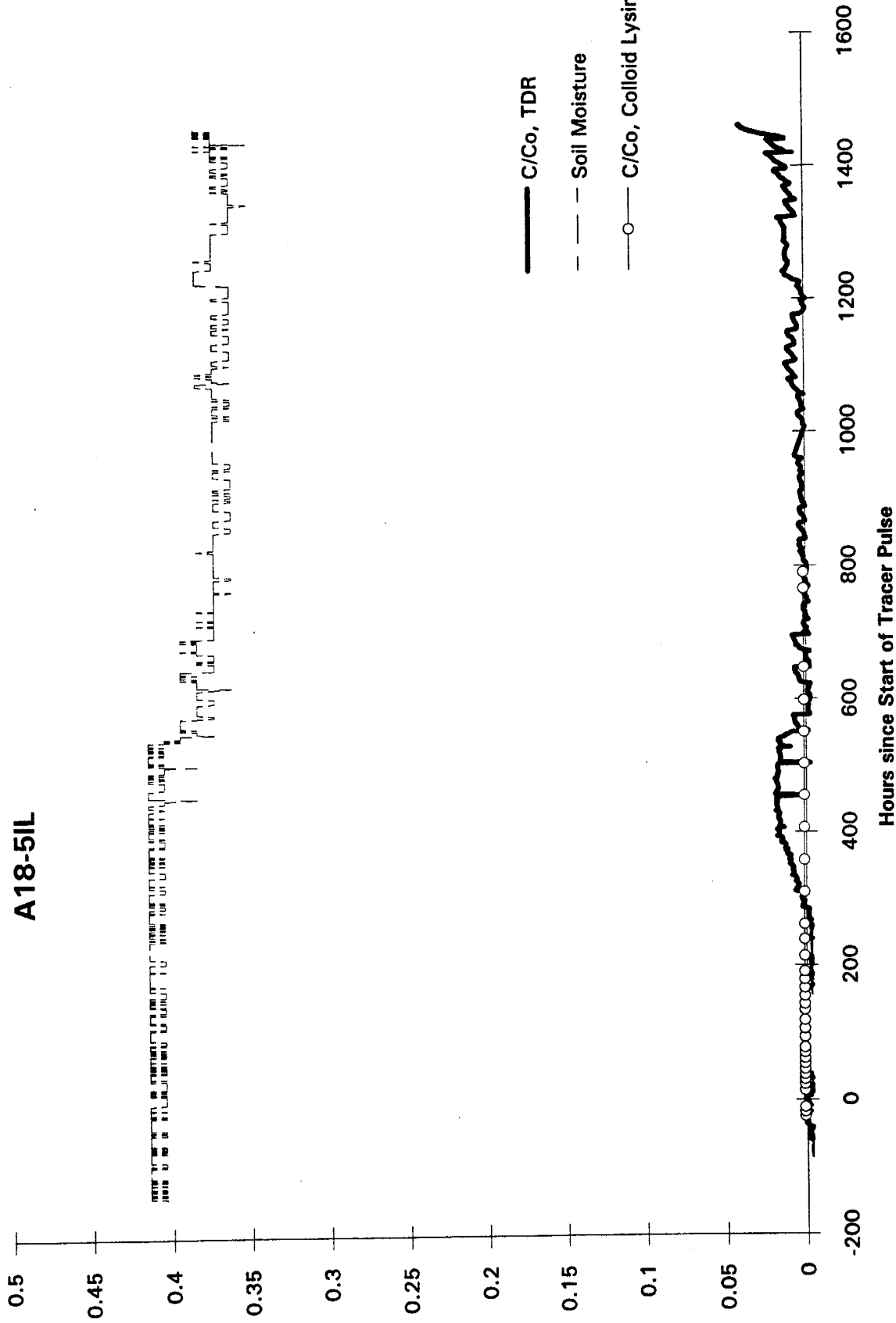
A16-40L

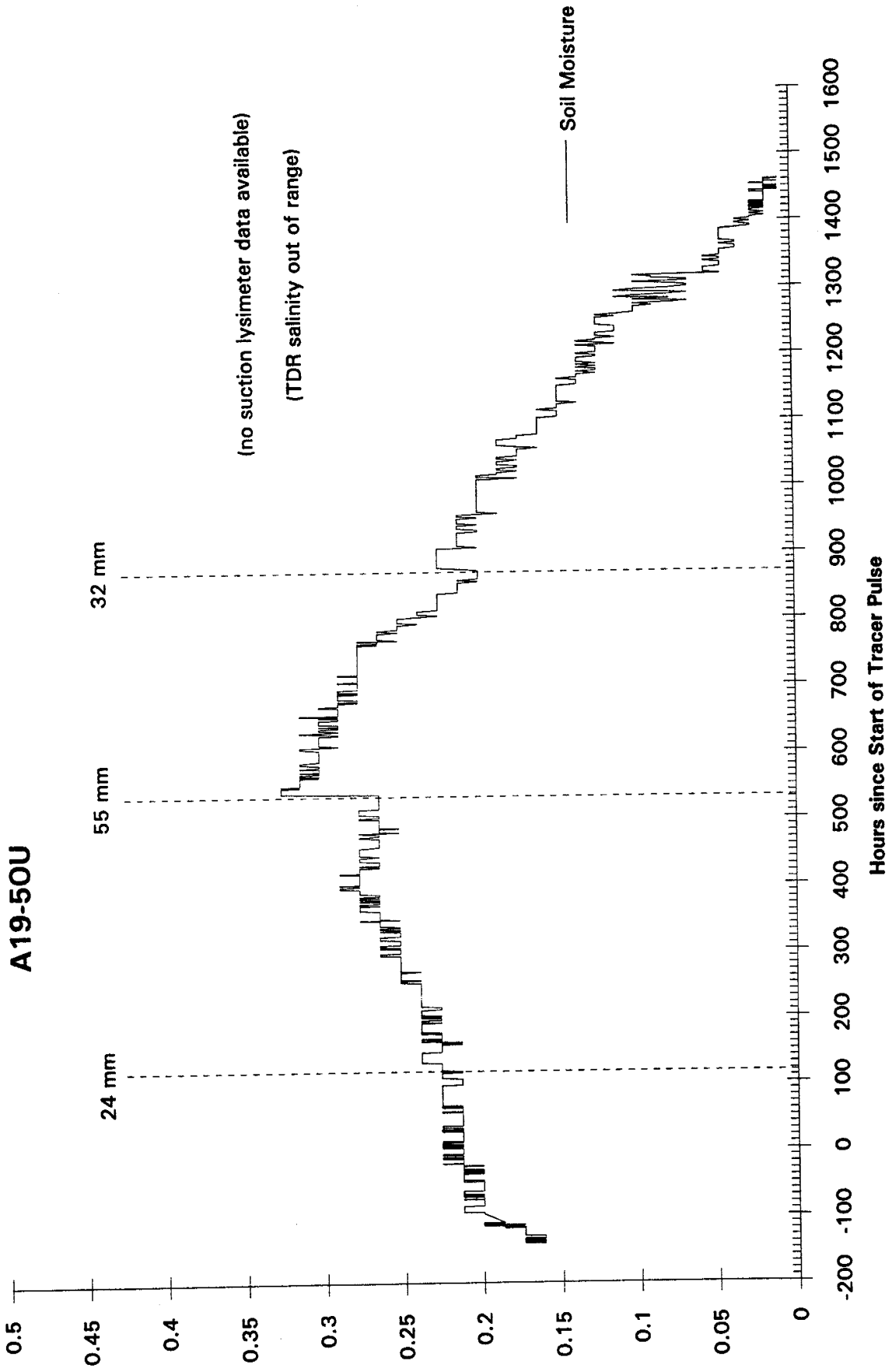


A17-5IU

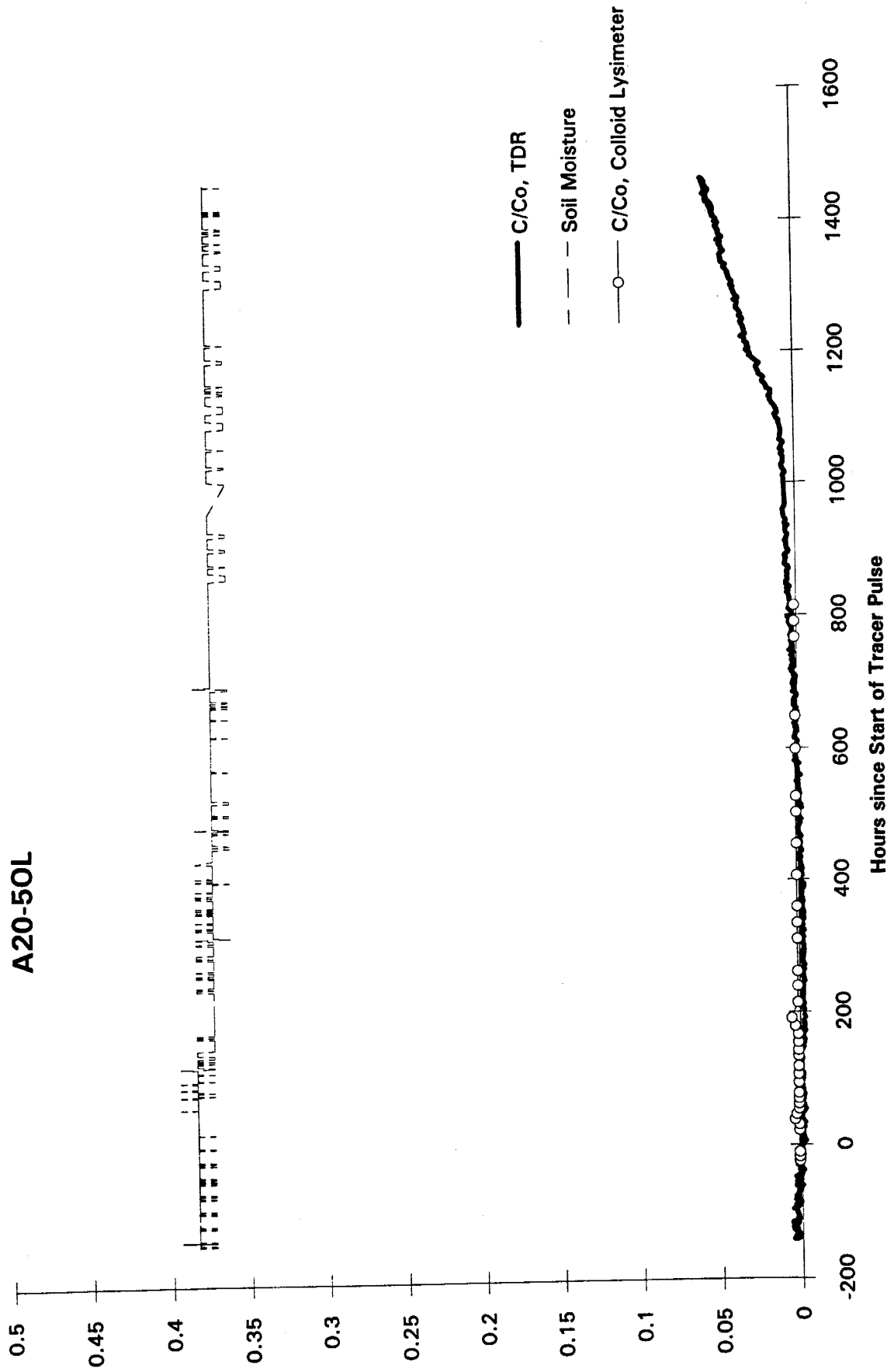


A18-5IL

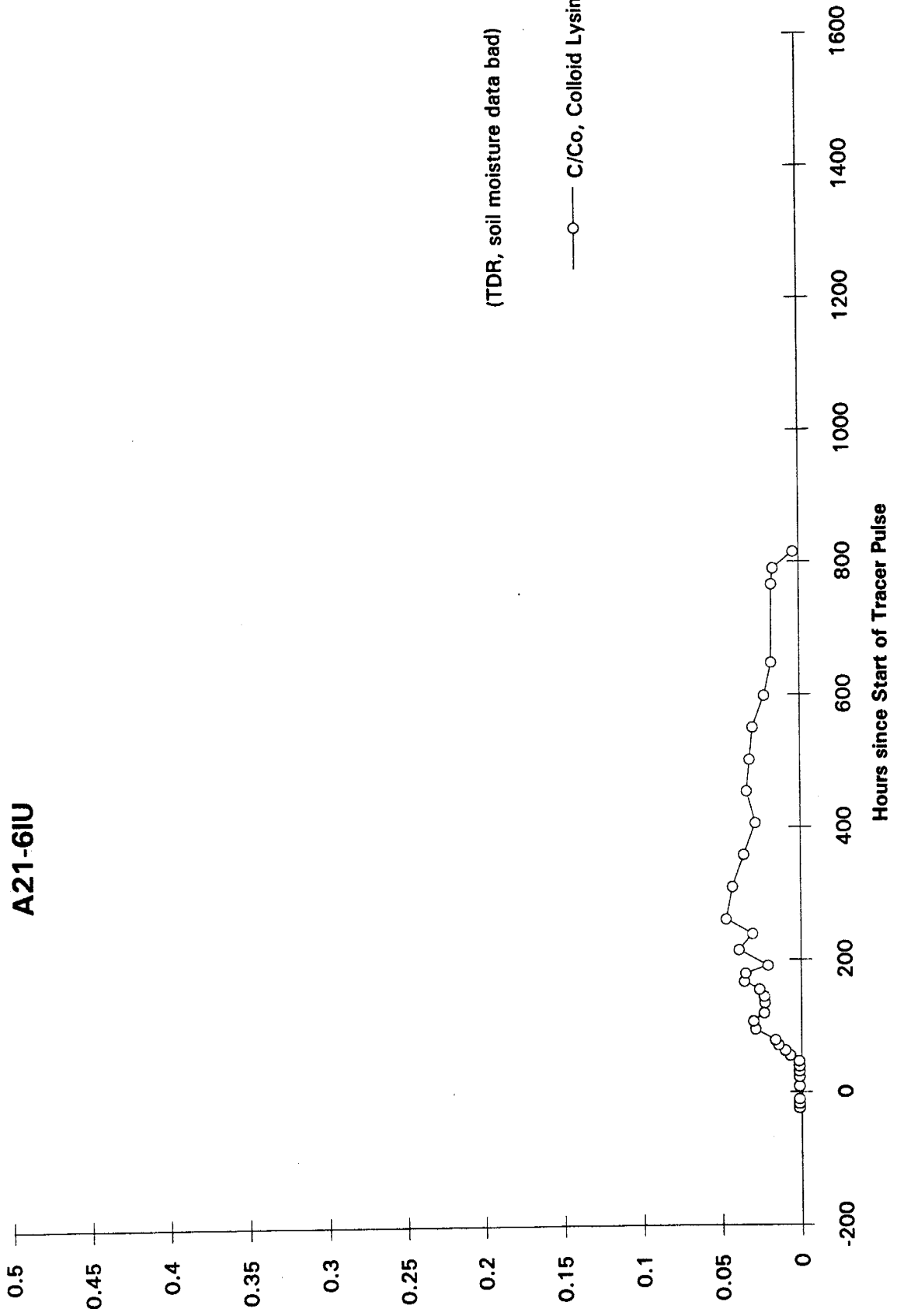




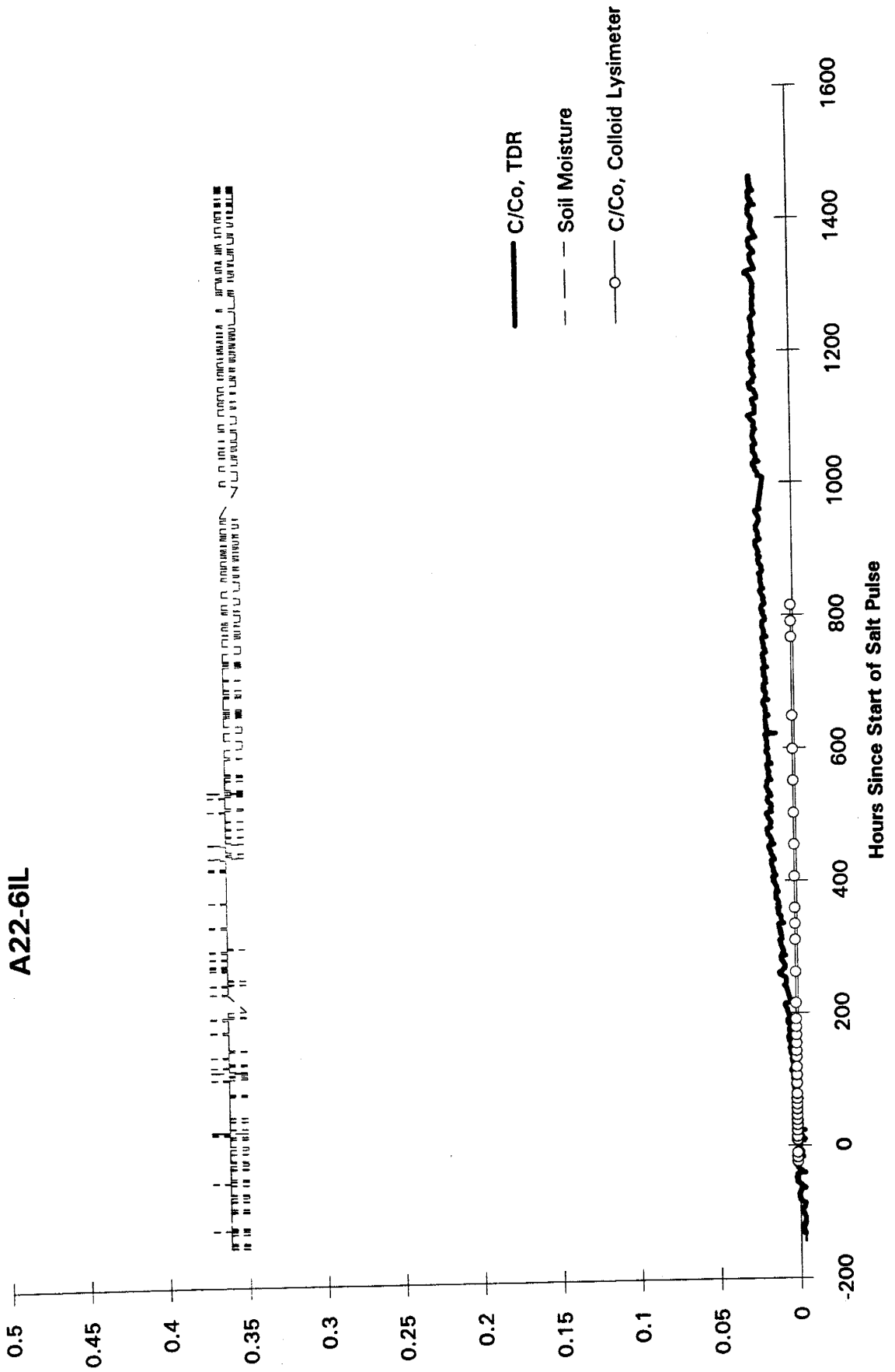
A20-50L

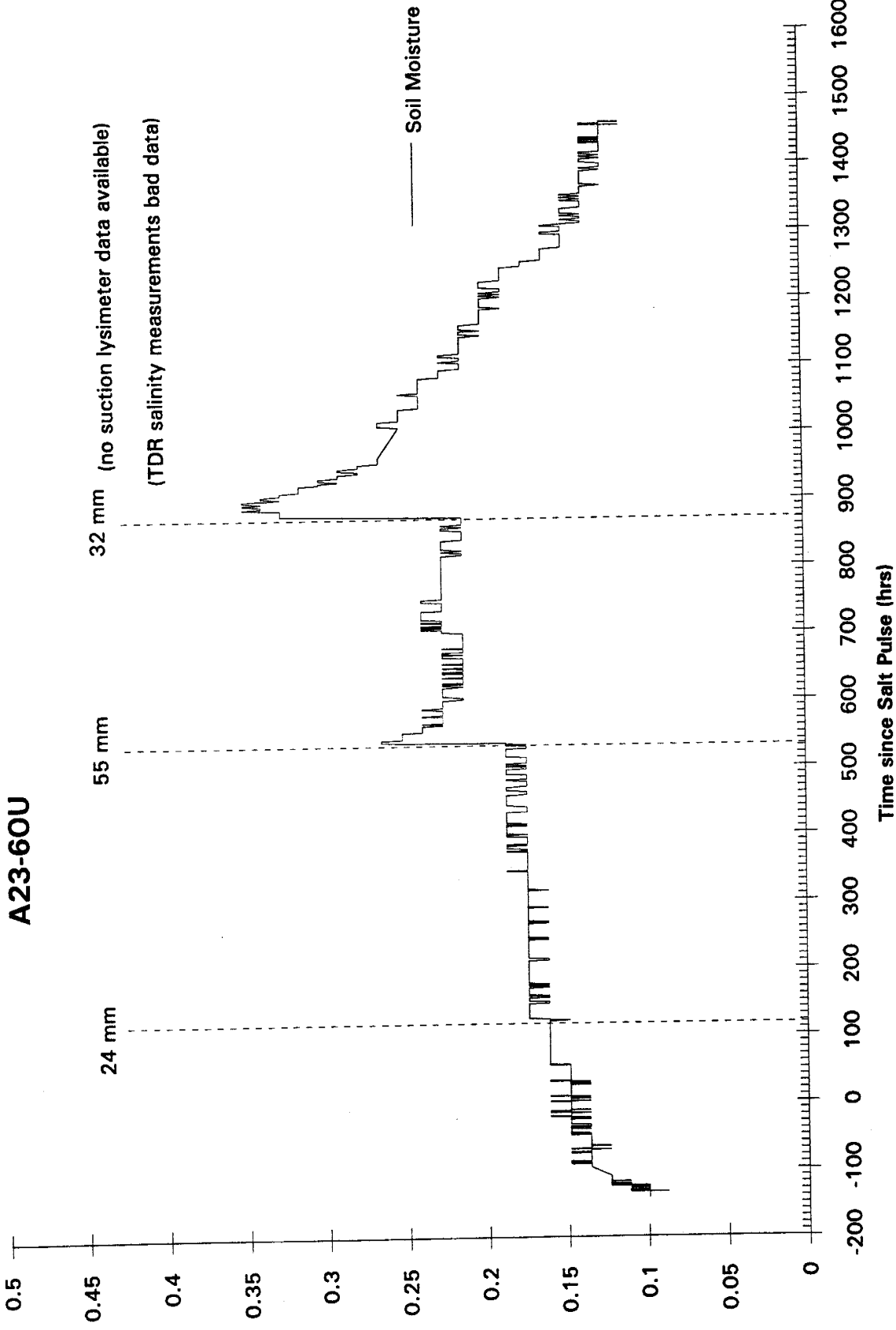


A21-6IU

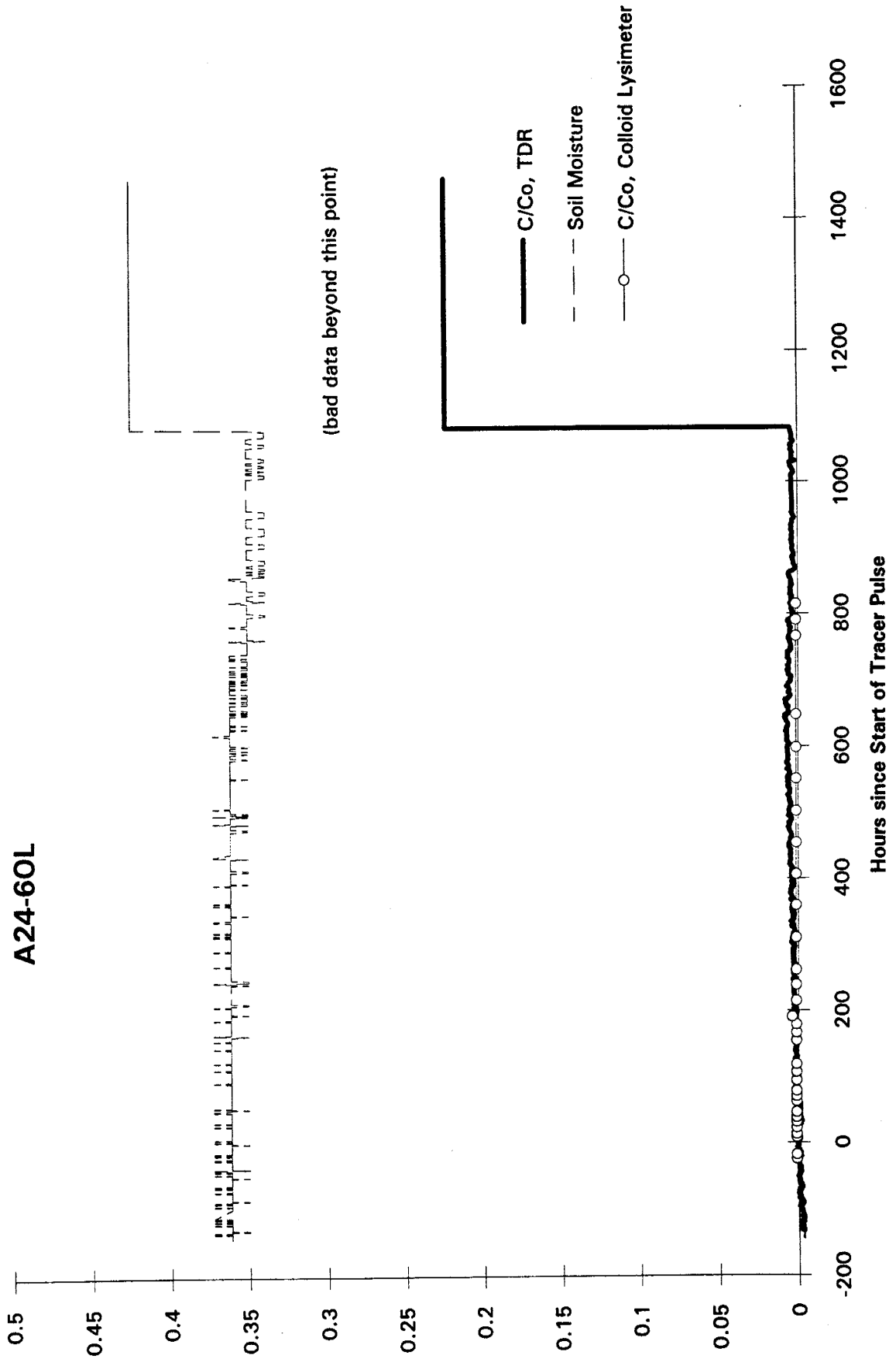


A22-6IL

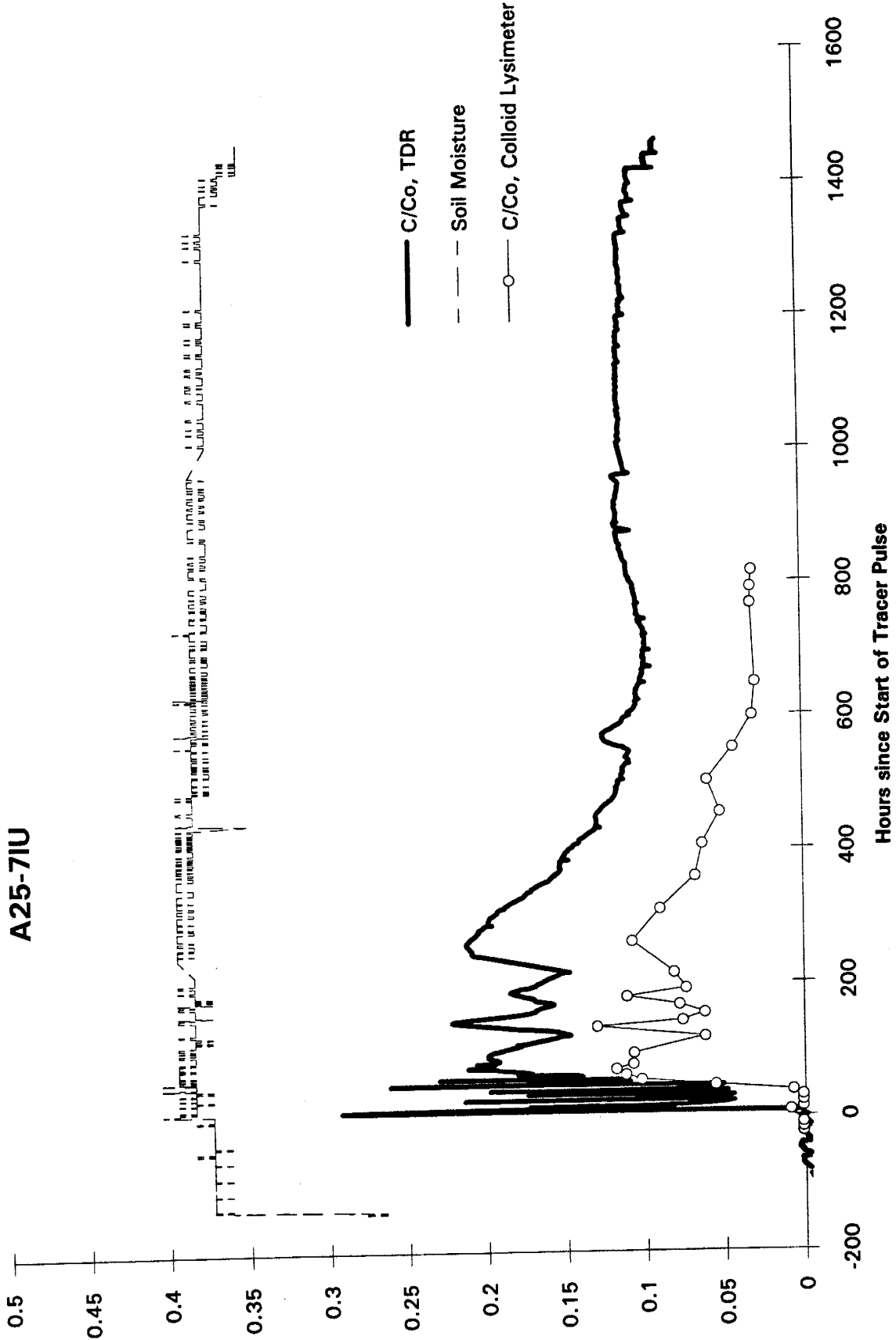




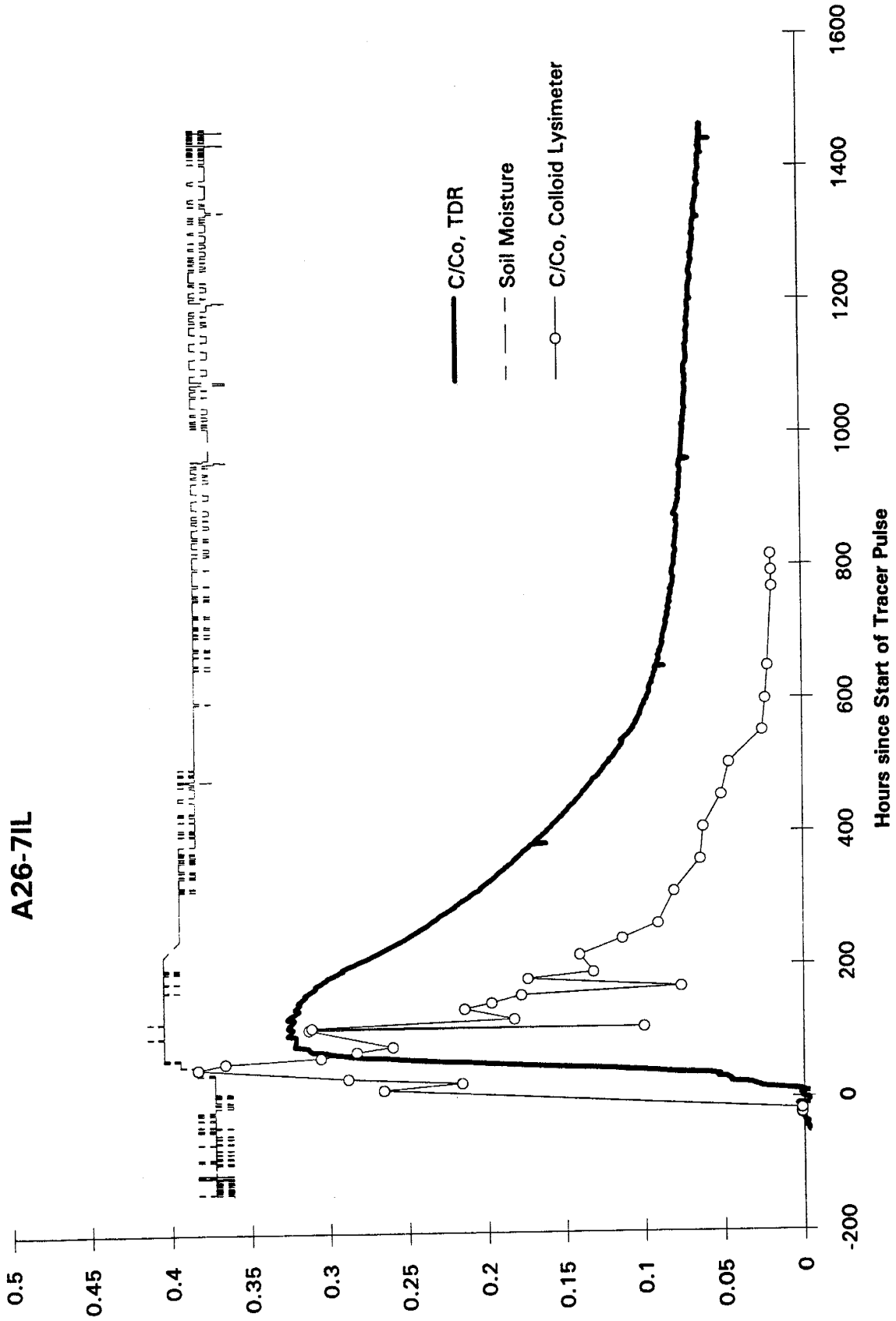
A24-60L



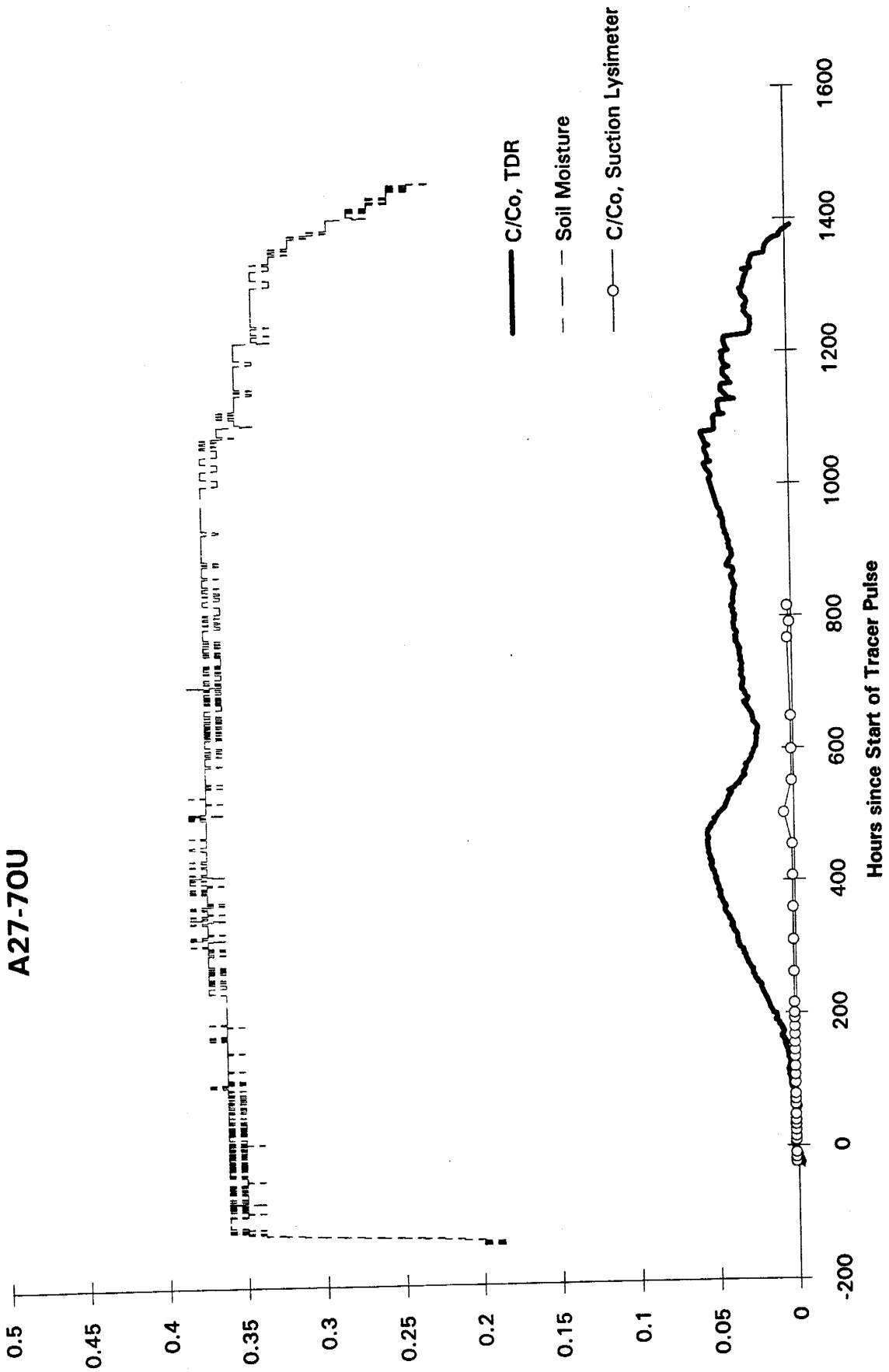
A25-7IU



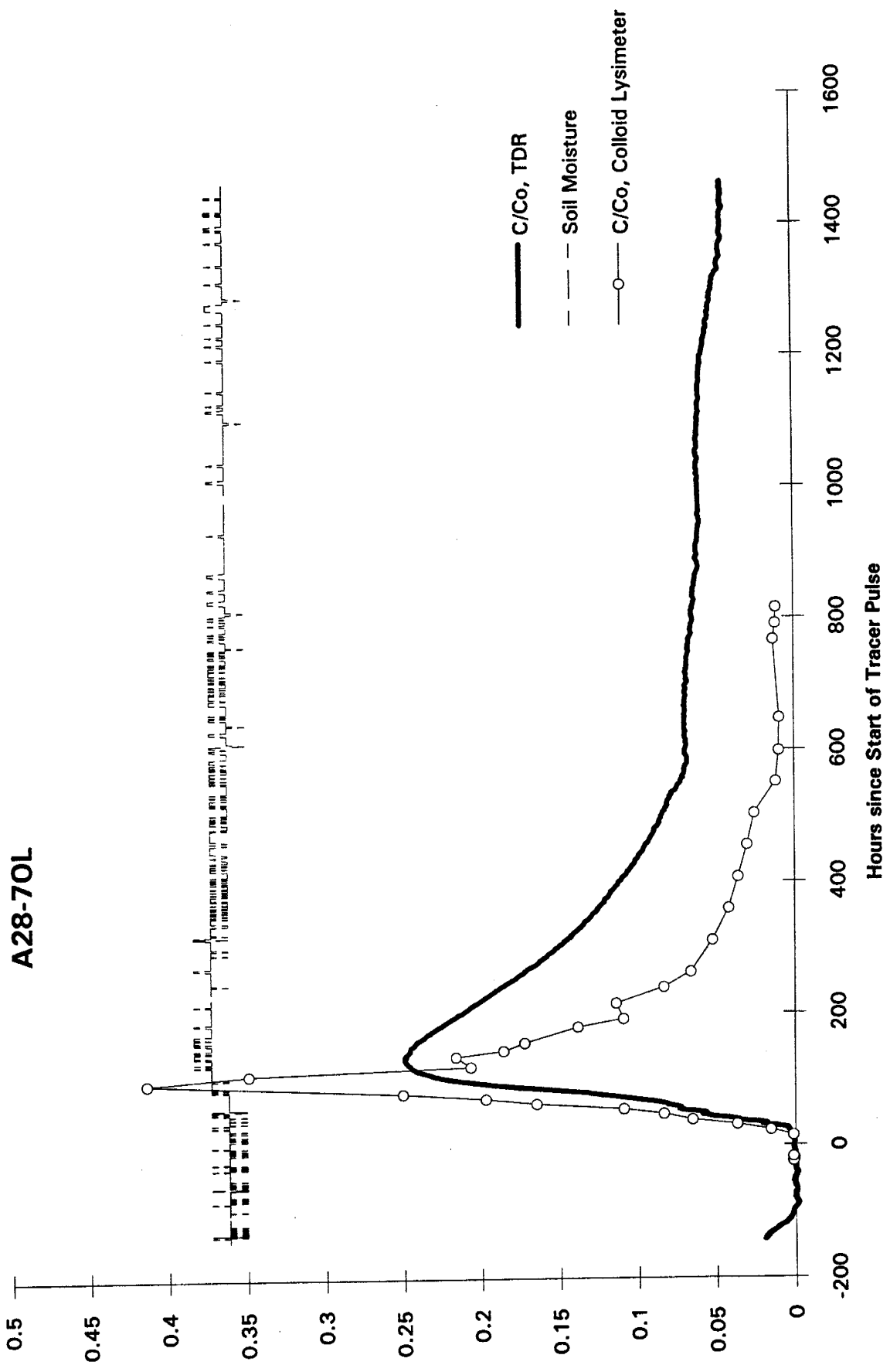
A26-7IL



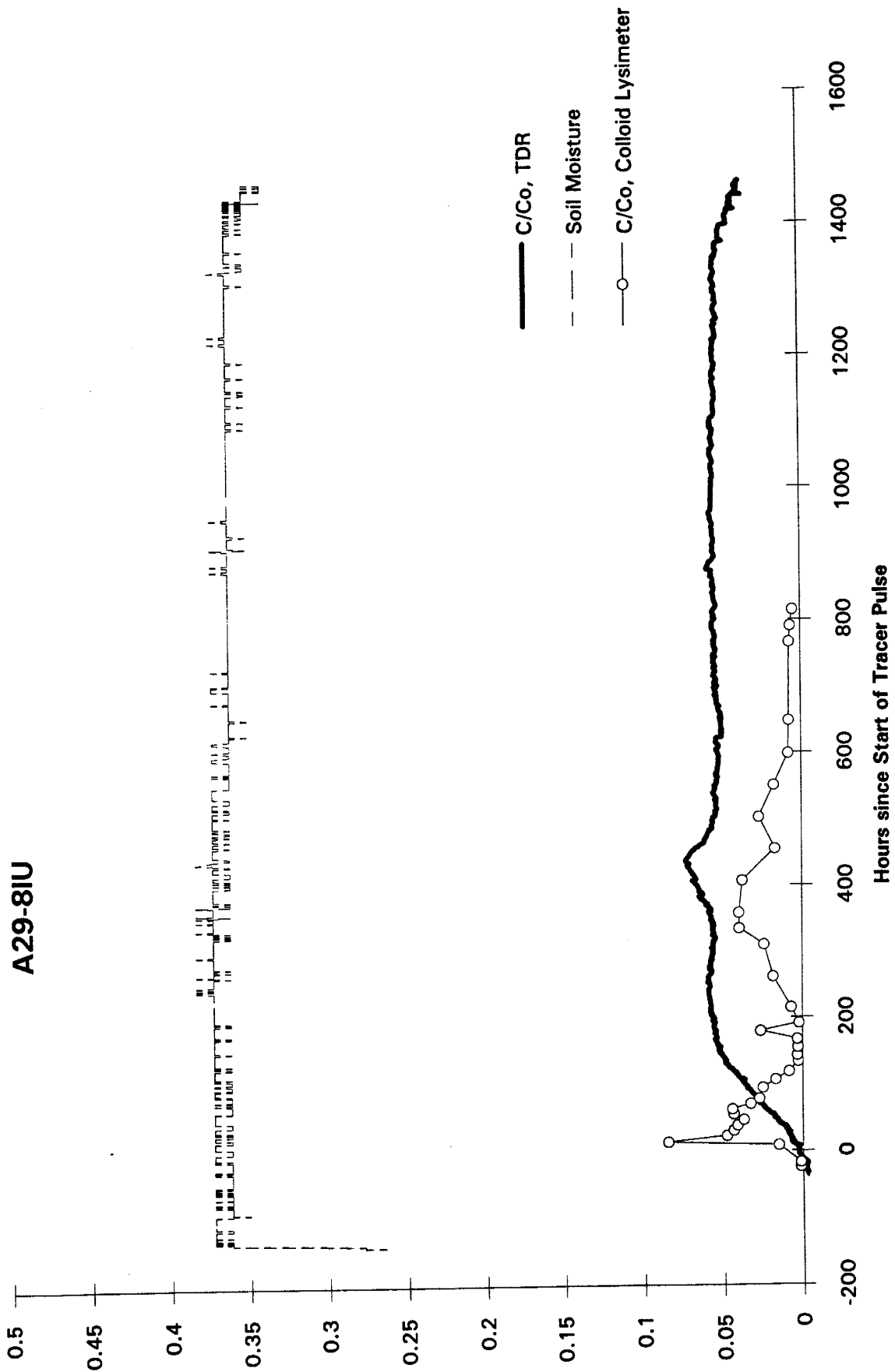
A27-70U



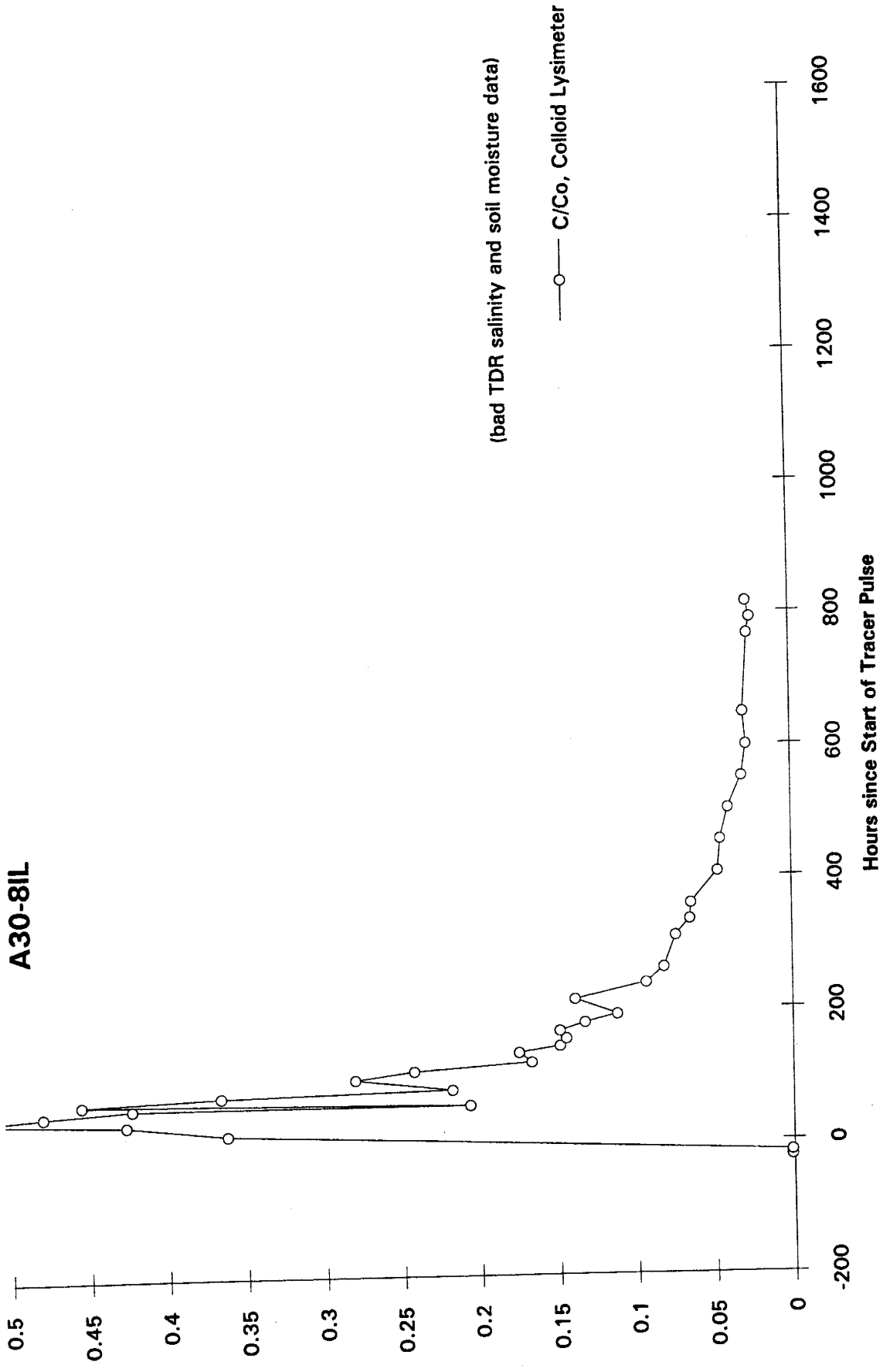
A28-70L



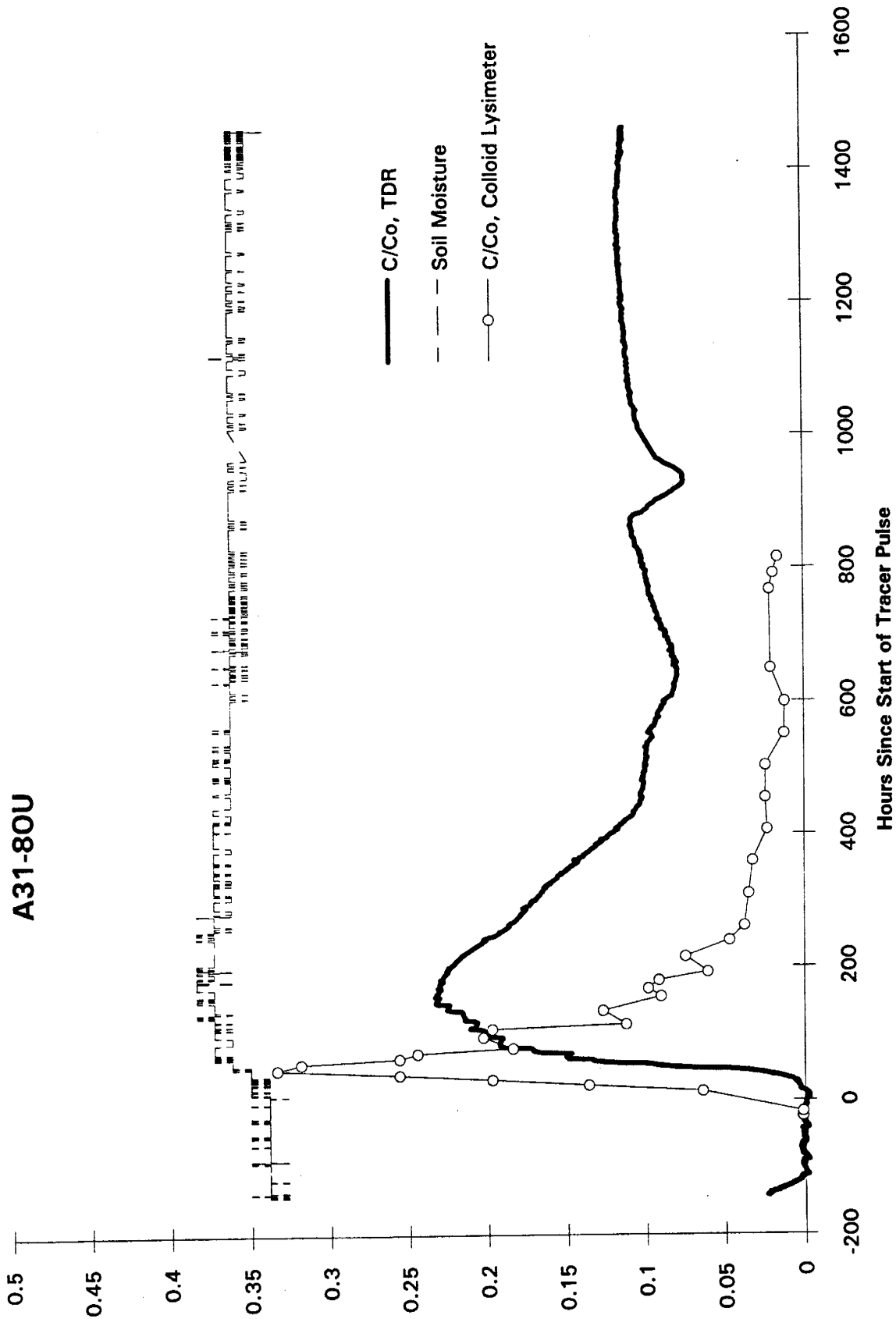
A29-8IU



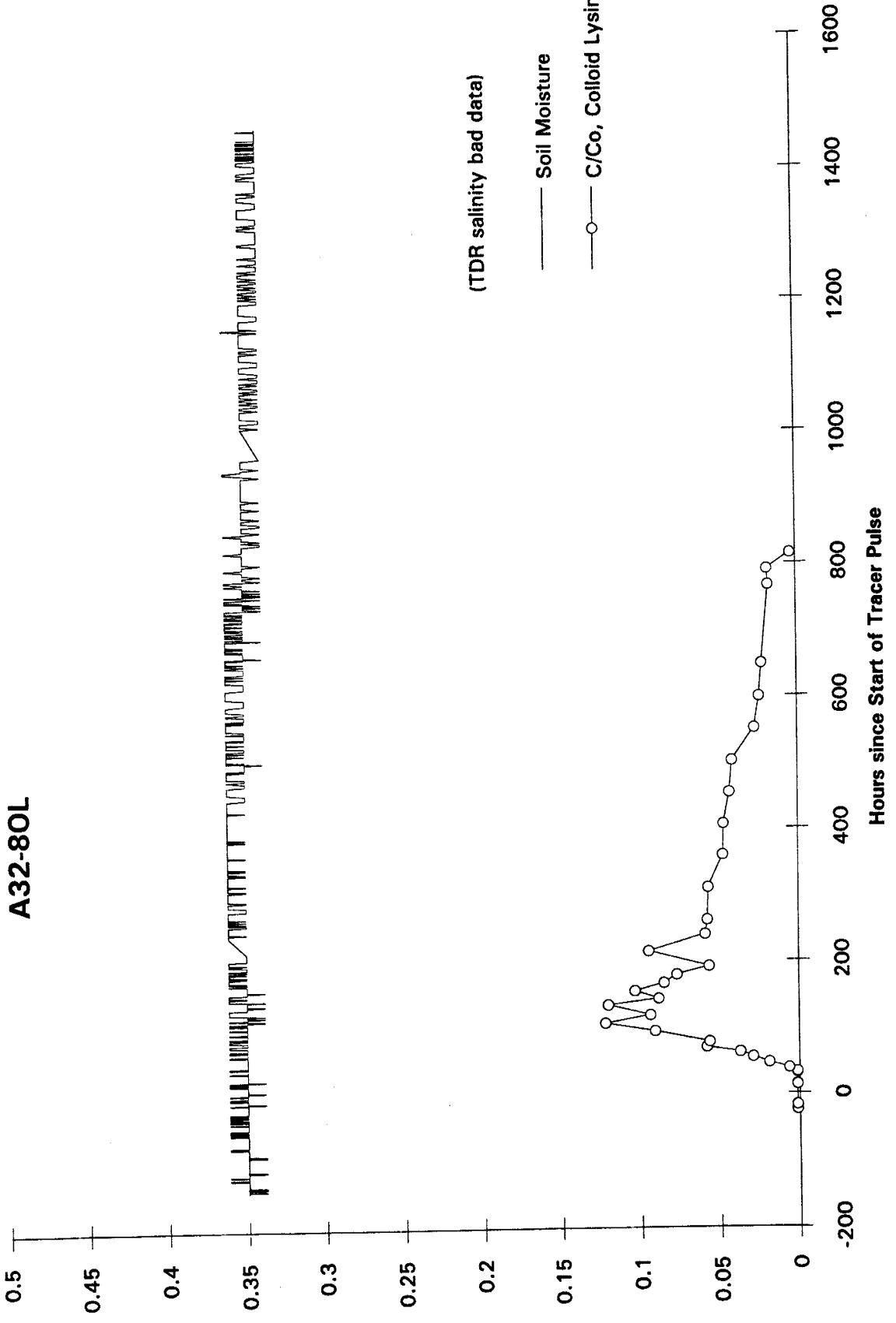
A30-8IL



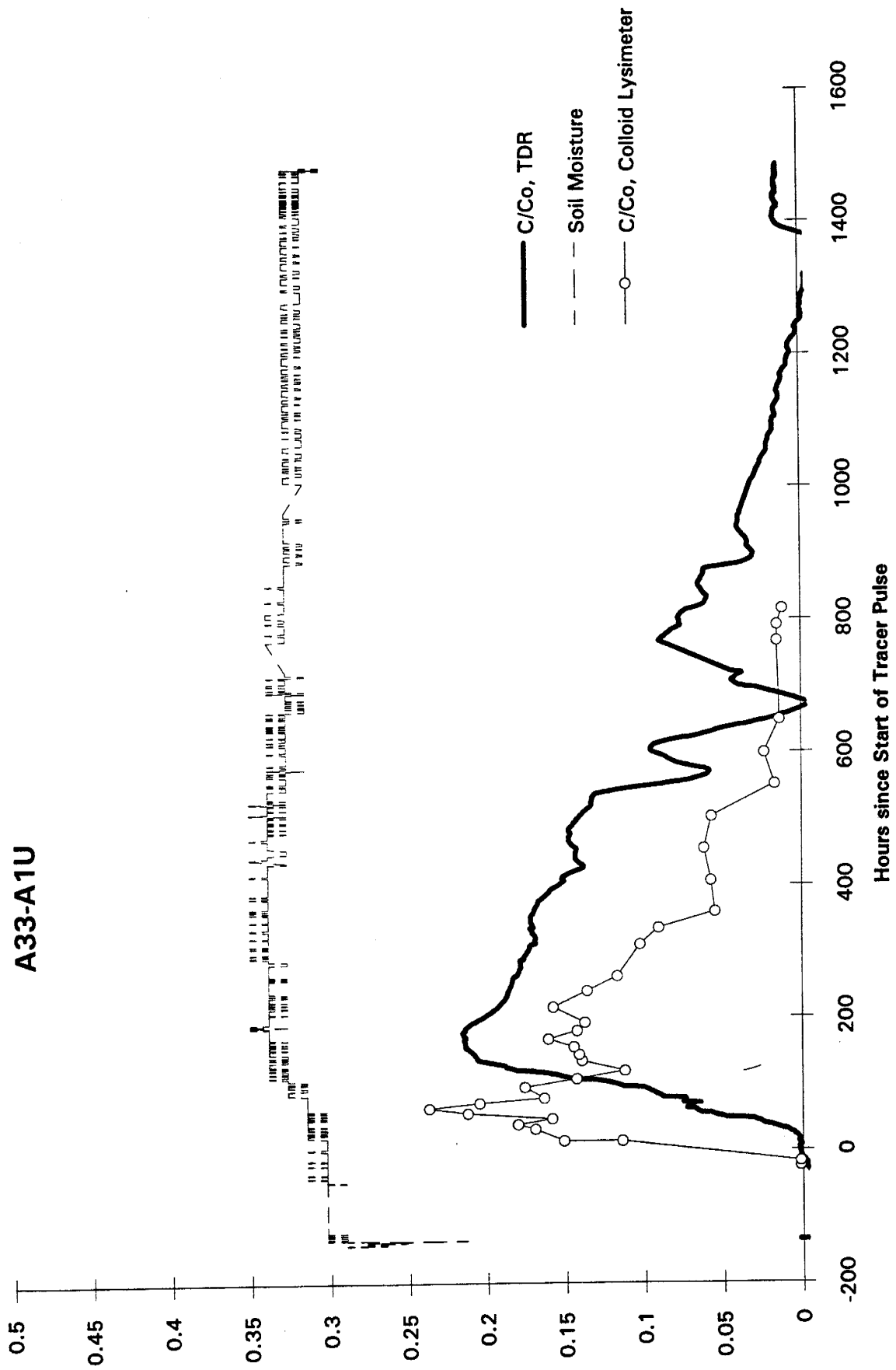
A31-80U



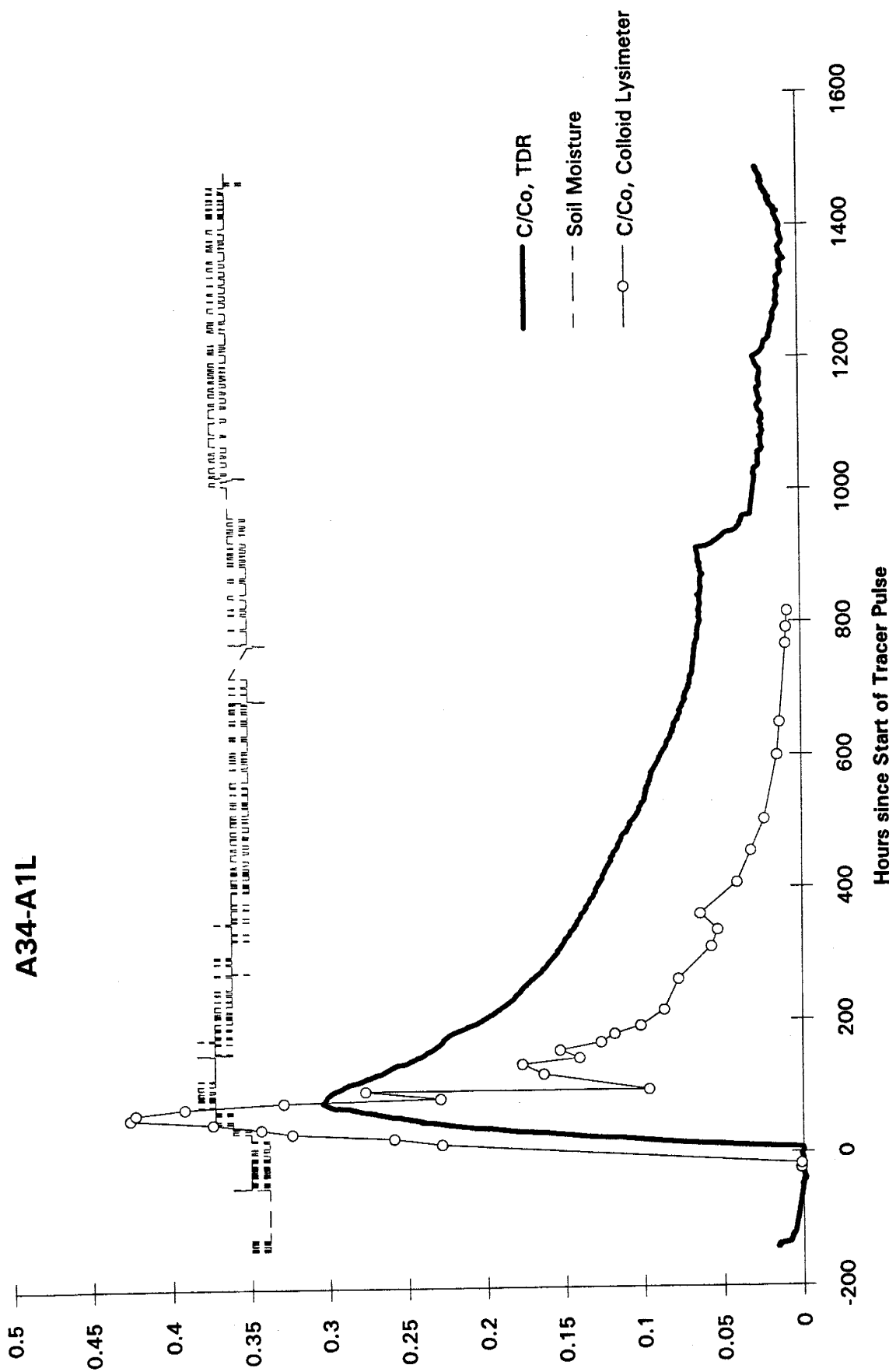
A32-80L



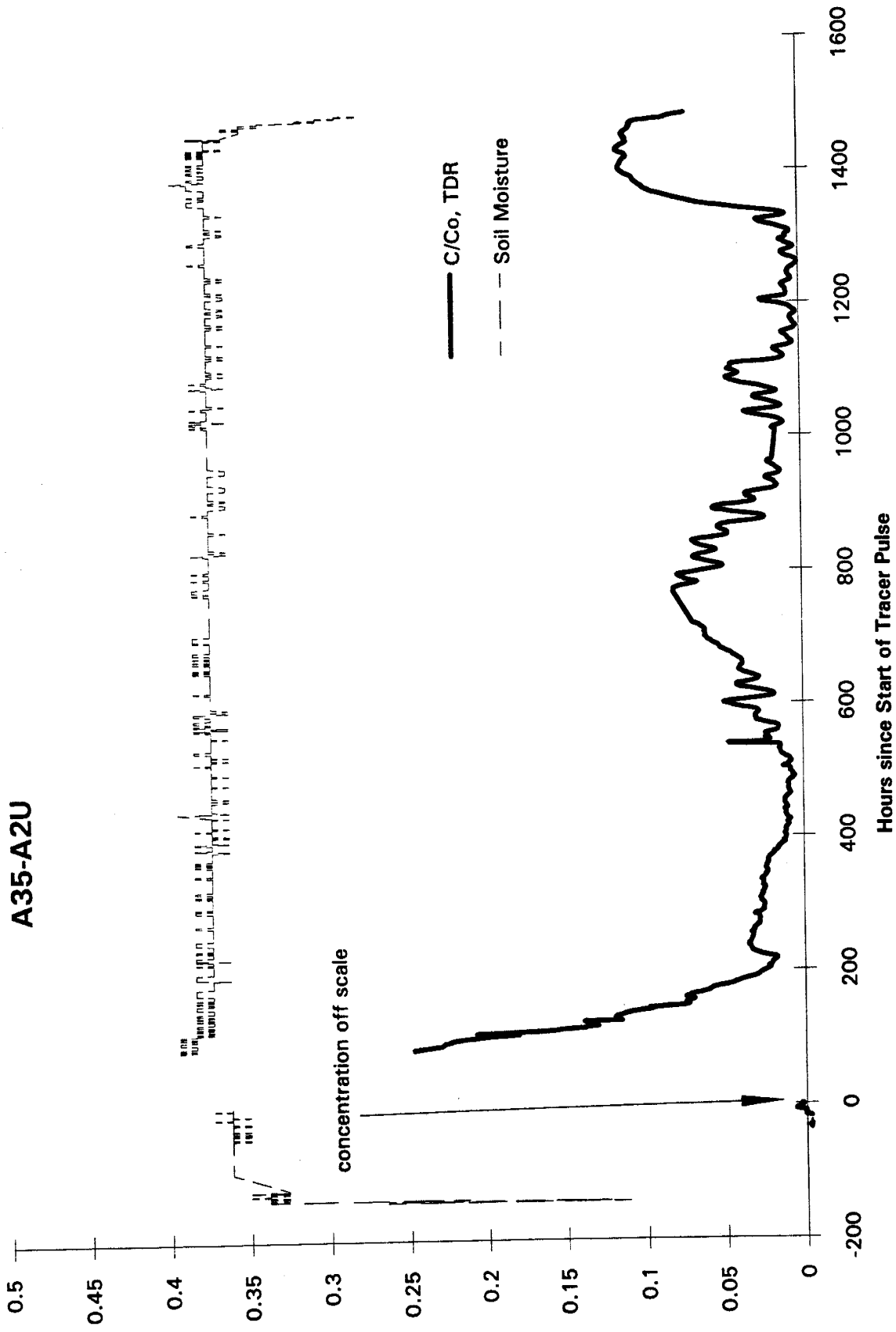
A33-A1U



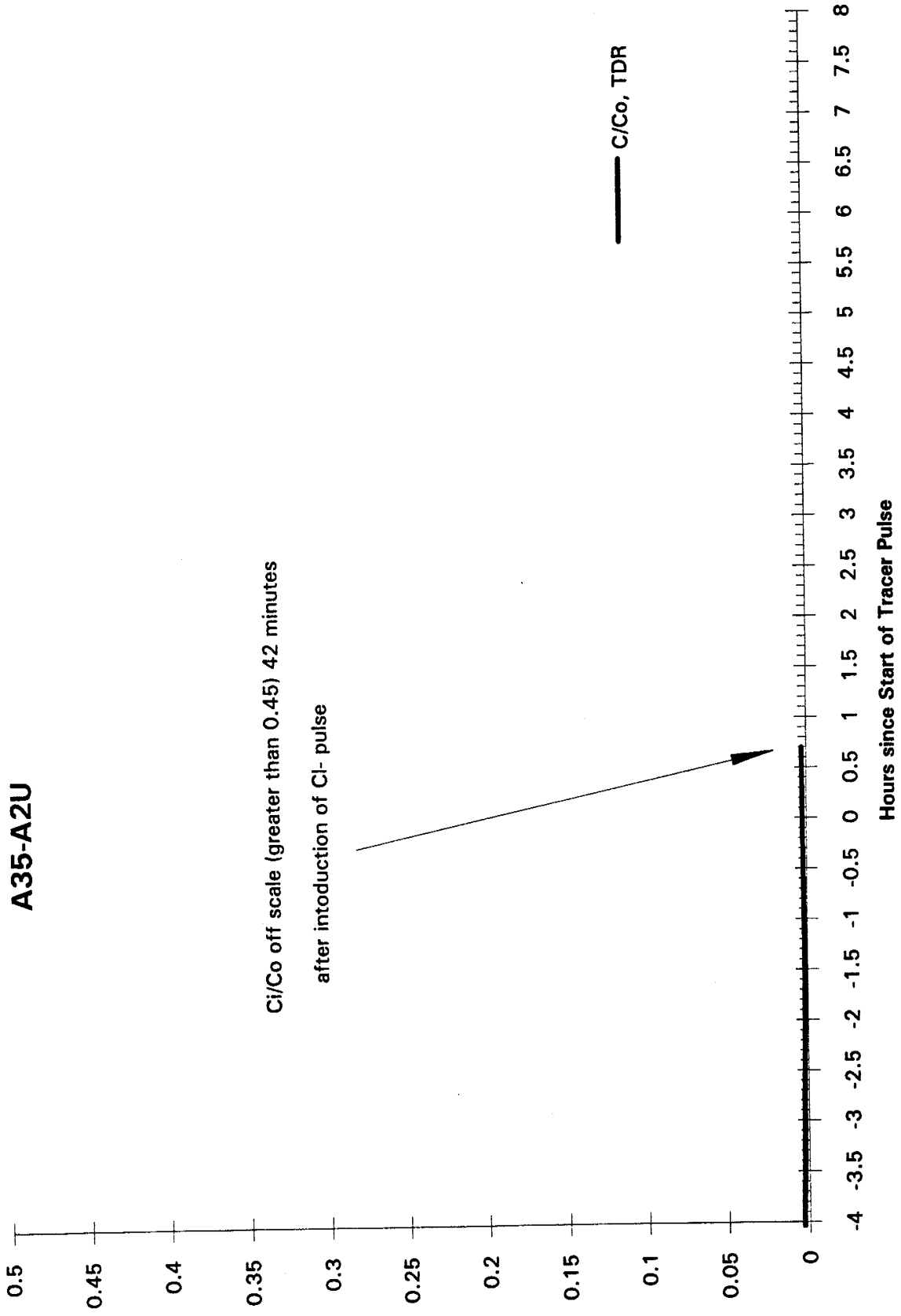
A34-A1L



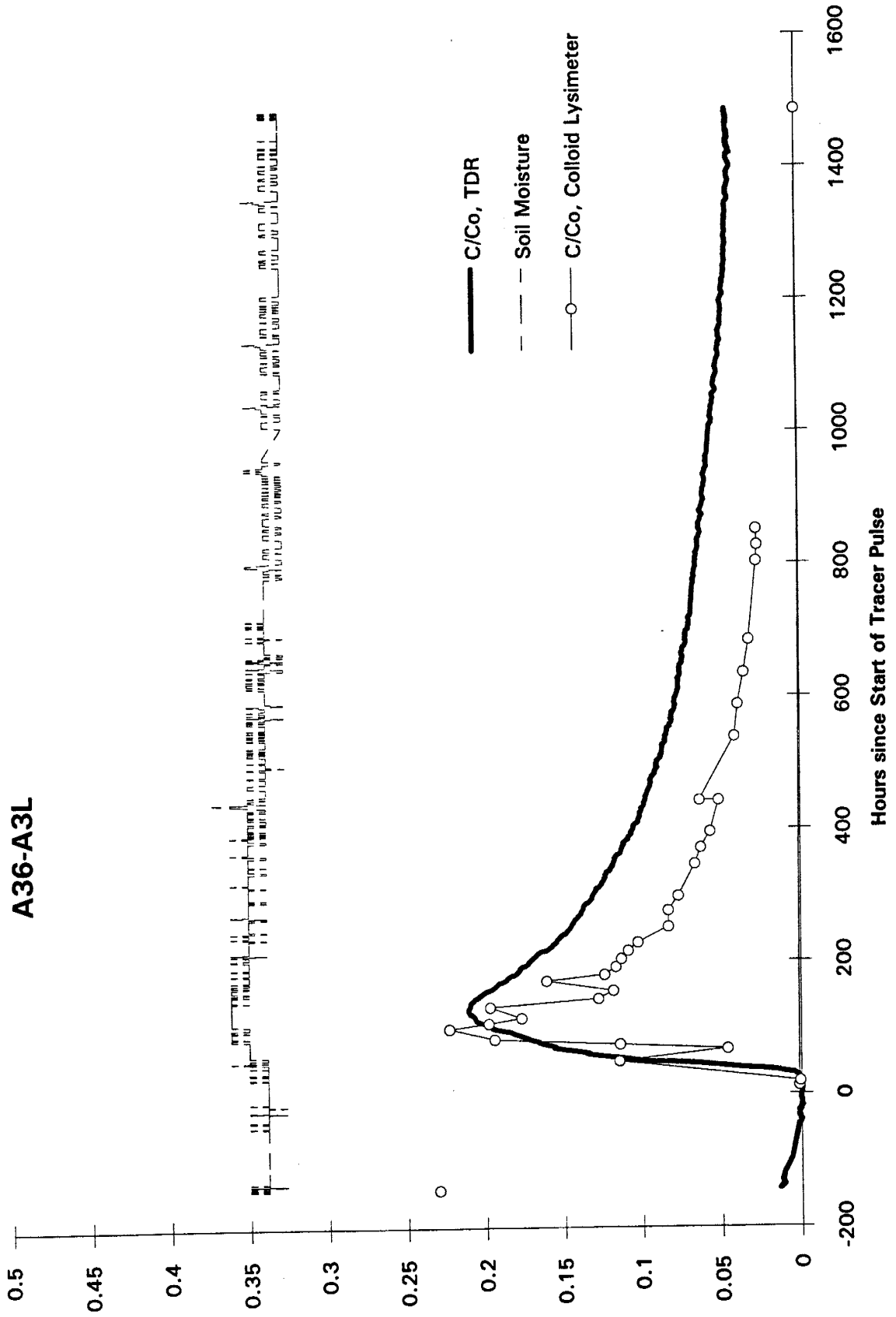
A35-A2U



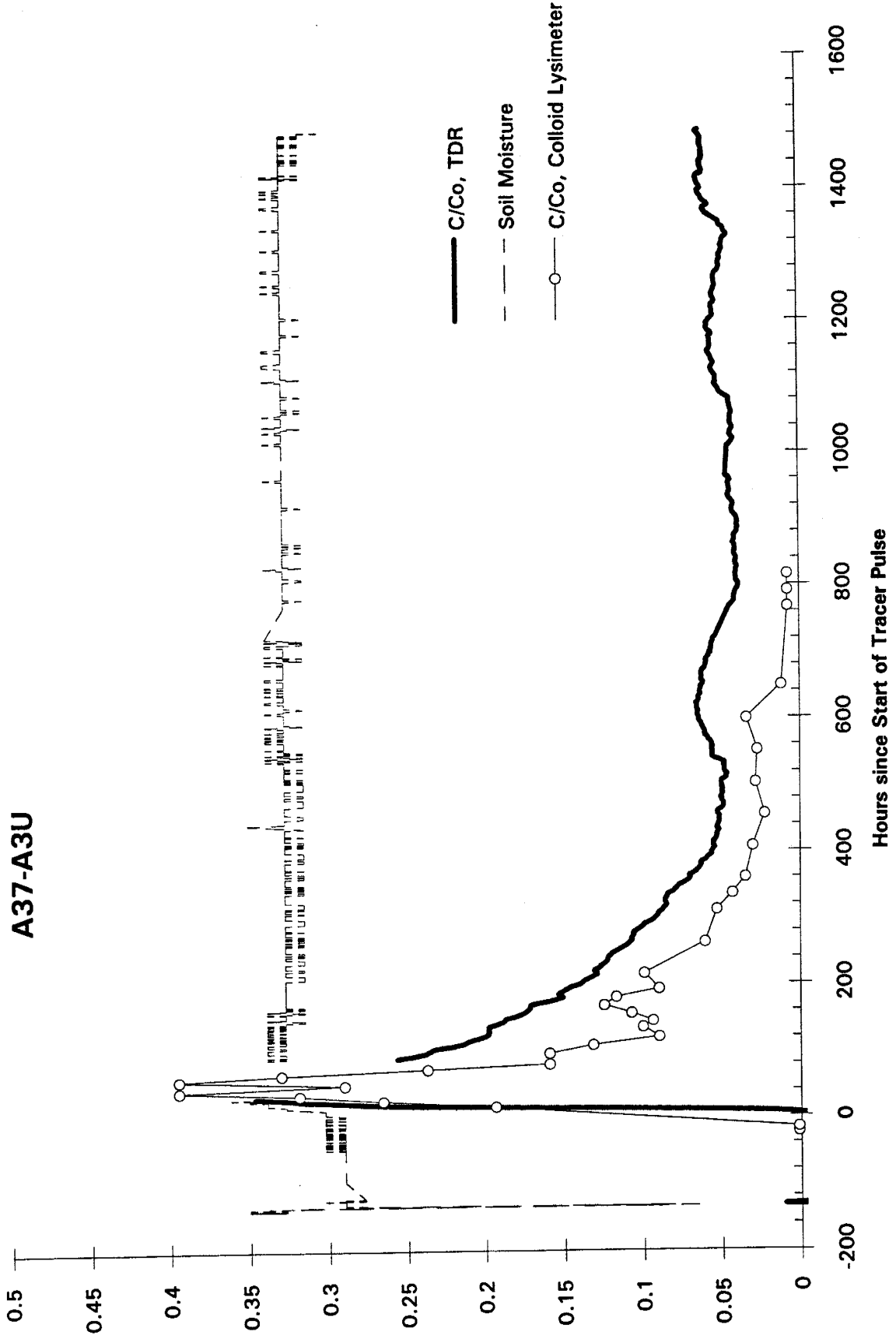
A35-A2U



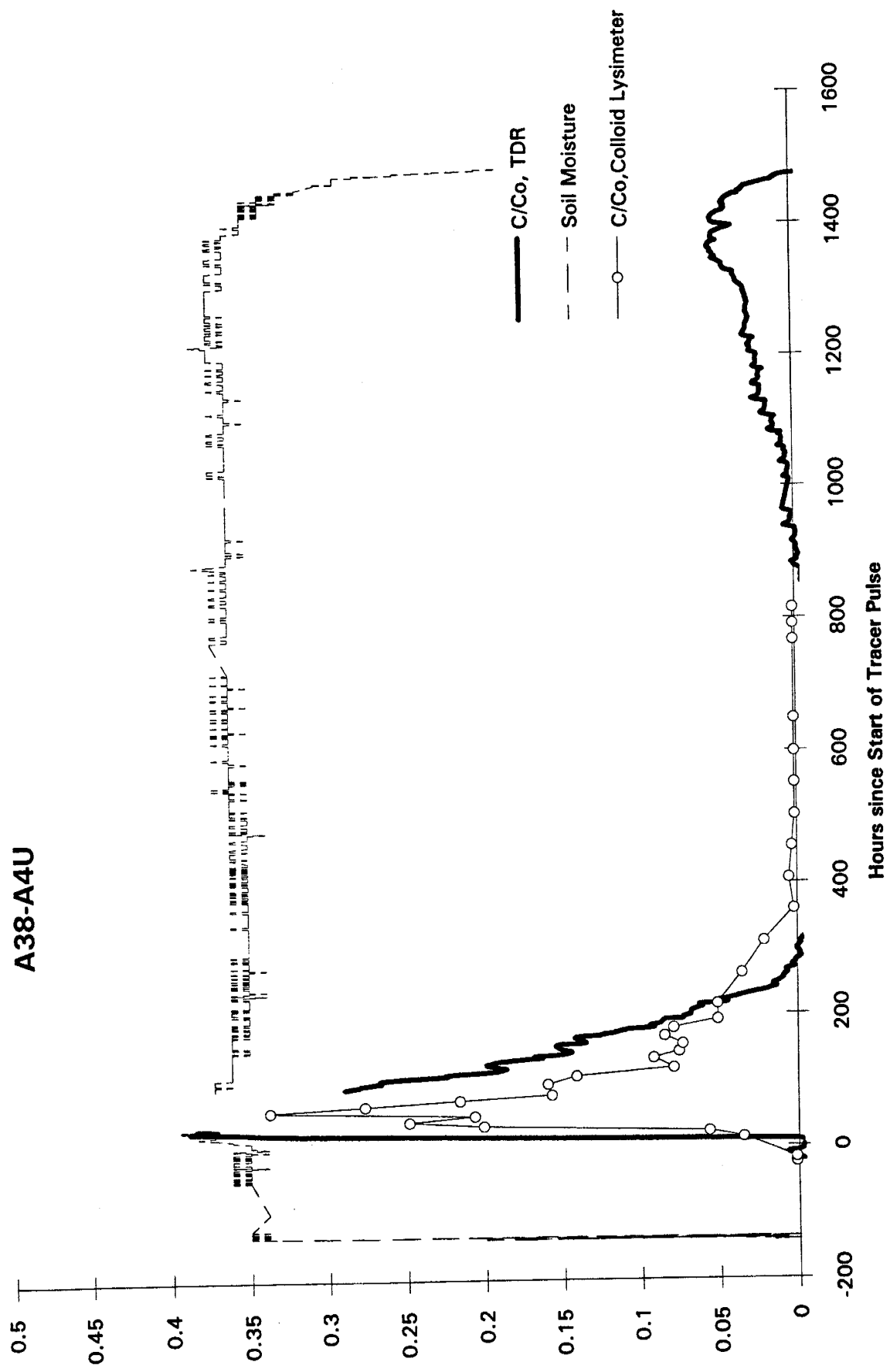
A36-A3L



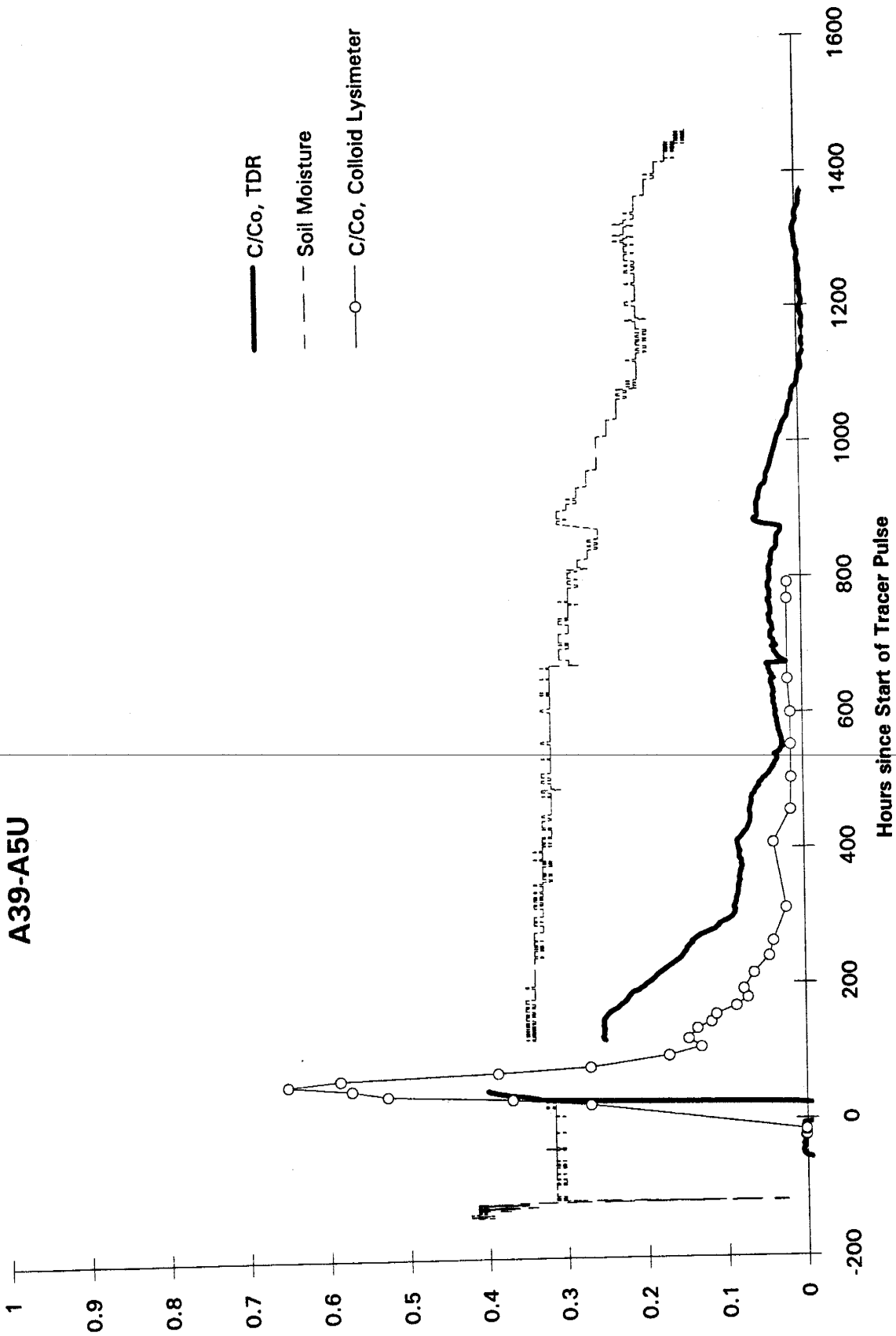
A37-A3U



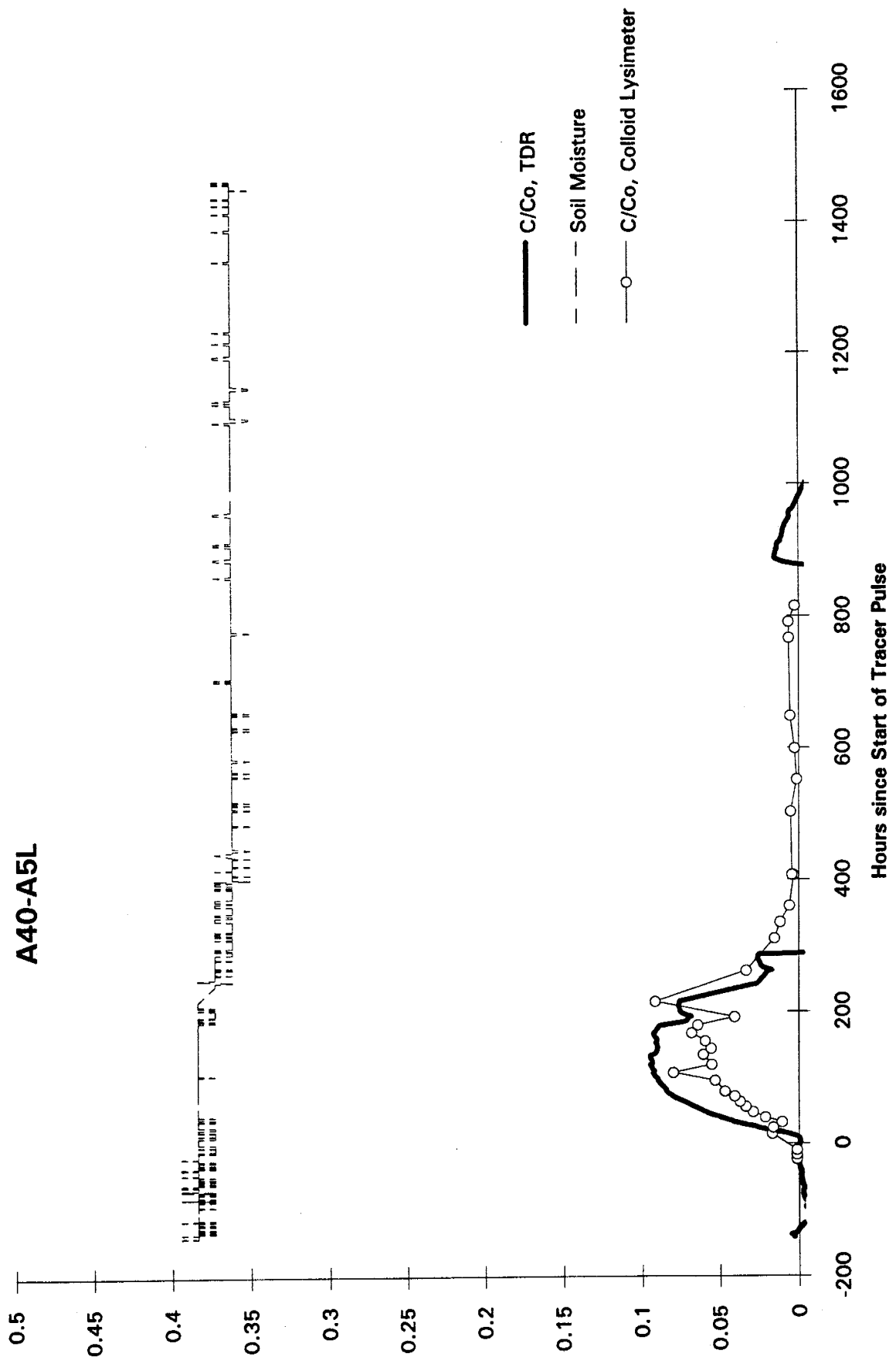
A38-A4U



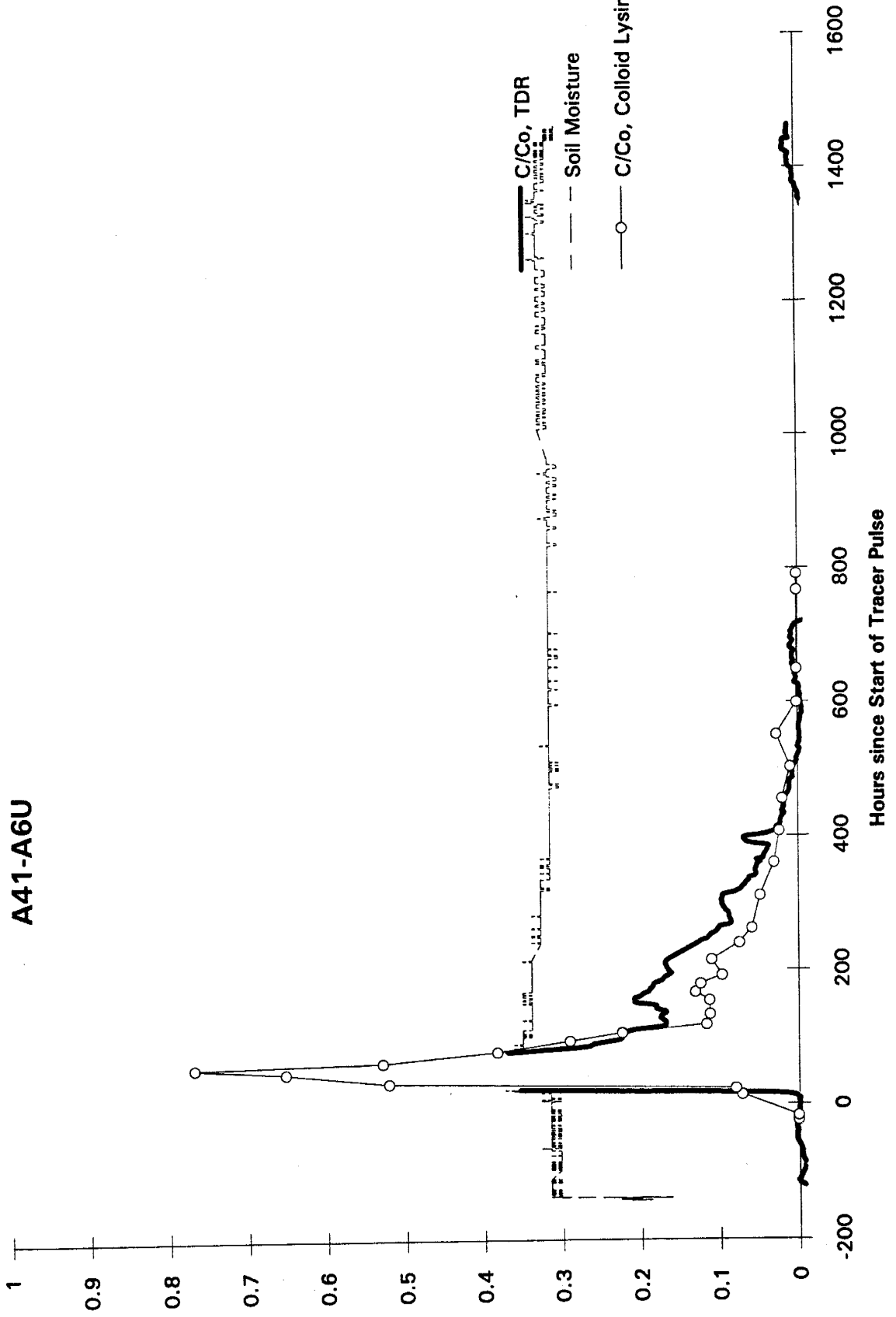
A39-A5U



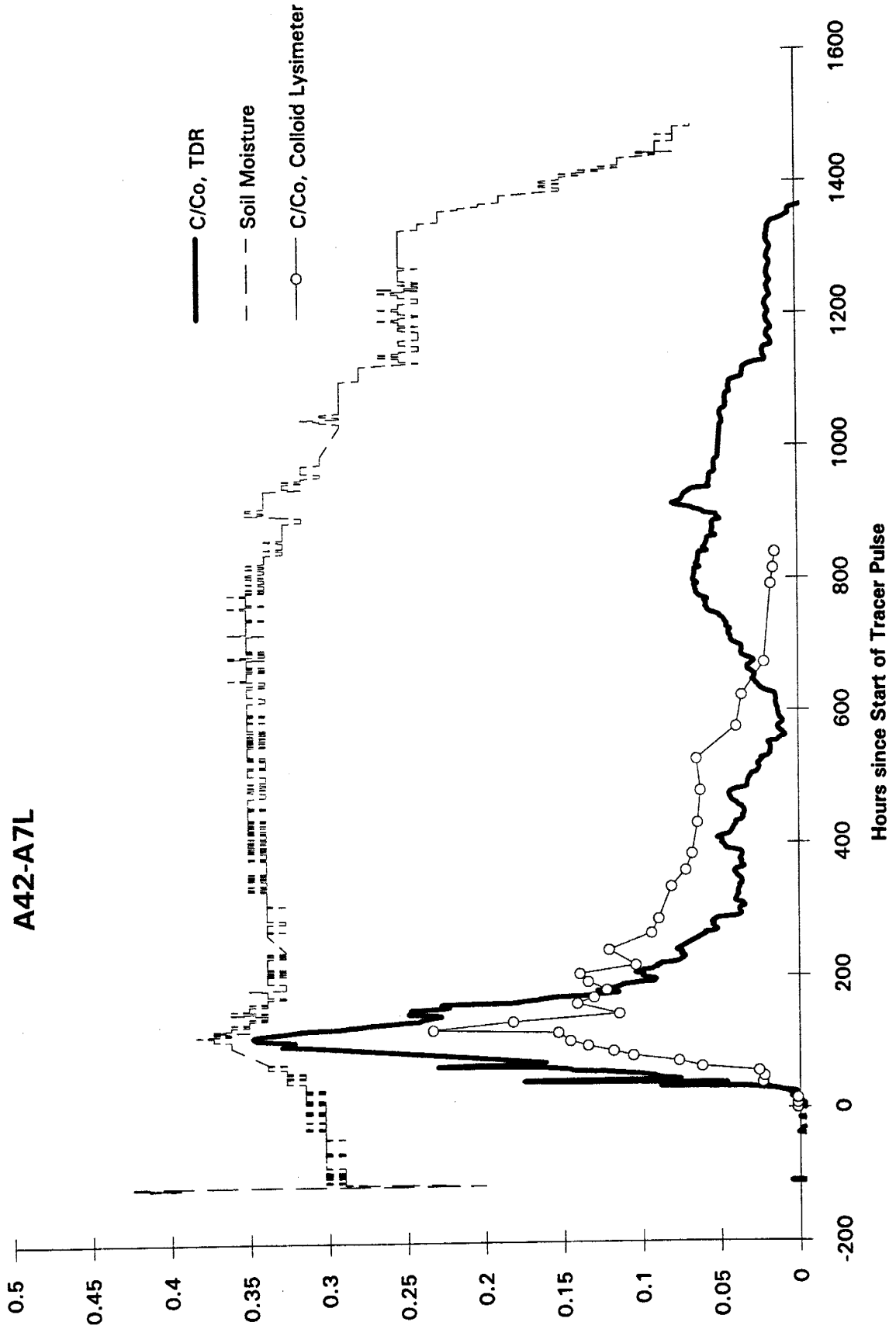
A40-A5L

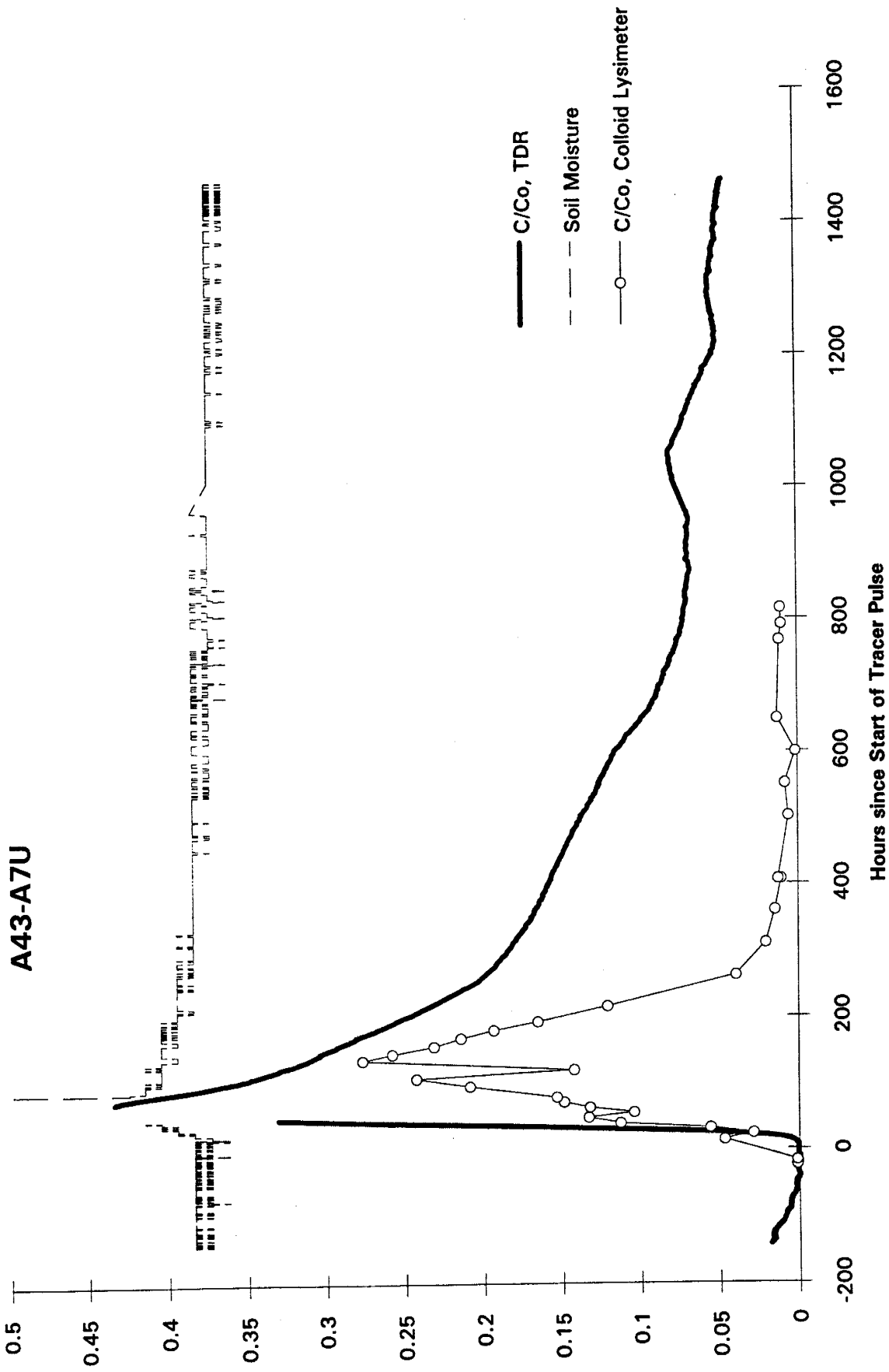


A41-A6U

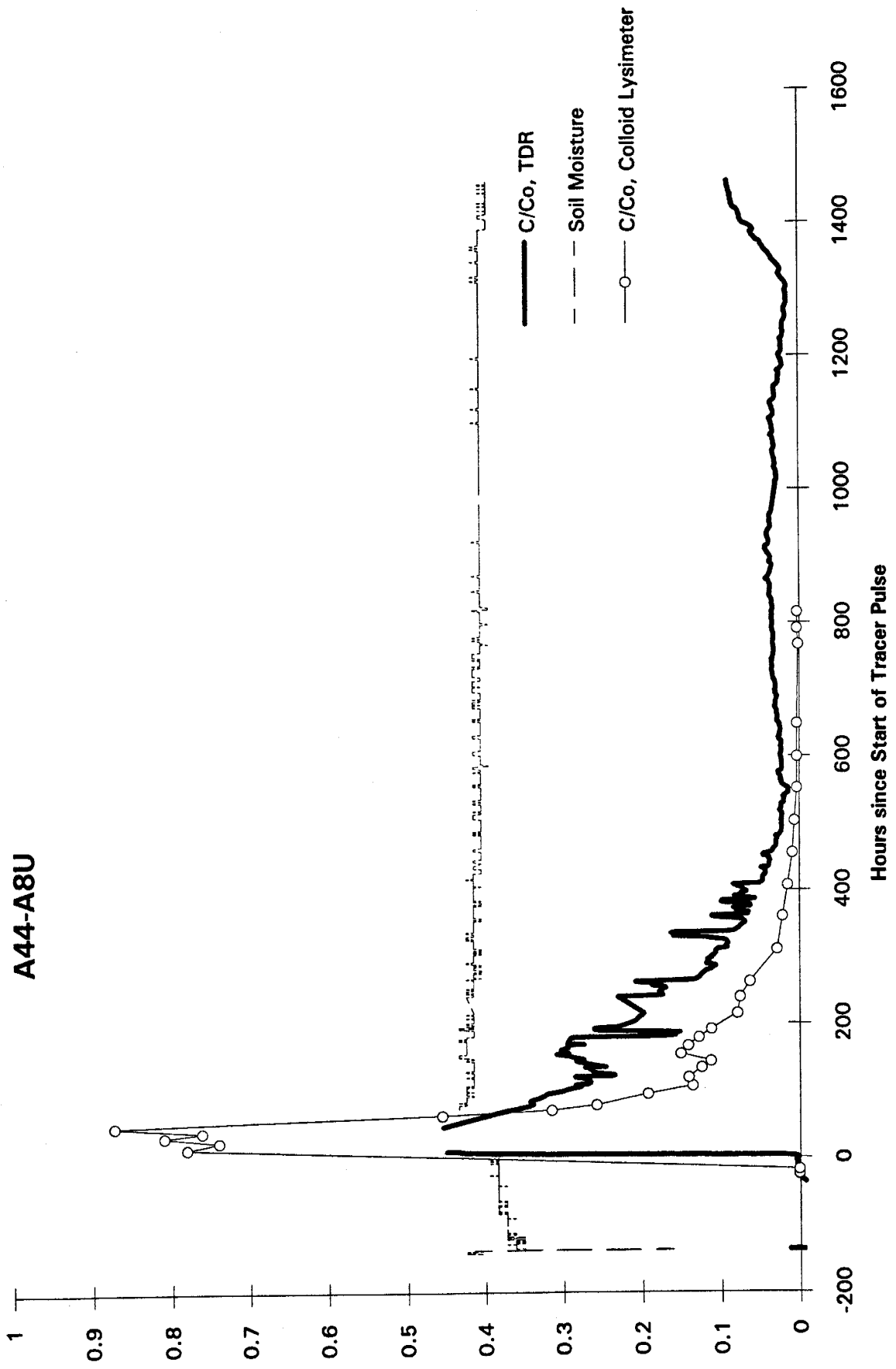


A42-A7L

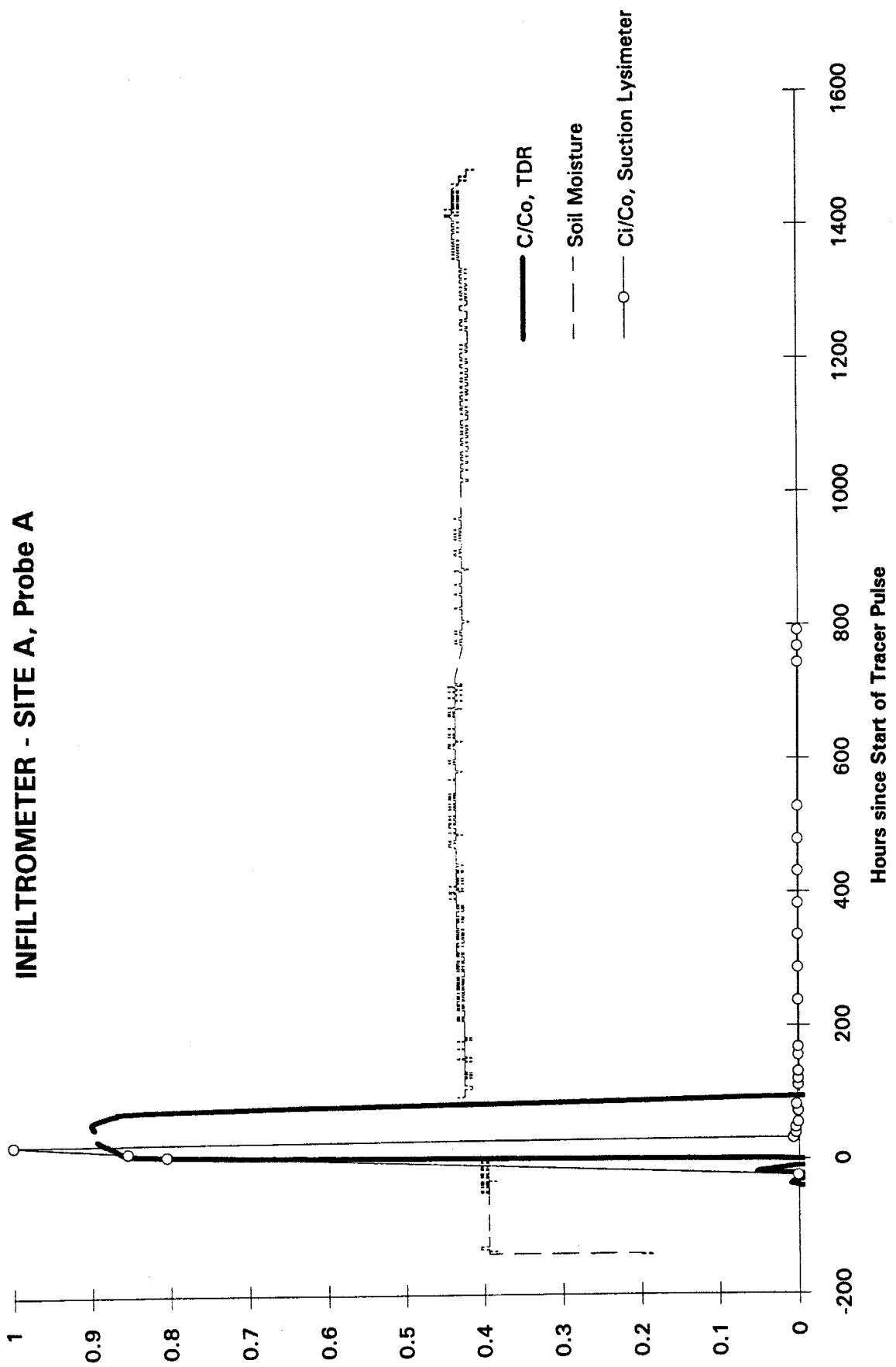




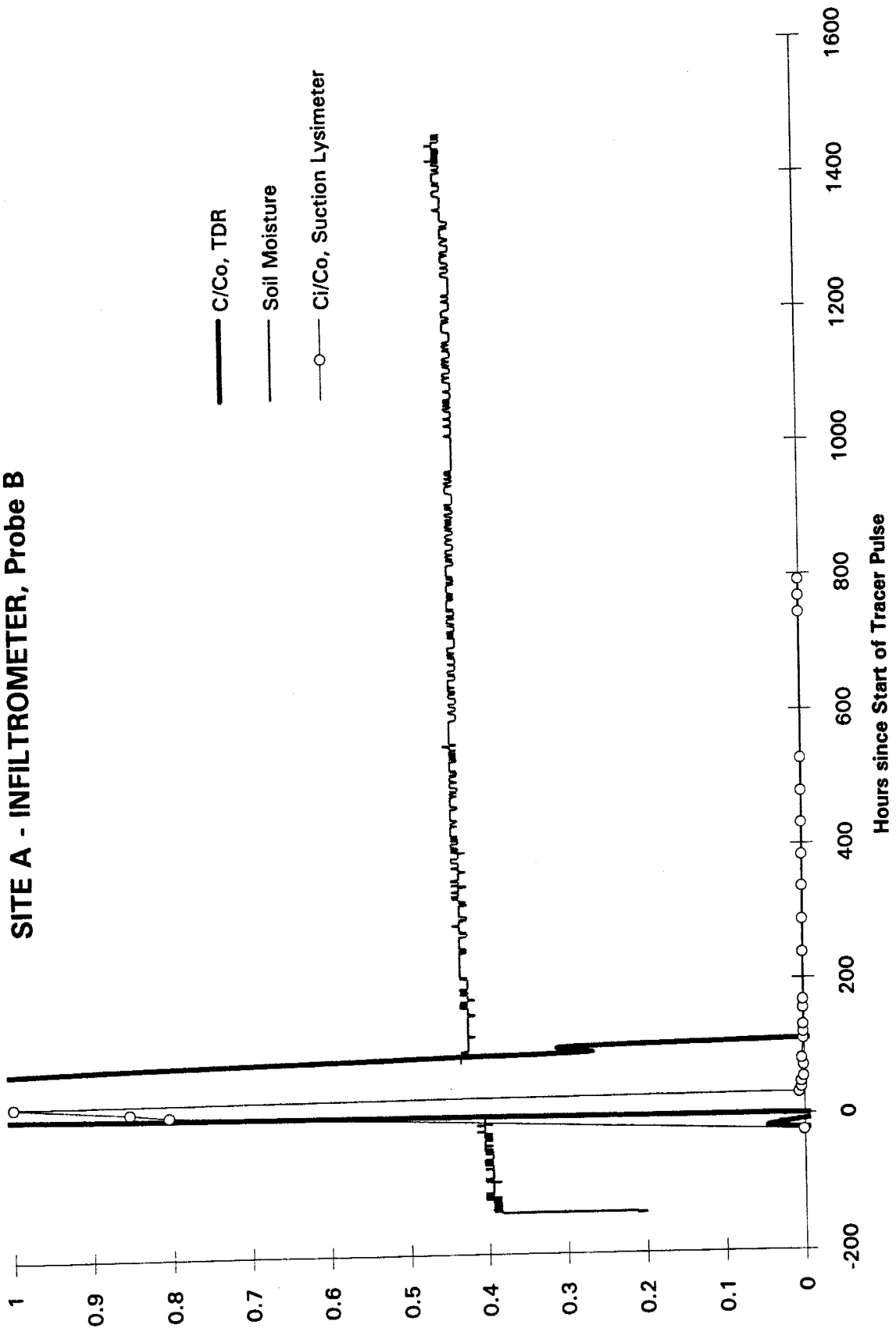
A44-A8U



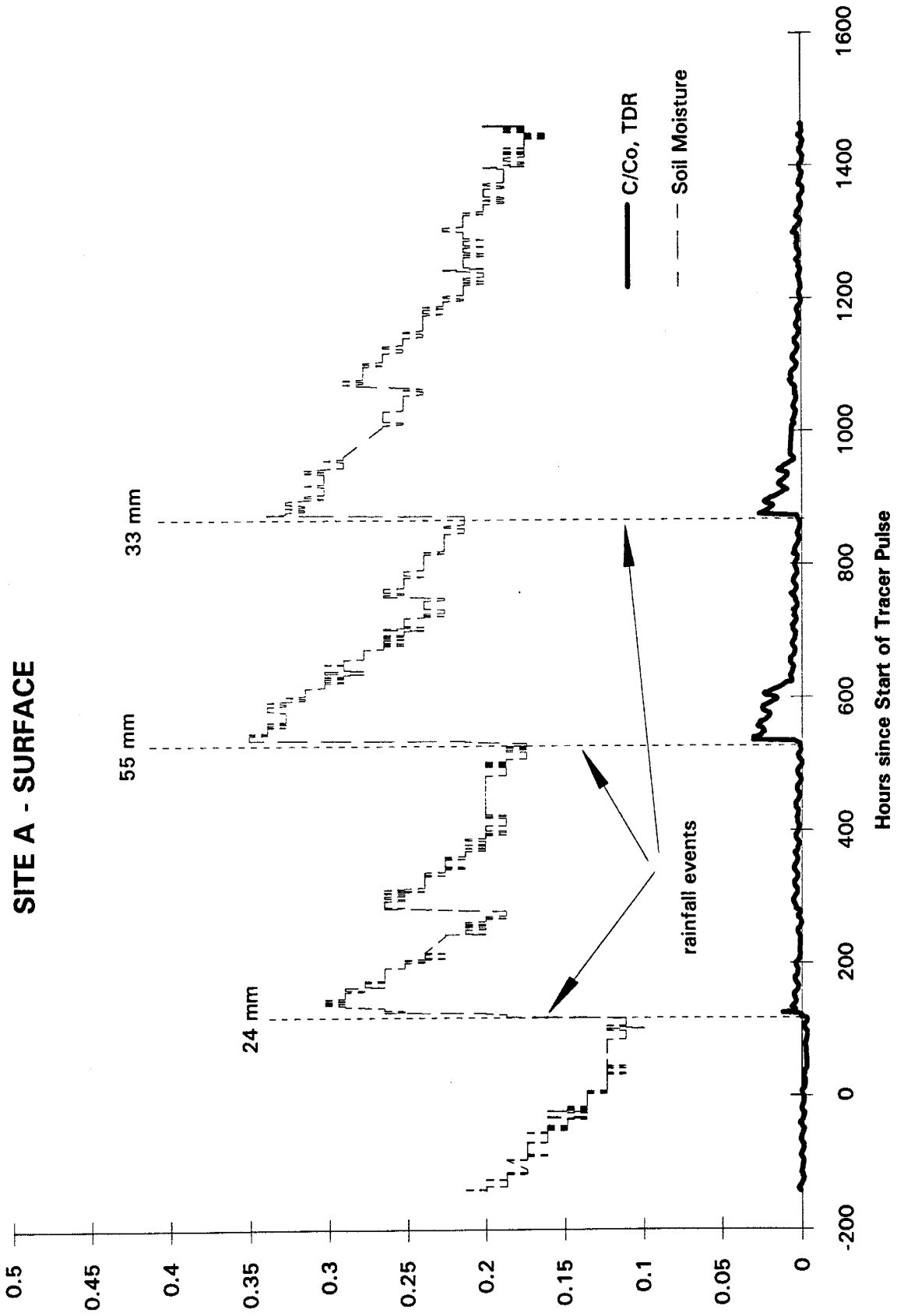
INFILTRMETER - SITE A, Probe A

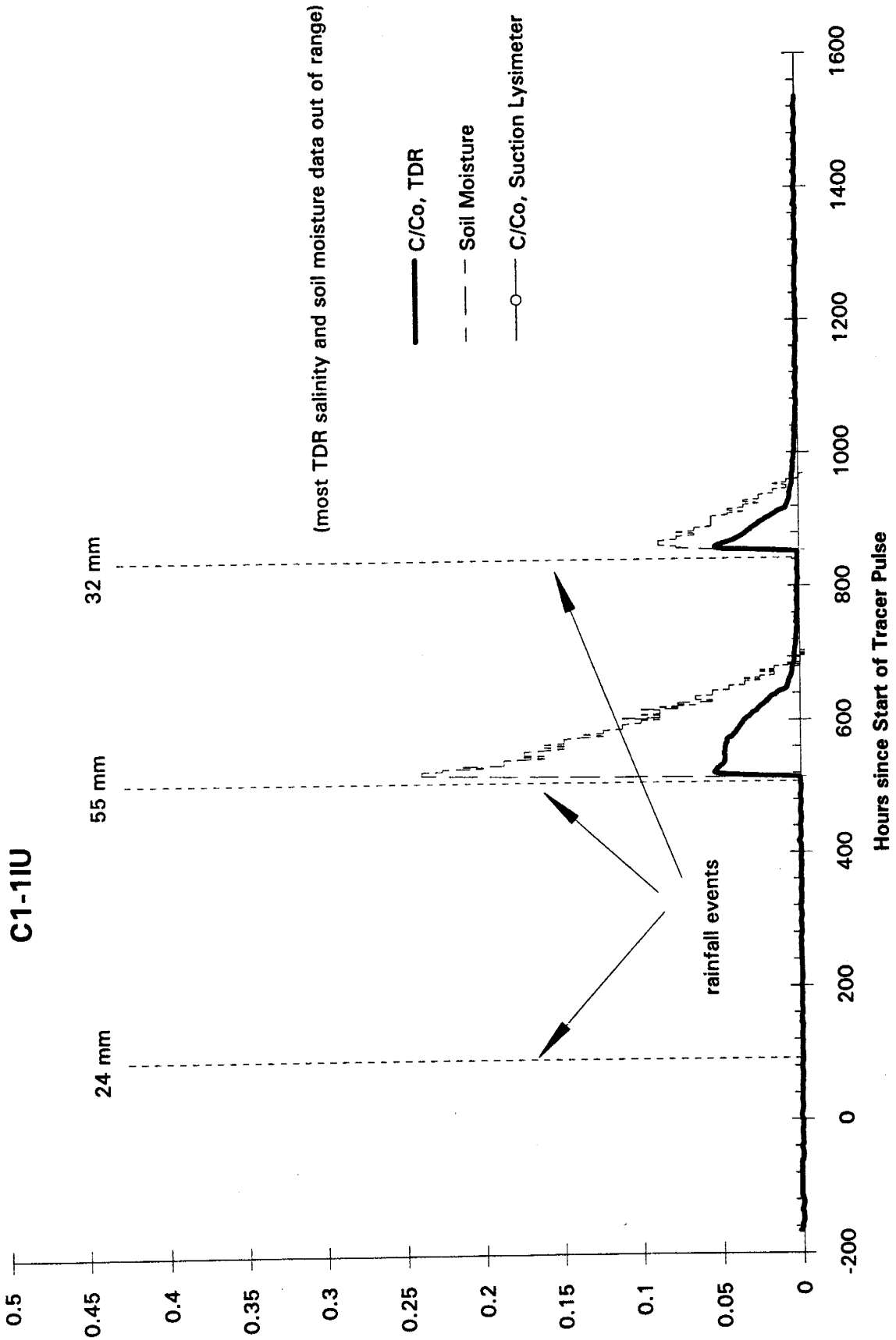


SITE A - INFILTRMETER, Probe B

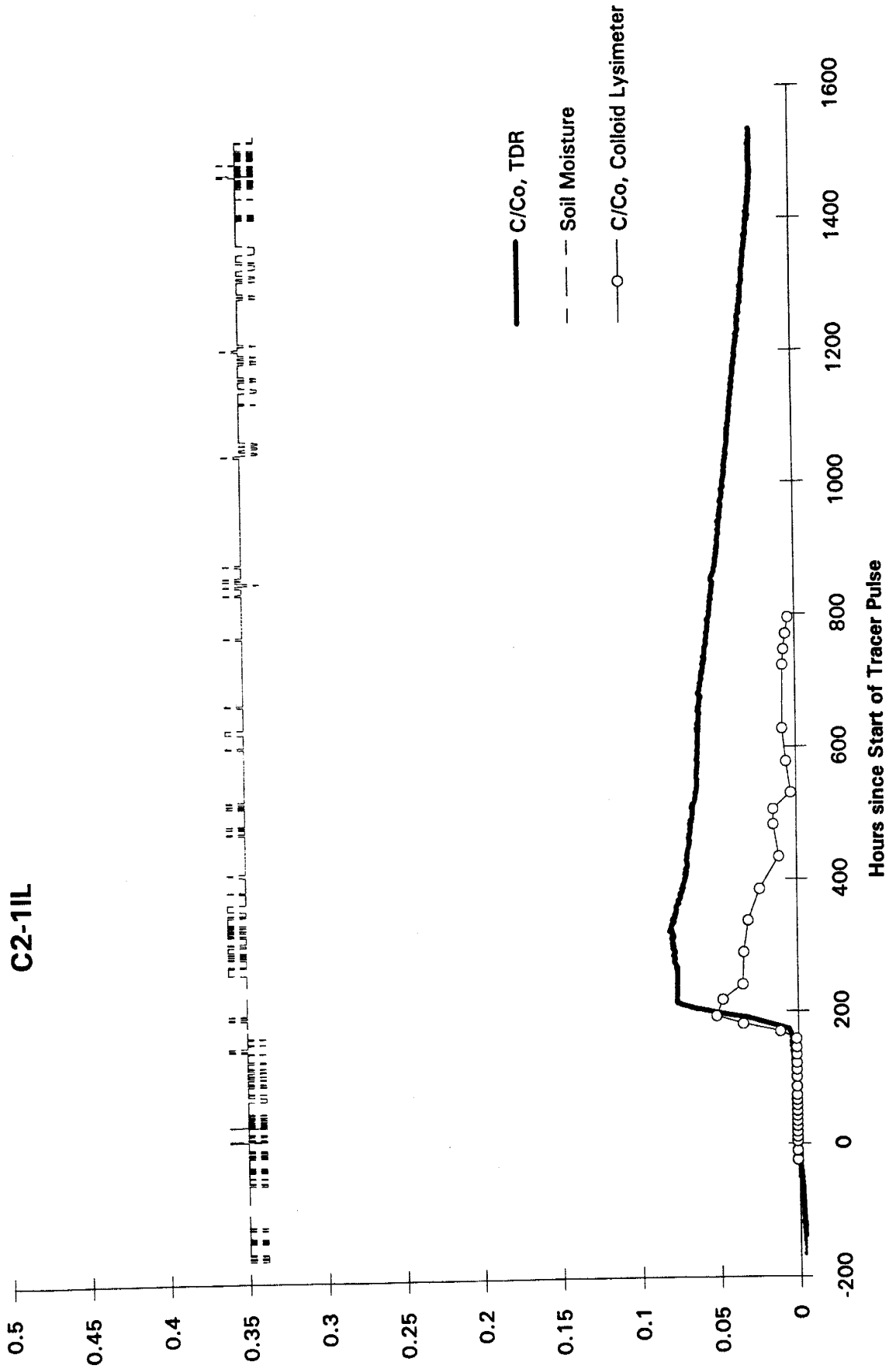


SITE A - SURFACE

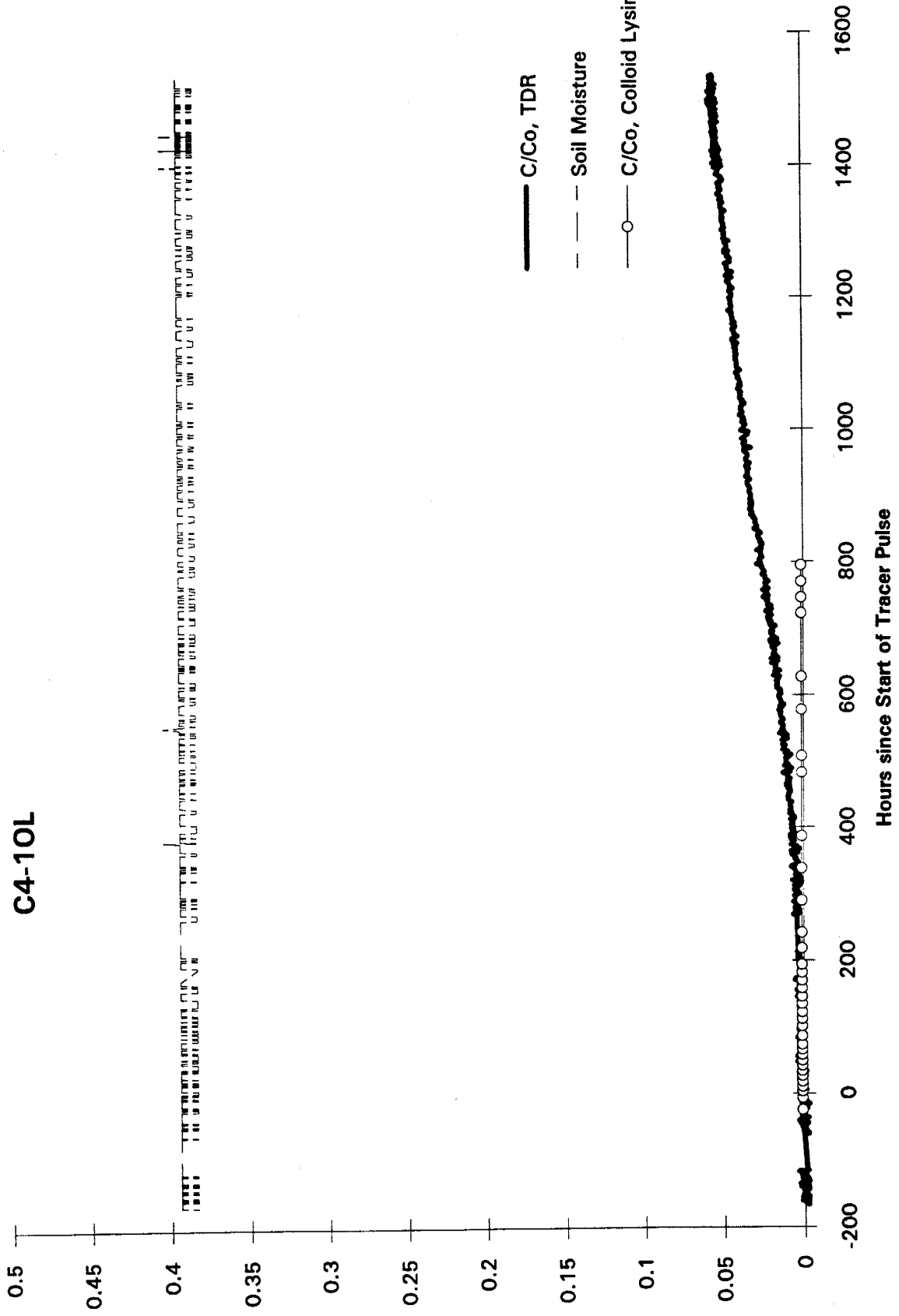


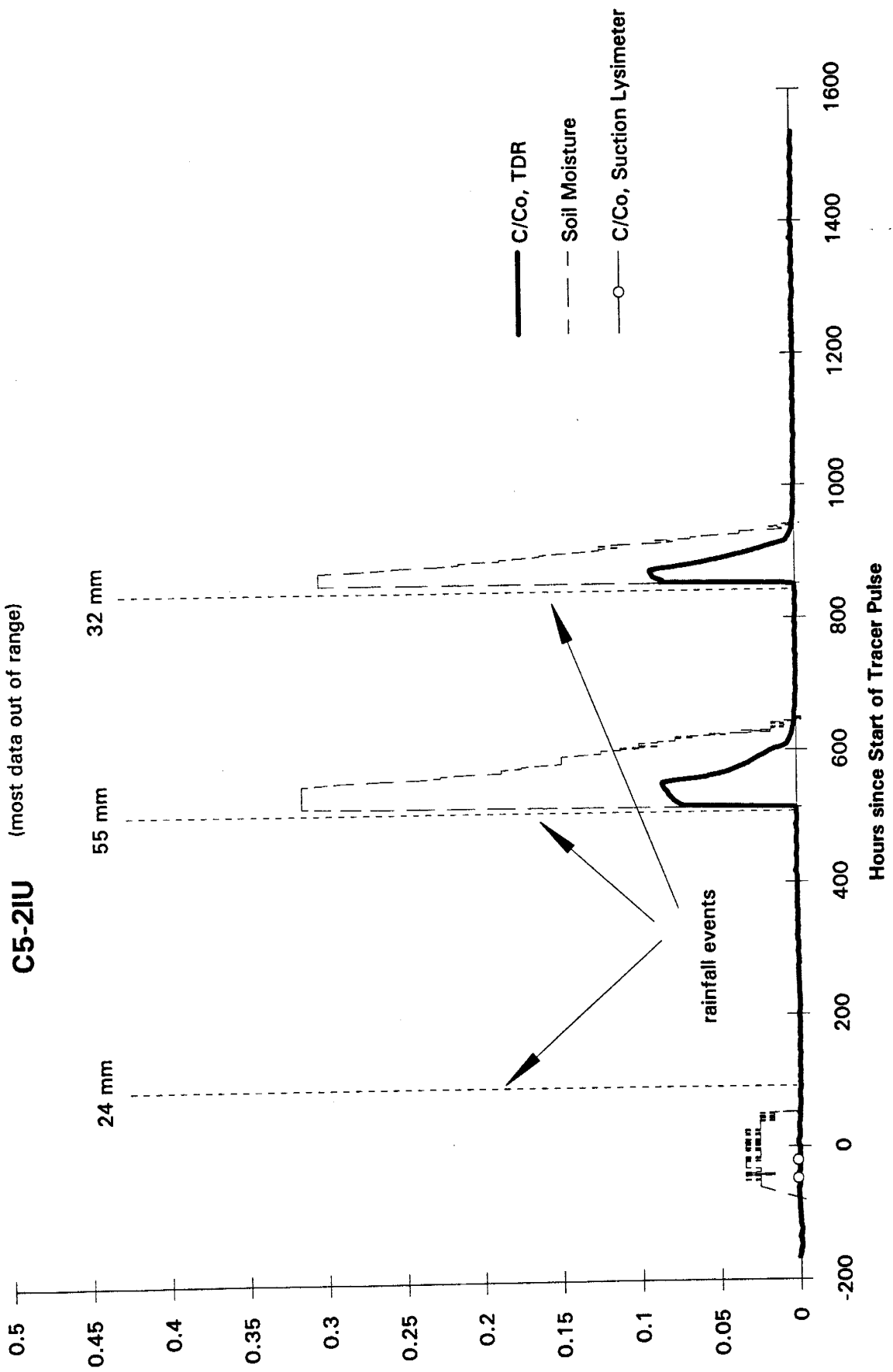


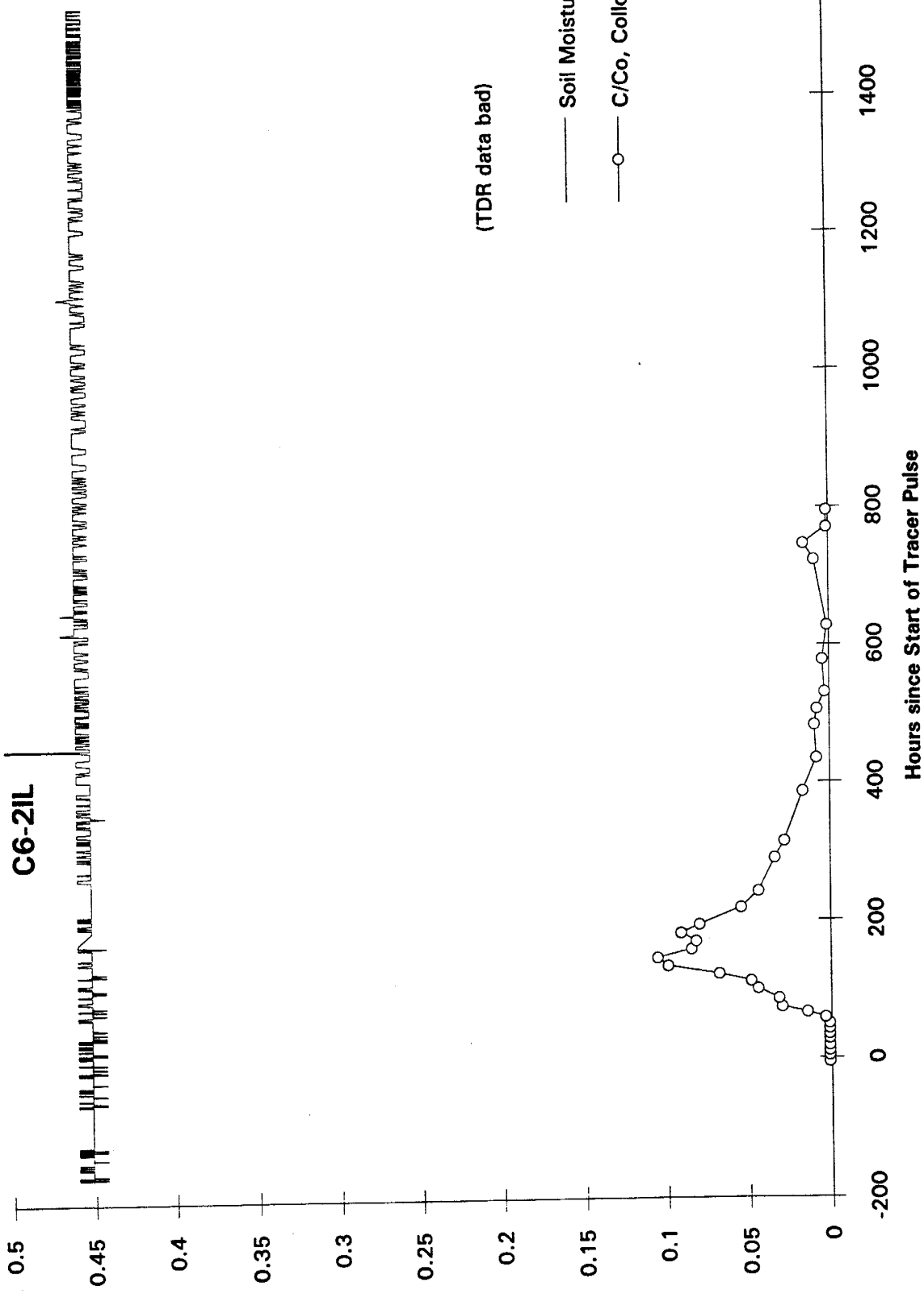
C2-11L



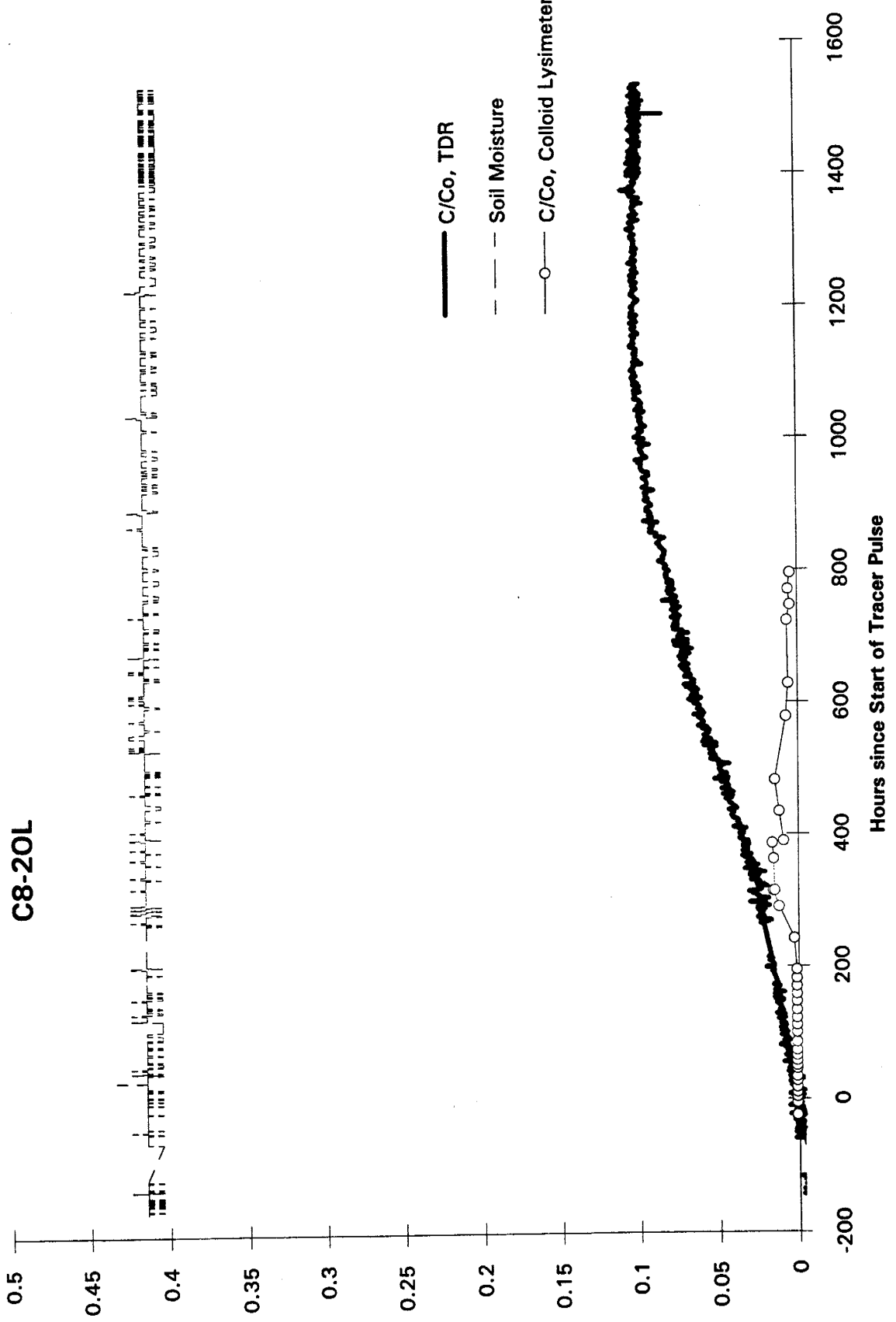
C4-10L

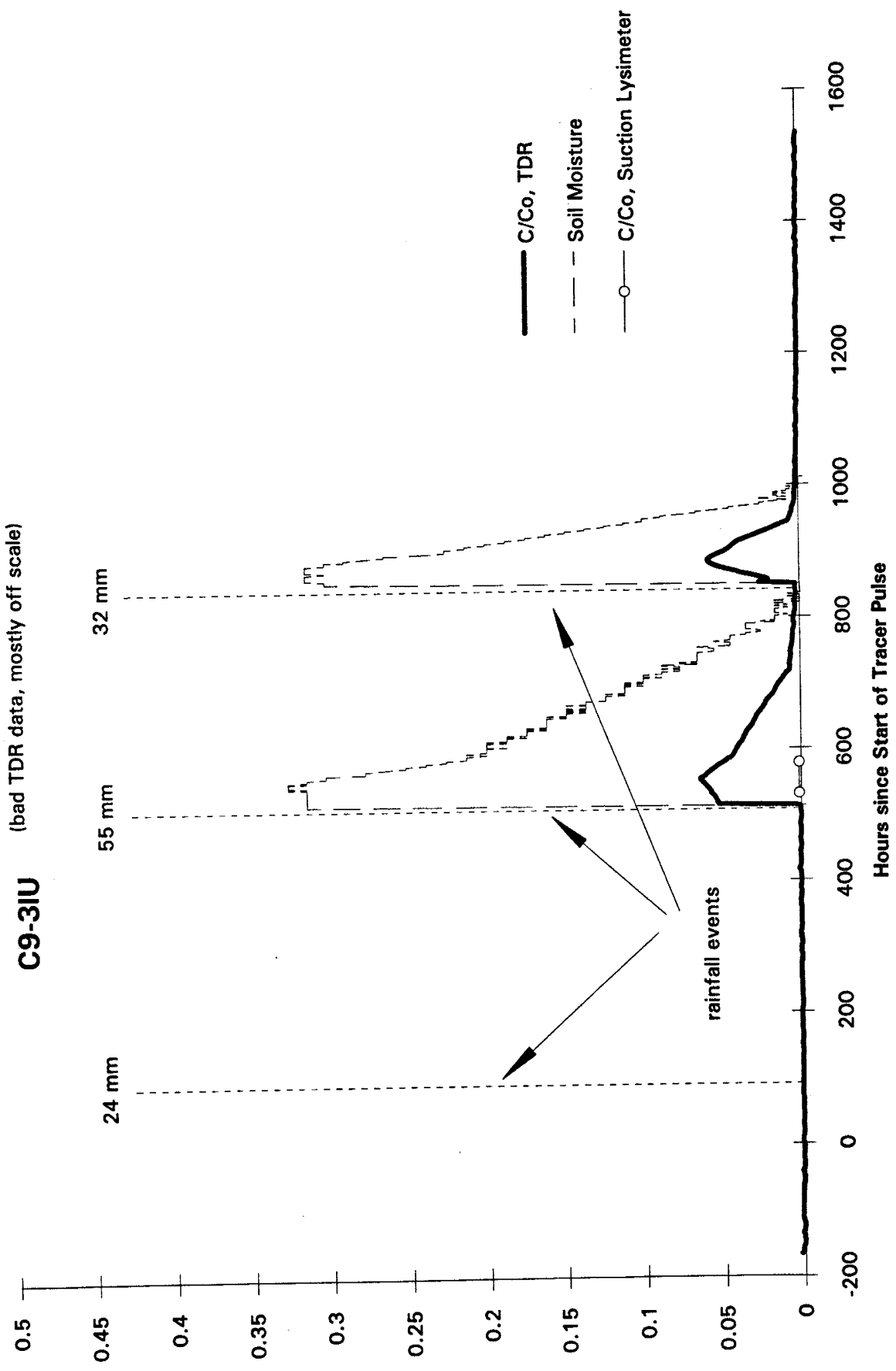




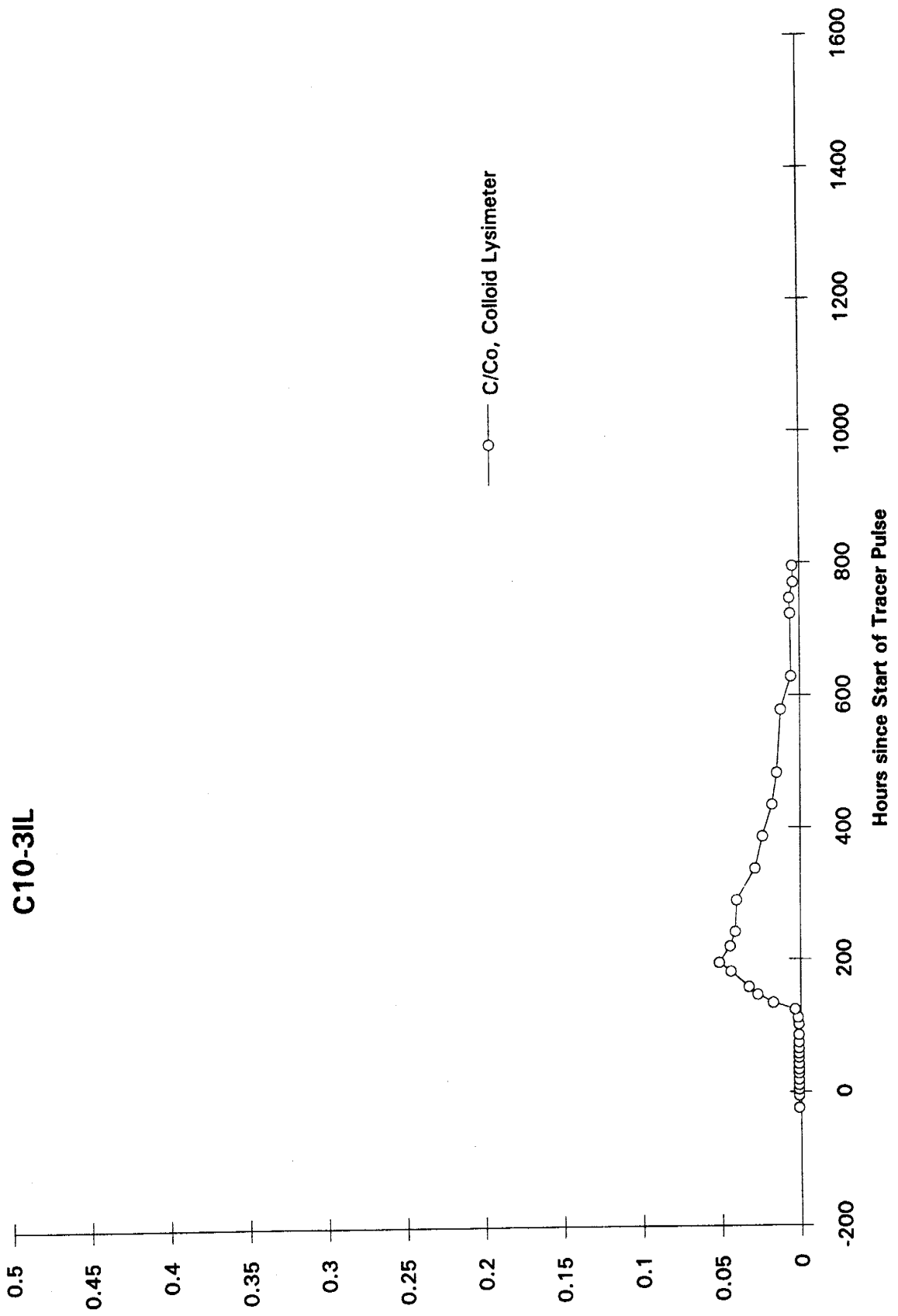


C8-20L

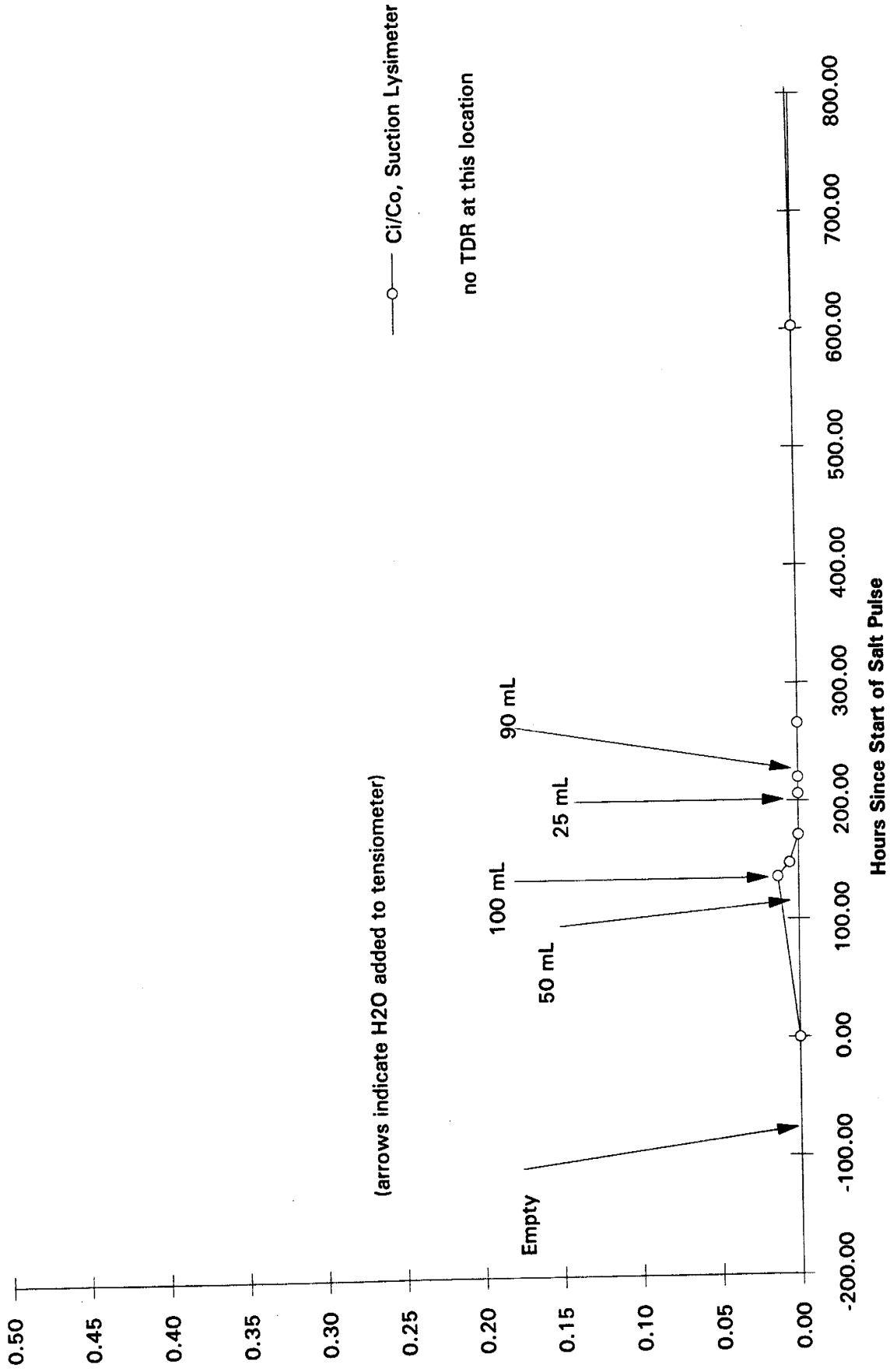




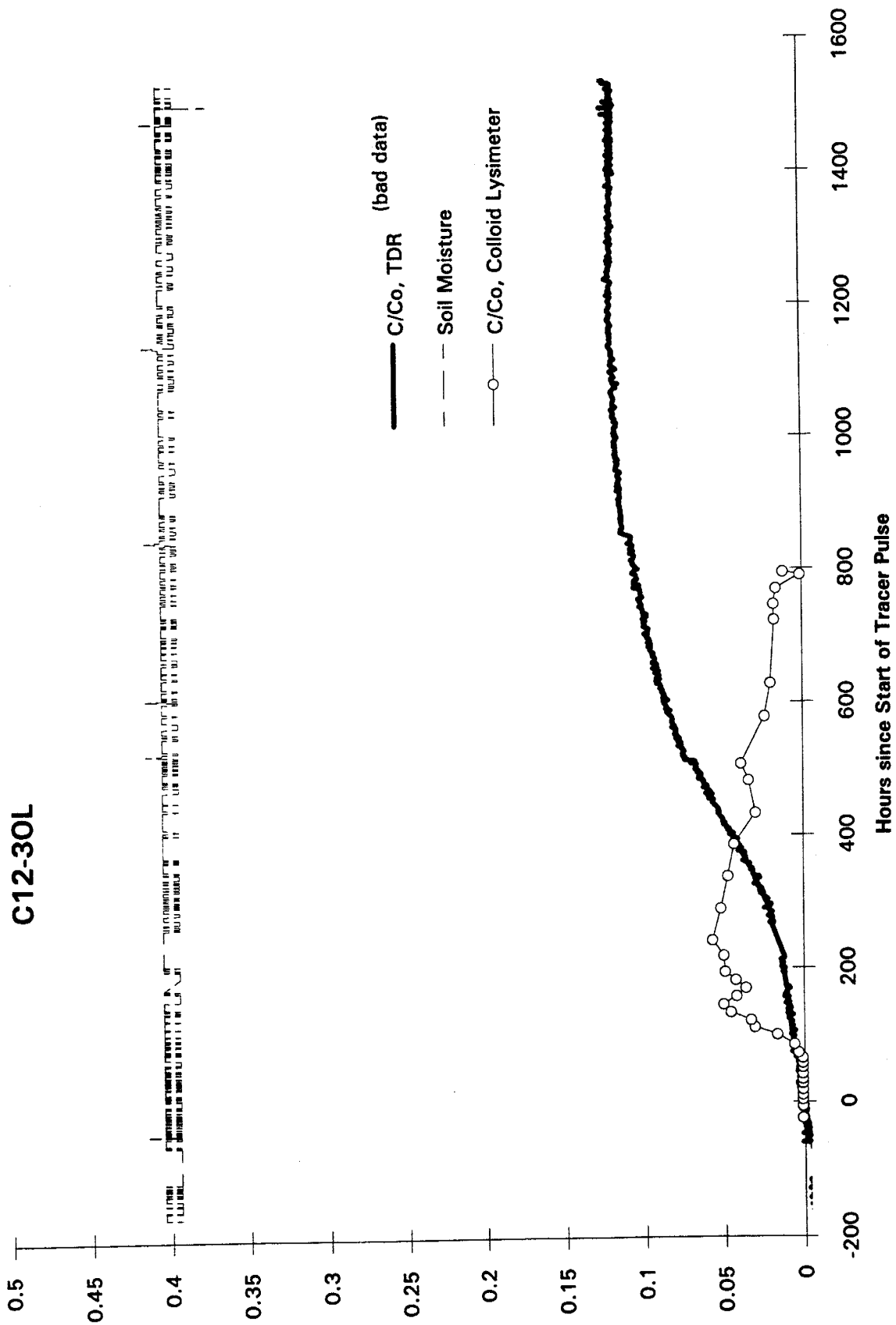
C10-3IL



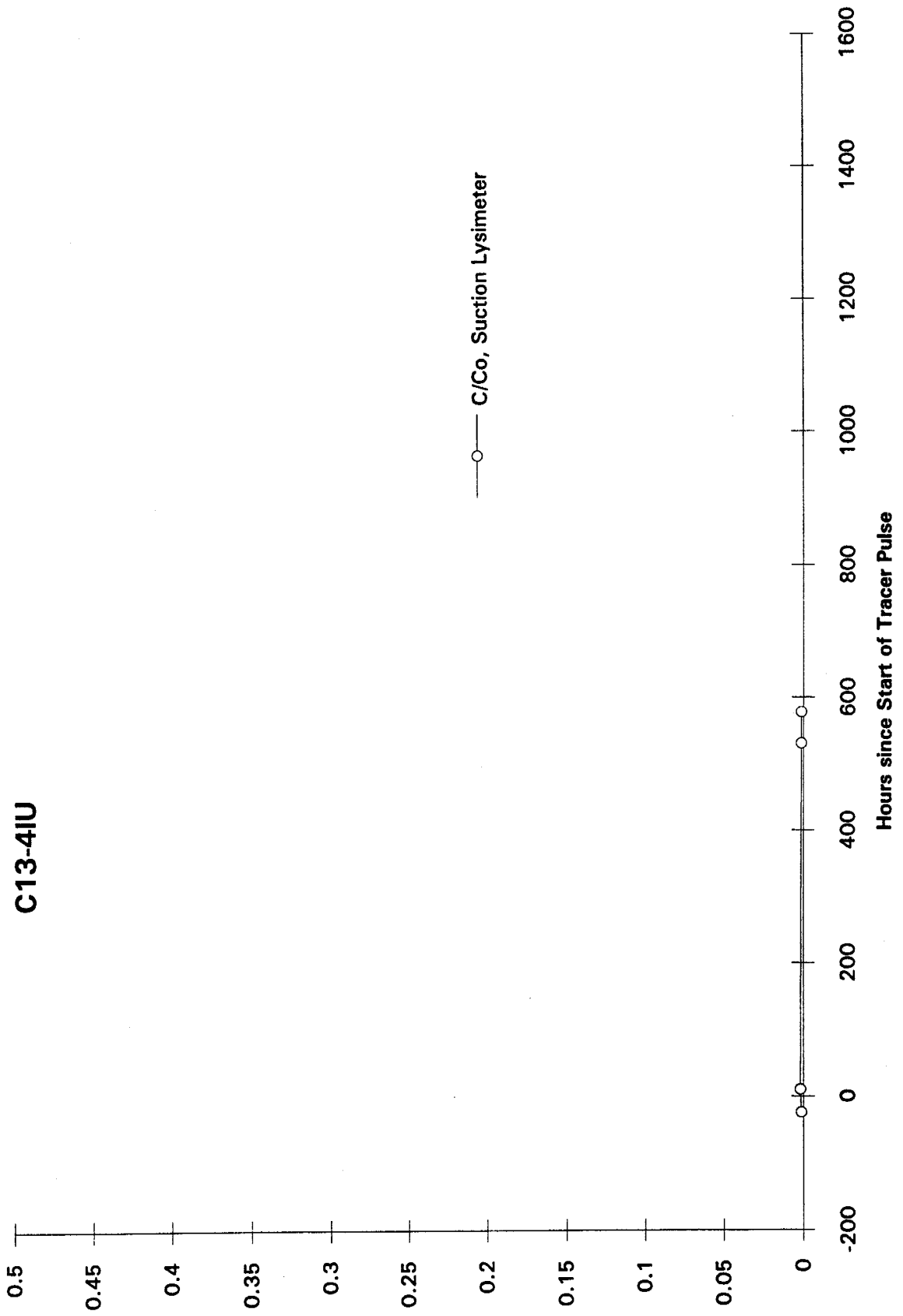
C11-30U

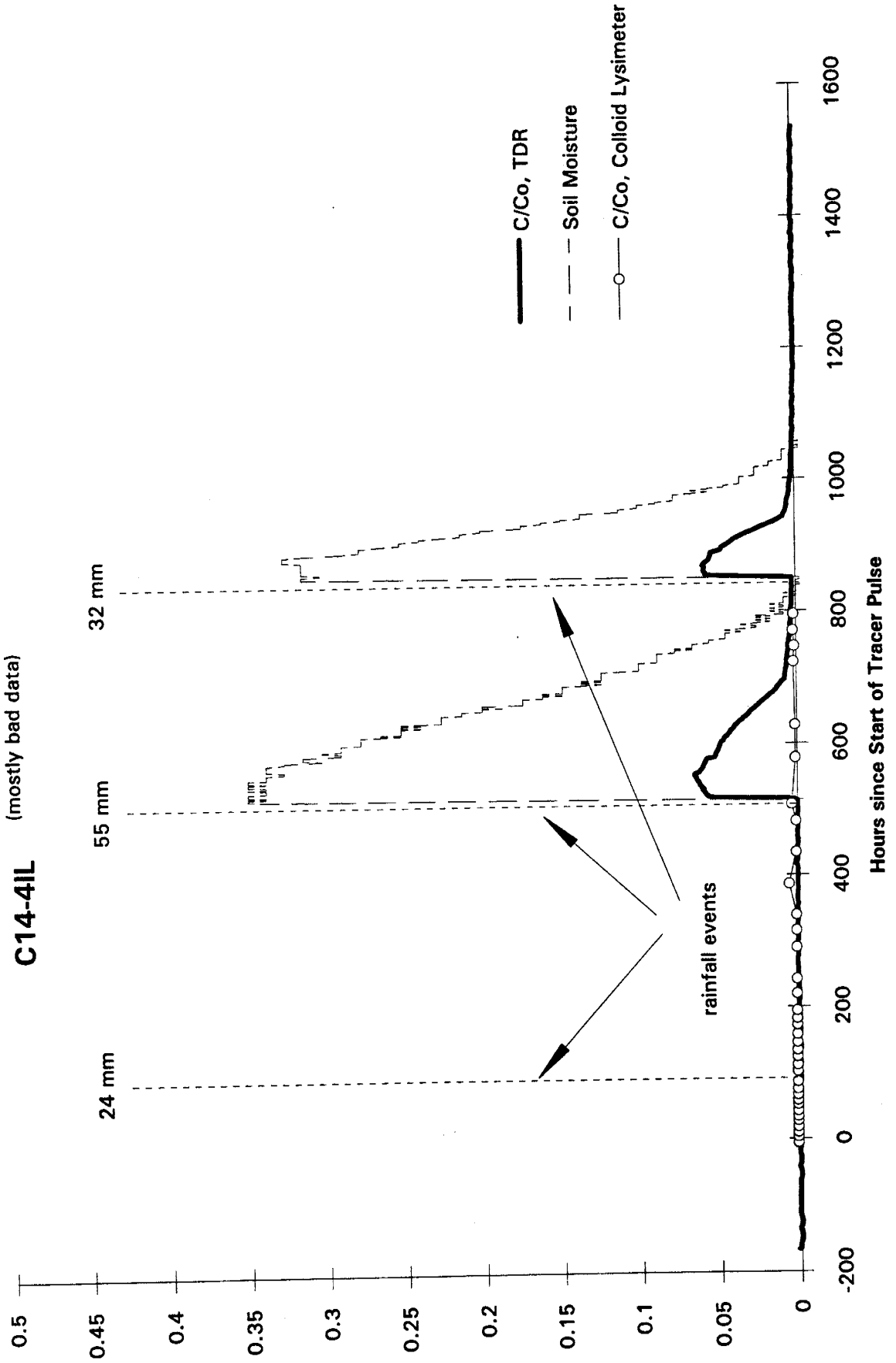


C12-30L

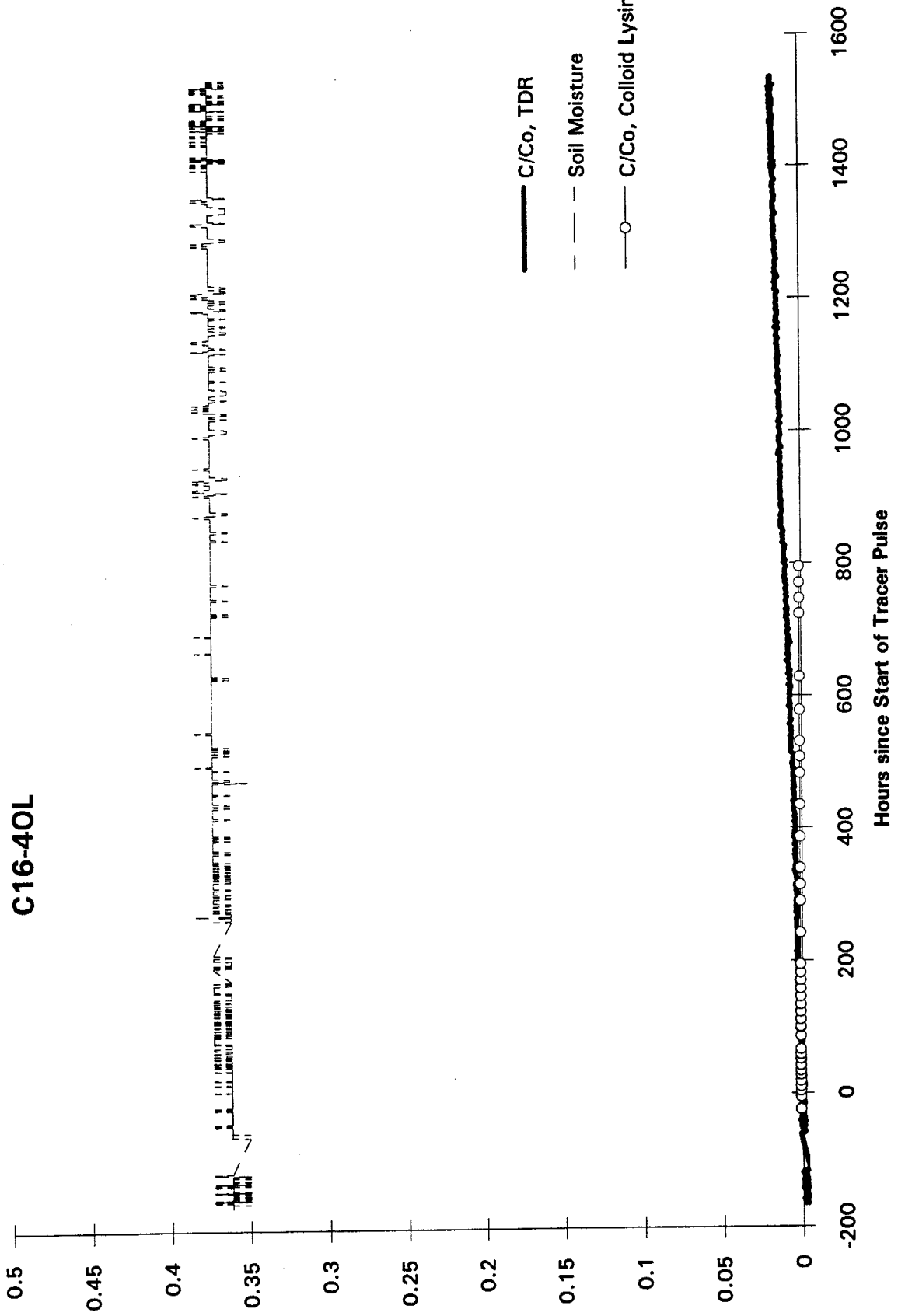


C13-4IU

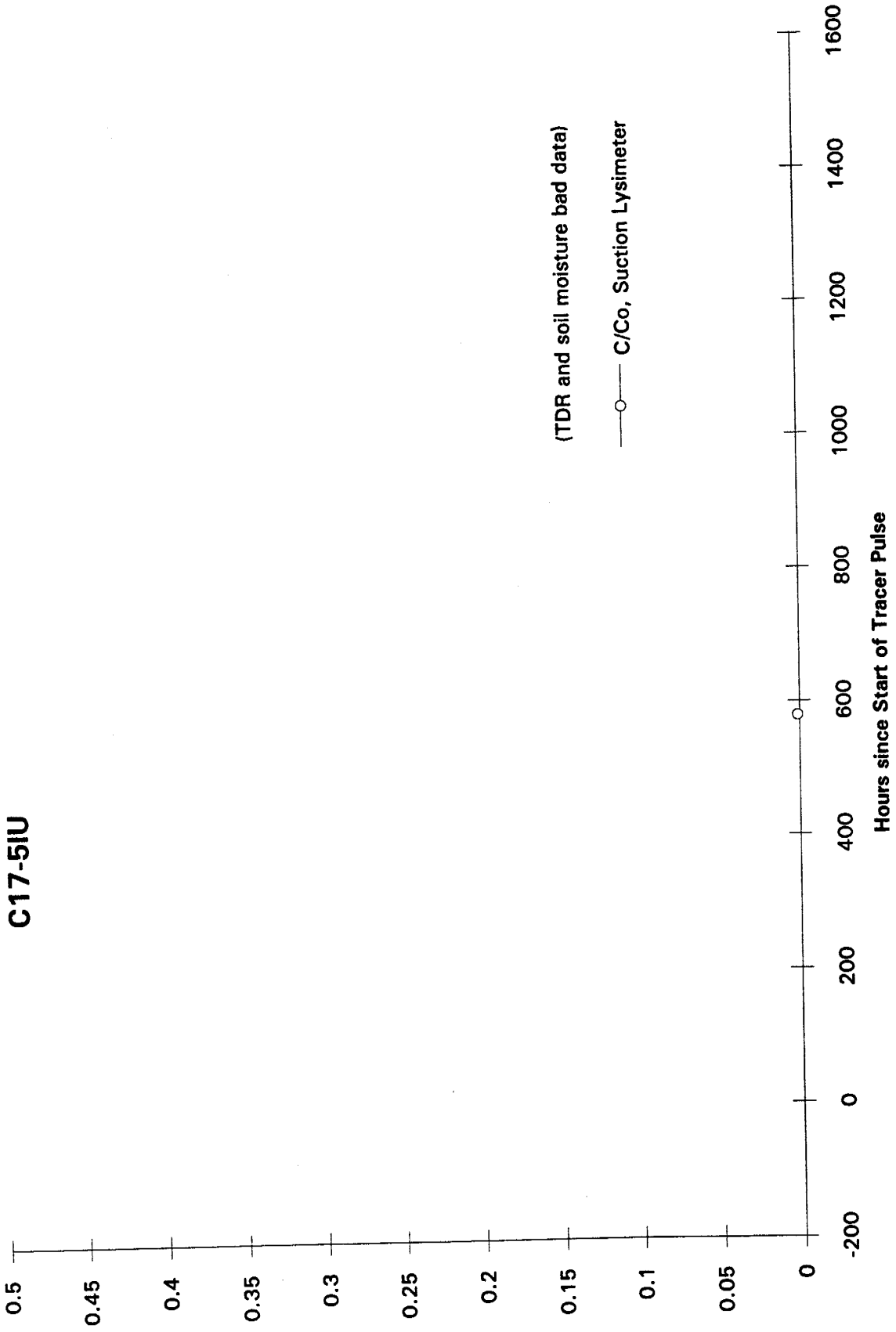


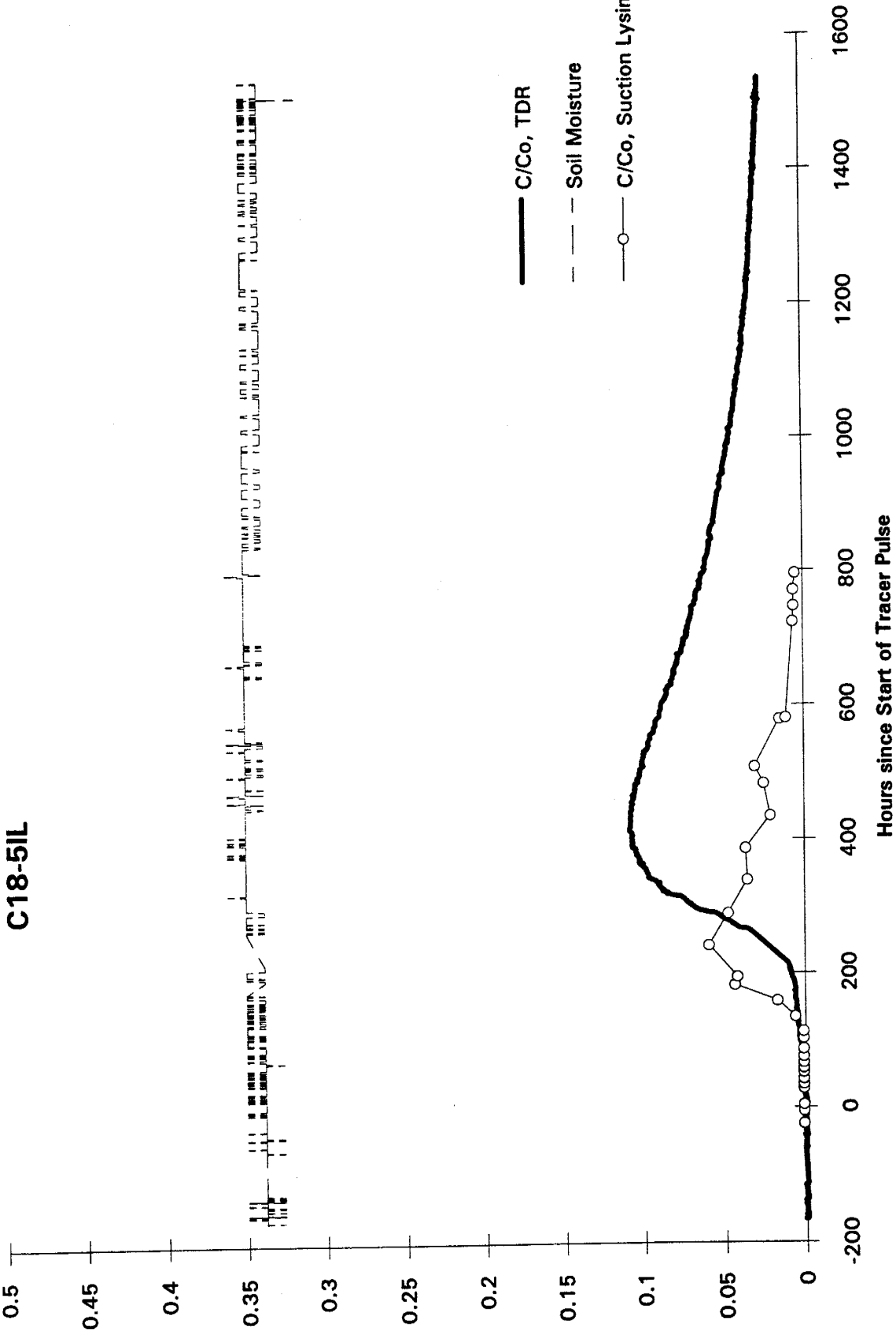


C16-40L

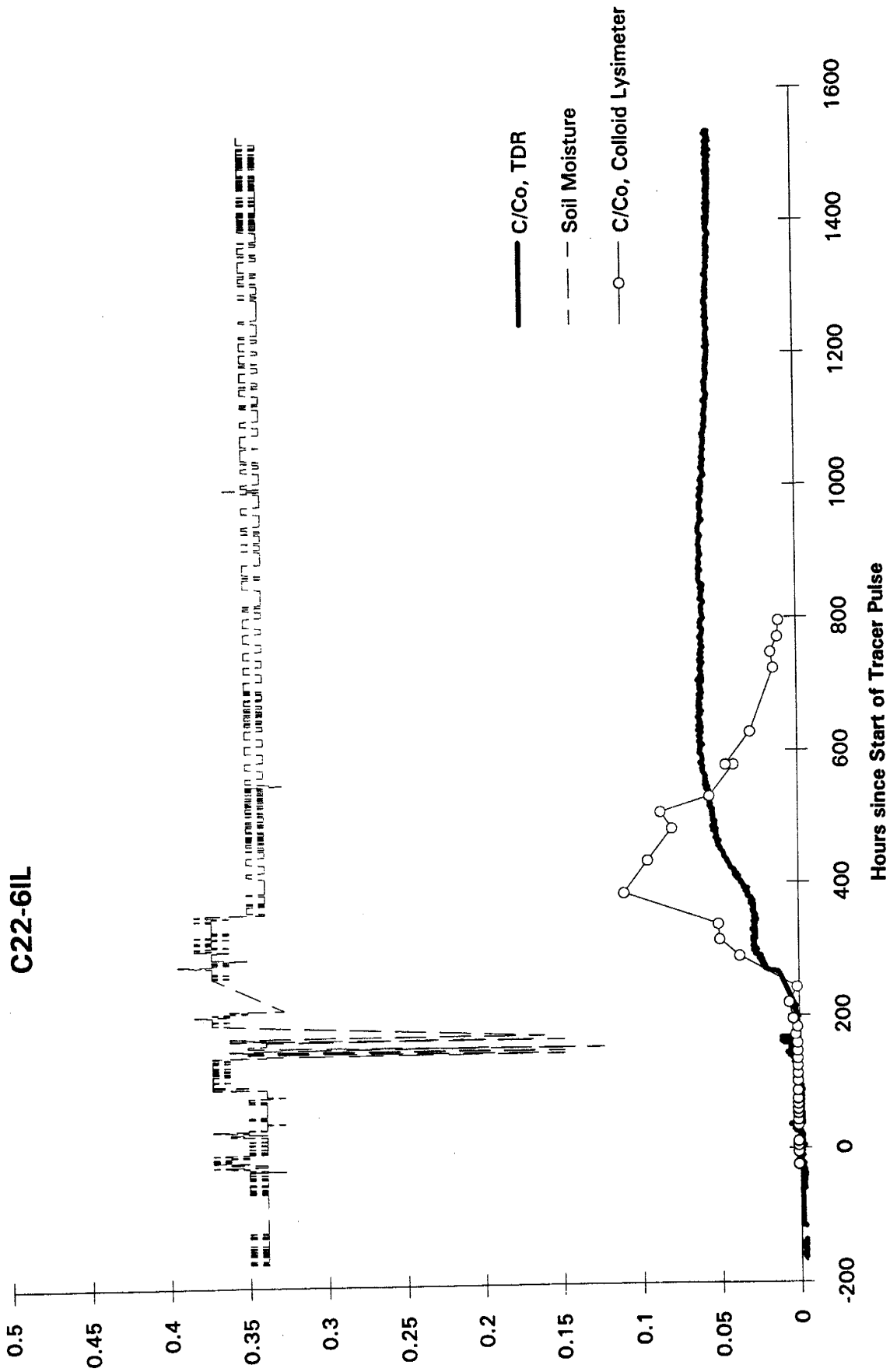


C17-5IU

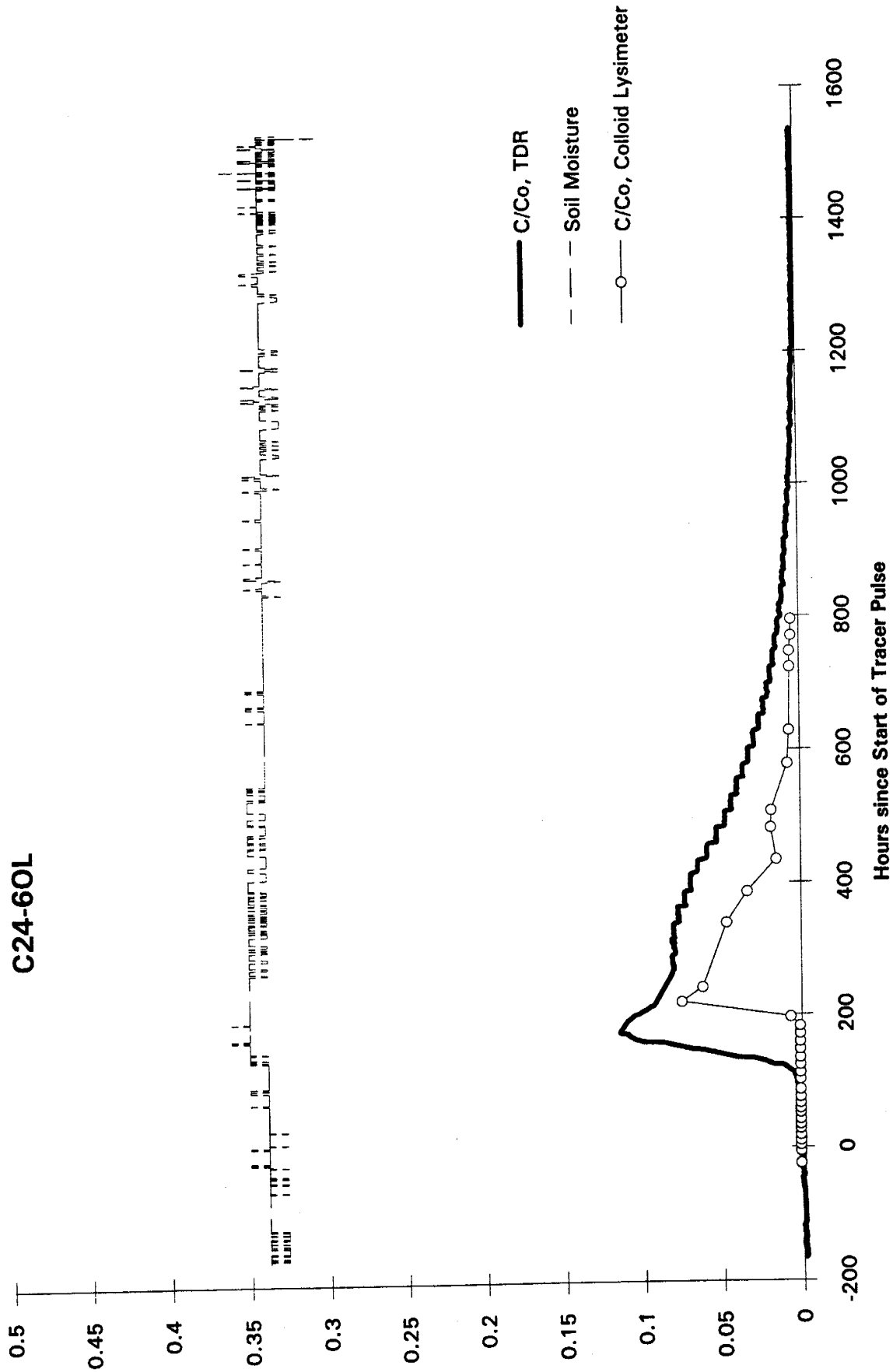


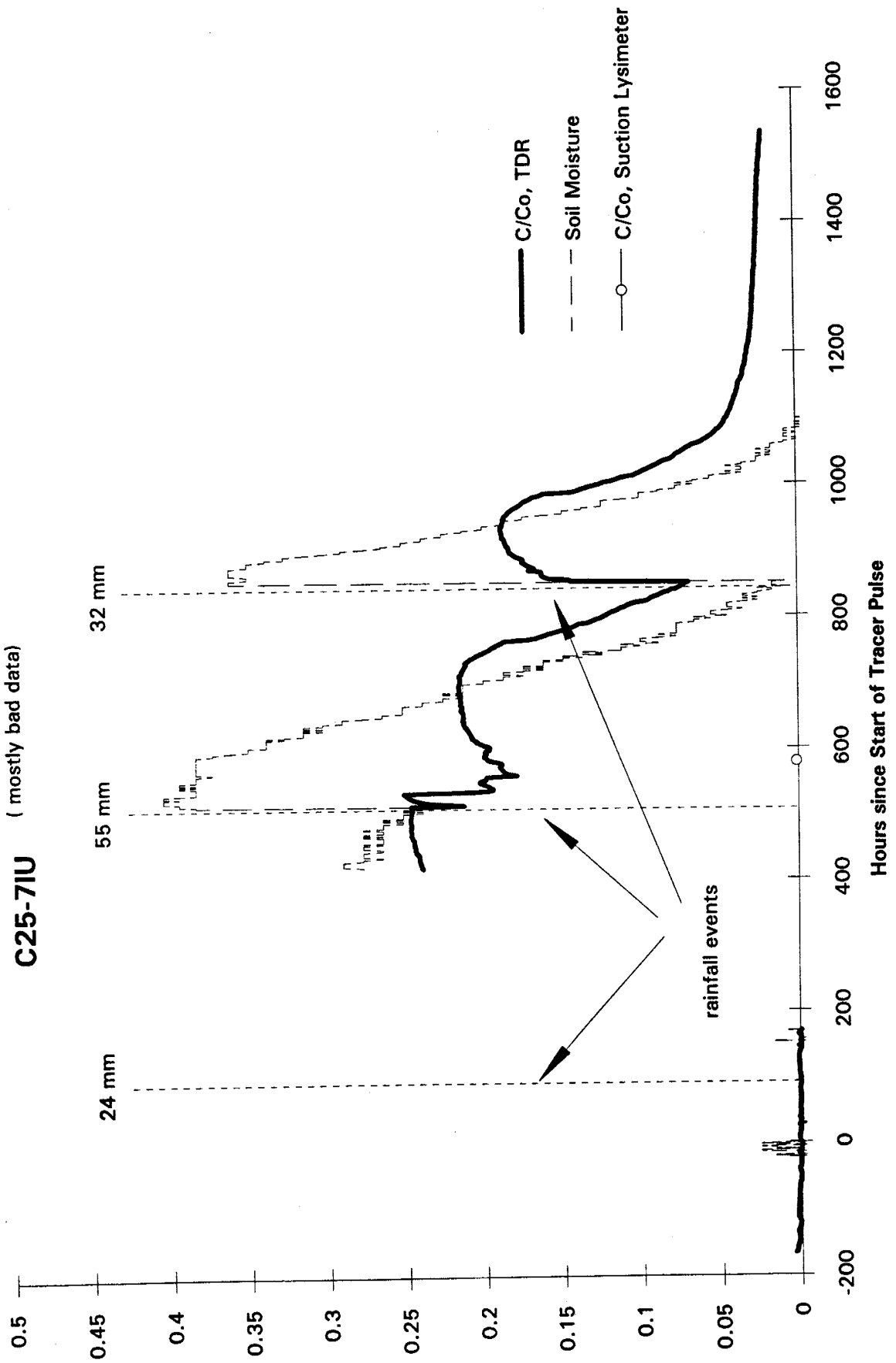


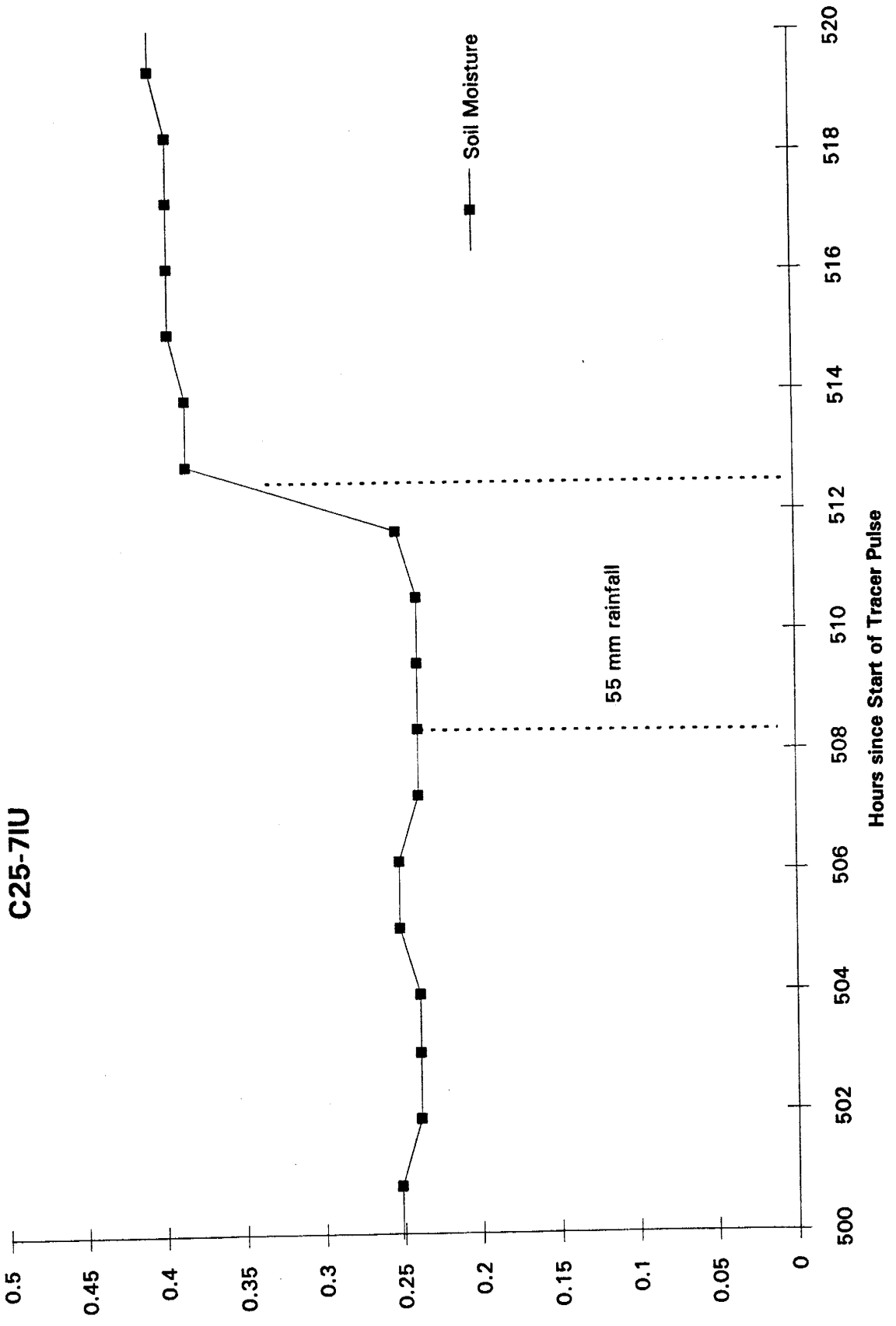
C22-6IL



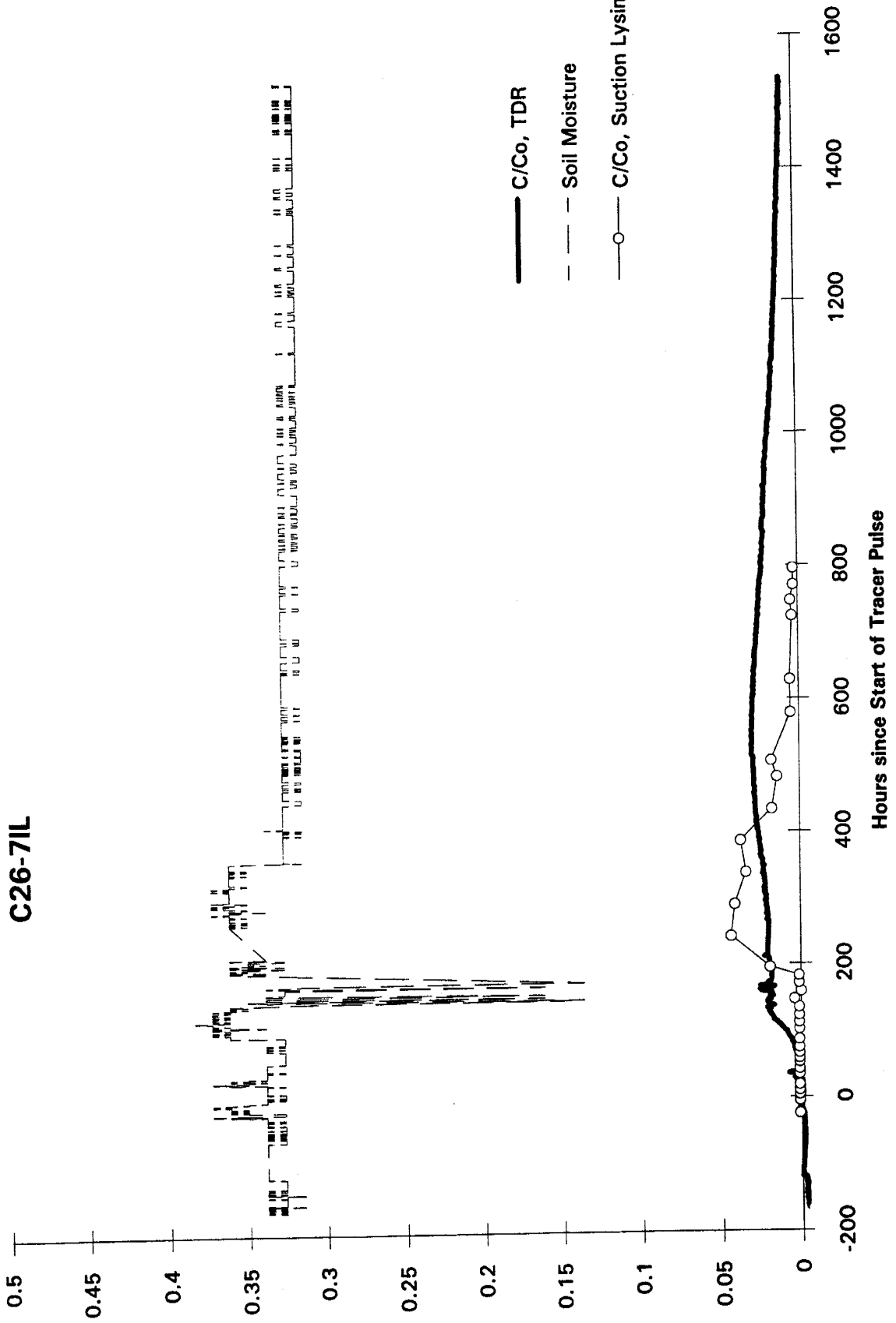
C24-60L

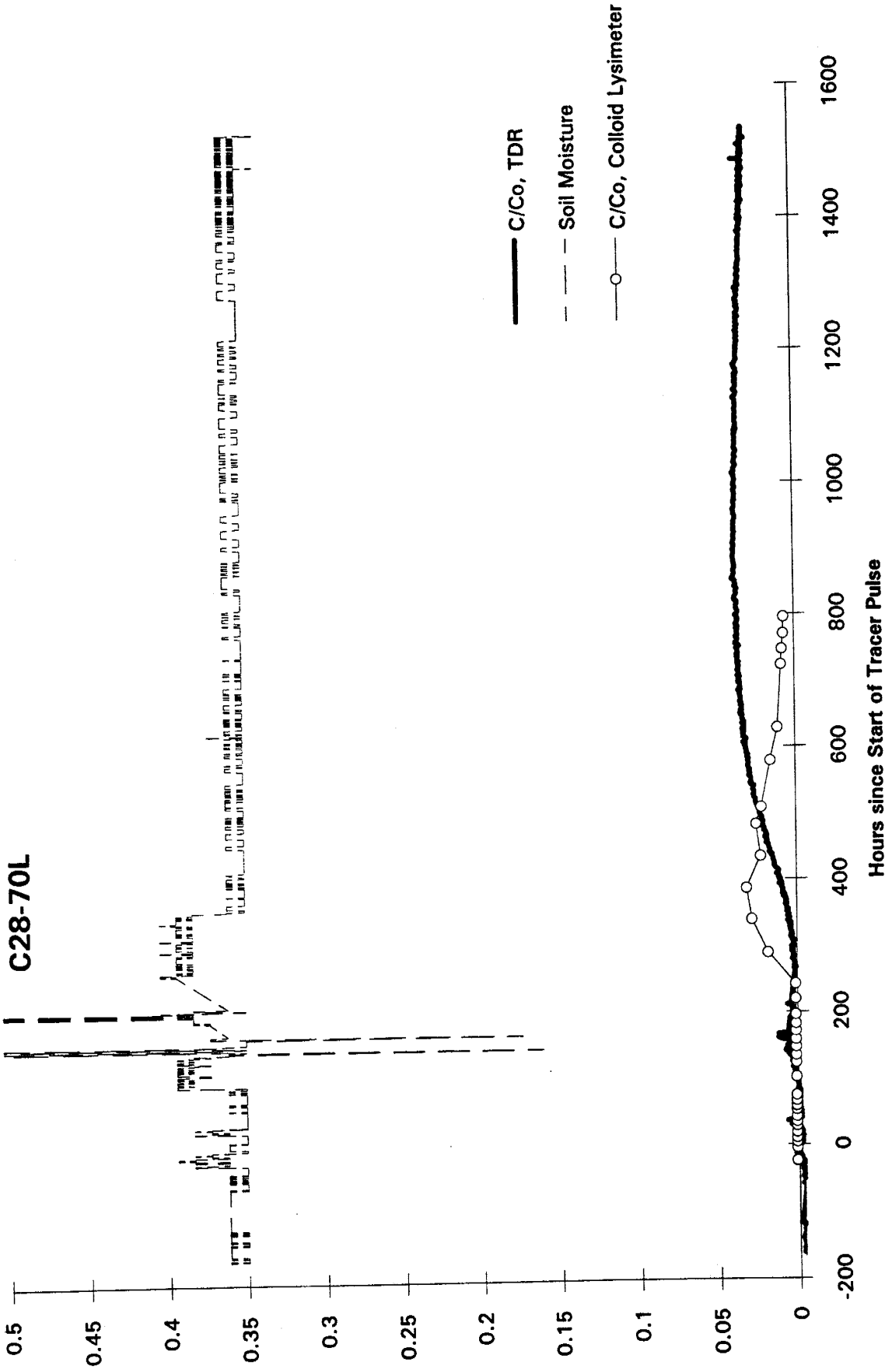




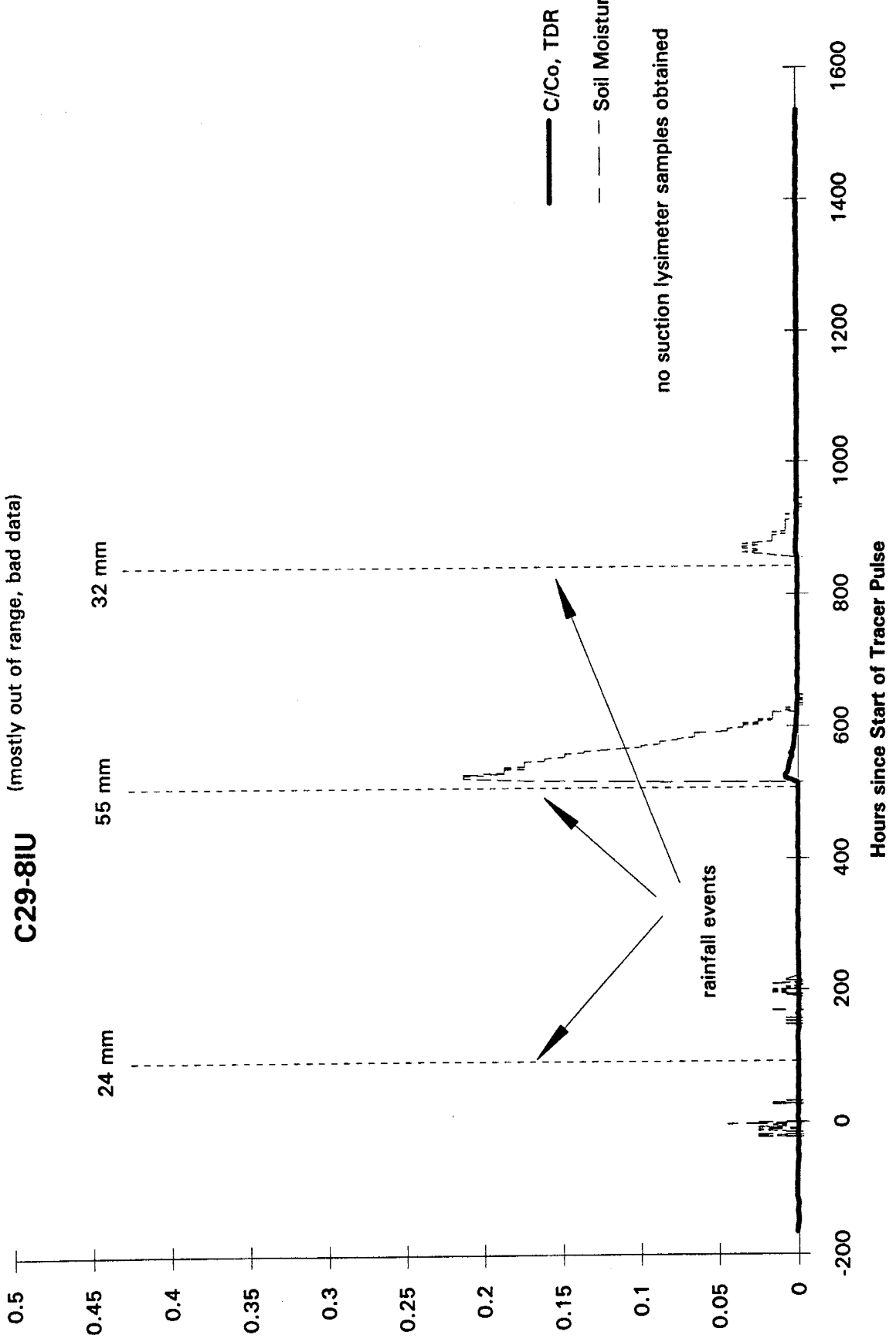


C26-71L

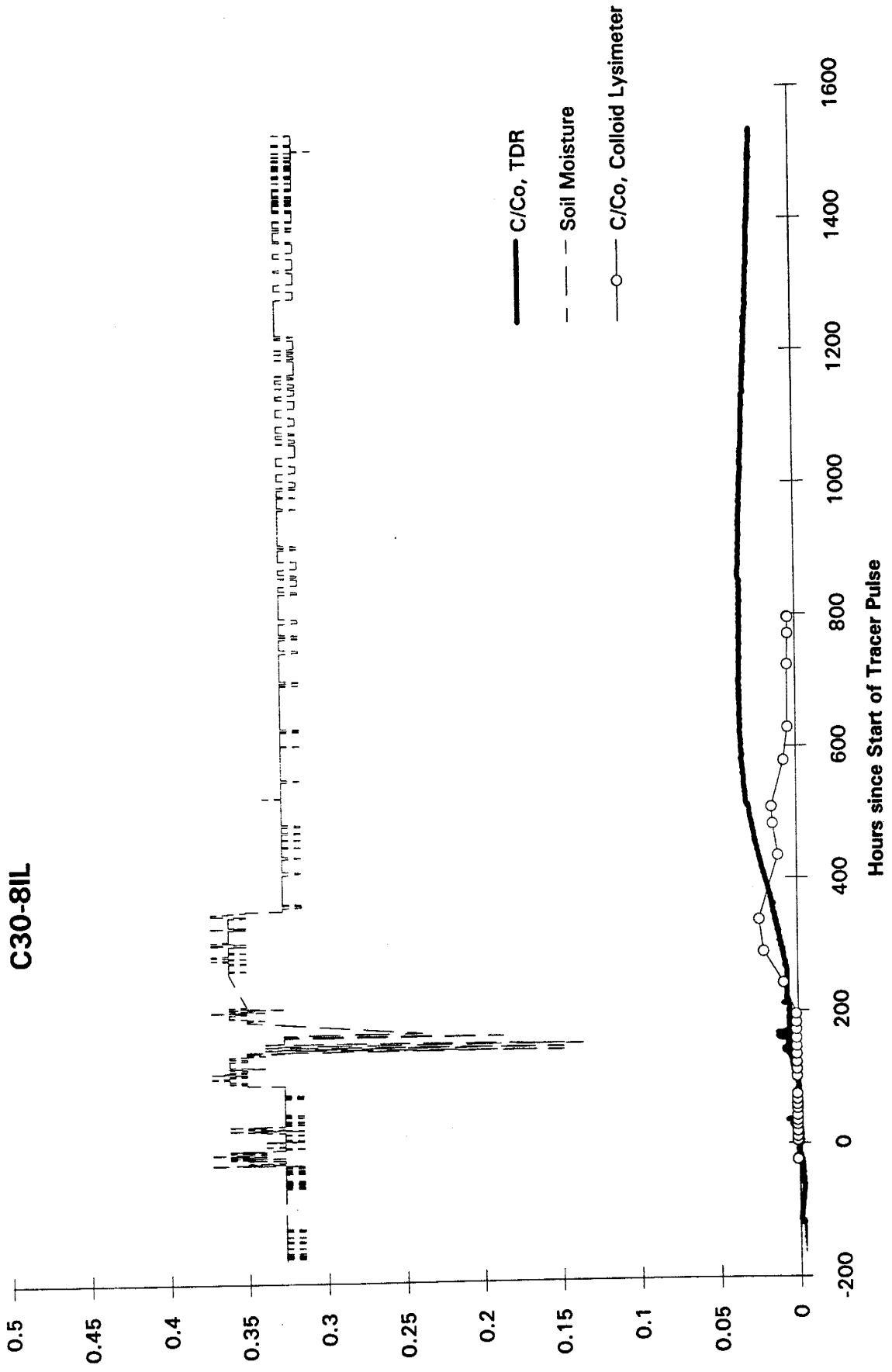


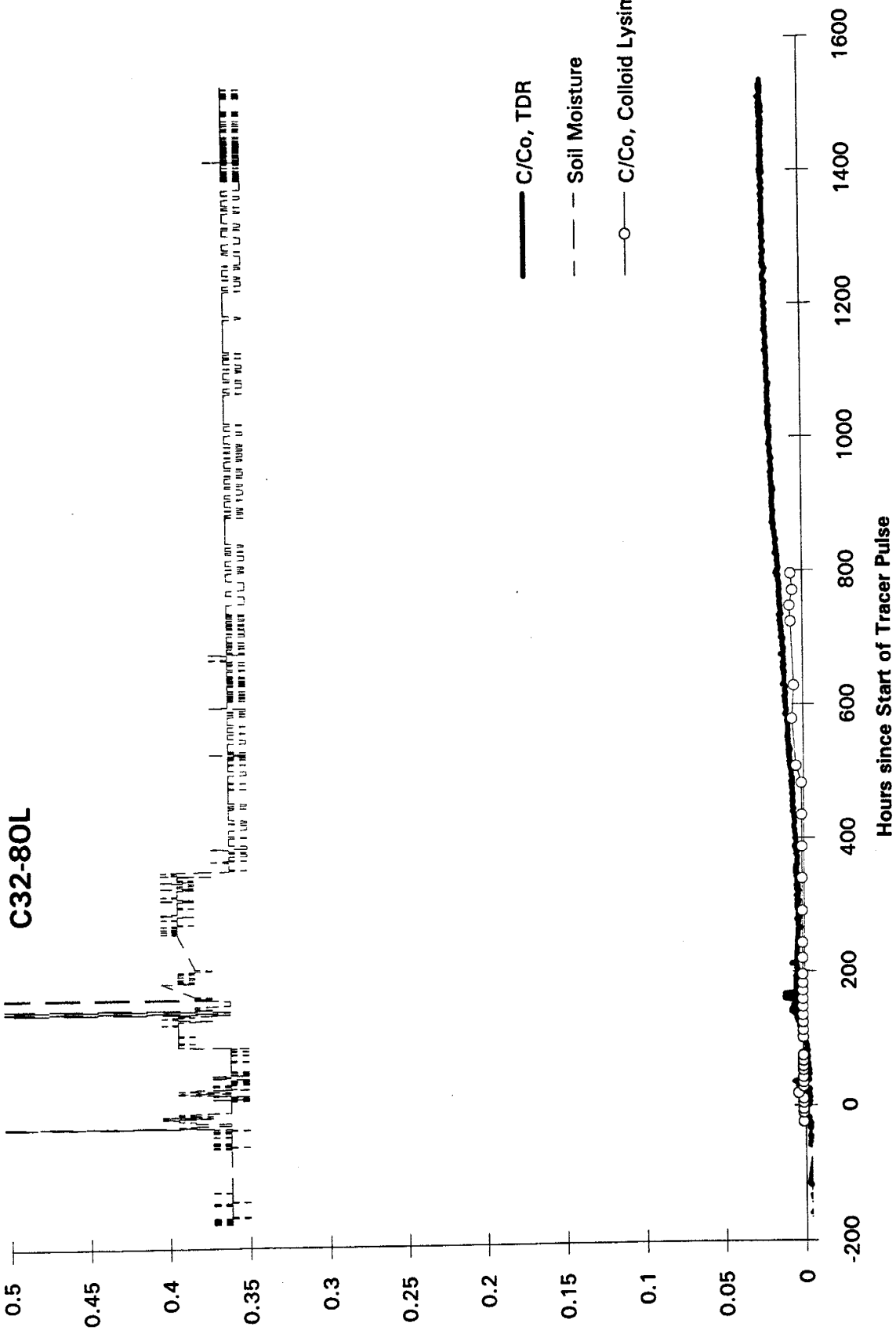


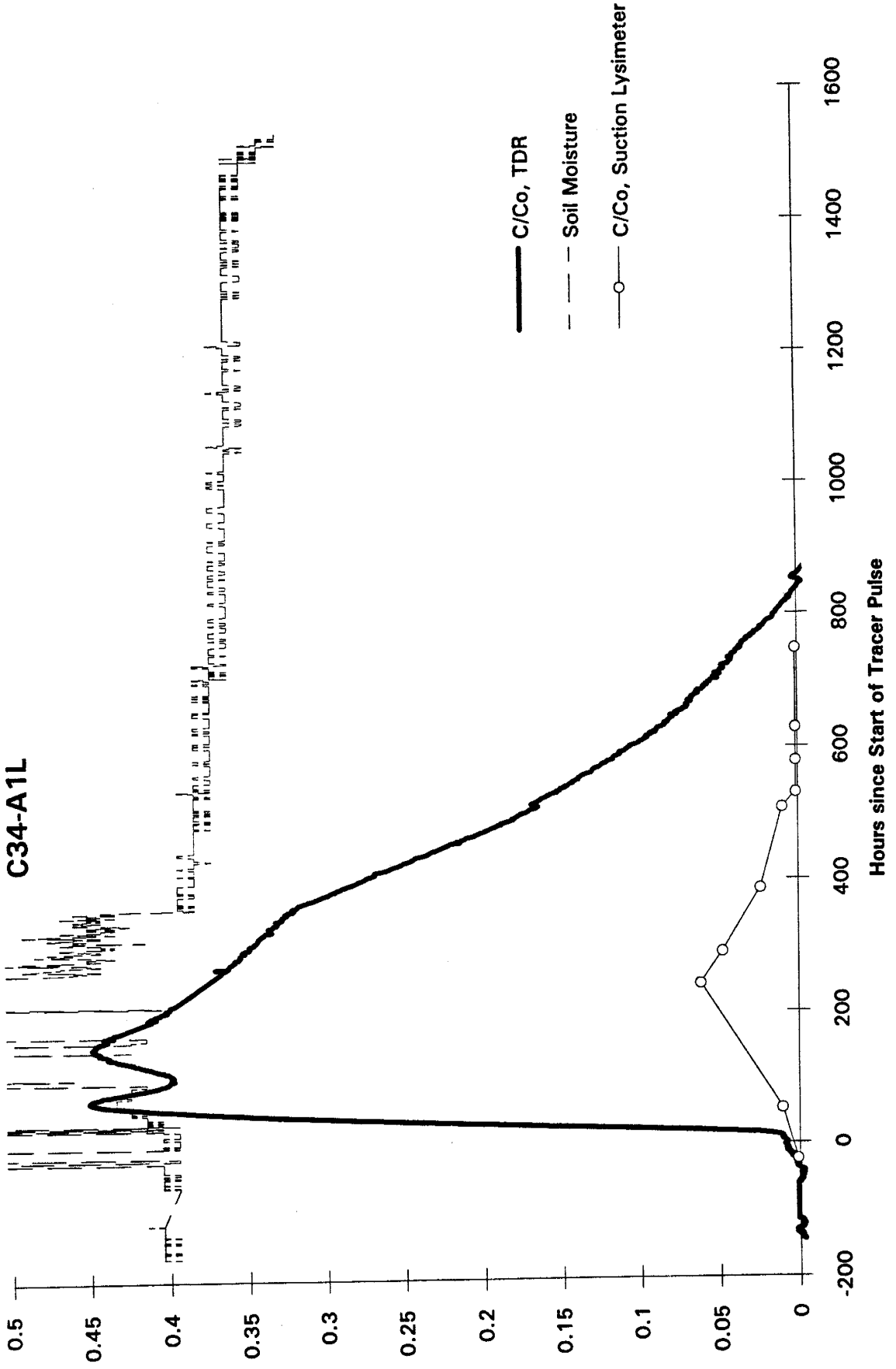
C29-8IU (mostly out of range, bad data)



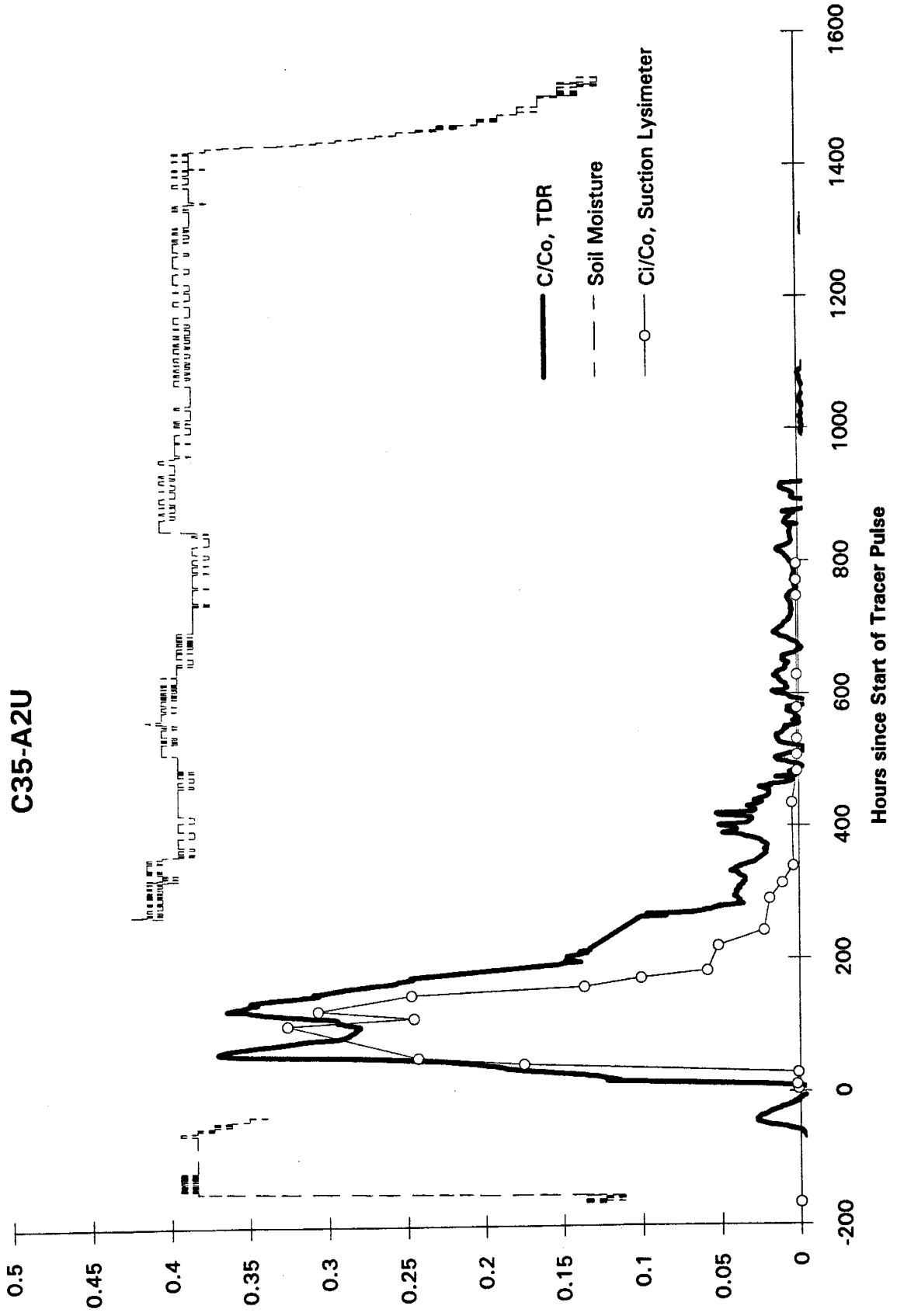
C30-81L



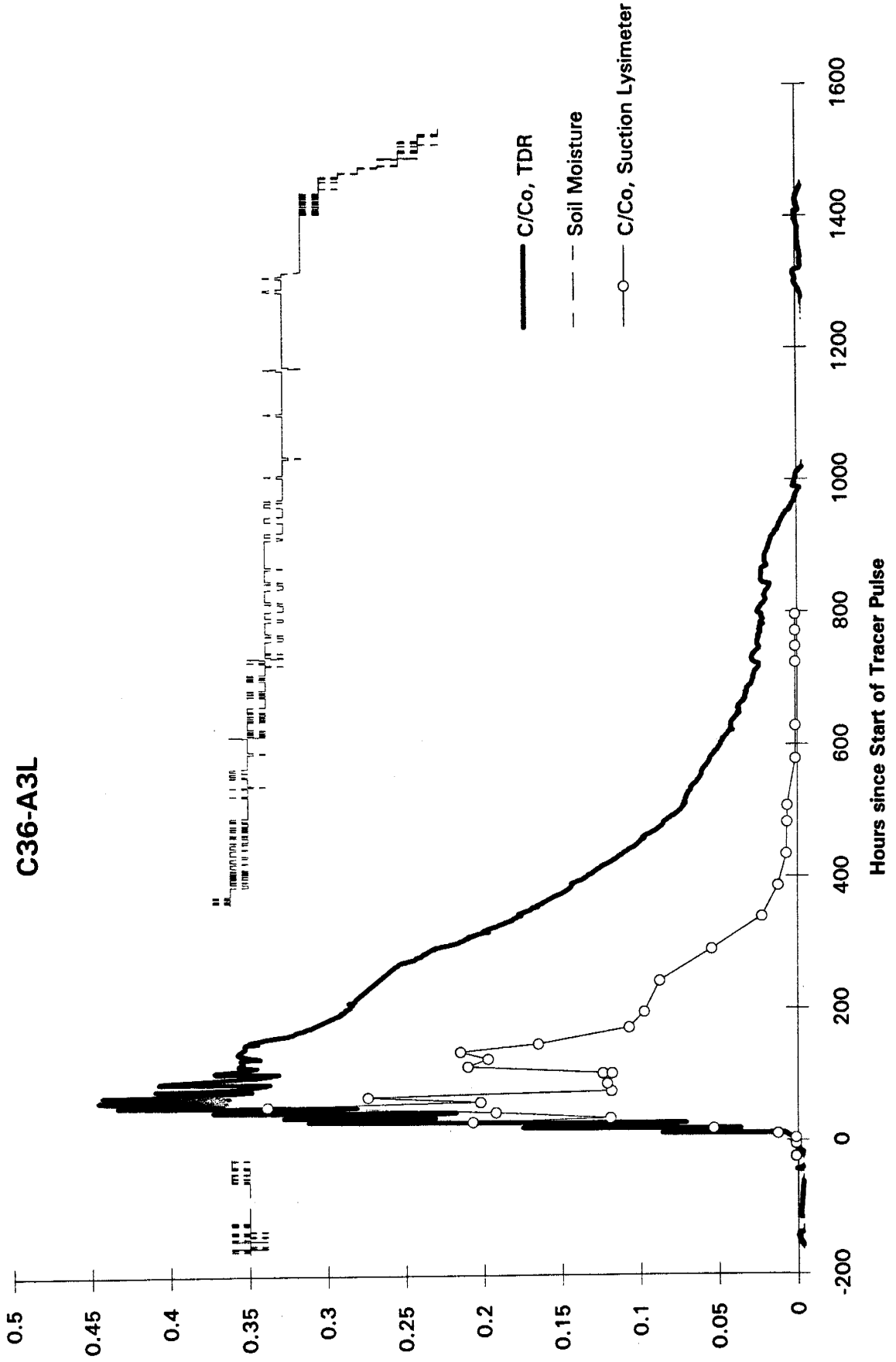


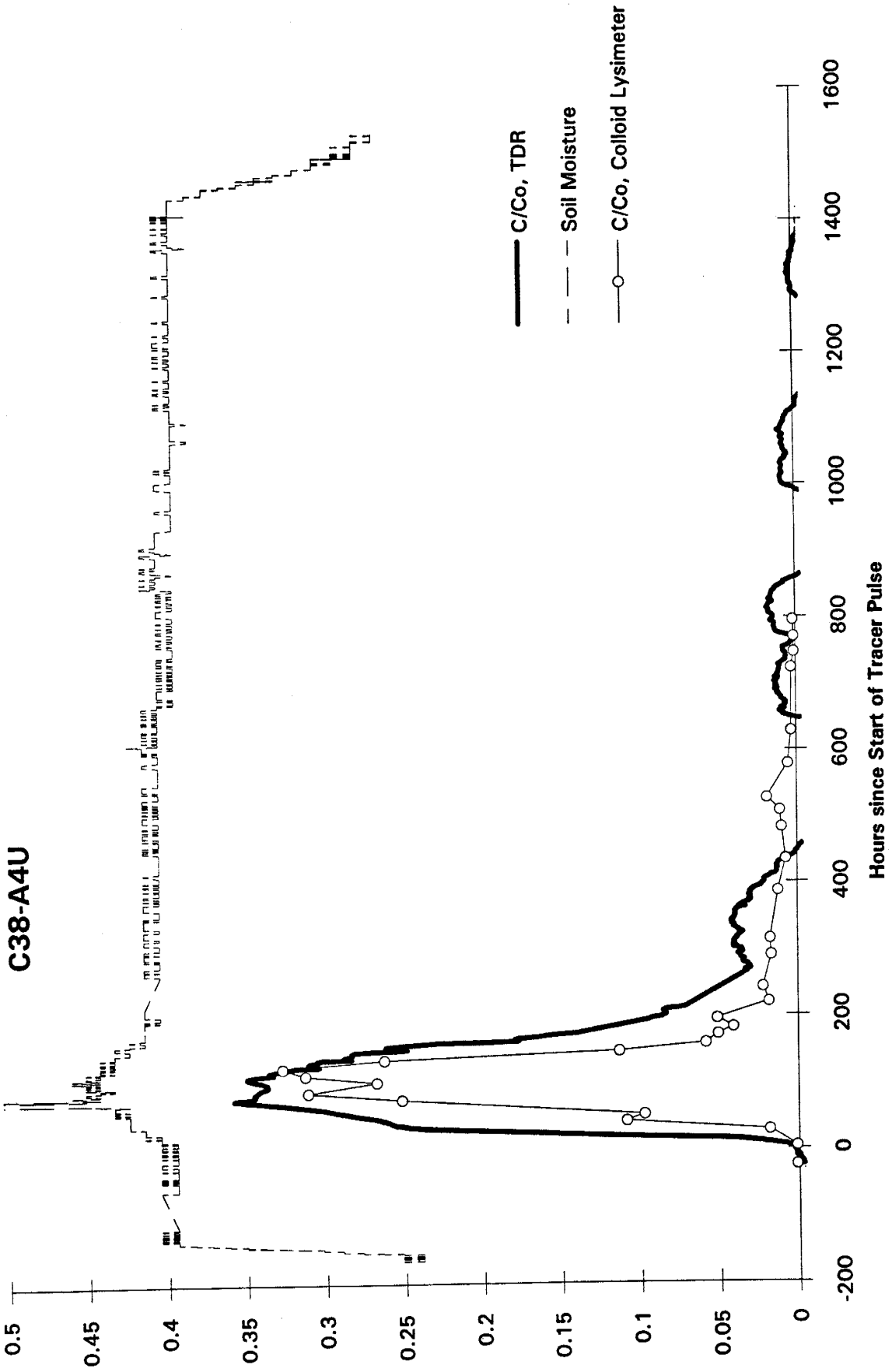


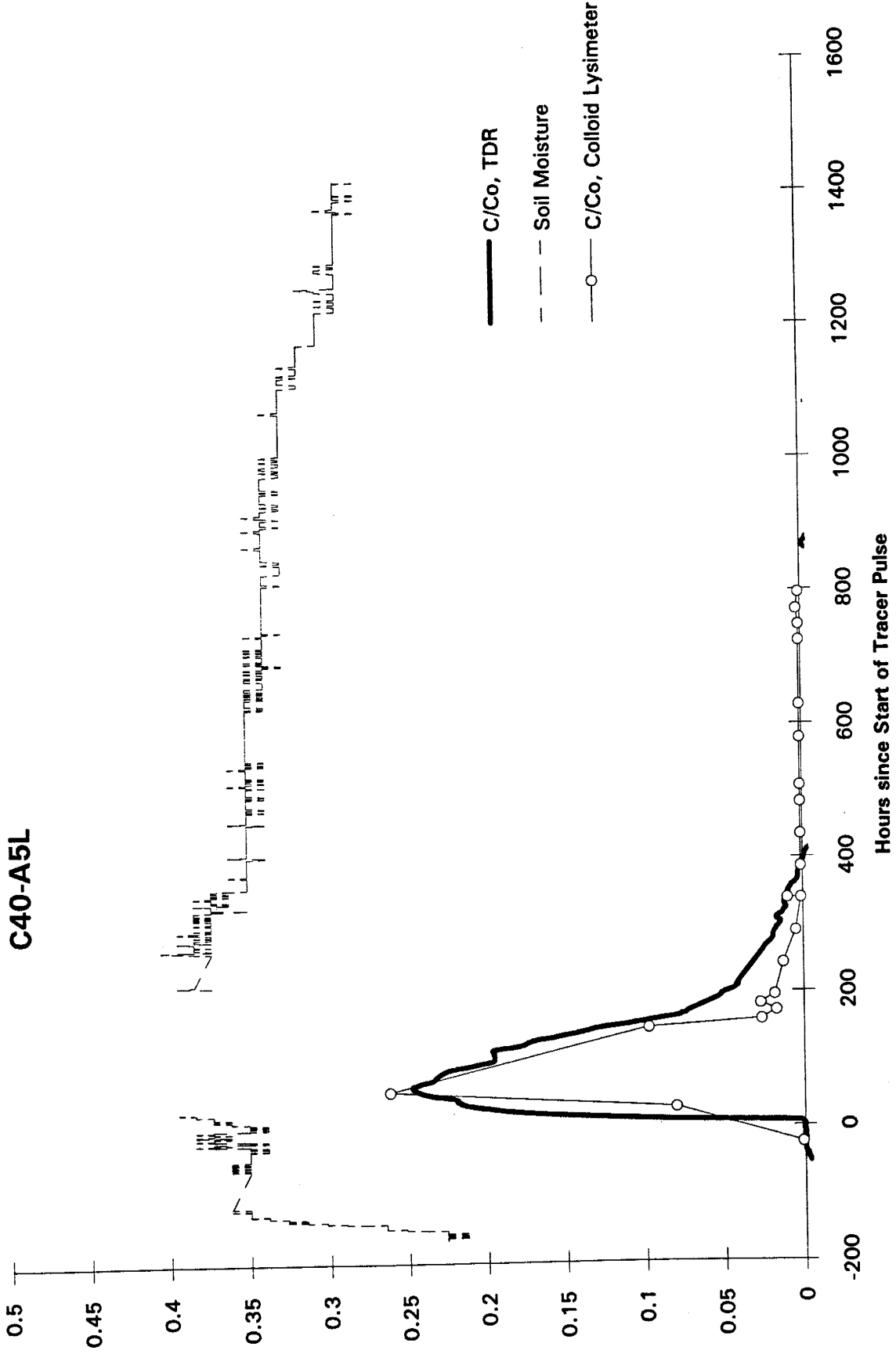
C35-A2U



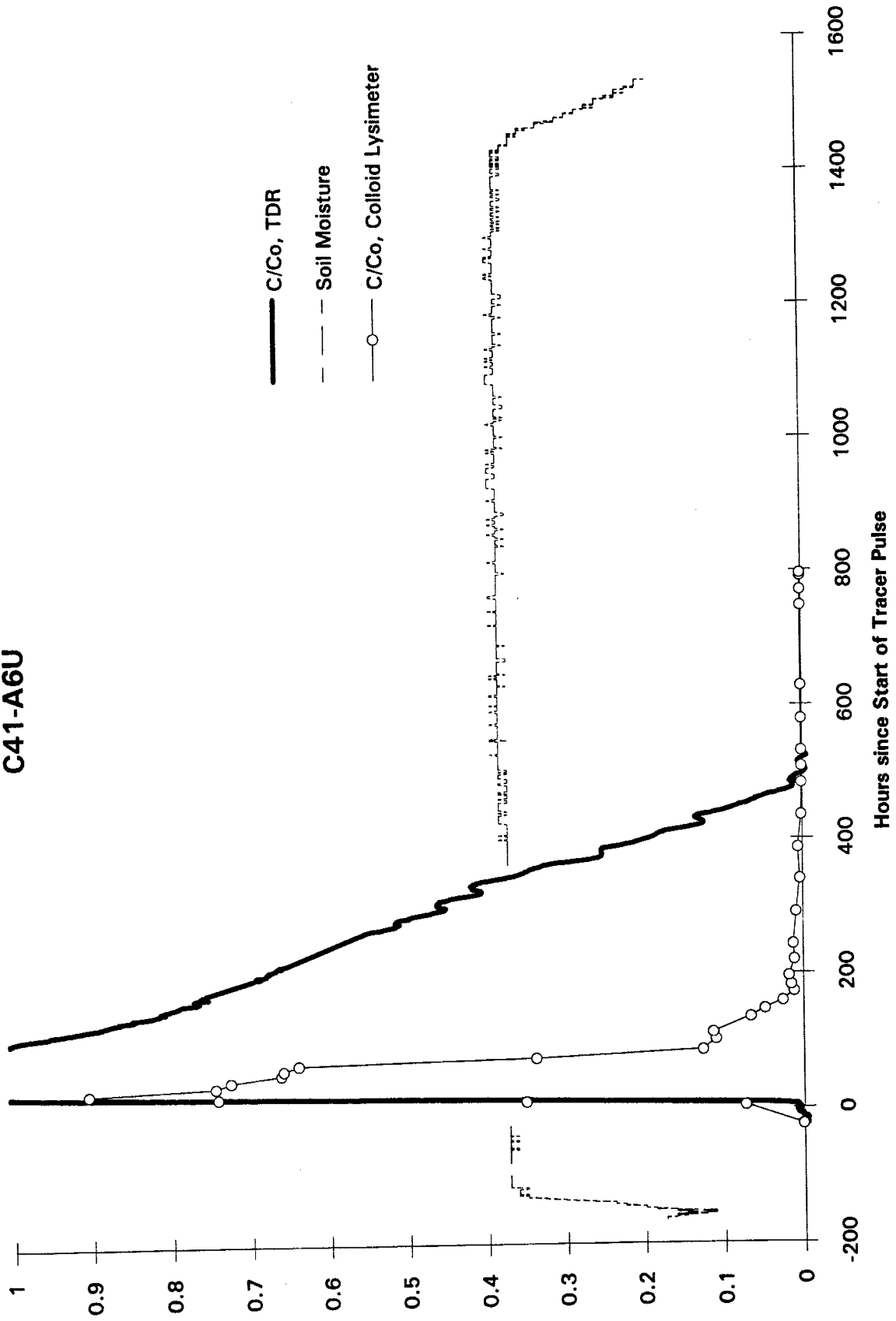
C36-A3L

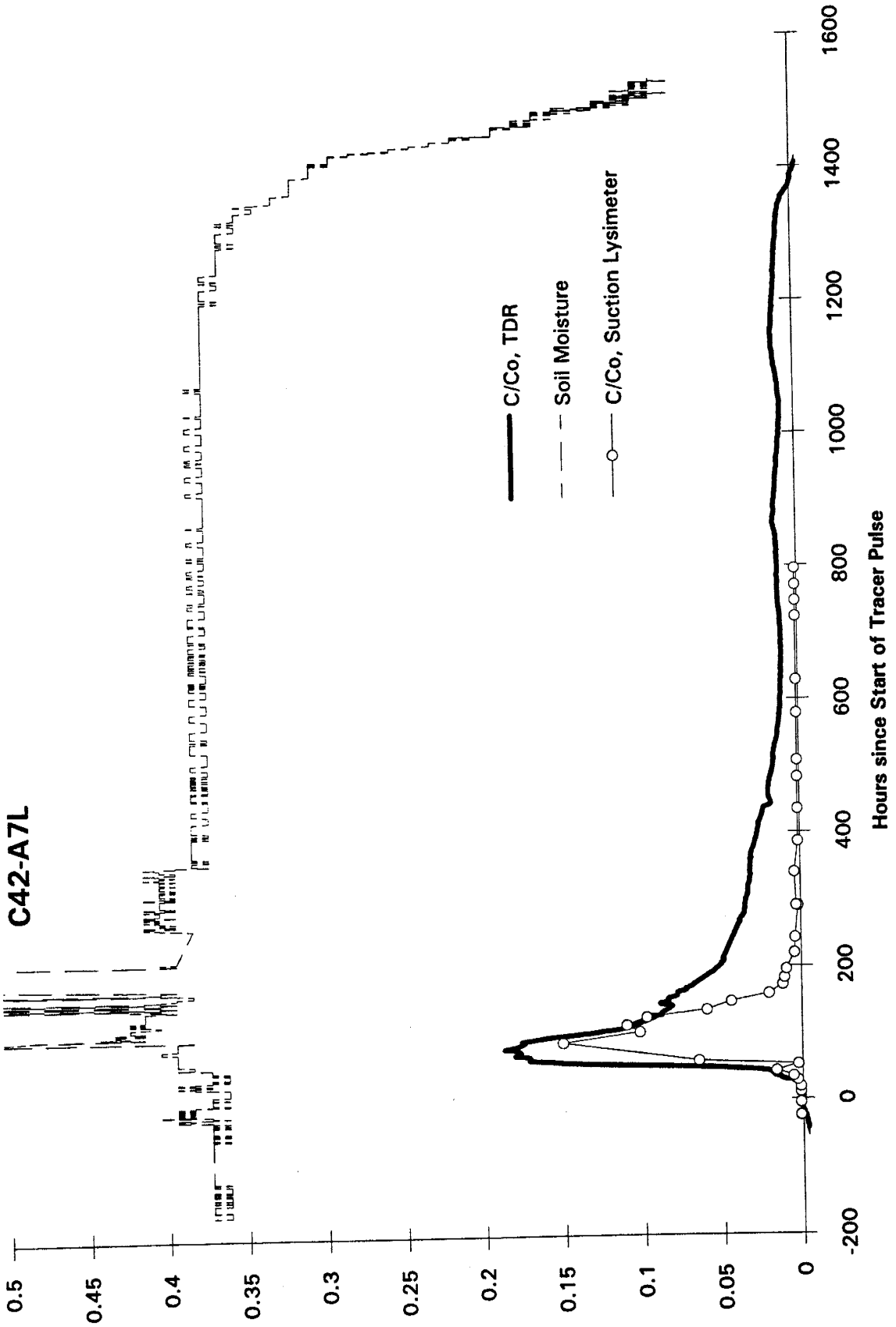




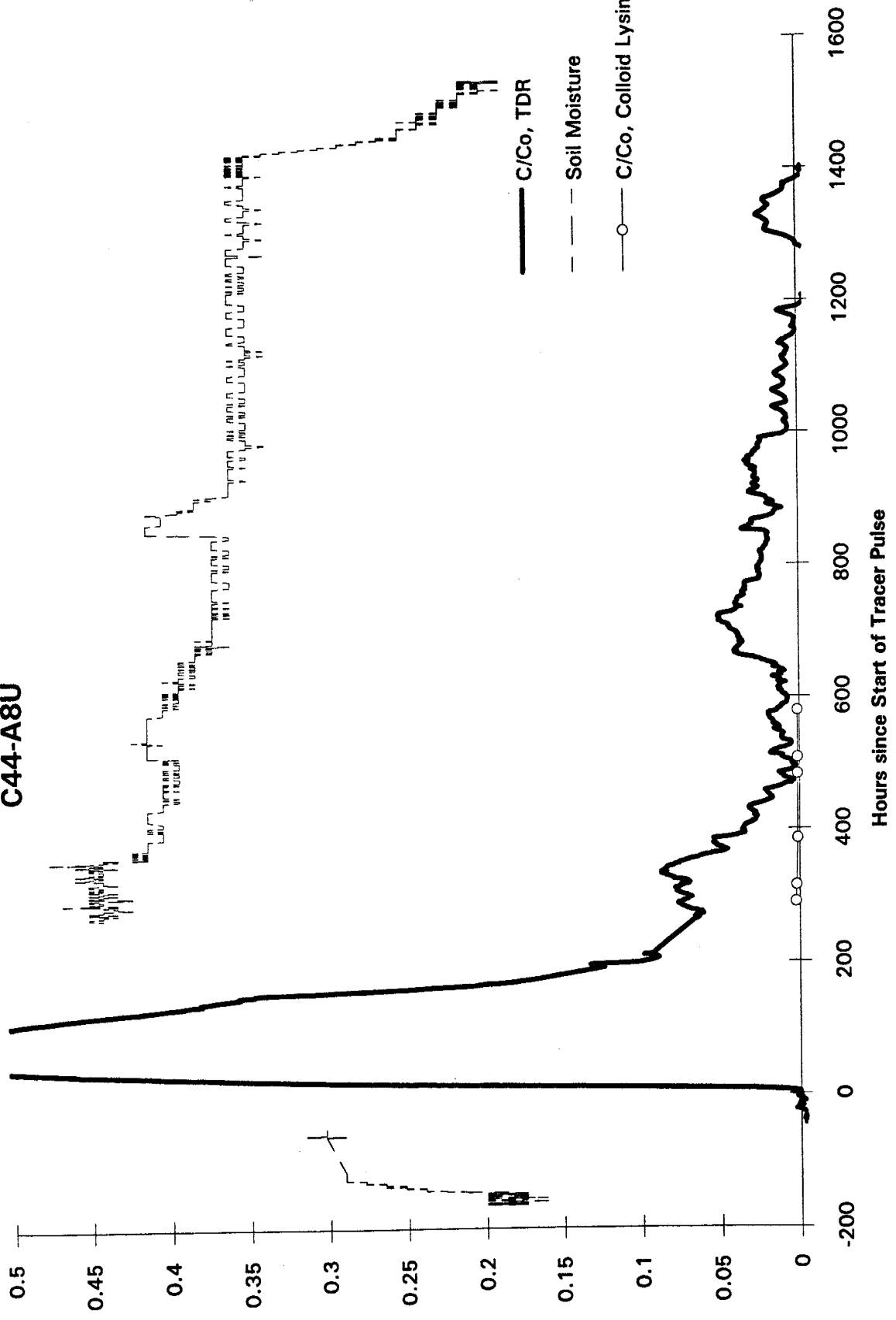


C41-A6U

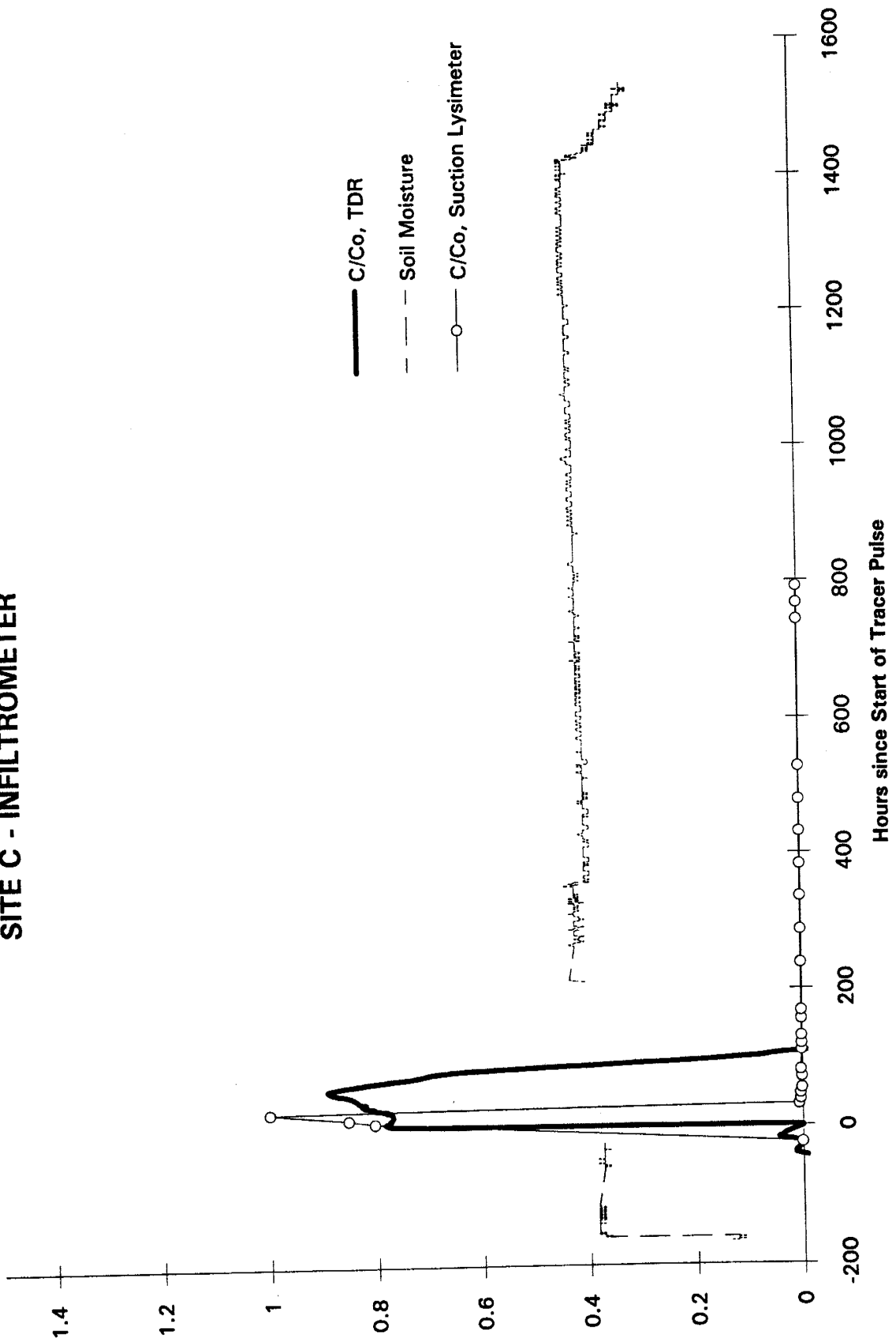


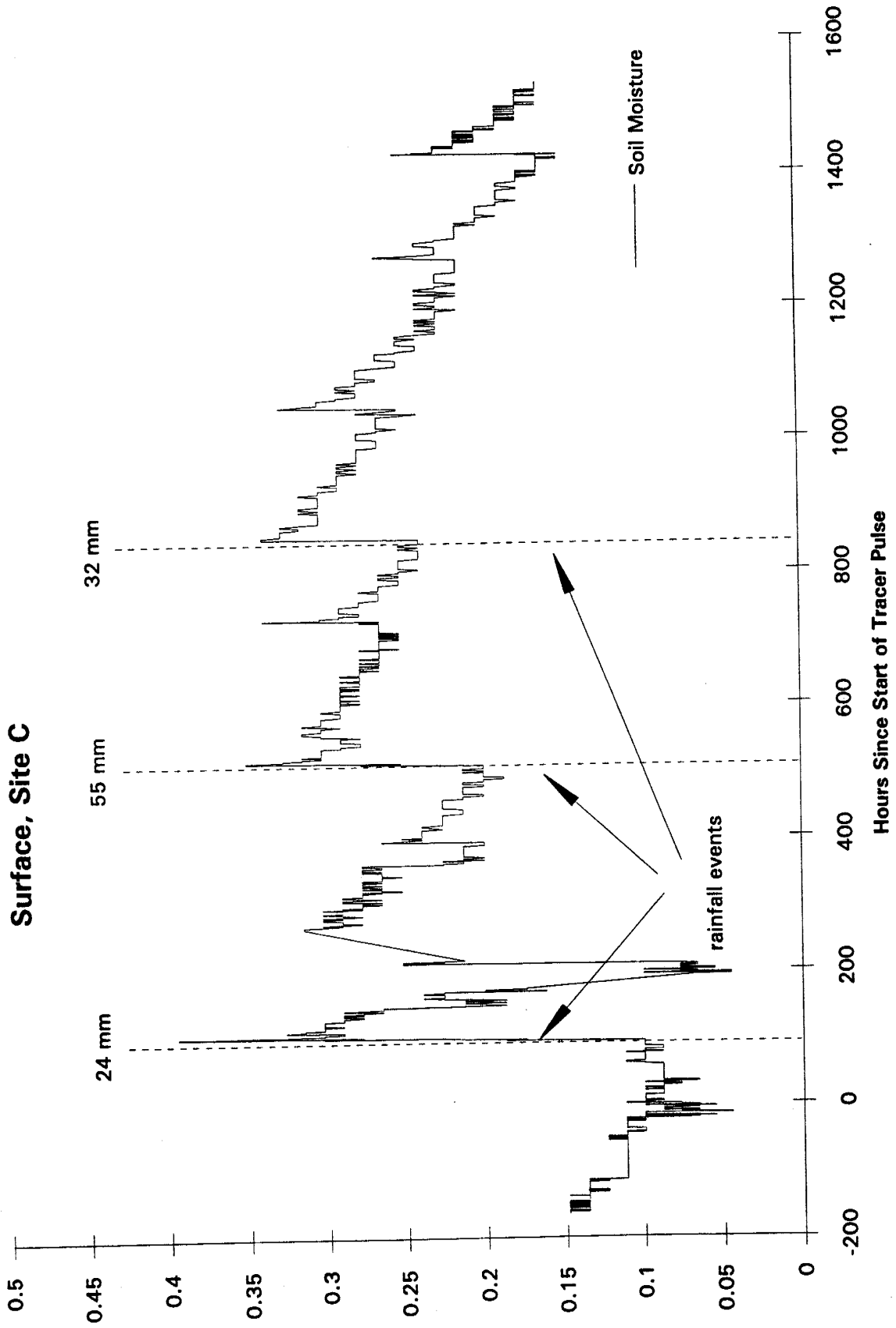


C44-A8U



SITE C - INFILTROMETER





Appendix V: Pressure Field

<u>Section</u>	<u>Page</u>
Data Acquisition Systems	2
Pressure Tensiometer and Transducer Array	2
Pressure Transducer Calibration and Data Reduction	2
Results	7
Tables	9
Figures	10
Graphs of Total Head at Sampling Points	
Site A	17
Site C	50

An automated data acquisition system coupled to a transducer-equipped tensiometer array was used to gather soil water pressures in time and space and to determine the shape of the overall pressure field. The following sections discuss data acquisition systems, construction and installation of the tensiometer array, data reduction, and results. A complete presentation of graphed total potentials in time at all sampling points is given at the end of this appendix.

Data Acquisition Systems

Two data acquisition systems for monitoring and recording transducer mV readings in time were installed at both Site A (the Clay Site) and Site C (the Sand Site). Each system monitored one half of the sampling points at a site and consisted of a Campbell Scientific 21XL datalogger with two SM416 sixteen channel multiplexers housed in a weatherproof fiberglass enclosure. MicroSwitch PC126 series 0-5 PSI differential pressure transducers were used to monitor water height inside the 500-gallon reservoir tanks, and to monitor the pressure field surrounding the infiltrometer. Sensor excitation and data transmission from external pressure sensors were carried over 22-AWG two-pair shielded cable. All connections were sealed with Con-X-All watertight connectors.

Pressure Transducer and Tensiometer array

Tensiometers were arranged in a concentric ring sampling array surrounding the infiltrometer and approximately 5 cm above the body of each TDR probe (Figures 1 and 2). 1/2" PVC pipe maintained a water column to a point above the ground surface where resin-encased modular pressure transducer units with 20.3 cm cables were inserted into the tees of each tensiometer (Figure 3). These transducer units were connected to the multiplexers with 12.2 m cables. A Texas Electronics TE525M tipping bucket rain gage was installed at Site A (the Clay Site) to collect rainfall measurements and connected to the datalogger also monitoring transducers.

A Compaq LTE 486SX/25 laptop computer was used for downloading programs to the datalogger and uploading data files from datalogger storage modules. Power to each system was provided by a Solarex MSX10 15 volt, 8.9 amp regulated solar collector to recharge the datalogger internal Ni-Cad batteries. Backup power was supplied by a 12-volt deep cycle marine battery.

Pressure Transducer Calibration and Data Reduction

All pressure transducers were calibrated in groups of fifteen by connection to a pressure chamber, referenced to a previously calibrated transducer. The measurements of the reference transducer, #05PSI127, had been previously confirmed with reference to a two meter hanging water column manometer. A Soil Moisture Systems (mbar) Tensimeter was connected to the chamber as well for confirmation of the Tensimeter measurements and transducer readings.

As the mV readings of each transducer were shown to respond in a linear manner to changes in actual pressure, a multiplier and an offset were calculated for each pressure transducer. During the Transport Processes Characterization Tests (TPCTs), the raw millivolt readings from the transducers were recorded at fifteen minute intervals and later converted to pressure head in centimeters of water at the transducer. Each mV reading was the average of twenty-five repeated

measurements. The calibrated offset and multiplier for each transducer was first used to convert transducer readings to cm H₂O at the transducer:

$$y = mx + b \text{ where}$$

- y = pressure head in centimeters of water at the transducer
- x = transducer millivolt readings
- m = slope of the mV to centimeters of water regression line
- b = intercept of the regression line

A typical graph of pressure head at the transducer versus mV readings is shown in Figure 4, together with the regression equation used to convert mV transducer readings to cm H₂O. The resulting y-values could either be converted to the height of water in the reservoir tanks or the pressure head in centimeters of water at the tensiometer tip. Off-scale transducer readings (-99999) which occurred during sampling periods when 40 - 80 PSI suction was applied to soil water samplers or which occurred for other reasons were deleted.

Calculation of pressure and total potential

For the tensiometers, the pressure head in centimeters of water at the transducer was added to the vertical length of the water column from the transducer to tensiometer tip to obtain pressure head at the tensiometer porous cup. The elevation of the porous cups above mean sea level (MSL) was then added to the pressure head readings to obtain total potential referenced to MSL.

$$\Psi_{\text{tip}} = \Psi_{\text{transducer}} + L$$

[measurements in meters of H₂O]

$$h_{\text{MSL}} = \Psi_{\text{tip}} + z$$

- where
- $\Psi_{\text{transducer}}$ = pressure head at the transducer converted from millivolt readings
 - L = length of the tensiometer from the transducer to the tensiometer tip
 - Ψ_{tip} = pressure head at the tensiometer tip
 - z = elevation above mean sea level
 - h_{MSL} = total hydraulic potential above mean sea level at the tensiometer tip

The total potential was then used to plot changes in the pressure field with time and as a response to rainfall events (See last section of this appendix).

Transducer and Tensiometer Errors

Numerous problems were encountered with tensiometers. Of the 44 tensiometers installed at Site A, 22 malfunctioned for all or a considerable portion of the infiltration test. Of the 22 malfunctioning tensiometers, 11 were the result of leaks in the tensiometers, due either to leakage

at the couplings or to degraded septae. 5 transducers malfunctioned for portions of the test. 6 showed major inconsistencies (greater than 15 cm difference) in pressure readings compared to manual Tensimeter readings. The most common problems encountered were:

1. Leakage and cracks in some tensiometers resulted in failure to maintain pressure.
2. Transducers came loose from tensiometers due to jostling during sampling, resulting in failure to maintain pressure.
3. Pressure readings of -99999 indicated negative pressure greater than the transducer capacity, usually but not always incurred during sampling.

Table 1 lists tensiometers and probable causes for problems.

Tensiometer accuracy

Transducer pressure readings were compared to the readings obtained from a Soil Moisture Systems Tensimeter at five different times during the test. Tensimeter readings were taken by inserting a needle through the septum capping the top end of the polycarbonate sight glass (Figure 4). A total of one hundred seventy-five comparisons were made. Eighty-six of those comparisons were discarded because they were taken when transducer readings were off scale due to soil water sampling, tensiometers were leaking or inoperable, or transducers were malfunctioning. The remaining eighty-nine transducer and Tensimeter pressure readings were compared, compensating for the difference in water column height between the top of the water column (the Tensimeter level) and the transducer level (Figure 3). The results (in cm of H₂O) show an average Tensimeter minus transducer difference of 6.49 cm, with a minimum difference of -44.65 cm, a maximum of 48.45 cm, and a standard deviation of 10.74 cm.

In the twenty-four cases where the water level in the tensiometer was below the transducer, both Tensimeter and transducers read the pressure in the air gap between the top of the water column and the septum. Readings by the two measurement systems should be equal. In these cases, the average Tensimeter minus transducer difference was 5.97 cm, with a minimum of -0.95 cm, a maximum of 16.15 cm, and a standard deviation of 5.24 cm. The difference in readings may be attributed primarily to the introduction of atmospheric air pressure into the tensiometer when the Tensimeter needle was inserted through the sight glass septum, resulting in a higher (less negative) reading. Increases of 2 to 20 cm of H₂O in consecutive readings were experienced during laboratory tests when the Tensimeter needle was immediately reinserted into an operating tensiometer. The variance in magnitude of error was inversely proportional to the volume of air gap between the water surface and the sight glass septum (Figure 3).

Effects of soil water sampling on tensiometer readings

During sampling, personnel would apply 40 to 80 PSI suction to draw water into the lysimeters and colloid samplers. As the sampling units were collocated with the tip of the tensiometers, a drop in pressure was noted in most properly functioning tensiometers at sampling times. As discussed above, the resulting drop in pressure often caused the 0 - 5 PSI pressure transducers to go off scale. After sampling, the pressure would gradually return to the level that existed prior to sampling.

Diurnal Fluctuations

Diurnal fluctuations in potential were noted in all functioning tensiometers. An increase in potential was observed on most days beginning at approximately noon and lasting until approximately 6 P.M., when potentials again decreased. The fluctuations ranged from 2 cm to as much as 25 cm, with most ranging between 3 and 6 cm. These fluctuations can be caused by barometric, temperature, or gravitational effects, and instrument error.

The regularity of the fluctuations throughout the entire test and across both TPCTs eliminates random equipment error. Effects on equipment from the daily increase in temperature would peak at approximately 3:00 P.M. (1500). Data transmission cables were buried approximately 6 inches below the soil surface except for the last two feet extending into the multiplexer and datalogger housing, and signal loss through heating of signal transmission wiring would be small. Laboratory tests showed that heating of the signal transmission cabling results in increased resistance, lowering of the magnitude of the transducer mV readings. This yields a resultant decline in the calculated potential rather than the observed increase in head when temperatures rose. Effects from temperature changes on the multiplexers in the closed datalogger/multiplexer housings would also likely exhibit a similar effect.

Pressure changes in the sight glass air gap (See Figure 3) can result from changes in both ambient temperature and solar energy intensity. The tensiometers were shielded from solar energy with aluminized insulated covers (See Appendix VI, Plate 9). The graph of diurnal changes illustrated in Figure 6 at sampling point A1-1IU, shows a rise in measured head during the afternoon, when ambient temperature and sunlight effects were peaking. This is the result that would be noted if rising temperatures in the air gap were a cause of erroneous measurements of soil water potential. As the temperature and pressure in the tensiometer sight glass air gap increased, the transducer would reflect a higher mV reading (greater cm of H₂O potential). The lack of immediate increase during the warming morning hours and the continuation of the increase after peak ambient temperature and solar intensity (at roughly 3 P. M.) may be attributed to temperature time lag because of the aluminized insulation shielding the tensiometers.

Discounting weather effects, barometric pressures should drop along with air temperatures at night. A drop in barometric pressure, assuming a real response from the aquifer, will result in a rise in the water table. A drop in barometric pressure, assuming no real change in the water table height in the unconfined aquifer, can also result in an increase in the pressure transducer mV readings and a corresponding increase in tensiometer measurement of total water potential. Either a real or transducer caused increase may contribute to the time lag noted in the discussion of temperature effects above.

It is also possible that effects from the gravitational pull of the sun and moon may also influence barometric pressures and aquifer water levels, and that the diurnal fluctuations are therefore real. However, the fluctuations do not display the variability in time that would be expected from gravitational effects. Of the possible causes for the diurnal fluctuations, the most likely is daily temperature change, though changes in barometric pressure may also play a minor role.

Response to soil water sampling

The response to sampling can also be used to estimate the extent of sampling point connection to the atmosphere or a water source (fast transport pathway). At sampling point A16-4OL (Figure 7), the fluctuations in head appear almost solely due to sampling, and there is little diurnal fluctuation. Sampling point A16-4OL appears to be isolated not only from atmospheric effects but also any ready source of water to replace that removed during sampling, taking as long as 10 hours to return to pre-sampling levels. Sampling site A1-1IU (Figure 6) returns to pre-sampling levels within thirty minutes, indicating either a ready source of water or connection to the atmosphere.

Results

Long time patterns of total potential change

Plots of changes in total potential with time at the individual instrument locations in both Site A and Site C (the Sand Site) exhibit trends mimicking the change in infiltration rate (Figure 5). This pattern may be caused by changes in boundary conditions, air entrainment, evapotranspiration, and drainage.

Air entrainment and mounding of water under a recharge basin have been noted by Hantush (1967) and Muckel (1959). The pattern of infiltration rate in time experienced during the test is strikingly close to that of Figure 18 in Muckel (1959). Muckel attributes the pattern to the dissolution of entrained air followed by microbial contamination of water passages, and would be supported by the algae growth in this test (Refer to Appendix II - Infiltration). The corresponding declines in both infiltration rate and total potential we experienced are not accounted for in his model.

Barring sufficient recharge, decline of the total potential during the summer months is to be expected because of increased evapotranspiration. Conservative estimates by the Blaney-Criddle, Radiation, and Penman methods for reference ET yield values of 7.0 to 8.5 mm per day during late June and early July. The total rainfall of 192 mm measured at the site over the months of June, July, and August (to mid month) is less than half of a conservatively estimated 400 mm of evapotranspiration.

The rise and decline in infiltration rate with a corresponding rise and decline in total potential supports the proposition that algae constriction of water passages at the upper (infiltrator) boundary combine with drainage from the lower boundaries of the flow system to control the patterns of change in infiltration rate and head. Assuming that drainage from the lower boundary is unchanged, infiltration rate and total potential would rise after the introduction of the Cl⁻ tracer as algae contamination of the system is reduced. As the Cl⁻ tracer is flushed from the system (300 to 500 hours after the start of the pulse), algae growth rates would increase, and infiltration rates and total potentials would again decline.

It should also be remembered that the flow systems at both sites were well drained with numerous zones of preferential flow (Refer to Appendix VI - Dye Pulse and Excavation) and that infiltration rates were many orders of magnitude higher than calculated solely on the basis of media properties (See Appendix II - Infiltration). Even without algal contamination or evapotranspiration, water levels encountered in late May and early June will be higher than those found in later summer months, without ample recharge. Barring a decrease in conductivity at the infiltrator surface, the decrease in head at the lower boundary would result in a higher gradient and higher infiltration rates, rather than the lower infiltration rates experienced.

Response to Sampling

Effects of the suction pressures generated during soil water sampling procedures were also evident (Figures 6 and 7). The changes in total head due to soil water sampling were not constant at all sampling sites. Fast return to pre-sampling heads (Figure 6) indicated that some sampling points were well connected to either air (by macropores to the surface) or water (transport pathways). Some instrument locations demonstrated precipitous drops that required long times to re-equilibrate (Figure 7), indicating that the sampling points were not well connected to either an air or water supply and could not easily replace the sampled water volume.

Rainfall events

A striking correlation is exhibited between changes in the pressure field and rainfall events. Three major rainfall events occurred during the test period which were reflected in changes in the total potential. Effects of rainfall were reflected within an hour in the pressure transducer readings. The response at Site A is virtually instantaneous throughout the instrument array for all three rainfall events. The second and third rainfall events are universally noted at Site C, though response to the first rainfall event at Site C is rarely noted. The 55.1 mm rainfall event raised the total hydraulic potential by 30 to 40 cm on average at Site A. The most extreme change measured at a functioning tensiometer was an increase of 55 cm at location A26-7IL. The magnitude of the change in head (~35 cm) during the three rainfall events is much greater than the actual rainfall (~5 cm), even considering an unsaturated pore volume of .35.

Bianchi and Haskell (1966), and McWhorter, (1971) have noted and discussed this phenomenon in shallow unconfined aquifers. They attribute this aberrant rise in the measured water table to the increase in pressure from the entrainment of air between the water table and an advancing infiltration front from the saturated surface layer. Given the dominance of macropore and preferential flow and the well-drained nature of the system, we feel it more likely that the cause is the preferential filling of macropores by the infiltrating water. The low air entry values of the relatively large size pores would result in rapid escape of air from any volume of media between the water table and a "rain-saturated" surface layer. Figures 8 and 9 display typical potential rise and rainfall event correlation at both Site A and Site C. Figure 10 is a smaller time scale presentation of the rainfall response of two sampling points in the same vertical instrument borehole at Site A. The rapid rise and slow decrease in the potential is more representative of the gradual flow of water out of the system than a release of trapped air. The relatively fast response of the pressure potential at both the upper level of the tensiometer array and the lower (Figure 10) also argues that media to 3 m depths were well connected to the surface. Also, had an increase in pressure in a trapped air volume been the cause of the apparent rise in head, there should be no difference between upper and lower sampling points in either the magnitude or time of rise.

Diurnal fluctuations

Diurnal fluctuations are believed to result primarily from temperature changes within the tensiometer itself, with a possible slight effect from barometric pressure changes. Diurnal fluctuations therefore identified tensiometers sensitive or not sensitive to atmospheric changes, but do not necessarily indicate sampling points connected to the atmosphere or macropores.

Sampling Location	Function? (Y/N)	Reason for Malfunction
A1-1IU	Y	
A2-1IL	Y	
A3-1OU	N	Invalid data thru Hour 925
A4-1OL	Y	
A5-2IU	N	Leakage
A6-2IL	N	Leakage
A7-2OU	Y	
A8-2OL	N	Leakage
A9-3IU	Y	
A10-3IL	N	Leakage from Hour 825
A11-3OU	Y	
A12-3OL	N	Leakage
A13-4IU	N	Leakage
A14-4IL	Y	
A15-4OU	Y	Leakage from Hour 1450
A16-4OL	N	Tensiometer/Transducer
A17-5IU	N	Leakage
A18-5IL	N	Invalid Data
A19-5OU	N	Leakage
A20-5OL	N	Tensiometer/Transducer
A21-6IU	Y	Invalid Data from Hour 1400
A22-6IL	N	Leakage

Sampling Location	Function? (Y/N)	Reason for Malfunction
A23-6OU	Y	
A24-6OL	N	Tensiometer/Transducer
A25-7IU	Y	
A26-7IL	Y	
A27-7OU	Y	
A28-7OL	Y	Invalid Data from Hour 1275
A29-8IU	Y	
A30-8IL	Y	*Leakage from Hour 1000
A31-8OU	N	Invalid Data
A32-8OL	N	Invalid Data
A33-A1U	Y	
A34-A1L	N	Tensiometer/Transducer
A35-A2L	N	Invalid Data
A36-A3L	Y	
A37-A3U	N	Tensiometer/Transducer
A38-A4L	N	Leakage
A39-A5U	Y	
A40-A5L	Y	Invalid Data Hours 100-300
A41-A6L	N	Leakage
A42-A7L	Y	Invalid Data Hours 100-300
A43-A7U	N	Tensiometer/Transducer
A44-A8L	Y	

Table 1. Tensiometer malfunctions, Site A

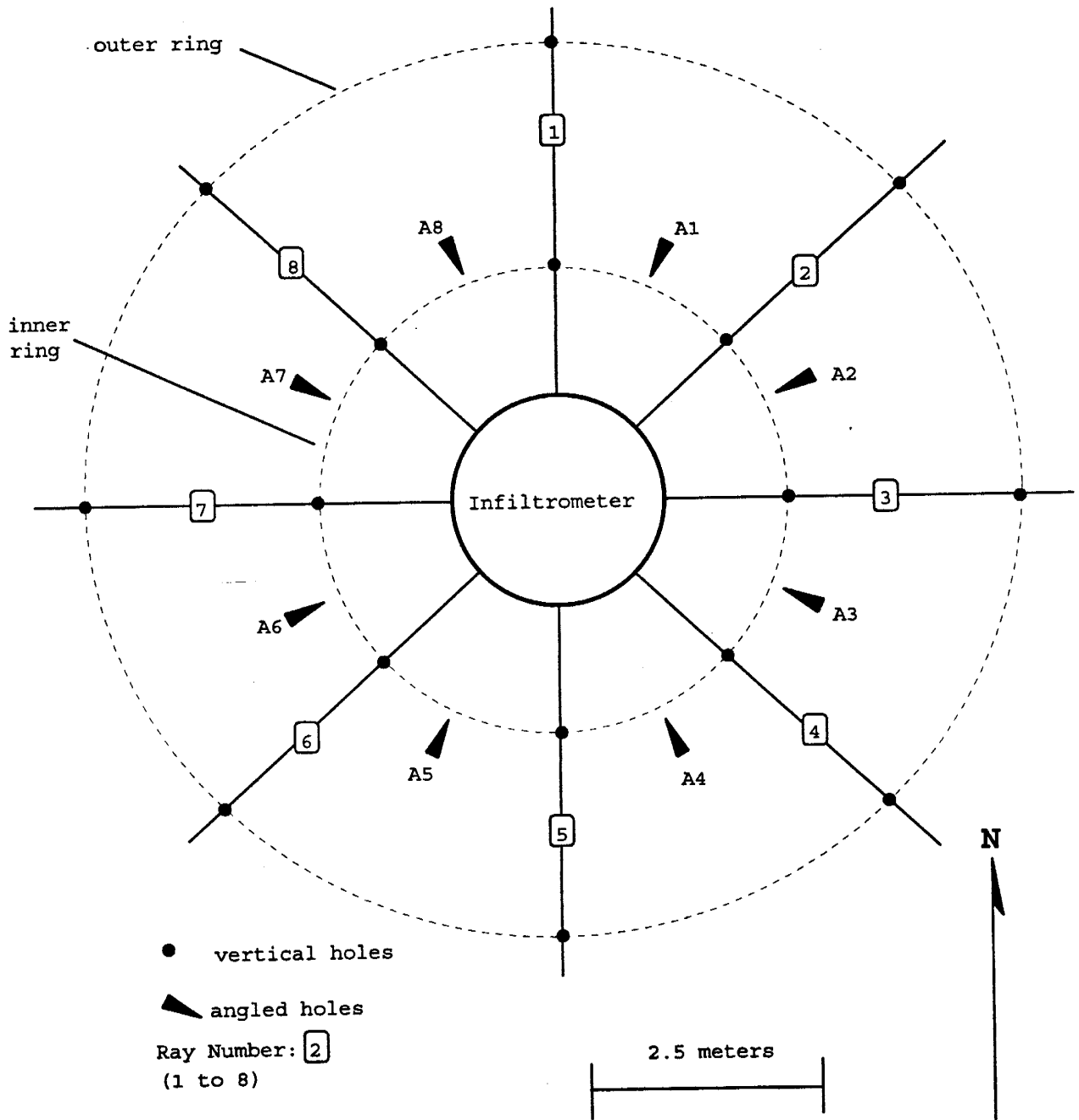


Figure 1. Site instrumentation array.

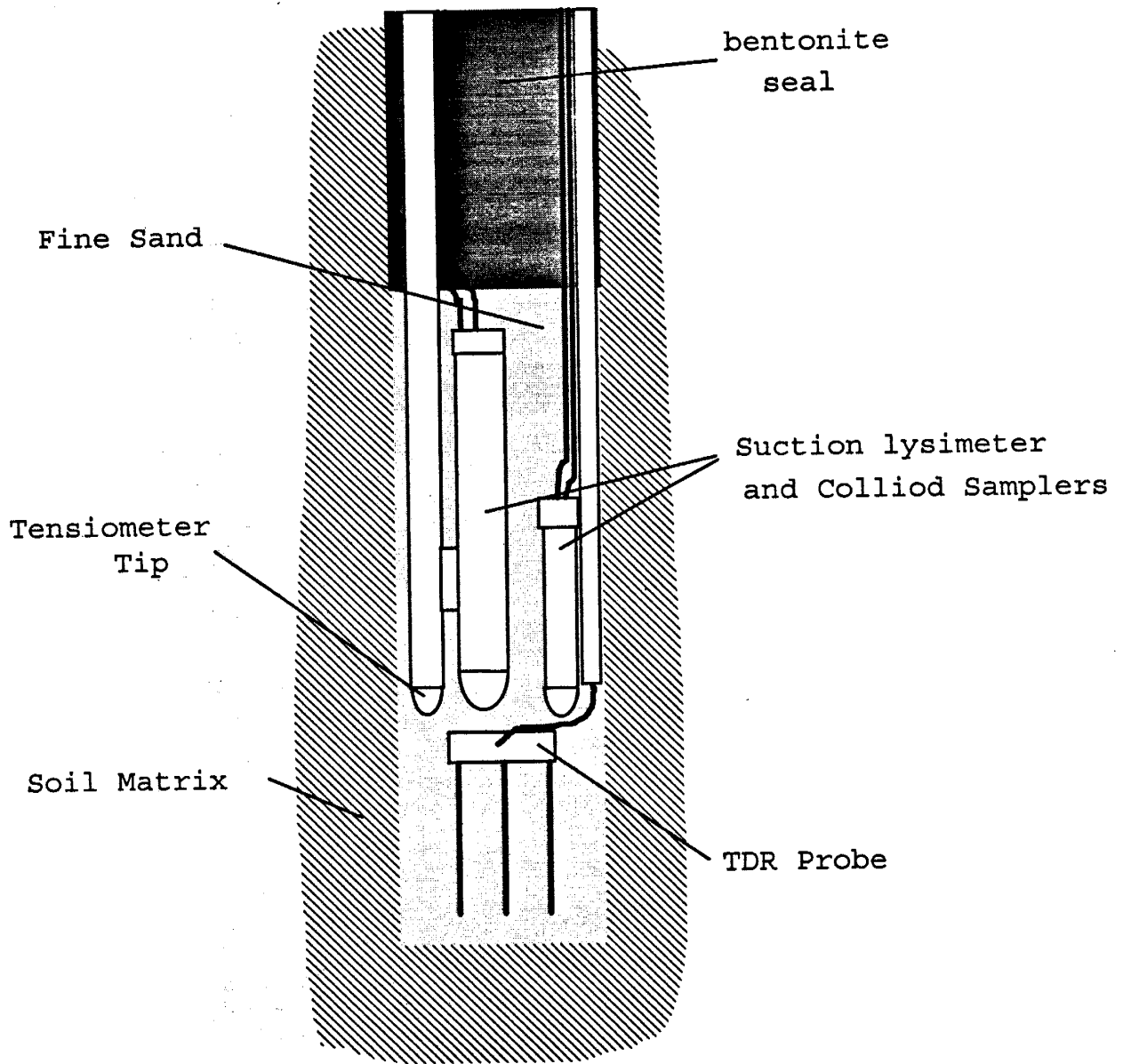


Figure 2. Sampling point instrumentation package.

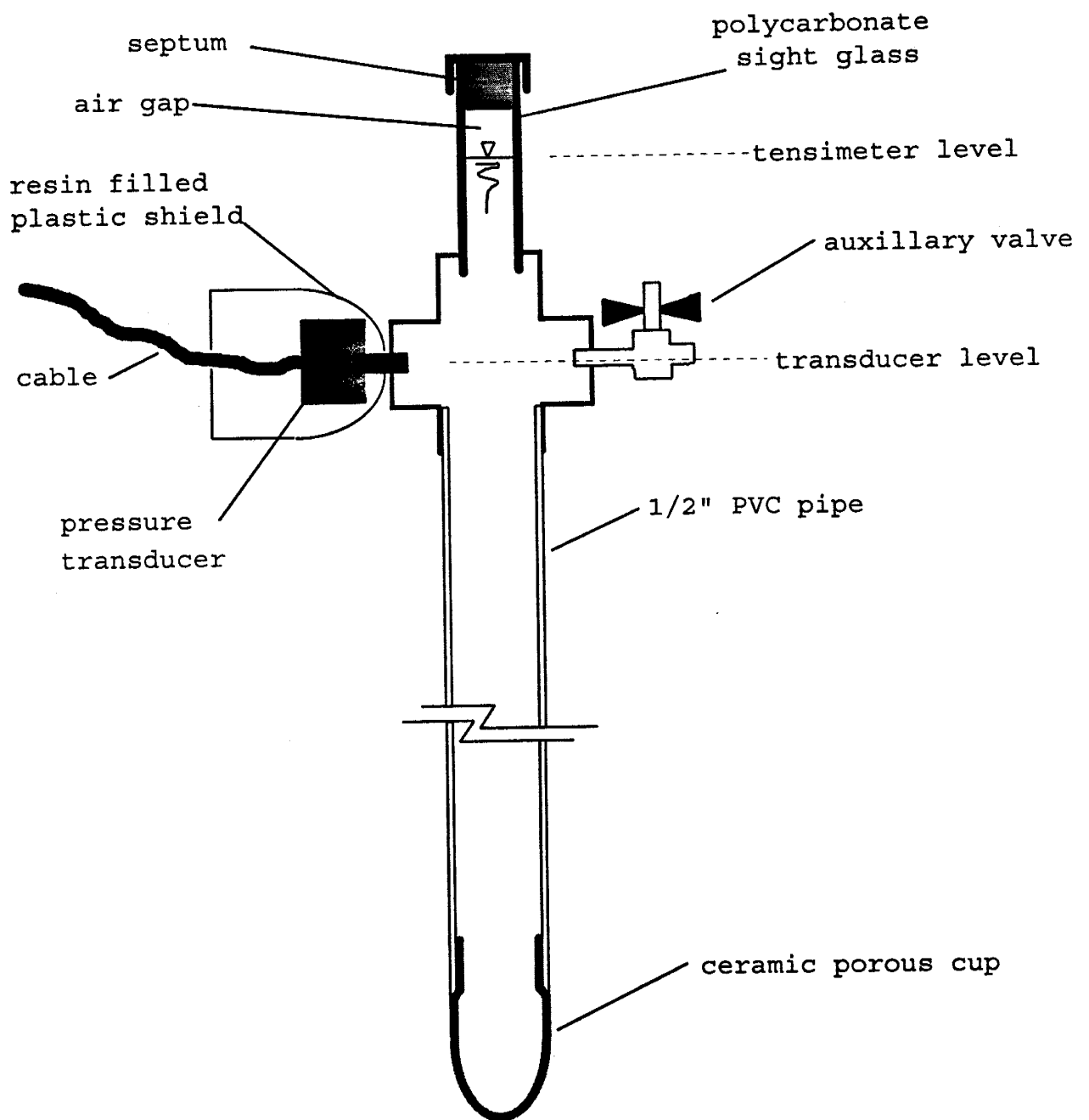


Figure 3. Tensiometer construction

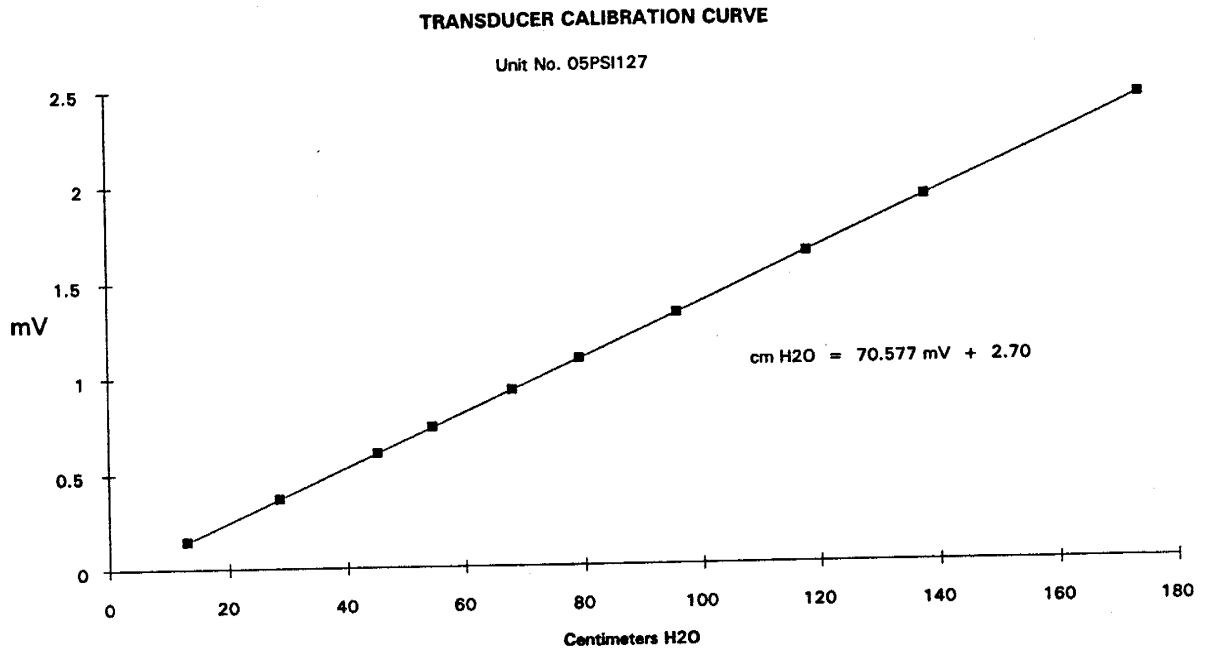


Figure 4. Transducer Calibration.

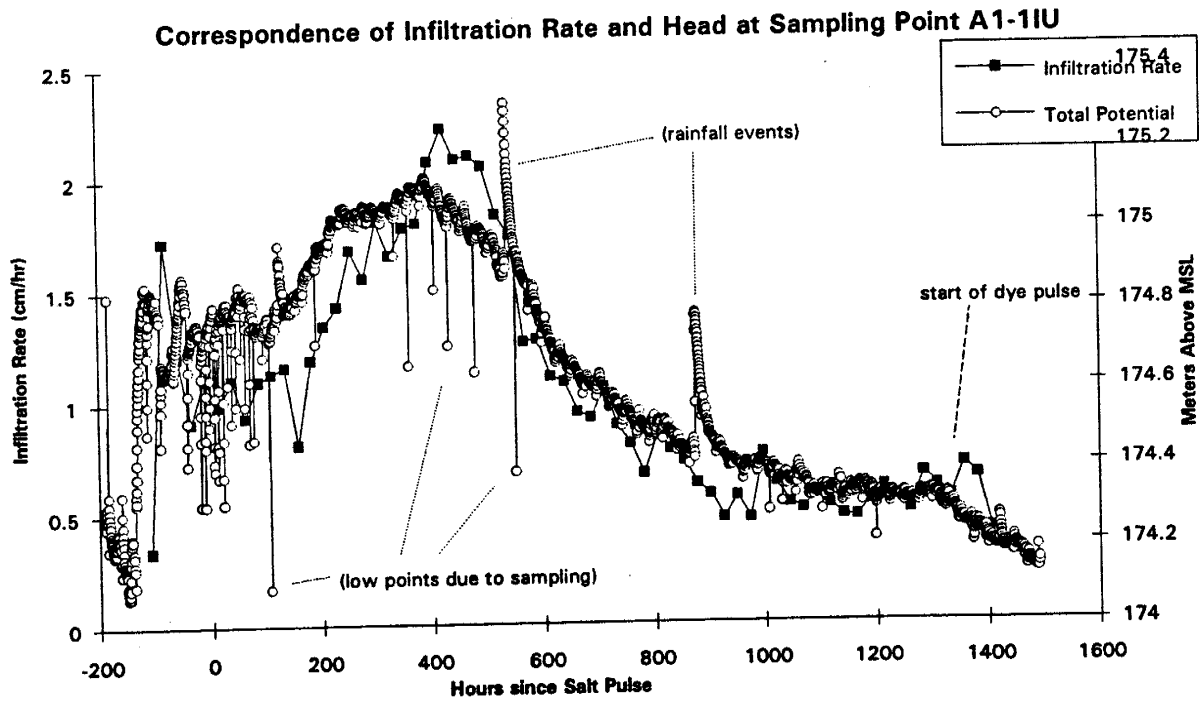


Figure 5. Correspondence of trends between infiltration rate and changes in total potential.

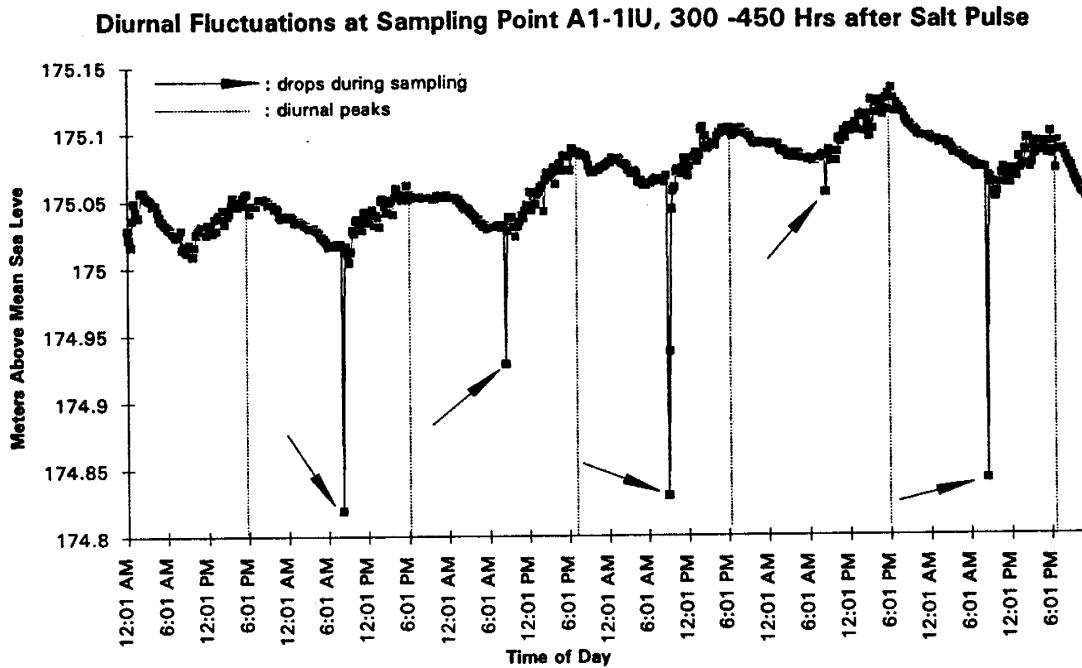


Figure 6. Diurnal piezometric head fluctuations and rapid return after sampling.

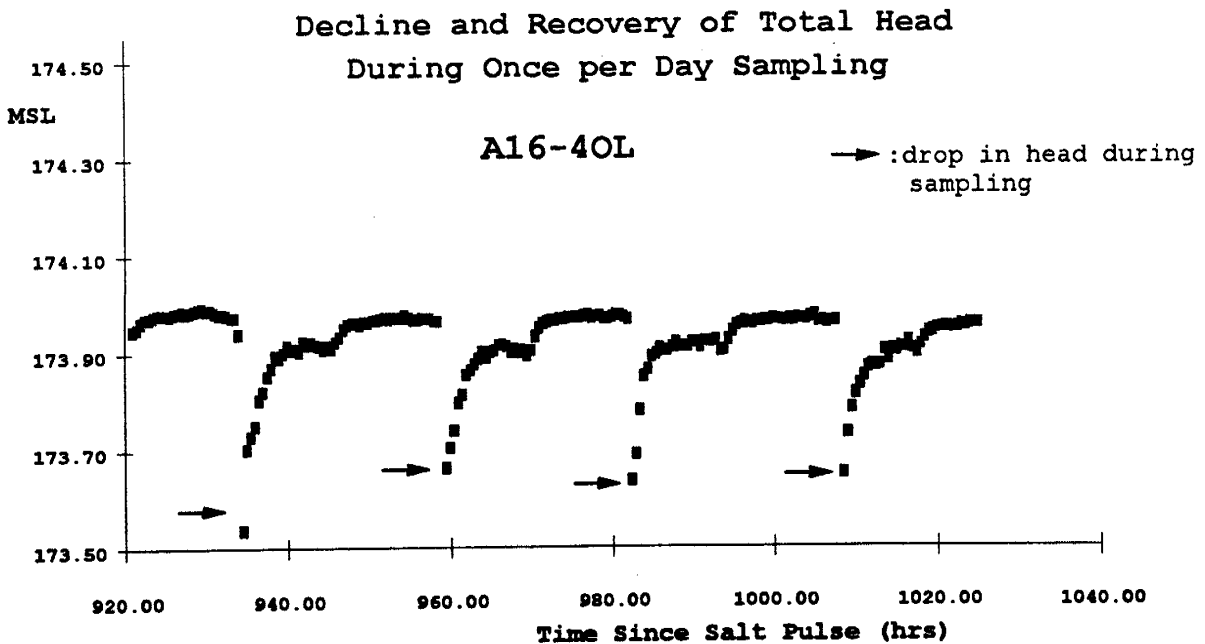


Figure 7. Depression of head during sampling and slow return.

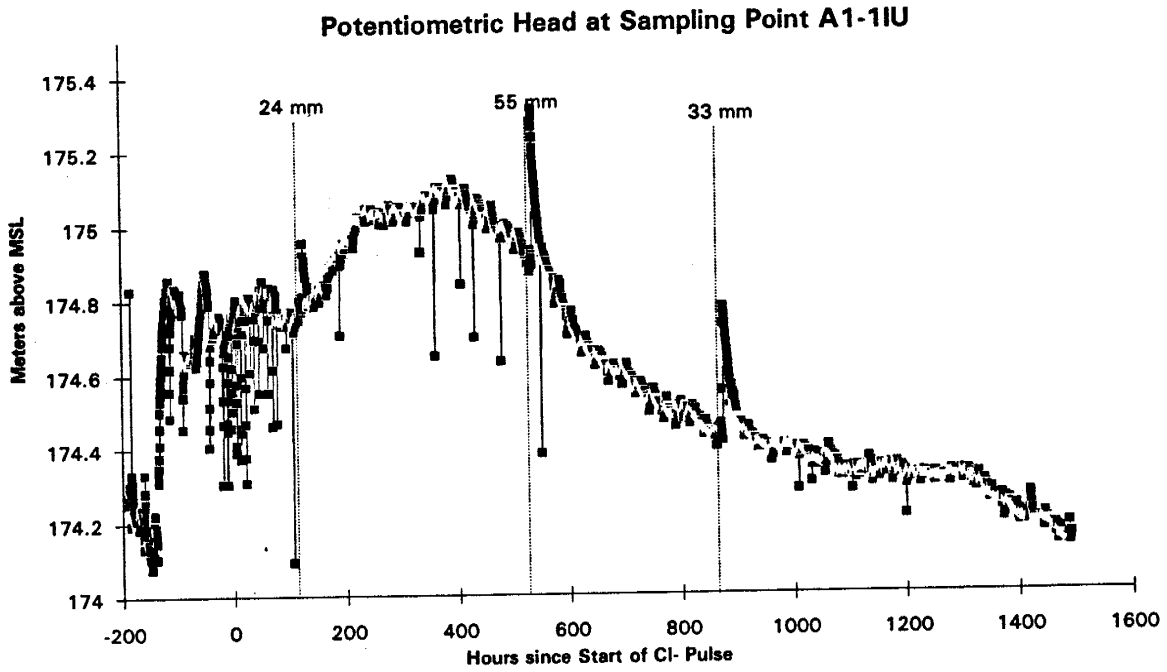


Figure 8. Total potential in time and rainfall events at sampling point A1-1IU, Site A.

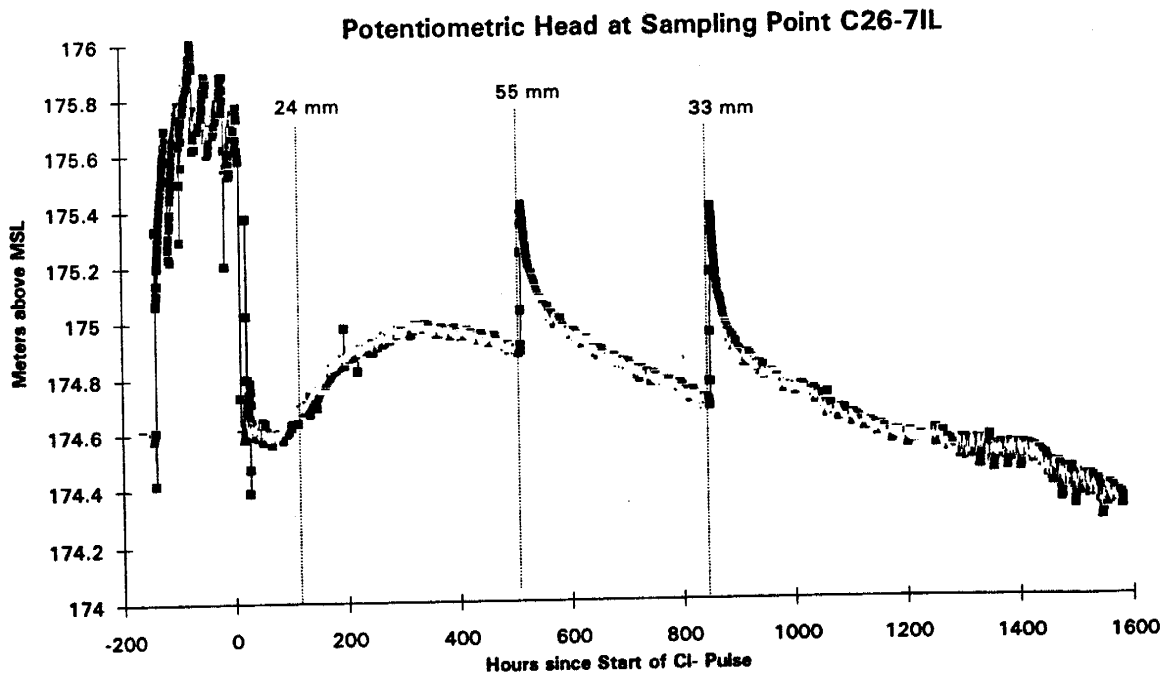


Figure 9. Correlation of head rise and rainfall events at sampling point C26-7IL, Site C.

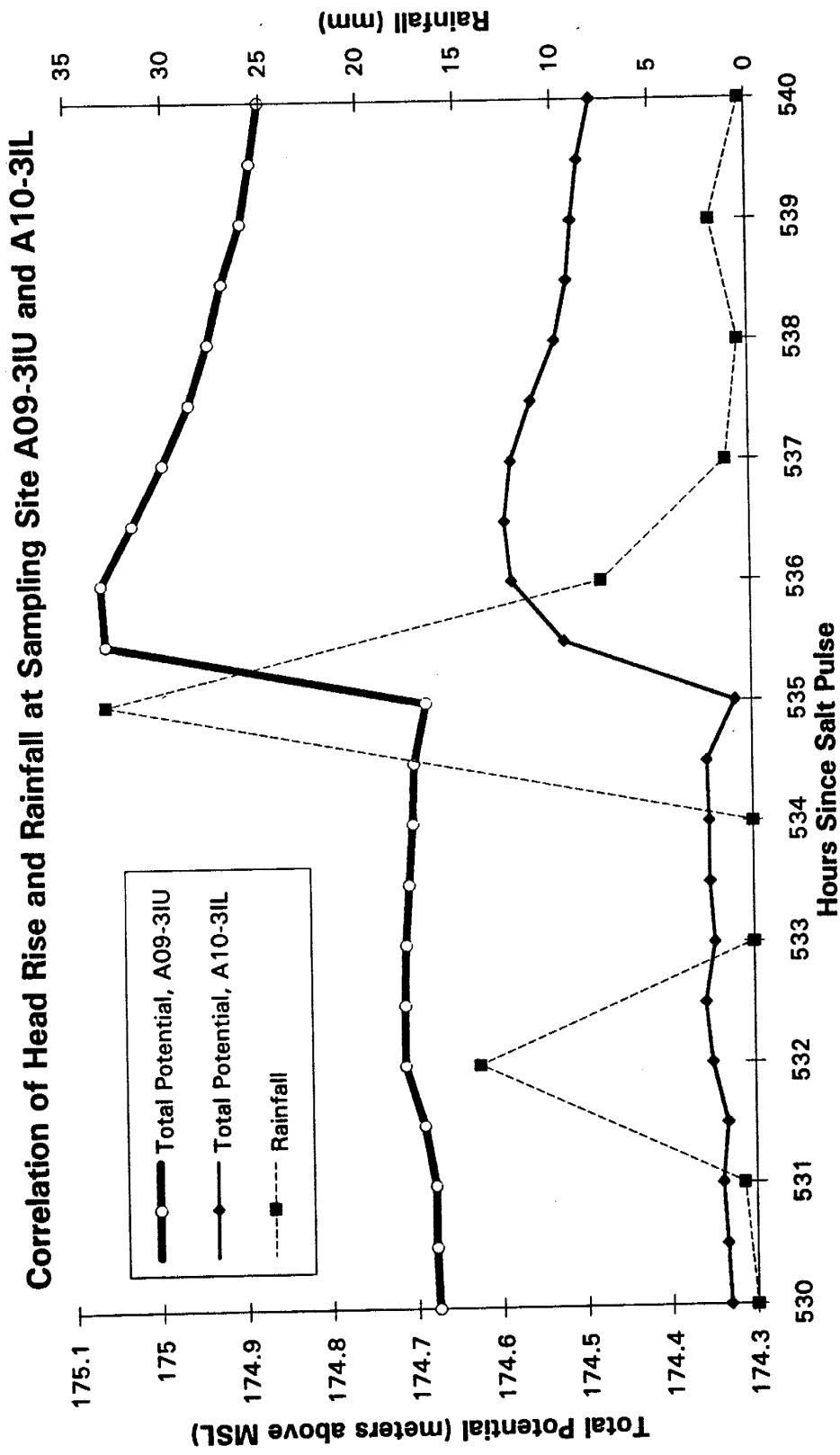
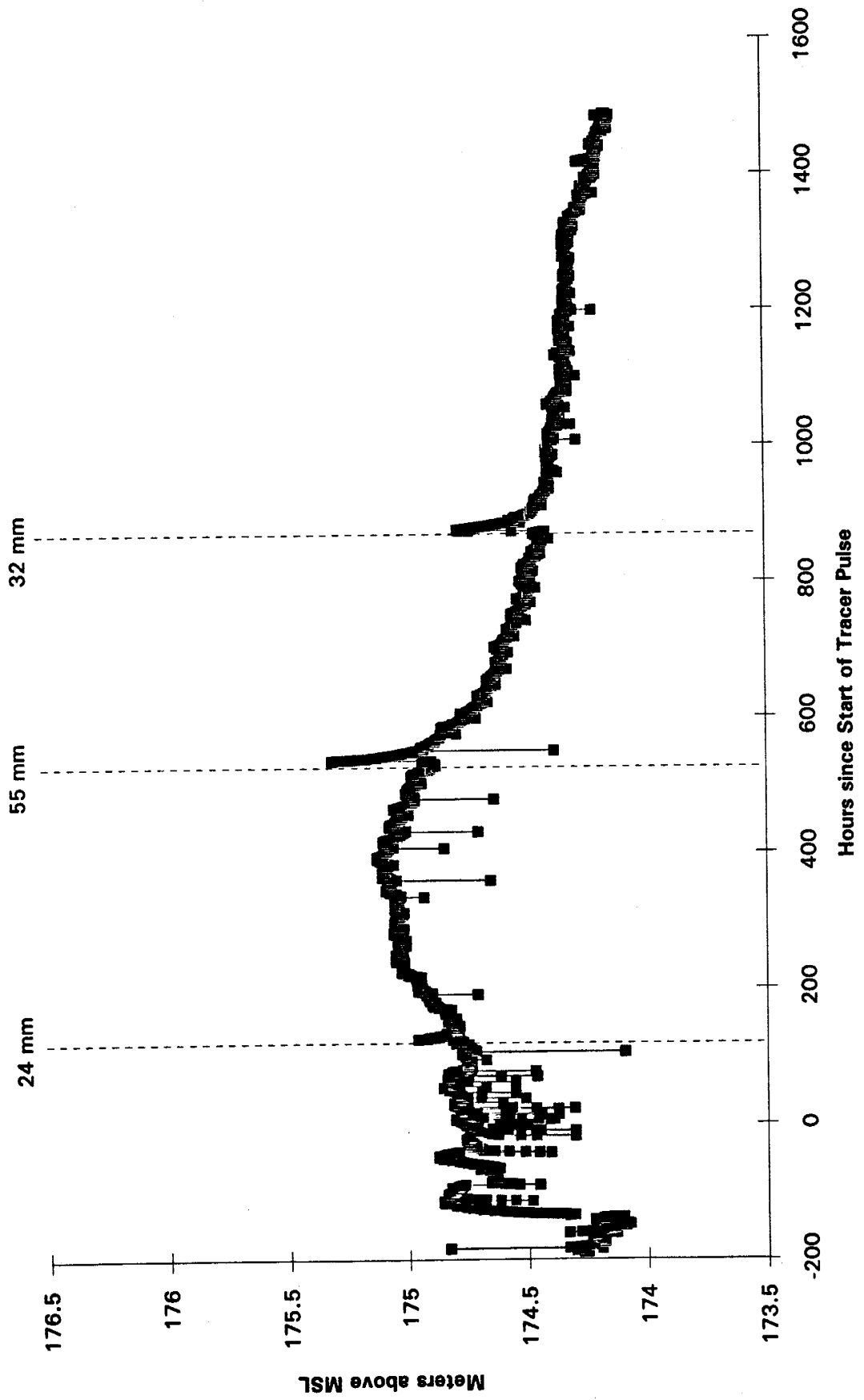
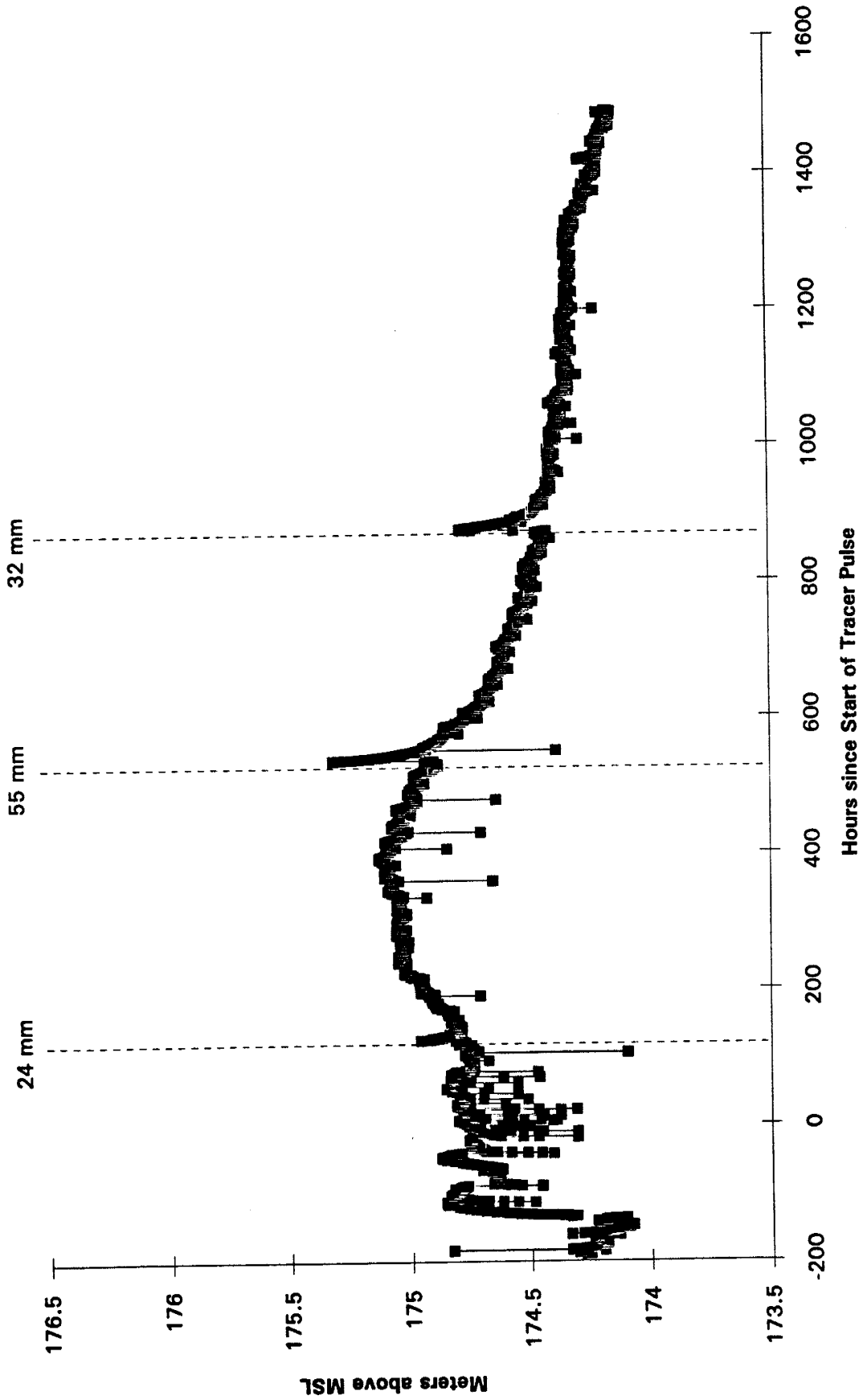


Figure 10. Pressure head response to rainfall event at lower level (3 m) sampling point A10-3IL and at upper level (2 m) sampling point A09-3IU.

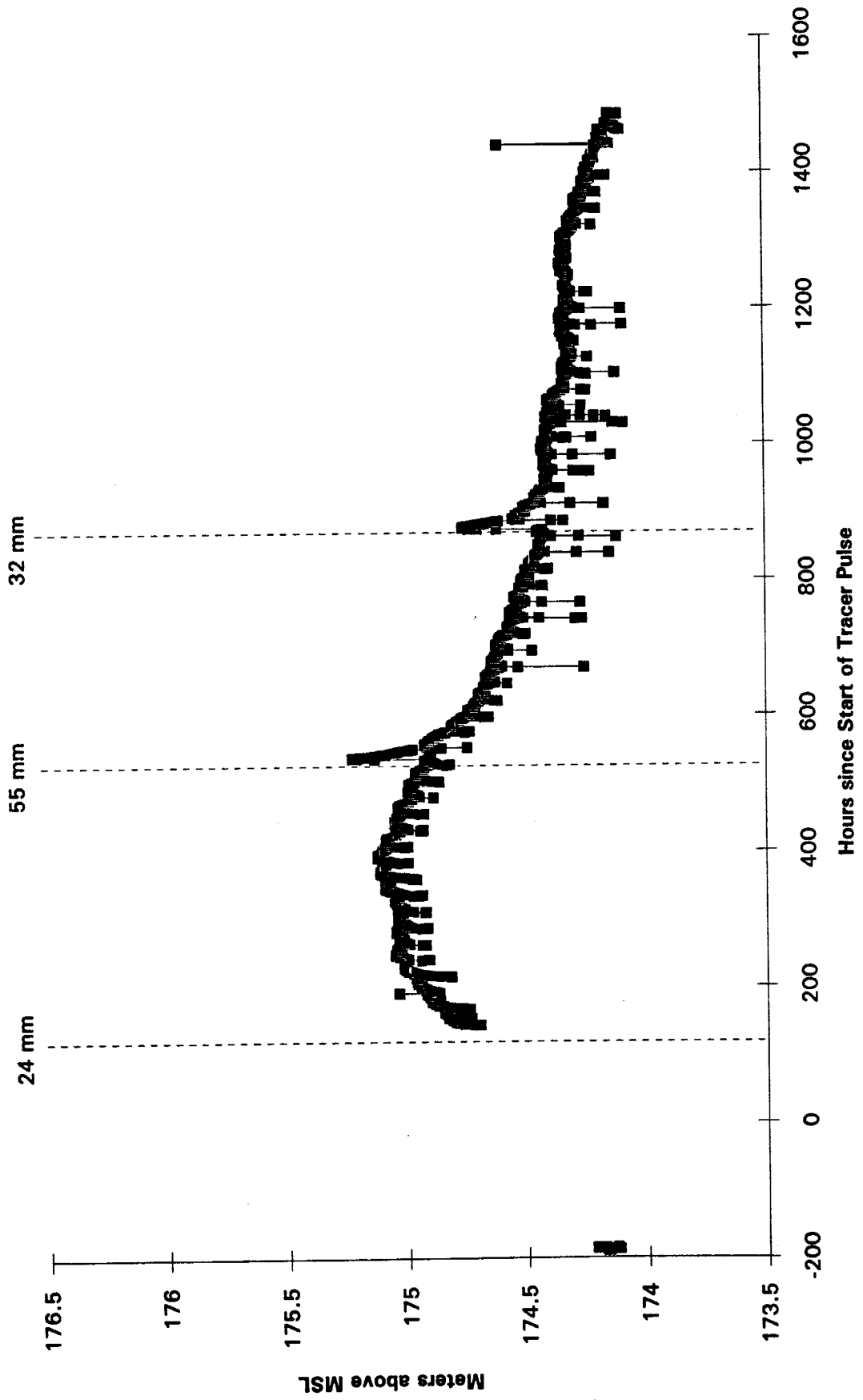
A01-1IU



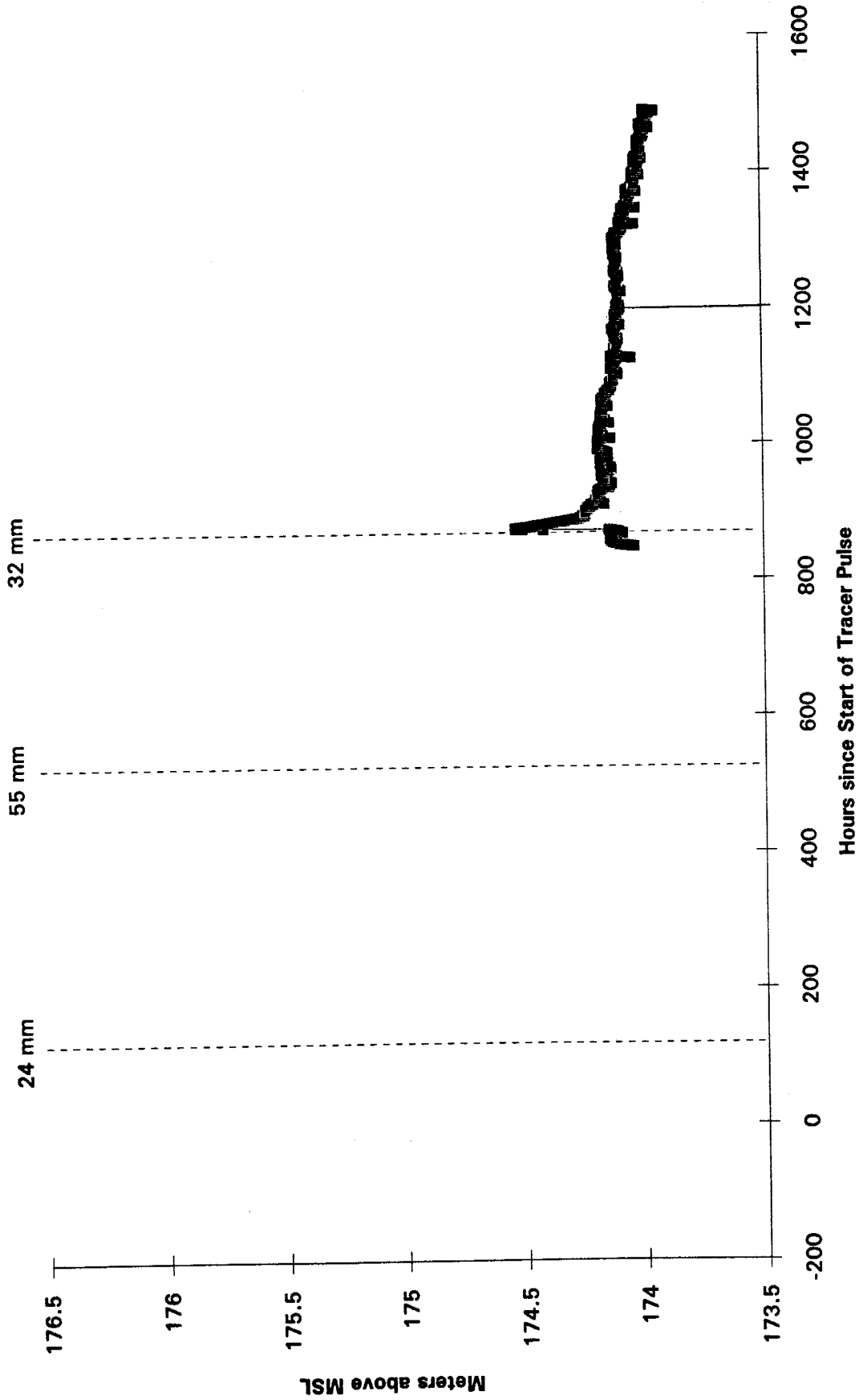
A01-1IU



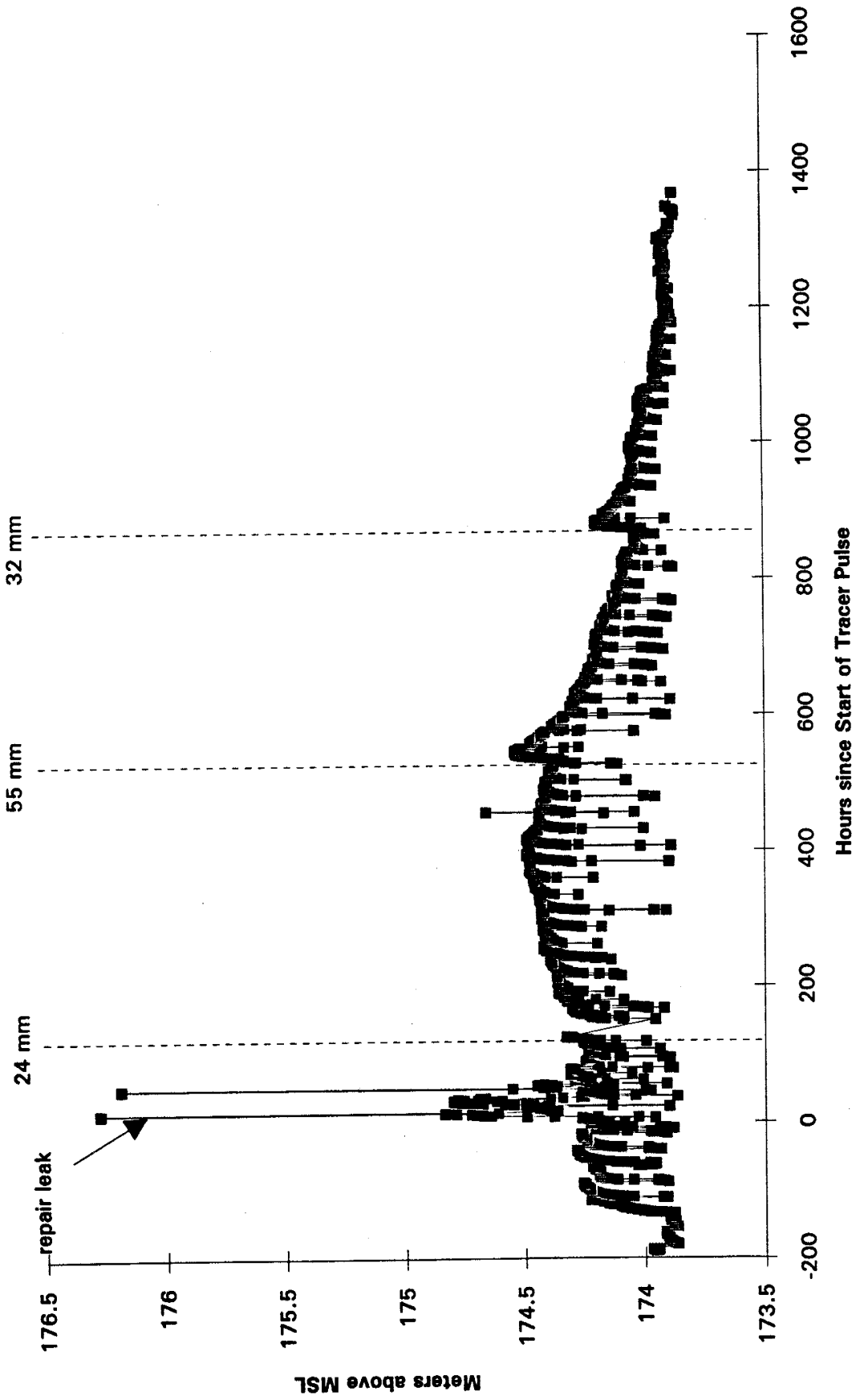
A02-11L



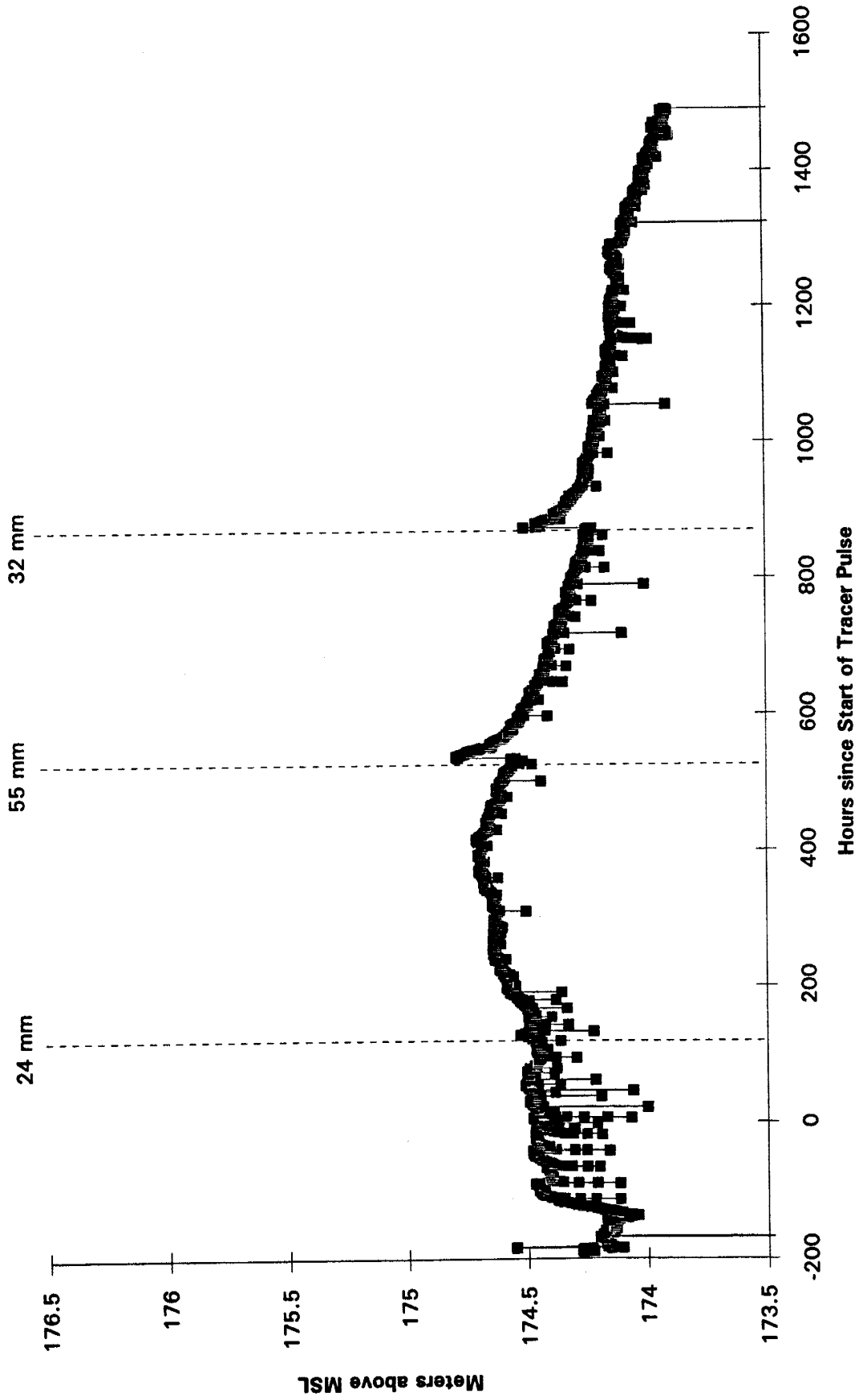
A03-10U



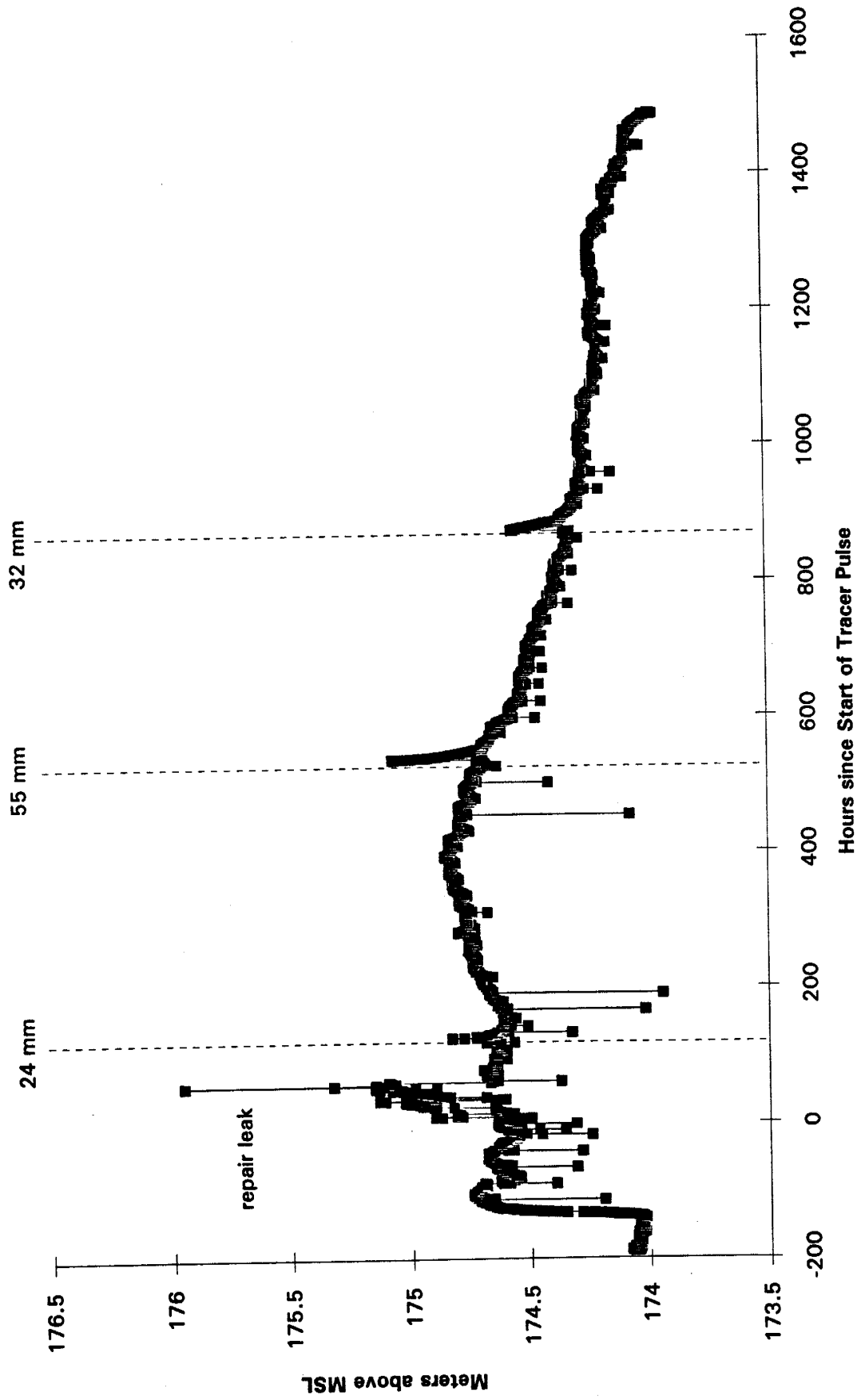
A04-10L



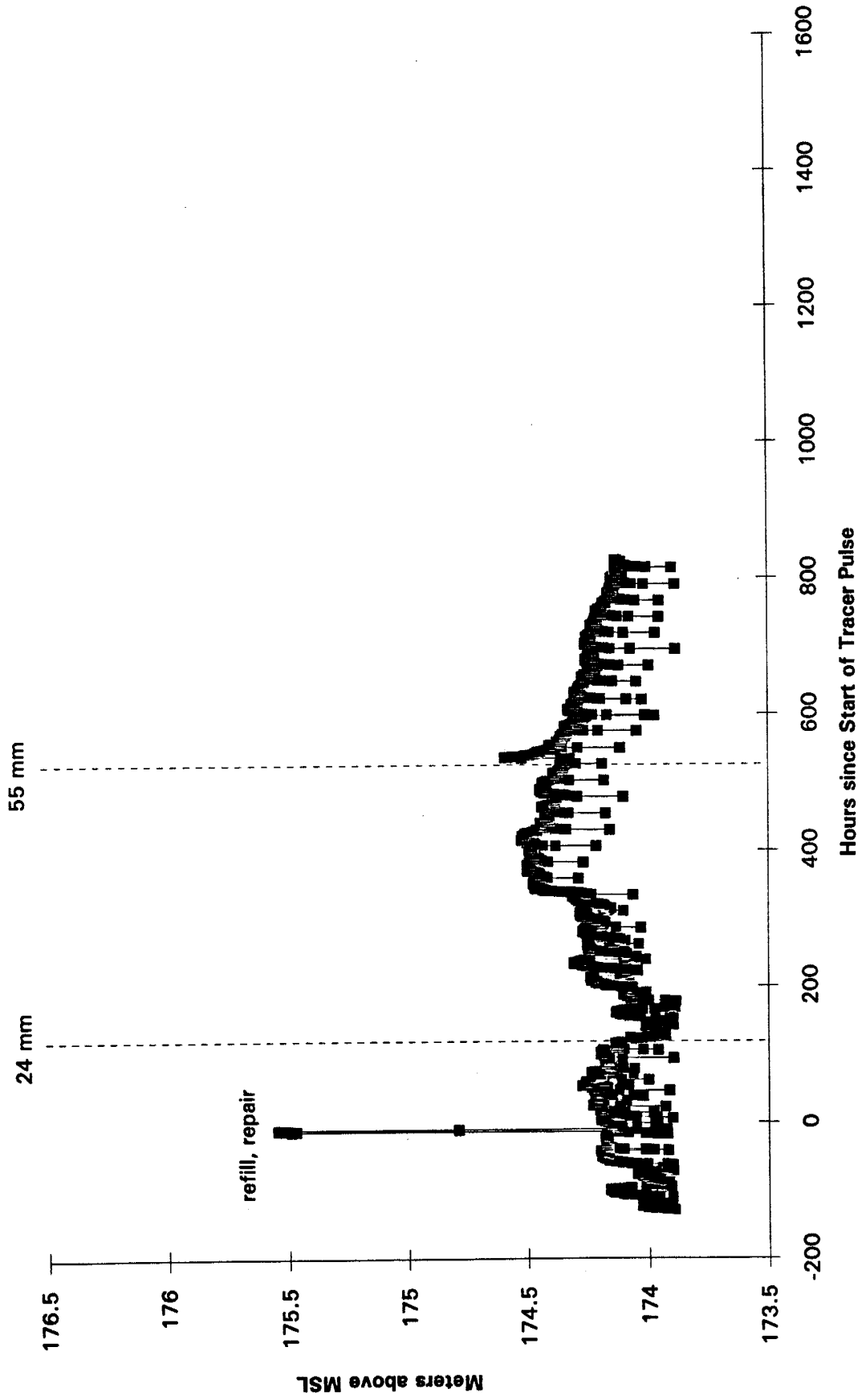
A07-20U



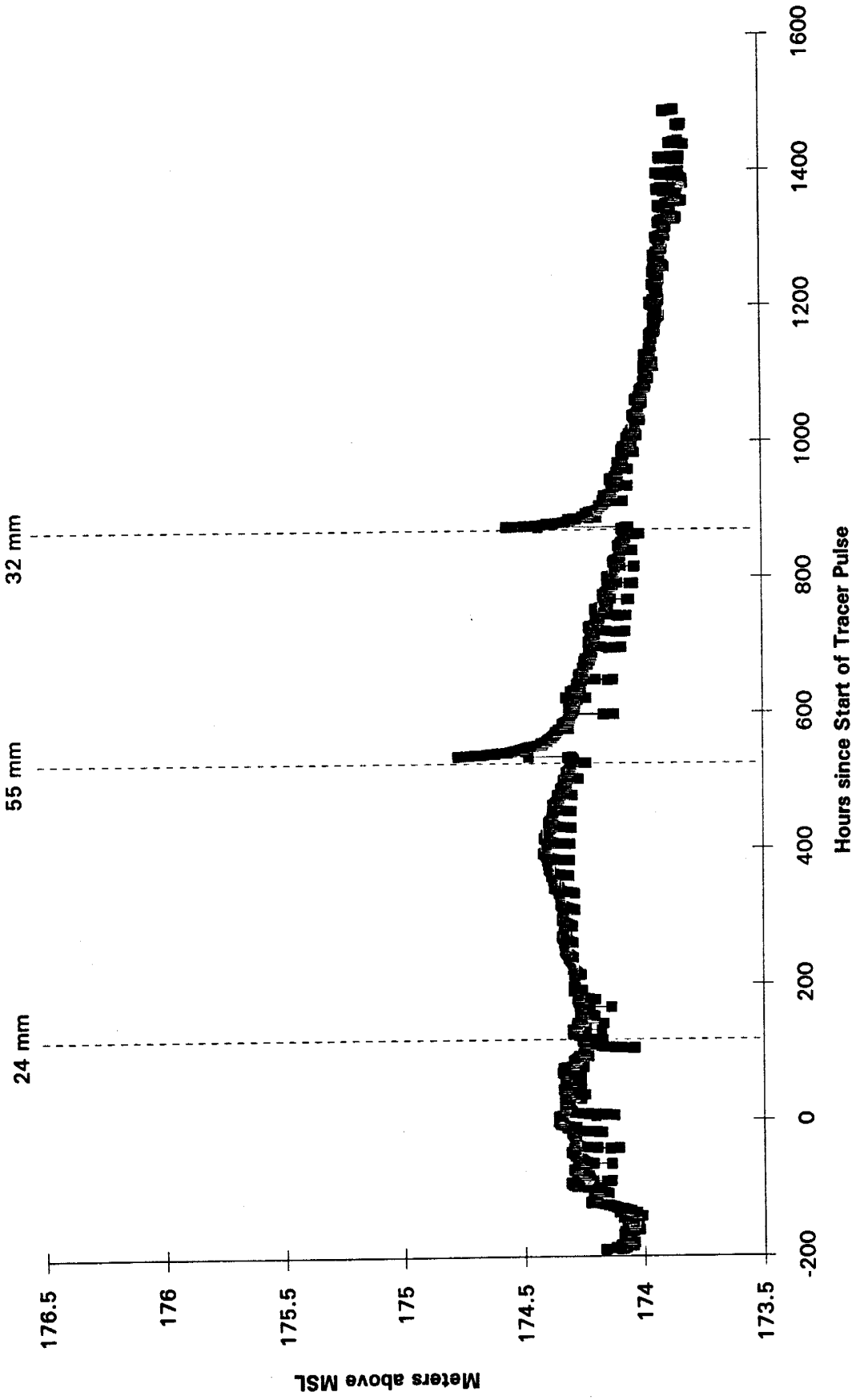
A09-3IU



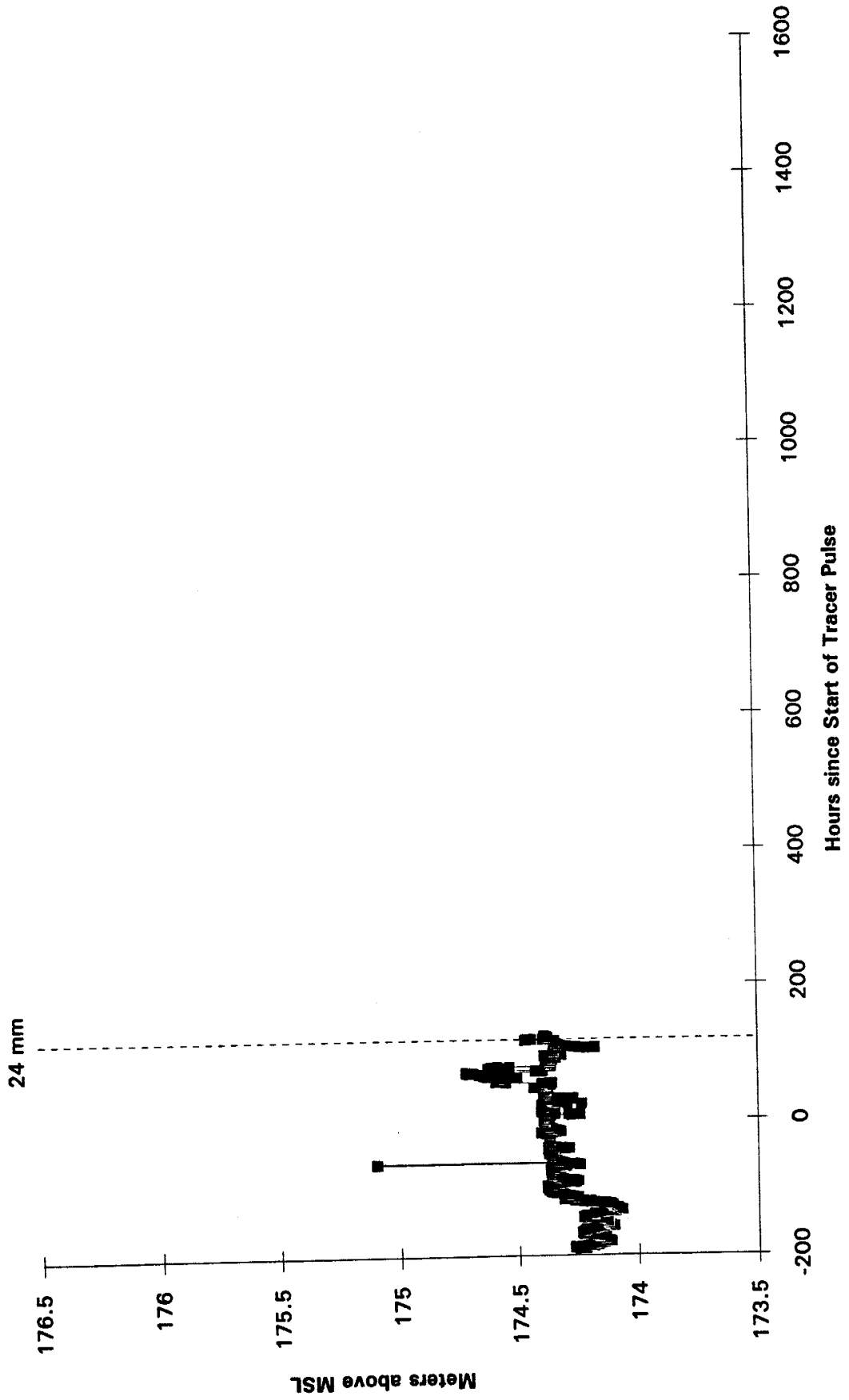
A10-3IL



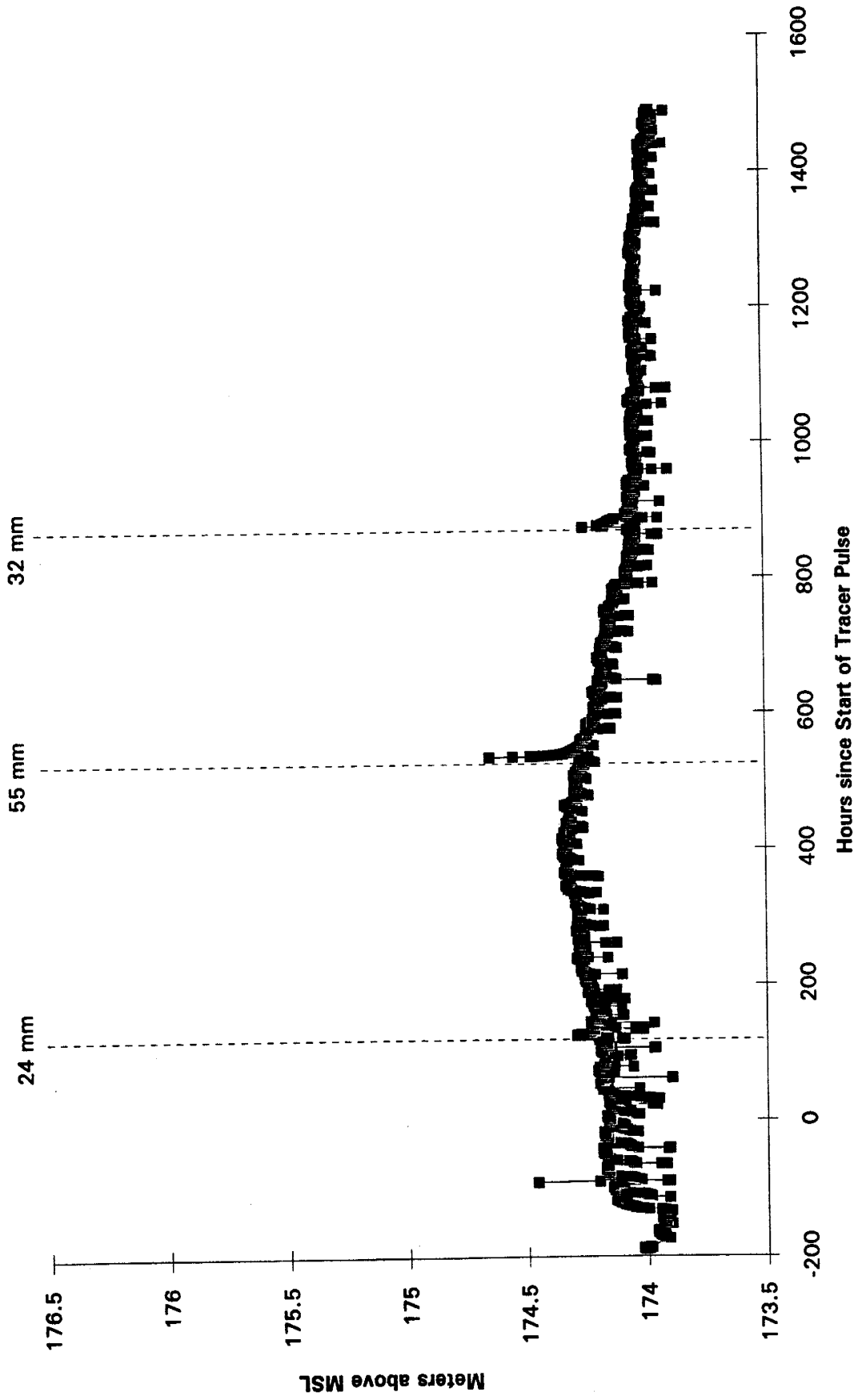
A11-30U



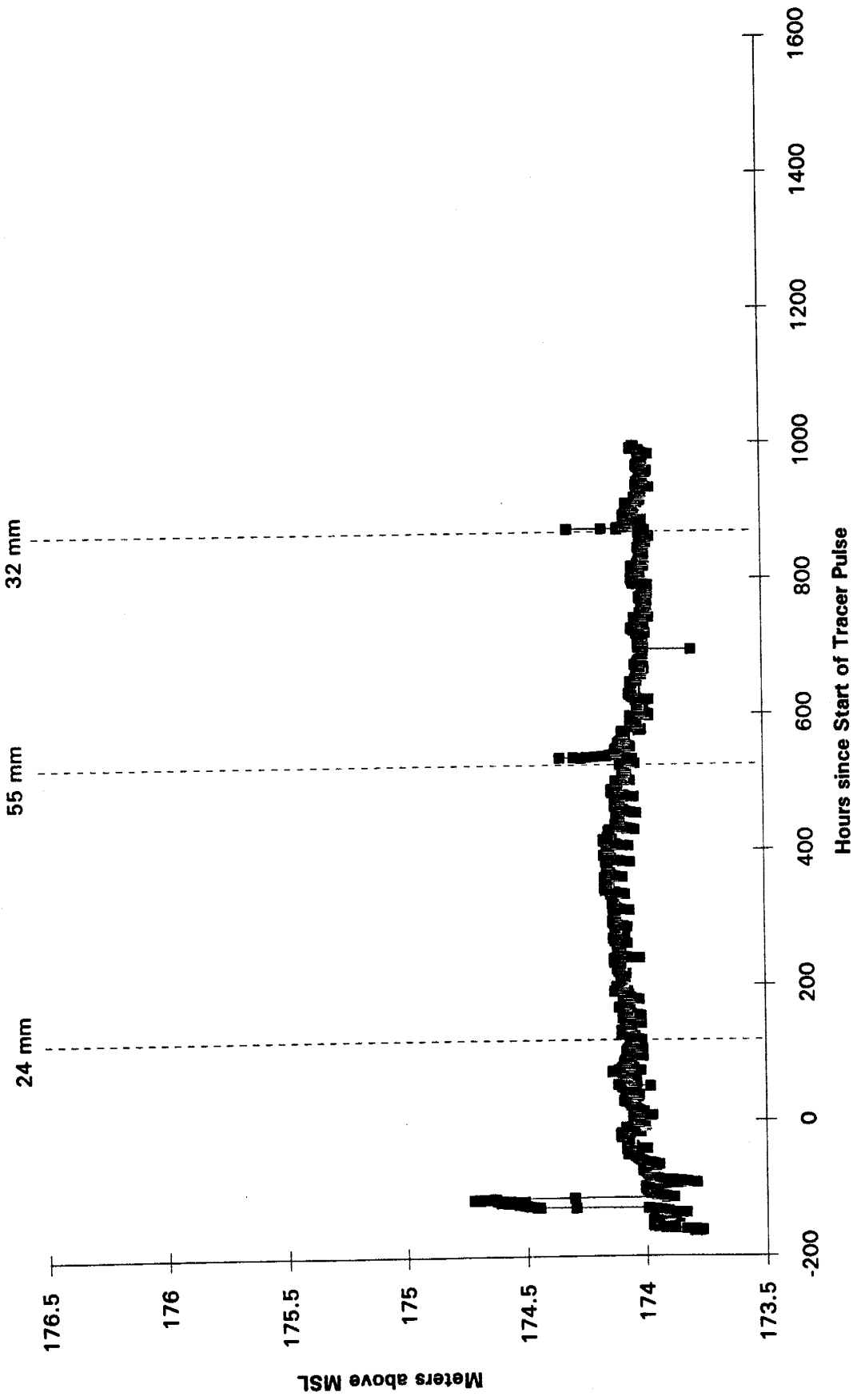
A13-4IU



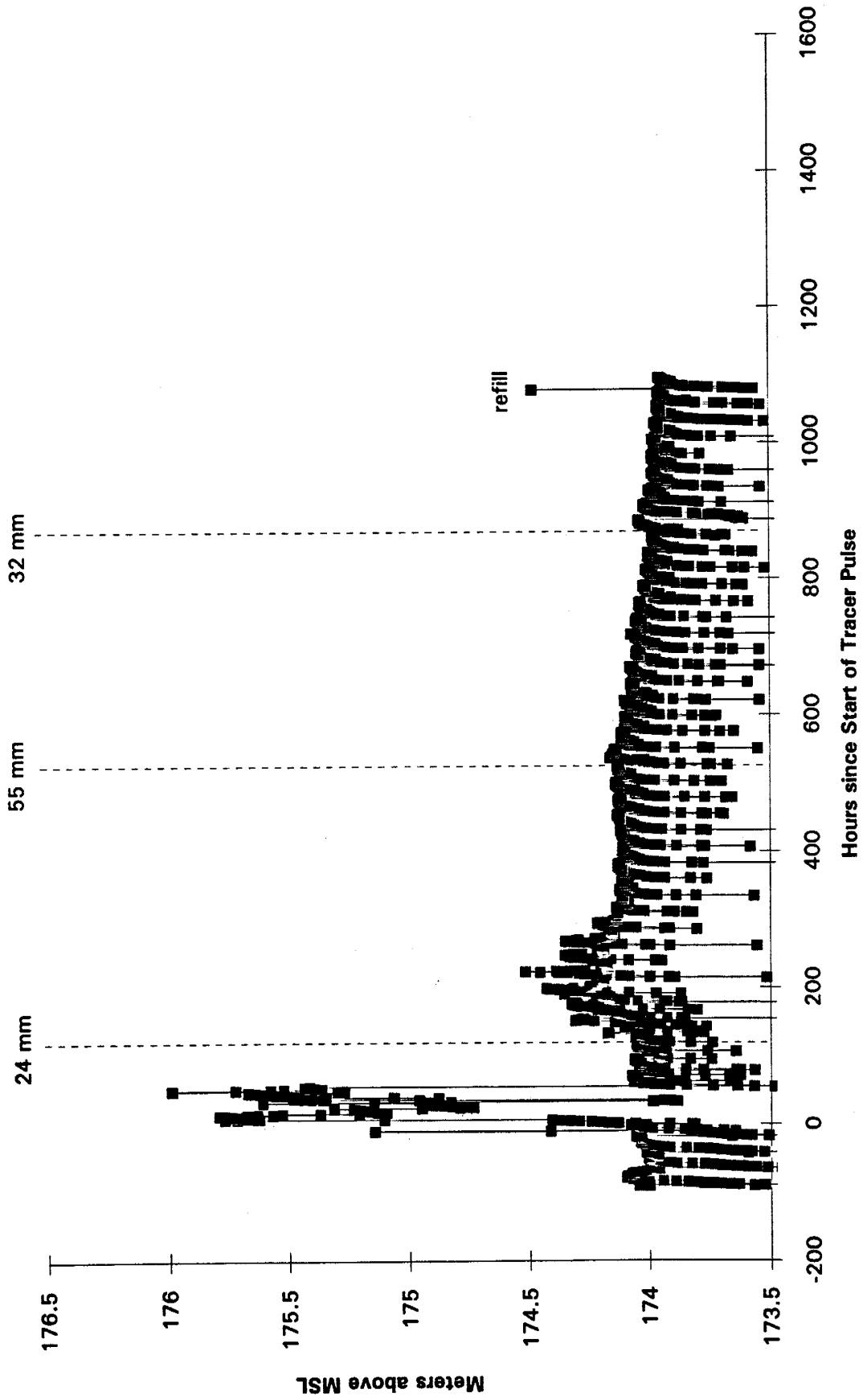
A14-4IL



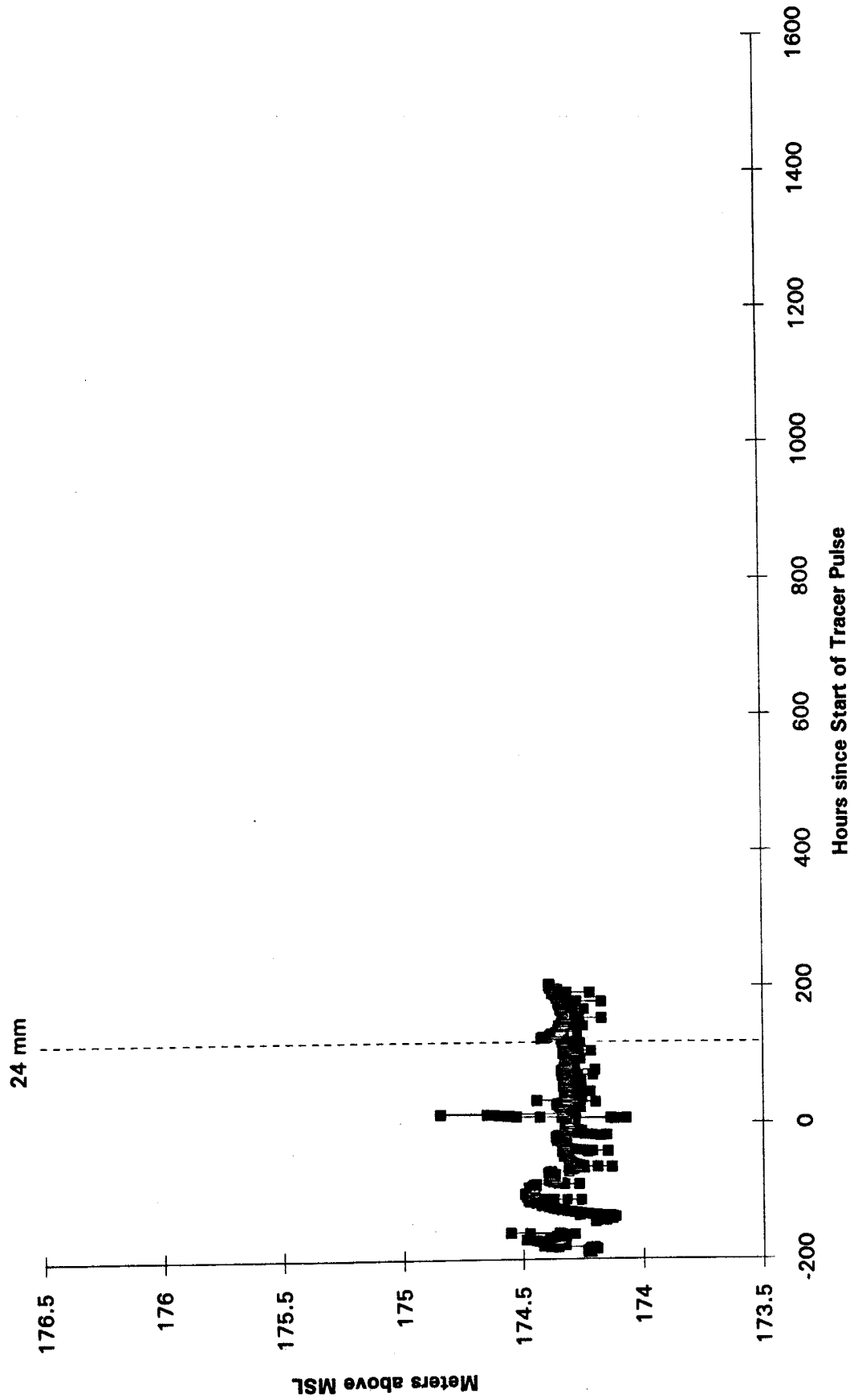
A15-40U



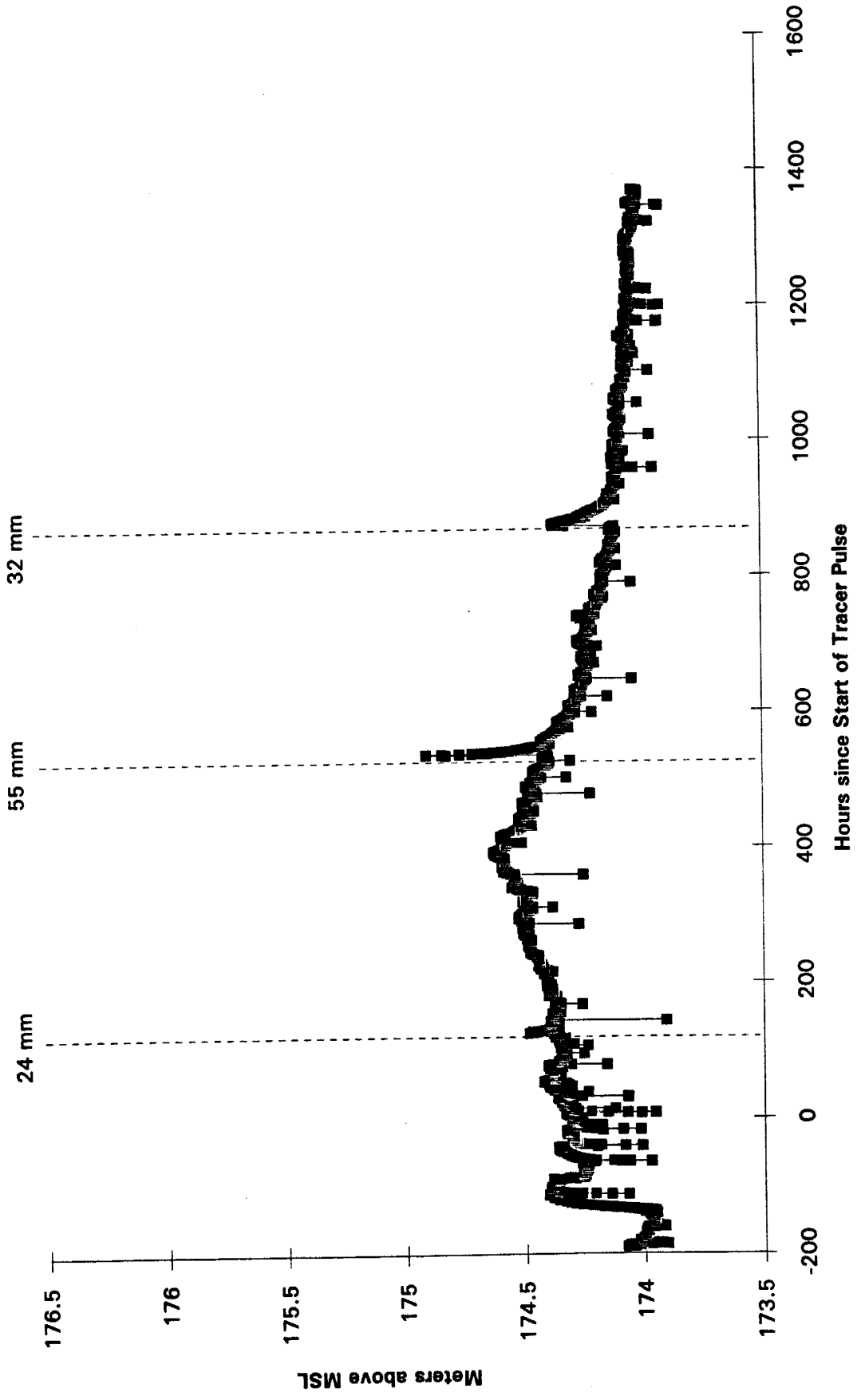
A16-40L



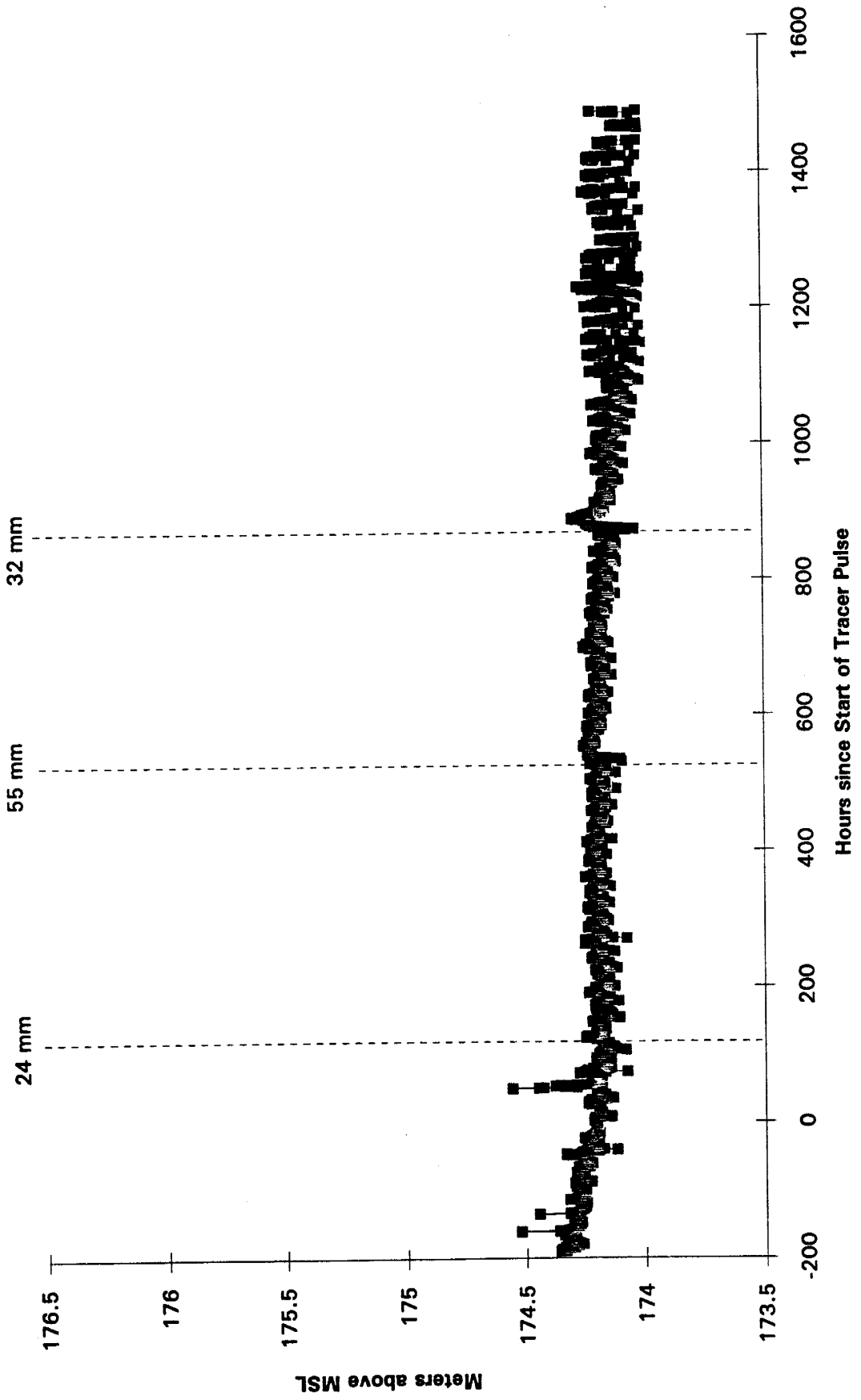
A17-5IU



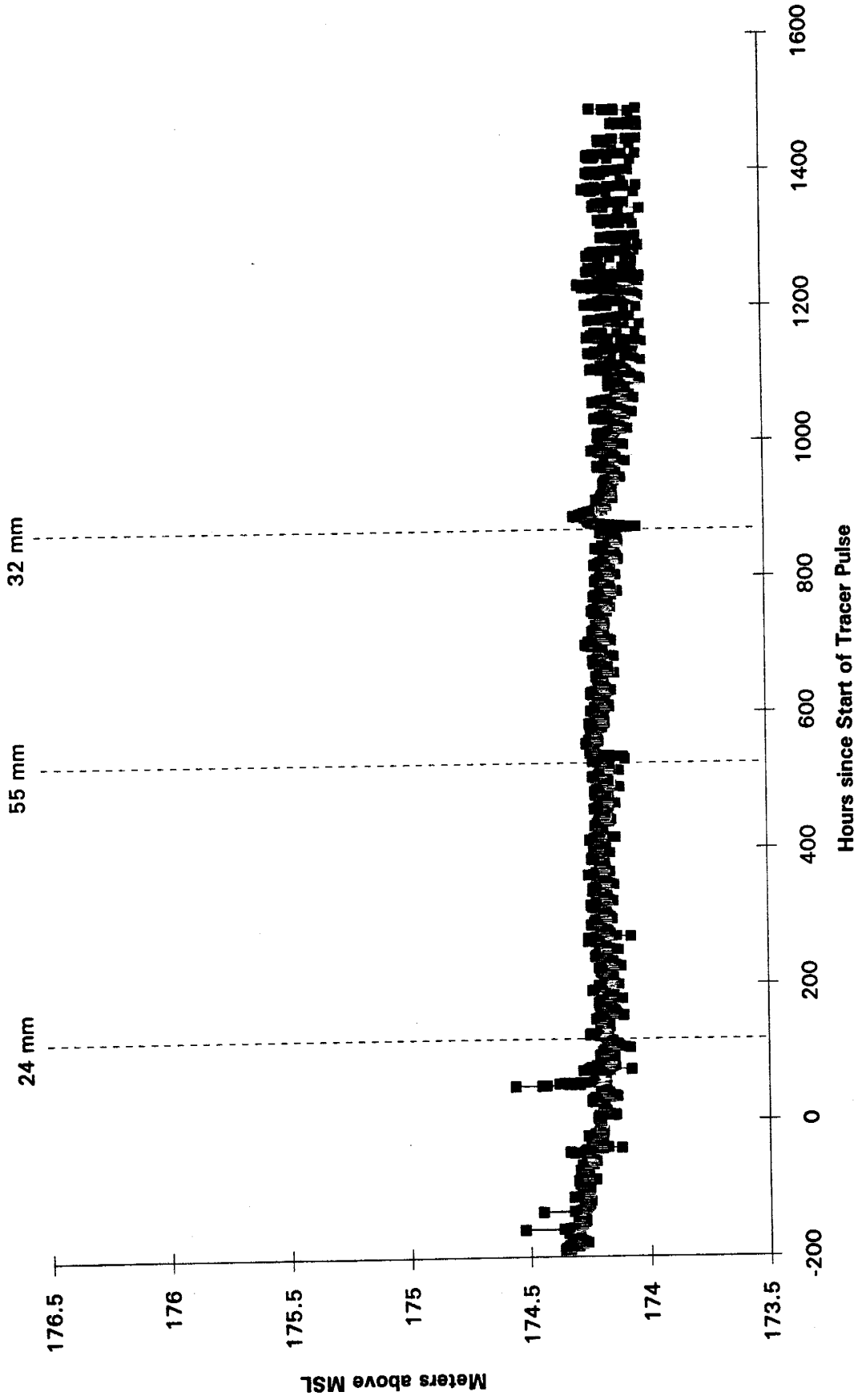
A21-6IU



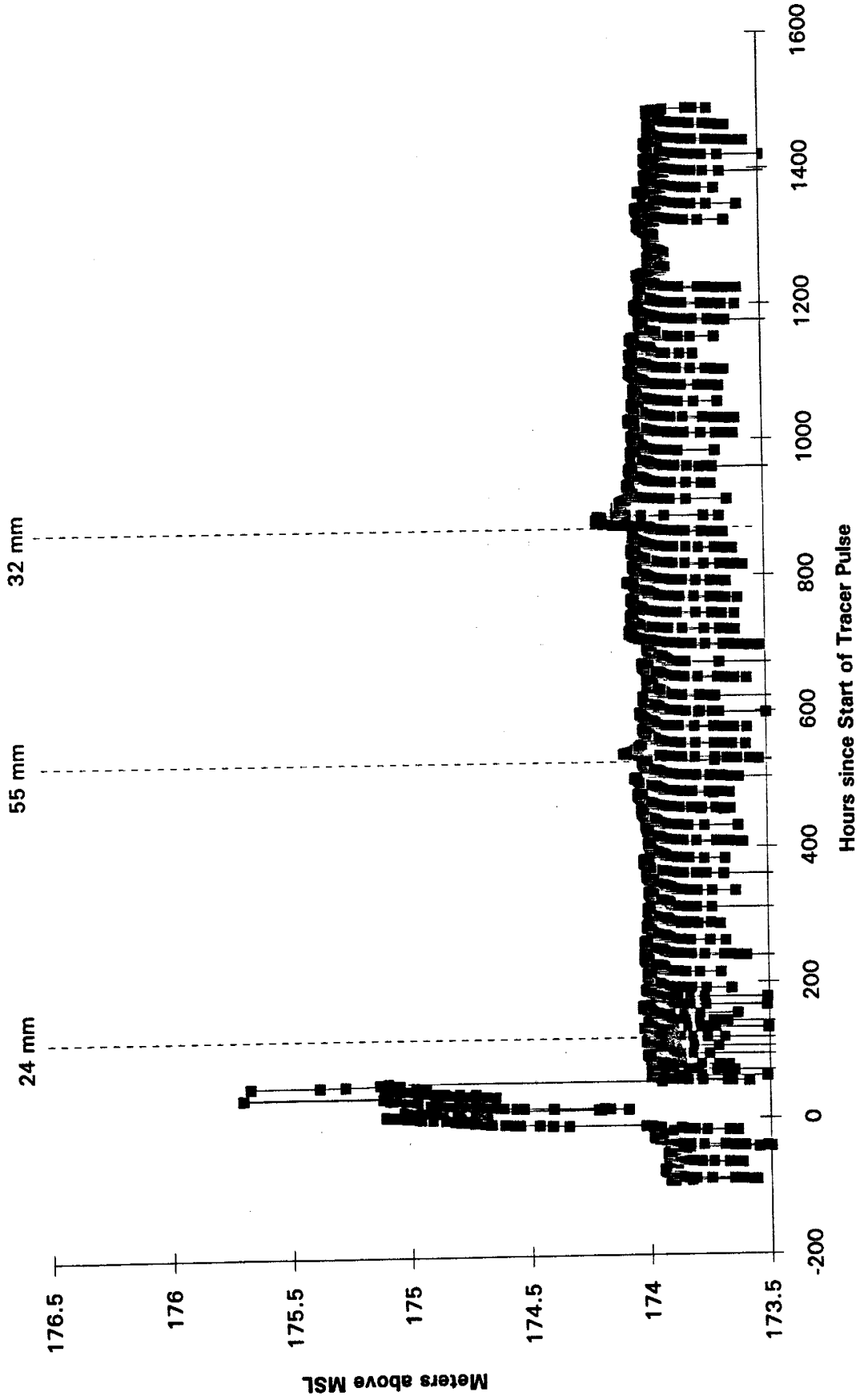
A23-60U



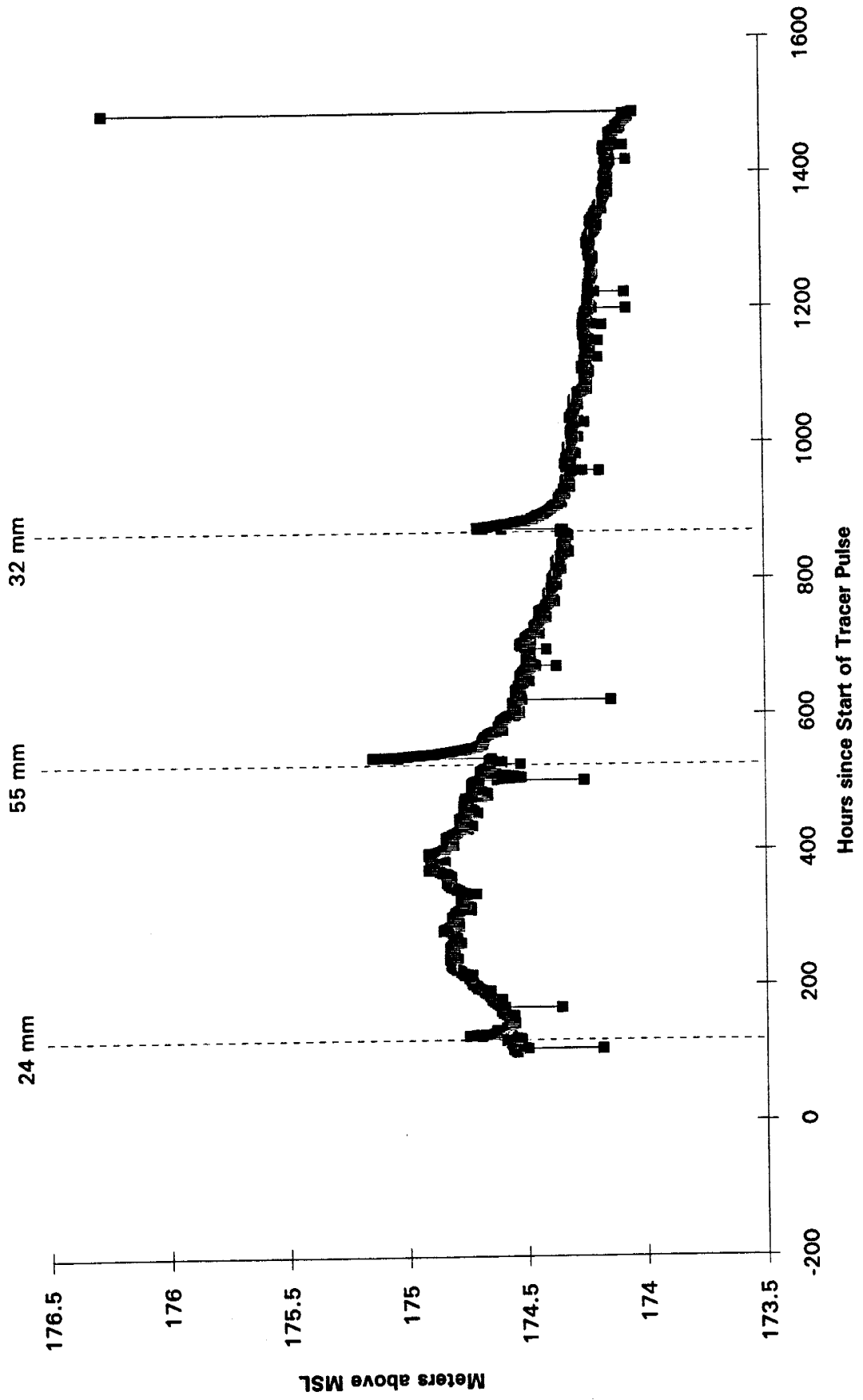
A23-60U



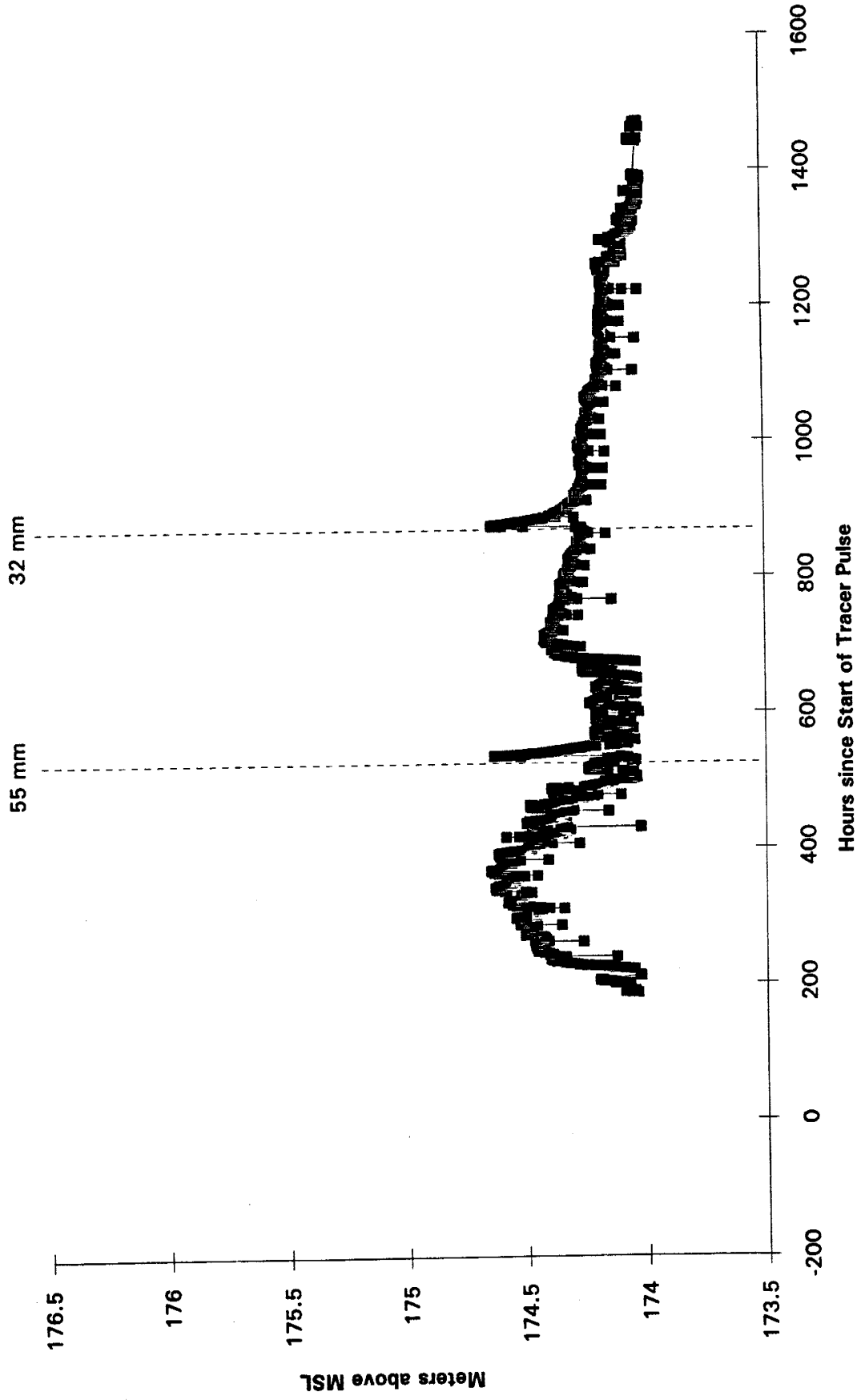
A24-60L



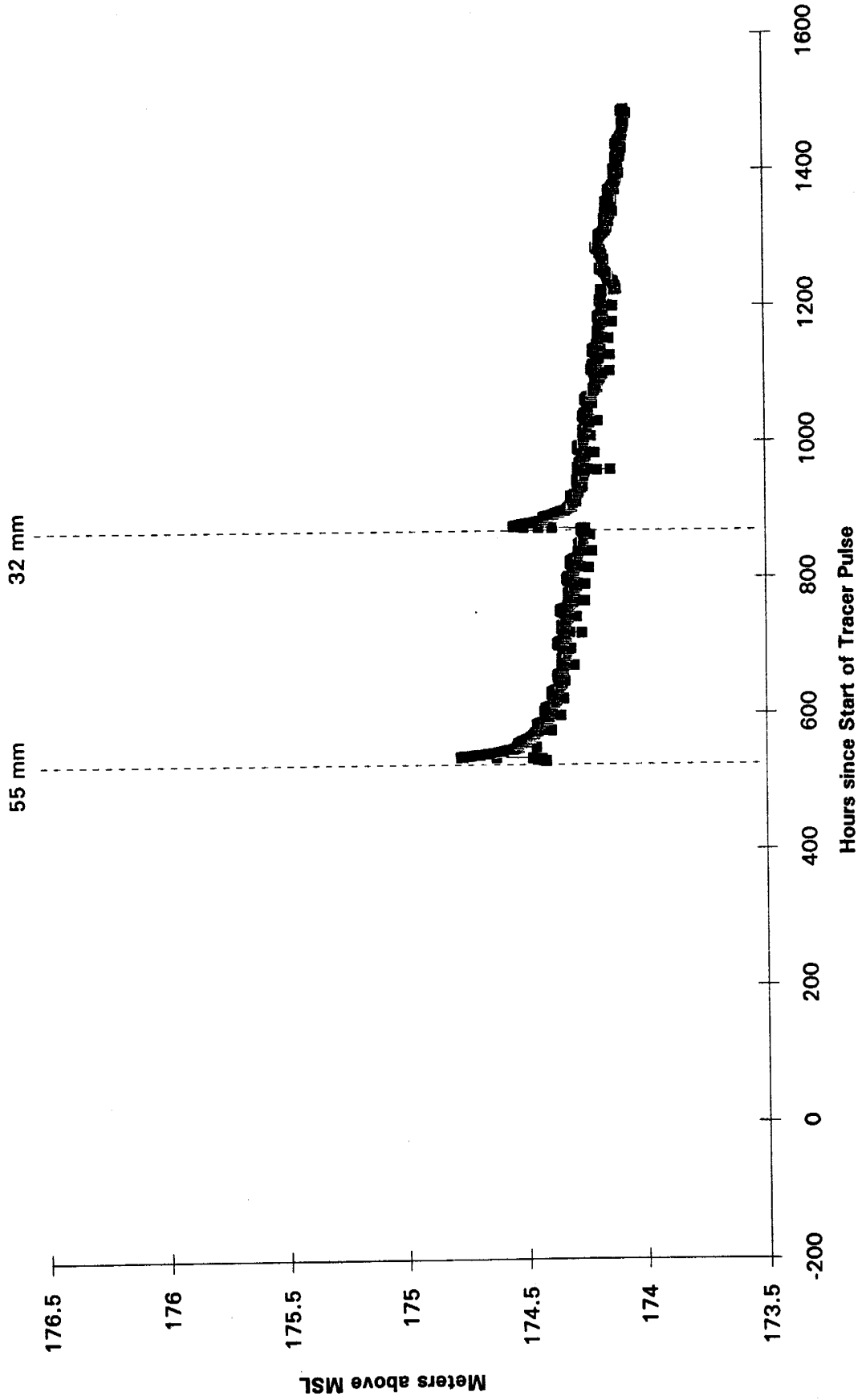
A25-7IU



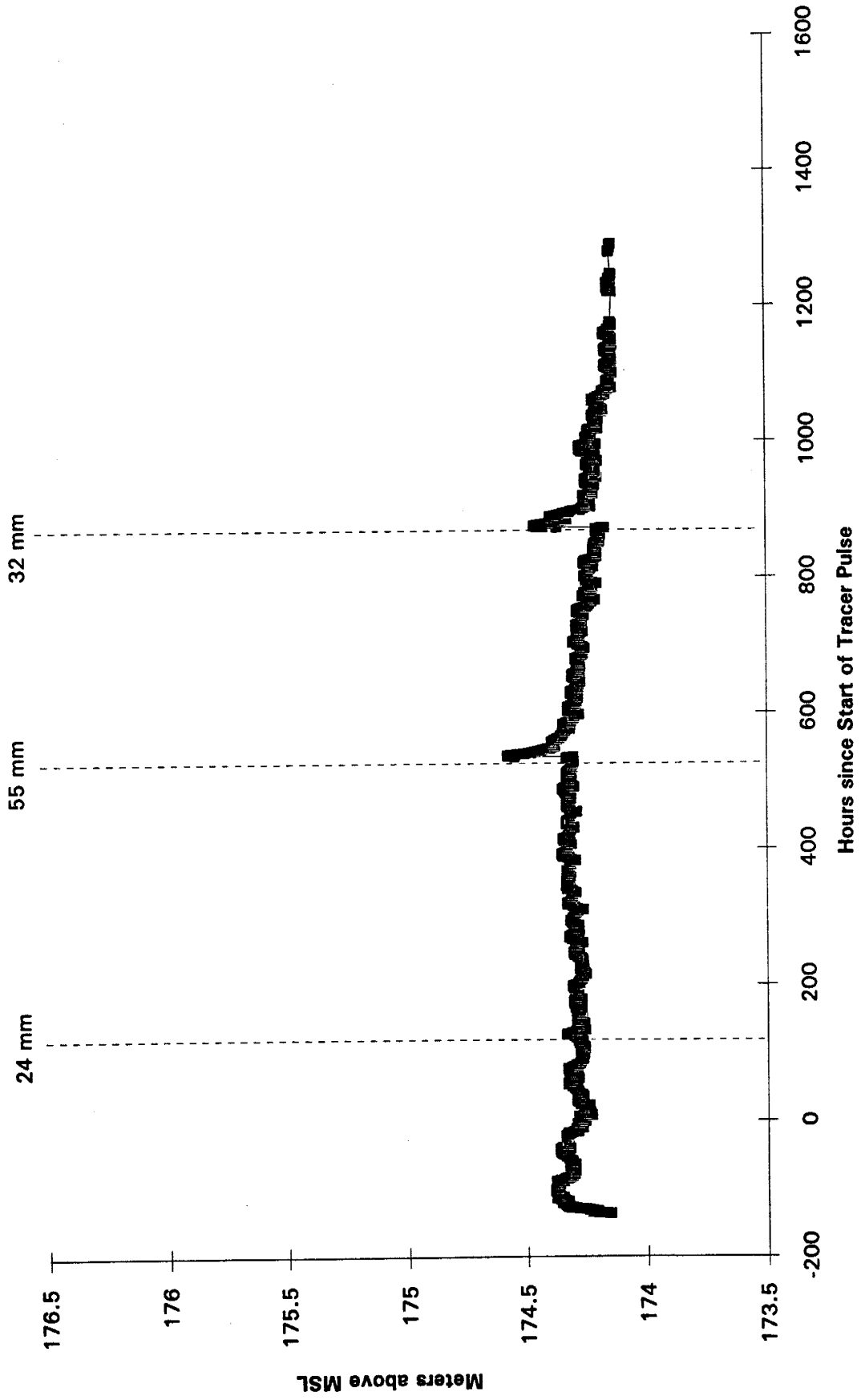
A26-7IL



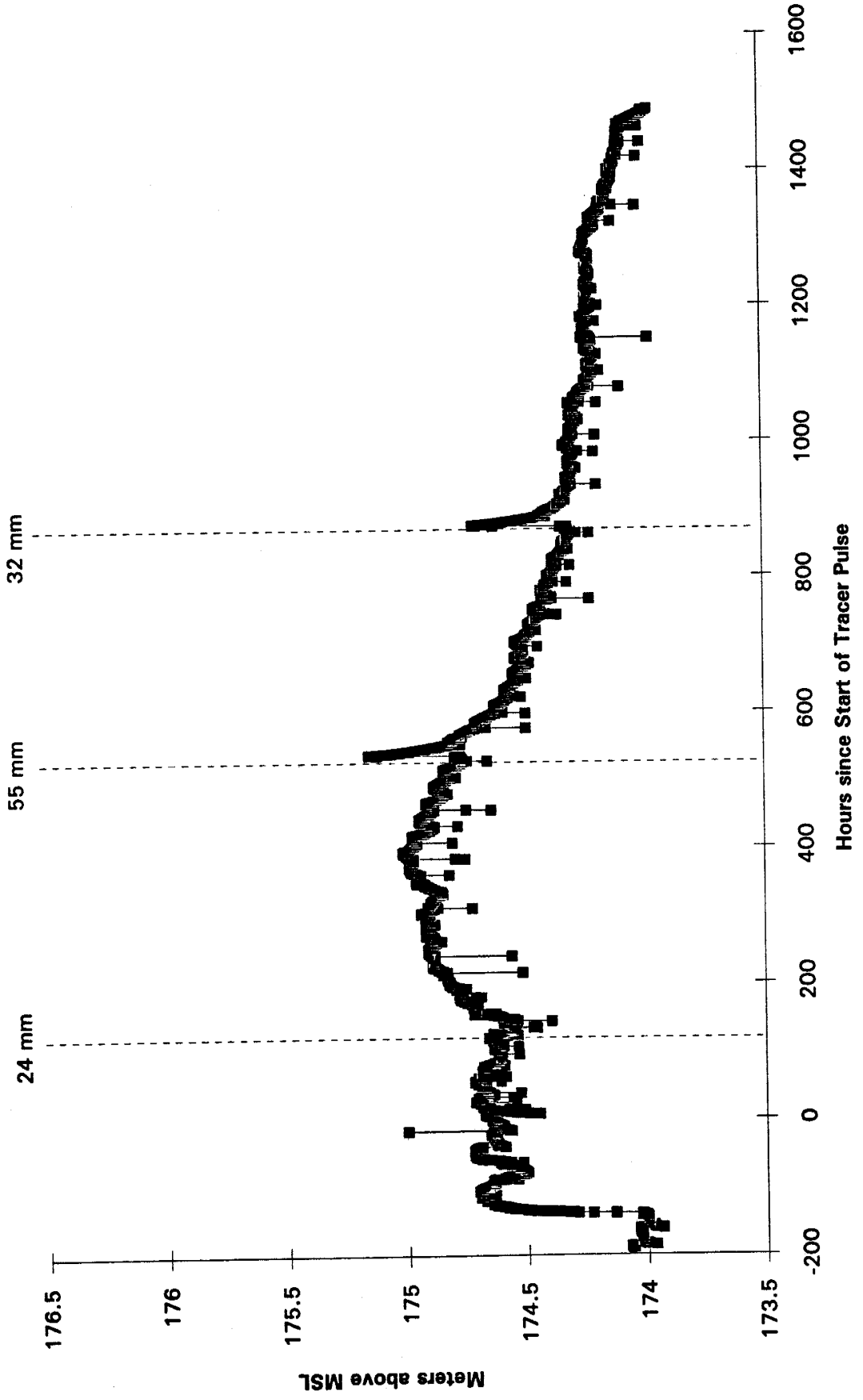
A27-70U



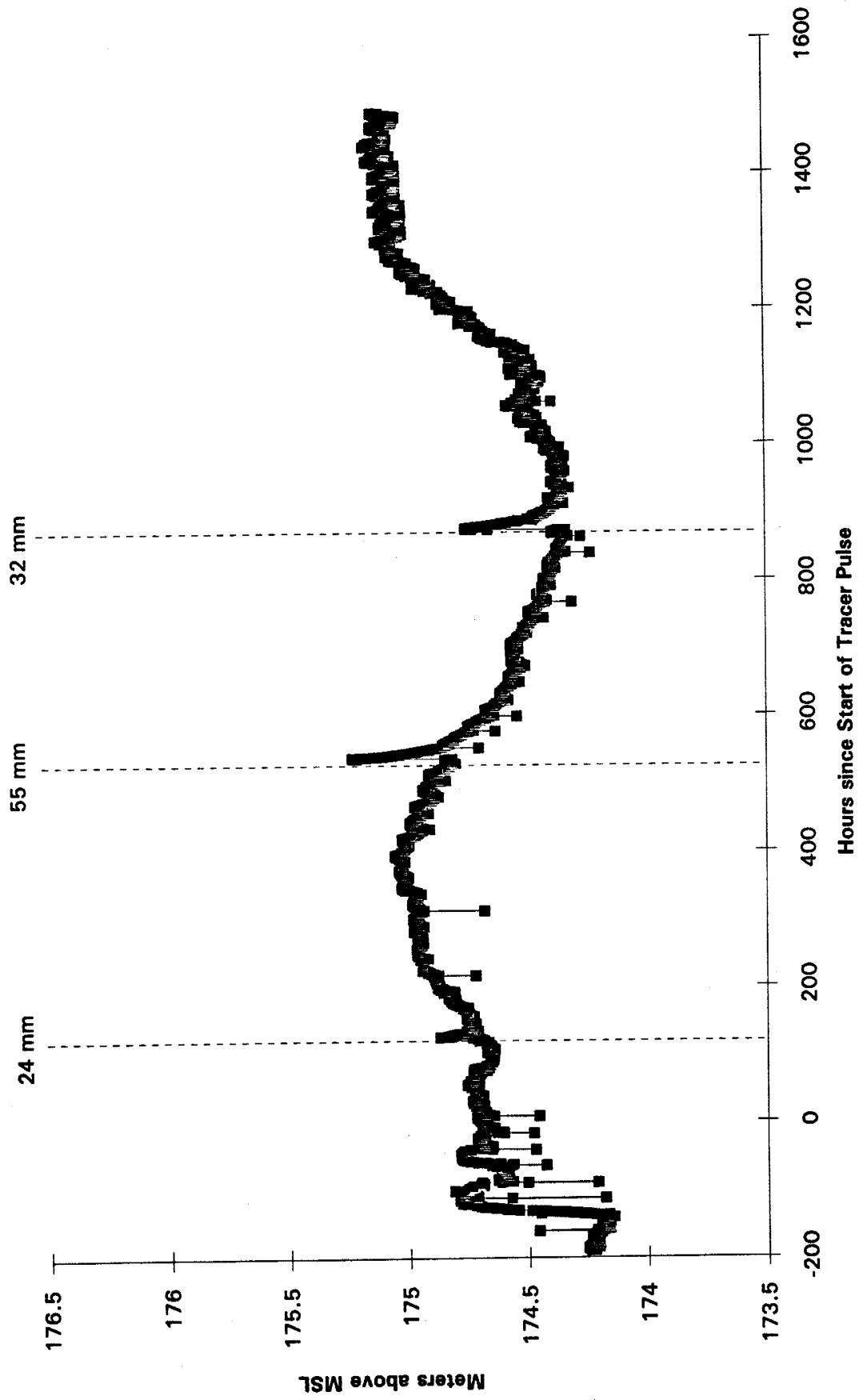
A28-70L



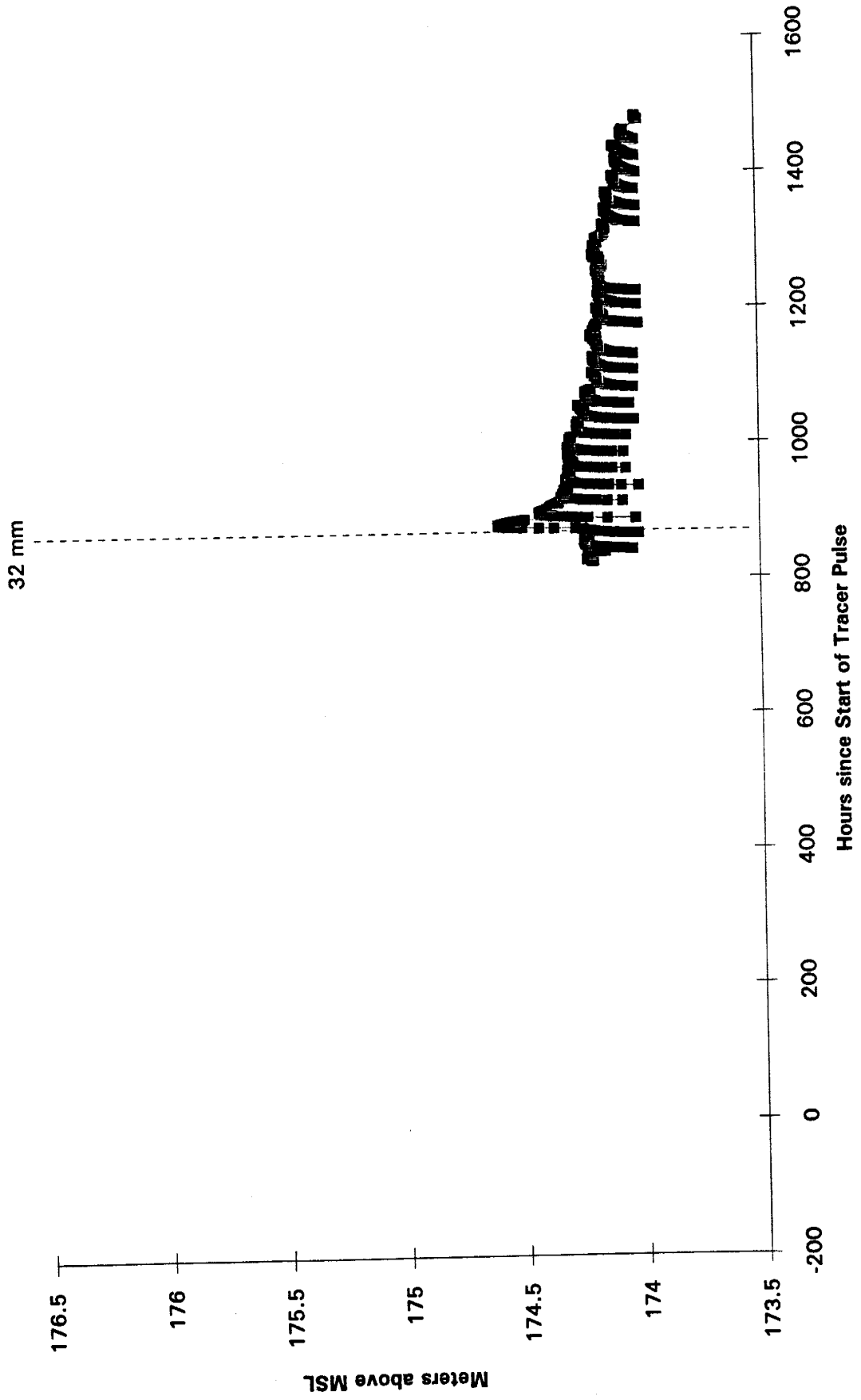
A29-8IU



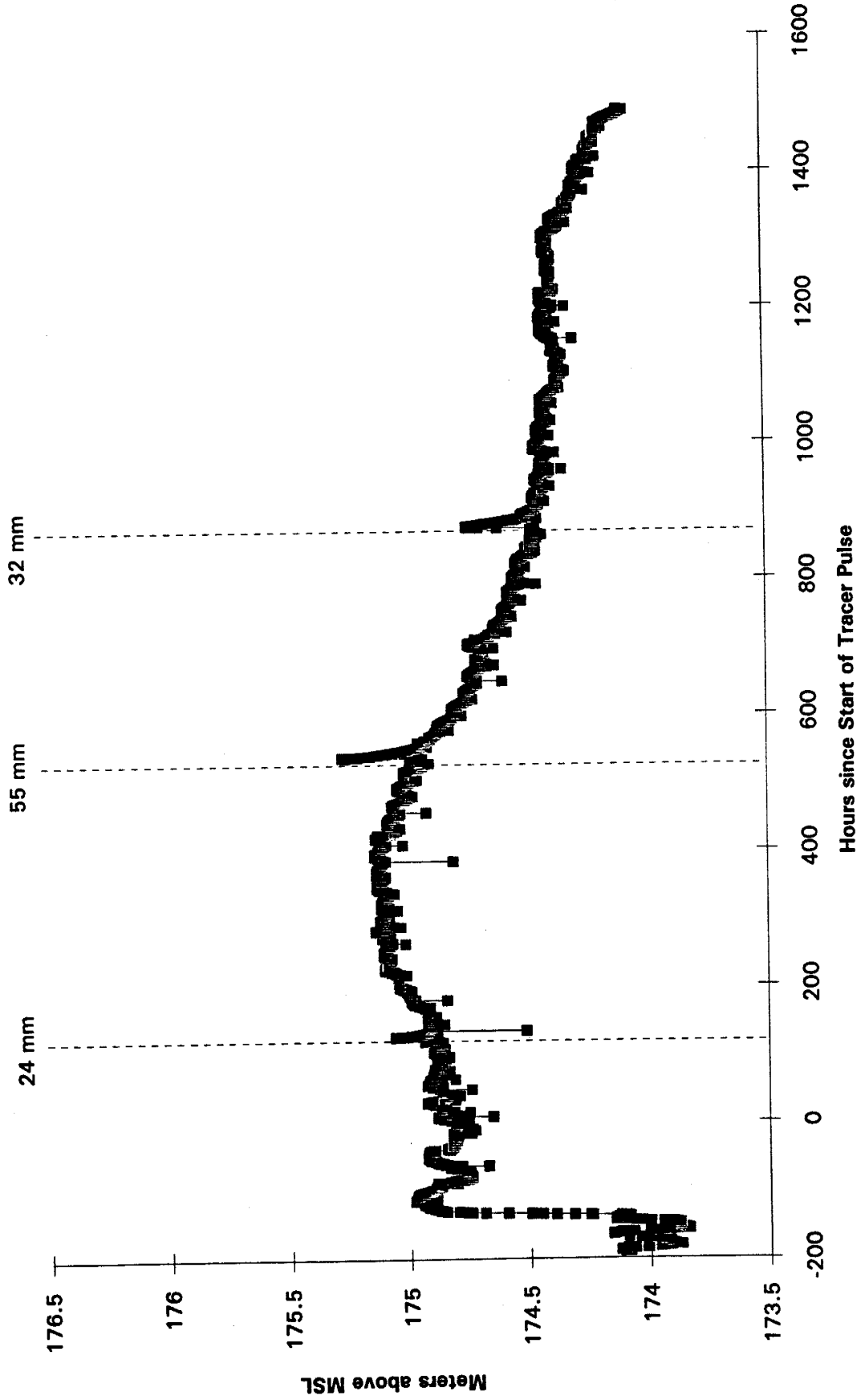
A30-8IL



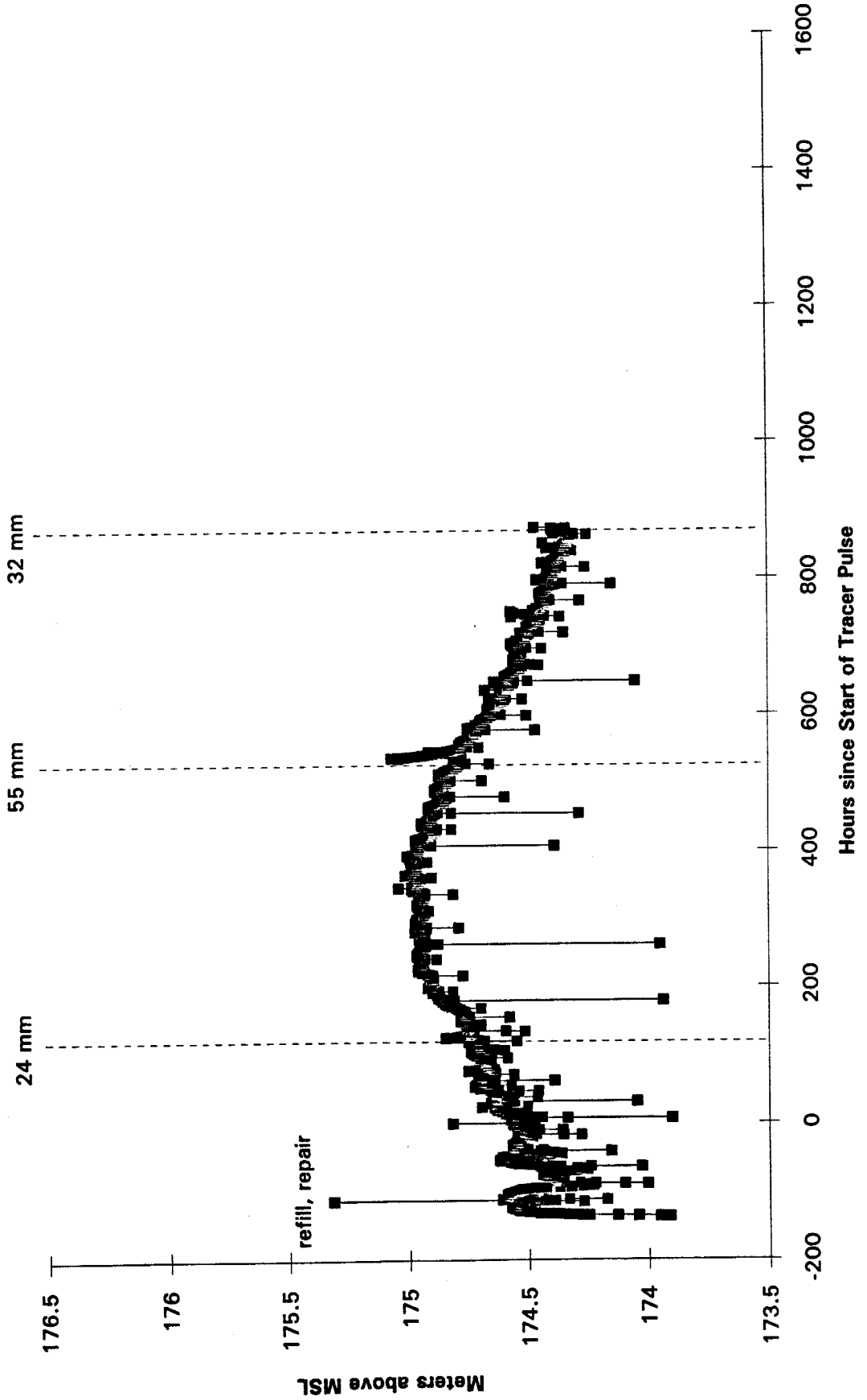
A32-80L



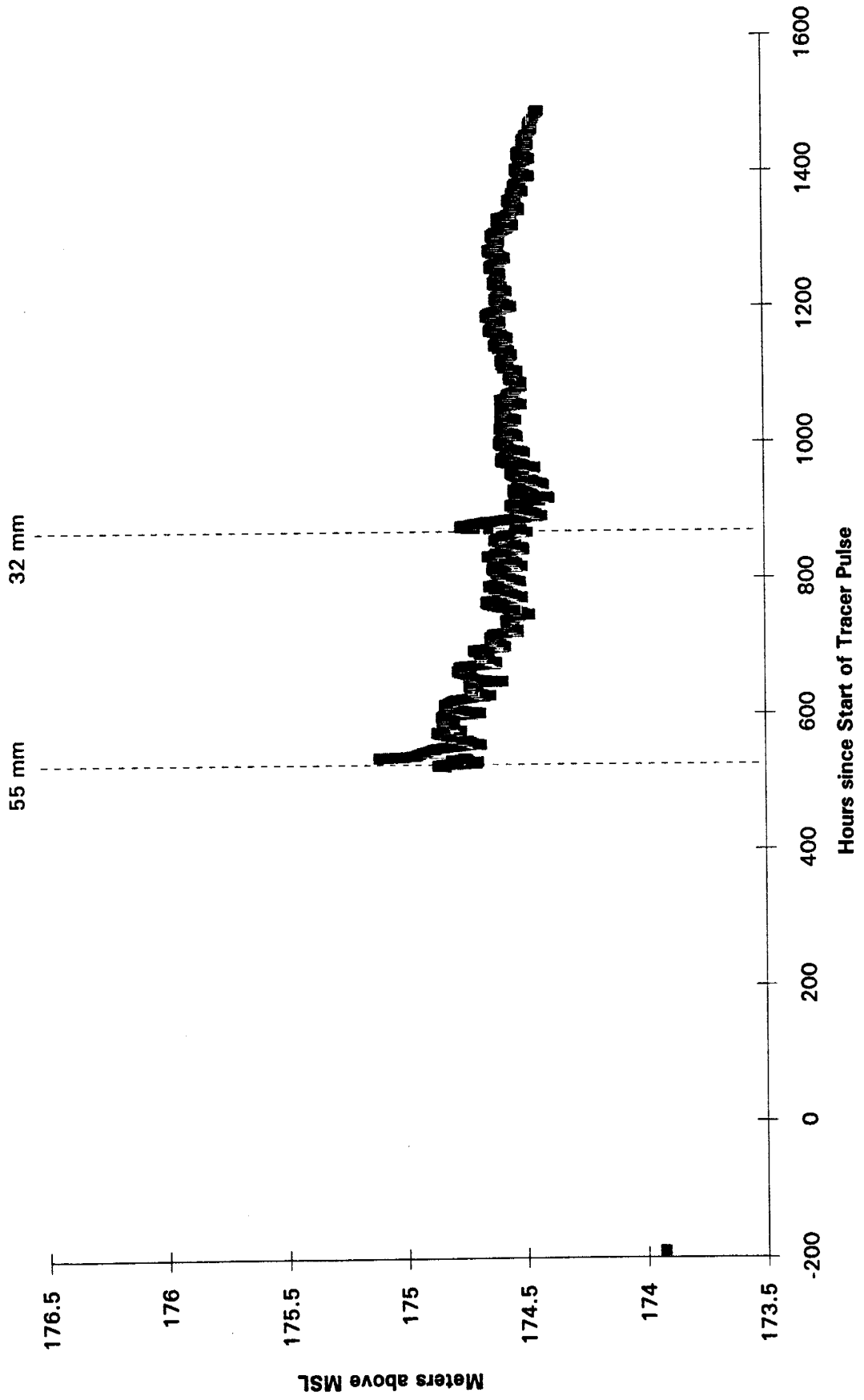
A33-A1U



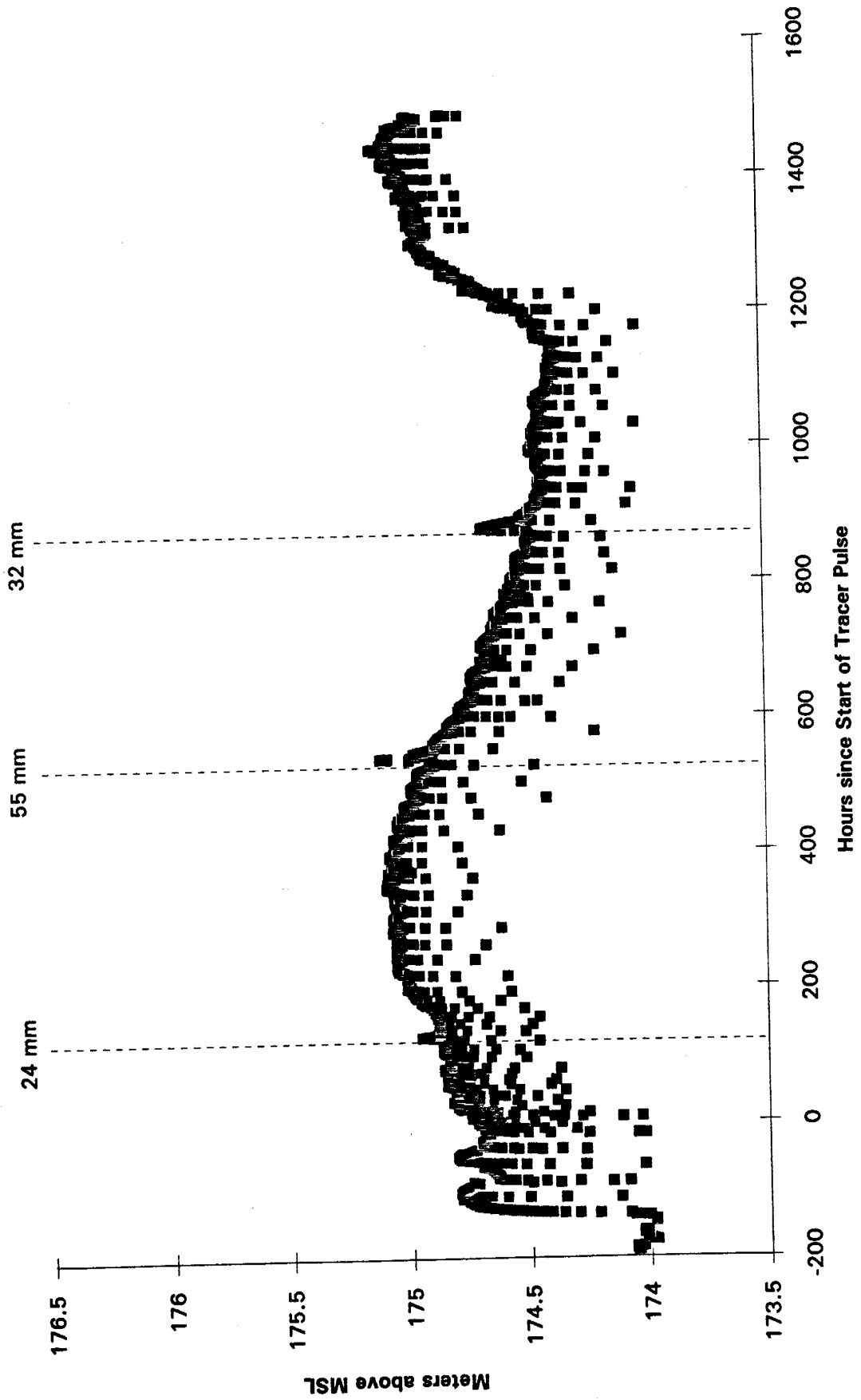
A34-A1L



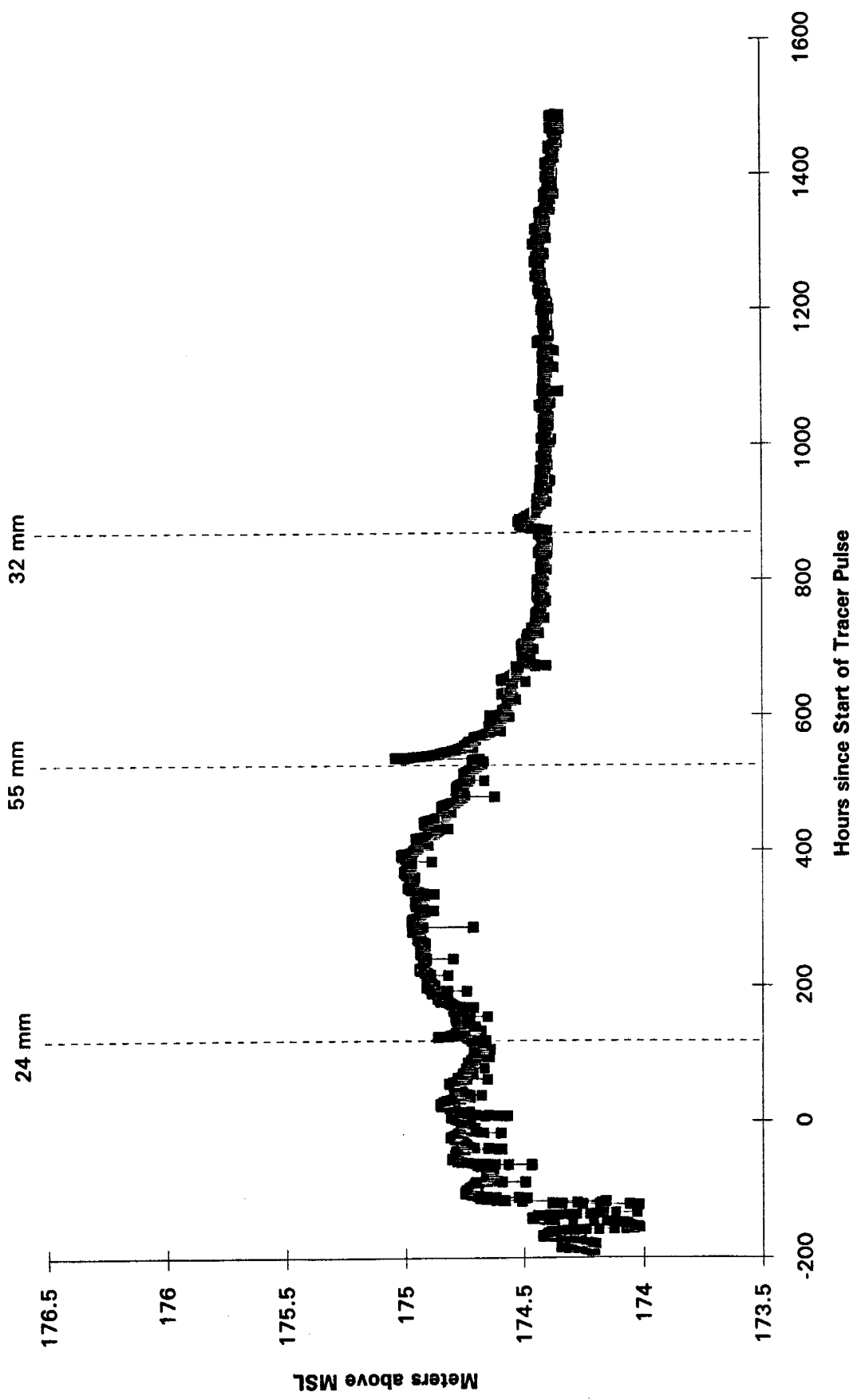
A35-A2U



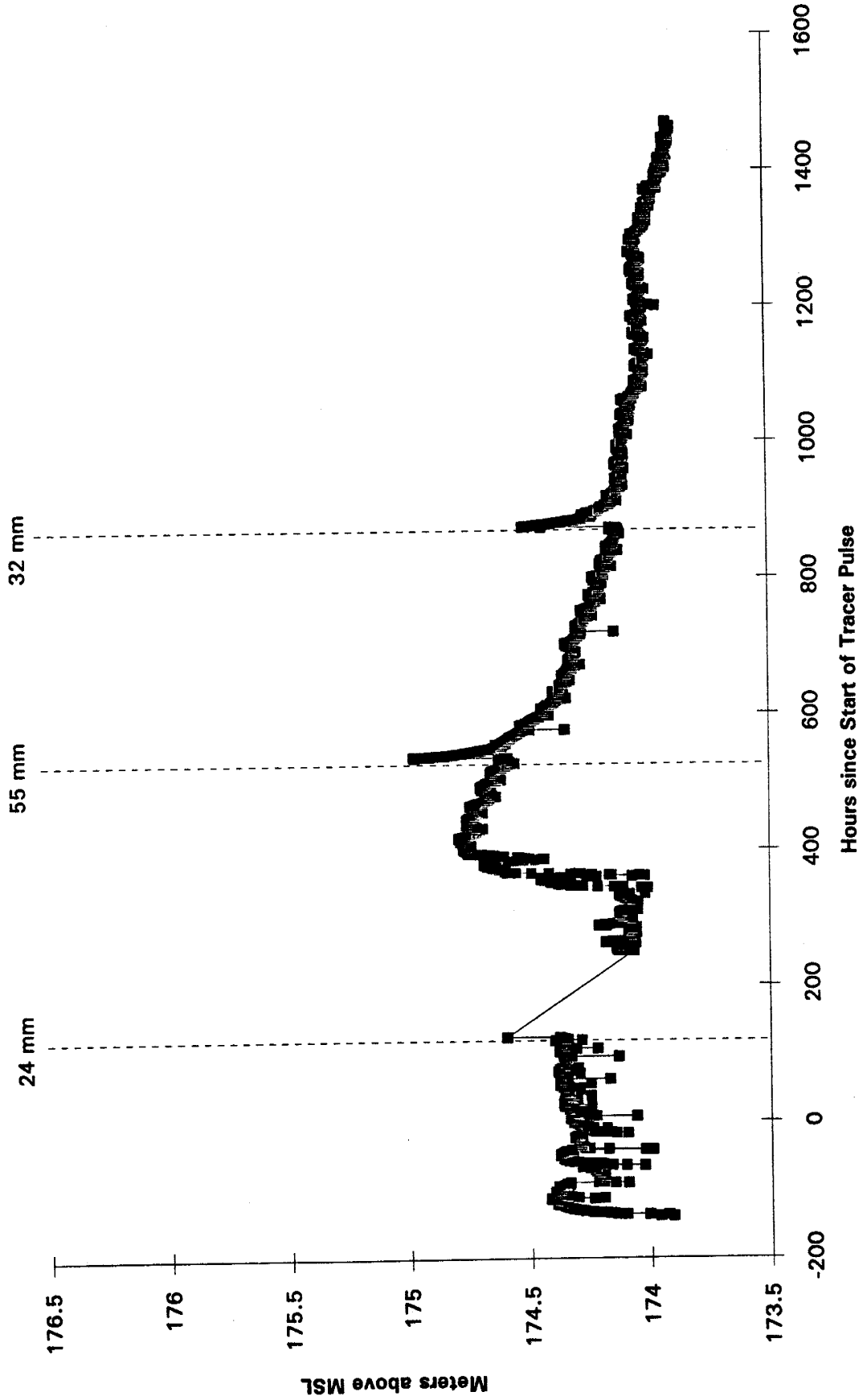
A36-A3L



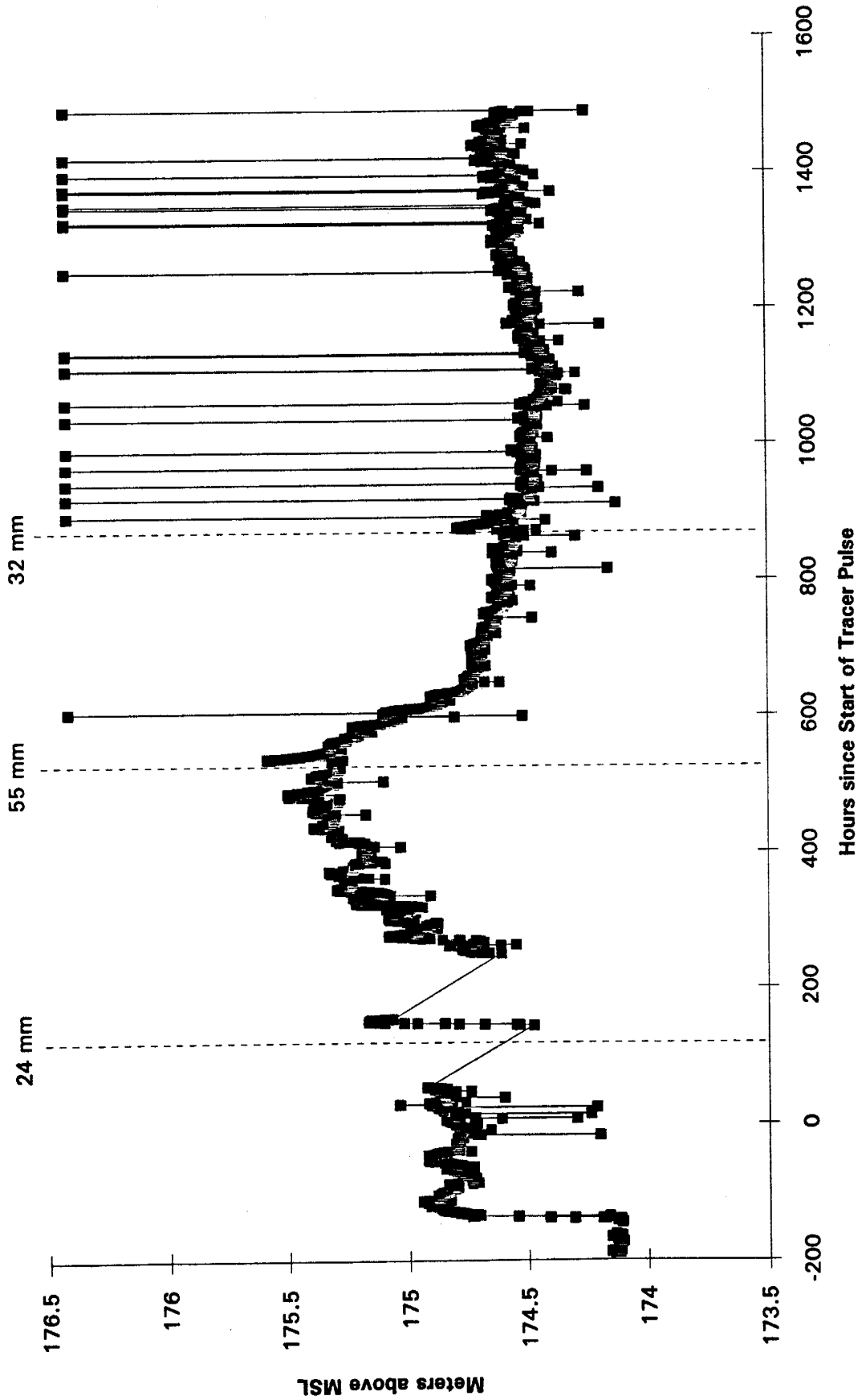
A39-A5U



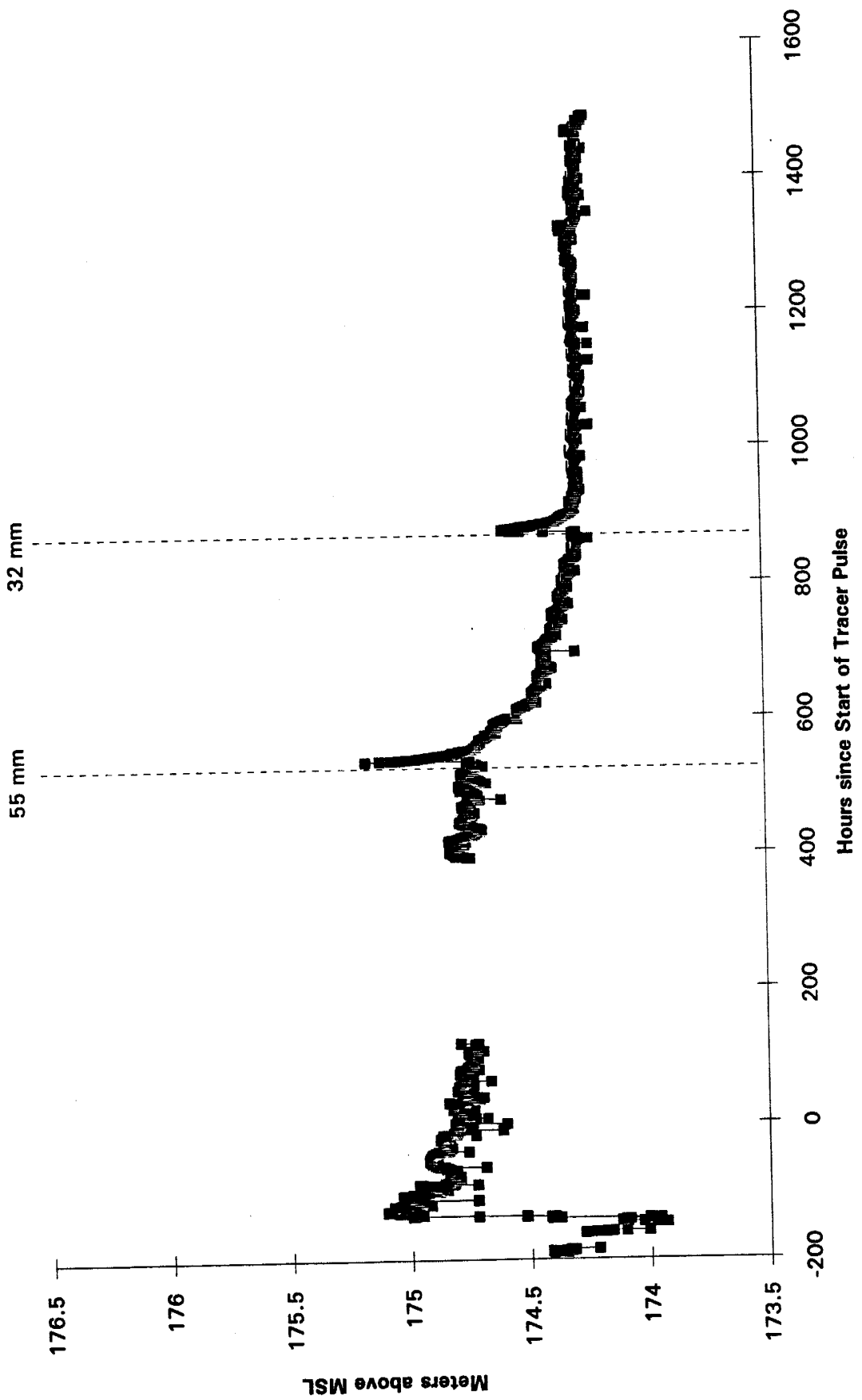
A40-A5L



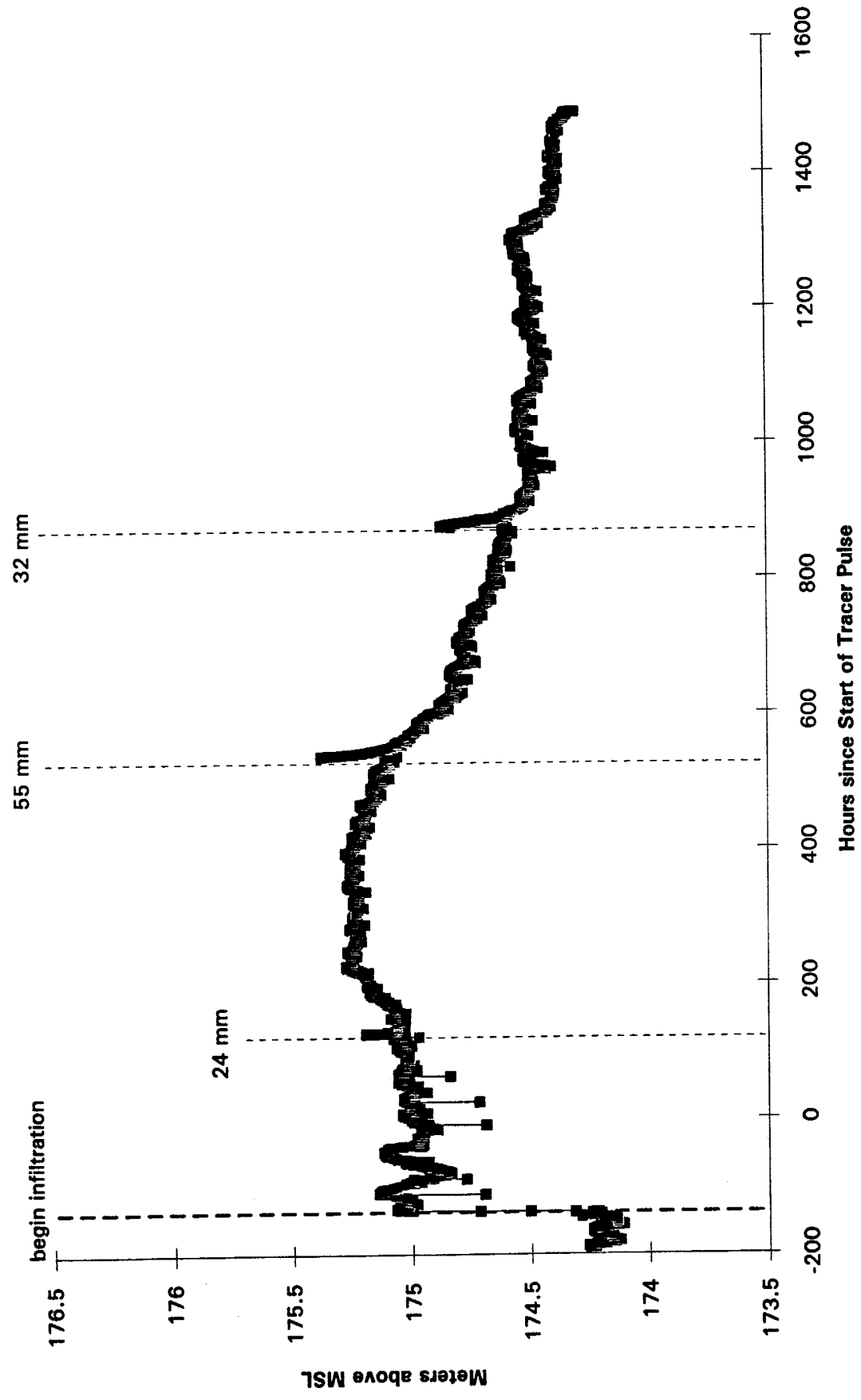
A42-A7L



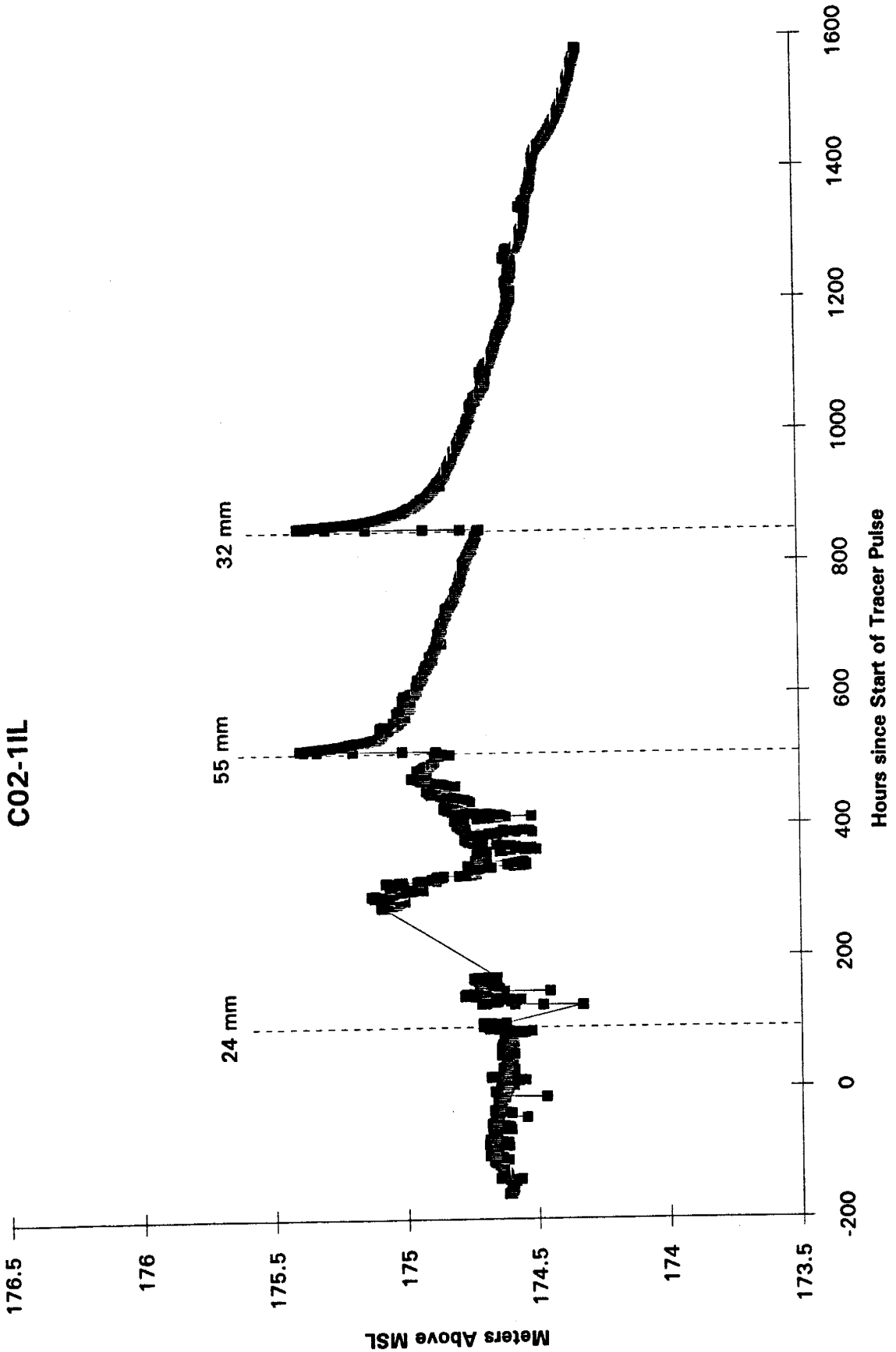
A43-A7U



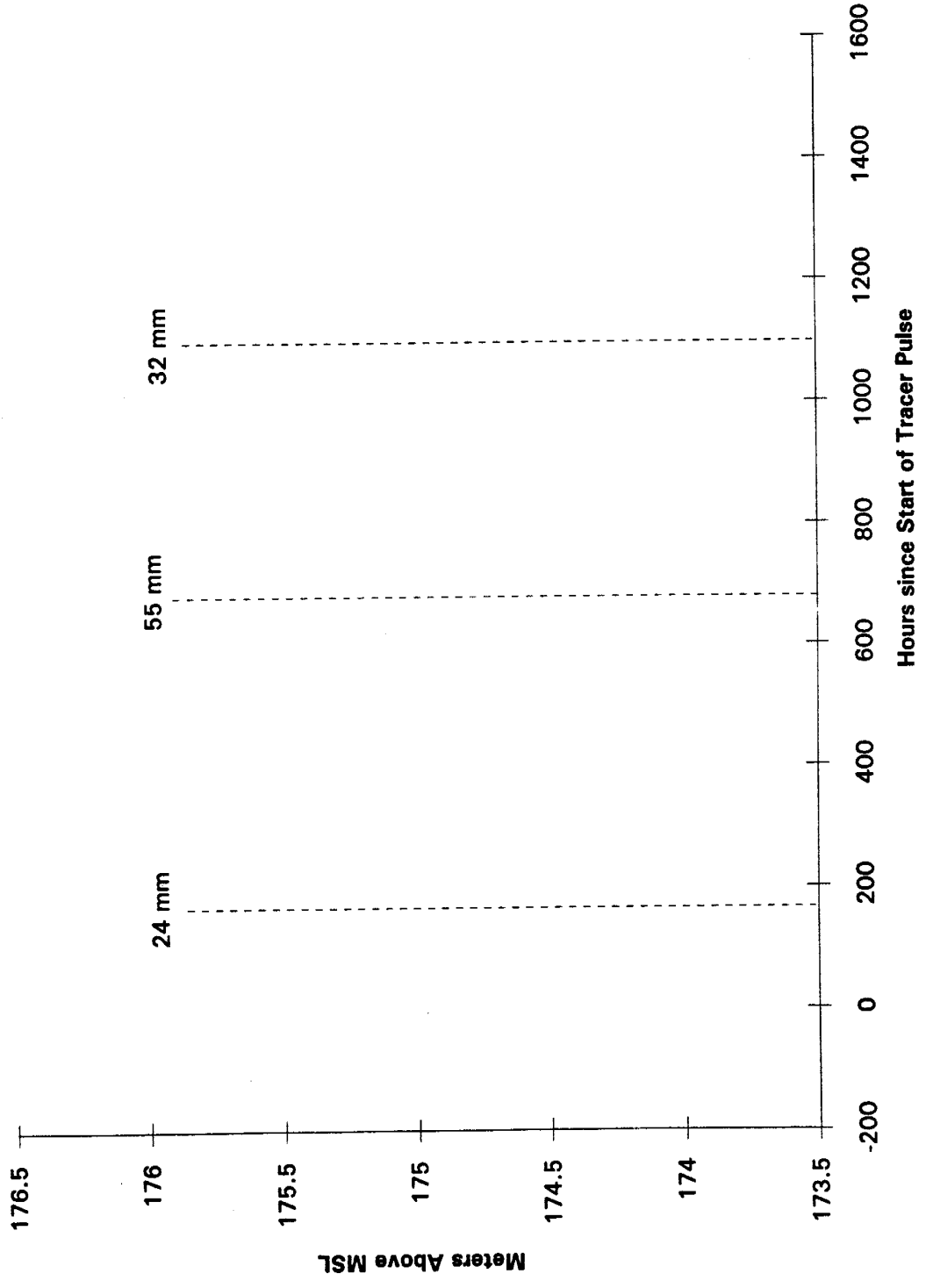
A44-A8U



C02-11L

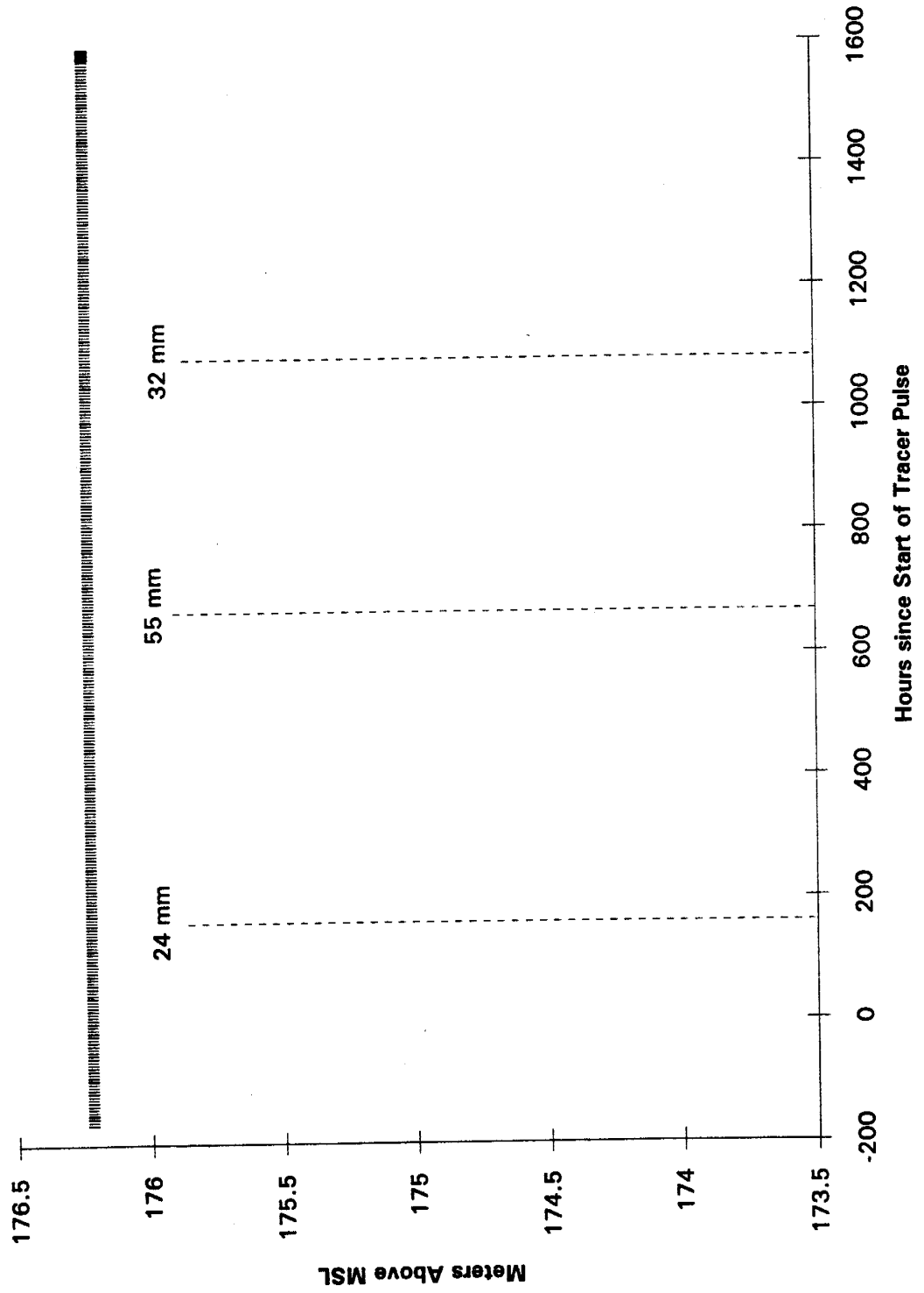


C04-10L



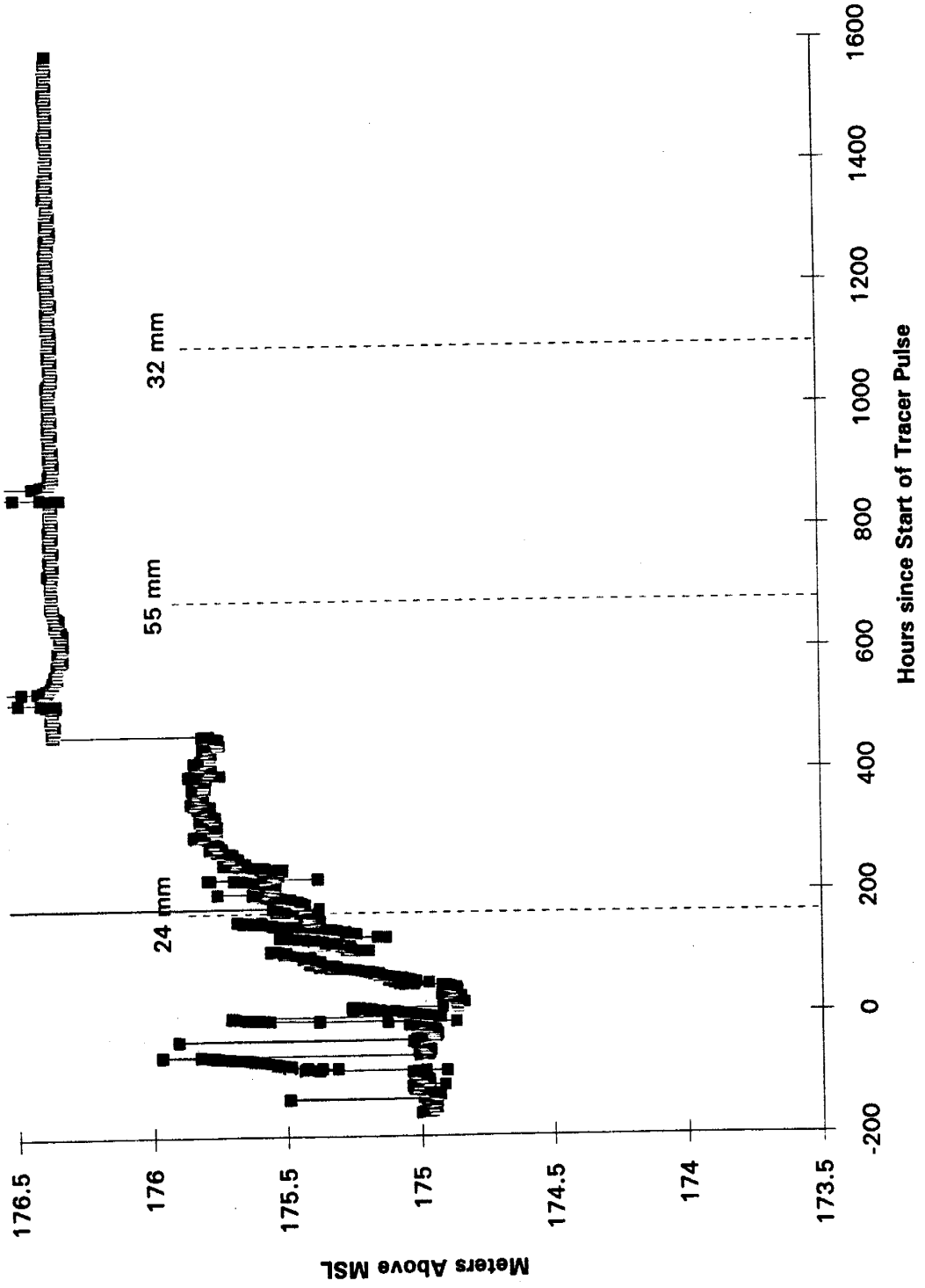
■ C04-10L

C06-2IL



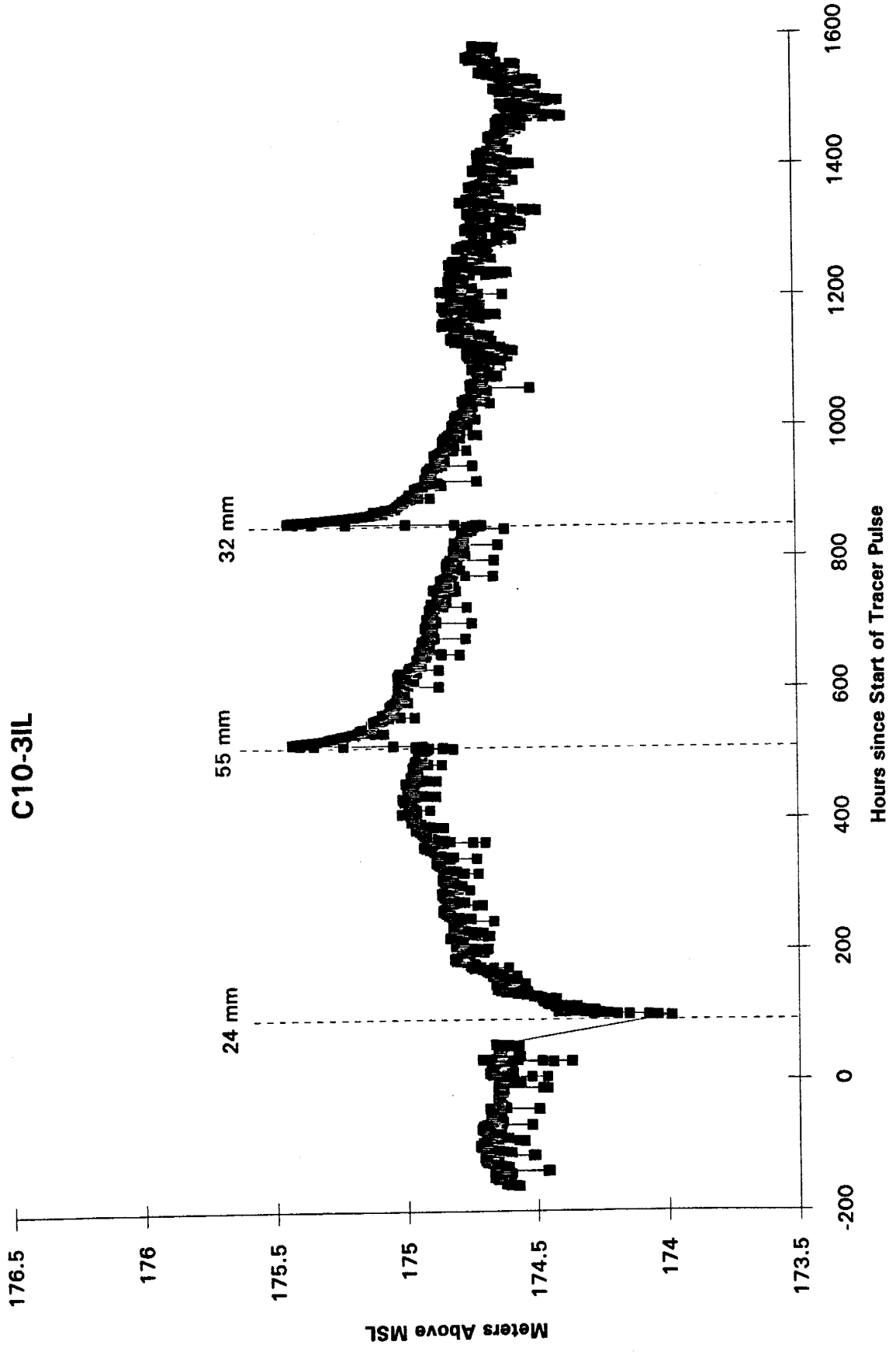
■ C06-2IL

C08-20L

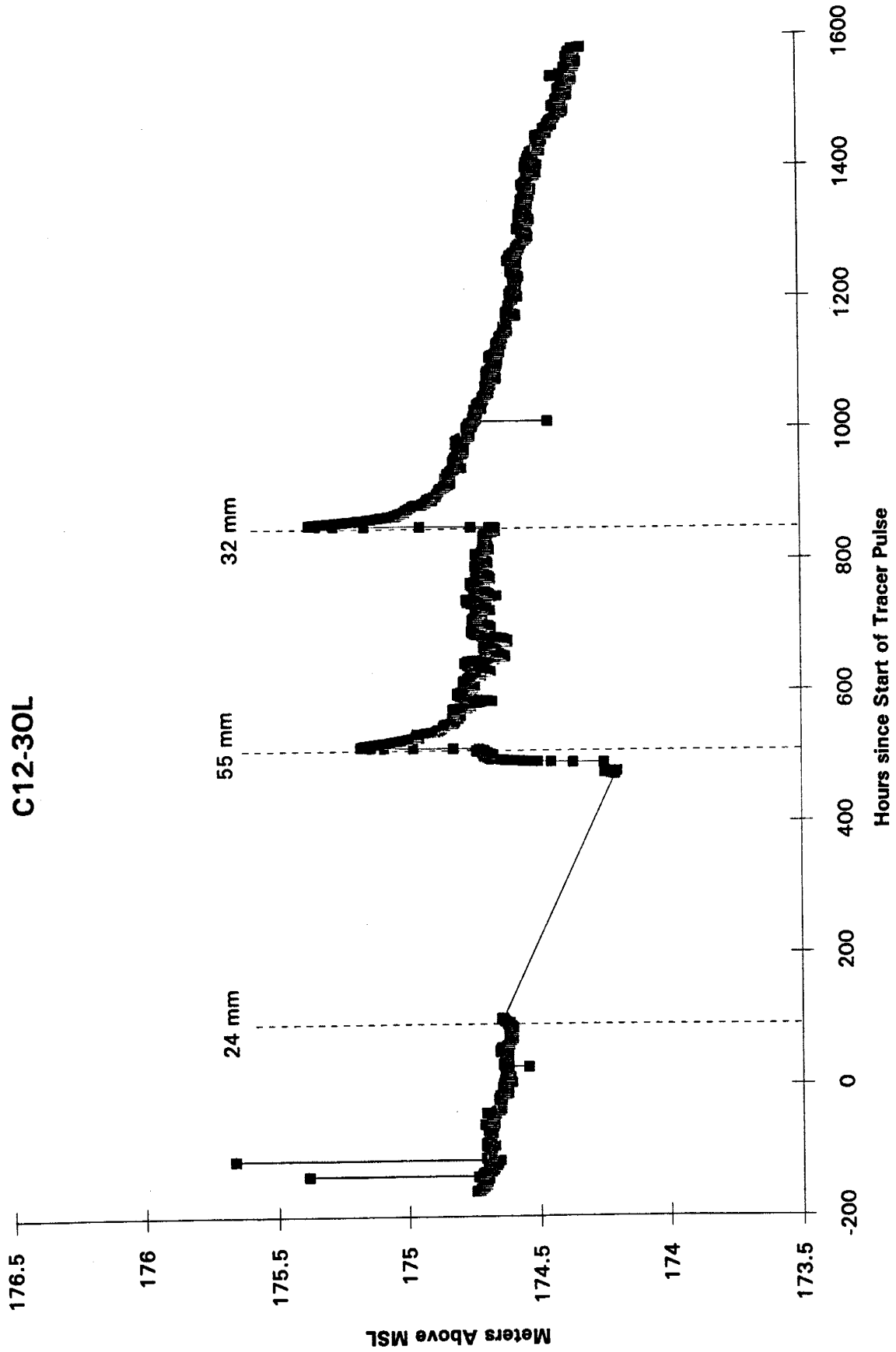


■ C08-20L

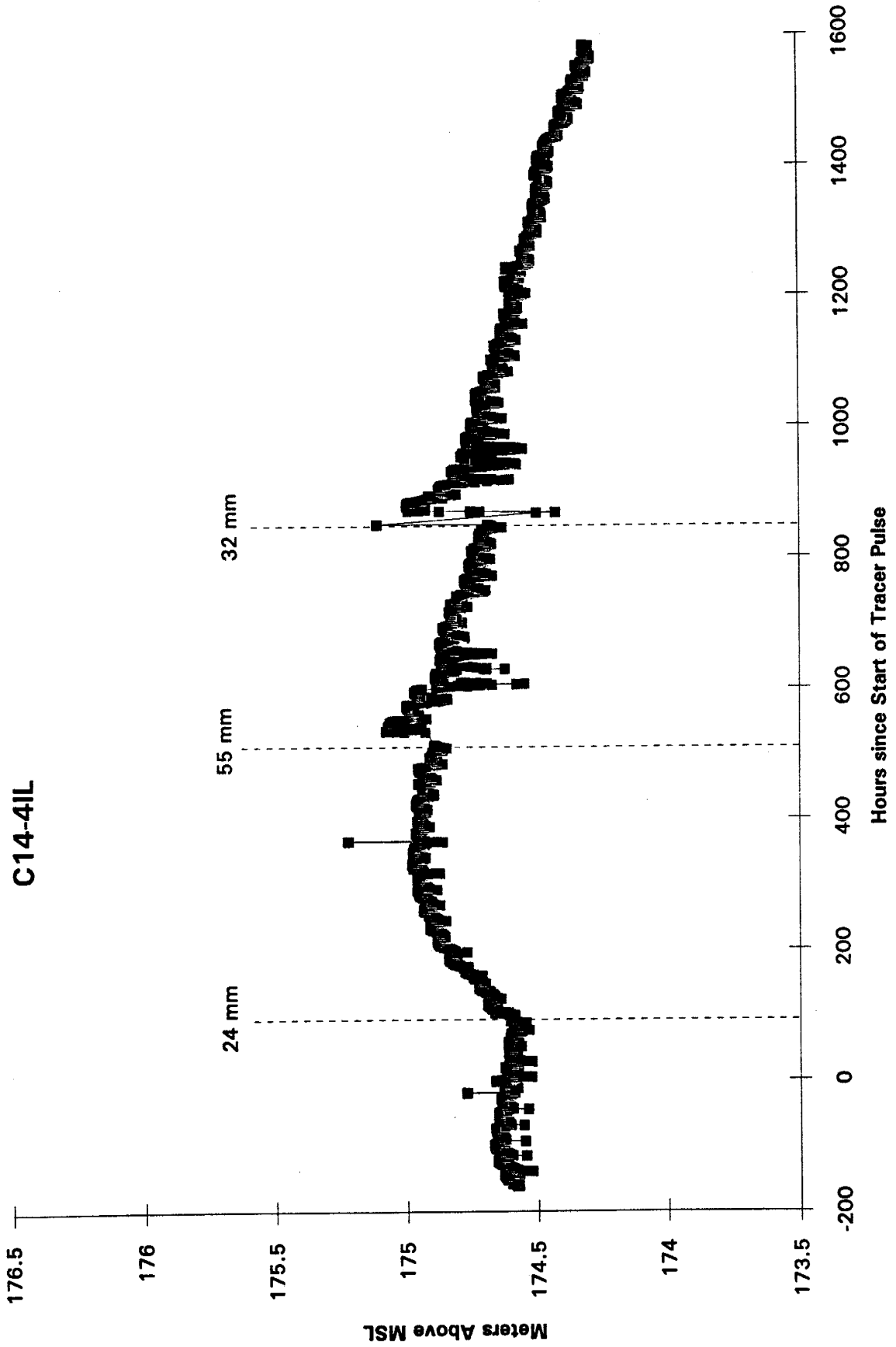
C10-3IL



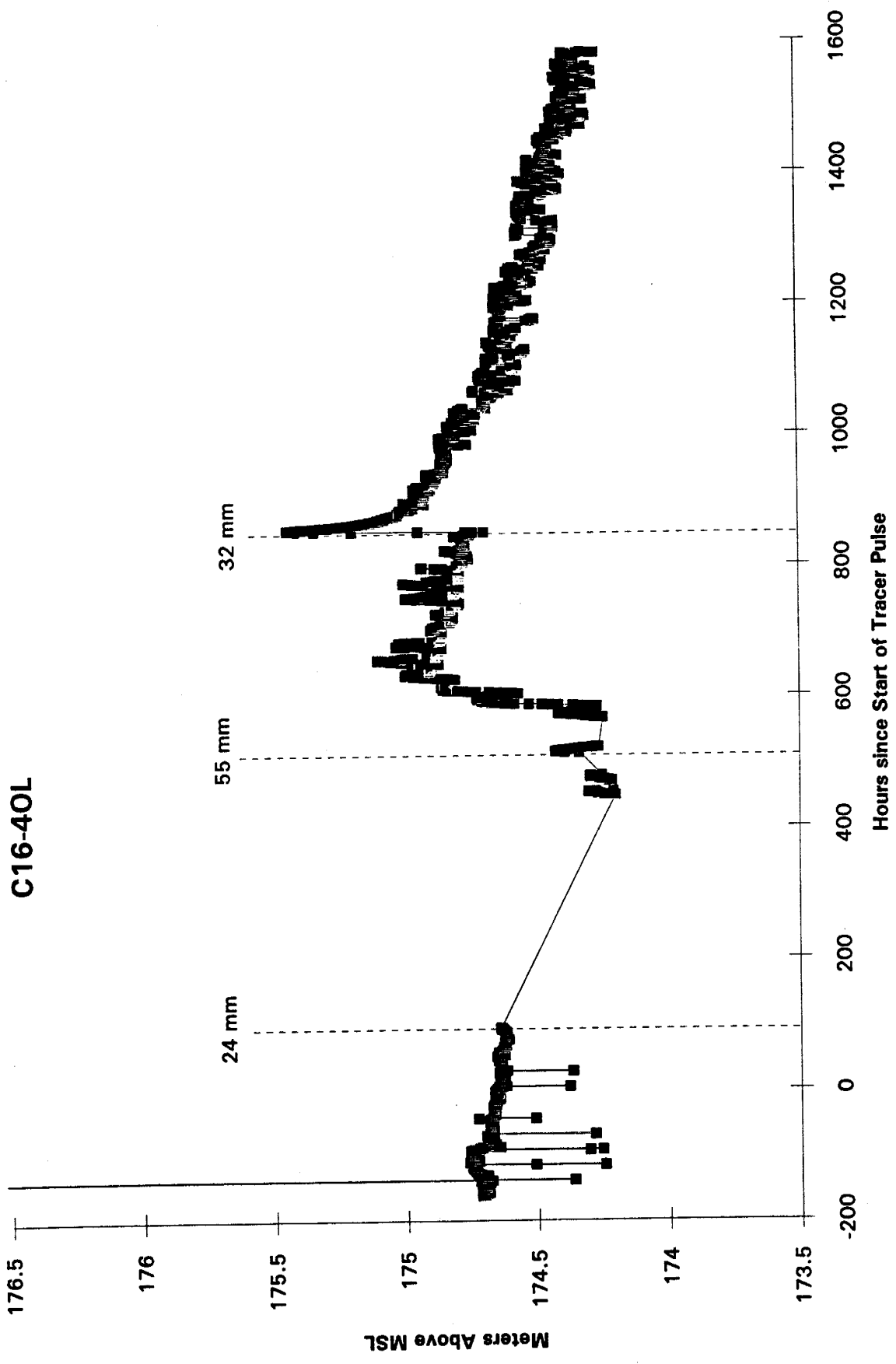
C12-30L



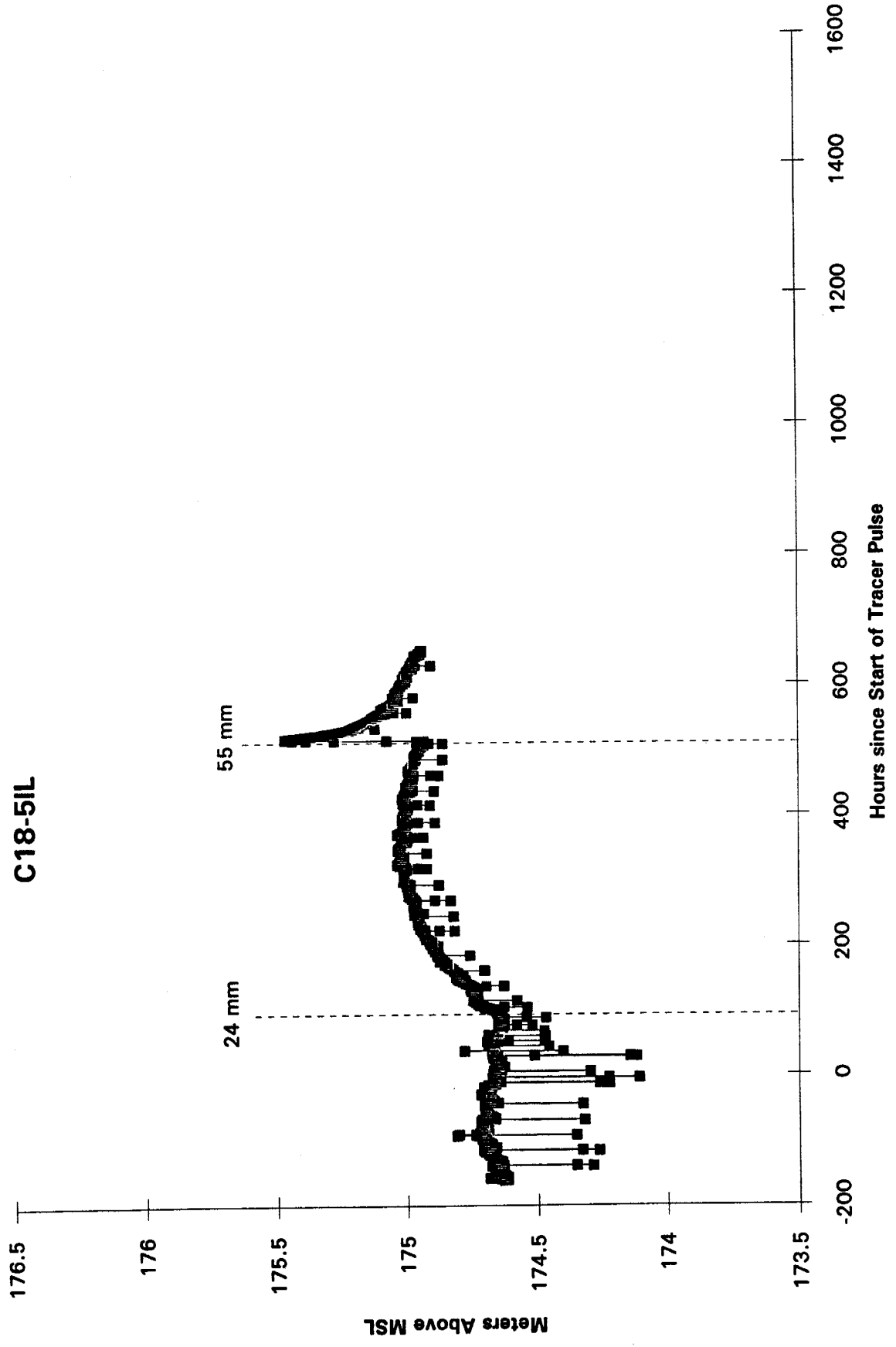
C14-4IL



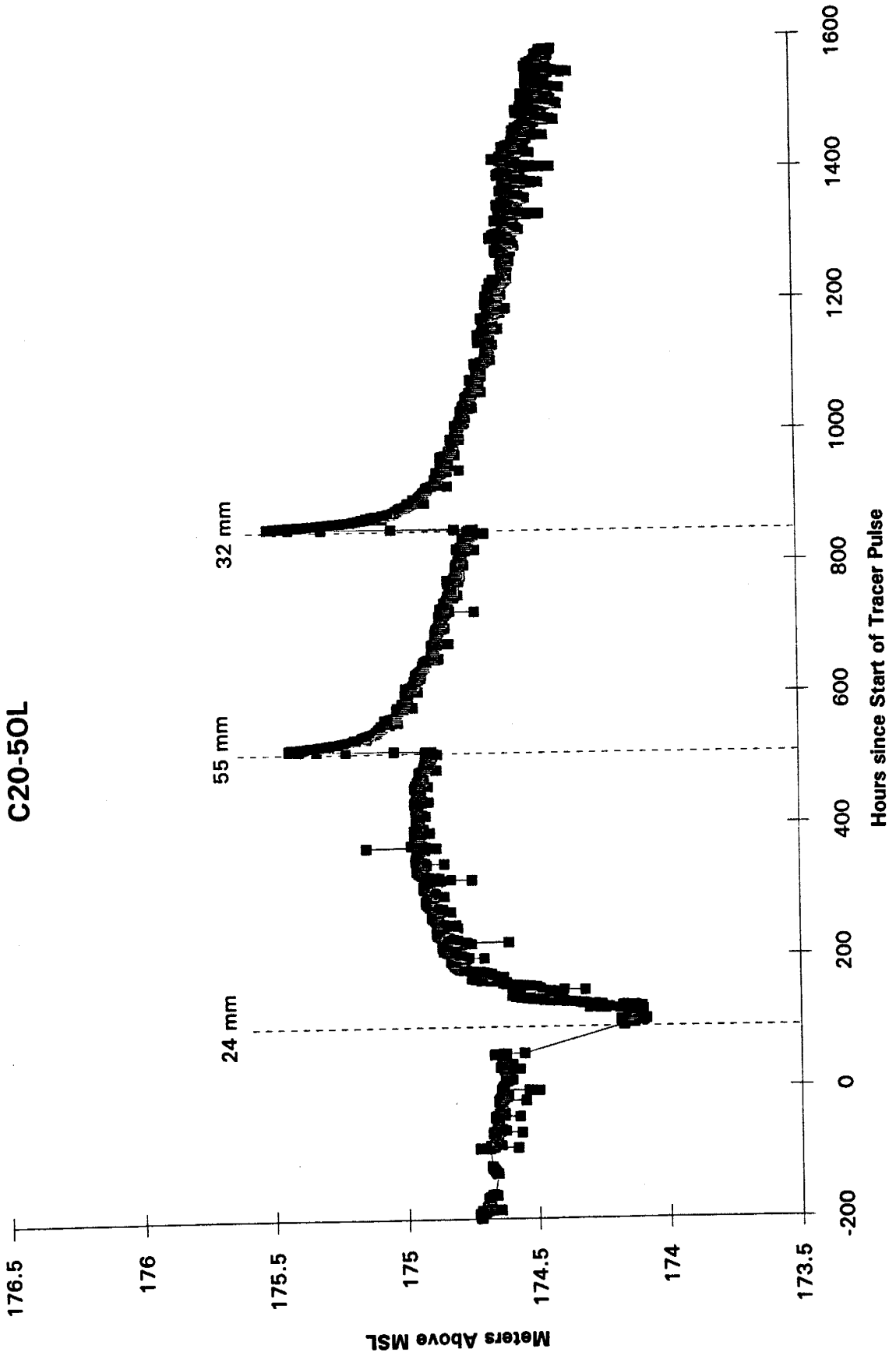
C16-40L



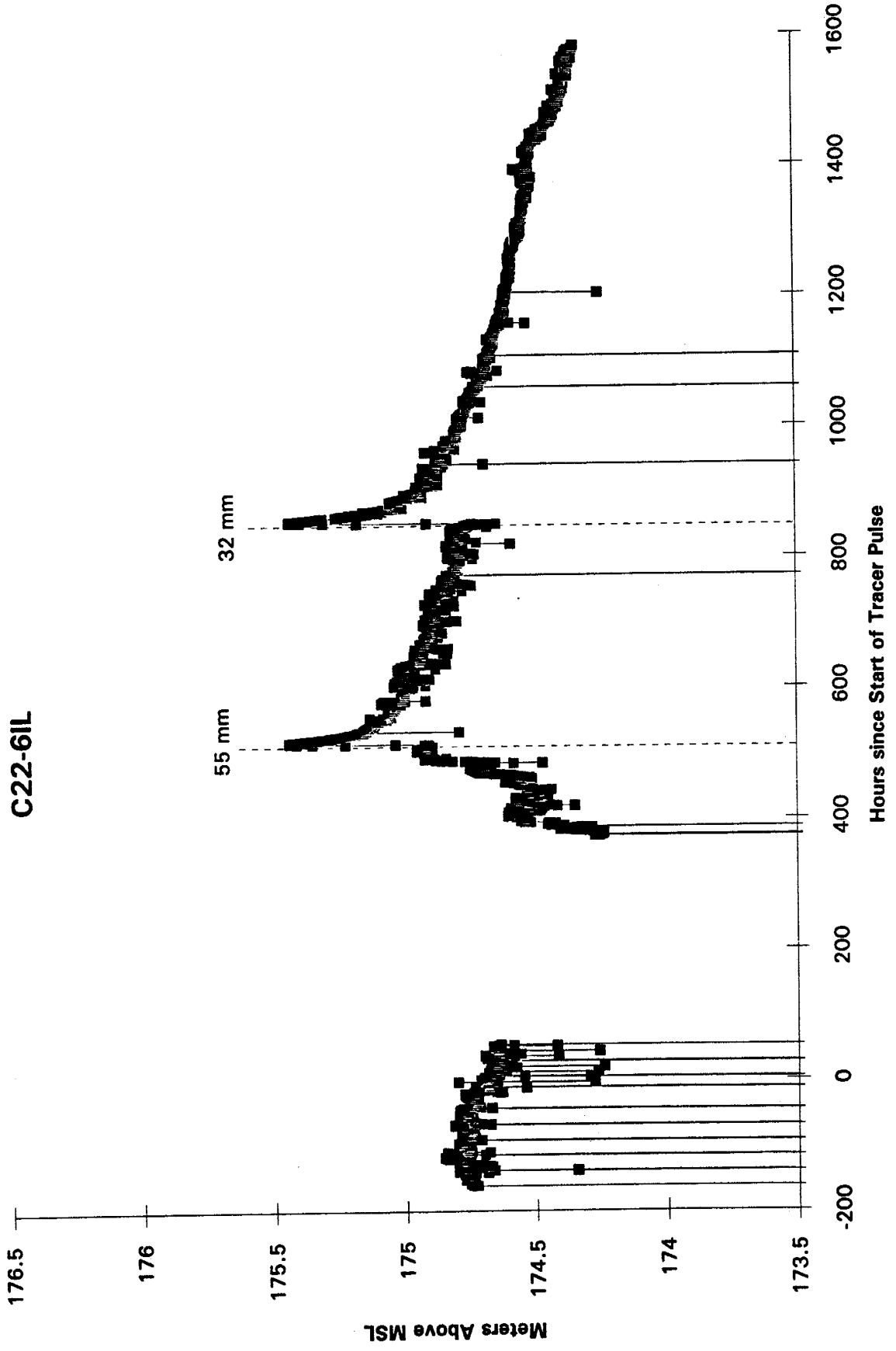
C18-5IL



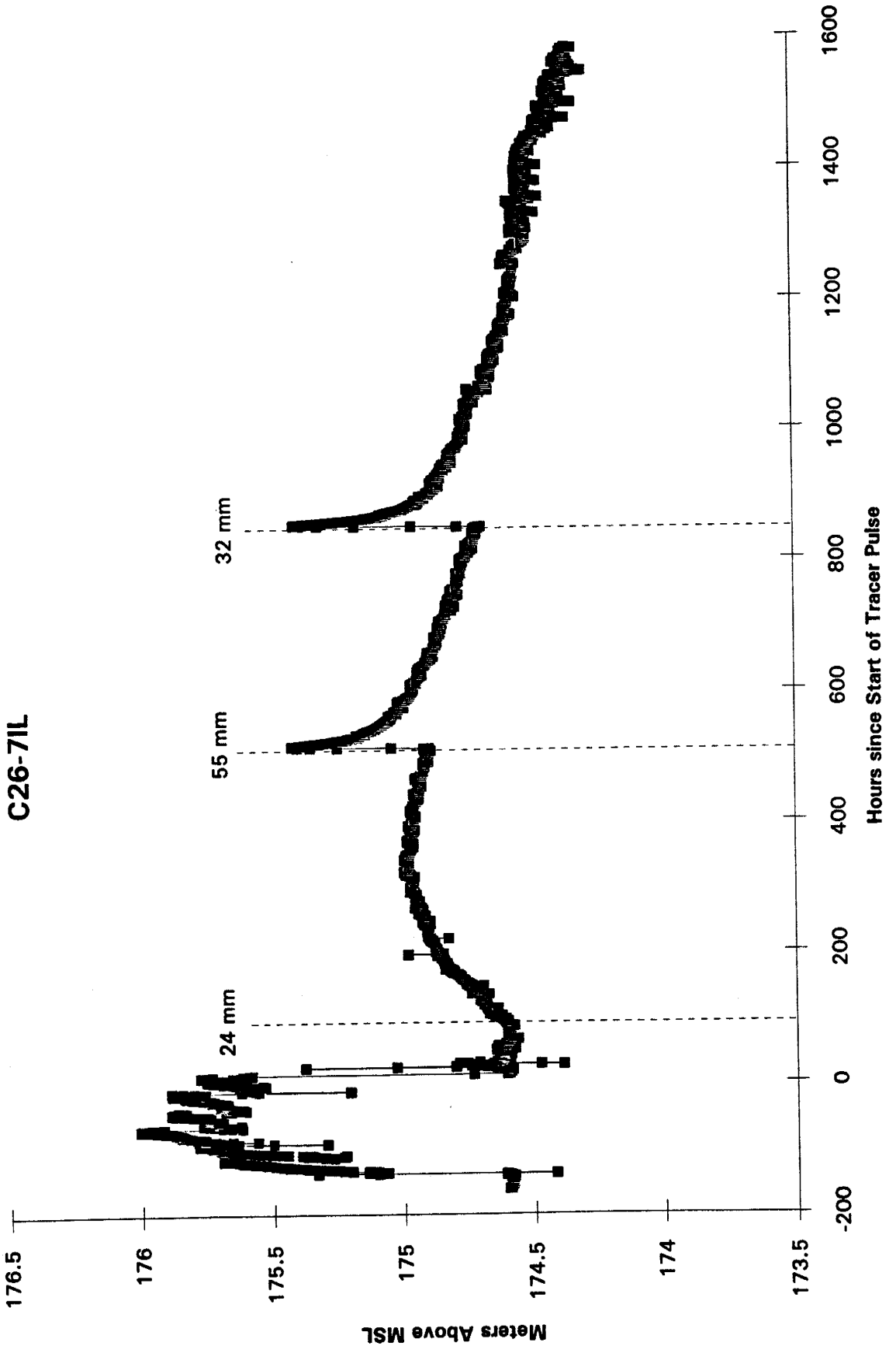
C20-50L



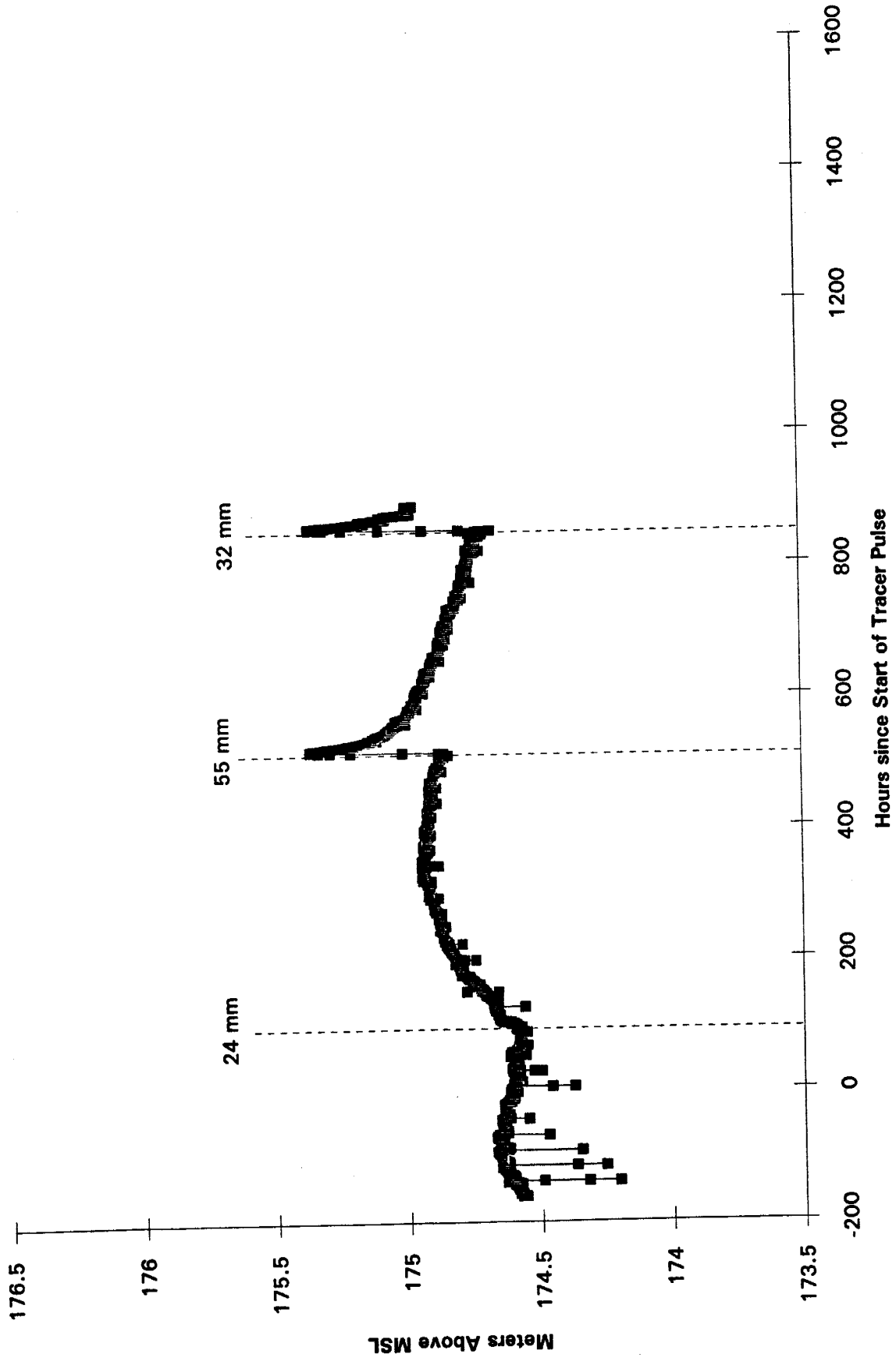
C22-61L



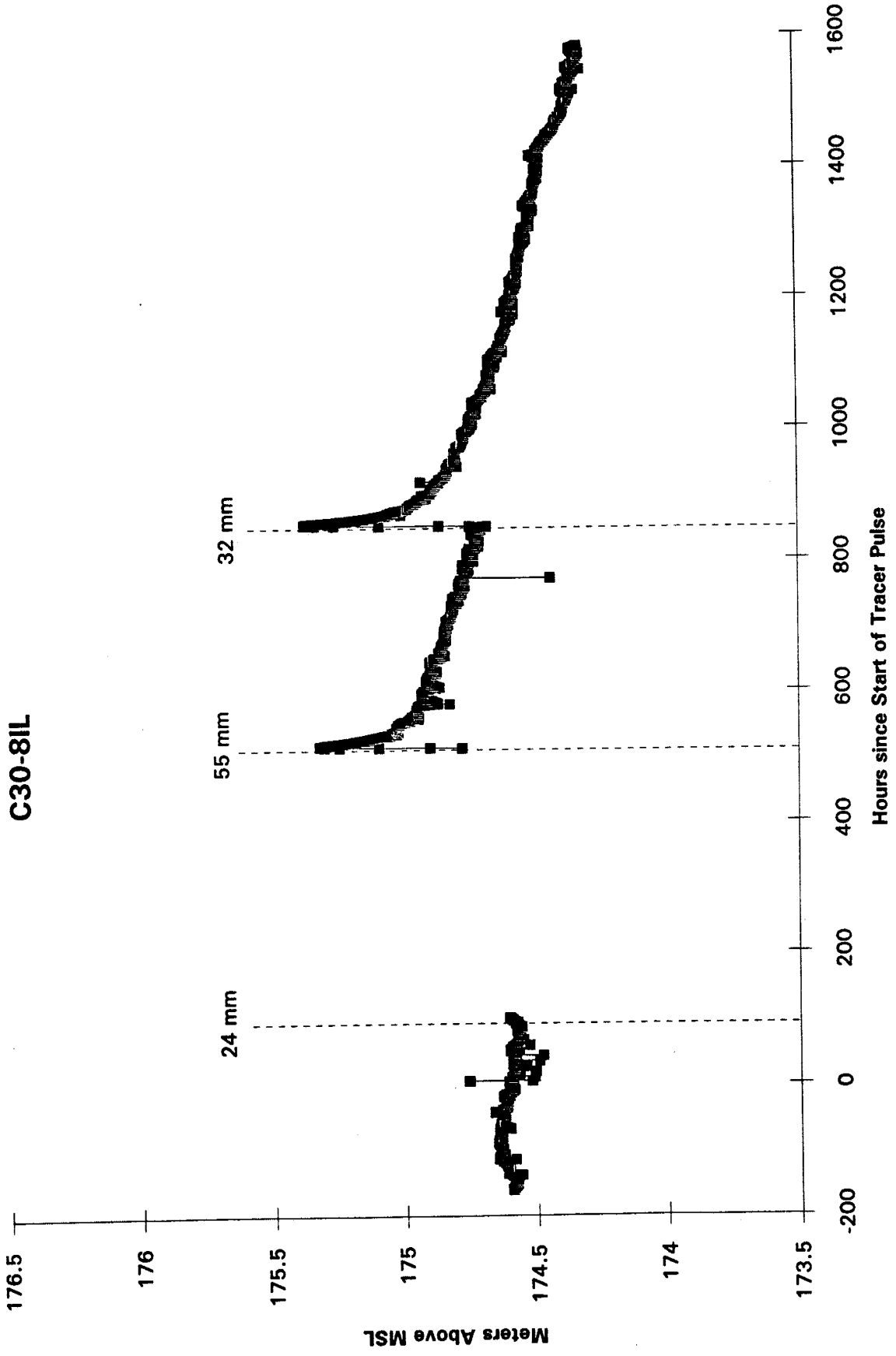
C26-7IL



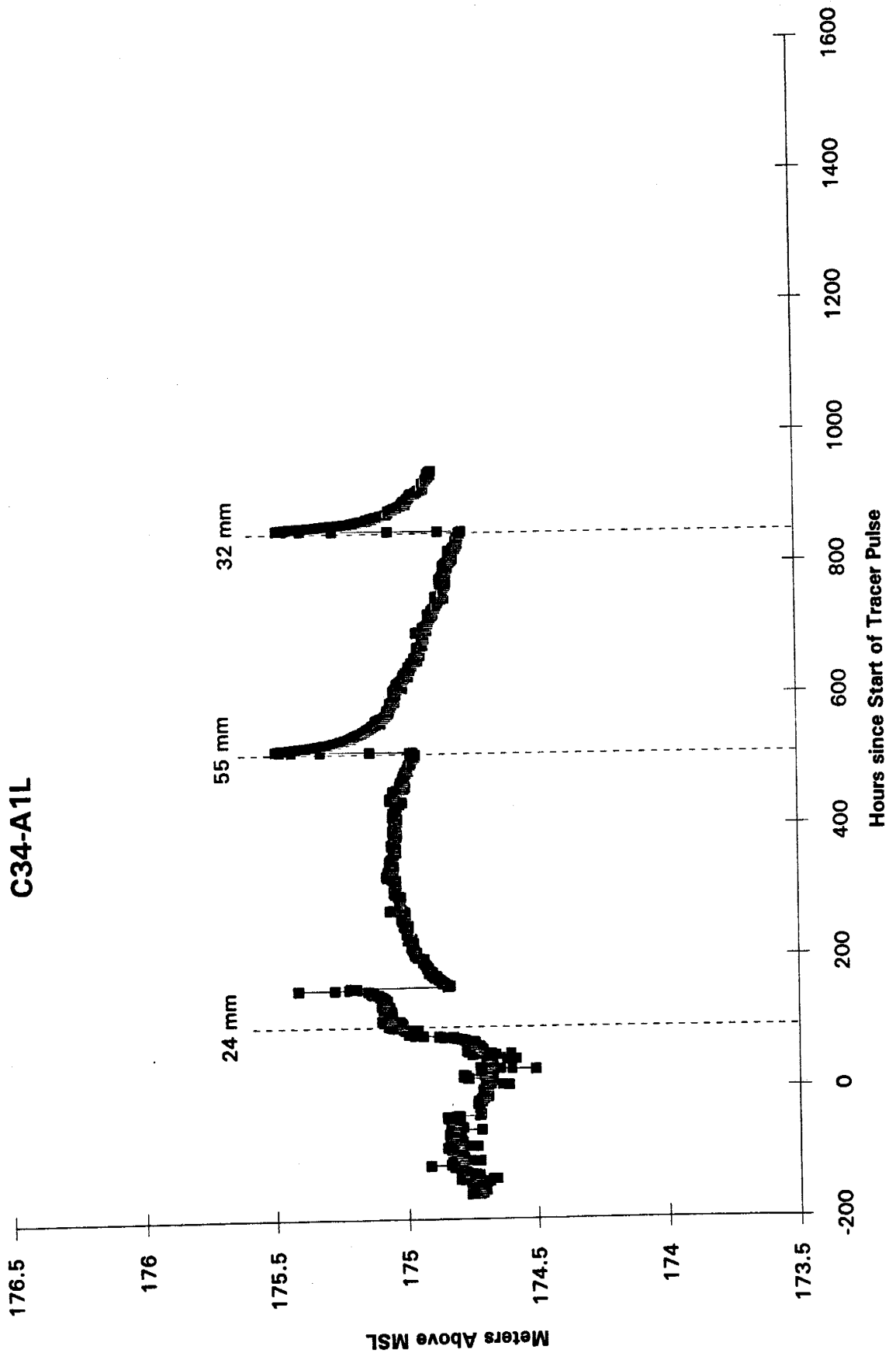
C28-70L

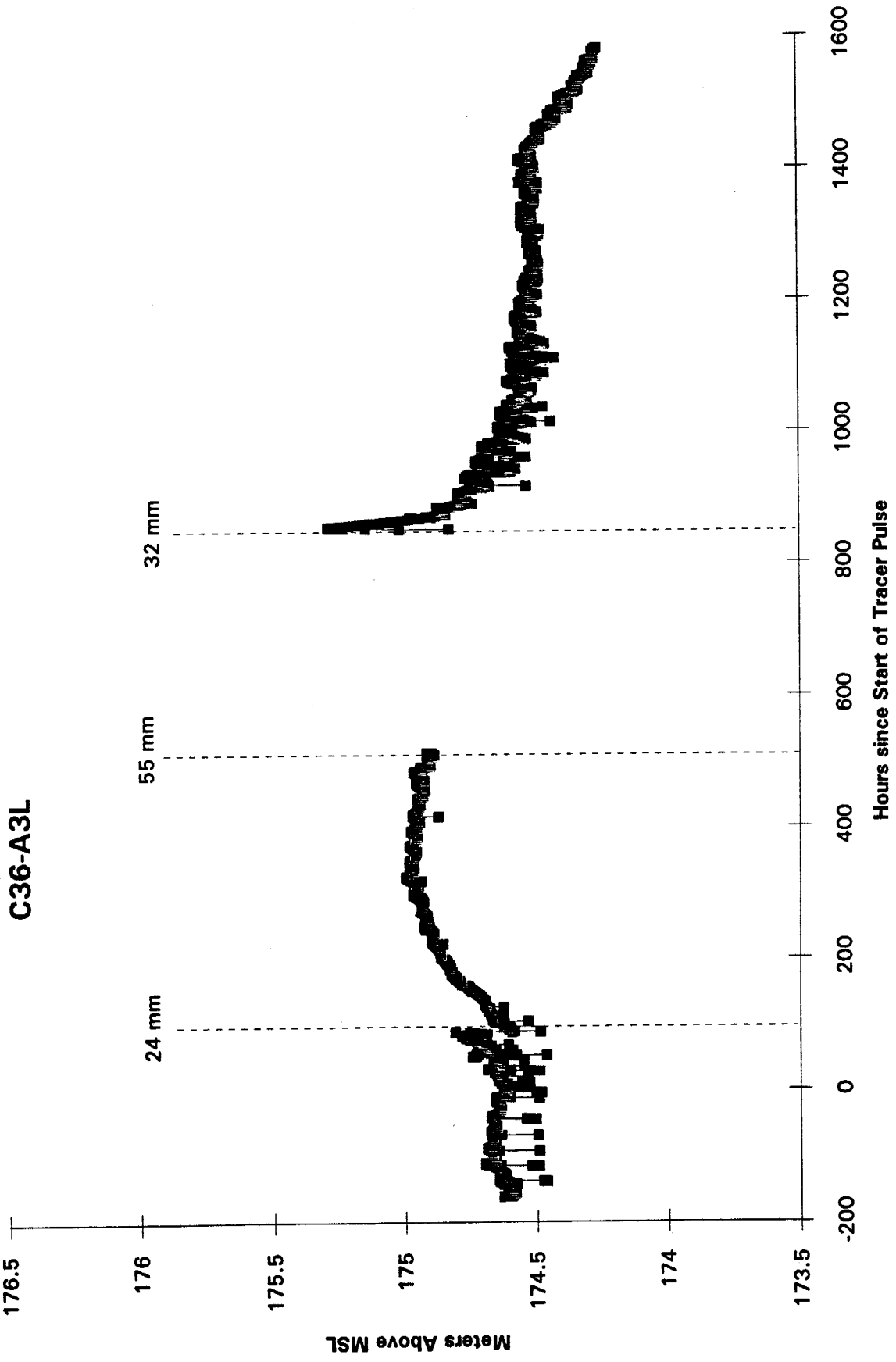


C30-8IL

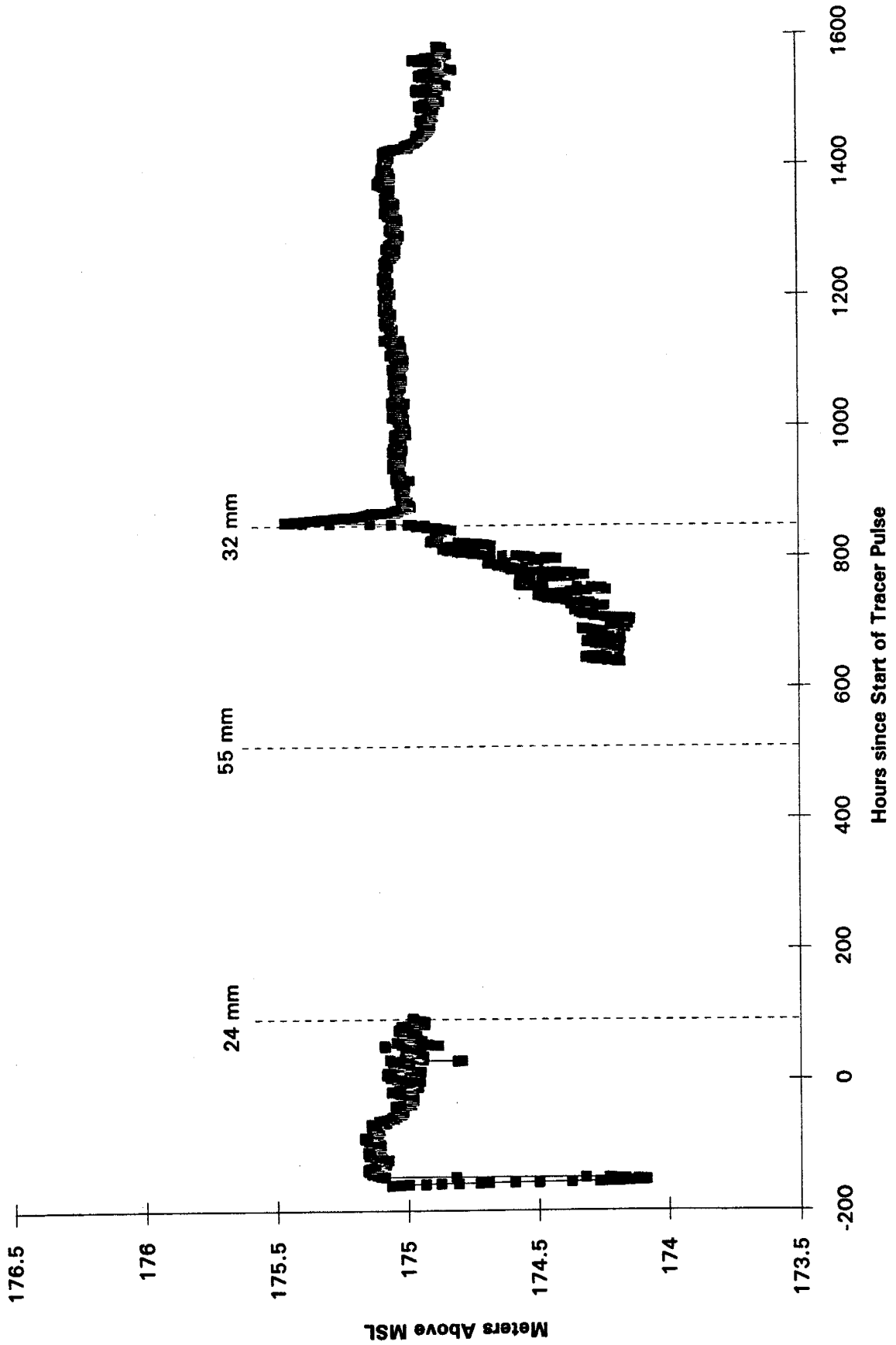


C34-A1L





C42-A7L



Appendix VI. Dye Pulse and Site Excavation

<u>Section</u>	<u>Page</u>
Dye Pulse	2
Excavation methods	2
Site A excavation	3
Media Heterogenieties	4
Bioturbation	5
Results	6
Tables	8
Figures	9
Plates	10

This appendix discusses the dye pulse and subsequent excavation of Site A (the Clay Site). The dye pulse and excavation allowed visualization of fast transport pathways and zones of preferential flow and the inspection of the hydrostratigraphic units (See Appendix I) removed from the erosional dynamics occurring in outcrop. The excavation process, heterogeneities, bioturbated features, and results are described. The plates referred to are presented in the last section of this appendix.

Dye pulse

At 17:30, August 15, a 4.0 grams/liter solution of FD&C red dye #3 was prepared by adding 12.0 kg of dye powder to 800 gallons of water in the reservoir tanks at Site A. Introduction of the dye pulse was begun while normal infiltration was underway to ensure that dye transport closely mirrored saturated flow processes (Plate 13).

At 08:30, August 17, an additional 1.4 kg dye was added to the remaining 650 gallons, resulting in a final concentration of 4.5 grams/liter. At 11:30, August 20, with 400 gallons of dyed water remaining in the reservoir tanks, all infiltration at Site A was terminated. Flow at Site C (Sand Site), where no dye had been introduced, was also terminated at this time to ensure that water introduced at Site C would not affect Site A.

Excavation methods

Excavation of Site A was begun on August 22, and completed on August 27, 1994. The site was excavated by both back hoe and detailed hand examination. Excavation of the south half of the infiltrometer surface was begun by hand (Plates 17 and 18). Beginning the next day, the back hoe was used to excavate a circular trench between the inner and outer sampling rings (See Plates 21 to 23). The trench was widened inward until it met the infiltrometer surface (Plate 24). The resulting 2 meter wide by 2 meter high cake shaped pillar was then hand reduced (Plates 25 to 39). After the back hoe had expanded and deepened the resulting pit, the fresh surface was given a detailed examination using hand tools. The hand excavated surface was then mapped and photographed, and the back hoe was used to expose fresh surface at a greater depth and width. The sides of the pit were sloped for safety reasons, and resulted in an even greater area being exposed to detailed hand examination.

The process of back hoe excavation of one to two foot layers followed by detailed hand inspection of exposed surfaces was repeated throughout the excavation process, allowing detailed visualization of subsurface transport pathways and processes. The final size of the excavation was approximately twenty meters across at the top, sloping to a 5.5 meter diameter floor at a depth of approximately six meters. A 1.5 meter by 2 meter pit (gouge) was dug by the back hoe into the bottom of the pit floor as a final excavation (Plates 100 to 102), but no personnel hand examined it due to safety regulations. After completion of excavation, photographing, and mapping, the pit was refilled with the excavated materials.

The remainder of this section is an overview of the findings of the excavation.

Site A (Clay Site) excavation

The site was first excavated by hand to a depth of one foot over the south half of the area inside the infiltrometer. It was apparent that the majority of dye was captured by the organic growth in the first foot of soil (Plate 19). The soil inside the infiltrometer below this depth presented a mottled pink to red color (Plate 20). A back hoe was then used to excavate a circular trench approximately 1 meter wide by 1.5 meters deep between the inner and outer sampling rings (Plate 22). No signs of preferential flow or fast transport flowpaths were visible on bottom or the inside or outside wall of this trench (Plate 41). The layer of blocky structured clays (Unit 4) under the surface topsoils and loess (Unit 5) was penetrated by this excavation. The excavation was widened to about 6 meters diameter and the remaining pillar under the infiltrometer was excavated by hand (Plate 27). As the diameter of the pillar was reduced, it was apparent that virtually all the flow from the infiltrometer was directed vertically through Units 5 and 4 (topsoil and blocky structured clays) via zones of preferential flow, fractures, root tubes, and wormholes (Plates 28 to 39). One dye-filled wormhole directly intercepted sampling point A35-A2U at a depth of approximately six and one-half feet (Plate 30). The complete excavation of the pillar under the infiltrometer revealed numerous instances of fracture, root, and wormhole fast transport pathways bypassing volumes of undyed matrix (Plates 31 to 38).

Excavation by back hoe was resumed after the central pillar was completely excavated. The pit was widened to approximately 6 meters with a depth of 2 meters (Plate 43). The media at this depth was primarily bedded, oxidized clays (Unit 3). The flow was still predominantly vertical through fractures and macropores, though flowpaths began to spread horizontally along bedding planes in the clays (Plate 54). No dyed flow was found on the outside walls of the excavation.

After examination at this level, back hoe excavation resumed. At a depth of 2.1 meters, a crayfish hole filled with dyed water was exposed (Plate 40) and excavation by the back hoe was halted. In addition to the 2 cm by 3 cm crayfish hole, hand excavation of the 3 meter by 3 meter floor revealed numerous active fractures and zones of preferential flow through silty sand stringers (Plates 44 and 45). At the beginning of the test in June, this depth had been approximately 1.5 meters below the water table, as defined by the elevation of standing water in augered instrument and sampling boreholes. During the excavation in August, the media was still fully saturated, and dyed water could be seen in active fractures and preferential flow zones of sand or silty sand diamict of hydrostratigraphic Unit 6. The matrix surrounding active flowpaths was stained with pink dye. This depth was the upper boundary of a strata of oxidized clays containing carbonate filled fractures. Many of the carbonate deposits encountered were stained a light pink color, indicating radial flow through this unit. During excavation of the media at this depth, the base of the capillary fringe (standing water) was observed to drop from less than 2.0 meters below the surface to at least 6.1 meters below the surface (into Unit 5) in less than forty-eight hours, verifying that the system was well drained.

The excavation by back hoe and hand continued through the remaining oxidized, bedded clays (Unit 3). Increasing areal spread of dye intrusions was observed. The clay colors gradually but irregularly changed with depth from yellow oxidized clays to brownish gray and gray clays

of the unoxidized clays of Unit 2 (Plates 50 to 53). Active transport pathways were pervasive, and included sandy zones of preferential flow, active fractures and complexes of crayfish burrows (Plates 52, 56, and 73). Walls and floors of crayfish burrows and complexes were often stained with red dye (Plate 81).

In close proximity to sampling point A28-7OL, a sand stringer at 2.8 meters was discovered which discharged dyed water (Plate 77). Further excavation revealed connection to a large silty sand body (mixture of Units 6 and 4) located in the Northwest quadrant of the site and apparently inserted by glacial processes into beds of oxidized silty clays of Unit 3 (Plate 76).

The next major unit excavated was the bedded, unoxidized gray clay (Unit 2) at about 2.9 meters to 3.0 meters depth. Crayfish burrows transported dye into this unit (Plate 83), but did not penetrate lower. When first viewed, this unit appeared massive. Hand excavation revealed that this unit was structured with beds and laminations, and contained both horizontal and vertical transmissive fractures and sand inclusions (Plates 50 to 52). These fractures typically had oxidized surfaces, and contained medium and fine sands. Some of the vertical fractures were up to a cm in width (Plate 68). Excavation into this unit revealed instances of saturated sand stringers. At this depth, the dyed water had been diluted to the extent that the dye was almost imperceptible, and no distinct dyed water could definitely be determined as coming from any of the sand stringers encountered.

The last major unit (Unit 1, massive unoxidized clay) was encountered at depths between 3.4 meters to 5 meters. This unit contained no definite bedding planes, and had an increasing cobble and pebble content with depth. This unit exhibited all the features of a geologically reworked glacial till deposit: isolated sand channels and stringers (Plate 102), random cobble and pebble inclusions (Plate 102), no visible layering or bedding, and deformation features (Plate 53). The depth of this unit at Site A is unknown, but extends at least to 5.5 meters, which is the deepest penetration made by the back hoe. A substantial sand stringer in this unit was encountered at about 5.2 meters (Plate 102). When back hoe excavated samples of this Unit 1 were broken open, they often split along planes that appeared to be shear or remnant bedding features. These fracture planes were typically covered with a fine sand, indicating significant flow had occurred at some time in the past. A few of these fracture planes contained red dye from a secondary dye pulse (Plate 55) initiated after excavation to approximately 3 meters, affirming that flow was possible through this unit (Plate 103).

During the excavation, large cores were taken from most units for later hydrologic laboratory analysis (Plates 60 to 67 and 95 to 99).

Media Heterogeneity

Besides the heterogeneity of the vertical progression from soils to oxidized clays to oxidized bedded clays to unoxidized bedded clays to massive unbedded clays, there are the large silty sand body in the northwest quadrant of the site (Plates 74 and 94) and the frequent intrusive sand channels and stringers (Unit 6) encountered at all depths during the excavation (Plates 44, 52, and 102 and Figure 1). Other heterogeneities encountered were the greater abundance of layered oxidized clays with interbedded carbonate deposits in the south and southeast section

of the site and the greater number of silty sand zones in the North and Northwest octants of the site.

Bioturbation

As noted above, bioturbation produced major flow pathways (Figure 1). Root and wormholes were ubiquitous throughout the first 2 meters of the excavation. Crayfish burrows appeared in many cases to follow pre existing fractures in the bedded clays. Complexes of crayfish burrows stained with red dye (Plate 82) were found at depths from just below the surface to 3.2 meters (Plate 83). These depths are well below the perched water table during the spring and summer months. A fifteen minute cursory inspection of the surrounding field surface discovered three instances of crayfish burrows (Plates 104 to 109). Geologists mapping the local outcrops reported numerous instances of crayfish habitation throughout the area.

Results

Dye tracer

Dye movement was observed through the topsoils and loess (Unit 5) and underlying blocky structured silty clays (Unit 4) via fractures, root holes, crayfish burrows, and worm holes. Dye movement was vertical through these units, with no evidence of lateral spread encountered during the excavation. Sampling location A35-A2U, approximately 2 meters below the infiltrometer ring, was directly intercepted by a worm hole beginning just beneath the infiltrometer surface. The soil water sampler at that location was inoperable, but the wormhole and sampling site contained dark red dye (Plate 30). 42 minutes after the introduction of the salt pulse, C_i/C_o ratios from the TDR trace at that sampling point went almost instantaneously from 0 to off scale (greater than .45) indicating that the Cl^- tracer transport via this fast transport pathway reached a depth of 2 meters at high concentration in less than one hour (Figure 28). Concentrations of Cl^- tracer traveling this same path may have spread laterally through the bedded clays of Unit 3 and contributed to the early arrival of high concentrations at the lower inner Northeast sampling point (A6-2IL) (Discussed in Appendix IV). The early disappearance of Cl^- concentrations from this area may be due to the fast arrival of clean infiltrated water down the same fast transport pathway following the termination of the Cl^- tracer pulse.

Bioturbation

Bioturbation was a major factor in transport at Site A. Ubiquitous wormholes (Plates 29, 30, 31, and 39), root holes (Plates 31 to 34), and crayfish burrows (Plates 80 to 84) transported dye past the depths of the oxidized bedded clays (Unit 3) and into the layered unoxidized clays (Unit 2) near the deepest extent of the excavation. The lack of dyed transport pathways on the outside walls of the initial trench dug around the infiltrometer (Plate 23), and the preponderance of dyed root and wormholes discovered during the dismantling of the pillar beneath the infiltrometer also attest to the importance of bioturbation in aiding vertical flow processes through the upper three hydrostratigraphic units. The low salinity concentrations encountered at sampling points and the corresponding large number of active bioturbated features in the South, Southwestern, and Southeastern octants of the site evince the possibility that transport of the majority of flux in those regions passed through such bioturbated fast transport pathways, eluding the sampling points entirely.

The Hagen-Poiseuille equation for macropore flow (See Table 1), calculates the flux through macropores. While laminar flow, a circular cross section, and other assumption inherent in this solution will not be fully realized in flow through the bioturbated pathways, the formula provides an estimate of the transport potential. At a conservative gradient estimate of .01, only eleven small root holes of 1 mm radius would be required accommodate the maximum infiltrated flux through the infiltrometer. 2 wormholes of 1.5 mm radius could accommodate the entire flux through the infiltrometer at maximum infiltration rates. One large root hole of 2 mm radius would have the capacity to transport more than one and one-half the maximum flux through the infiltrometer. A single crayfish hole of the common 2 cm x 3 cm dimensions encountered during excavation of Site A is able to accommodate over forty-five times the maximum flux through the infiltrometer. When the perched water table is below some portion

of these bioturbated fast transport features, and the surrounding media is still essentially saturated, the gradients between the surface and the perched water table may approach 1.0 for vertical macropores. This was the situation encountered during the site installation in late May and early June and during excavation in August. The potential for fast transport of contaminants through bioturbated macropores to the perched water table during or immediately after intense rainfall events is great.

N = a dimensionless shape factor

R = diameter of passage

The Hagen-Poiseuille equation: $q = -\frac{N \rho_w g R^2}{\mu} \nabla h$ where $\rho_w, g =$ density of water, acceleration of gravity

For a circular tube, this becomes:

$$q = -\frac{\rho_w g r^2}{8\mu} \nabla h \quad \text{where } r = \text{tube radius} \\ \text{all others as above}$$

To approximate pore tortuosity and roughness, we used a conservative equation of:

$$q = -\frac{\rho_w g r^2}{12\mu} \nabla h. \quad \text{The results for a range of pore sizes and } \nabla h\text{'s:}$$

$\nabla h = .01$:

	r (m)	μ (kg/ms)	q(m/s)	Q (m3/s)	Qinfl (maximum)	% of Maximum Q
very small root:	0.0005	9E-07	0.002286	1.795E-09	3.1678E-05	0.01
small root:	0.001	9E-07	0.009144	2.873E-08	3.1678E-05	0.09
wormhole:	0.0015	9E-07	0.020575	1.454E-07	3.1678E-05	0.46
medium root:	0.002	9E-07	0.036577	4.596E-07	3.1678E-05	1.45
crayfish burrow:	0.015	9E-07	2.057466	0.0014543	3.1678E-05	4591.04

$\nabla h = .1$:

	r	μ	q(m/s)	Q (m3/s)	Qinfl (maximum)	% of Maximum Q
very small root:	0.0005	9E-07	0.022861	1.795E-08	3.1678E-05	0.06
small root:	0.001	9E-07	0.091443	2.873E-07	3.1678E-05	0.91
wormhole:	0.0015	9E-07	0.205747	1.454E-06	3.1678E-05	4.59
medium root:	0.002	9E-07	0.365772	4.596E-06	3.1678E-05	14.51
crayfish burrow:	0.015	9E-07	20.57466	0.0145434	3.1678E-05	45910.41

$\nabla h = 1$:

	r	μ	q(m/s)	Q (m3/s)	Qinfl (maximum)	% of Maximum Q
very small root:	0.0005	9E-07	0.228607	1.795E-07	3.1678E-05	0.57
small root:	0.001	9E-07	0.91443	2.873E-06	3.1678E-05	9.07
wormhole:	0.0015	9E-07	2.057466	1.454E-05	3.1678E-05	45.91
medium root:	0.002	9E-07	3.657718	4.596E-05	3.1678E-05	145.10
crayfish burrow:	0.015	9E-07	205.7466	0.1454337	3.1678E-05	459104.08

Table 1. Potential fluxes through various size bioturbated passages at three possible gradients

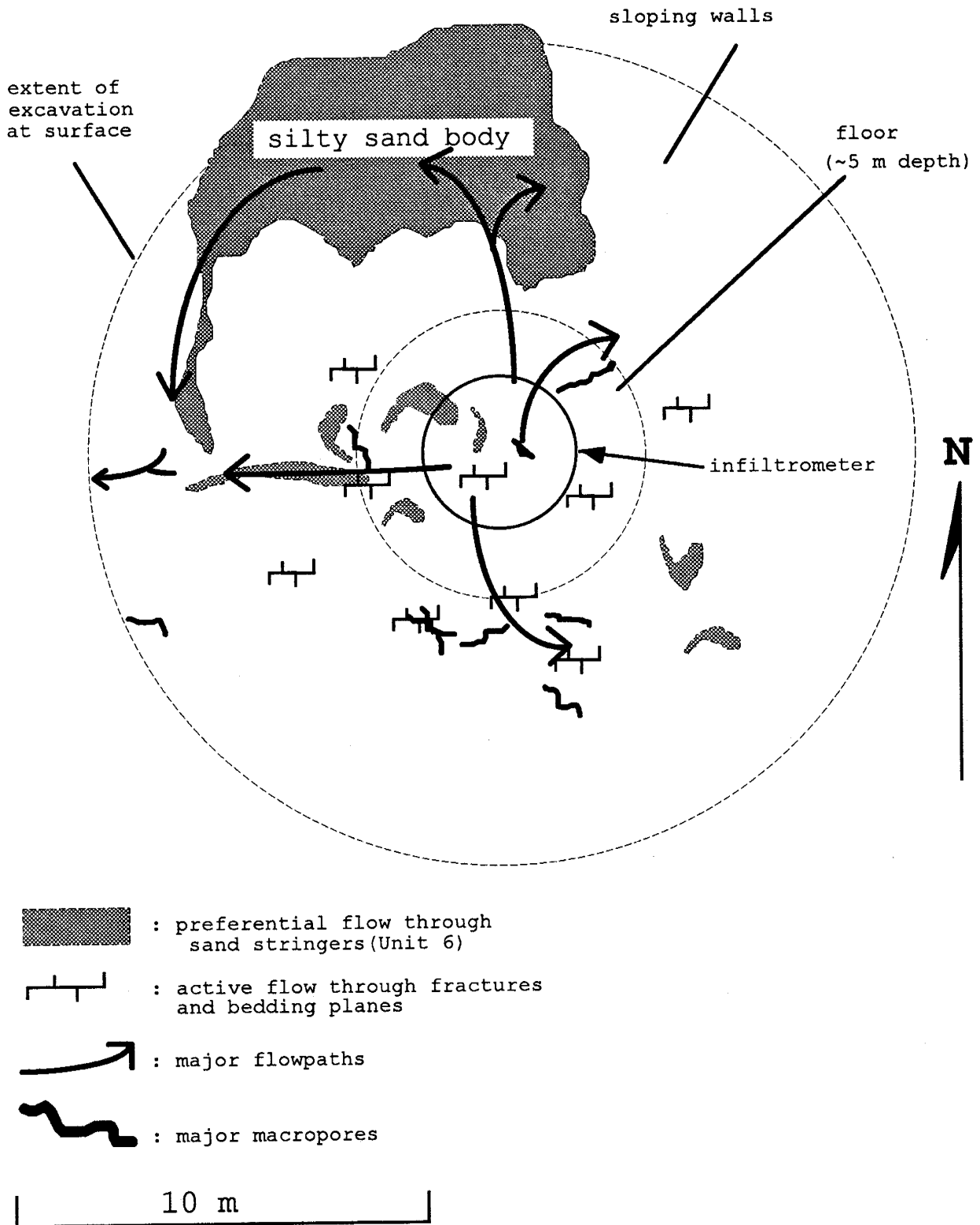


Figure 4. Plan view of major macropores, fractures, and zones of preferential flow found during excavation at the Clay Site. Noted features are integrated over the depth of the excavation.



Plate 1. View of Sites A (Clay Site) and Site C (Sand Site) in early June, 1994. Site A and Paddy's Run is to the right, Site C is to the left. Between the two sites are the 2500 gallon main supply tanks which feed the two 500 gallon site supply tanks located at each site.



Plate 2. Site C before instrumentation showing staked borehole locations, infiltrometer, and the two 500 gallon site supply tanks.



Plate 3. Main supply tanks. The water filter manifold is in the foreground between the two rows of 55 gallon drums.

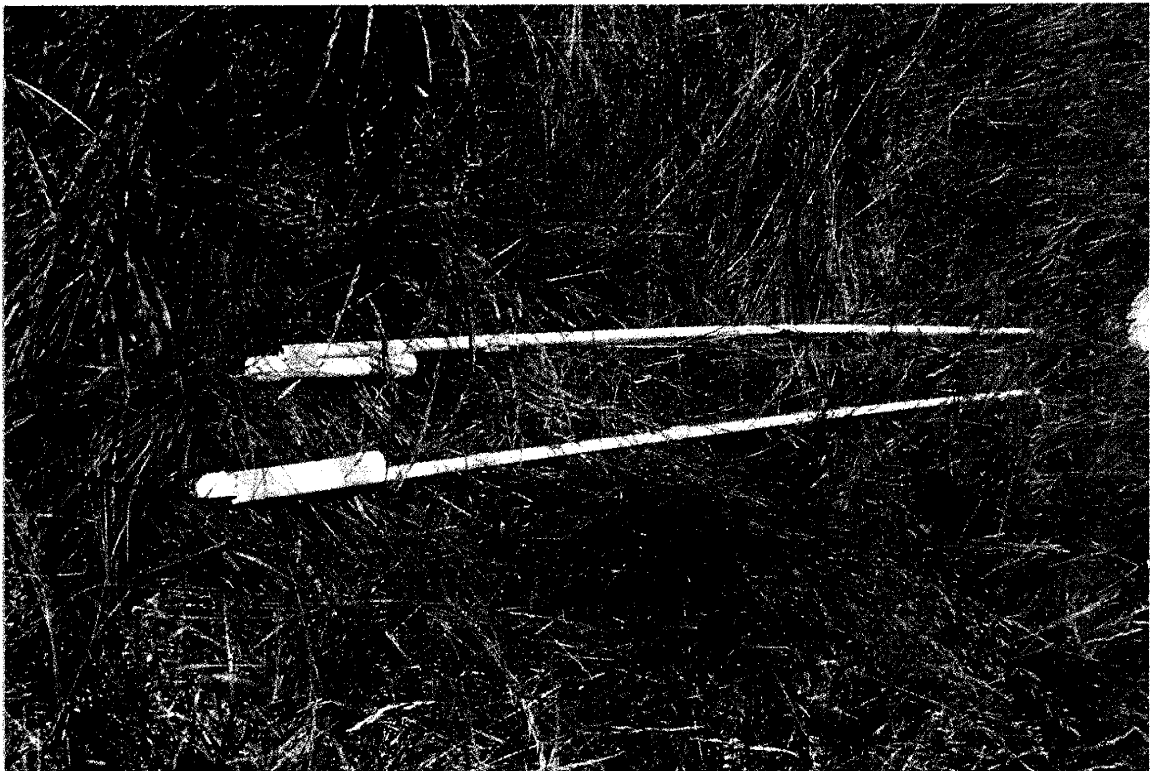


Plate 4. Suction lysimeter type soil water samplers prior to installation. They are taped to the 3/8" PVC pipe used to protect the TDR coaxial signal transmission cable.

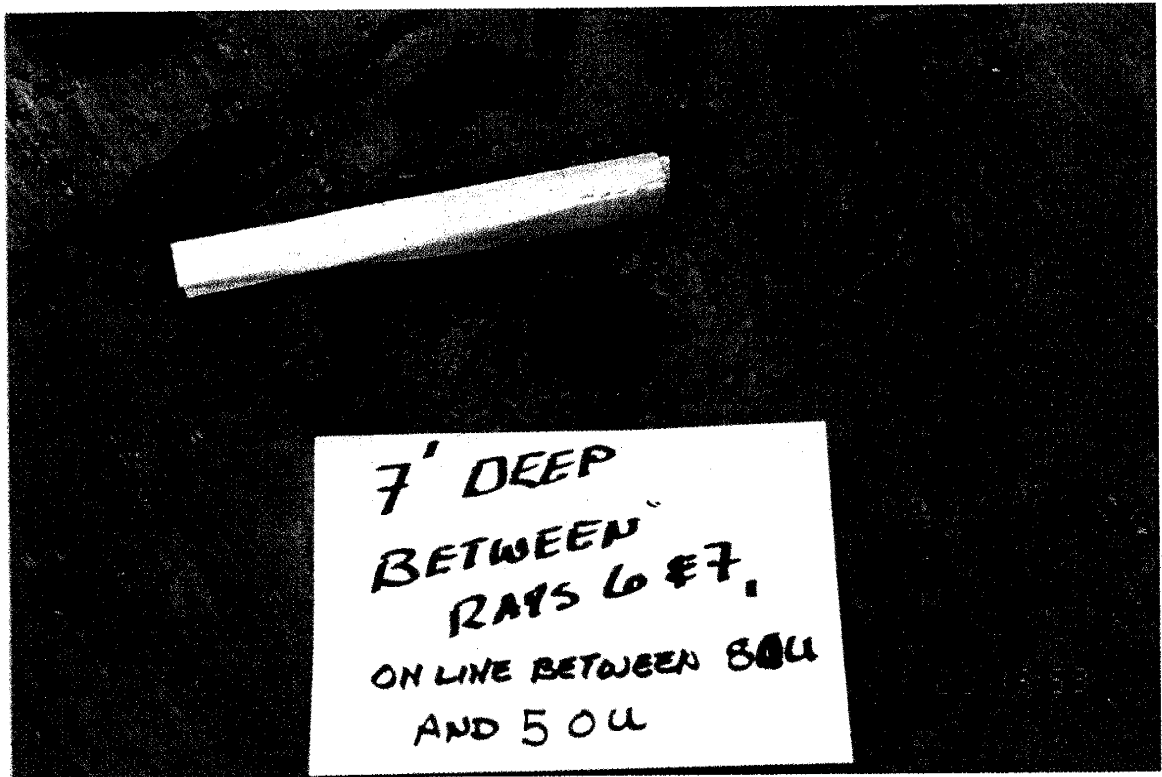


Plate 40. Crayfish burrow at approximately 2.2 m depth in layered oxidized clays of Unit 3. Note the pink dye on the rolled up note card.

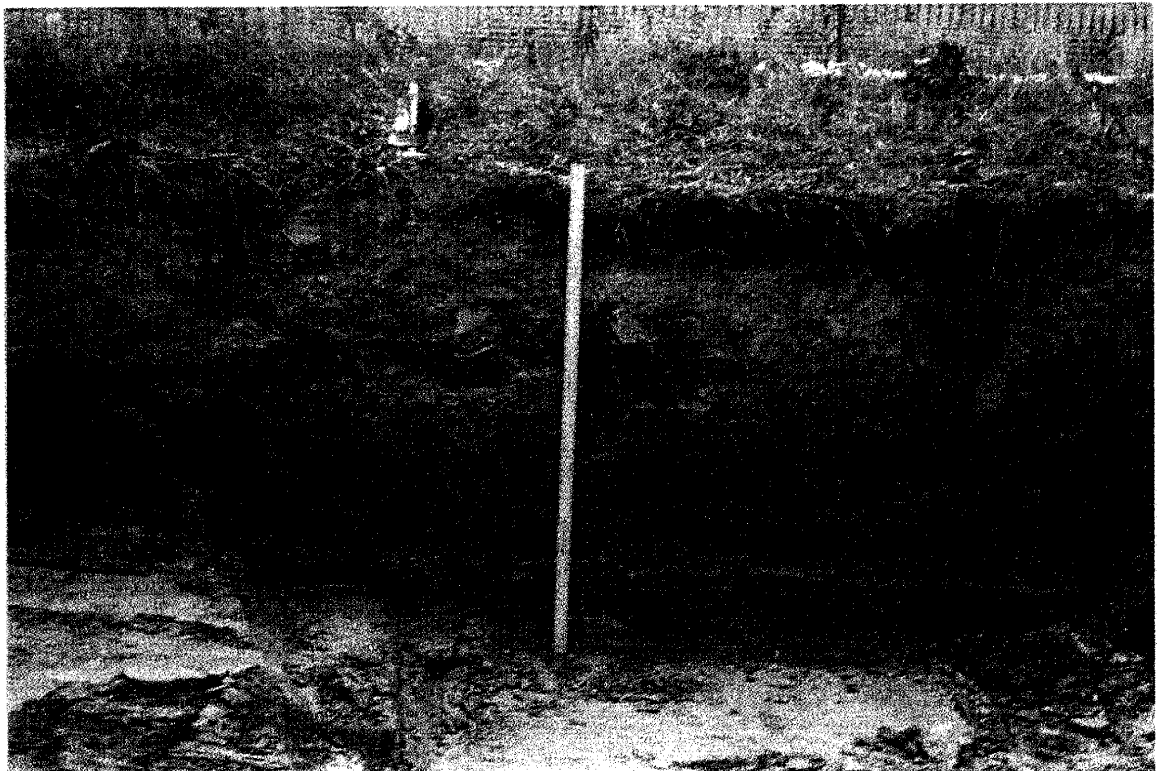


Plate 41. Unstained floor and exterior walls of 1.3 m deep excavation at outer sampling ring.



Plate 5. Instrument installation at Site A by Sandia Labs and FERMCO personnel.

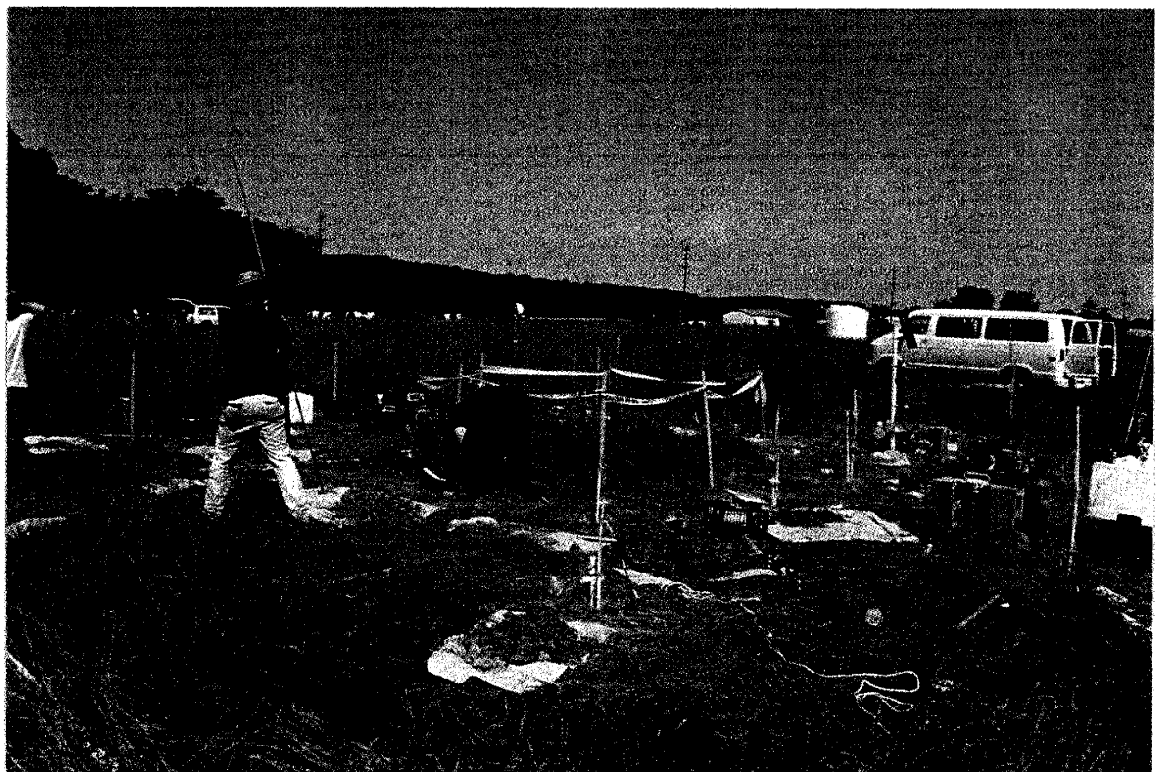


Plate 6. Instrument installation and borehole augering.

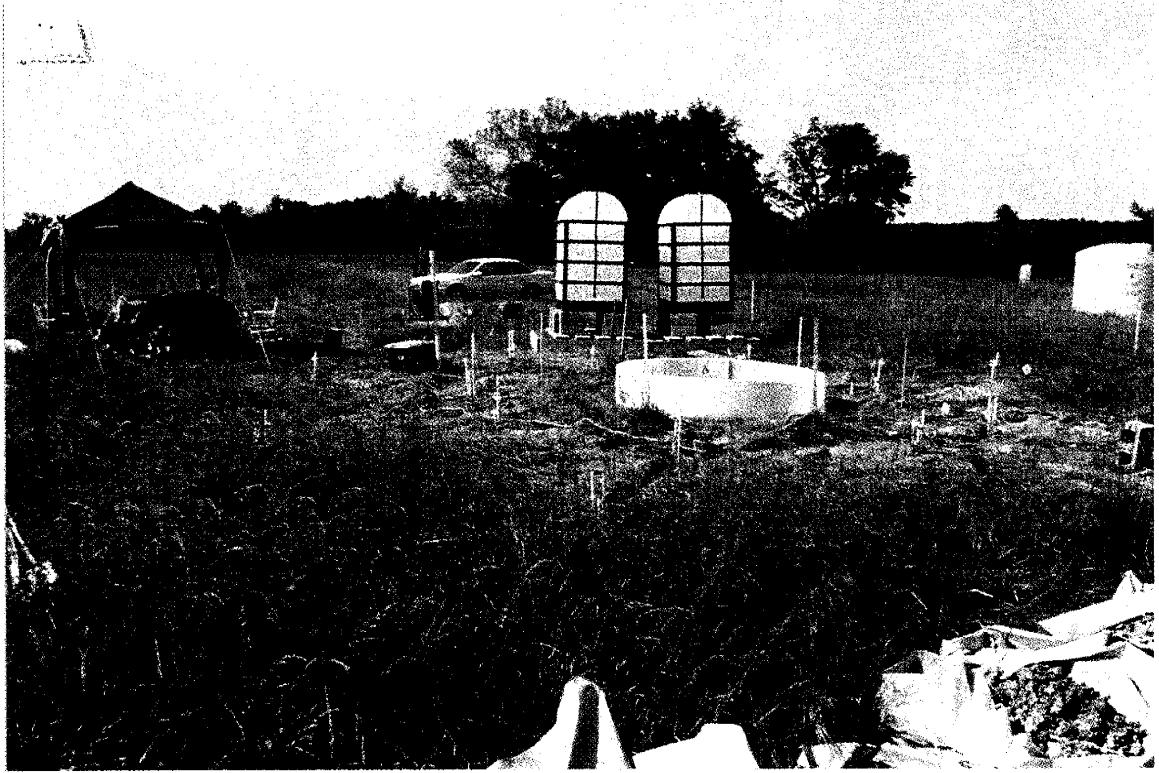


Plate 7. Site C, with instrument packs installed. Installed tensiometers (white piping) can be seen at sampling locations.



Plate 8. Installation of TDR and tensiometer transducer array. The traducer multiplexers and datalogger station is contained in the gray box with solar panel in center of picture. A TDR system is being assembled at left.



Plate 9. Site A with infiltrator ring, transducer, and TDR systems in place. The tensiometers at some sampling points have been covered with aluminized insulation. The two site supply tanks at left have not yet been plumbed to the infiltrator.

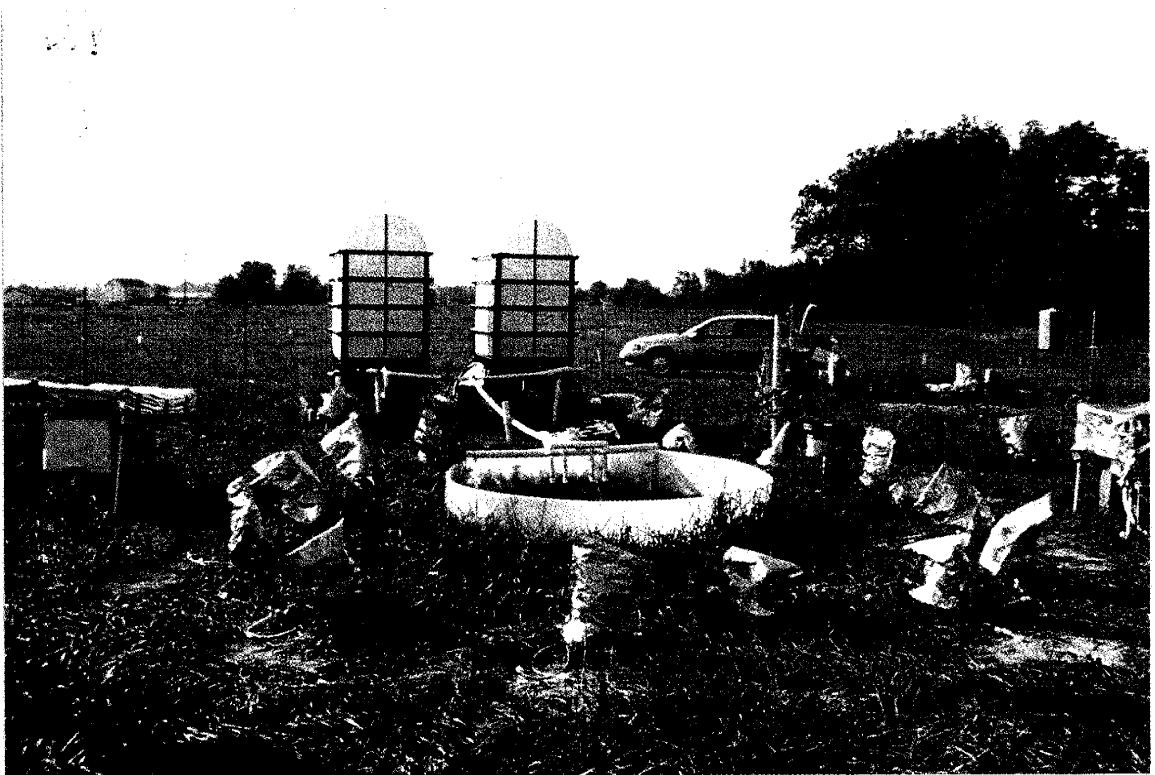


Plate 10. Site A, fully operational. Aluminum cloth sunscreens shield TDR stations at right and left from summer sun.



Plate 11. Water supply manifold from site supply tanks to the infiltrometer. Note the live grass in the infiltrometer after two months of constant infiltration, possible only if unsaturated conditions are present.

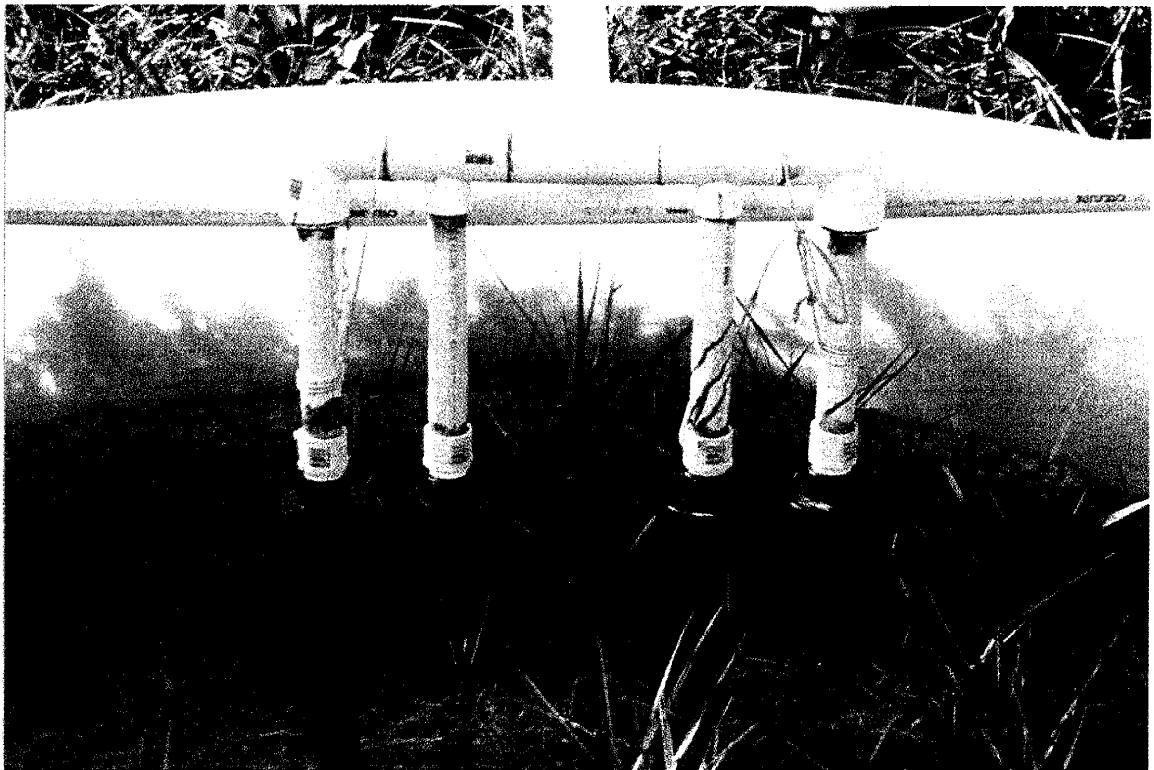


Plate 12. Close up of infiltrometer water supply manifold and float valves.



Plate 13. Start of Dye pulse into Site A on August 15, 1994. 400 gallons of dyed water was infiltrated.



Plate 14. Dye pulse spreading across infiltrometer.



Plate 15. Disassembly of Site A on the morning of August 22, 1994 after termination of dye pulse and infiltration.



Plate 16. Dye covering infiltrometer surface after removal of the infiltrometer ring.

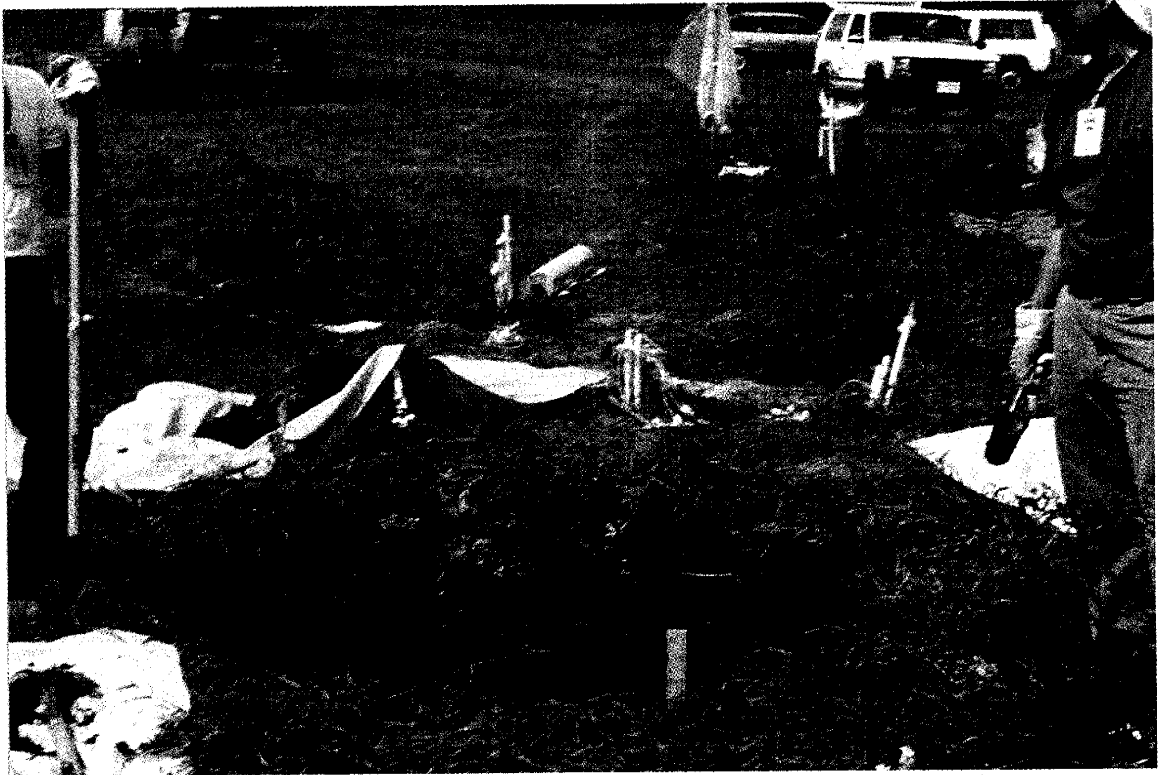


Plate 17 (above). Beginning hand excavation of infiltrometer surface.



Plate 18 (right). Hand excavation of south half of Site A infiltrometer surface.



Plate 19. Excavated south half of Site A infiltrometer surface. Note the preponderance of dye capture in the organic zone of the topsoil (Unit 5).

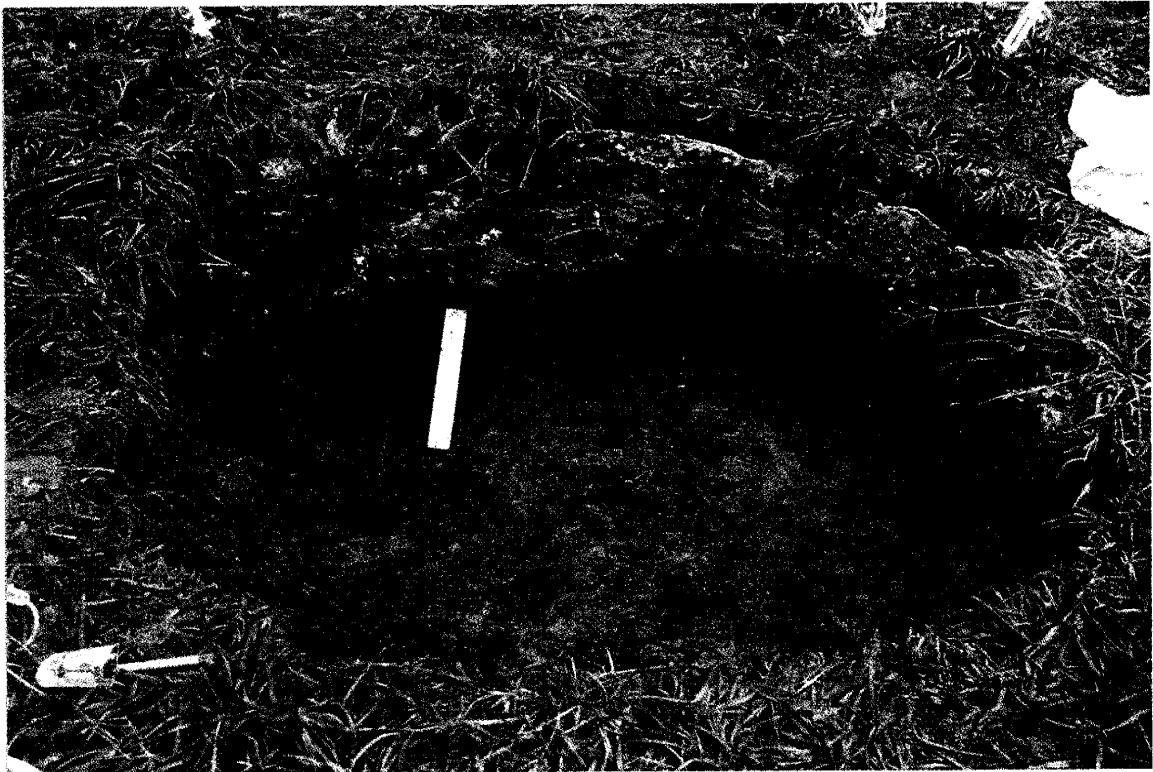


Plate 20. South half of Site A infiltrometer surface excavated to a depth of one foot. Note the dye capture in the organic zone and topsoils (Unit 5) and the preferential movement into the beginning of the blocky structured silty clays (Unit 4).

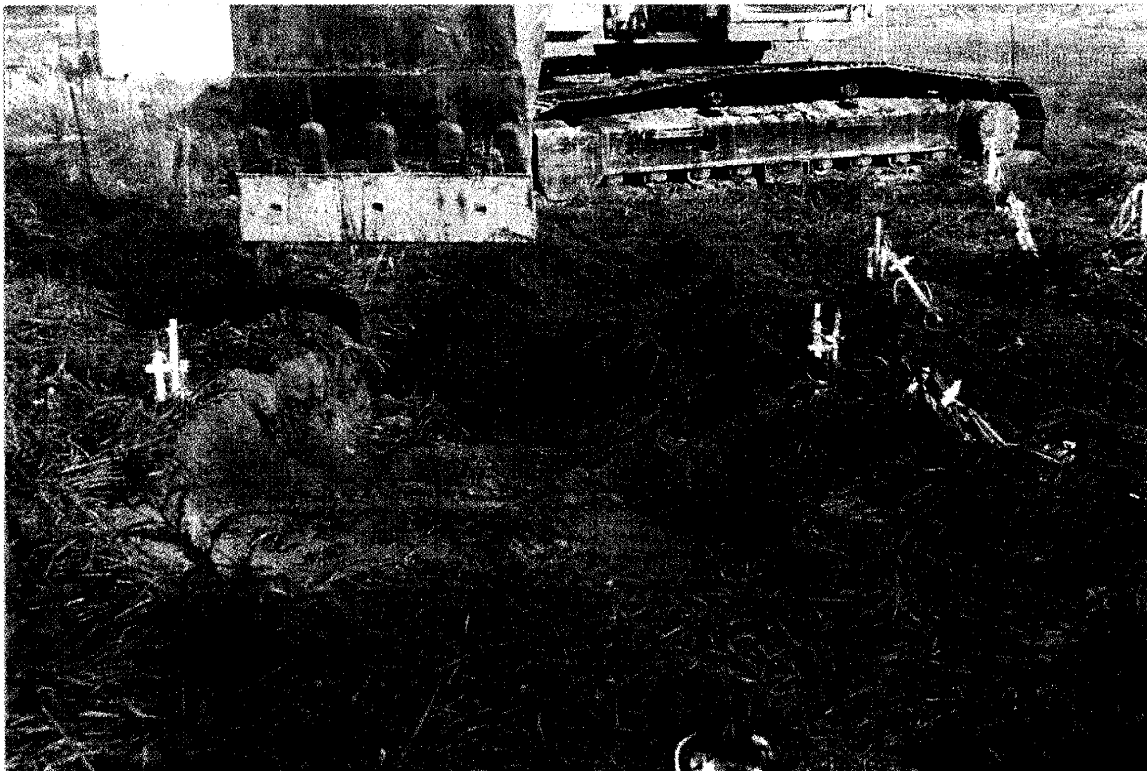


Plate 21. Beginning of trench between inner and outer rings of the instrumentation array (refer to Figure 3). Morning of August 23, 1994.



Plate 22. Back hoe trenching between inner and outer sampling rings.



Plate 23. Completed 1.2 m deep trench between inner and outer sampling rings (See Figure 3). No dye was found on the inner or outer walls or the bottom of this trench.

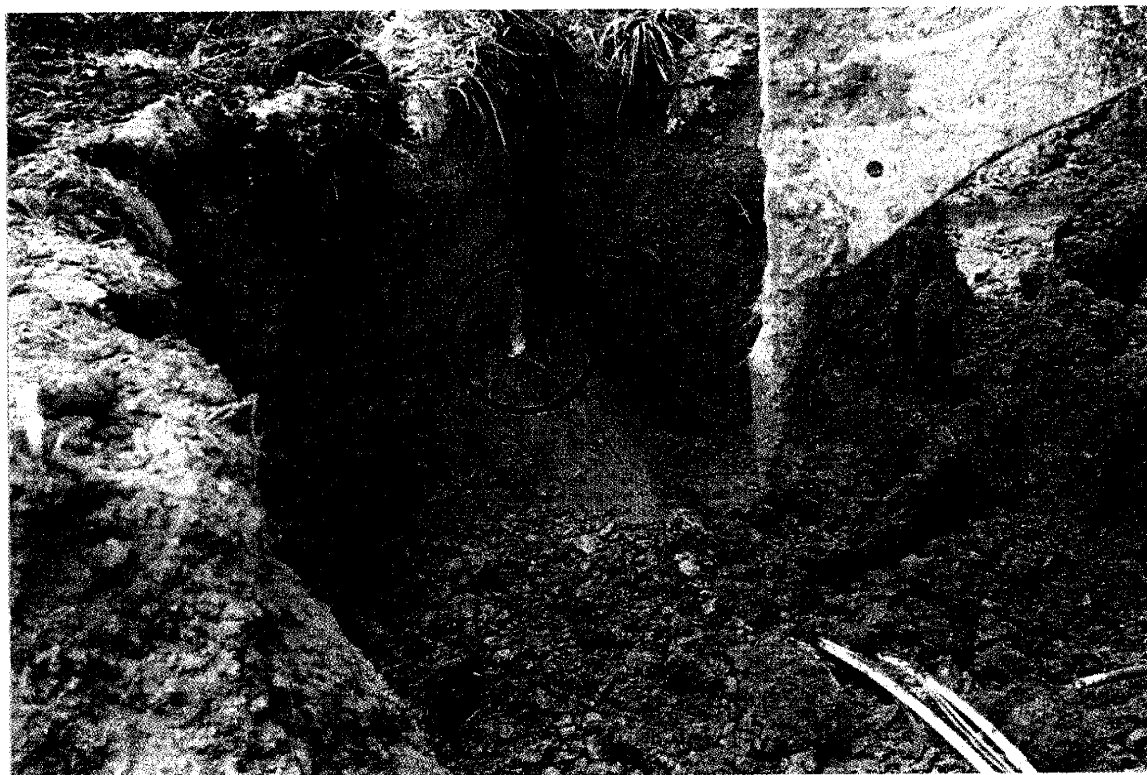


Plate 24. Enlargement of the trench towards the infiltrometer surface. An angled instrument hole showing the light bentonite filler and blue sampling tubes is circled

Plate 25 (right). Beginning of the excavation of the pillar under the infiltrometer.

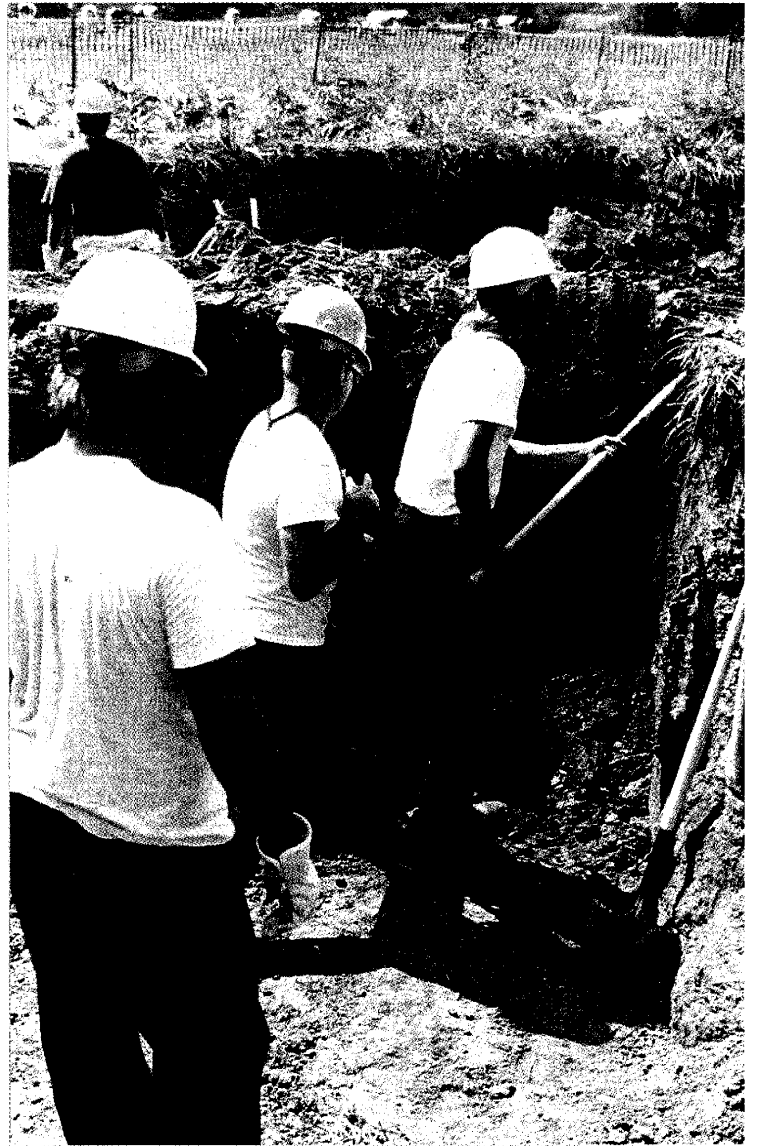


Plate 26 (below). Back hoe excavation between the infiltrometer and the outer sampling ring.





Plate 27(above). Remaining pillar under the infiltrometer surface. The white feature at the bottom center of the infiltrometer is the top of the sand pack of sampling point A35-A2L.

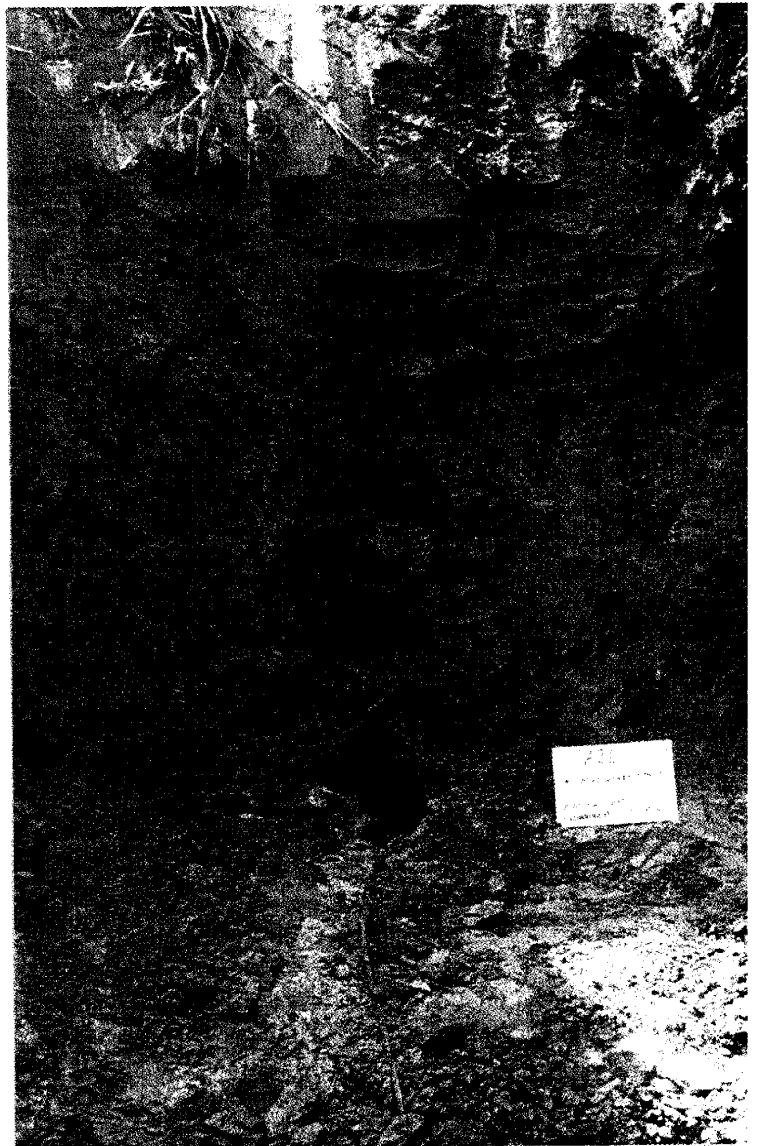


Plate 28 (right). Dye stained matrix following worm hole transport pathway to sampling point A35-A2L.

Plate 29 (right). Wormhole filled with red dye excavated in pillar under infiltrometer surface.



Plate 30 (below). Wormhole filled with red dye intercepted by sampling point A35-A2L. The Cl⁻ tracer pulse arrived in forty-two minutes and in high concentration at this sampling point 2 m below the infiltrometer.

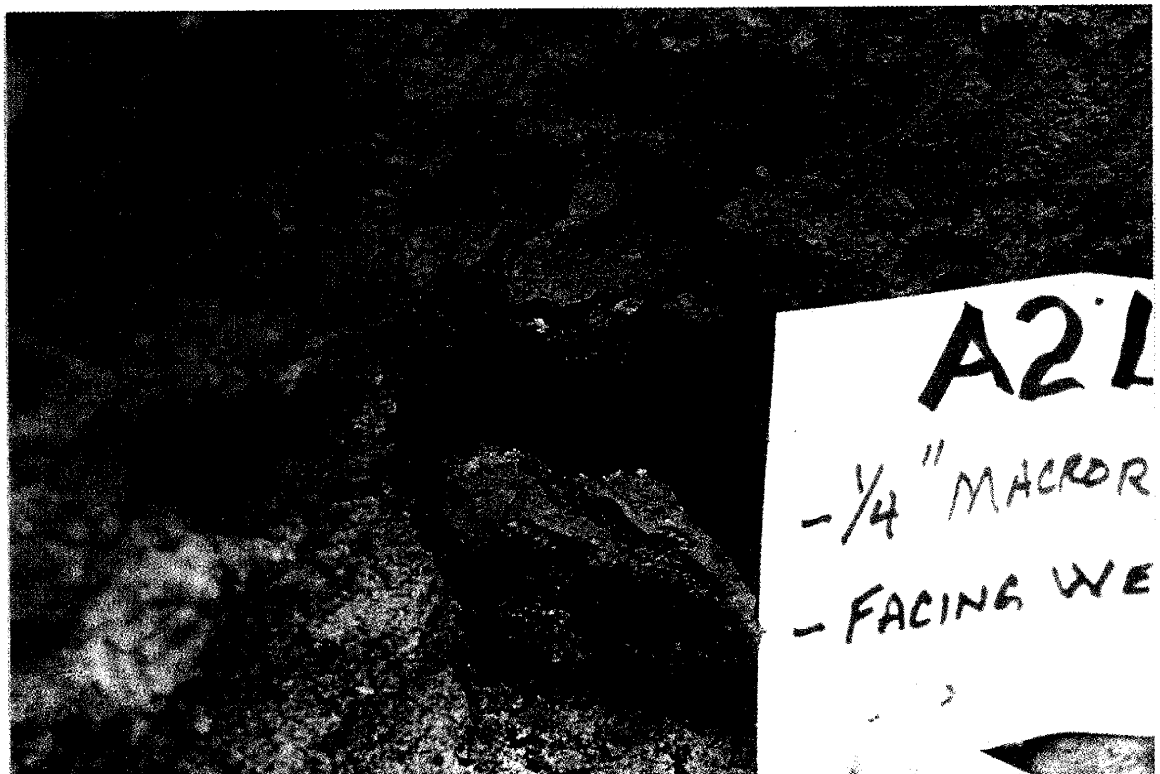


Plate 31 (right). Active root and worm holes through Unit 4 in the pillar underneath the infiltrometer.

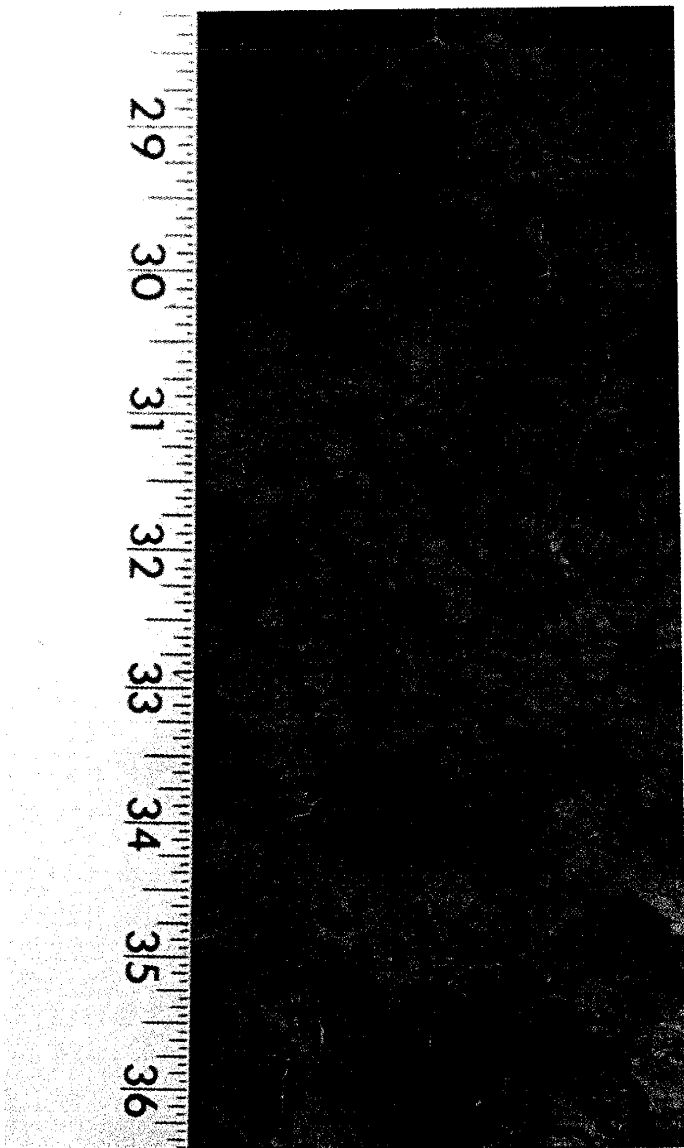
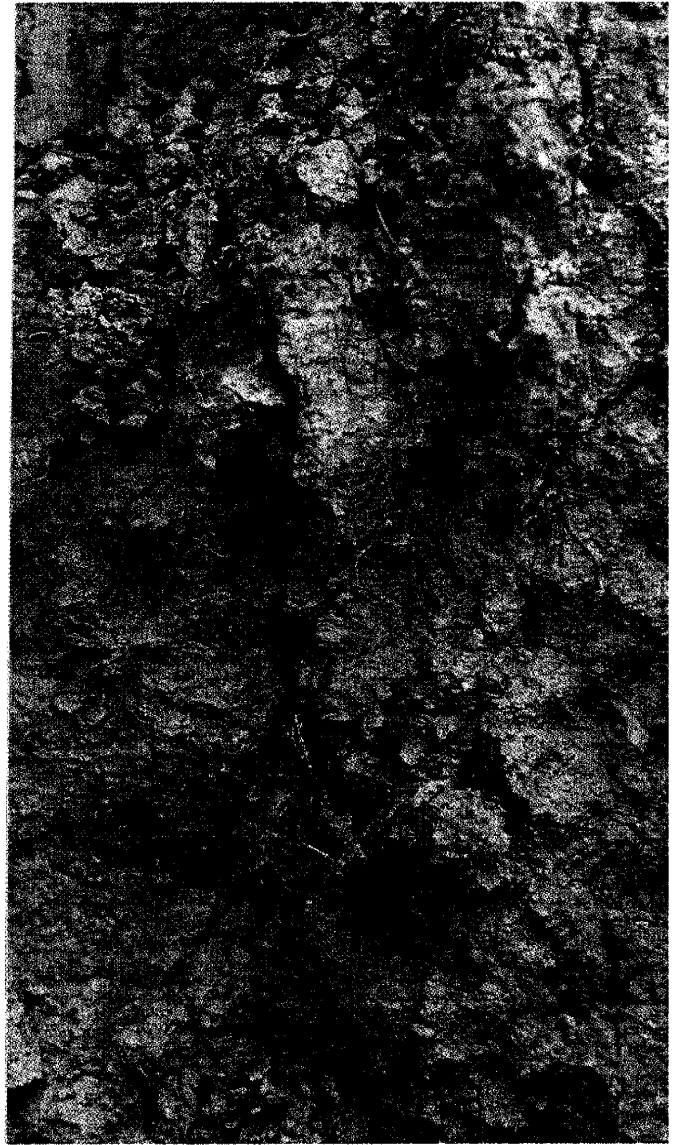


Plate 32 (left). Active root holes and fractures in Unit 4.



Plate 33 (left). Excavation of the pillar under the infiltrometer showing dye stained fracture surfaces.



Plate 34. Dyed matrix surrounding root hole.

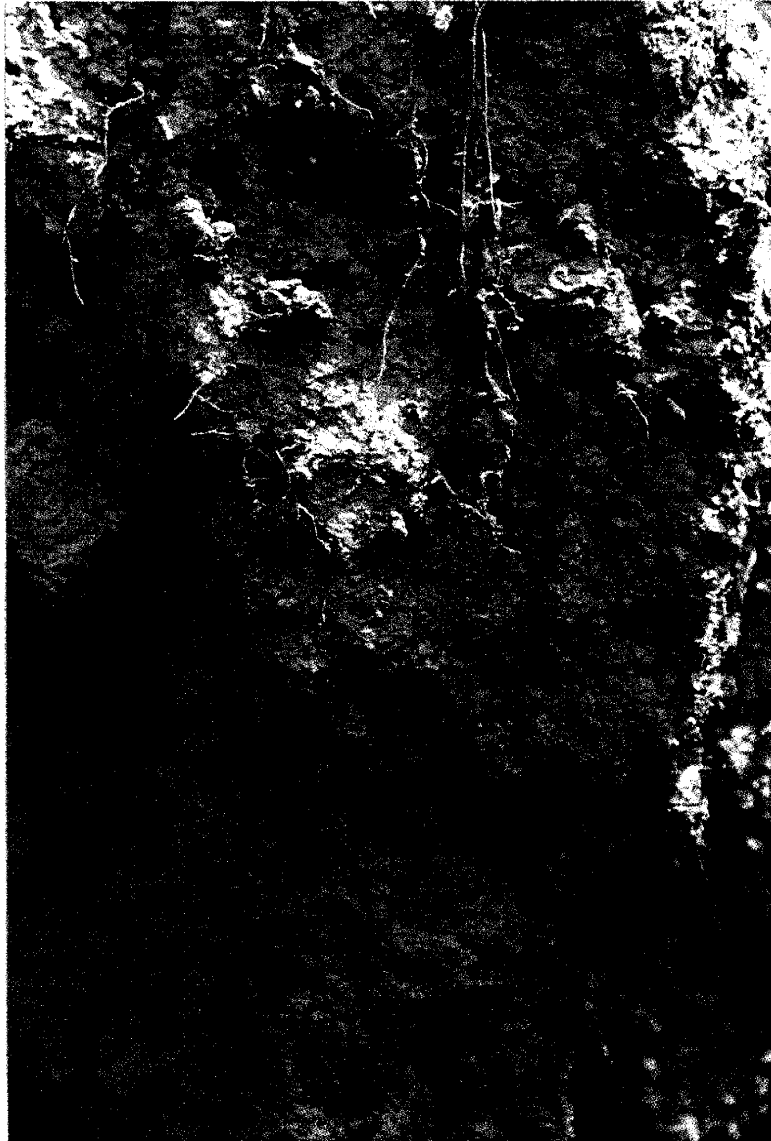


Plate 35. The burrow at the top of the photo is a 2 cm x 3 cm crayfish burrow .3 m below surface in pillar beneath infiltrometer.

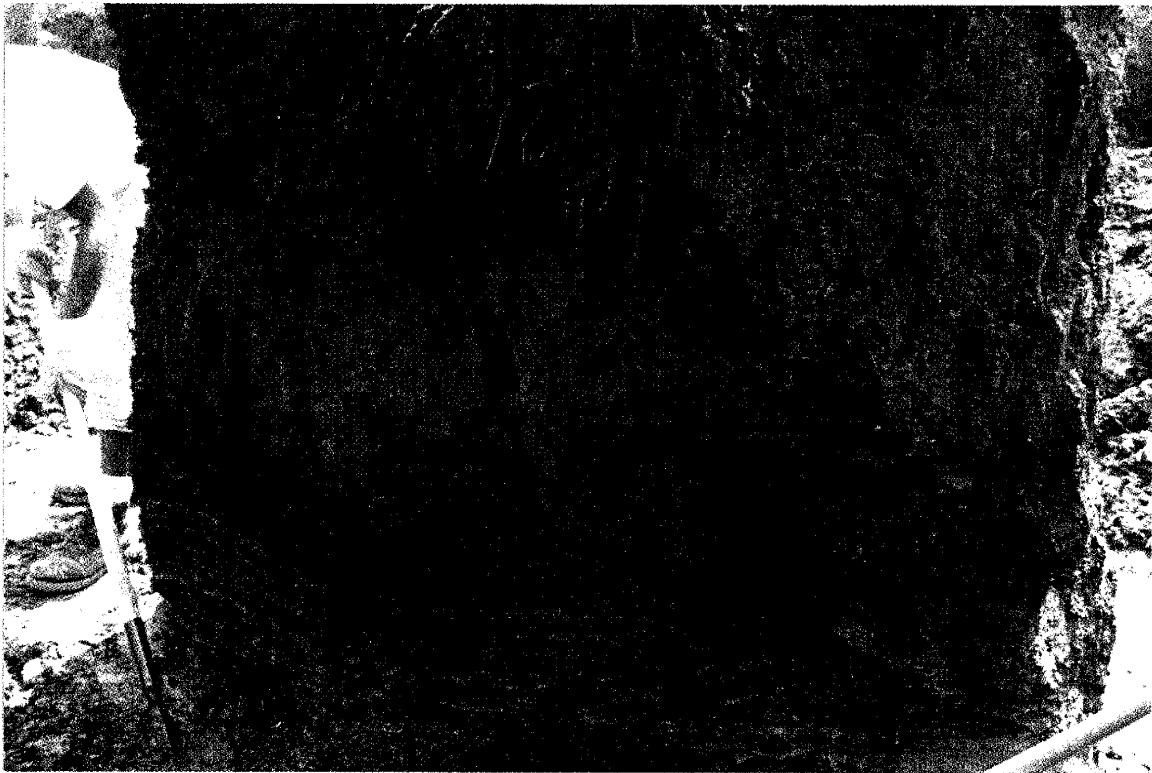


Plate 36 (above). Preferential flowpaths in pillar beneath infiltrometer. Note light colored bands of carbonate deposits at base of pillar (Unit 3).

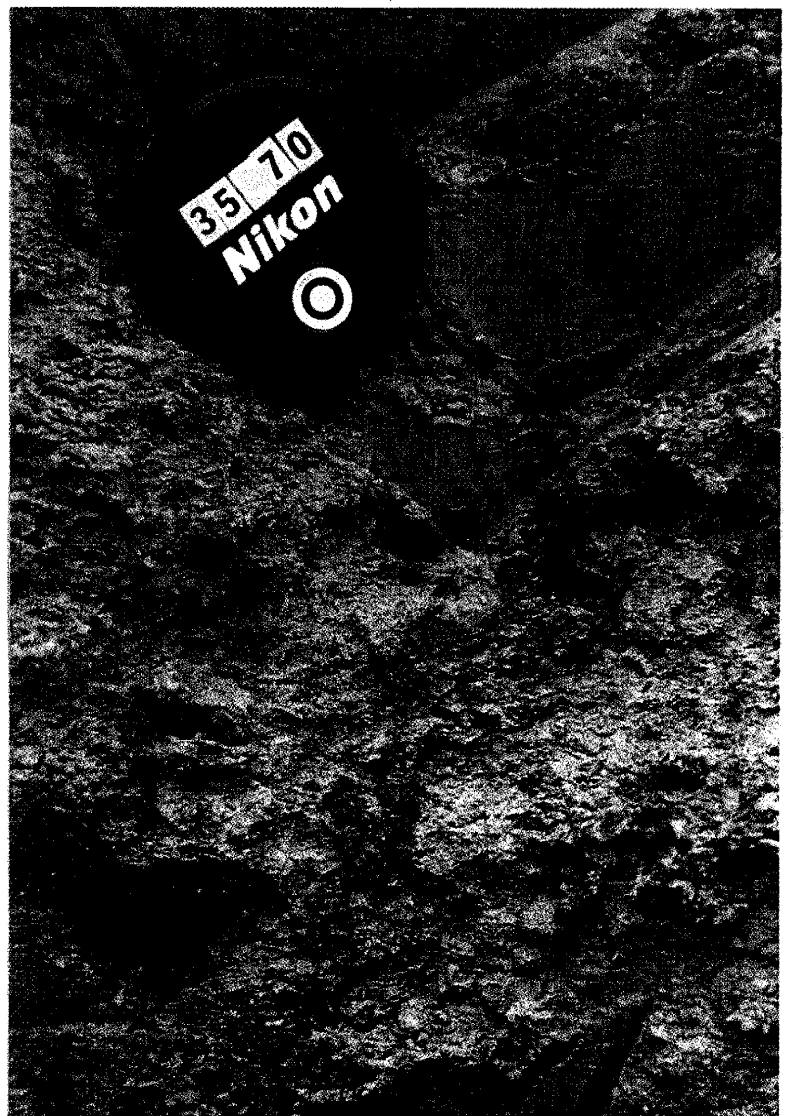


Plate 37 (right). Stained root holes and matrix in Unit 4.

Plate 38 (right). Dye flow along fracture planes, roots holes in Unit 4 beneath infiltrrometer pillar.



Plate 39 (below). Macropore in Unit 5 just beneath infiltrrometer surface.

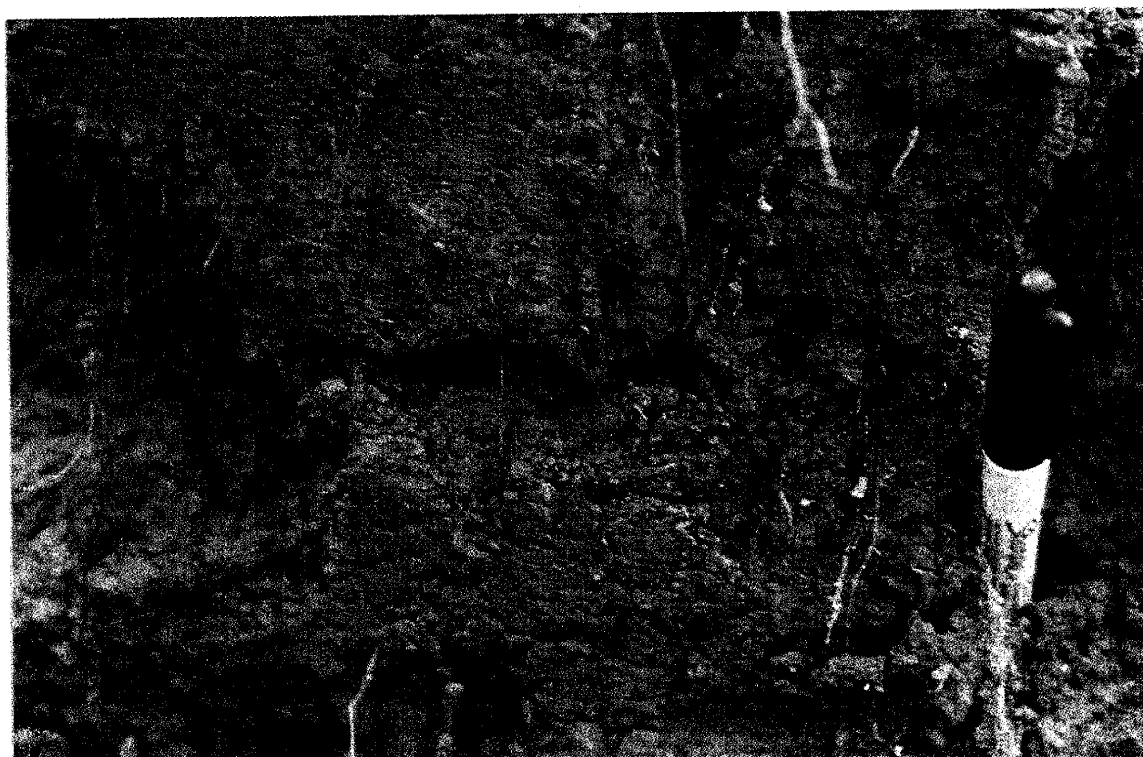




Plate 42. Morning prayers led by Keith The Lugubrious.



Plate 43. Back hoe excavation and sloping of pit sides.

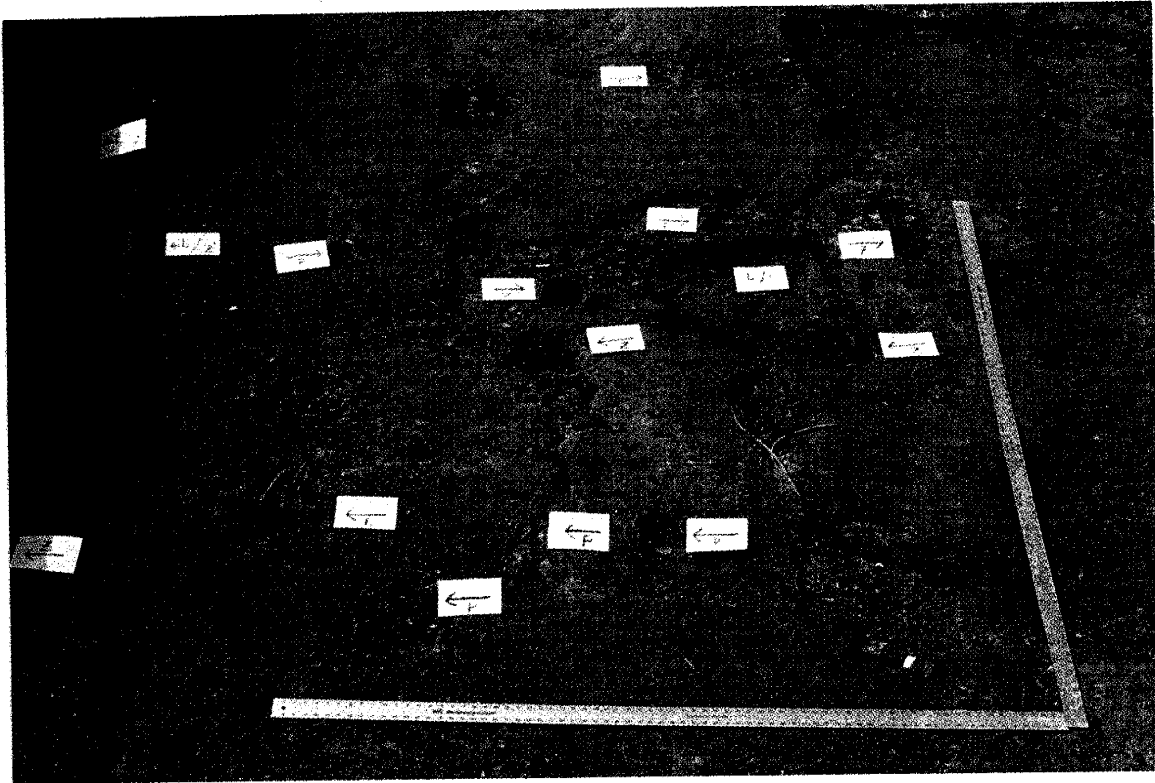


Plate 44 (above). 4" x 6" note cards indicate macropores, sandy zones of preferential flow and active fractures at approximately 2.2 m depth in oxidized layered clays of Unit 3.

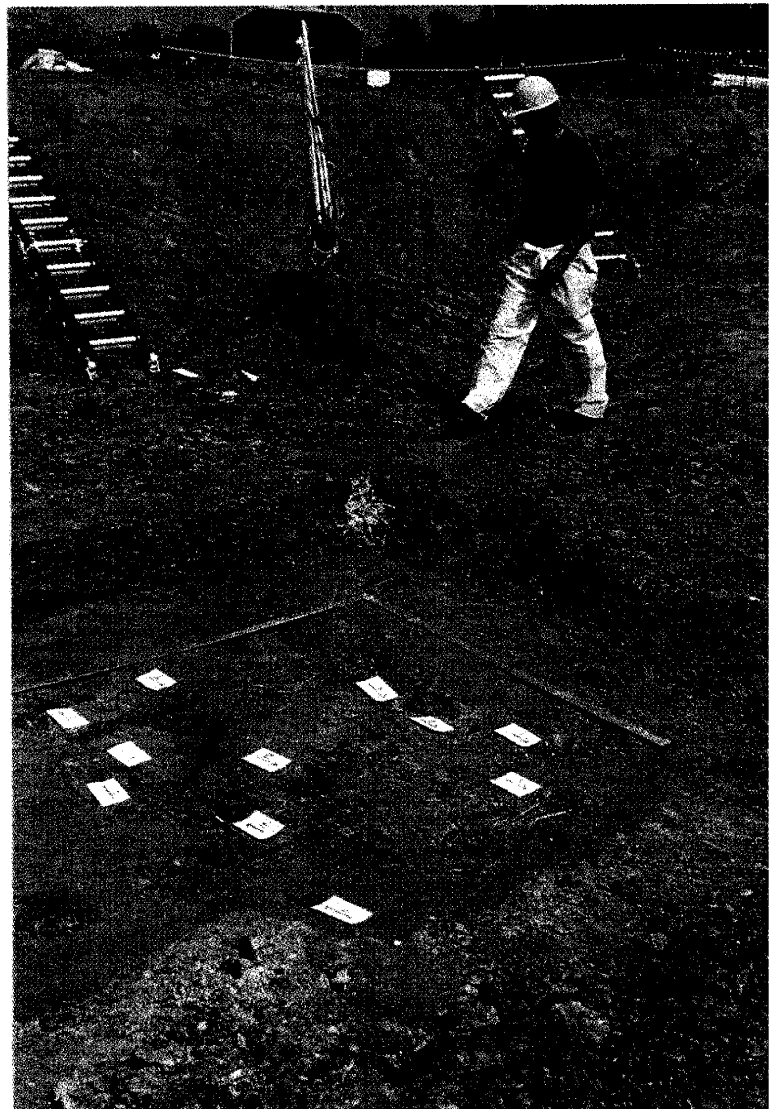


Plate 45 (right). Macropores, zones of preferential flow and active fractures at approximately 2.2 m depth in oxidized layered clays of Unit 3.

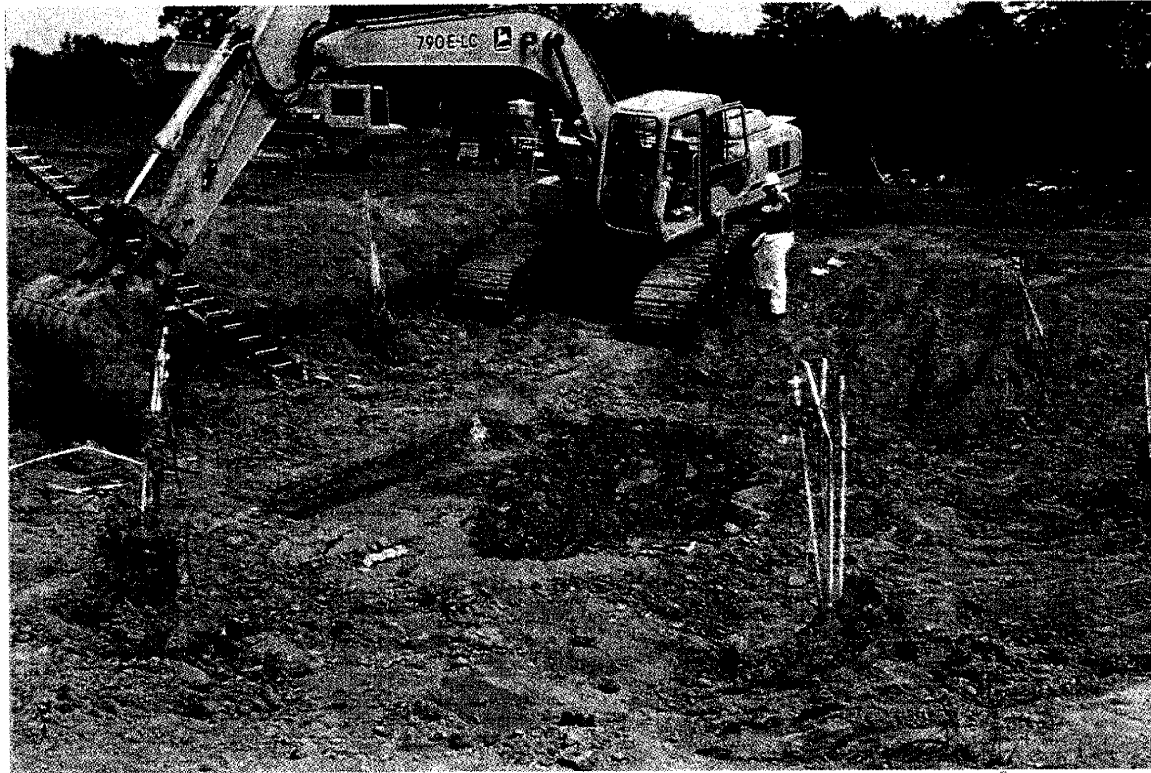


Plate 46. Widening and deepening of excavation.

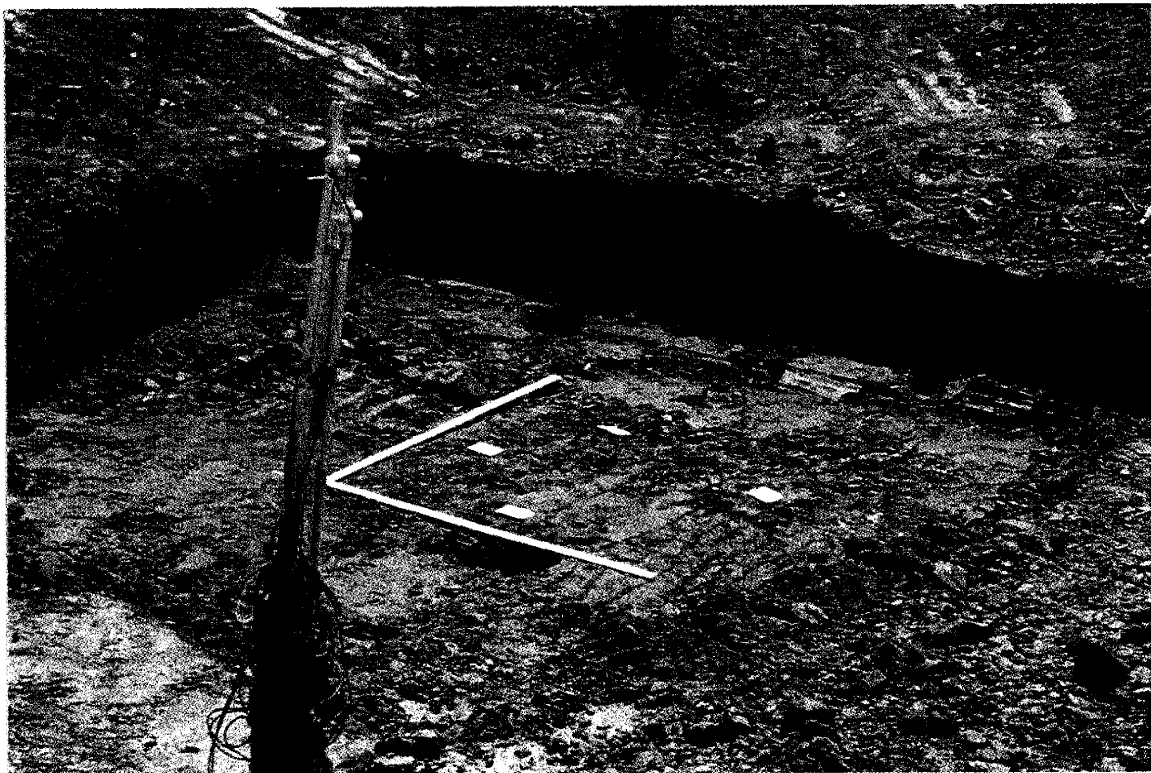


Plate 47. Note cards indicate macropores, fractures, and sandy inclusions at approximately 2.5 m depth. Note the layered oxidized clays and carbonate layers.



Plate 48. Deepening excavation to the top of Unit 2, layered unoxidized clays.

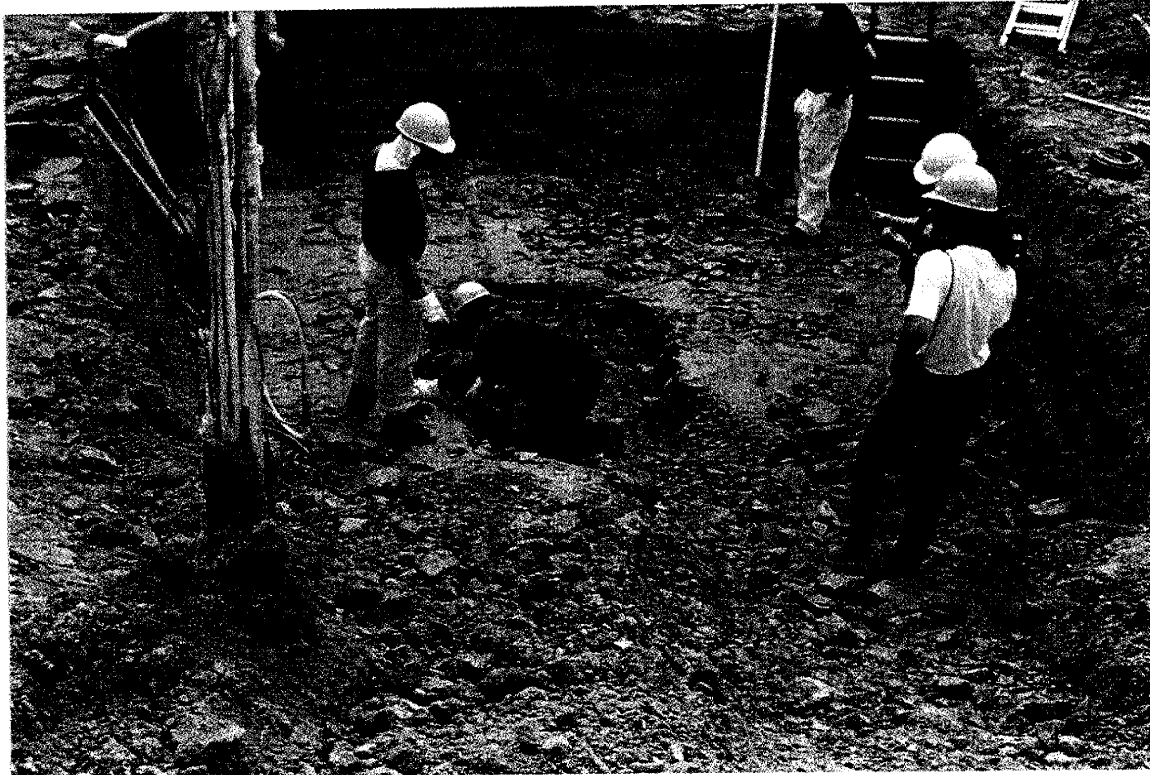


Plate 49. Hand excavation into the unoxidized, layered clays of Unit 2. The PVC tubing and cables of both an upper and lower sampling point are visible to the left. Note the bentonite seal at the base.

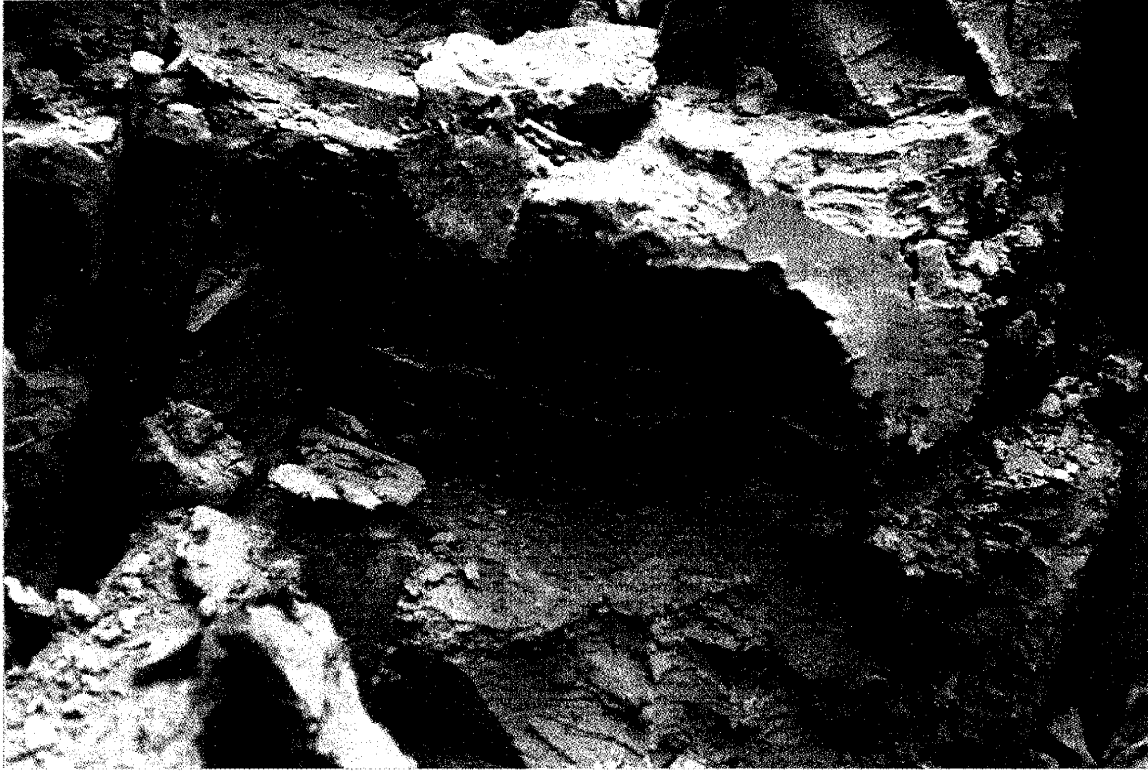


Plate 50. Oxidized vertical fracture surface in the unoxidized layered clays of Unit 2.



Plate 51. Unoxidized layered clays of Unit 2. Note the oxidized fracture surfaces and bedding planes.

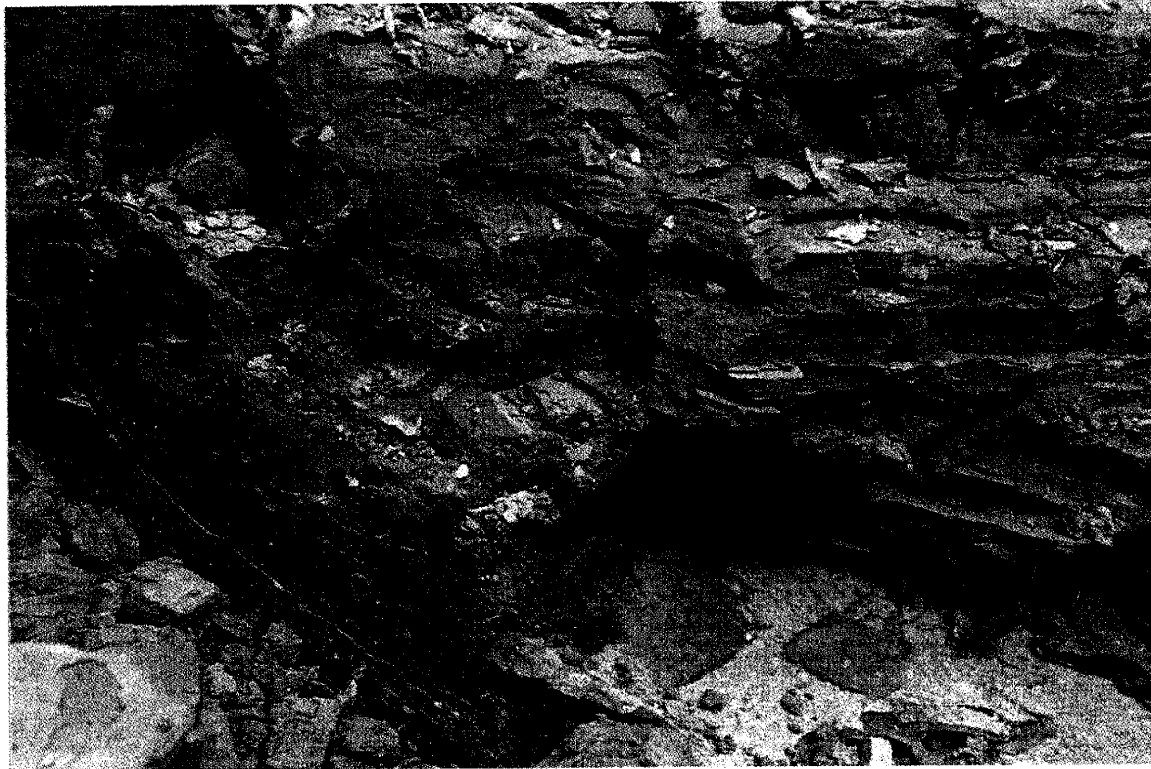


Plate 52. Tight beds in the layered unoxidized clays of Unit 2. A sand inclusion is visible in the lower center of the plate.



Plate 53. Deformation features in the massive unoxidized clays of Unit 1.

Plate 54 (right). Large vertical and horizontal fractures in layered oxidized clays of Unit 3.

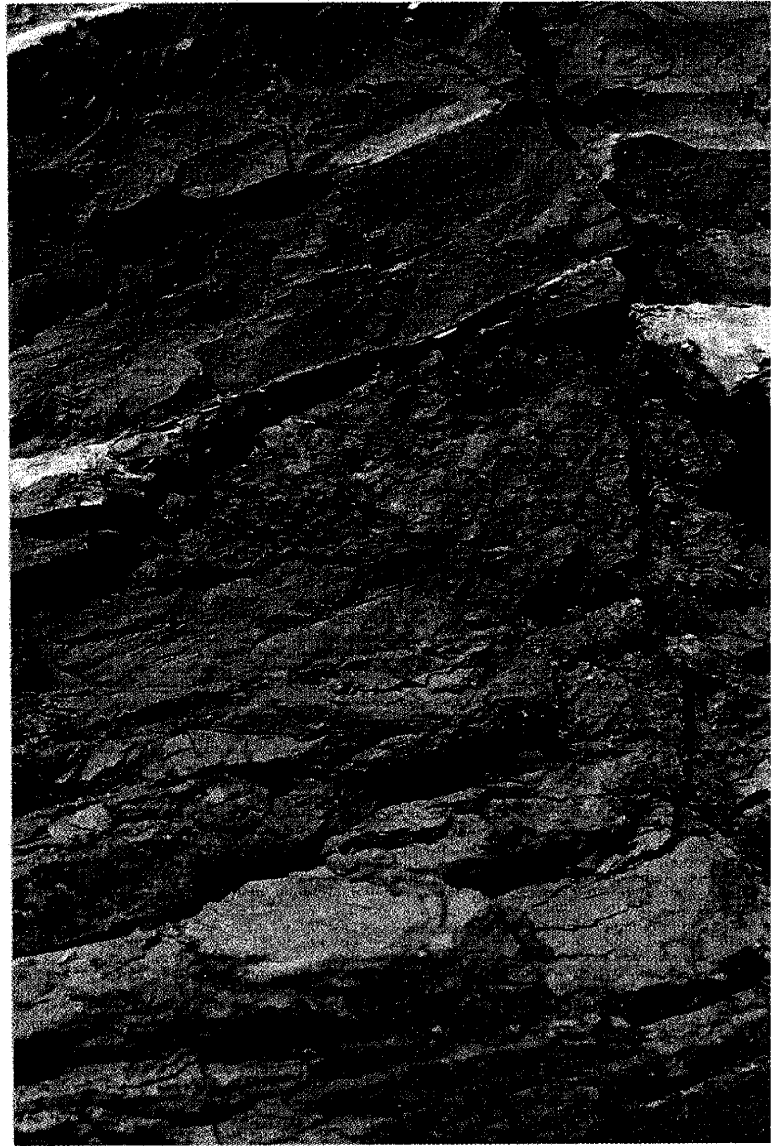


Plate 55 (below). Dye pit at top of Unit 1 (massive unoxidized clays). Depth approximately 3.2 m.



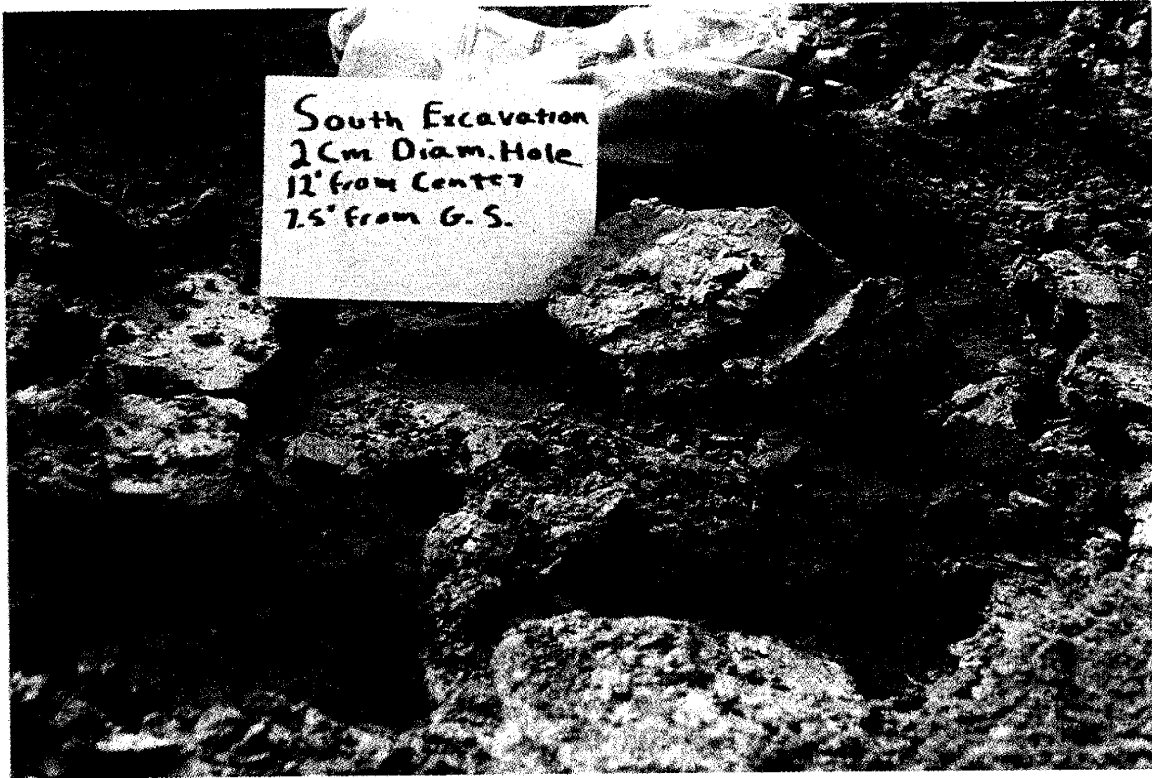


Plate 56. Crayfish burrows at south end of excavation.

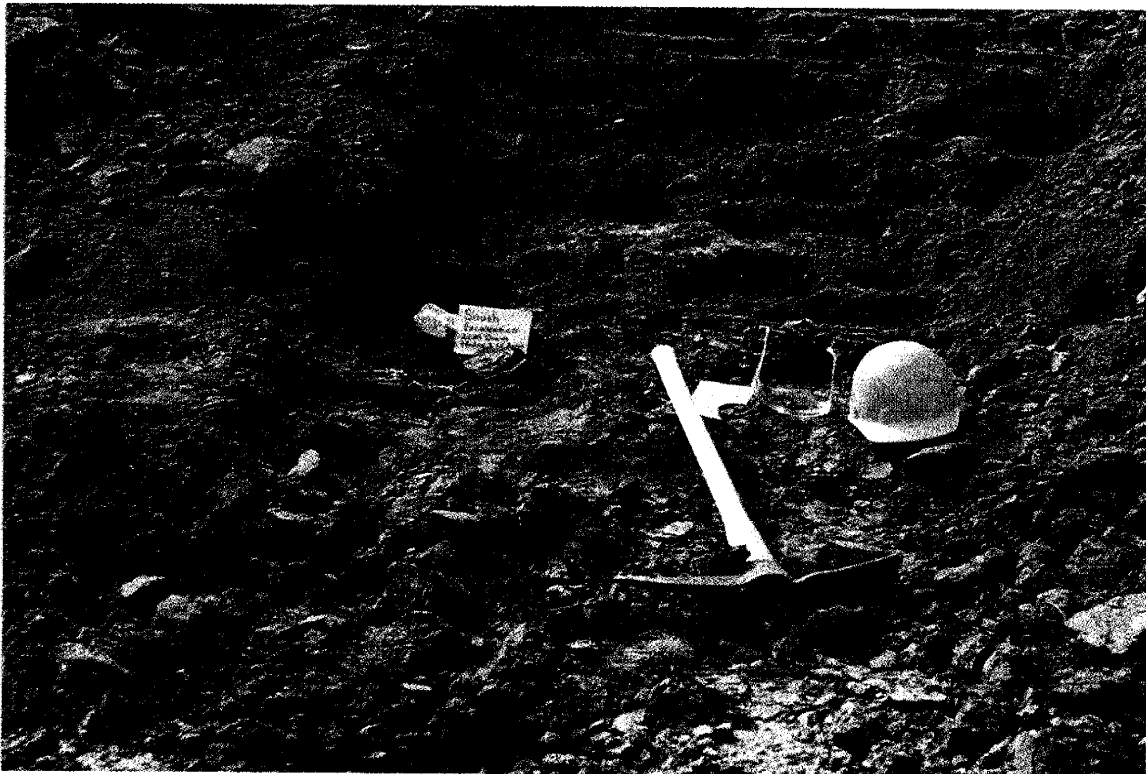


Plate 57. Hand excavated transect through strata at south of excavation.

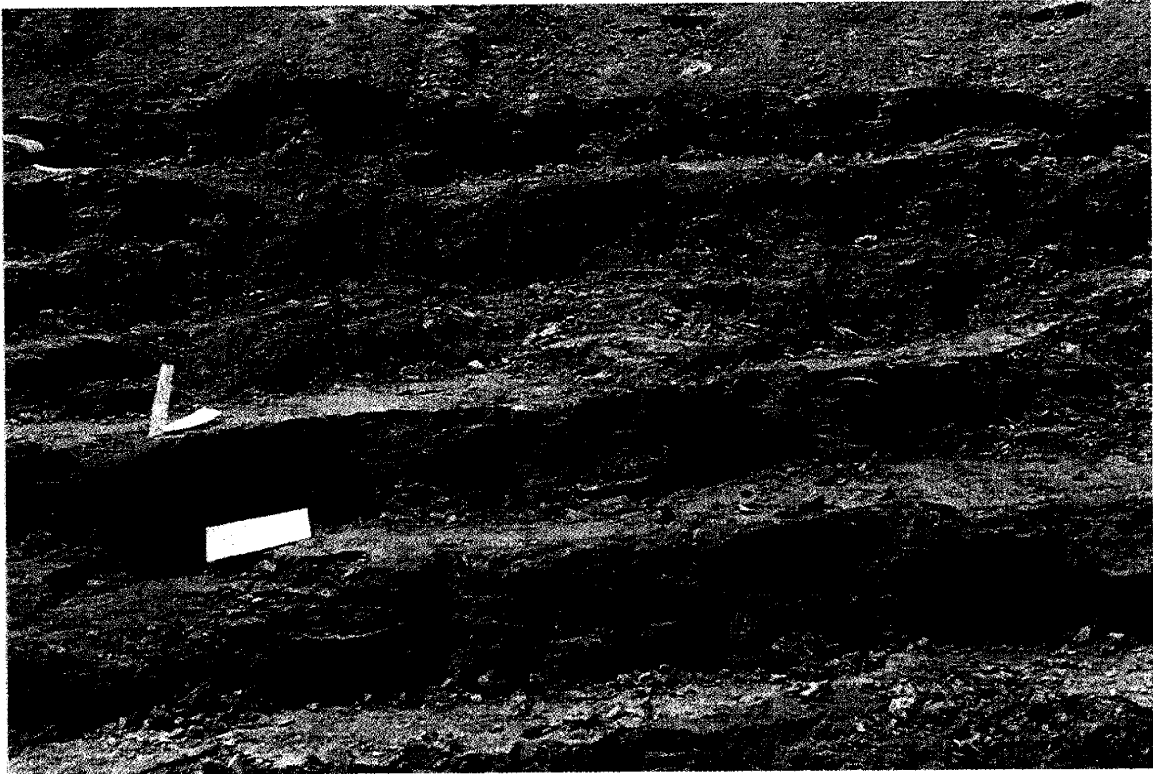


Plate 58. Terraced hand excavation of sloping sides of excavation.



Plate 59. Back hoe excavation and sloping of sides. The blue tarp was put in place to prevent movement of the remnants of the dye pit.

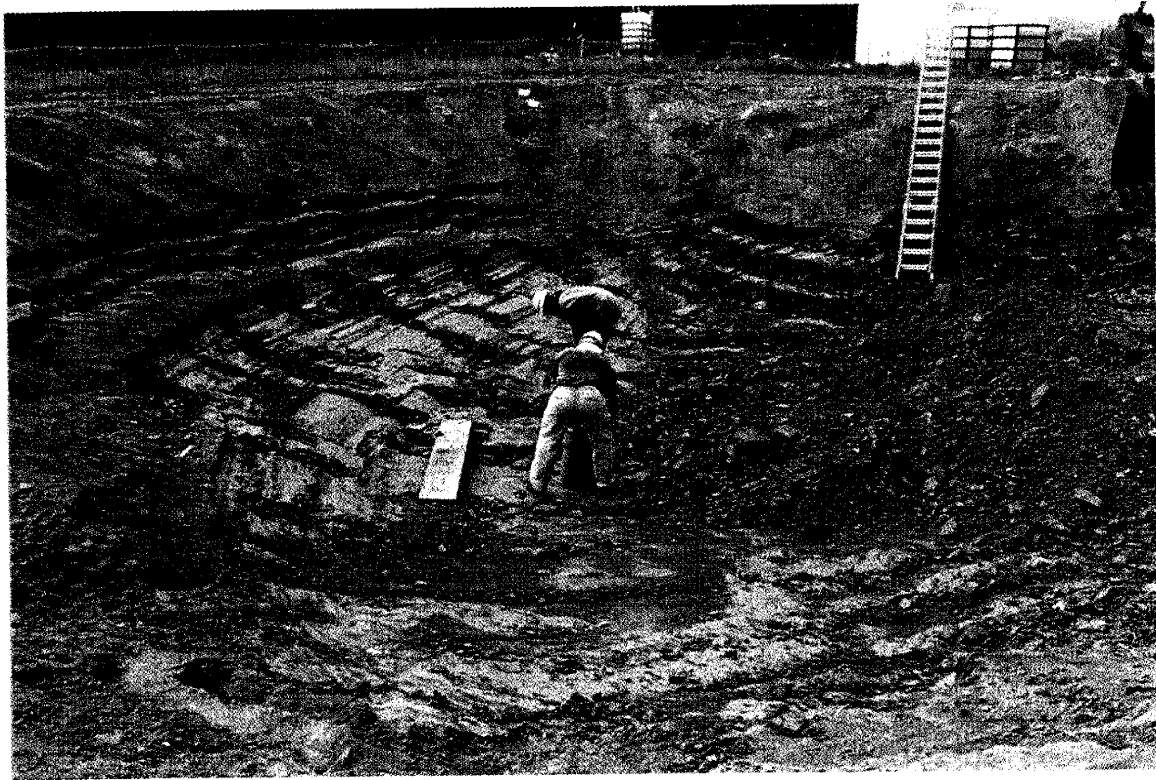


Plate 60. Placing 12" plastic pipe used in obtaining cores from Unit 2.



Plate 61. Back hoe used to press pipe into media for core samples.

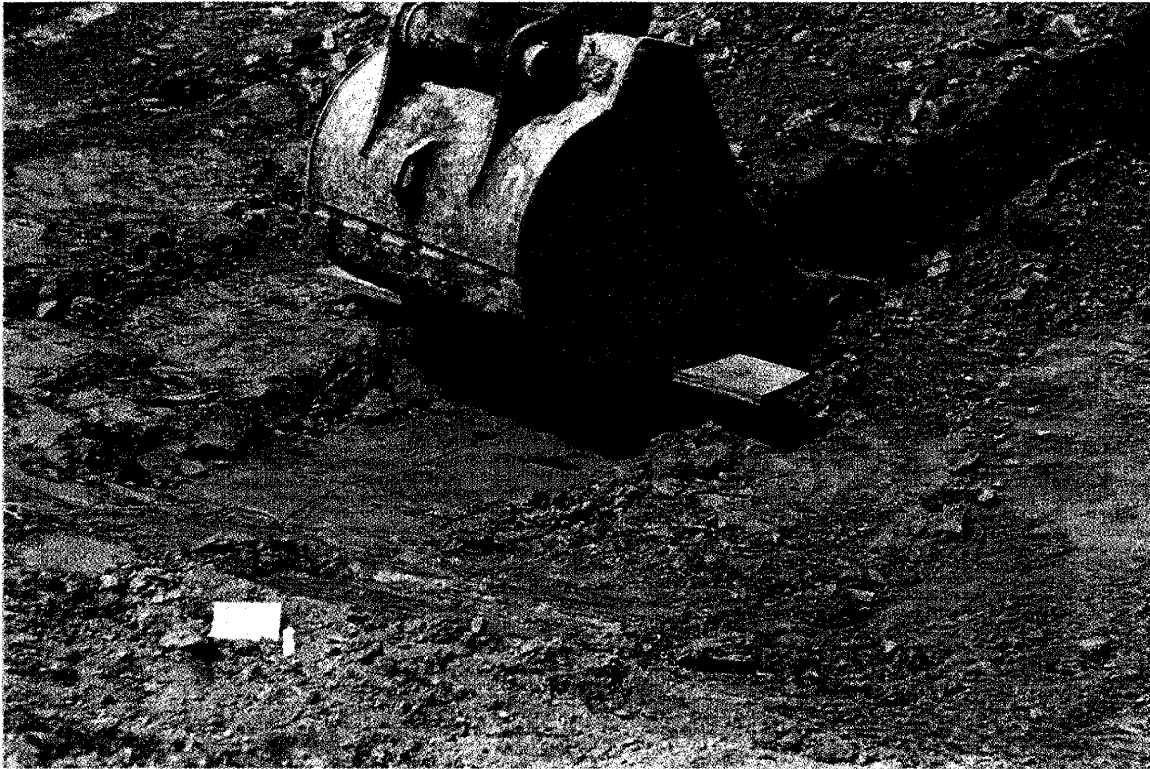


Plate 62. Pipe pressed into clays to obtain "undisturbed" samples.

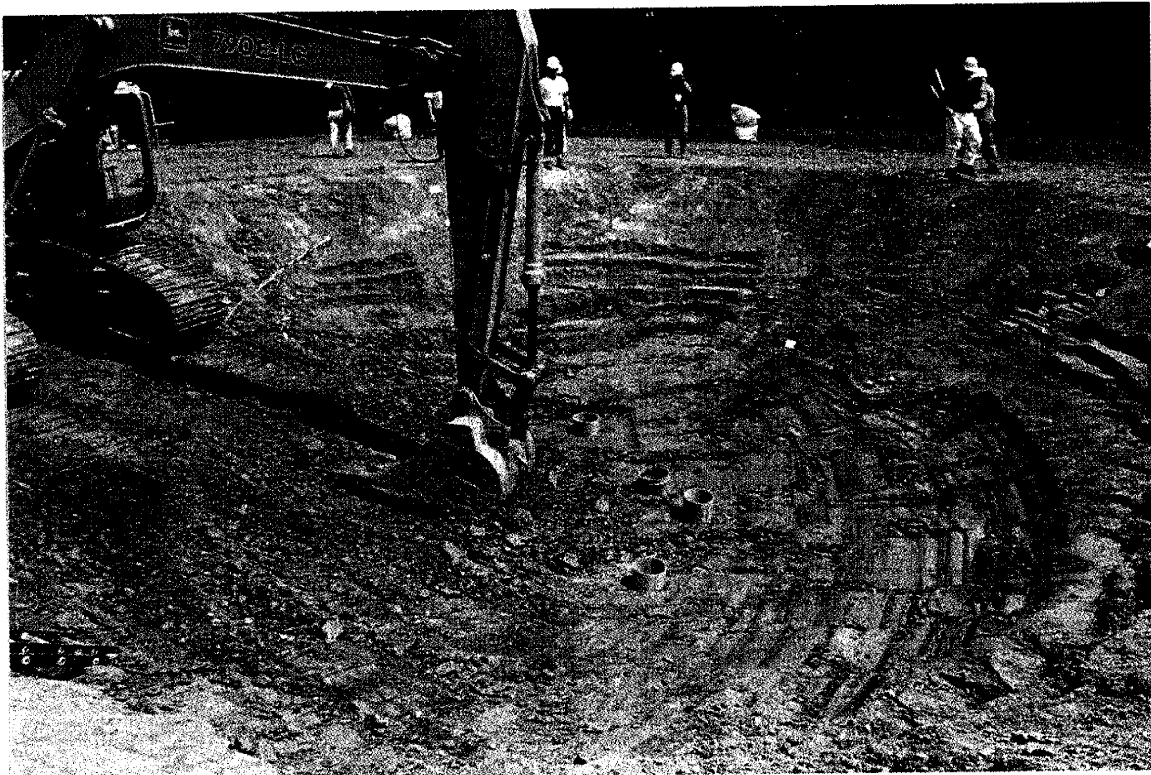


Plate 63. First four cores in place.



Plate 64 (above). Close up of first four cores before removal.



Plate 65 (right). Back hoe removing core samples.



Plate 66 (above). Core removed from Unit 2. Beds and laminations are obvious.



Plate 67 (right). Excavation after core samples removed.

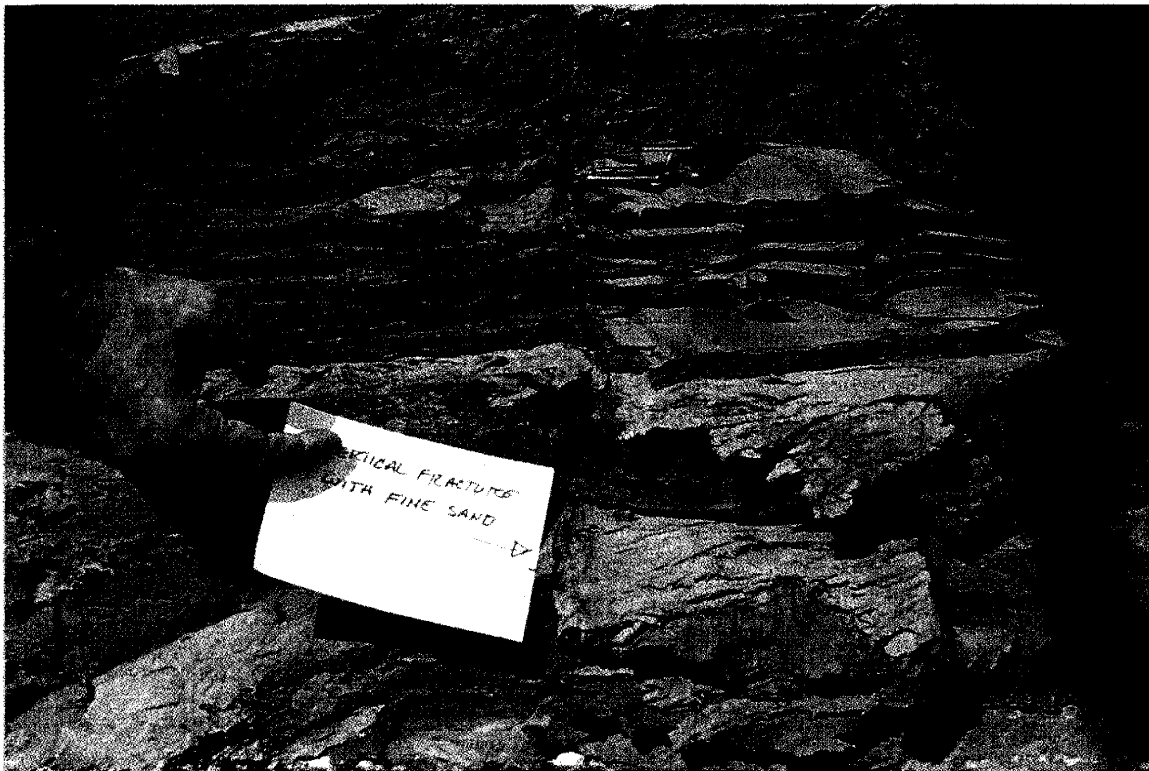


Plate 68. Vertical fracture in Unit 2 filled with fine and medium sands. Found during hand excavation of Unit 2 (layered unoxidized clays) in the SW quadrant of the site.



Plate 69. Deepening and widening the excavation, morning of August 26, 1994.



Plate 70. Hand terracing of sloped excavation sides.

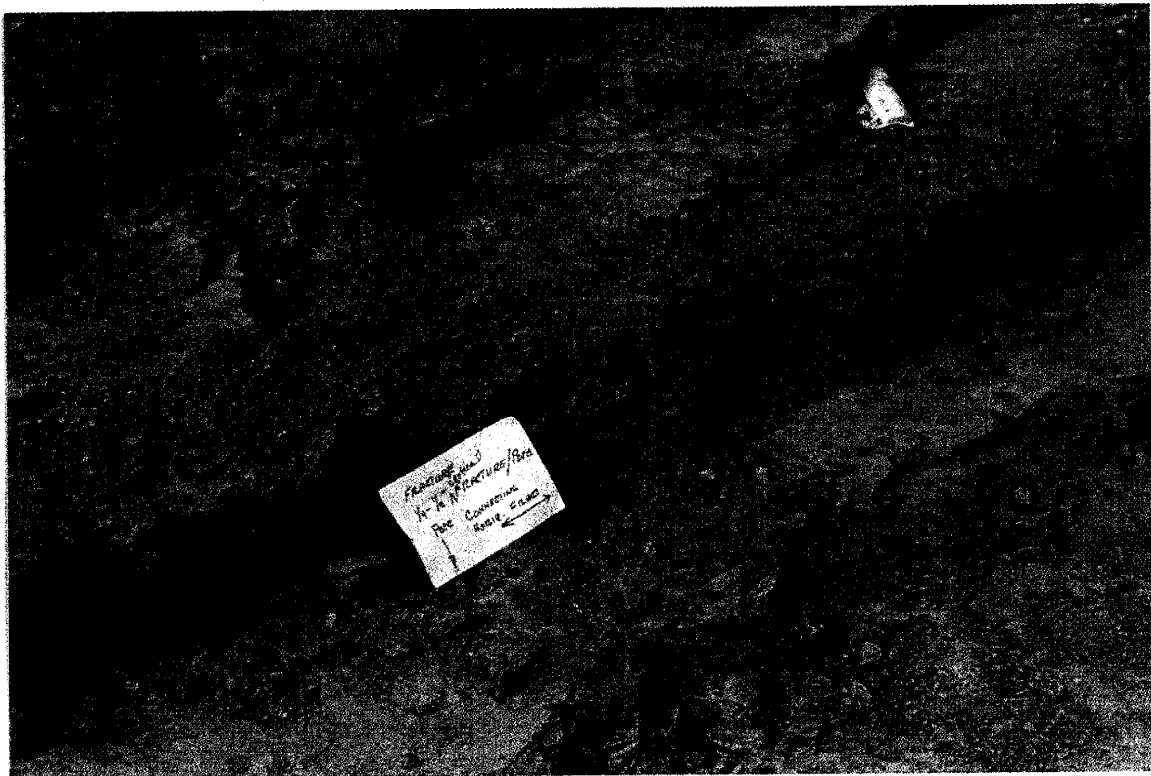


Plate 71. Active fractures and crayfish burrows in Unit 3. Depth approximately 2.3 m. The burrows appeared to follow pre existing fractures and bedding planes.



Plate 72. Mud crack casts in oxidized, layered clays of Unit 3.



Plate 73. Pink dyed fractures between the beds of Unit 2 (unoxidized layered clays). Depth approximately 3 m.



Plate 74. Close up of the large silty sand body in the NW quadrant of the site.



Plate 75. Large filled macropore in the silty sand body in the NW quadrant of the site. The pore is between the 4" x 6" note card and the film container cap.

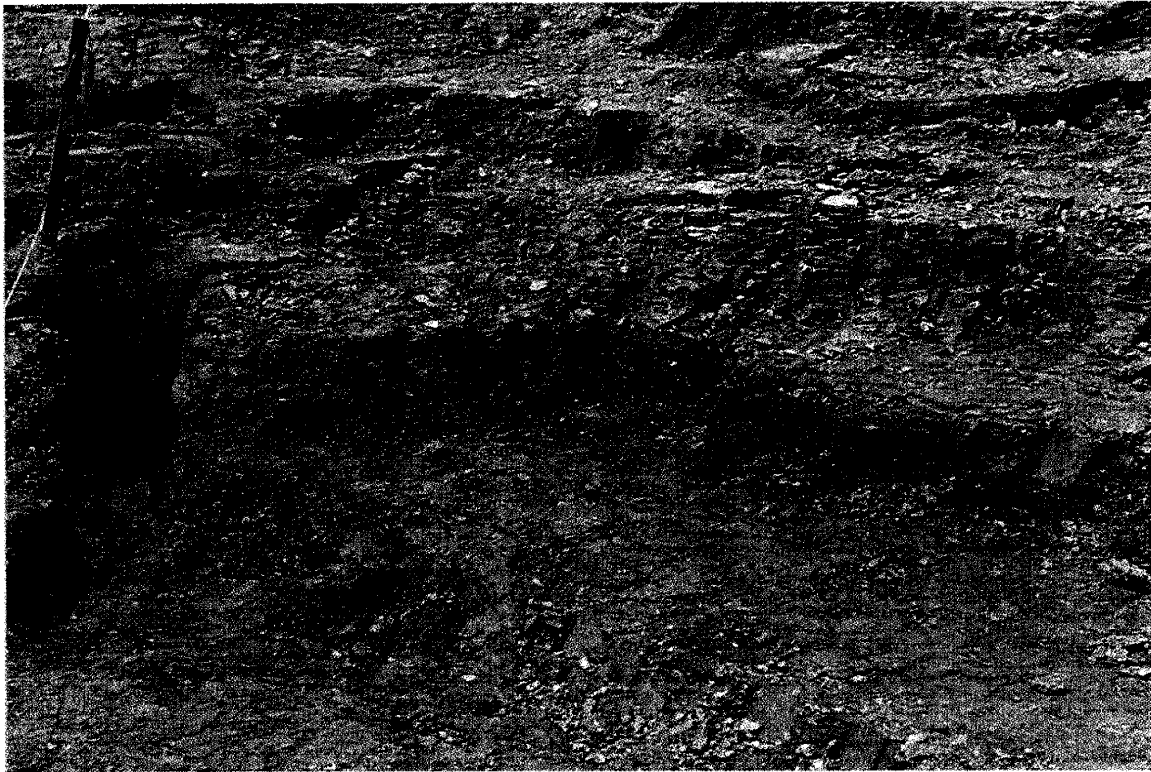


Plate 76. Facing west. The silty sand body in the center of the photo is seen wedged between clays of Unit 4 above and Unit 3 below.



Plate 77. Pink dye (lower right center) can just be seen in the bottom of the trench at sampling site A28-7OL at the far west of the site. The water was moving through a sand stringer originating in the silty sand body in the NW quadrant.

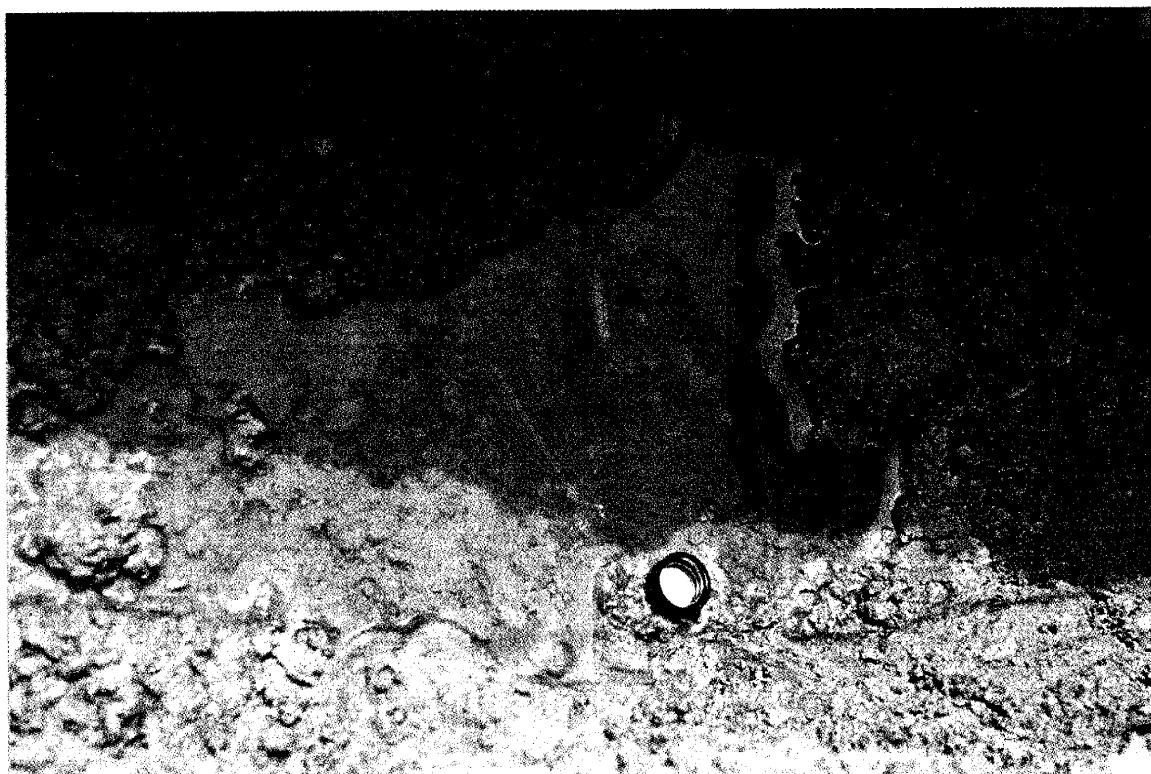


Plate 78 (above). Close up of the pink water emerging from the sand stringer at sampling site A28-7OL.



Plate 79 (right). Beds of Unit 3 (oxidized layered clays). Slightly dyed carbonate deposits can be found between beds and in fractures.

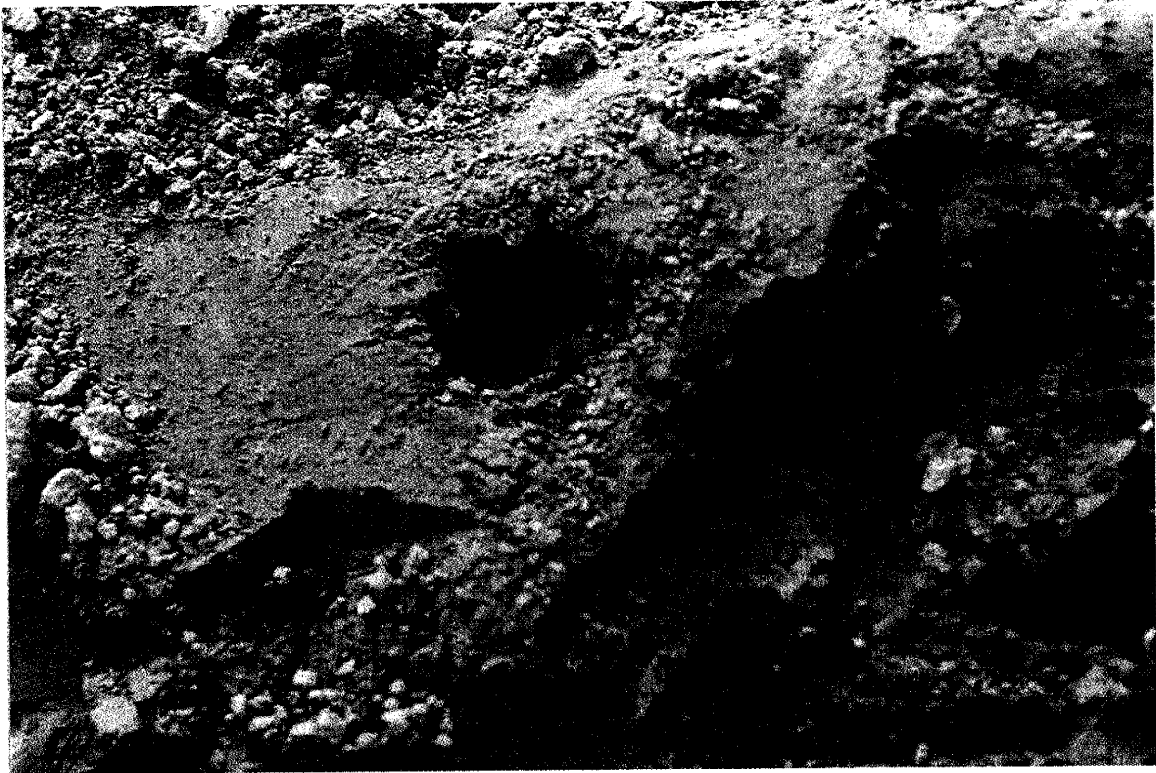


Plate 80. Pink dyed crayfish burrow at approximately 2 m depth.



Plate 81. Crayfish hole in Unit 3 (oxidized layered clays).



Plate 82. Complex of crayfish burrows in Unit 3 (layered oxidized clays) at south of site. Depth approximately 2.5 m.



Plate 83. Crayfish burrow in Unit 2 (unoxidized layered clays).



Plate 84 (above). Large crayfish burrow or possible mouse burrow at 75° angle from vertical, just below surface at far west edge of the excavation. This burrow dropped straight down at least 4 feet, then turned toward center of the site..

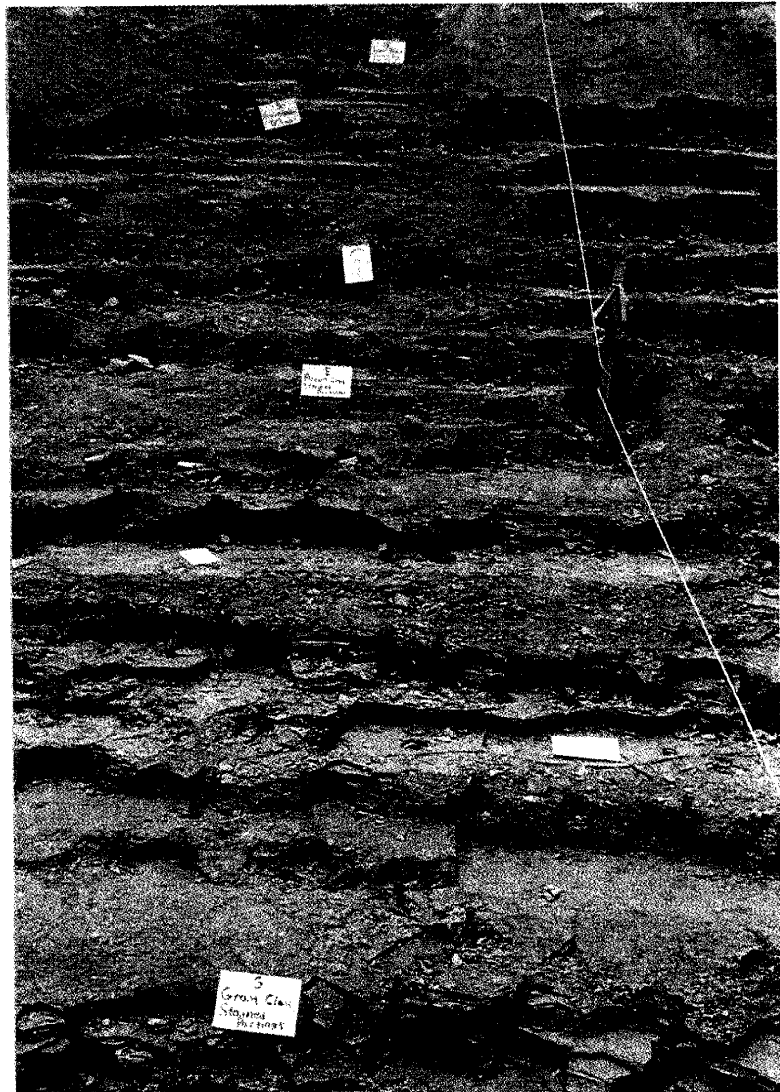


Plate 85 (right). Transect from Unit 2 (layered unoxidized clays) to surface (Unit 5 topsoils) at south of excavation.

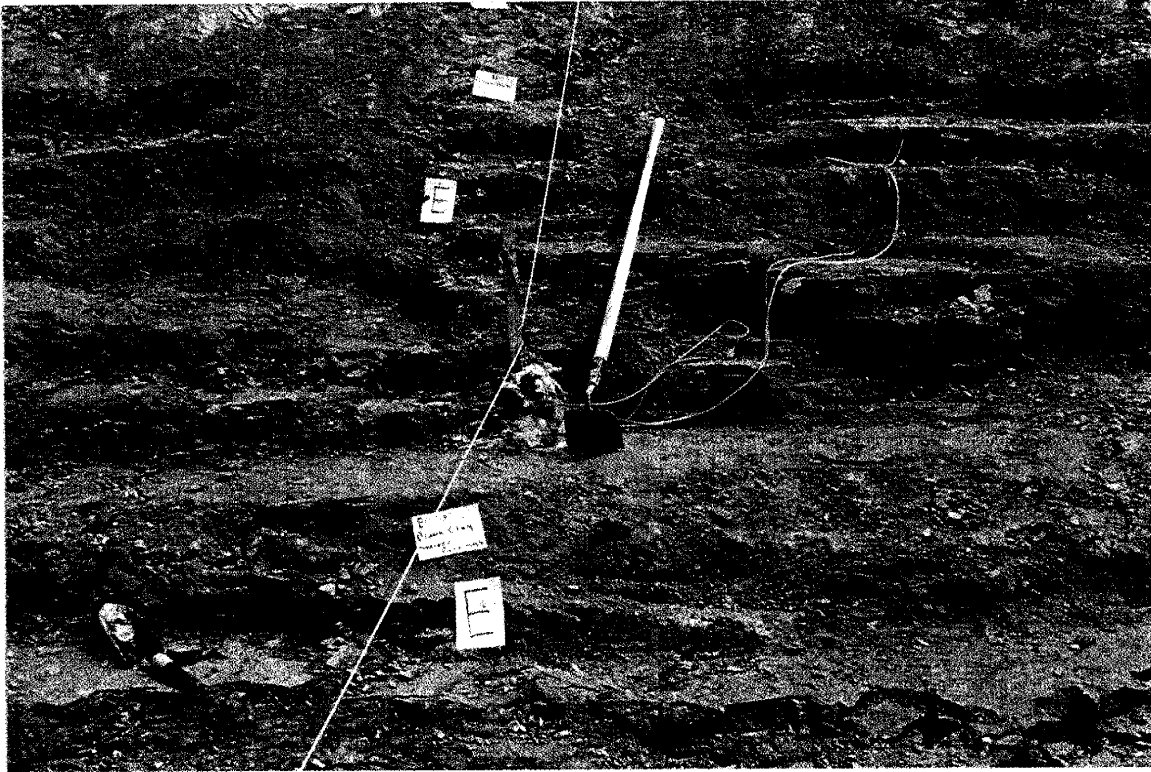


Plate 86. Hand terracing of east side of excavation. Sandpack and sampling tubes from a soil water sampler can be seen in the center of the plate.

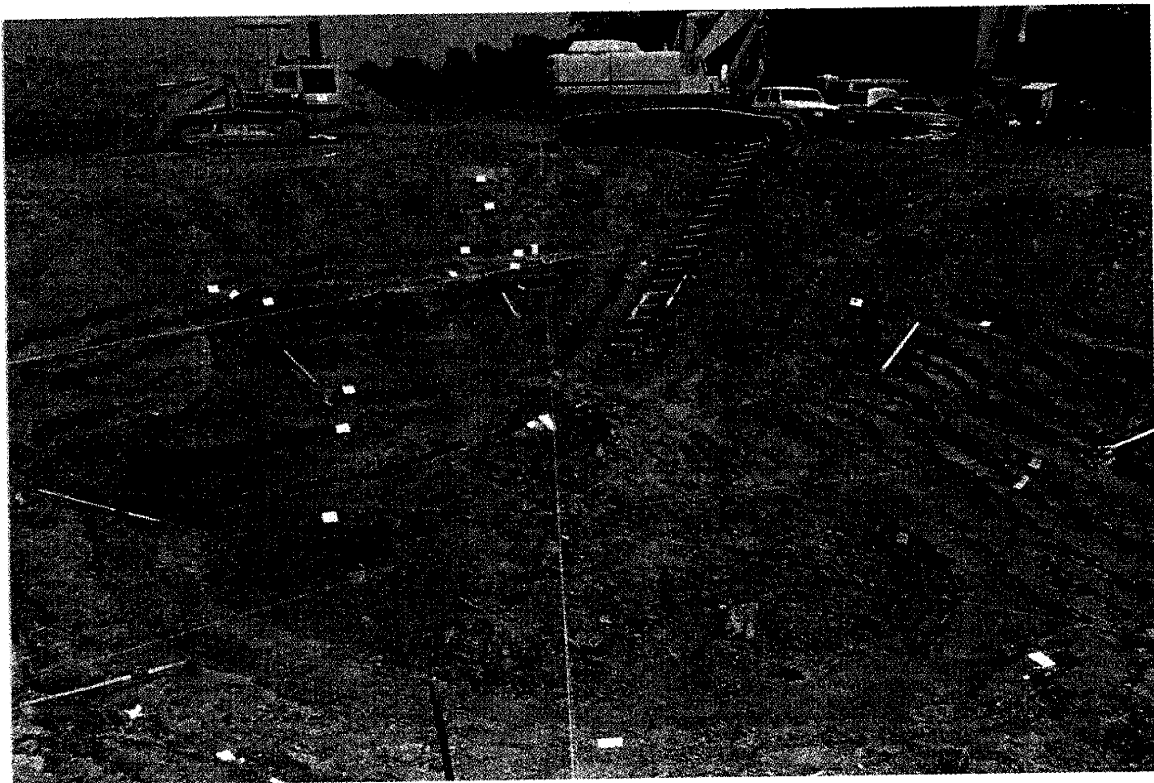


Plate 87. View of the excavation at noon, August 26, 1994. Facing North. The excavated material can be seen in the large pile behind the bulldozer. The silty sand body in the NW quadrant is outlined

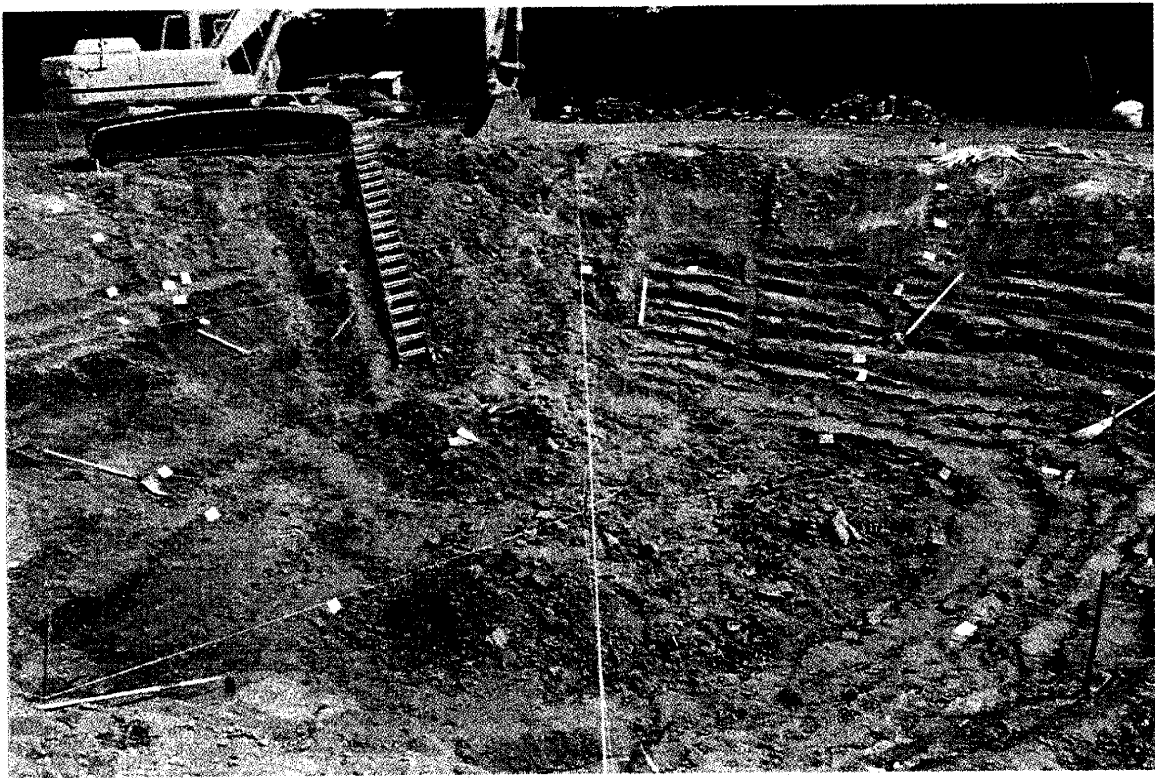


Plate 88. View of the excavation on August 26, 1994, facing NE.

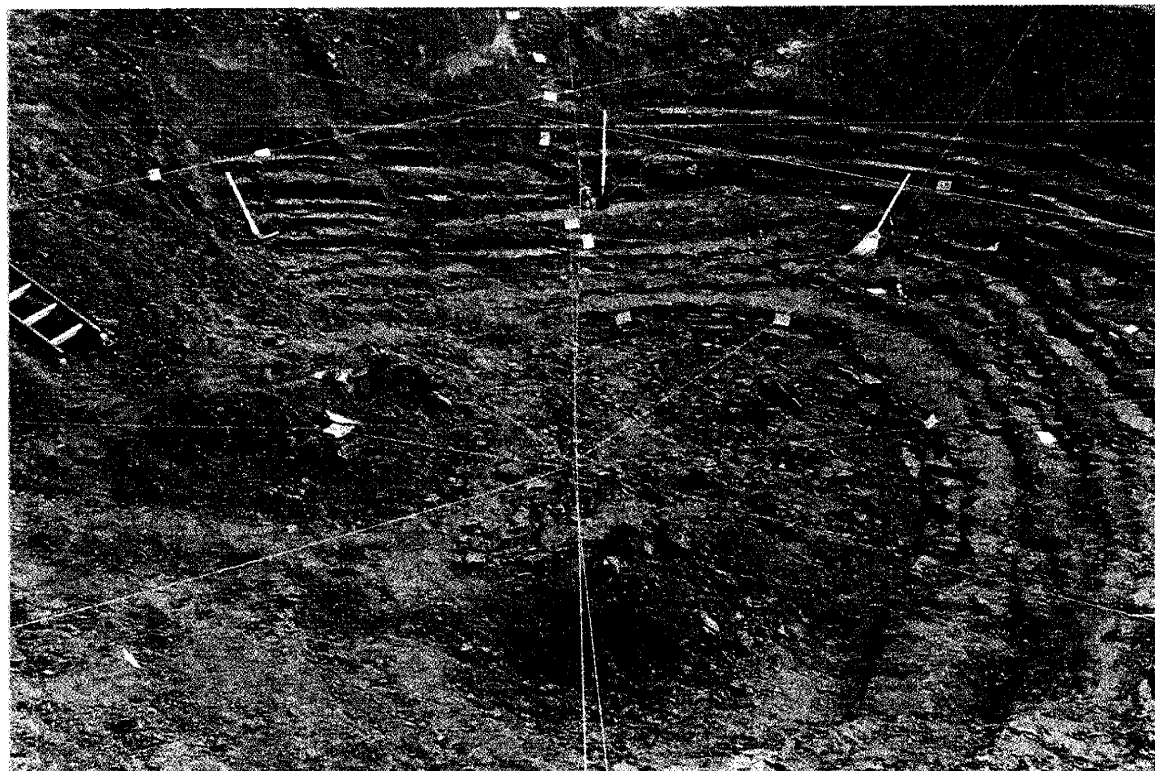


Plate 89. View of the excavation at noon on August 26, 1994, facing East.

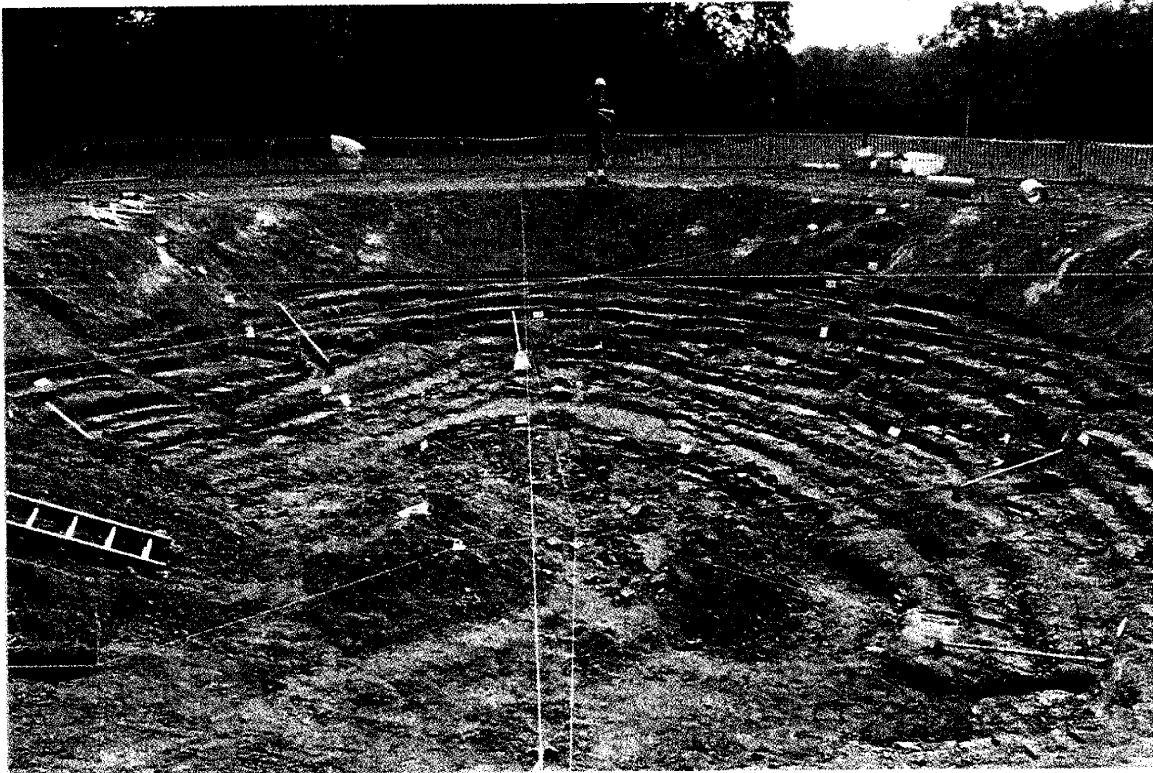


Plate 90. View of the excavation at noon on August 26, 1994, facing SE.

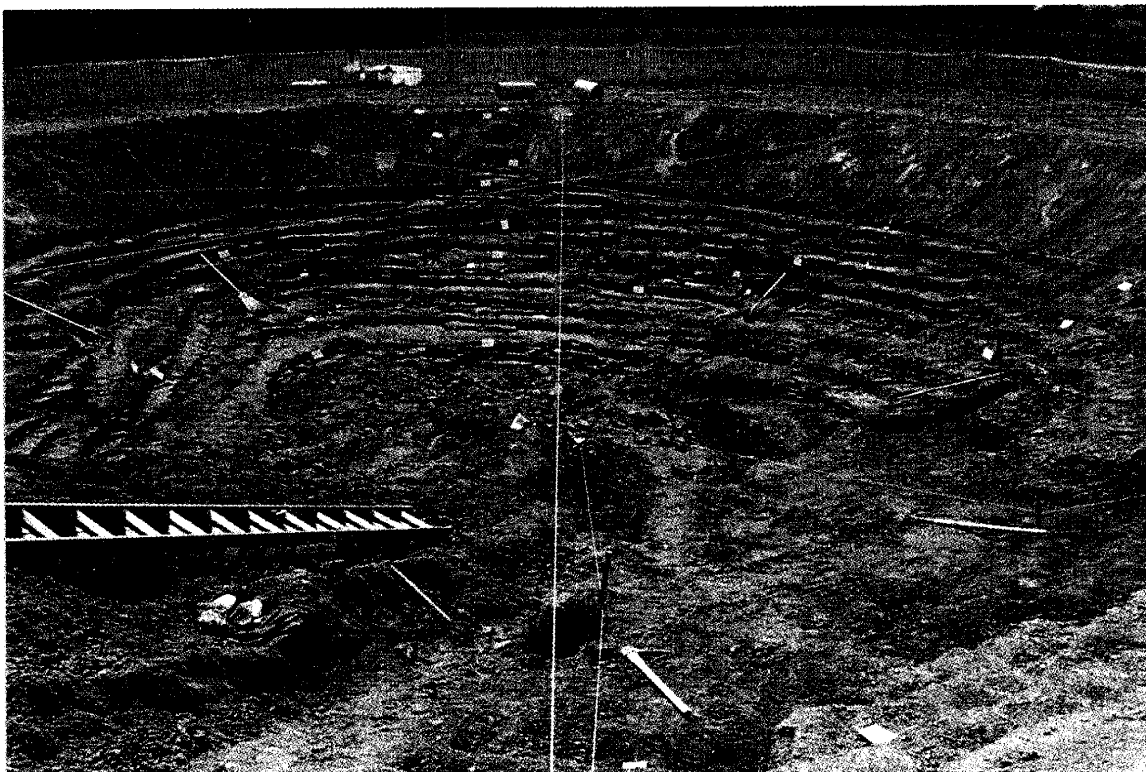


Plate 91. View of the excavation at noon on August 26, 1994, facing South.



Plate 92. View of the excavation at noon on August 26, 1994, facing SW.

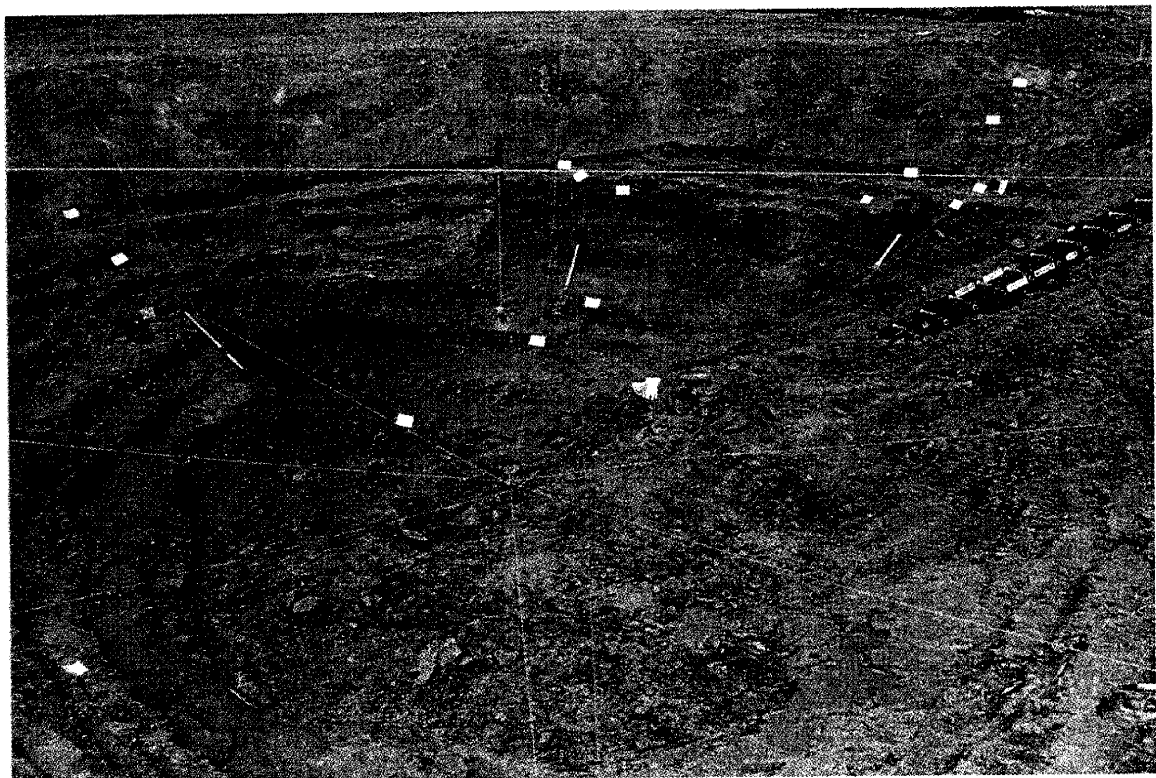


Plate 93. View of the excavation at noon on August 26, 1994, facing West.

Plate 94 (right). View of the silty sand body in the NW quadrant of the site, at noon on August 26, 1994.



Plate 95 (below). Core sampling by back hoe.





Plate 96. View inside a finished vertical core.



Plate 97. Back hoe insertion of horizontal core.

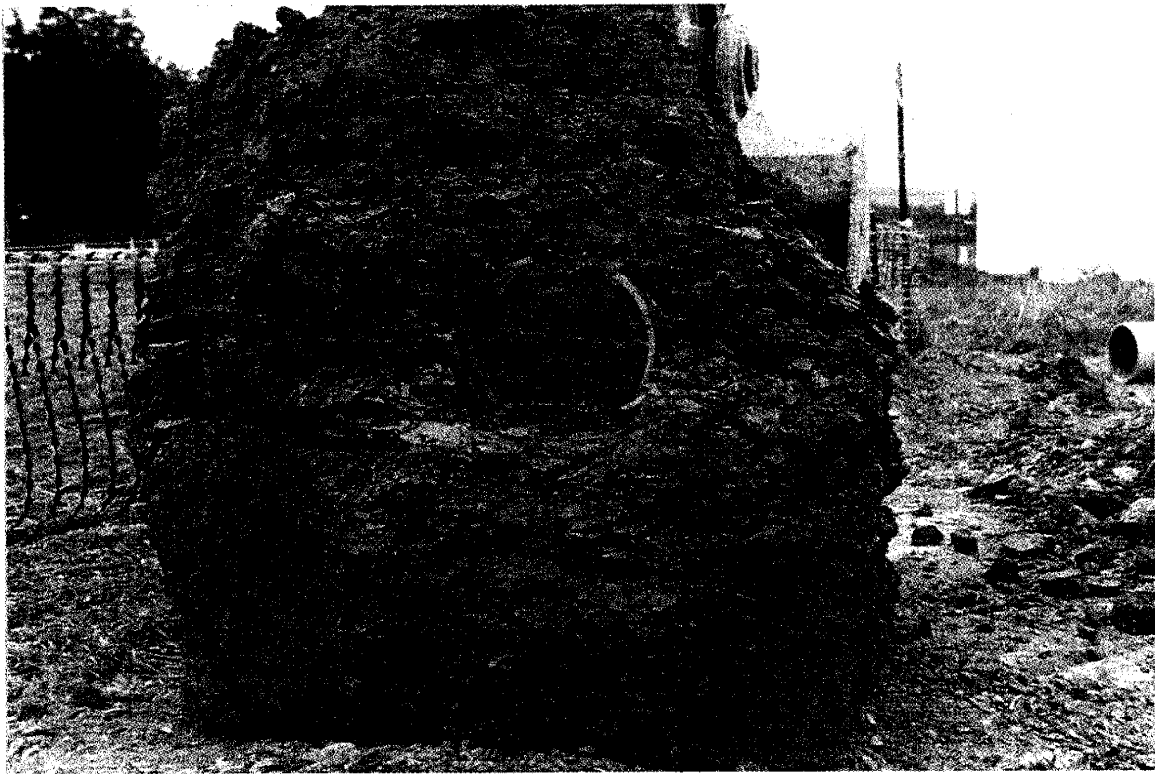


Plate 98. Extracted horizontal core from Unit 3.



Plate 99. Close up of extracted horizontal core.

Plate 100 (right). Back hoe gouge into the massive unoxidized clay of Unit 1.

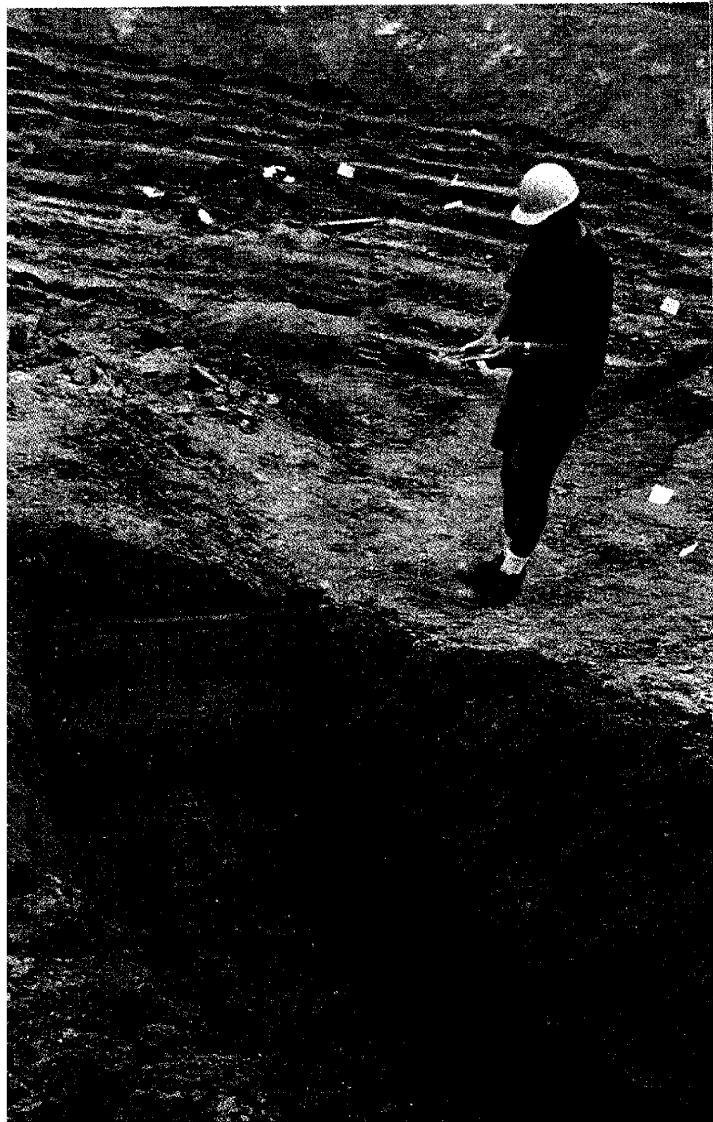
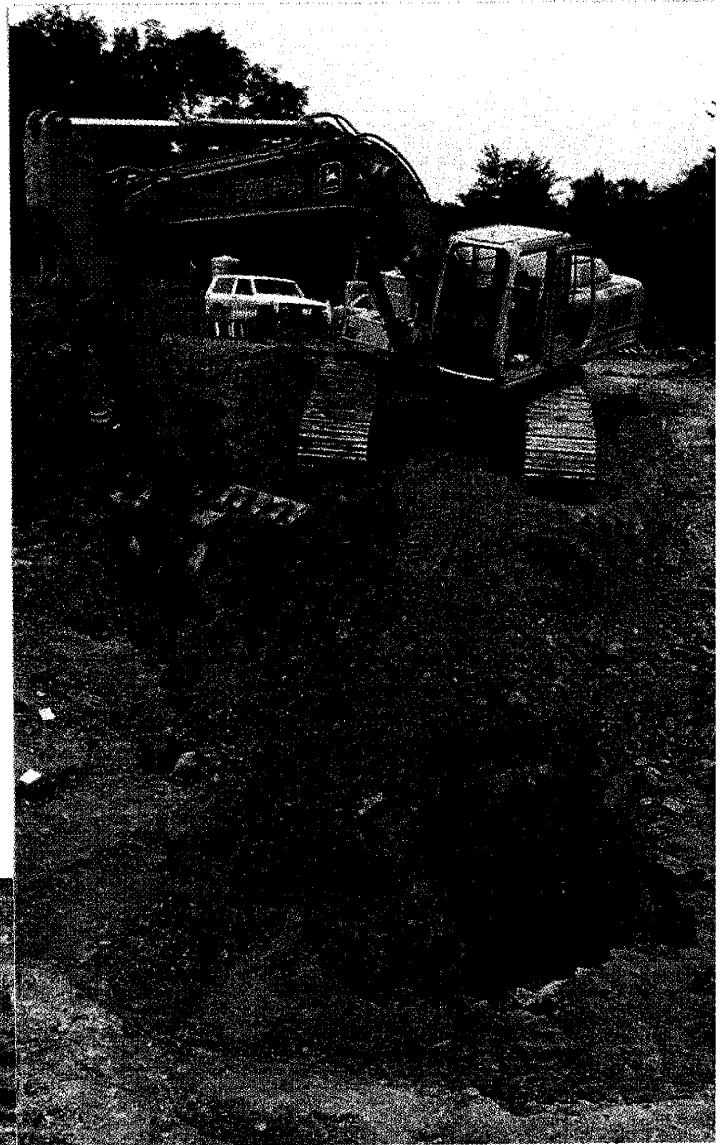


Plate 101 (left). Back hoe gouge into the massive unoxidized clay of Unit 1.

Plate 102 (right). Gravels, cobbles, and sand inclusion in Unit 1. The depth is approximately 6 m.



Plate 103 (below). Dye along fracture plane of a sample excavated from the massive unoxidized clays of Unit 1.



Plate 104 (right) . Covered opening
of crayfish burrow #1 at surface.



Plate 105 (below). Crayfish burrow #1
15 cm below surface.

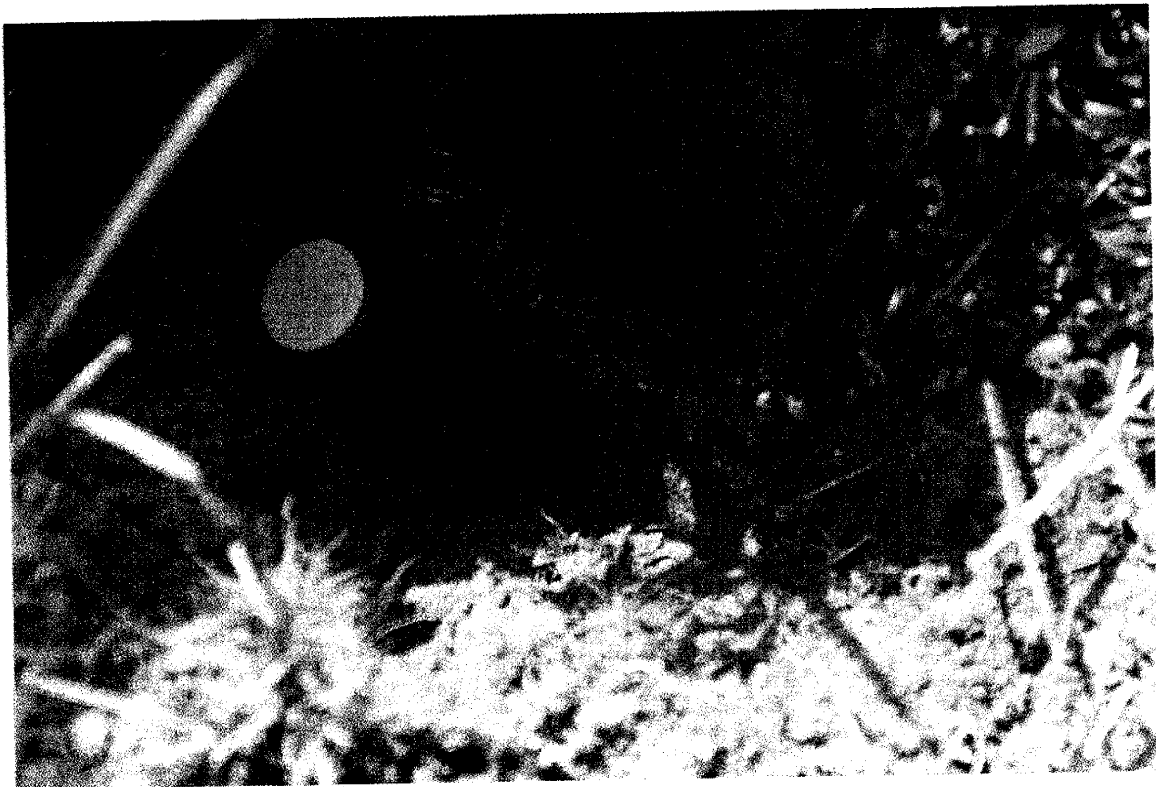




Plate 106. Covered surface opening of crayfish burrow #2.



Plate 107. Crayfish burrow #2.



Plate 108. Crayfish burrow #3. This is the third crayfish burrow found in a cursory 15 minute examination of the field surface surrounding the infiltration sites.



Plate 109. Crayfish burrow #3.



Plate 110. Sites A and C after termination of the Subsurface Transport Pathways Characterization Test. Facing East Southeast towards Paddy's Run and the main FERMCO plant. The two 500 gal site supply tanks of Site C are seen to the right, and the backhoe and Site A are to the left. The excavated material seen in the large dirt pile was repacked into the Site A excavation.